Universiteit Gent, Faculteit Toegepaste Wetenschappen
Vakgroep Bouwkundige Constructies
Ghent University, Faculty of Engineering
Department of Structural Engineering

CONSTRUCTIEF GEDRAG EN ONTWERP VAN BETONCONSTRUCTIES VERSTERKT MET UITWENDIG GELIJMDE VEZELCOMPOSIETWAPENING

STRUCTURAL BEHAVIOUR AND DESIGN OF CONCRETE MEMBERS STRENGTHENED WITH EXTERNALLY BONDED FRP REINFORCEMENT

Stijn MATTHYS

LABORATORIUM MAGNEL VOOR BETONONDERZOEK
MAGNEL LABORATORY FOR CONCRETE RESEARCH

Proefschrift tot het verkrijgen van de graad van
Doctor in de Toegepaste Wetenschappen, richting Bouwkunde
Academiejaar 1999-2000

Thesis in fulfilment of the requirements for the degree of
Doctor of Applied Sciences, option Structural Engineering
Academic year 1999-2000

CONSTRUCTIEF GEDRAG EN ONTWERP VAN BETONCONSTRUCTIES VERSTERKT MET UITWENDIG GELIJMDE VEZELCOMPOSIETWAPENING

STRUCTURAL BEHAVIOUR AND DESIGN OF CONCRETE MEMBERS STRENGTHENED WITH EXTERNALLY BONDED FRP REINFORCEMENT

Universiteit Gent, Faculteit Toegepaste Wetenschappen
Vakgroep Bouwkundige Constructies
Ghent University, Faculty of Applied Sciences
Department of Structural Engineering

CONSTRUCTIEF GEDRAG EN ONTWERP VAN BETONCONSTRUCTIES VERSTERKT MET UITWENDIG GELIJMDE VEZELCOMPOSIETWAPENING

STRUCTURAL BEHAVIOUR AND DESIGN OF CONCRETE MEMBERS STRENGTHENED WITH EXTERNALLY BONDED FRP REINFORCEMENT

Stijn MATTHYS

LABORATORIUM MAGNEL VOOR BETONONDERZOEK
MAGNEL LABORATORY FOR CONCRETE RESEARCH

Proefschrift tot het verkrijgen van de graad van
Doctor in deToegepaste Wetenschappen, richting Bouwkunde
Academiejaar 1999-2000

Thesis in fulfilment of the requirements for the degree of
Doctor of Applied Sciences, option Structural Engineering
Academic year 1999-2000

Promotor – *Supervisor*
Prof. Dr. Ir. L. Taerwe
Universiteit Gent, Vakgroep Bouwkundige Constructies
–
Prof. Dr. Ir. L. Taerwe
Ghent University, Departement of Structural Engineering

Onderzoeksinstelling – *Research institute*
Universiteit Gent, Vakgroep Bouwkundige Constructies
Laboratorium Magnel voor Betononderzoek
Technologiepark-Zwijnaarde 9
9052 Gent
–
Ghent University, Departement of Structural Engineering
Magnel Laboratorium for Concrete Research
Technologiepark-Zwijnaarde 9
B-9052 Ghent

Beursverlenende instantie – *Research grant offered by*
Vlaams Instituut voor de bevordering van het Wetenschappelijk-Technologisch Onderzoek in de Industrie (IWT)
Bischoffsheimlaan 25
1000 Brussel
–
Institute for the Promotion of Innovation by Science and Technology in Flanders (IWT)
Bischoffsheimlaan 25
B-1000 Brussels

"The thinking that we are has brought us to where we have already been.
In order to go somewhere else, we must think in a different way."

Albert Einstein

Dedicated to Els, Tijmen and Siebe

Preface

This doctoral study concerns advanced composite reinforcement for concrete structures and more specifically its use as externally bonded reinforcement to repair and strengthen existing structures. As a novel reinforcing material for concrete, these composites were brought to my attention as an engineering student, reading an article about 'the house of the future'. A few years later, Prof. L. Taerwe offered me the opportunity to perform a graduation thesis on the 'structural behaviour of prefabricated concrete slabs pretensioned with advanced composites'. As a result, I became active in this research field, first as a final year student, after graduating in 1994 as a research assistant and in 1996 as a doctoral researcher.

The work presented in this report is based on the research I conducted over the last four years with a doctoral research grant provided by the IWT (Vlaams Instituut voor de bevordering van het Wetenschappelijk-Technologisch Onderzoek in de Industrie - Institute for the Promotion of Innovation by Science and Technology in Flanders) of the Flemish Community. The work has been carried out at the Magnel Laboratory for Concrete Research, Department of Structural Engineering of Ghent University. In addition to the IWT, also the Research Fund of Ghent University, the Volvo Fund, the Fund for Scientific Research – Flanders and the European Community (TMR Programme) are acknowledged for their financial support. The companies B.K. International, ECC, Resiplast, Sika, Sumitomo Europe, Syncoglas and S&P Clever Reinforcing Company are gratefully recognized for providing test material.

During my doctoral study several persons gave me their support and contributed to the experimental and analytical studies. First of all, I am very grateful to my supervisor Prof. Luc Taerwe, director of the Magnel Laboratory for Concrete Research, who gave me the opportunity to perform research on an innovative topic, yet closely related to building practice. I appreciate very much his support and many suggestions during the whole research project, as well as the useful discussions we had. Also, I am thankful for the international dimension he gave to this research project, resulting in the participation of the author to several conferences and workshops, membership in international task groups and study visits to other research institutes. I want to thank Prof. Paul Thomas for being there with his pragmatic ideas and thinking. A word of thanks is also addressed to the visiting researchers, Paolo Serra, Hossam Khalil, and Ramiro Sanchez-Lopez and the graduation students, Jeroen Depla, Peter De Meyer and Katrien Audenaert, who participated in some of the research. Especially, I want to recognize my colleagues and the foreign guests, for the friendly and the professional contacts.

With respect to the experimental work, I am indebted to the technical staff of the laboratory, who made it possible to perform quite a lot of large scale experiments. A special word of thanks is also addressed to the administrative staff for their friendly support and for being helpful when needed.

In the framework of this study I was able to meet many people abroad. In this respect, I want to thank Drs. T. Triantafillou, S. Rizkalla, C. Burgoyne, B. Täljsten, G. Manfredi, R. Tepfers, K. Pilakoutas and many others for the interesting conversations and feed-back I had with them. Especially, I appreciate the pleasant and interesting time during the meetings of fib (International Federation for Structural Concrete) Task Group 9.3 "FRP Reinforcement for Concrete Structures" and CUR (Civieltechnisch Centrum Uitvoering Research en Regelgeving) Task Group C97B-1 "Regelgeving voor versterken van betonconstructies met behulp van uitwendige koolstofvezellijmwapening [Rules for the strengthening of concrete structures using externally bonded carbon fibre reinforced polymer reinforcement]", as well as during my short study stays at the University of Manitoba (Canada), Chalmers University (Sweden), the Royal Institute of Technology in Stockholm (Sweden) and the University of Artois (France).

Finally, I want to thank my family, close friends and colleagues who encouraged and supported me in a more personal way. Special thanks go to my wife Els, who supported me in so many ways.

Ghent, September 2000
Stijn Matthys

Abstract

This thesis deals with several aspects of the structural behaviour and the design of reinforced concrete members strengthened with externally bonded fibre reinforced polymer reinforcement. Both analytical and experimental work are presented, focussing on the development of design guidelines.

In the first chapter, an introduction is given on fibre reinforced polymer (FRP) materials as structural reinforcement for concrete and more specifically as externally bonded reinforcement to strengthen existing structures. Briefly, the use of FRP in concrete construction, its history, benefits and some particular aspects of using this novel reinforcing material are mentioned. The repair and strengthening with externally bonded FRP reinforcement (FRP EBR) is discussed, demonstrating the efficiency and attractiveness of this technique among which the advantages and disadvantages of this technique. The problem statement and consequently the aim and the outline of this thesis are presented.

In Chapter 2, a description is given of FRP materials and their characteristics, the FRP systems available for externally bonded reinforcement and the techniques to apply them to the concrete. It is demonstrated that FRP reinforcement forms a group of materials, with high performance characteristics, which strongly depend on the assembly of the constituent materials. In general, the FRP EBR systems are very strong and durable. Nevertheless, when evaluating the properties of different types of FRP, EBR systems based on carbon fibre reinforced polymers (CFRP) exhibit the best characteristics.

The performed experimental and analytical studies concerning the structural behaviour of concrete elements strengthened with FRP EBR are reported in Chapters 3 till 6. These chapters correspond to the four test programmes which have been conducted, dealing with flexural and shear strengthening of reinforced concrete beams, strengthening of tensile members (to investigate tension stiffening and cracking behaviour) and confinement of axially loaded columns. The experiments were mainly conducted on large scale elements, varying several parameters with respect to the strengthening materials, the amount of external reinforcement and the strengthening lay-out or configuration. Based on the experimental work, an insight is obtained in the structural behaviour of the strengthened members. The feasibility and efficiency of externally bonded FRP reinforcement to strengthen concrete structures is clearly demonstrated. From the analytical verifications, existing models have been verified and extended to predict the influence of externally bonded FRP reinforcement. These calculation models deal with both the ultimate state and serviceability behaviour. It appears that the structural behaviour of the strengthened concrete members can be predicted in an accurate way.

Based on the derived models and a literature review regarding the models for FRP bond failure, Chapter 7 gives detailed provisions for the design of the strengthened members. In this extensive chapter, the basis of design, the safety concept, the design models and procedures and some special design considerations are provided for concrete members

strengthened in flexure and shear, axially loaded confined columns and strengthened tensile members. From this chapter it appears that, compared to new structures, the design of concrete members strengthened with externally bonded reinforcement is more complex. To assure structural safety, suggestions with respect to design failure modes, ductility and accidental loss of FRP EBR are formulated. It is demonstrated that the design of strengthened flexural members is often governed by the serviceability limit state and that special attention should be paid to the ultimate limit state verification of bond failure. To gain better insight into the design aspects, a parametric study concerning flexural strengthening is presented.

In the last chapter, the conclusions of the doctoral study are summarized and an outlook on the future use and development of the FRP EBR technique is given. Some suggestions for continued research are made.

Table of contents

Notations

Roman upper case letters

A_c	cross-sectional area of concrete
$A_{c,eff}$	effective concrete area in tension
A_e	cross-sectional area of effectively confined concrete
A_f	cross-sectional area of FRP reinforcement
A_g	gross cross-sectional area
A_r	cross-sectional area of reinforcement
A_s	cross-sectional area of longitudinal steel reinforcement
A_{s1}	cross-sectional area of longitudinal tensile steel reinforcement
A_{s2}	cross-sectional area of longitudinal compressive steel reinforcement
A_u	cross-sectional area of unconfined concrete
A_{wf}	cross-sectional area of FRP shear reinforcement
A_{ws}	cross-sectional area of steel shear reinforcement
C_i	constant
D	diameter of cylinder or column
D_i	constant
E_a	modulus of elasticity of adhesive
E_c	modulus of elasticity of concrete
$E_{c\ell II}$	modulus of elasticity of concrete at origin of second branch (circumf. direction)
$E_{c\ell 1}$	modulus of elasticity of concrete of first branch (circumferential direction)
$E_{c\ell 2}$	modulus of elasticity of concrete of second branch (circumferential direction)
E_{cII}	modulus of elasticity of concrete at origin of second branch
E_{c1}	modulus of elasticity of concrete of first branch
E_{c2}	modulus of elasticity of concrete of second branch
$E_{c\infty}$	modulus of elasticity of concrete for long-term loading
E_{el}	elastic energy
E_f	modulus of elasticity of FRP
$E_{f,comp}$	modulus of elasticity of FRP in compression
E_{fib}	modulus of elasticity of fibres
E_{fk}	characteristic value of modulus of elasticity of FRP
$E_{fk0.05}$	lower bound characteristic value (5 % fractile) of E-modulus of FRP
$E_{fk0.95}$	upper bound characteristic value (95 % fractile) of E-modulus of FRP
$E_{f,tens}$	modulus of elasticity of FRP in tension
E_{fu}	modulus of elasticity of FRP at ultimate stage
E_i	tangent modulus of elasticity of concrete at origin in the axial (i = c) or circumferential (i = cℓ) direction
E_{iII}	modulus of elasticity of concrete at origin of second branch
E_{i1}	modulus of elasticity of concrete of first branch

E_{i2} modulus of elasticity of concrete of second branch
E_{mat} modulus of elasticity of matrix
E_r modulus of elasticity of reinforcement
E_s modulus of elasticity of steel
E_{sec} secant modulus of elasticity
$E_{sec,M}$ $= f_{ccM}/\varepsilon_{cc1M}$
$E_{sec,Md}$ $= f_{ccMd}/\varepsilon_{ccMd}$
$E_{sec,u}$ secant modulus of elasticity at ultimate stage
$E_{sec,ud}$ secant modulus of elasticity at ultimate limit state
E_{sec1} $= f_{cc}/\varepsilon_{cc1}$
$\Sigma(EA)$ axial stiffness of the tension reinforcement
G_a shear modulus of adhesive
G_f fracture energy
I_c moment of inertia of transformed (cracked) section
I_{co} moment of inertia of transformed (cracked) section before strengthening
I_f moment of inertia about the centroid of FRP
I_{o2} moment of inertia of transformed cracked section before strengthening
I_1 moment of inertia of transformed uncracked section
I_2 moment of inertia of transformed cracked section
K_{conf} parameter expressing the stiffness and effectiveness of the confining device
K_{confx} K_{conf} in x-direction
K_{confy} K_{conf} in y-direction
K flexural stiffness
L distance between support and end of FRP
$\overline{M}$ moment line of a beam with a point load Q = 1 at midspan
M(x) moment at distance x
M_{Ad} design value of resisting moment of the accidental situation
M_{cr} cracking moment
M_d design value of moment
M_{dS} design value of moment of strengthened member
M_{fib} fibre mass per area
M_k characteristic value of moment
M_{kg} moment due to dead load
M_{kq} moment due to life load
M_{Rbd} resisting design moment corresponding with V_{Rbd}
M_{Rd} resisting design moment
M_{RdS} resisting design moment of strengthened member
M_{RdU} resisting design moment of unstrengthened member
M_{Rpd} design value of moment corresponding with V_{Rpd}
M_{Sd} acting design moment
$M_{x=0}$ moment acting on section corresponding to end of EBR
M_y moment at which internal steel starts yielding
M_{yd} design value of moment at which internal steel starts yielding

M_o	acting moment during strengthening
M_{serS}	service moment of stengthened beam under rare load combination, obtained from M_{RdS}
M_{serU}	service moment of unstengthened beam under rare load combination, obtained from M_{RdU}
N	applied tensile force or acting load
N_c	force in concrete
N_{cr}	cracking load
$N_{cr,exp}$	cracking load (experimental)
$N_{cr,m}$	$= (N_{cr,n} + N_y)/2$
$N_{cr,n}$	load beyond which concrete element is in stabilized cracking phase
N_f	force in FRP
N_{fa}	FRP force to be anchored
N_{fad}	design value of FRP force to be anchored
$N_{fa,max}$	maximum FRP force which can be anchored
$N_{fad,max}$	design value of maximum FRP force which can be anchorage
N_{fd}	acting design force in FRP
$N_{fQu}(\ell_{t,max})$	acting force at distance $\ell_{t,max}$ from end of FRP, when reaching ultimate load
N_{Rd}	resisting design force
N_{Rfd}	resisting design force in FRP
N_{Rsd}	resisting design force in steel
N_r	$= N_s + N_f$
N_{rd}	$= N_{sd} + N_{fd}$
N_{ref}	(ultimate) load of reference specimen
N_{rk}	$= M_k/z_e$
N_{Sd}	acting design force
N_{Srd}	acting design force in reinforcement
N_s	force in steel
N_{sd}	acting design force in steel
N_{s1}	force in tensile steel reinforcement
N_{s2}	force in compressive steel reinforcement
N_u	ultimate load
$N_{u,exp}$	ultimate load (experimental)
N_y	load after yielding of the internal steel reinforcement
$N_{y,exp}$	load after yielding of the internal steel reinforcement (experimental)
Q	point load
Q_{ana}	ultimate load (analytical verification)
Q_{cal}	ultimate load (calculated)
Q_{cr}	cracking load
$Q_{cr,exp}$	cracking load (experimental)
Q_{exp}	ultimate load (experimental)
Q_f	force in FRP
Q_{k1}	service load, from ultimate limit state assuming full composite action

Q_{k2}	service load, from ultimate limit state verifying loss of composite action
Q_{k3}	service load, from stress limitations
Q_{k4}	service load, from deflection limitations
Q_{k5}	service load, from crack width limitations crack width
Q_{max}	maximum load
Q_{ref}	(ultimate) load of reference specimen
Q_{ser}	service load
Q_u	ultimate load
$Q_{u,ref}$	ultimate load of reference specimen
Q_y	load at which the steel starts yielding
Q_o	load at which the FRP EBR is applied
R	curvature of the helix, or radius of cylinder or column
T	temperature
T_g	glass transition temperature
V_c	shear capacity of concrete
V_{ck}	concrete shear contribution at service load
V_{cr}	shear force causing shear cracking
V_d	acting design shear force
$V_{f,exp}$	FRP shear contribution (experimental)
V_k	shear force at service load
V_R	resisting shear capacity
V_{Rbd}	resisting design shear force at which bond failure is initiated
V_{Rd}	resisting design shear capacity
V_{Rd1}	resisting design shear capacity of the concrete
V_{Rd2}	resisting design shear capacity of the concrete in diagonal compression
V_{Rp}	resisting shear force at which shear crack peeling is initiated
V_{Rpd}	resisting design shear force at which peeling initiates
V_{Sd}	acting design shear force
V_u	ultimate shear capacity
$V_{u,ref}$	ultimate shear capacity of reference specimen
V_{wf}	resisting shear capacity of FRP shear reinforcement
V_{wfd}	resisting design shear capacity of FRP shear reinforcement
V_{ws}	resisting shear capacity of steel stirrups
V_{wsd}	resisting design shear capacity of steel stirrups
$V_{x=0}$	shear force acting on section corresponding to end of EBR

Roman lower case letters

a	maximum deflection, or shear span
a_c	length governing critical flexural shear crack of unstrengthened member
a_g	maximum deflection due to self weight

a_L	fictitious shear span
a_ℓ	horizontal distance over which the moment line is shifted
a_{lim}	maximum allowable deflection
a_Q	maximum deflection due to the point loads
a_v	distance from major load to support
a_1	deflection in uncracked state
a_2	deflection in fully cracked state
$(a / \ell)_{max}$	ratio of the allowable deflection over the span length ℓ
b	width of concrete member
b′	clear width between the rounded corners
b_f	total width of the bonded FRP
b_w	minimum width of the section (width of the web)
b_o	constant
c_F	factor related to the fracture energy
d	effective depth of the member, or thickness of the bond layer
d′	clear depth between the rounded corners
d_1	distance between tension face and tensile steel reinforcement
d_2	distance between compression face and compressive steel reinforcement
f_c	concrete compressive cylinder strength
f_{cb}	bond shear strength of the concrete
f_{cbd}	design bond shear strength of the concrete
f_{cbk}	characteristic bond shear strength of the concrete
f_{cc}	compressive strength of the confined concrete
f_{ccd}	design value of the confined concrete compressive strength
f_{ccM}	confined concrete strength assuming constant confining pressure $\sigma_{\ell u}$
f_{ccMd}	confined concrete strength assuming constant confining pressure $\sigma_{\ell ud}$
$f_{c,cube}$	concrete compressive strength measured on cubes
f_{cd}	design value of concrete compressive strength
f_{ck}	characteristic value of concrete compressive strength
f_{cm}	mean concrete compressive cylinder strength
$f_{c,prism}$	concrete compressive strength measured on prisms
f_{ct}	concrete tensile strength
f_{ctk}	characteristic value of concrete tensile strength
$f_{ctk0.05}$	lower bound characteristic tensile strength
$f_{ctk0.95}$	upper bound characteristic tensile strength
f_{ctm}	mean concrete tensile strength
f_{co}	unconfined concrete strength
f_f	FRP tensile strength
$f_{f,comp}$	FRP compressive strength
f_{fd}	design value of the FRP tensile strength
$f_{f,eff}$	effective strength of the FRP
$f_{fd,eff}$	effective design strength of the FRP

f_{fib}	tensile strength of the fibres
f_{fk}	characteristic value of the FRP tensile strength
f_{fm}	mean value of the FRP tensile strength
$f_{f,tens}$	$= f_f$
f_{wy}	yield stress of the stirrups
f_{wyd}	design value of yield stress of the stirrups
f_y	yield stress of the steel reinforcement
f_{yd}	design value of the yield stress of the steel reinforcement
f_{yk}	characteristic value of the yield stress of the steel reinforcement
$f_{o,c}$	intercept stress
$f_{o,c\ell}$	intercept stress (circumferential direction)
$f_{o,i}$	stress at the intercept of the second slope with the stress axis
g	self weight
h	total depth of the member
h_f	flange depth
k	constant
k_b	size factor
k_c	factor relating to compaction of concrete
k_e	confinement effectiveness coefficient
k_{e1}	confinement effectiveness coefficient, for partial wrapping
k_{e2}	confinement effectiveness coefficient, for account fibre orientation
k_{e3}	confinement effectiveness coefficient, for shape of cross-section
k_f	$= (\sin \alpha_f + \cos \alpha_f)$
k_M	coefficient depending on the loading type
k_s	$= (\sin \alpha_s + \cos \alpha_s)$
k_v	factor relating maximum moment and shear force
k_α	factor relating crack width assumed tensile member to maximum crack width
k_1, k_2	coefficients
ℓ	span length of the beam, or overlap joint length
ℓ_b	bonded length
$\ell_{cr,n}$	transfer length at stabilized cracking
ℓ_f	transfer length of FRP reinforcement (based on mean bond stress)
ℓ_r	transfer length
ℓ_{rf}	transfer length of FRP reinforcement
ℓ_s	transfer length of steel rebars (based on mean bond stress)
ℓ_t	available anchorage or transfer length
$\ell_{t,max}$	maximum anchorage or transfer length
ℓ_1	distance between the point load Q and the support
ℓ/d	ratio of span length to effective depth
$(\ell/d)_{max}$	maximum ratio of span length to effective depth

m	$= M_{kq}/M_{kg}$, for unstrengthened (U) or strengthened (S) member
m_i	mass fraction of constituent i
n	power
n_c	curve-shaped parameter
$n_{c\ell}$	curve-shaped parameter (circumferential direction)
n_i	curve-shaped parameter that mainly controls the curvature in the transition zone between the first and second branch
p	pitch of the helix
r	radius, or $= E_c/(E_c-E_{sec1})$
r_c	radius of rounded corners
$1/r$	curvature
$1/r_u$	curvature at failure
$1/r_y$	curvature at start of yielding of steel reinforcement
s	centre to centre spacing of the FRP, or slip, or adhesive thickness
s'	clear spacing between the FRP reinforcement
s_f	spacing of FRP shear reinforcement
$s_{f,max}$	maximum allowable spacing of the FRP reinforcement
s_{rm}	mean crack spacing
s_{rm}^{exp}	mean crack spacing (experimental)
$s_{r,max}$	maximum crack spacing
$s_{r,max}^{exp}$	maximum crack spacing (experimental)
s_s	spacing of steel stirrups
s_u	ultimate slip
s_1	slip corresponding to $\tau_{b,max}$
t	(total) thickness of FRP reinforcement
t_{df}	equivalent dry-fibre thickness
u	bond perimeter
u_f	bond perimeter of the FRP reinforcement
u_s	bond perimeter of the steel reinforcement
v	vertical crack displacement
v_{fib}	fibre volume fraction
v_i	volume fraction of constituent i
v_{mat}	matrix volume fraction
w	horizontal crack displacement
w_{crit}	critical crack width at which there is no longer aggregate interlock contribution
w_f	crack width at level of FRP reinforcement
w_h	horizontal component of the crack width
w'_i	clear distance between the rounded corners
w_k	characteristic value of the crack width
w_{lim}	maximum allowable crack width

w_m	mean crack width
w_s	crack width at level of steel reinforcement
w_v	vertical component of the crack width
x	depth of the compression zone, or $= \varepsilon_c/\varepsilon_{cc1}$, or distance
x_e	depth of the compression zone (linear elastic analysis)
x_{lim}	maximum allowable depth of compression zone (ductility requirement)
x_o	neutral axis depth before strengthening
y_u	ultimate deflection at midspan
y_{ref}	ultimate deflection at midspan of reference specimen
z	lever arm between total tensile force and compression force
z_e	lever arm between (linear elastic analysis)
z_f	lever arm between FRP tensile force and compression force
z_s	lever arm between steel tensile force and compression force

Greek upper case letters

Γ	reduced moment of inertia of transformed cross-section
Γ_f	parameter
Γ_o	reduced moment of inertia of transformed cross-section, prior to strengthening
Γ_1	reduced moment of inertia of transformed cross-section, uncracked state
Γ_2	reduced moment of inertia of transformed cross-section, cracked state
ΔM_d	variation of the design moment
ΔN_f	variation of the FRP force
ΔN_{fd}	variation of the design value of the FRP force
ΔT	temperature change
Δx	small distance
$\Delta\sigma_{f,cr}$	FRP stress increase at first cracking
Ø	(mean) diameter of the steel reinforcement
Φ_r	global load safety factor for the rare load combination
Φ_{qp}	global load safety factor for the quasi-permanent load combination

Greek lower case letters

α	reduction factor, or angle of shear reinforcement with respect to longitudinal axis
α_f	$= E_f/E_c$, or angle of FRP shear reinforcement with respect to longitudinal, or fibre orientation with respect to the circumferential direction

α_s	$= E_s/E_c$, or angle of steel stirrups with respect to longitudinal axis
$\alpha_{T,CFRP}$	coefficient of thermal expansion of FRP
$\alpha_{T,concrete}$	coefficient of thermal expansion of the concrete
α_1, α_2	parameter expressing confined concrete strength
α_{1d}, α_{2d}	parameter expressing the design value of confined concrete strength
β	coefficient which relates mean and characteristic value of crack width, or $= \beta_1\beta_2$, or parameter depending on the unconfined concrete properties
β_{fe}	coefficient which relates mean and characteristic value of ε_{fue}
β_t	factor taking into account the type of loading
β_1	coefficient taking into account the bond characteristics of the reinforcement
β_2	coefficient taking into account the loading type
γ_c	material safety factor for the concrete
$\gamma_{c,axial}$	material safety factor for the concrete under uniaxial compression
γ_g	load safety factor for the dead load
γ_f	material safety factor for the FRP
γ_M	partial safety factor for the materials
γ_q	load safety factors for the life load
γ_s	material safety factor for the steel
$\gamma_{s,axial}$	material safety factor for the steel under uniaxial compression
δ_G	distance from the compression face to the centroid of the compression force divided by the depth of the compression zone (stress block centroid coefficient)
$\delta_{1/r}$	curvature ductility index
$\delta_{1/r,min}$	minimum curvature ductility index
ε_c	concrete strain at the extreme compression fibre
ε_{ccMd}	axial strain of confined concrete corresponding with f_{ccMd}
ε_{ccu}	ultimate axial strain of confined concrete
ε_{ccud}	design value of ultimate axial strain of confined concrete
ε_{cc1}	axial strain of confined concrete at maximum load
ε_{cc1M}	axial strain of confined concrete corresponding with f_{ccM}
$\varepsilon_{c,exp}$	measured axial concrete strain
$\varepsilon_{c\ell}$	circumferential concrete strain
$\varepsilon_{c\ell II}$	circumferential concrete strain at the origin of second branch
$\varepsilon_{c\ell 1}$	circumferential concrete strain at maximum load
$\varepsilon_{c\ell u}$	circumferential ultimate concrete strain
$\varepsilon_{c\ell u,fit}$	circumferential ultimate concrete strain, calculated to fit experimental results
ε_{cm}	mean concrete strain
ε_{cr1}	tensile strain of the uncracked state, with $N = N_{cr}$
ε_{cr2}	tensile strain of the fully cracked state, with $N = N_{cr}$

ε_{cu}	ultimate concrete strain at the extreme compression fibre
ε_{cII}	concrete strain at the origin of second branch
ε_{co}	initial concrete strain
ε_{c1}	axial concrete strain at maximum load
ε_{f}	FRP reinforcement strain
$\varepsilon_{f,eff}$	effective FRP tensile strain
ε_{fm}	mean FRP reinforcement strain
$\varepsilon_{f,min}$	minimum required ultimate FRP strain to assure sufficient ductility
ε_{fQu}	midspan FRP strain at ultimate load
ε_{fu}	ultimate FRP strain
$\varepsilon_{fu,c}$	FRP strain in the critical section at ultimate stage
ε_{fud}	design value of the ultimate FRP strain
ε_{fue}	effective ultimate FRP strain
$\varepsilon_{fue,d}$	design value of the effective ultimate FRP strain
$\varepsilon_{fu,eff}$	effective failure strain of the FRP wrapping reinforcement
ε_{fum}	mean value of the ultimate FRP strain
ε_{i}	strain of the concrete in the axial (i = c) or circumferential (i = cℓ) direction
ε_{iII}	strain at the origin of the second branch
ε_{m}	mean value of the strain
ε_{mu}	mean ultimate strain
ε_{r}	reinforcement strain
$\varepsilon_{rm,r}$	mean strain of the reinforcement with respect to the surrounding concrete
ε_{r2}	reinforcement strain in the cracked section
ε_{s}	steel reinforcement strain
ε_{sm}	mean steel reinforcement strain
$\varepsilon_{s,min}$	minimum required ultimate steel strain to assure sufficient ductility
ε_{su}	ultimate strain of the steel reinforcement
ε_{s1}	steel tensile reinforcement strain
ε_{s2}	steel compressive reinforcement strain
ε_{y}	yield strain of the steel reinforcement
ε_{yd}	design value of the yield strain of the steel reinforcement
ε_{yk}	characteristic value of the yield strain of the steel reinforcement
ε_{o}	initial strain at the extreme tensile fibre before strengthening
ε_{1}	strain corresponding to the uncracked state
ε_{2}	strain corresponding to the fully cracked state
ζ, ζ', ζ_b	distribution or tension stiffening coefficients
ζ_l	boundary condition
η	= h/d
η_a	= M_{serS}/M_{Ak}
η_e	effectiveness factor
$\eta_e f_{fd}$	design value of the effective FRP strength of the confining reinforcement

η_S	$= M_{RdS}/M_{RdU}$
η_o	$= M_o/M_{serU}$
θ	angle between the diagonal shear crack and the member longitudinal axis
κ_f	ratio of the recorded mean tensile strain at ultimate load ε_{mu} to the mean ultimate FRP strain ε_{fu} obtained from tensile tests
λ	parameter
μ_{dS}	reduced acting design moment of the strengthened member
μ_{RdS}	reduced resisting design moment of the strengthened member
μ_{RdU}	reduced resisting design moment of the unstrengthened member
μ_u	dilation rate (change of circumferential strain with respect to the axial strain)
υ	coefficient taking into account the load configuration and span of the beam
ν	Poisson ratio
ν_f	Poisson ratio of the FRP
ν_{fib}	Poisson ratio of the fibres
ν_{mat}	Poisson ratio of the matrix
ξ	$= x/d$
ξ_b	bond parameter
ρ	reinforcement ratio
$\rho_{c,eff}$	ratio of the effective concrete area in tension
ρ_{eq}	equivalent reinforcement ratio
ρ_f	volumetric ratio of the FRP wrapping reinforcement, or density of the fibre composite
ρ_{fx}	ratio representing the quantities of transverse confining reinforcement in the x direction
ρ_{fy}	ratio representing the quantities of transverse confining reinforcement in the y direction
ρ_i	density of the constituent i
ρ_l	longitudinal reinforcement ratio
ρ_r	reinforcement ratio for either steel (r = s) or FRP reinforcement (r = f), or $= A_s/A_{c,eff}$
ρ_s	steel reinforcement ratio
ρ_{sg}	$= A_s/A_g$
$\rho_{s,min}$	minimum reinforcement ratio of the internal steel
$\rho_{w,eq}$	equivalent shear reinforcement ratio
ρ_{wf}	FRP shear reinforcement ratio
ρ_{ws}	steel shear reinforcement ratio
σ	stress
σ_c	concrete stress
σ_{ccu}	ultimate compressive stress of confined concrete
σ_{ccud}	design value of the ultimate compressive stress of confined concrete
$\sigma_{c,exp}$	measured axial concrete stress

σ_{cII}	concrete stress at the origin of the second branch
σ_f	FRP stress
σ_{fib}	fibre stress
σ_ℓ	lateral confining stress on the concrete
$\sigma_{\ell,circ}$	confinement stress per unit width exerted by circular FRP wrapping reinf.
$\sigma_{\ell,spiral}$	confinement stress per unit width exerted by helicoïdal FRP wrapping reinf.
$\sigma_{\ell u}$	maximum lateral confinement stress
$\sigma_{\ell ud}$	design value of maximum lateral confinement stress
$\sigma_{\ell ux}$	maximum lateral confining stresses in the x direction
$\sigma_{\ell uxd}$	design value of maximum lateral confining stress in the x direction
$\sigma_{\ell uy}$	maximum lateral confining stresses in the y direction
$\sigma_{\ell uyd}$	design value of maximum lateral confining stress in the y direction
$\sigma_{\ell x}$	lateral confining stress in the x direction
$\sigma_{\ell y}$	lateral confining stress in the y direction
σ_{mat}	matrix stress
σ_{max}	maximum stress
σ_r	stress in the tensile reinforcement (steel or FRP)
σ_s	stress in the tensile steel reinforcement
σ_{s2}	stress in the compressive steel reinforcement
σ_{ws}	tensile stress in the steel stirrups
τ	shear stress
τ_{ad}	design value of mean shear strength obtained through lap shear tests
τ_{am}	mean shear strength obtained through lap shear tests
τ_b	bond shear stress
τ_{bm}	mean bond shear stress
$\tau_{b,max}$	maximum bond shear stress
$\tau_{c,max}$	maximum shear stress in the concrete
τ_{cza}	shear stress mobilised in compression zone and in shear crack (aggregate interlock)
τ_{fm}	mean bond stress of the FRP reinforcement
τ_m	mean shear stress
τ_{max}	maximum shear stress
τ_{sm}	mean bond stress of the steel reinforcement
τ_{Rdl}	design value of resisting shear stress of concrete
τ_{Rm}	mean resisting shear stress
τ_{Rp}	resisting shear stress corresponding with initiation of peeling
τ_{Rpd}	design value of resisting shear stress at initiation of peeling
τ_{Rpk}	characteristic value of resisting shear stress at initiation of peeling

φ	ratio of the critical crack width at which there is no longer an aggregate interlock contribution to the mean crack spacing
ϕ	creep coefficient
χ	coefficient relating the dowel action to the axial stiffness of the reinforcement
ψ	ratio of the average over the maximum concrete compressive stress (stress block area coefficient)
ψ_2	load combination factor with respect to the quasi-permanent load combination
ω	constant

Important abbreviations

FRP	fibre reinforced polymer
FRP EBR	externally bonded FRP reinforcement
AFRP	aramid fibre reinforced polymer
CFRP	carbon fibre reinforced polymer
GFRP	glass fibre reinforced polymer
HFRP	hybrid fibre reinforced polymer
RC	reinforced concrete
SLS	serviceability limit state
ULS	ultimate limit state
AS	accidental situation
EC1	Eurocode 1
EC2	Eurocode 2

SAMENVATTING

Deze samenvatting geeft een overzicht van de voornaamste aspecten van het proefschrift, dat handelt over de versterking van structurele betonelementen met uitwendig gelijmde vezelcomposietwapening ('externally bonded fibre reinforced polymer reinforcement' of FRP EBR). De voor- en nadelen, de eigenschappen en de toepassing van deze versterkingstechniek worden besproken, alsook het uitgevoerd experimenteel onderzoek en de analytische verificaties. Ontwerprichtlijnen worden voorgesteld voor gewapend betonelementen versterkt in buiging en dwarskracht en axiaal belaste kolommen omwikkeld met FRP EBR.

1 Inleiding

1.1 Vezelcomposietwapening voor beton

De ontwikkeling van lichte vezels met hoge sterkte en stijfheid in de jaren veertig was het begin van een sterke opgang van de vezelcomposietmaterialen. Aanvankelijk slechts aangewend voor hoogwaardige toepassingen binnen de ruimtevaart en vliegtuigindustrie, groeide de interesse voor vezelcomposietmaterialen ook binnen een groter aantal sectoren van de industrie, waaronder de bouwsector. In de betonbouw is de aanwending van vezelcomposiet- of 'fibre reinforced polymer' (FRP) elementen, voornamelijk als structurele wapening, uitgegroeid tot één van de meest veelbelovende nieuwe technieken [1-4]. Immers, uitgesproken voordelen zoals o.a. een hoge axiale sterkte, een uitstekende corrosieweerstand en een laag soortelijk gewicht, maken deze FRP materialen aantrekkelijk voor zowel gewapend, voorgespannen als uitwendig versterkt beton. De aanwending van deze niet-metallische wapening biedt mogelijkheden waarbij hoogwaardige eigenschappen en duurzaamheid centraal staan.

De aangewende vezelcomposiet- of FRP wapeningen zijn opgebouwd uit sterke, dunne, continue vezels van niet-metallische aard ingebed in een matrix (harsbinder, vulstoffen en additieven). Voor de vezels wordt veelal uitgegaan van koolstofvezels, aramidevezels en glasvezels. Men spreekt respectievelijk van CFRP, AFRP en GFRP. De harsbinder bestaat bijvoorbeeld uit epoxy, vinylester of onverzadigd polyester. Fig. S-1 geeft een uitvergroot beeld van een CFRP (de diameter van één vezel bedraagt ongeveer 7 μm). Het spanning-rek diagram van enkele FRP elementen in vergelijking met gangbaar betonstaal en voorspanstaal wordt gegeven in Fig. S-2.

1.2 Versterken van betonconstructies

In de meeste geïndustrialiseerde landen, is de hedendaagse bouwkundige infrastructuur (bruggen, wegen, utiliteitsbouw, enz.) in zeer belangrijke mate uitgebouwd. Het onderhouden, herstellen en versterken van structurele elementen is dan ook van groot belang en brengt jaarlijks belangrijke investeringen met zich mee.

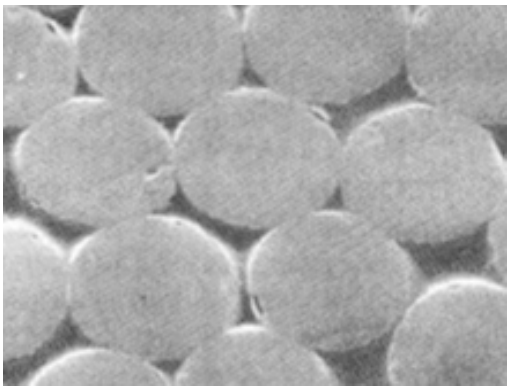

Fig. S-1 *Uitvergroting van een koolstofvezelcomposiet*

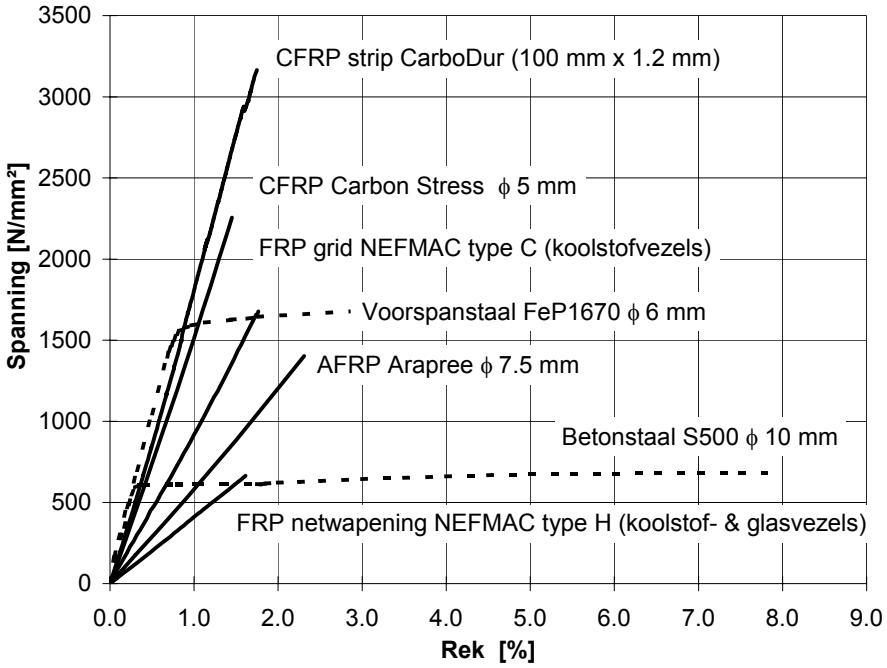

Fig. S-2 *Spanning-rek diagram van enkele FRP elementen in vergelijking met staal*

De noodzaak om bestaande constructies te herstellen en versterken bestaat met name vanwege diverse redenen.

- Verandering in functie en gebruik: het aanbrengen van openingen (vb. voor het plaatsen van leidingen en liftkokers), herbestemming van lokalen, toenemende belasting en frequentie van gebruik, enz.
- Uitwendige beschadiging door mechanische invloeden: impakt-belasting, explosie, sleet, heien van palen dicht bij bestaande gebouwen, bronbemaling, aardbeving, enz.
- Uitwendige of inwendige beschadiging door omgevingsinvloeden: corrosie van wapening, vriesschade, alkali-silica-reactie, inwerking van agressieve reagentia, brandschade, enz.
- Onvoorziene beschadiging door menselijke fouten (vb. doorboren van wapening of voorspanwapening bij het aanbrengen van signalisatie).

- Veranderingen in normen en ontwerprichtlijnen waardoor structurele elementen niet langer de beoogde veiligheidsmarges bezitten conform deze nieuwe normen.
- Fouten bij het ontwerp (foutieve detaillering, conceptiefouten en berekeningsfouten) of de uitvoering.

Voor het herstellen en versterken van structurele elementen kunnen een aantal verschillende technieken aangewend worden naargelang de specifieke situatie en de aard van de constructie. Eén van deze technieken, die veelvuldig toegepast wordt vanwege zijn efficiëntie, betreft uitwendig gelijmde staalwapening. Als alternatief wordt deze techniek recent ook met groot commercieel succes toegepast op basis van vezelcomposietwapening, met jaarlijks honderden toepassingen wereldwijd [1].

1.3 Probleemstelling en internationale stand van zaken

Uit de vele internationale onderzoeksprojecten, waaronder het onderzoek uitgevoerd aan het Laboratorium Magnel voor Betononderzoek, blijkt zeer duidelijk dat de aanwending van composietmaterialen in de betonbouw vele mogelijkheden biedt [1-7]. Dit getuigen ook de toepassingen die de laatste vijf à tien jaar (voornamelijk in Japan, USA, Canada, Duitsland en Zwitserland) werden gerealiseerd. Wat betreft nieuwe betonconstructies, gewapend of voorgespannen met FRP, dienen deze toepassingen vooralsnog als demonstratieprojecten beschouwd te worden. Daarentegen, wat betreft het versterken van bestaande constructies met uitwendig gelijmde vezelcomposietwapening kent het aantal praktische toepassingen in vele landen een exponentiële groei.

De aanzienlijke interesse in FRP wapening zal slechts blijvend in succesvolle toepassingen resulteren, indien voldoende inzicht bekomen wordt in het structureel gedrag van betonelementen gewapend, voorgespannen of versterkt met FRP en indien ontwerprichtlijnen beschikbaar zijn. In verband hiermee lopen in Japan, Noord-Amerika en Europa diverse initiatieven [8-10]. Met betrekking tot deze initiatieven, is er noodzaak aan fundamenteel onderzoek inzake rekenregels, analytische modellen en ontwerprichtlijnen voor de aanwending van structurele FRP wapening voor betonconstructies. Dit geldt in het bijzonder voor de versterking van betonconstructies met uitwendig gelijmde vezelcomposiet-wapening. Inderdaad, gezien de efficiëntie, de eenvoud en de flexibele toepasbaarheid van uitwendig gelijmde vezelcomposietwapening, is de commerciële interesse bijzonder groot, evenals de vraag naar uniforme ontwerprichtlijnen.

1.4 Doelstelling en onderwerp

Met het onderzoeksproject wordt beoogd het structureel gedrag en de modellering van gewapend betonelementen versterkt met uitwendig gelijmde vezelcomposietwapening te bestuderen. Dit met het doel ontwerprichtlijnen voor de aanwending en dimensionering van gelijmde vezelcomposietwapening te formuleren.

Gezien de omvang en het grote aantal ontwerpaspecten die in de praktijk kunnen voorkomen, werd het onderwerp gelimiteerd tot die aspecten die de meerderheid van de ontwerpproblemen uitmaken:

- Versterking van gewapend betonelementen (voor voorgespannen beton zijn bijkomende aspecten van toepassing) door middel van niet voorgespannen FRP wapening, die aangebracht wordt met een lijm op polymeerbasis (vb. epoxy).
- Versterking op buiging en dwarskracht van gewapend betonelementen zoals balken en platen, inrijgen van axiaal belaste kolommen en versterken van trekkers uit gewapend beton.

2 Uitwendige versterking met gelijmde vezelcomposietwapening

2.1 Algemeen

Uitwendige versterking van betonconstructies met opgelijmde staalplaten werd ontwikkeld in het midden van de jaren zestig [11] en is sinds jaren uitgegroeid tot een efficiënte en wereldwijd veel toegepaste methode [11,12]. Deze techniek bevat echter inherent enkele nadelen die in het licht van de recentste evoluties op het gebied van materiaaltechnologie betere alternatieven moet toelaten. Een dergelijke innovatie die sinds een aantal jaren met stijgend succes wordt toegepast (zoals blijkt uit de vele toepassingen die wereldwijd worden gerealiseerd) betreft de aanwending van vezelcomposietwapening als uitwendig opgelijmd versterkingsmiddel [13].

Deze versterkingstechniek bestaat erin dat bijkomende wapening wordt aangebracht aan een bestaande constructie met het doel hetzij de draagkracht ervan te herstellen of te verhogen, hetzij om aan bepaalde eisen in verband met de gebruikstoestand te voldoen. De vezelcomposietwapening wordt uitwendig aan de betonconstructie bevestigd door middel van een structurele verlijming (indien nodig kunnen bijkomende mechanische verankeringen voorzien worden). In hetgeen volgt wordt de term ‘uitwendig gelijmde vezelcomposiet-wapening’ (‘externally bonded FRP reinforcement’) ook aangeduid met de afkorting FRP EBR.

Voor aanwending als uitwendig gelijmde wapening, bestaan de FRP elementen uit dunne prefab strippen en laminaten, die reeds uitgehard zijn, of uit vellen en weefsels, die in situ geïmpregneerd worden en uitharden. De vezels zijn parallel en (overwegend) unidirectioneel georiënteerd. Laminaten en weefsels waarbij de vezels in twee of meer richtingen zijn georiënteerd worden eveneens toegepast. Het spanning-vervorming gedrag van FRP en staalwapening voor uitwendige verlijming, wordt vergeleken in Fig. S-3. Aangezien vezelcomposieten een materialengroep op zich vormen, met soms sterk uiteenlopende eigenschappen (zelfs voor een zelfde type vezel), zijn de curven in Fig. S-3 louter indicatief. Meestal wordt, gezien hun uitmuntende eigenschappen, gebruik gemaakt van CFRP (FRP op basis van koolstofvezel), doch ook FRP EBR op basis van glasvezel (GFRP) of aramidevezel (AFRP) worden toegepast.

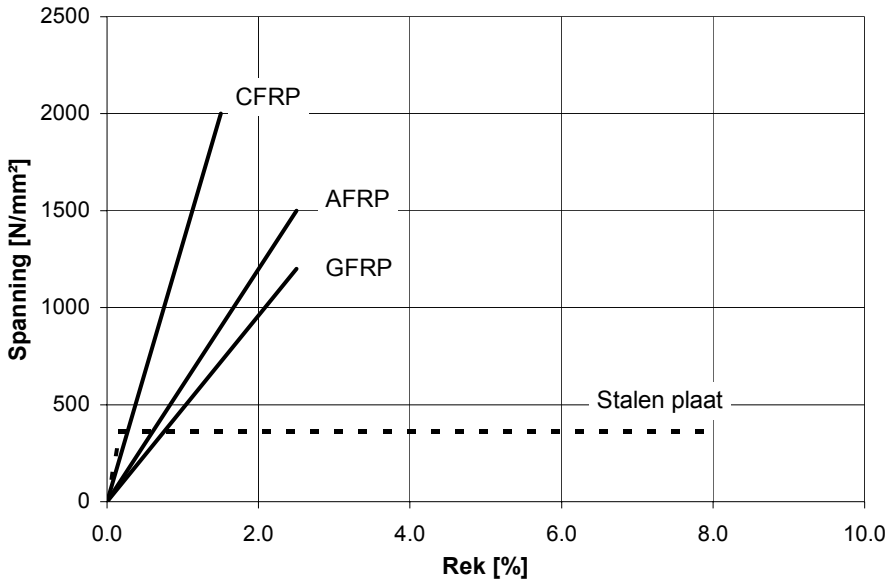

Fig. S-3 *Spanning-rek gedrag van gelijmde wapening*

2.2 Voor- en nadelen van FRP EBR

De aanwending van vezelcomposietwapening in plaats van staal biedt, zowel qua uitvoering als qua structureel gedrag, mogelijkheden tot een betere optimalisatie van de uitwendige versterking met opgelijmde wapening. Deze optimalisatie leidt bovendien in vele gevallen tot een reductie van de globale kostprijs, en dit ondanks de hogere kostprijs van de vezelcomposietmaterialen zelf. De volgende punten verduidelijken dit.

- Staalplaten dienen beschermd te worden tegen corrosie. Evenwel ontstaat dikwijls na verloop van tijd corrosie op het verlijmde staaloppervlak waardoor de composietwerking tussen de staalplaat en de betonconstructie in het gedrang komt. FRP materialen daarentegen bezitten een goede corrosieweerstand.
- Door hun gewicht kunnen staalplaten enkel in beperkte lengten aangewend worden (maximaal 6 à 10 m) en zijn ze moeilijk verhandelbaar. Bij grotere lengten zijn voegen, die een delicaat punt in het ontwerp en de uitvoering vormen, noodzakelijk. Bovendien is dikwijls een zware stelling nodig wat bv. onderdoorgaand verkeer onmogelijk maakt en een belangrijke meerkost met zich meebrengt. De quasi in onbeperkte lengten beschikbare FRP laminaten daarentegen zijn bijzonder licht en flexibel in gebruik.
- FRP materialen (voornamelijk CFRP) gedragen zich zeer goed onder wisselende belasting.
- Ook voorgespannen FRP wapening kan verlijmd worden. Hierdoor kunnen aanwezige trekspanningen, scheuropeningen en doorbuigingen gereduceerd worden. Deze techniek is echter nog in een experimenteel stadium.
- De aanwending van FRP wapening is, meer nog dan deze van staalplaten, ook vanuit esthetisch oogpunt aantrekkelijk. Hun geringe dikte heeft nagenoeg geen invloed op de vrije hoogte en na overschilderen zijn ze bijna niet meer te onderscheiden. Het aanbrengen van extra afwerkingslagen (bepleistering, spuitbeton, enz.) is bovendien mogelijk.

De nadelen van FRP zijn de hoge materiaalkostprijs (deze wordt dikwijls gecompenseerd door de winst in arbeidskost of snellere heringebruikname), de lage transversale sterkte (wat maakt dat FRP elementen gevoelig zijn voor impact of vandalisme) en bepaalde duurzaamheidsproblemen die mogelijk kunnen optreden voor sommige types FRP. Echter, globaal beschouwd bezitten FRP materialen en CFRP in het bijzonder een zeer hoge duurzaamheid.

2.3 Toepassingsmogelijkheden en FRP EBR systemen

FRP EBR kan met grote eenvoud verlijmd worden op o.a. beton, staal, hout en baksteen. Deze techniek wordt dan ook aangewend bij het versterken van balken, platen, wanden en kolommen van o.a. bruggen en gebouwen. Toepassing is echter ook mogelijk in andere gevallen zoals bijvoorbeeld het omrijgen van schoorstenen of het versterken van schalen en tunnelgewelven. De FRP wapening is daarbij, naast de aangewende vezelsoort en vezelrichtingen, in diverse types en systemen beschikbaar, aangepast aan de vereisten van de te versterken constructie. Men onderscheidt in hoofdzaak de zogenaamde 'prefab' (reeds uitgehard) en 'wet lay-up' (in situ impregnatie en uitharding) types, weergegeven in Fig. S-4. FRP EBR systemen bestaan uit de FRP wapening die aangebracht dient te worden en de lijm nodig voor de aanwending. Gezien de vele mogelijkheden inzake materiaalcomponenten, vorm en toepassingstechniek, zijn velerlei FRP EBR systemen commercieel beschikbaar.

Een overzicht van de belangrijkste eigenschappen en enkele typische kenmerken van 'prefab' en 'wet lay-up' systemen is gegeven in Tabel S-1.

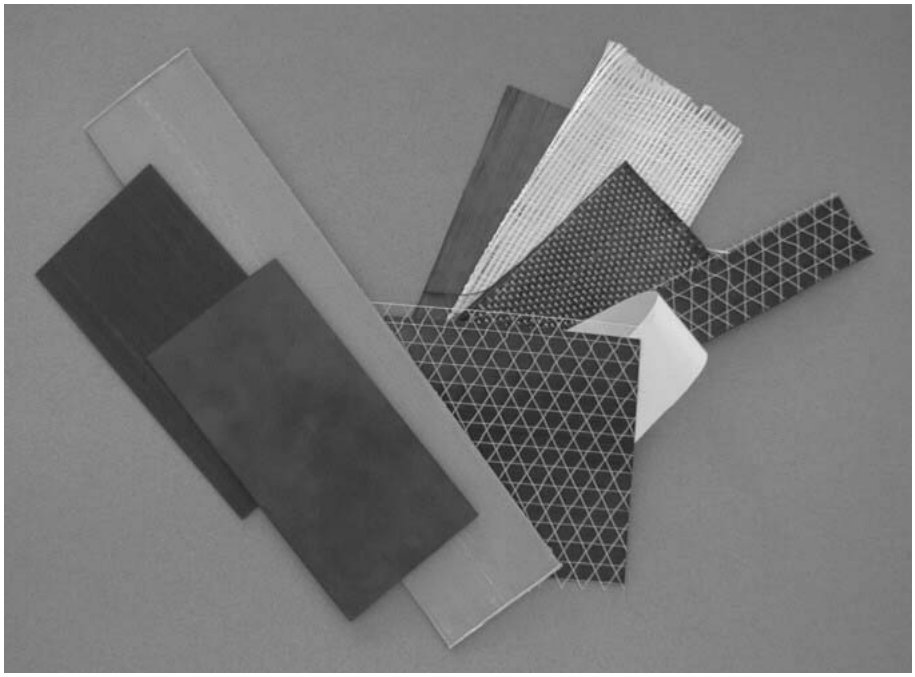

Fig. S-4 *'Prefab' (rechts) en 'wet lay-up' (links) FRP voor uitwendige verlijming*

Tabel S-1 *Typische kenmerken van FRP EBR systemen*

	PREFAB (PRE-CURED)	**WET LAY-UP (IN-SITU CURING)**
Vorm	Strippen en laminaten	Vellen en weefsels
Dikte	Ongeveer 1.0 tot 1.5 mm	Ongeveer 0.1 tot 0.5 mm
Lijm	Thixotrope lijm voor de aanhechting	Lijm met lage viscositeit voor de impregnatie en aanhechting
Vezelvolume	Ongeveer 70 %	Ongeveer 30 % (na impregnatie)
Aanwending	Eenvoudige verlijming van de geprefabriceerde elementen	Verlijming en impregnatie van de FRP (vormgeving in-situ)
Toepasbaarheid	Indien niet voorgevormd enkel voor vlakke oppervlaktes	Ongeacht de vorm, hoeken dienen afgerond te worden
Aantal lagen	Meestal 1 laag, meerdere lagen mogelijk	Meestal meerdere lagen
Oppervlakte oneffenheid	De prefab elementen en de thixotrope lijm laten een zeker oneffenheid toe	Dikwijls is een uitvlakmortel nodig i.v.m. onthechting door oneffenheden
Eenvoud in gebruik	Eenvoudig toepasbaar, beter kwaliteitsgarantie (prefab systeem)	Zeer flexibel in gebruik, meer noodzaak aan kwaliteitscontrole
Kwaliteits-controle	Verkeerde toepassing of slechte uitvoering = verlies aan composietwerking tussen de FRP EBR en de betonconstructie, gebrekkige lange-duur integriteit van het systeem, enz.	

2.4 Toepassingstechnieken

De gangbaar aangewende basistechniek bestaat in de manuele toepassing van de FRP wapening door verlijming met het betonelement, waarbij de aanhechting wordt verwezenlijkt door middel van de polymerisatie van een twee-componenten lijm (meestal epoxy) die kan uitharden bij omgevingstemperatuur. Daarnaast bestaan er ook diverse specifieke technieken zoals o.a. gerobotiseerd omwikkelen van kolommen en schoorstenen, het gebruik van prefab FRP schalen in combinatie met expansieve mortel, het gebruik van prepreg (pre-impregnated) FRP dat kan uitharden met behulp van verwarmingselementen of infra-rood straling, enz.

Een overzicht van de basistechniek is weergegeven in Tabel S-2.

3 Structureel gedrag van betonelementen versterkt in buiging

3.1 Aard van de proeven

Het structureel gedrag van gewapende betonbalken versterkt in buiging met CFRP strippen werd bestudeerd aan de hand van negen balken met een overspanning van 3.8 m [14-18]. Fig. S-5 geeft de afmetingen van de balken en de proefopstelling. Een overzicht van alle proefparameters wordt gegeven in Tabel S-3. De betonbalken werden dusdanig opgevat dat steeds een buigingsbreuk zou bekomen worden (overdimensionering naar dwarskracht-sterkte), gekenmerkt door verbrijzeling van het beton na het vloeien van het staal en (met uitzondering van balk BF 9) vóór het bezwijken van de FRP wapening.

Tabel S-2 *Aanwending van vezelcomposietlaminaten*

VOORAFGAANDE HERSTELLINGEN	Verwijder slechte betonzones, verifieer onvolkomenheden en potentiële schademechanismen, enz. Voorzie gepaste herstellingen.	
OPPERVLAKTE-VOORBEREIDING	BETON	Ruw zetten oppervlak (vb. zandstralen). Verifieer de oneffenheid en vlak uit indien nodig. Oppervlak stofvrij en droog maken.
	FRP	Indien gespecificeerd licht opschuren oppervlak, reinigen van het oppervlak (vet- & stofvrij), enz. Echter, dikwijls wordt FRP 'gebruiksklaar' geleverd.
AANBRENGEN FRP EBR	PREFAB	Aanwenden epoxy op het beton. Aanwenden epoxy op het laminaat (dakvormig). Verlijming laminaat (tot overtollige epoxy vrijkomt).
	WET LAY-UP	Aanbrengen epoxy op het beton (undercoating) Inrollen (verlijming en impregnatie) van het laminaat. Verdere impregnatie van het laminaat (overcoating).
AFWERKING	Schilderen, bezetten, enz. (vb. esthetische redenen en brandveiligheid).	
KWALITEITSCONTROLE (voorafgaand, tijdens en na de aanwending)		

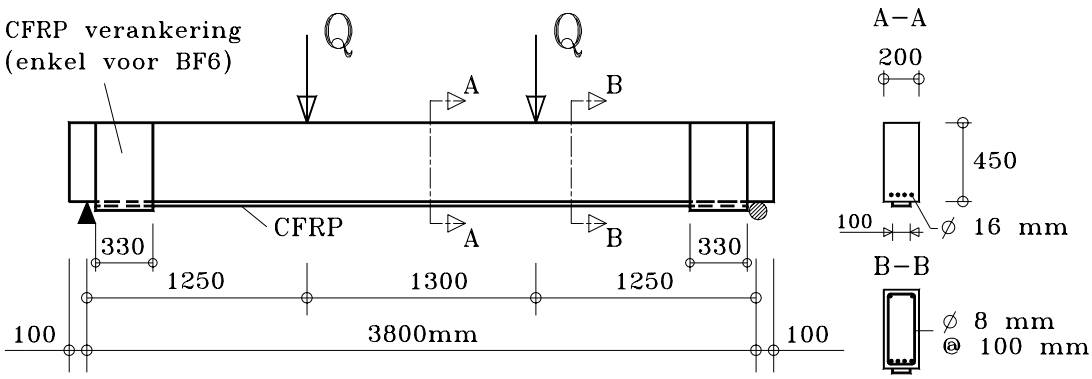

Fig. S-5 *Proefopstelling gewapende betonbalken versterkt in buiging*

Een eerste reeks balken (BF1 t.e.m. BF6), met een geometrisch wapeningspercentage ρ_s = 0.96 %, werd versterkt met één laag prefab CFRP (breedte 100 mm, dikte 1.2 mm), ρ_f = 0.14 %. Aan de hand van deze proefreeks werd de invloed nagegaan van het versterken van initieel gescheurde balken en het versterken onder belasting. Het aanbrengen van een extra verankering ter plaatse van de stripuiteinden (Fig. S-5) werd bestudeerd bij balk BF6. Voor een tweede reeks balken (BF7 t.e.m. BF9), met een wapeningspercentage ρ_s = 0.48 %, werden twee types laminaat aangewend: één laag prefab CFRP, ρ_f = 0.14 % voor balk BF8 en twee lagen wet lay-up CFRP (breedte 100 mm, equivalent droge-vezeldikte 0.111 mm), ρ_f = 0.026 % voor balk BF9.

De karakteristieken van het betonstaal en de CFRP laminaten worden gegeven in Tabel S-4. Het aangewende beton had een gemiddelde cilinderdruksterkte van 32.8 N/mm^2 op 28 dagen ouderdom. Meer gedetailleerde informatie inzake de materiaaleigenschappen is opgenomen in Appendix B.

Tabel S-3 *Proefparameters gewapend betonbalken versterkt in buiging*

Balk	**Wijze van versterken**	f_{cm} [N/mm^2]	ρ_s [%]	ρ_f [%]	**Voorafgaande belasting** [kN]	**Last tijdens het versterken** [kN]
BF1	Onversterkt (ref.)	33.7	0.96	-	-	Eigengewicht
BF2	Versterkt(1)	36.5	0.96	0.14	-	Eigengewicht
BF3	Versterkt(1)	34.9	0.96	0.14	-	Eigengewicht
BF4	Vooraf gescheurd/versterkt(1)	30.8	0.96	0.14	110	Eigengewicht
BF5	Versterkt (1) onder belasting	37.4	0.96	0.14	110	110
BF6	Versterkt(1) & extra verankering(2)	35.9	0.96	0.14	-	Eigengewicht
BF7	Onversterkt. (ref.)	38.5	0.48	-	-	Eigengewicht
BF8	Versterkt(1)	39.4	0.48	0.14	-	Eigengewicht
BF9	Versterkt(3)	33.7	0.48	0.026	-	Eigengewicht

(1) CarboDur 100 mm x 1.2 mm, (2) Replark 330 mm x 0.111 mm, (3) 2 lagen Replark 100 mm

Tabel S-4 *Eigenschappen (gemiddelde waarden) wapening bepaald d.m.v. van trekproeven*

Type	**Nominale afmetingen** [mm]	**Vloei-grens** [N/mm^2]	**Trek-sterkte** [N/mm^2]	**Breuk-rek** [%]	**E-modulus** [N/mm^2]
Betonstaal S500	Ø 16	590	690	12.4	200000
CarboDur S1012	100 x 1.2	-	3200	1.85	159000(1)
Replark MRK-M2-20	100 x 0.111	-	3500	1.25	233000(1)

(1) Tangensmodulus aan de oorsprong

3.2 Voornaamste proefresultaten

De bezwijkbelasting Q_u, het bekomen versterkingseffect t.o.v. de referentiebalken en het breukaspect worden gegeven in Tabel S-5. Het belasting-doorbuiging gedrag van de balken is weergegeven in Fig. S-6 en Fig. S-7.

Tabel S-5 *Proefresultaten en analytische verificatie bij volledige composietwerking*

Balk	**Experimenteel**				**Analytische verificatie**		
	Q_u [kN]	**Q_u/Q_{ref}** [-]	**Breuk aspect**	**y_u/y_{ref} [-]**	**Q_u** [kN]	**Breuk aspect**	**Q_{exp}/Q_{ana}** [-]
BF1	144.2	1.00	Y/B	1.00	141.8	Y/B	1.02
BF2	185.0	1.28	O(Y)/B	0.76	200.2	Y/B	0.92
BF3	186.0	1.29	O(Y)/B	0.87	196.7	Y/B	0.95
BF4	184.2	1.28	O(Y)/B	0.84	187.3	Y/B	0.98
BF5	177.0	1.23	O(Y)/B	0.97	191.8	Y/B	0.92
BF6	183.0	1.27	O(Y)/B	0.74	198.9	Y/B	0.92
BF7	80.7	1.00	Y/B	1.00	78.2	Y/B	1.03
BF8	111.3	1.38	O(Y)	0.38	165.8	Y/B	0.67
BF9	95.8	1.19	O(Y)/B	0.63	97.0	Y/F	0.99

Y/B: vloeien wapening gevolgd door verbrijzeling van het beton
Y/F: vloeien wapening gevolgd door breuk van de FRP wapening
O(Y): onthechting van de FRP (na vloeien van de wapening)

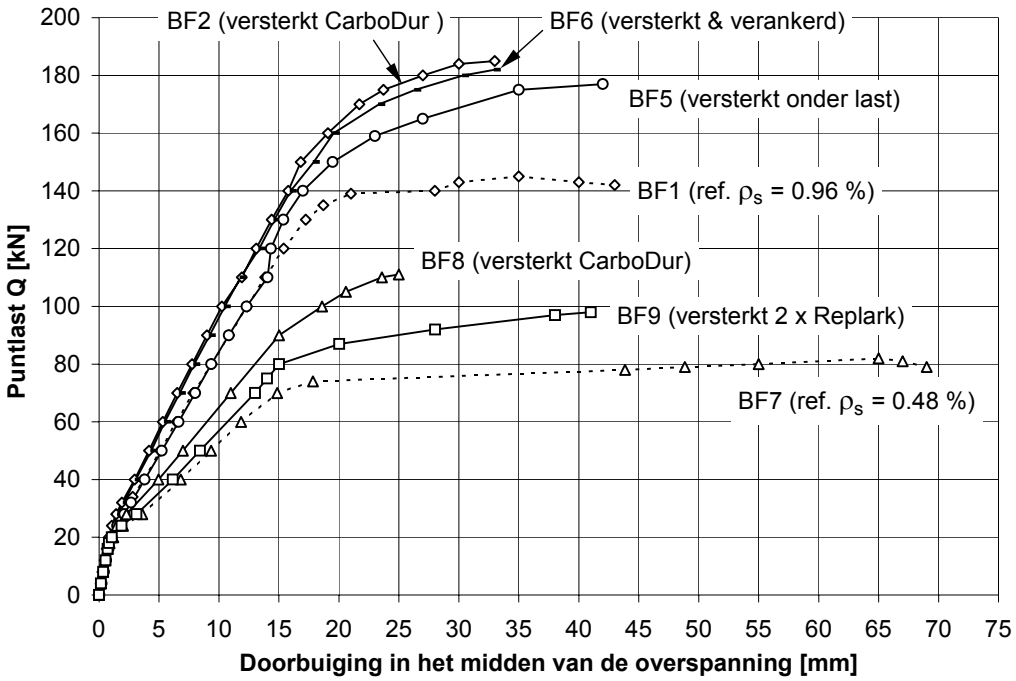

Fig. S-6 *Belasting-doorbuiging gedrag van balken BF1, BF2, BF5, BF6 en BF7-BF9*

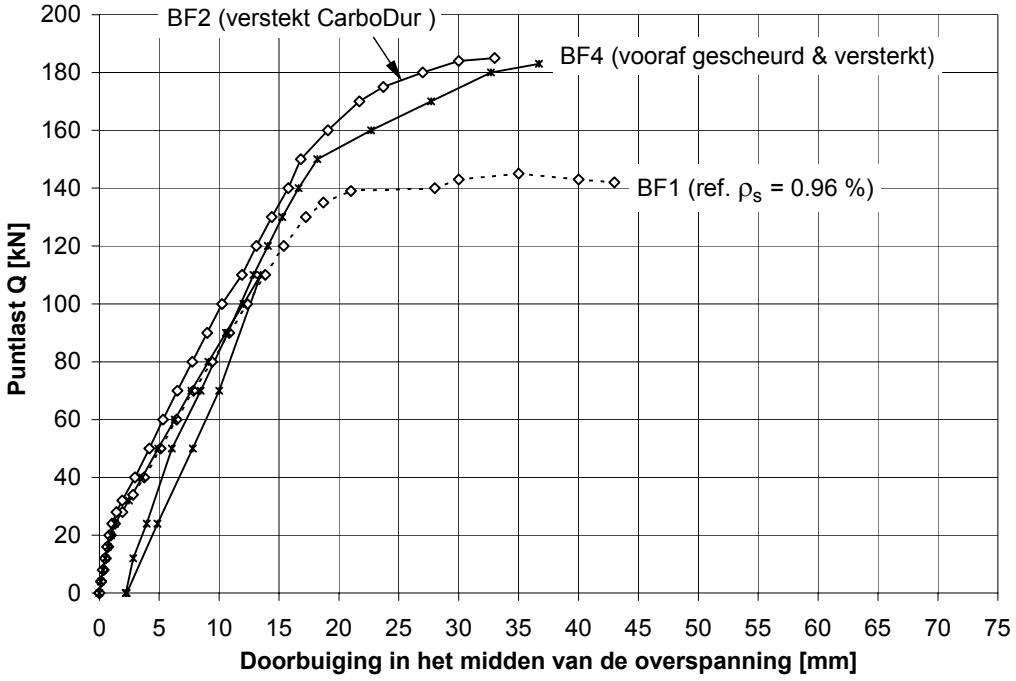

Fig. S-7 *Belasting-doorbuiging gedrag van balken BF1, BF2 en BF4*

Vergelijking van de bekomen resultaten toont duidelijk aan dat een aanzienlijke verhoging van de bezwijkbelasting bekomen wordt voor de versterkte balken. Ook de stijfheid in gescheurde toestand neemt toe, echter corresponderend met een zekere afname in de ductiliteit (plastische vervormbaarheid). Dit laatste wordt in Tabel S-5 weergegeven aan de hand van de verhouding van de maximale doorbuiging y_u van de versterkte balk t.o.v. de maximale doorbuiging y_{ref} van de referentiebalk.

Het bezwijkaspect van de versterkte balken wordt gekenmerkt door het vloeien van de wapening gevolgd door het voortijdig loskomen van de CFRP strip (Fig. S-8), resulterend (met uitzondering van balk BF8) in verbrijzeling van het beton in de drukzone. Het loskomen van de strip gebeurt dusdanig plots dat visueel niet vastgesteld kon worden waar de onthechting geïnitieerd wordt. Dit laatste aspect werd geverifieerd aan de hand van balk BF6 waarvoor de uiteinden van de strip extra verankerd werden. Echter, ook in dit geval werd bij vergelijkbare bezwijkbelasting onthechting bekomen, waaruit besloten werd dat deze niet het gevolg was van een verankeringsbreuk doch van het loskomen van de strip ter plaatse van een dwarskrachtscheur (afpelwerking t.g.v. vertikale verplaatsing van de scheurvlakken).

Fig. S-8 *Typisch bezwijkaspect van de versterkte balken door onthechting*

3.3 Analytische verificatie

3.3.1 Bezwijktoestand

In een eerste nazichtsberekening, werd de bezwijklast en het breukaspect van de balken nagegaan indien volledige composietwerking tussen het beton en de opgelijmde wapening verondersteld wordt. De berekening gebeurt conform Eurocode 2 [19], analoog zoals de berekening van onversterkte gewapend betonbalken. In de berekening wordt uitgegaan van de experimenteel bekomen materiaalsterktes en materiaalveiligheidscoëfficiënten gelijk aan 1. De resultaten van de berekening zijn weergegeven in Tabel S-5. Uit deze tabel blijkt dat de onthechting van de strippen, experimenteel bekomen, optrad (met uitzondering van BF8) nabij de verwachte breuk indien volledige composietwerking verondersteld wordt.

In een volgende nazichtsberekening werd de onthechting van de strippen analytisch geverifieerd. Zoals aangegeven in paragraaf 7.4.3.1. kan onthechting geïnitieerd worden door (een combinatie van) diverse factoren. Hierbij dienen in hoofdzaak de onthechting aan de uiteinden van de FRP EBR (verankeringsbreuk) en de onthechting bij scheuroverbrugging nagegaan te worden. Verankeringsbreuk werd nagerekend conform paragraaf 7.4.3.2. Uitgaande van de materiaalkarakteristieken kan de maximale FRP kracht $N_{fa,max}$ bepaald worden die kan verankerd worden door de verlijming aan de FRP-uiteinden, alsook de

bijhorende verankeringslengte $\ell_{t,max}$. Uitgaande van een klassieke berekening op basis van evenwichtsvergelijkingen en compatibiliteit van vervormingen, werd eveneens de optredende kracht $N_{fQu}(\ell_{t,max})$ bepaald. Dit is de kracht in de strip op een afstand $\ell_{t,max}$ van het uiteinde, bij het bereiken van de experimentele breukbelasting Q_u. Zoals aangegeven in Tabel S-6, is de optredende kracht $N_{fQu}(\ell_{t,max})$ merkelijk lager dan de weerstandbiedende kracht $N_{fa,max}$. Verankeringsbreuk blijkt dus niet kritiek te zijn voor de beproefde balken.

Tabel S-6 *Verificatie van verankeringsbreuk*

Balk	$\mathbf{Q_{u,exp}}$ [kN]	$\mathbf{N_{fa,max}}$ [kN]	$\mathbf{\ell_{t,max}}$ [mm]	$\mathbf{N_{fQu}(\ell_{t,max})}$ [kN]	$\mathbf{N_{fa,max}/N_{fQu}(\ell_{t,max})}$ [-]
BF2	185.0	48.5	166	21.4	2.27
BF3	186.0	47.6	169	21.7	2.19
BF4	184.2	45.1	179	21.9	2.05
BF5	177.0	49.0	164	20.4	2.40
BF6	183.0	> 48.2	-	-	-
BF8	111.3	50.1	161	23.0	2.18
BF9	95.8	24.4	89	5.2	4.68

Onthechting bij scheuroverbrugging is voornamelijk kritiek bij dwarskrachtscheuren. Dit is het gevolg van de vertikale verplaatsing van de scheurvlakken, die een rechtstreekse afpelwerking van de FRP EBR veroorzaakt. Een model voor deze bezwijkvorm werd opgesteld in [20] en geeft de weerstandbiedende dwarskracht waarbij afpellen wordt geïnitieerd:

$$V_{Rp} = \tau_{cza} b\left(x + (h - x)\left(1 - \frac{\varepsilon_o + \varepsilon_f}{\varphi}\right)\right) + \chi\Sigma(EA) \qquad \text{(S-1)}$$

met,

- τ_{cza} de schuifspanning die overgedragen wordt in de drukzone en in de scheur (d.m.v. ‘aggregate interlock’),
- x de hoogte van de drukzone,
- $(\varepsilon_o + \varepsilon_f)$ de rek in de meest getrokken vezel (rek in de FRP EBR, met inbegrip van de initiële rek ε_o vóór versterken),
- $\varphi = w_{crit}/s_{rm}$ de verhouding van de kritieke scheuropening waarbij geen ‘aggregate interlock’ bijdrage meer optreedt tot de gemiddelde scheurafstand,
- χ een coëfficiënt die de deuvelwerking van de wapening relateert met de axiale stijfheid van de wapening,
- $\Sigma(EA) = E_sA_s + E_fA_f$ de axiale stijfheid van de wapening (E is de elasticiteitsmodulus en A is de doorsnede van de wapening).

De grootheden x en $(\varepsilon_o + \varepsilon_f)$ kunnen bepaald worden aan de hand van evenwichtsvergelijkingen en compatibiliteit van de vervormingen en zijn een functie van de

aangrijpende belasting. Dit impliceert dat vergelijking (S-1) dient opgelost te worden door middel van een iteratie. De modelparameters τ_{cza}, φ en χ werden bepaald aan de hand van een experimentele kalibratie (de hiervoor aangewende data zijn opgenomen in Appendix C) en bedragen respectievelijk 0.71 N/mm^2, 25.1 10^{-3} en 0.75 10^{-3}.

Aangezien vergelijking (S-1) complex is om te berekenen, kan als alternatief ook gebruik gemaakt worden van vergelijking (S-2), die bekomen werd door een lineaire regressie van de experimentele data:

$$V_{Rp} = \tau_{Rp} bd \quad \text{waarbij} \quad \tau_{Rp} = (0.54 + 151\rho_{eq}) \quad [\text{N/mm}^2] \tag{S-2}$$

met, $\rho_{eq} = \rho_s + (E_f/E_s)\rho_s$ het equivalent wapeningspercentage.

Resultaten van de analytische verificatie op basis van vergelijkingen (S-1) en (S-2) zijn weergegeven in Tabel S-7. Beide formules geven een vrij goede voorspelling van de experimentele breuklast. De spreiding op de resultaten is het grootst voor vergelijking (S-2).

Tabel S-7 *Verificatie van afpellen t.p.v. dwarskrachtscheuren*

Balk	Q_u [kN]	$Q_p^{(1)}$ [kN]	$Q_u/Q_p^{(1)}$ [-]	$Q_p^{(2)}$ [kN]	$Q_u/Q_p^{(2)}$ [-]
BF2	185.0	185.9	1.00	180.0	1.03
BF3	186.0	185.8	1.00	180.0	1.03
BF4	184.2	185.5	0.99	180.0	1.02
BF5	177.0	182.2	0.97	180.0	0.98
BF6	183.0	185.9	0.98	180.0	1.02
BF8	111.3	122.3	0.91	119.5	0.93
BF9	95.8	96.9	0.99	108.4	0.88

(1) Vergelijking (S-1), (2) vergelijking (S-2)

3.3.2 Rekken in de wapening

Op basis van een klassieke berekening in een gescheurde doorsnede [19], werden o.a. de rekken in de wapening nagerekend onder toenemende belasting. Zoals blijkt uit Fig. S-9 en Appendix C, wordt (met uitzondering van lage belastingen waar de doorsnede nog niet gescheurd is) een nauwkeurige voorspelling bekomen.

3.3.3 Doorbuigingen

Krommingen en uitgaande daarvan doorbuigingen, werden nagerekend met inbegrip van het 'tension stiffening' effect (zie ook paragrafen 5 en 7.4.4). De resultaten van de berekeningen zijn weergegeven in Appendix C en in Fig. S-10 (voor balken BF1 en BF2). Een nauwkeurige voorspelling wordt bekomen.

3.3.4 Scheuropeningen

Gebaseerd op het model besproken in paragraaf 5, dat rekening houdt met het verschillend hechtingsgedrag van de staal en de FRP wapening, werden de scheuropeningen nagerekend.

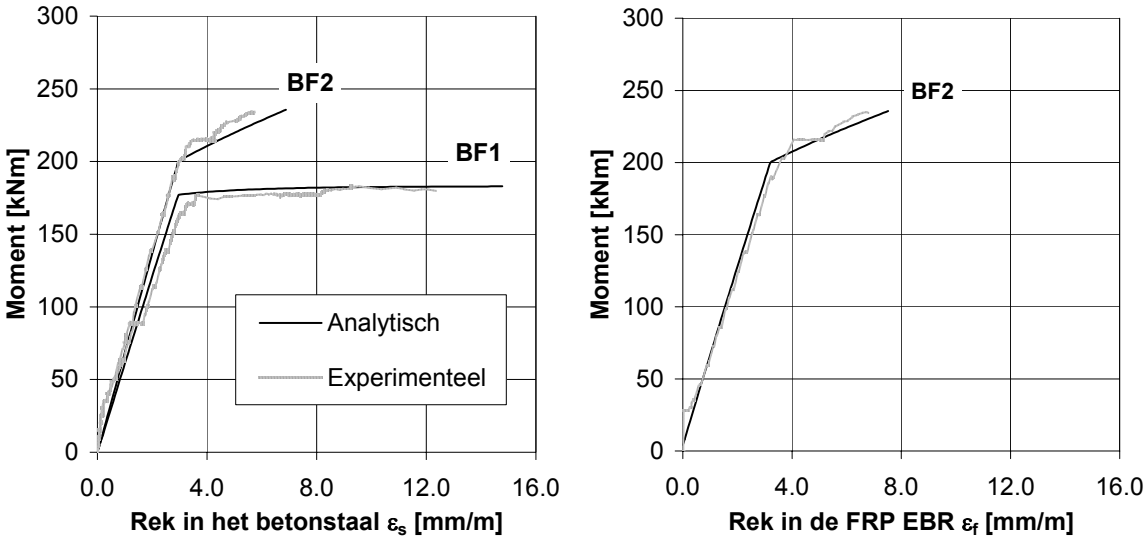

Fig. S-9 *Rekken in de langswapening van balken BF1 en BF2*

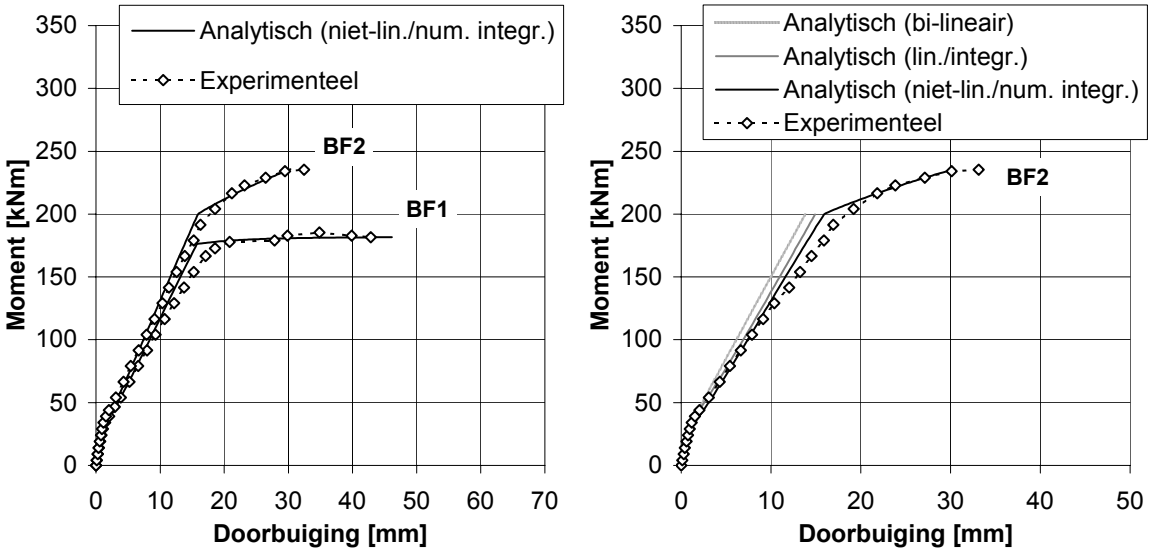

Fig. S-10 *Doorbuigingen van balken BF1 en BF2*

De resultaten van de berekening zijn opgenomen in Appendix C, evenals in Fig. S-11 voor balken BF1 en BF2. Relatief nauwkeurige voorspellingen worden bekomen. Aangezien het model voor de berekening van de scheuropening bedoeld is voor belastingsniveau's overeenstemmend met de gebruiksbelasting, is de nauwkeurigheid voor hoge belastingen minder goed.

3.3.5 Rekken en schuifspanningen langsheen de FRP wapening

Analoog zoals uiteengezet in paragraaf 3.3.2, werd de FRP rek langsheen de lengte van de strip nagerekend. Alhoewel deze berekening geen rekening houdt met lokale rekvariaties nabij scheuren, wordt een goed beeld van het globaal gedrag bekomen (Fig. S-12). Voor de berekening wordt uitgegaan van de verschoven momentenlijn (om rekening te houden met de toename in trekspanning t.g.v. dwarskrachtscheuren).

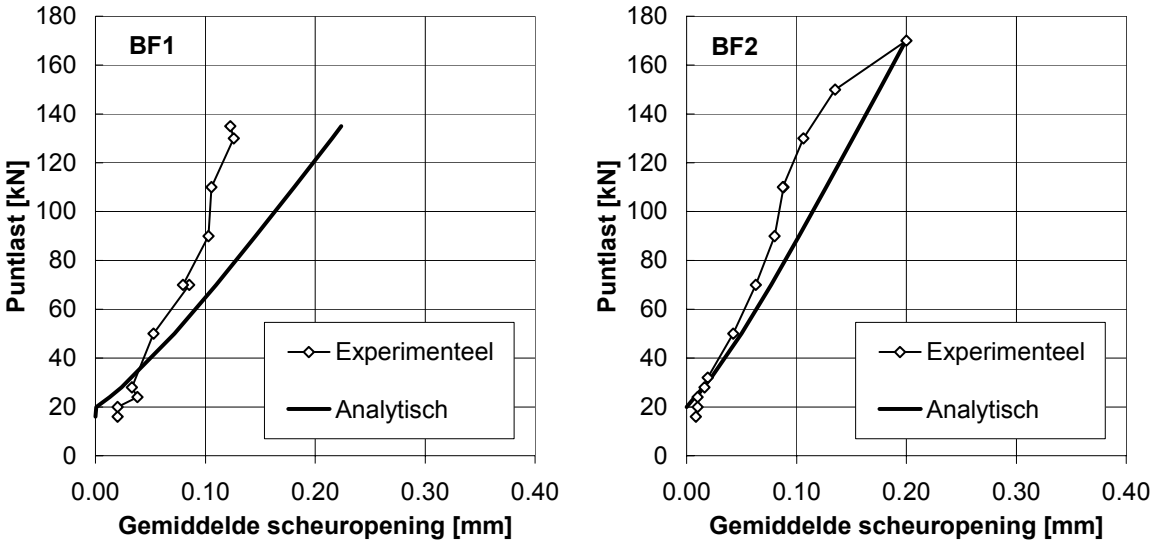

Fig. S-11 *Verificatie van de gemiddelde scheuropening*

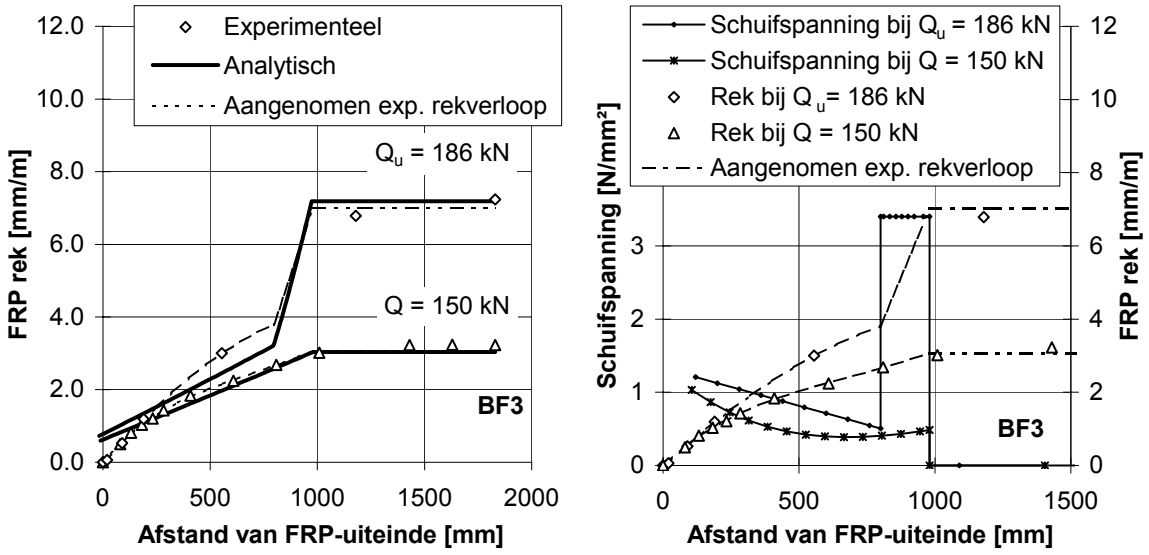

Fig. S-12 *Verificatie van het rekverloop en berekende schuifspanningen*

Zoals blijkt uit Fig. S-12, stemt het berekende rekverloop (met uitzondering van de verankeringszone) relatief goed overeen met het opgemeten rekverloop. Eveneens wordt vastgesteld dat de rekken in de FRP wapening sterk toenemen na het vloeien van het betonstaal (Q = 150 kN in Fig. S-12 is juist voor het bereiken van de vloeigrens). Dit is ook geïllustreerd in Fig. S-32.

De variatie van de kracht $\Delta N_f = \Delta\varepsilon_f E_f A_f$ langsheen de strip, vormt evenwicht met de hechtschuifspanningen τ_b in de lijm. Het verband tussen beide wordt gegeven door:

$$\tau_b = \frac{\Delta\varepsilon_f}{\Delta x} E_f t \qquad \text{(S-3)}$$

met t de dikte van de FRP wapening. Uit de berekende schuifspanningen (Fig. S-12) blijkt dat hechtschuifspanningsconcentraties voorkomen in de verankeringszone en, na het vloeien van de inwendige staalwapening, nabij de puntlast. De hechtsterkte $\tau_{max} \approx 1.8 f_{ctm}$ (met f_{ctm} de gemiddelde treksterkte van het beton) wordt echter niet overschreden.

3.4 Besluiten

Uit het experimenteel en analytisch onderzoek op de gewapend betonbalken versterkt in buiging met FRP EBR, kan het volgende besloten worden:

- Door het uitwendig versterken met CFRP laminaten kan men de bezwijklast aanzienlijk verhogen. Voor de beproefde balken werd een versterkingsfactor van 1.2 tot 1.4 bekomen. Voorafgaande scheurvorming in de balk lijkt weinig invloed te hebben op de sterktetoename.
- Indien men een balk onder een initiële belasting plaatst en dan pas versterkt, zal de versterkingsfactor slechts in geringe mate afnemen. Balk BF5, belast voor het versterken met 1.7 keer de gebruikslast van de referentiebalk, bezweek bij een slechts 4 % lagere breuklast in vergelijking met een analoge balk versterkt onder enkel zijn eigengewicht. Versterkingen aangebracht bij belaste constructies zijn bijgevolg goed mogelijk.
- De versterkte balken in dit proefprogramma bezweken door onthechting van de uitwendig gelijmde FRP wapening. Op basis van analytische verificatie kan gesteld worden dat deze onthechting werd geïnitieerd ter plaatse van dwarskrachtscheuren.
- Door de uitwendige versterking met CFRP verhoogt eveneens de stijfheid van de balken en wordt een fijner scheurpatroon ontwikkeld (kleinere scheuropeningen).
- De ductiliteit van de versterkte balken nam in belangrijke mate af (25 % tot 68 %), doch bleef hoger dan het minimum gespecificeerd in paragraaf 7.3.3.
- Het structureel gedrag van de balken (breukaspect, bezwijkbelasting, krommingen en doorbuigingen, scheuropeningen, enz.) kan op relatief goede en eenvoudige wijze theoretisch nagerekend worden. Enkel de voorspelling van onthechting van de uitwendig gelijmde FRP wapening is enigszins bewerkelijk, gezien de vele invloedsfactoren.
- Een model voor de verificatie van onthechting ter plaatse van dwarskrachtscheuren of buigscheuren in zones met belangrijke dwarskrachten, werd voorgesteld.

4 Structureel gedrag van betonelementen versterkt in dwarskracht

4.1 Aard van de proeven

Aan de hand van zeven balken (BS1 t.e.m. BS7) - overgedimensioneerd in buiging - werd nagegaan in welke mate dwarskrachtversterking met CFRP wapening kan verwezenlijkt worden [14-18, 21]. Fig. S-13 geeft de afmetingen van de balken en de proefopstelling. Voor de balken BS1 en BS2 bedraagt de beugelafstand 200 mm, voor de balken BS3 t.e.m. BS7 is de beugelafstand dubbel zo groot. Voor de dwarskrachtversterking werden diverse configuraties aangenomen, zoals aangegeven in Fig. S-13 en Tabel S-8. Op balk BS4 na, werd slechts een beperkte hoeveelheid uitwendige vezelcomposietwapening aangebracht teneinde ook na versterking nog een dwarskrachtbreuk te bekomen en aldus het effect van de versterking beter te kunnen onderzoeken.

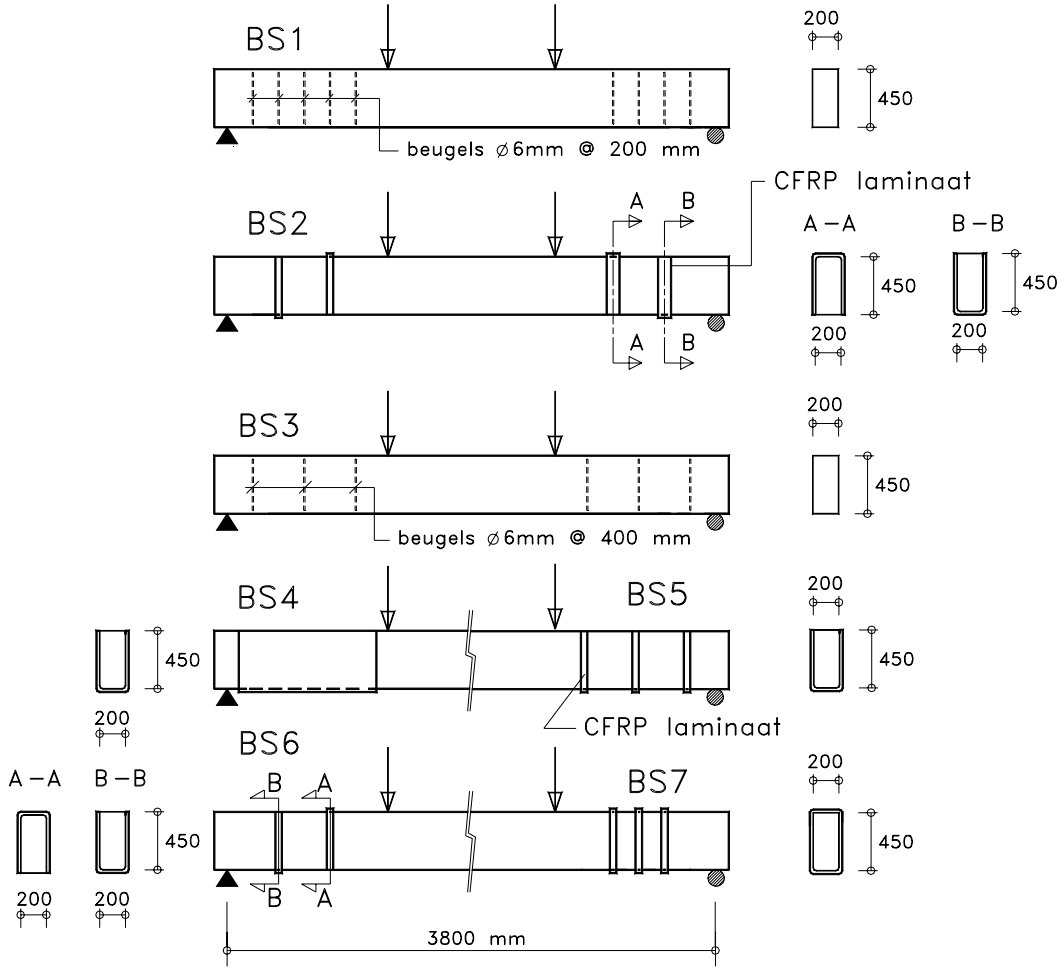

Fig. S-13 *Proefopstelling gewapende betonbalken versterkt in dwarskracht*

Tabel S-8 *Proefparameters en bezwijktoestand van de balken versterkt in dwarskracht*

Balk	**Wijze van versterken** (zie Fig. S-13)	f_{cm} [N/mm^2]	**Beugels** [mm]	**Breedte FRP** [mm]	**Pas FRP** [mm]	Q_u [kN]	**Breuk aspect**	Q_u/Q_{ref} [-]
BS1	Onversterkt (ref.)	35.0	Ø 6 at 200	-	-	206.3	D	1.00
BS2	2 strippen (∪&∩ vorm)	33.8	Ø 6 at 200	50/100[(1)]	400	247.5	O/D	1.20
BS3	Onversterkt (ref.)	37.5	Ø 6 at 400	-	-	136.6	D	1.00
BS4	Volledig (∪vorm)	38.4	Ø 6 at 400	1070	-	252.0	B	1.84
BS5	3 strippen (∪vorm)	36.0	Ø 6 at 400	50	400	170.0	O/D	1.24
BS6	2 strippen (∪&∩ vorm)	35.8	Ø 6 at 400	50	400	166.7	O/D	1.22
BS7	3 strippen (gesloten vorm)	34.7	Ø 6 at 400	50/100[(1)]	200	235.5	D	1.72

[(1)] Breedte verschillend in beide dwarskrachtoverspanningen

D: dwarskrachtbreuk

O/D: onthechting van (een aantal van) de strippen gevolgd door dwarskrachtbreuk

B: buigingsbreuk t.g.v. het vloeien van de langswapening gevolgd door verbrijzeling van het beton

De versterking werd bekomen door het U-vorming verlijmen van de vezelcomposiet-wapening. Hierbij werd geopteerd voor wet lay-up CFRP (Tabel S-1), dat flexibel is bij aanwending. De hoeken van de betonbalken werden afgerond met een straal van ongeveer 30 mm, ter plaatse van de uitwendige wapening.

Een overzicht van alle proefparameters wordt gegeven in Tabel S-8. De karakteristieken van het betonstaal en de CFRP wapening worden gegeven in Tabel S-9. Het aangewende beton had een gemiddelde cilinderdruksterkte van 35.0 N/mm^2 op 28 dagen ouderdom. Meer gedetailleerde informatie inzake de materiaaleigenschappen is opgenomen in Appendix B.

Tabel S-9 *Eigenschappen (gemiddelde waarden) wapening bepaald d.m.v. van trekproeven*

Type	**Nominale afmetingen** [mm]	**Vloei-grens** [N/mm^2]	**Trek-sterkte** [N/mm^2]	**Breuk-rek** [%]	**E-modulus** [N/mm^2]
Betonstaal S500	Ø 6	560	590	5.1	200000
	Ø 20	530	620	11.9	200000
Replark MRK-M2-20	100 x 0.111	-	3500	1.25	233000(1)

(1) Tangensmodulus aan de oorsprong

4.2 Voornaamste proefresultaten

De bezwijkbelasting Q_u, het bekomen versterkingseffect t.o.v. de referentiebalken en het breukaspect worden vermeld in Tabel S-8. Het scheurpatroon bij bezwijken en het breuk-aspect zijn eveneens weergegeven in Fig. S-14.

Beschouwing van de proefresultaten toont aan dat een belangrijke dwarskrachtversterking kan gerealiseerd worden en, indien voldoende uitwendige wapening aangebracht wordt, dat een dwarskrachtbreuk kan vermeden worden (zie balk BS4). Afhankelijk van de hoeveelheid uitwendige dwarskrachtwapening, neemt de bezwijklast met 20 % tot 84 % toe. De dwarskrachtbreuk die bekomen wordt voor de balken (uitgezonderd BS4) is gekenmerkt door een grote diagonale dwarskrachtscheur die zich plotseling vormt bij een puntlast van ongeveer 100 kN en die verder groeit tot dwarskrachtbreuk bekomen wordt. Het breukaspect van de versterkte balken wordt, op de balken BS4 en BS7 na, gekenmerkt door een onthechting van de vezelcomposietwapening. Dit is het gevolg van de relatief hoge krachten die opgewekt worden in de laminaten, in combinatie met de beperkte verankeringslengte die beschikbaar is over de hoogte van de balk. Door de laminaten bijvoorbeeld in een gesloten lus aan te wenden (balk B7) wordt extra verankering bekomen.

Balk BS2 bezweek in de rechter dwarskrachtoverspanning, ondanks de grotere breedte van de CFRP wapening (100 mm i.p.v. 50 mm in de linker dwarskrachtoverspanning). Dit bijzonder resultaat is het gevolg van de grote afstand tussen de puntlast en de dichtst nabij gelegen FRP dwarskrachtstrip. Deze afstand bedraagt 1.1 keer de nuttige hoogte van de balk, wat de vorming van een dwarskrachtscheur toelaat in deze onversterkte zone. Gezien de variabiliteit van de betonsterkte (en een mogelijk licht asymmetrische belasting van de puntlasten), blijkt de breuk voor deze balk in de rechter dwarskrachtoverspanning op te treden.

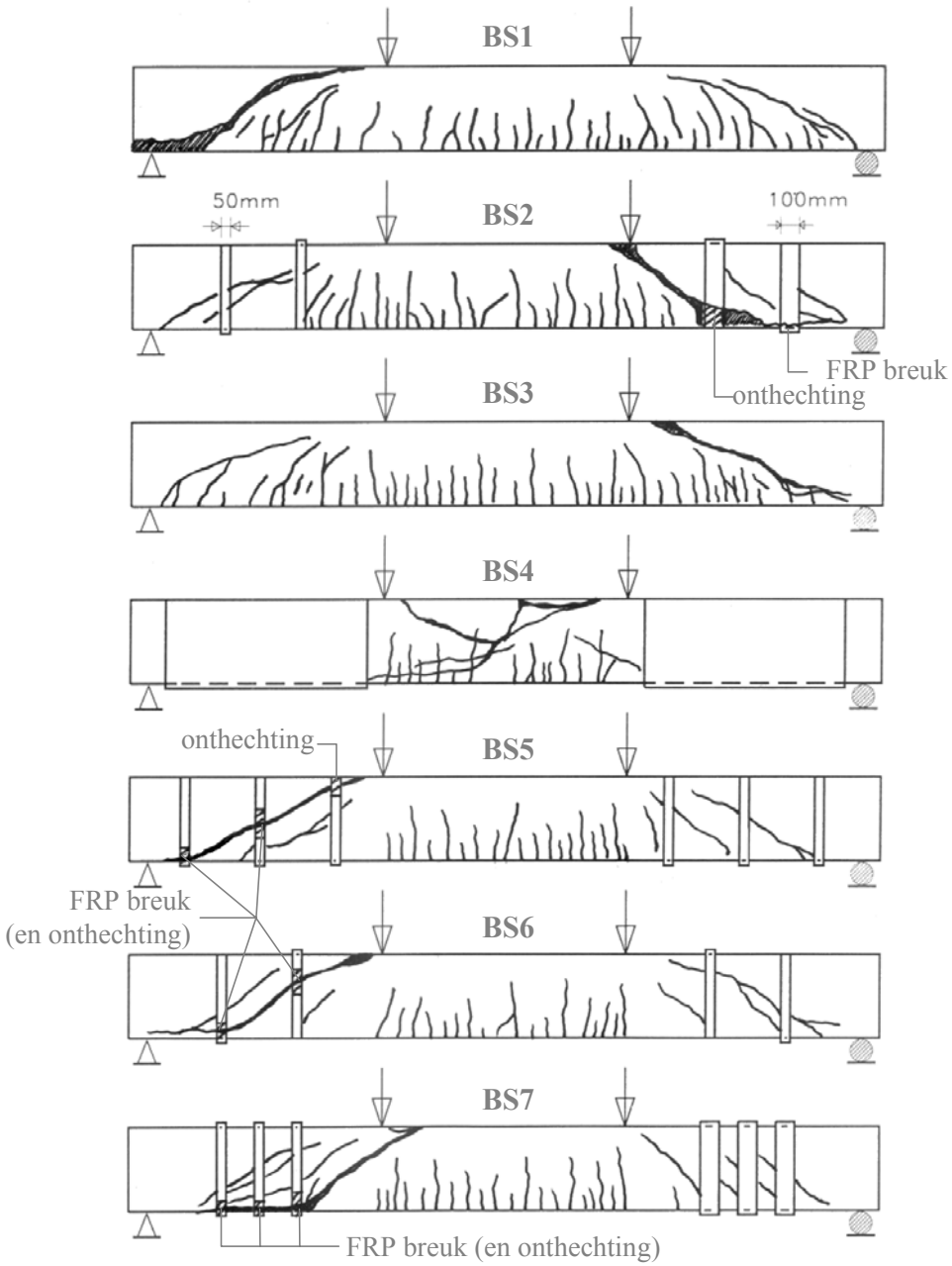

Fig. S-14 *Breukaspect van de balken BS*

Door middel van rekstroken werd de rek in de FRP wapening opgemeten op diverse locaties in de dwarskrachtoverspanning. De resultaten van deze metingen en de locaties van de rekstroken zijn weergegeven in Appendix D. De rekken opgemeten voor balk BS2, voor de FRP dwarskrachtstrip nabij de linkse puntlast, zijn eveneens weergegeven in Fig. S-15. Uit deze figuur blijkt dat slechts significante waarden opgemeten worden na het vormen van de kritieke dwarskrachtscheur. Verder blijkt ook de variatie van de FRP rek langsheen de lengte van de strip. Nabij de verwachte locatie van de dwarskrachtscheur (sg 5 en sg 6) worden de hoogste waarden opgemeten. Merkelijk lagere waarden worden opgetekend voor de rekstroken die verder van de dwarskrachtscheur gelokaliseerd zijn (sg 7 en sg 8).

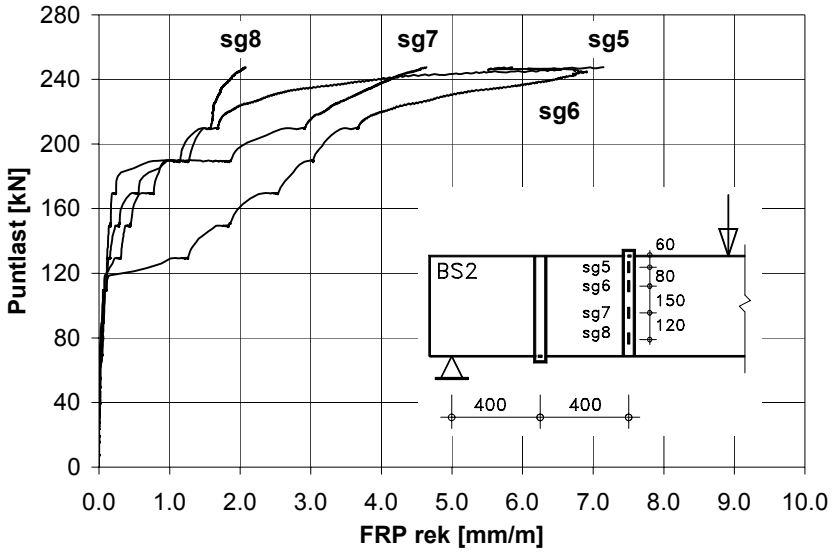

Fig. S-15 *Opgemeten FRP rekken voor één van de strippen van balk BS2*

4.3 Analytische verificatie

4.3.1 Dwarskrachtsterkte

De dwarskrachtcapaciteit V_R van de versterkte gewapend betonbalken werd geëvalueerd aan de hand van het superpositiebeginsel:

$$V_R = V_c + V_{ws} + V_{wf} \tag{S-4}$$

met, V_c, V_{ws} en V_{wf} de bijdragen tot de dwarskrachtsterkte van het beton, de stalen beugelwapening en de uitwendige FRP dwarskrachtwapening, respectievelijk.

De dwarskrachtsterkte van de vezelcomposietwapening kan, analoog zoals bij de inwendige stalen beugels, bepaald worden door toepassing van de veralgemeende vakwerk-analogie:

$$V_{wf} = \frac{A_{wf}}{s_f} 0.9 d E_f \varepsilon_{f,eff} \left(\cot\theta + \cot\alpha_f\right) \sin\alpha_f \tag{S-5}$$

met, A_{fw} de doorsnede van de FRP dwarskrachtwapening, s_f de asafstand (beugelpas) tussen de FRP wapening (voor volledige verlijming met FRP is s_f gelijk aan de breedte b_f van de aangewende vezelcomposietwapening), $\varepsilon_{f,eff}$ de effectieve FRP breukrek conform paragraaf 4.3.2, θ de helling van de dwarskrachtscheur ten opzichte van de langsas van de balk (normaal aangenomen als 45°) en α_f de hoek tussen de (hoofd)richting van de vezels en de langsas van de balk (90° voor de beproefde balken).

In vergelijking (S-4) wordt impliciet aangenomen dat de bijdrage van het beton niet significant verandert in vergelijking met niet versterkte betonelementen. De vraag kan niettemin gesteld worden of dit het geval is. Immers, door de grote scheuropeningen bij hoge belastingen (scheuren overbrugd door de FRP, doch waarbij de inwendige stalen beugels reeds vloeien), treedt mogelijk een verminderde 'aggregate interlock' en dus betonbijdrage op. Daar tegenover staat, dat het inrijgende effect van de FRP dwarskrachtwapening mogelijk

een positieve bijdrage heeft. Alhoewel dit niet expliciet onderzocht werd in het proefprogramma, werd experimenteel geen aanduiding gevonden van een gewijzigde dwarskrachtsterkte van het beton voor de versterkte balken. Mocht dit toch het geval zijn, dan wordt dit effect (door de aard van de kalibratie van $\varepsilon_{f,eff}$, paragraaf 4.3.2) impliciet verrekend in de bijdrage V_{wf}.

Resultaten van de analytische verificatie volgens vergelijking (S-4) (voor $\theta = 45°$) zijn weergegeven in Tabel S-10. De hierbij aangewende pas van de FRP wapening bedraagt 400 mm voor balken BS2 en BS6, 300 mm voor balk BS5 en 200 mm voor balk BS7. Ondanks de benaderende methode voor de bepaling van $\varepsilon_{f,eff}$, blijkt uit Tabel S-10 dat de dwarskrachtsterkte vrij nauwkeurig kan voorspeld worden (de spreiding is analoog voor de versterkte en de niet versterkte balken).

Tabel S-10 *Verificatie van de dwarskrachtsterkte*

Balk	**Wijze van versterken**	V_u [kN]	V_c [kN]	V_{ws} [kN]	$\varepsilon_{f,eff}$ [mm/m]	V_{wf} [kN]	V_R [kN]	V_u/V_R [-]
BS1	Onversterkt (ref.)	210.6	133.6	60.2	-	-	193.8	1.09
BS2	2 strippen (∪&∩ vorm)	251.8	129.6	60.2	8.54	24.4	214.2	1.18
BS3	Onversterkt (ref.)	140.9	141.7	30.2	-	-	171.8	0.82
BS4	Volledig (∪ vorm)	256.3	B	B	B	B	B	B
BS5	3 strippen (∪ vorm)	174.3	136.9	30.2	6.52	24.8	191.9	0.91
BS6	2 strippen (∪&∩ vorm)	171.0	136.2	30.2	8.56	24.4	190.8	0.90
BS7	3 strippen (gesloten vorm)	239.8	136.6	30.2	8.12	46.4	213.2	1.12

$V_u = Q_u + g\ell/2$, met g het eigengewicht; B: buigingsbreuk

4.3.2 Effectieve FRP breukrek

Uit het experimenteel onderzoek blijkt dat de FRP rek varieert langsheen de dwarskrachtscheur, dat lokaal onthechting optreedt aan beide zijden van de scheur en dat, naargelang de beschikbare verankeringslengte, FRP onthechtingsbreuk kan optreden. Hieruit volgt dat de bijdrage van de FRP dwarskrachtwapening gerelateerd is aan een effectieve breukrek $\varepsilon_{f,eff}$ die in de meeste gevallen lager is dan de eigenlijke FRP breukrek ε_{fu} bekomen uit uniaxiale trekproeven. De modellering van deze effectieve breukrek $\varepsilon_{f,eff}$ is gezien de complexe aard en de interactie van de invloedsfactoren moeilijk en vergt verder onderzoek naar deze aspecten. Daarom werd voor een meer deterministische aanpak gekozen, zoals gesuggereerd in [22,23]. Hierbij wordt door middel van een regressie-analyse $\varepsilon_{f,eff}$ experimenteel gekalibreerd. Er wordt uitgegaan van het verschil in bezwijkbelasting van een versterkt en een onversterkt element. Aangenomen wordt dat dit verschil gelijk is aan de dwarskrachtbijdrage $V_{f,exp}$ van de FRP wapening. Uit vergelijking (S-5) en met $\theta = 45°$, wordt dan de corresponderende waarde van $\varepsilon_{f,eff}$ berekend. Gebaseerd op deze methode worden in [22,24] formules voorgesteld voor $\varepsilon_{f,eff}$ in functie van de parameter $E_f\rho_{wf}$.

Deze betrekkingen werden op basis van de proefresultaten van 70 experimenten (het eigen onderzoek en data gevonden in de literatuur, Appendix D), geverifieerd. Om met een aantal

bijkomende aspecten rekening te houden werd een nieuwe kalibratie uitgevoerd. Voor FRP dwarskrachtwapening die mechanisch verankerd wordt in de drukzone of die het element volledig omwikkelt, wordt $\varepsilon_{f,eff}$ bekomen als:

$$\varepsilon_{f,eff} = 0.72\varepsilon_{fu} e^{-0.0431\Gamma_f} \tag{S-6}$$

waarbij,

$$\Gamma_f = \frac{E_f \rho_{wf}}{f_{cm}^{2/3}(a/d)} \tag{S-7}$$

met f_{cm} en E_f uitgedrukt in N/mm^2 (Γ_f in (N/mm^2)$^{1/3}$), $\rho_{wf} = A_{wf}/(s_f b_w)$, a/d de verhouding van de dwarskrachtoverspanning tot de nuttige hoogte en b_w de breedte van de balk. Voor FRP dwarskrachtwapening die enkel aan de zijvlakken van het element aangebracht wordt, geldt:

$$\varepsilon_{f,eff} = 0.56\varepsilon_{fu} e^{-0.0455\Gamma_f} \tag{S-8}$$

In het geval van U-vormige FRP dwarskrachtwapening waren onvoldoende data beschikbaar om een verband te bekomen en moet eveneens uitgegaan worden van vergelijking (S-8).

In Fig. S-16 worden de vergelijkingen (S-7) and (S-8) vergeleken met de experimentele data. Alhoewel een duidelijke trend waarneembaar is, is de spreiding relatief groot.

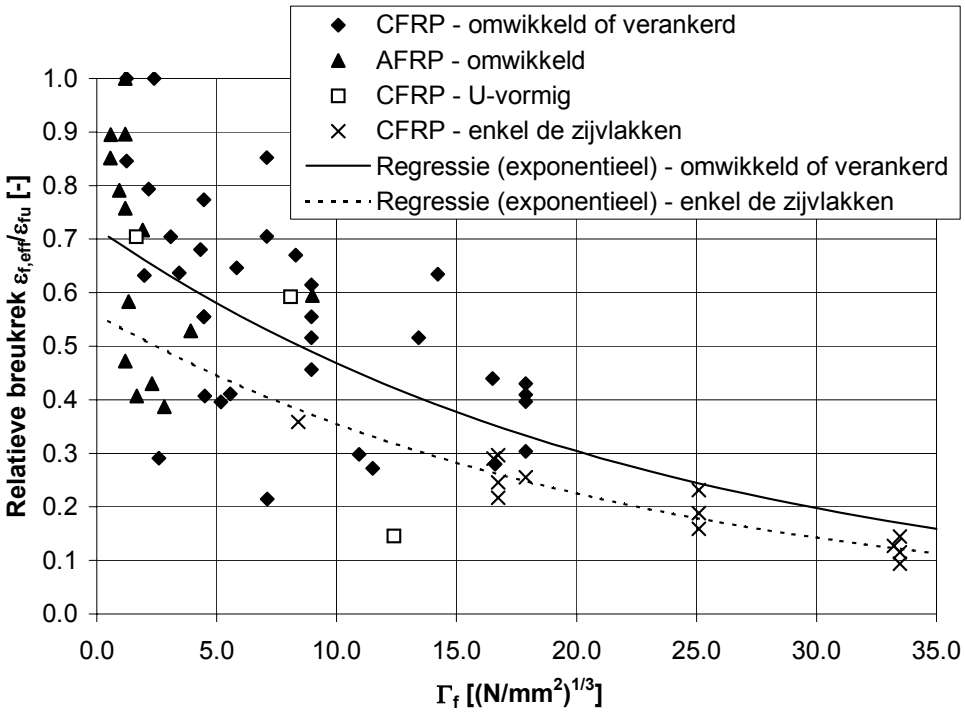

Fig. S-16 *Voorgestelde betrekkingen voor de effectieve FRP breukrek*

4.4 Besluiten

Uit de resultaten van de studie naar het gedrag van gewapend betonbalken versterkt op dwarskracht met FRP EBR kan het volgende besloten worden:

– De dwarskrachtsterkte kan aanzienlijk verhoogd worden zodat de balk niet meer bezwijkt onder dwarskracht maar onder buiging.

- De bijdrage van de FRP wapening tot de dwarskrachtsterkte is gerelateerd aan een effectieve breukrek die in de meeste gevallen kleiner is dan de FRP breukrek bekomen uit trekproeven.
- Verhoogde efficiëntie wordt bekomen indien onthechtingsbreuk van de FRP vermeden of uitgesteld kan worden.
- Het narekenen van de dwarskrachtsterkte van de FRP wapening kan gebeuren volgens de veralgemeende vakwerkanalogie (Mörsch).
- Een model voor de effectieve FRP breukrek, op basis van een experimentele kalibratie, werd voorgesteld. Uitgaande van dit model worden relatief nauwkeurige voorspellingen bekomen.

5 Tension stiffening en scheuroverbrugging

5.1 Aard van de proeven

Bij de proeven op betonbalken versterkt met FRP EBR in buiging bleek duidelijk dat zowel het bezwijkvermogen als de stijfheid in gescheurde toestand toenemen. Dit laatste aspect is maatgevend voor de gebruikgrenstoestand van de constructie en werd in detail bestudeerd aan de hand van 18 tension stiffening proeven [25,26]. Dit zijn trekproeven op wapeningsstaven die zijn ingebed in (versterkte) betonprisma's, zoals ook weergegeven in Fig. S-17. Een overzicht van de proefparameters is gegeven in Tabel S-11.

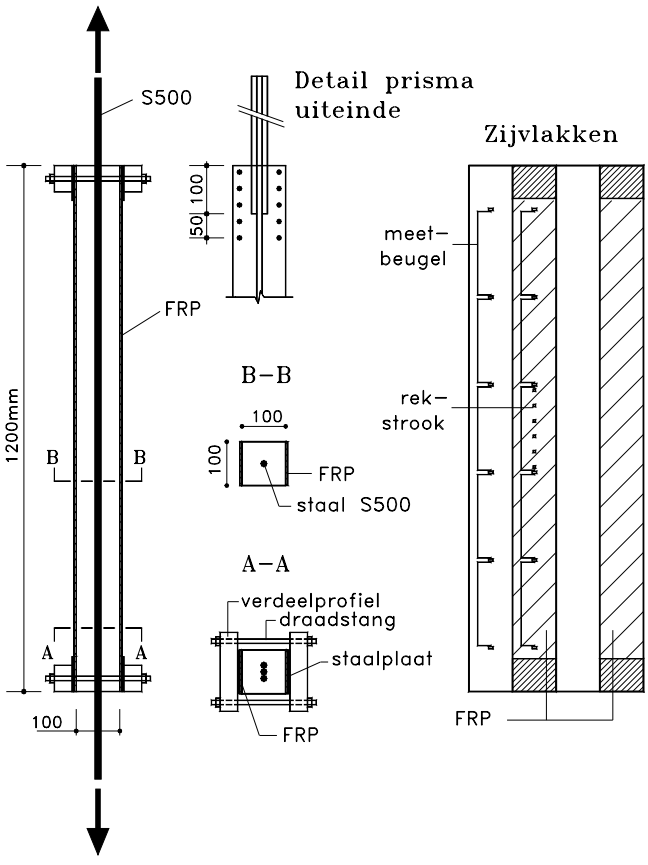

Fig. S-17 *Tension stiffening proefstukken*

Tabel S-11 *Proefparameters voor de tension stiffening proeven*

Reeks	Proefstuk	f_{cm} [N/mm^2]	Beton-staal	ρ_s [%]	FRP type	Aantal lagen	ρ_f [%]
T1	N(T1)/100/14/Ref.	36.2	Ø 14 mm	1.56	-	-	-
	N(T1)/100/14/C#1	36.2	Ø 14 mm	1.56	CFRP	1	0.23
	N(T1)/100/14/C#2	36.2	Ø 14 mm	1.56	CFRP	2	0.45
T2	N(T2)/100/14/C#1	32.3	Ø 14 mm	1.56	CFRP	1	0.23
	N(T2)/100/14/G#2	32.3	Ø 14 mm	1.56	GFRP	2	0.41
	N(T2)/100/14/G#5	32.3	Ø 14 mm	1.56	GFRP	5	1.02
T3	N(T3)/100/10/Ref.	32.5	Ø 10 mm	0.79	-	-	-
	N(T3)/100/10/C#1	32.5	Ø 10 mm	0.79	CFRP	1	0.22
	N(T3)/100/10/G#5	32.5	Ø 10 mm	0.79	GFRP	5	1.01
	N(T3)/100/10/C#4	32.5	Ø 10 mm	0.79	CFRP	4	0.90
T4	N(T4)/100/16/Ref.	30.3	Ø 16 mm	2.05	-	-	-
	N(T4)/100/16/C#1	30.3	Ø 16 mm	2.05	CFRP	1	0.23
	N(T4)/100/16/G#5	30.3	Ø 16 mm	2.05	GFRP	5	1.02
	N(T4)/100/14/C#3	30.3	Ø 14 mm	1.56	CFRP	3	0.68
T5	H(T5)/100/14/Ref.	96.0	Ø 14 mm	1.56	-	-	-
	H(T5)/100/14/C#1	96.0	Ø 14 mm	1.56	CFRP	1	0.23
	H(T5)/100/14/G#2	96.0	Ø 14 mm	1.56	GFRP	2	0.41
	H(T5)/100/14/G#3	96.0	Ø 14 mm	1.56	GFRP	3	0.61

Voor de inwendige wapening werd uitgegaan van betonstaal S500, met een diameter van respectievelijk 10 mm, 14 mm en 16 mm. De uitwendig gelijmde FRP wapening bestond uit één of meerdere lagen wet lay-up CFRP (Replark 100 mm x 0.111 mm) of GFRP weefsels (Roviglas G 100 mm x 0.100 mm). De eigenschappen van de wapening zijn weergegeven in Tabel S-12. Twee soorten beton werden aangewend. Een normale sterkte en een hoge sterkte beton, met een gemiddelde cilinderdruksterkte op 28 dagen van respectievelijk 32.8 N/mm^2 en 96.0 N/mm^2. Meer informatie inzake de materiaal-eigenschappen is beschikbaar in Appendix B.

Tabel S-12 *Eigenschappen (gemiddelde waarden) wapening bepaald d.m.v. van trekproeven*

Type	Nominale afmetingen [mm]	Vloei-grens [N/mm^2]	Trek-sterkte [N/mm^2]	Breuk-rek [%]	E-modulus [N/mm^2]
Betonstaal S500	Ø 10	590	670	-	200000
	Ø 14	550	630	-	200000
	Ø 16	590	690	-	200000
Replark MRK-M2-20	100 x 0.111	-	3500	1.25	233000[(1)]
Roviglas G	100 x 0.100	-	1300	2.07	57000[(1)]

[(1)] Tangensmodulus aan de oorsprong

5.2 Voornaamste proefresultaten

Voor de prisma's werd, naargelang de hoeveelheid en het type uitwendig gelijmde wapening, een versterkingsfactor bekomen tussen 1.3 en 3.0. Ten gevolge van de hoge hechtschuifspanningen aan de uiteinden van de gelijmde FRP wapening, werd voor de proefstukken van reeks T1 een verankeringsbreuk bekomen. Om dit verder te vermijden, werd voor de volgende reeksen een mechanische verankering toegepast (Fig. S-17) en trad breuk op in de FRP wapening (met uitzondering van twee proefstukken die lokaal bezweken in het beton aan het prisma-uiteinde).

De opgemeten gemiddelde vervormingen van de prisma's zijn weergegeven in Appendix E. Een vergelijking van het belasting-rek gedrag, op basis van het equivalent wapenings-percentage ρ_{eq}, is voor een aantal prisma's eveneens weergegeven in Fig. S-18. Het linkerdeel van deze figuur toont versterkte prisma's met een zelfde hoeveelheid inwendig betonstaal en een constant equivalent wapeningspercentage ($\rho_{eq} \approx 1.83$ %). De opgemeten curven vallen nagenoeg samen. In vergelijking met het referentieproefstuk ($\rho_s = 1.56$ %), wordt een merkbare verhoging van de stijfheid in de gescheurde toestand waargenomen en neemt de sterkte in belangrijke mate toe. Voor het prisma in hoge sterkte beton is de scheurlast hoger.

In het rechterdeel van Fig. S-18 zijn de vervormingen uitgezet voor prisma's met een toenemend equivalent wapeningspercentage. De stijfheid in de gescheurde toestand neemt toe met ρ_{eq}. De helling van de laatste tak van de curven (stijfheid in gescheurde toestand na het vloeien van de staalwapening) is nagenoeg identiek voor de drie prisma's met het zelfde type en hoeveelheid uitwendige wapening, ongeacht de hoeveelheid inwendige wapening.

Het scheurpatroon bij bezwijken, de gemiddelde scheuropening en scheurafstand worden vergeleken in Fig. S-19 en Fig. S-20 voor de prisma's N(T4)/100/16/Ref en N(T4)/100/16/C#1. Scheurpatronen en gemiddelde scheuropeningen van de prisma's zijn eveneens opgenomen in Appendix E.

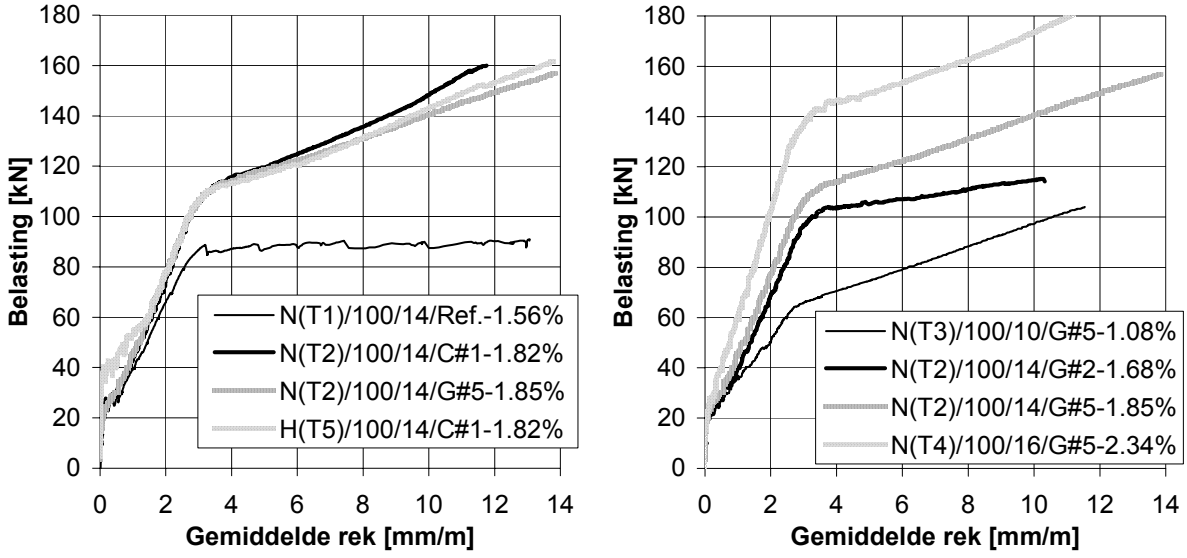

Fig. S-18 *Belasting-rek gedrag van een aantal prisma's in functie van* ρ_{eq}

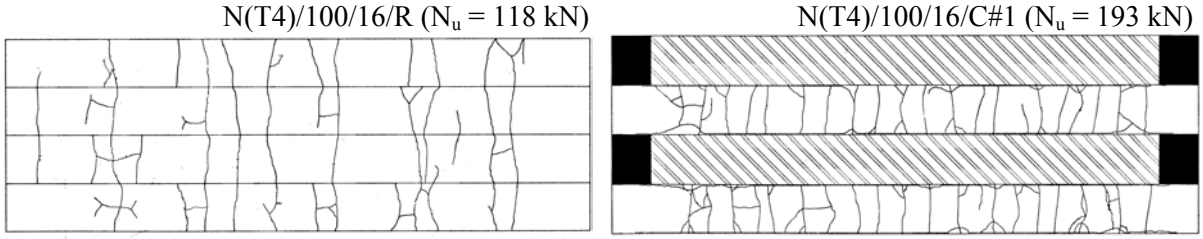

Fig. S-19 *Scheurpatroon bij bezwijken*

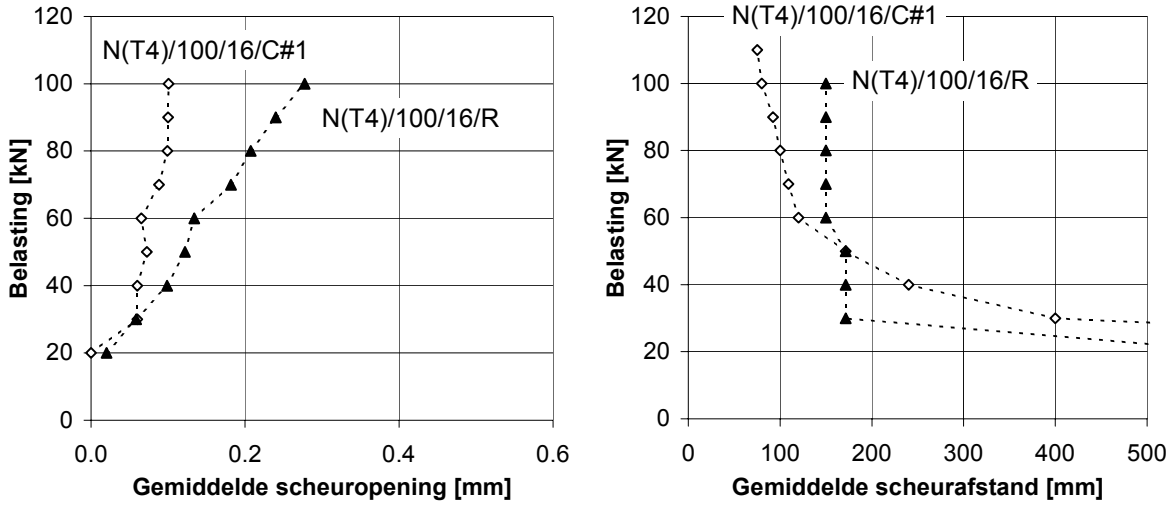

Fig. S-20 *Gemiddelde scheuropening en afstand*

Het scheurpatroon blijkt in belangrijke mate beïnvloed te worden door zowel de inwendige als de uitwendige wapening. Kleinere scheurafstanden worden bekomen bij toenemende wapenings-percentages, waarbij reeds een kleine hoeveelheid FRP een aanzienlijke vermindering van de scheurafstand met zich meebrengt. Een dicht scheurpatroon stemt overeen met kleinere scheuropeningen.

5.3 Analytische verificatie

5.3.1 Tension stiffening effect

Het belasting-rek gedrag van de prisma's, met inbegrip van het tension stiffening effect (bijdrage van het ongescheurd beton tussen de gescheurde doorsneden) werd analytisch geverifieerd conform [19]. Uitgaande van de ongescheurde (toestand 1) en de volledig gescheurde toestand (toestand 2), wordt de gemiddelde rek gegeven als:

$$\varepsilon_m = (1-\zeta)\varepsilon_1 + \zeta\varepsilon_2 \tag{S-9}$$

met ζ een verdeel- of tension stiffening coëfficiënt gedefinieerd als:

$$\begin{aligned} &\zeta = 0 && N < N_{cr} \\ &\zeta = 1-\beta_1\beta_2\left(\frac{N_{cr}}{N}\right)^n && N > N_{cr} \end{aligned} \tag{S-10}$$

met N de aangrijpende belasting, $N_{cr} = f_{ctm}A_c(1 + \alpha_s\rho_s + \alpha_f\rho_f)$ de scheurbelasting, α_s en α_f de verhouding van de elasticiteitsmodulus van de wapening t.o.v. deze van het beton, β_1 een

coëfficiënt die het aanhechtingsgedrag in rekening brengt (1 voor staal met hoge hechting) en β_2 een coëfficiënt voor de aard van de belasting (1 voor korte-duur belasting). De macht n bedraagt 2 [19]. Voor hoge sterkte beton wordt een betere nauwkeurigheid bekomen voor n gelijk aan 3 [27]. Aangezien de effecten van de inwendige en de uitwendige wapening moeilijk afzonderlijk te begroten zijn, werd aangenomen dat vergelijkingen (S-9) en (S-10) blijven gelden in het geval van een combinatie van staal en FRP wapening en dat de constanten β_1, β_2 en n van toepassing blijven. Met deze aannamen bleek een zeer goede overeenkomst bekomen te worden tussen de experimentele en analytische resultaten (Fig. S-21). De vervormingen ε_1 (in toestand 1) en ε_2 (in toestand 2) worden gegeven door:

$$\varepsilon_1 = N/(E_c A_c + E_s A_s + E_f A_f) \tag{S-11}$$

$$\begin{aligned} \varepsilon_2 &= N/(E_s A_s + E_f A_f) \quad \varepsilon_2 \le \varepsilon_y \\ \varepsilon_2 &= (N - A_s f_y)/E_f A_f \quad \varepsilon_2 > \varepsilon_y \end{aligned} \tag{S-12}$$

met ε_y de rek waarbij het vloeien van het staal aanvangt. Voor de referentieprisma's werd aangenomen dat het belasting-rek gedrag voor $\varepsilon_2 > \varepsilon_y$ horizontaal verloopt.

Resultaten van de analytische verificatie, voor een aantal van de prisma's, zijn weergegeven in Fig. S-21. Een nauwkeurige voorspelling van de gemiddelde rek wordt bekomen.

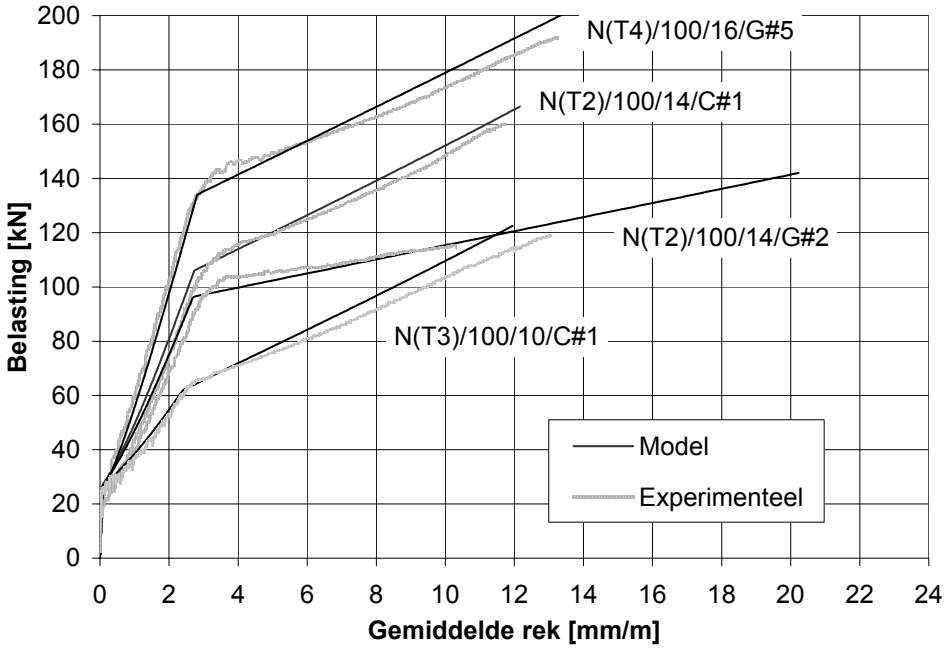

Fig. S-21 *Analytische verificatie van de gemiddelde rek*

5.3.2 Scheurafstand en scheuropeningen

In de gestabiliseerde scheurfase wordt de gemiddelde scheuropening gegeven door [19]:

$$\begin{aligned} w_m &= s_{rm}(\varepsilon_{rm} - \varepsilon_{cm}) \\ &= s_{rm}\varepsilon_{rm,r} \end{aligned} \tag{S-13}$$

met s_{rm} de gemiddelde scheurafstand en $\varepsilon_{rm,r} = \varepsilon_{rm}\zeta$ de gemiddelde rek in de wapening ten opzichte van het omringend beton. Deze laatste wordt gegeven door vergelijkingen (S-12) ($\varepsilon_2 < \varepsilon_y$) en (S-10). Voor de scheurafstand s_{rm} werden verschillende betrekkingen geverifieerd. Hieruit blijkt dat het belangrijk is expliciet rekening te houden met het verschillend aanhechtingsgedrag van de gecombineerde staal en FRP wapening. Dit kan analoog gebeuren zoals gespecificeerd in [28] voor voorgespannen beton. Aldus wordt de gemiddelde scheurafstand gegeven door [29]:

$$\begin{aligned} \ell_{cr,n} &= \frac{N_{cr}}{\tau_{sm} u_s} \frac{E_s A_s}{E_s A_s + \xi_b E_f A_f} \\ &= \frac{N_{cr}}{\tau_{fm} u_f} \frac{\xi_b E_f A_f}{E_s A_s + \xi_b E_f A_f} \end{aligned} \tag{S-14}$$

met u_s en u_f de aanhechtingslengte (in omtrekszin) van de wapening ten opzichte van het beton, $\tau_s = 1.80 f_{ctm}$ [28] en $\tau_f = 1.25 f_{ctm}$ [30] de gemiddelde hechtschuifspanning van het staal en de FRP en ξ_b een factor afhankelijk van de eigenschappen van de gecombineerde wapening:

$$\begin{aligned} \xi_b &= \frac{\tau_{fm} E_s A_s u_f}{\tau_{sm} E_f A_f u_s} \\ &= \frac{\tau_{fm} E_s Ø}{\tau_{sm} E_f 4t} \end{aligned} \tag{S-15}$$

met Ø de (gemiddelde) diameter van het betonstaal.

Met dit model wordt, zoals blijkt uit Fig. S-22 en Appendix E, een relatief nauwkeurige voorspelling bekomen van de gemiddelde scheurafstand en toegepast in vergelijking (S-13) van de gemiddelde scheuropening.

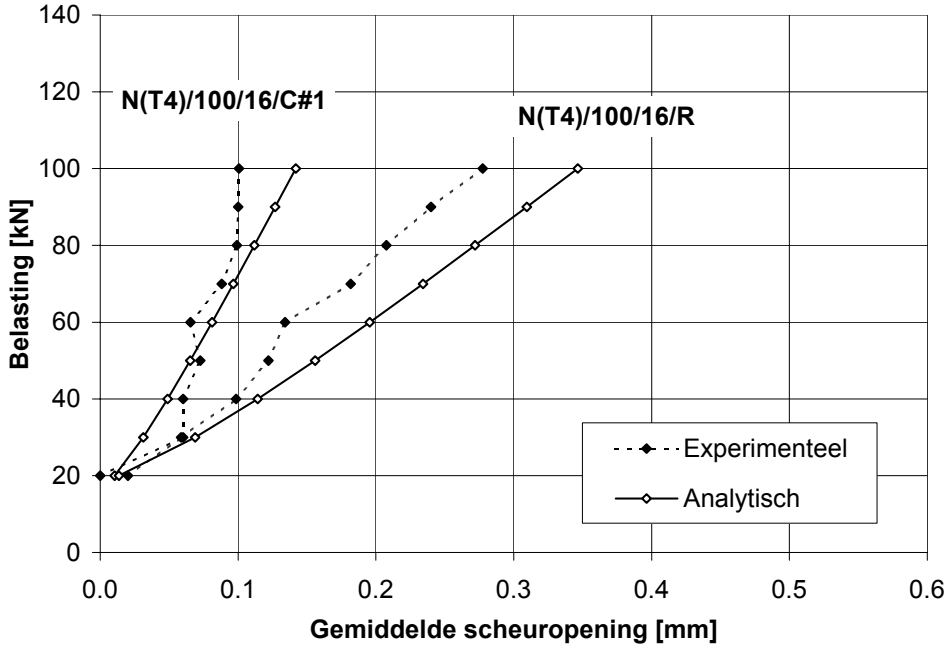

Fig. S-22 *Analytische verificatie van de gemiddelde scheuropening*

5.4 Besluiten

Uit de tension stiffening proeven en de analytische verificaties kan het volgende besloten worden:

- Een versterkingsfactor van 1.3 tot 3.0 werd bekomen voor de bezwijklast van de prisma's. Om onthechting ten gevolge van verankeringsbreuk te voorkomen, diende een bijkomende mechanische verankering toegepast te worden.
- Een merkbare toename in de stijfheid in de gescheurde toestand wordt bekomen door het aanbrengen van uitwendig gelijmde FRP wapening. De toename hangt in sterke mate af van het equivalent wapeningspercentage (met andere woorden van de hoeveelheid en de stijfheid van de wapeningen). De stijfheid in de gescheurde toestand na het vloeien van het betonstaal hangt voornamelijk af van de hoeveelheid en de stijfheid van de FRP wapening.
- Merkelijk lagere scheurafstanden en kleinere scheuropeningen worden bekomen voor de versterkte prisma's. In vergelijking met de onversterkte prisma's, gebeurt de ontwikkeling van het scheurpatroon op een meer gelijkmatige wijze.
- De gemiddelde rek van de prisma's, met inbegrip van het tension stiffening effect, kan nauwkeurig voorspeld worden volgens [19]. Voor de voorspelling van de scheurafstand blijkt het model in [29] het meest aangewezen.
- Op basis van deze modellen is eveneens een relatief nauwkeurige voorspelling mogelijk van de gemiddelde scheuropening.

6 Inrijgen van axiaal belaste kolommen

6.1 Aard van de proeven

Om de efficiëntie na te gaan van het inrijgen van beton door omwikkeling met FRP, werden proeven uitgevoerd op 15 cilinders en 11 kolommen [31,33]. Aan de hand van de proeven op omwikkelde cilinders werd de invloed nagegaan van al dan niet hechtende omwikkelingswapening. Met de drukproeven op kolommen werd de invloed nagegaan van het type en het aantal lagen FRP, de omwikkelingsconfiguratie (volledig of deels, cirkelvormig of helicoïdaalvormig) en de kolomdoorsnede (cirkelvormig of rechthoekig). Een overzicht van de proefparameters is gegeven in Tabel S-13 en Tabel S-14. De afmetingen en omwikkelingsconfiguratie van de kolommen is eveneens weergegeven in Fig. S-23.

Tabel S-13 *Proefparameters van de omwikkelde cilinders Ø150 mm x 300 mm*

Cilinder	**f_{cm} (28 dagen)** [N/mm^2]	**FRP type** [mm]	**Aantal lagen**	**Breedte** [mm]	**Omwikkeling** [mm]
R1-R3	34.8	-	-	-	-
C240b1-C240b3	34.8	C240	1	300	Volledig, hechtend
C240nb1-C240nb3	34.8	C240	1	300	Volledig, niet-hechtend
C640b1-C640b3	34.8	C640	1	300	Volledig, hechtend
C640nb1-C640nb3	34.8	C640	1	300	Volledig, niet-hechtend

Tabel S-14 *Proefparameters omwikkelde kolommen*

Kolom	Vorm doorsnede [mm]	f_{cm} (28 dagen) [N/mm^2]	FRP type [mm]	Aantal lagen	Breedte [mm]	Tussen-afstand [mm]	Spoed [mm]	Omwikkeling [mm]
K1	Ø 400	31.8	-	-	-	-	-	-
K2	Ø 400	34.3	C240	5	300	0	0	Volledig
K3	Ø 400	34.3	C640	4	300	0	0	Volledig
K4	Ø 400	39.3	TU600/20	6	200	0	0	Volledig
K5	Ø 400	39.3	TU600/20	2	200	0	0	Volledig
K6	Ø 400	35.8	TU600/20	4	200	200	0	Deels
K7	Ø 400	35.8	TU600/20	4	200	200	400	Deelsl
K8	Ø 400	39.1	TU360G160C/27G	4	50	0	0	Volledig
K9	355x355/r30	39.1	TU600/20	2	200	0	0	Volledig
K10	355x355/r15	37.7	TU600/20	2	200	0	0	Volledig
K11	250x500/r30	37.7	TU600/20	2	200	0	0	Volledig

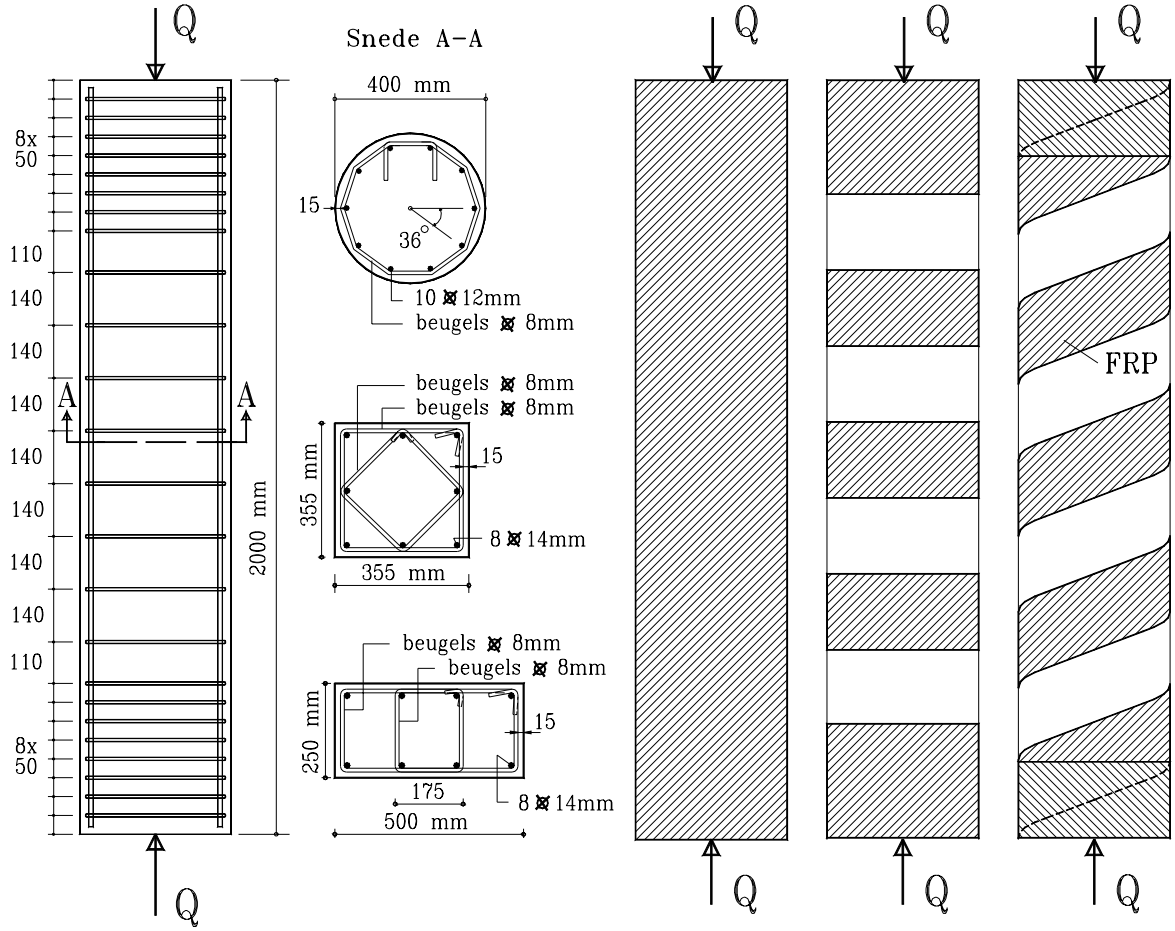

Fig. S-23 *Kolommen omwikkeld met FRP*

Verschillende types FRP werden aangewend: 2 soorten CFRP, een GFRP weefsel en een HFRP (hybride FRP) weefsel. De eigenschappen van de wapening zijn weergegeven in Tabel S-15. Het aangewende beton had een gemiddelde druksterkte op 28 dagen van 36.1 N/mm^2. Meer gedetailleerde informatie omtrent de materiaaleigenschappen is opgenomen in Appendix B.

Tabel S-15 *Eigenschappen (gemiddelde waarden) wapening bepaald d.m.v. van trekproeven*

Type	**Nominale afmetingen** [mm]	**Vloei-grens** [N/mm^2]	**Trek-sterkte** [N/mm^2]	**Breuk-rek** [%]	**E-modulus** [N/mm^2]
Rebar S500	Ø 8	560	610	2.77	200000
	Ø 12	620	720	8.73	200000
	Ø 14	560	630	9.97	200000
C-sheet 240 - Multipox T	300 x 0.117	-	2600	1.19	198000$^{(1)}$
C-sheet 640 - Multipox T	300 x 0.235	-	1100	0.22	471000$^{(1)}$
TU600/25 - PC5800	200 x 0.300	-	780	1.30	60000$^{(1)}$
TU360G160C/27G - PC5800	50 x 0.123	-	1100	0.96	97000$^{(1)}$

$^{(1)}$ Tangensmodulus aan de oorsprong

6.2 Voornaamste proefresultaten

6.2.1 Drukproeven op omwikkelde cilinders

Voor de met CFRP omwikkelde cilinders werd een versterkingsfactor bekomen tussen 1.17 en 1.32. De toename in sterkte is ongeveer gelijk voor de twee types aangewend CFRP. Dit komt omdat één laag van beide materialen ongeveer dezelfde kracht kan weerstaan (het product $\varepsilon_{c\ell u} E_f t$, met $\varepsilon_{c\ell u}$ de uiterste rek in omtrekszin, blijkt ongeveer gelijk te zijn voor beide materialen). In vergelijking met hechtende omwikkelingswapening, is de sterkte-toename voor niet-hechtende omwikkelingswapening geringer. Zoals ook blijkt uit de opgemeten vervormingen (Fig. S-24), komt dit doordat bij het bereiken van de druksterkte van het onversterkt beton, een zekere laterale uitzetting nodig is vooraleer de niet-hechtende omwikkelingswapening ten volle bijdraagt. Een analoog effect wordt bekomen voor hechtende omwikkelingswapening die holtes of onvolkomenheden bevat (ten gevolge van een slechte uitvoering).

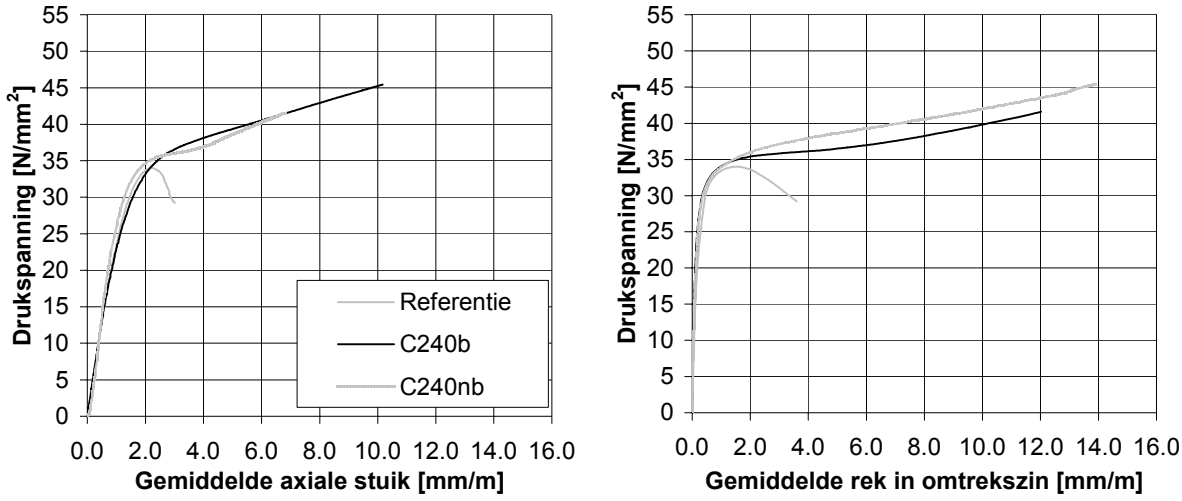

Fig. S-24 *Spanning-vervorming gedrag van omwikkelde cilinders*

6.2.2 Drukproeven op omwikkelde kolommen

Voor de omwikkelde kolommen werd een versterkingsfactor tussen 1.03 en 1.62 bekomen. Hieruit blijkt dat de efficiëntie van de FRP omwikkeling sterk afhangt van de proefparameters die werden gevarieerd.

In Fig. S-25 wordt het spanning-vervorming gedrag weergegeven (op basis van rekstrookmetingen) van de cirkelvormige kolommen, die volledig omwikkeld werden met FRP (de drukspanning is gerelateerd tot de oppervlakte A_g van de volledige kolomdoorsnede). De bekomen toename in sterkte hangt af van de hoeveelheid en de treksterkte van de omwikkelingswapening. Hoe hoger de stijfheid (hoeveelheid en E-modulus) van de omwikkelingswapening, hoe kleiner de toename in ductiliteit. Uit de proeven blijkt verder dat de efficiëntie van deels omwikkelde kolommen kleiner is dan deze van volledig omwikkelde kolommen. Dit komt omdat het beton niet ten volle ingeregen is. Vergeleken met cirkelvormig omwikkelen resulteert helicoïdaalvormig omwikkelen eveneens in een lagere efficiëntie. Dit komt omdat de vezels in het laatste geval minder efficiënt georiënteerd zijn om de laterale uitzetting van het beton tegen te werken. In Fig. S-26 wordt het gedrag vergeleken van een cirkelvormige en een vierkante kolom (met een zelfde oppervlakte van de doorsnede en omwikkeld met een zelfde type en hoeveelheid FRP). Aangezien bij vierkante of rechthoekige kolommen de steundruk voornamelijk aangrijpt in de afgeronde hoeken, is de efficiëntie merkelijk lager dan voor cirkelvormige kolomdoorsneden. De afrondingsstraal van de hoeken speelt hierbij een belangrijke rol.

De verhouding $\varepsilon_{c\ell u}/\varepsilon_{fum}$ van de opgemeten uiterste rek in omtrekszin tot de breukrek van de FRP (uit trekproeven), blijkt voor bijna alle kolommen een stuk kleiner te zijn dan 1 (zie Table 6-4 en Table 6.5), ondanks het feit dat steeds bezwijken van de FRP omwikkelingswapening optrad. Dit is het gevolg van de multi-axiale spanningstoestand waaraan de FRP onderworpen wordt, evenals van de spanningsconcentraties bij hoge belastingen. Deze spanningsconcentraties zijn het gevolg van de heterogene vervormingen van het sterk beschadigde doch nog steeds ingeregen beton, nabij de breuk.

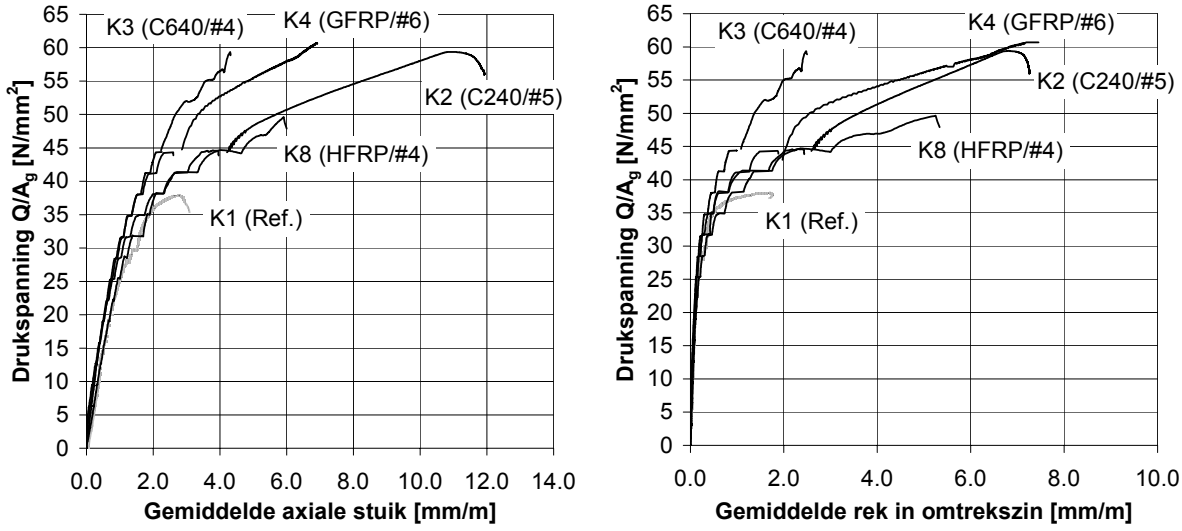

Fig. S-25 *Spanning-vervorming gedrag van cirkelvormige kolommen*

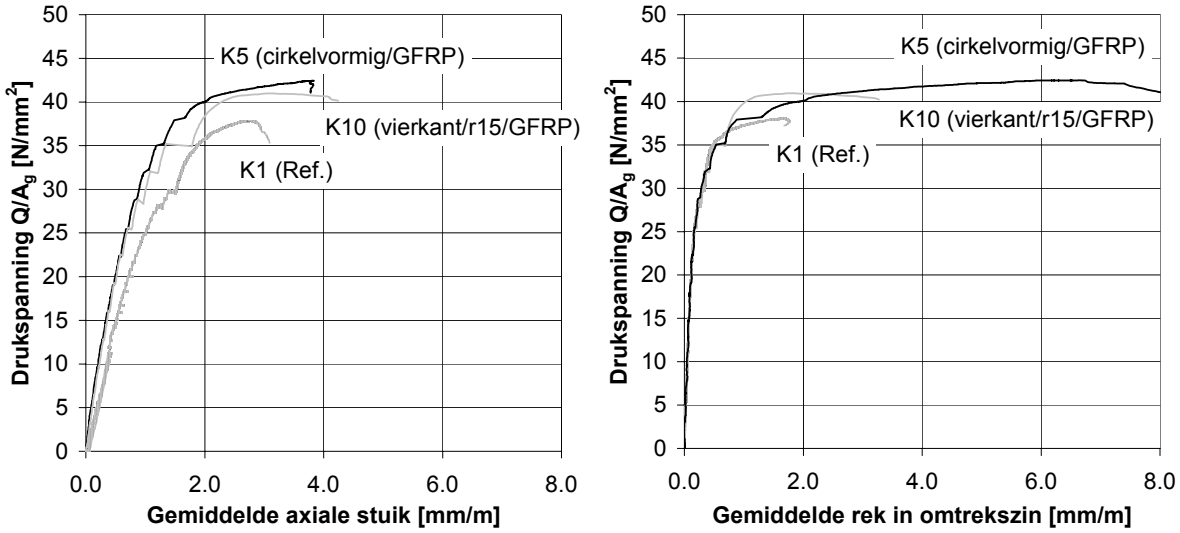

Fig. S-26 *Invloed van de vorm van de kolomdoorsnede*

6.3 Analytische verificatie

6.3.1 Probleemstelling

Diverse modellen, voornamelijk opgesteld voor het inrijgen met staal, zijn in de literatuur ter beschikking. Deze modellen blijken niet echt geschikt te zijn voor beton omwikkeld met FRP. Inderdaad, kenmerkend wordt in deze modellen aangenomen dat de steundruk constant is (wat juist is eens het staal vloeit). Voor de lineair elastische FRP materialen wordt echter een toenemende steundruk bekomen, naarmate de laterale uitzetting van het beton toeneemt. Bovendien blijkt de bezwijktoestand van beton omwikkeld met FRP in belangrijke mate af te hangen van de effectieve breukrek van de FRP omwikkelingswapening. Deze effectieve breukrek is meestal (een stuk) kleiner dan de breukrek van FRP bekomen uit trekproeven (zie paragraaf 6.2.2).

6.3.2 Steundruk

Beschouwing van een krachtenevenwicht van een cirkelvormige betondoorsnede omwikkeld met FRP, laat toe de steundruk als volgt te begroten (paragraaf 7.6.1.2):

$$\sigma_{\ell} = K_{conf}\,\varepsilon_{c\ell=f} \tag{S-16}$$

met K_{conf} een evenredigheidsfactor die de stijfheid van de omwikkelingswapening vertegenwoordigt en $\varepsilon_{c\ell=f}$ de rek van het beton in omtrekszin. Deze laatste kan, bij kwalitatieve en hechtende uitvoering, gelijk genomen worden aan de rek in de FRP omwikkelingswapening. De maximale steundruk wordt gegeven als:

$$\sigma_{\ell u} = K_{conf}\,\varepsilon_{fu,eff} \tag{S-17}$$

met $\varepsilon_{fu,eff}$ de effectieve FRP breukrek zoals gegeven in paragraaf 6.3.4.

De invloed van de omwikkelingsconfiguratie en de vorm van de kolomdoorsnede wordt in rekening gebracht door een efficiëntiefactor k_e die vervat wordt in K_{conf}. Hiervoor wordt verder verwezen naar paragraaf 7.6.1.2.

6.3.3 Spanning-vervorming gedrag van beton omwikkeld met FRP

Fig. S-27 geeft een schematische aanduiding van een model voor het spanning-vervorming gedrag van beton omwikkeld met FRP. Uitgaande van de rek in omtrekszin en de corresponderende steundruk van de omwikkelingswapening, kan het spanning-vervorming gedrag bepaald worden. De berekeningsmethode is in wezen een combinatie van verschillende modellen voor het uni-axiaal spanning-vervorming gedrag van omwikkeld beton, de laterale uitzetting van het beton, de steundruk uitgeoefend door de FRP omwikkelingswapening en een breukcriterium dat de effectieve FRP breukrek in acht neemt.

In de literatuur werden recent drie modellen voorgesteld voor het spanning-vervorming gedrag van beton omwikkeld met FRP [34-36]. Deze modellen zijn weergegeven in Appendix F en werden geverifieerd aan de hand van het experimenteel bekomen spanning-vervorming gedrag van de proefstukken. Resultaten van de analytische verificatie voor kolommen K2 en K6 zijn weergegeven in Fig. S-28. Uit deze verificatie wordt het volgende besloten:

- De resultaten van de drie modellen verschillen in belangrijke mate. De beste voorspellingen worden bekomen door het model van Spoelstra en Monti [34]. Dit model is evenwel complex om te berekenen (het model beschouwt de toenemende steundruk stapsgewijs, waarbij per stap een iteratieve berekening nodig is).
- Indien voor het breukcriterium uitgegaan wordt van een breukrek $\varepsilon_{fu} = f_f/E_f$ (met f_f de treksterkte van de FRP wapening), dan wordt de bezwijklast in de meeste gevallen overschat. Het is daarom van belang dat een gereduceerde breukrek in rekening gebracht wordt.

De analytische verificatie van alle proefstukken, volgens het model van Spoelstra en Monti en overeenkomstig een effectieve breukrek $\varepsilon_{fu,eff}$ (paragraaf 6.3.4), is weergegeven in Appendix F.

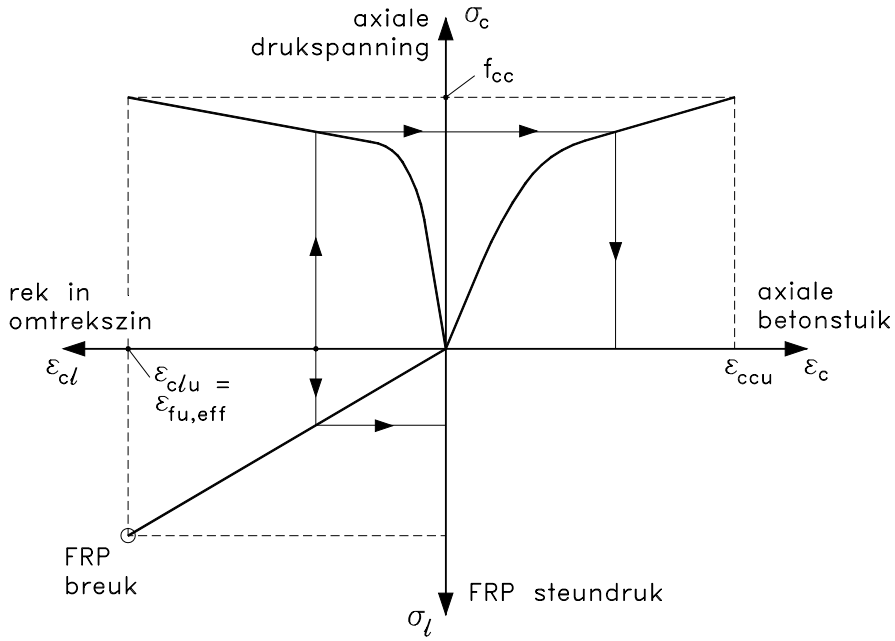

Fig. S-27 *Beton omwikkeld met FRP (toenemende steundruk)*

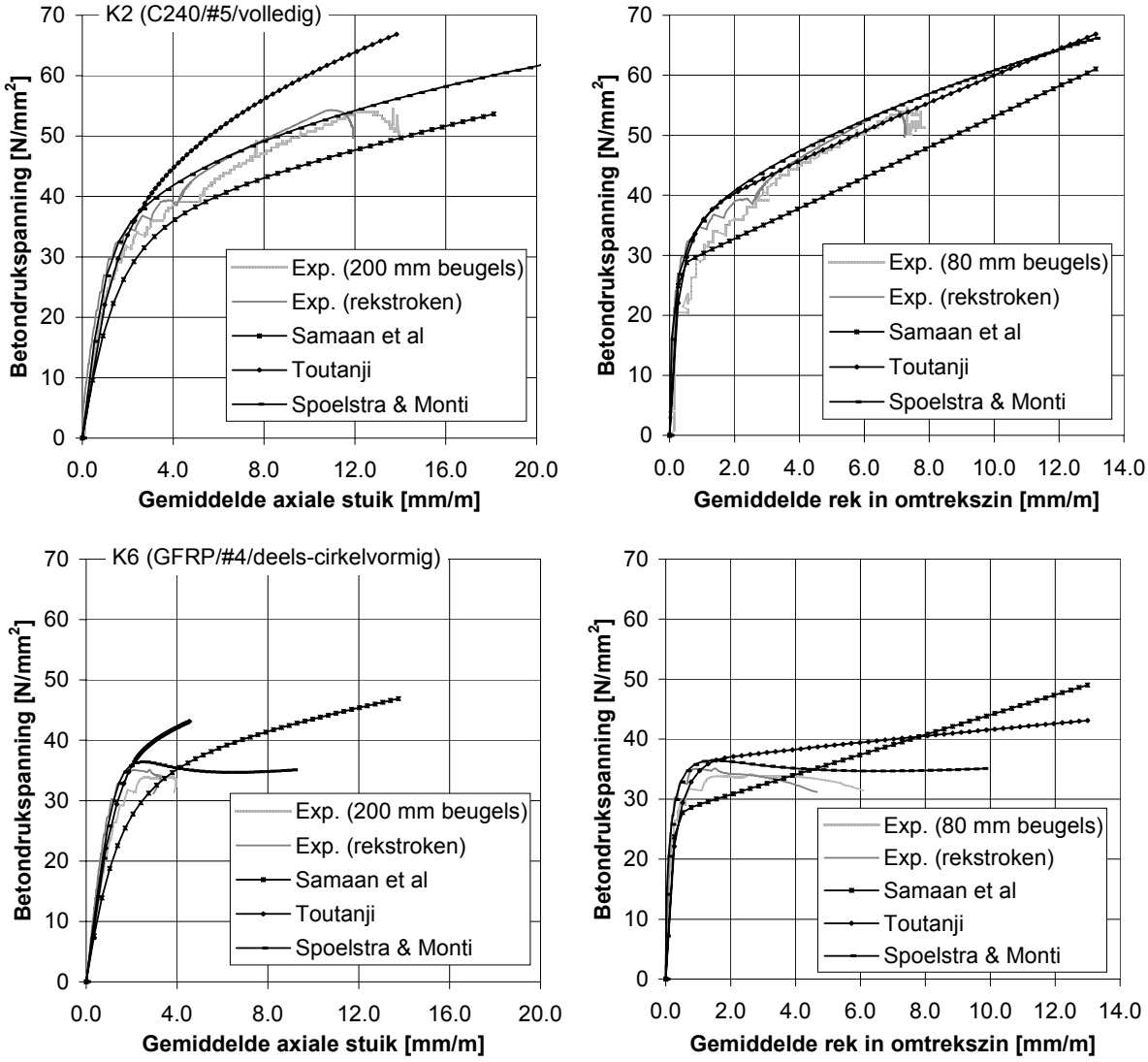

Fig. S-28 *Analytische verificatie voor kolommen K2 en K6*

6.3.4 Effectieve maximale steundruk

De gereduceerde breukrek die bekomen wordt voor FRP omwikkelingswapening kan in rekening gebracht worden aan de hand van de verhouding $\eta_e = \varepsilon_{fu,eff}/\varepsilon_{fu}$. De maximale steundruk wordt dan gedefinieerd als:

$$\sigma_{\ell u} = K_{conf} \frac{\eta_e f_f}{E_f} \tag{S-18}$$

waarbij η_e, gebaseerd op een beperkt aantal experimenten (Appendix F), gekalibreerd werd als (Fig. S-29):

$$\eta_e = 0.105(K_{conf})^{0.266} \tag{S-19}$$

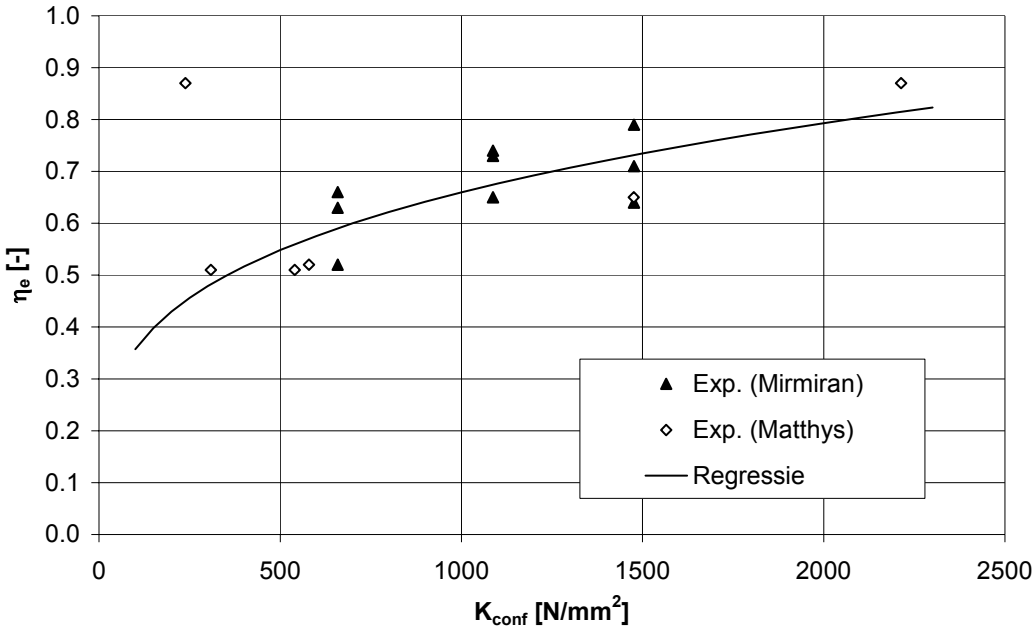

Fig. S-29 *Effectieve breukrek van FRP omwikkelingswapening*

6.3.5 Bezwijkbelasting

Uitgaande van de druksterkte f_{cc} van het met FRP omwikkeld beton, werd de maximale belasting van de proefstukken berekend als:

$$Q_{max} = f_{cc} A_c + \sigma_s A_s \tag{S-20}$$

met $\sigma_s = E_s \varepsilon_{cc1} \leq f_y$ de spanning in de stalen langswapening, ε_{cc1} de stuik van het beton corresponderend met f_{cc} en f_y de vloeigrens van het staal. Bij een voldoend hoge maximale steundruk ($K_{conf}/f_{co} > 3$, met f_{co} de druksterkte van het onversterkt beton) is de betonstuik ε_{cc1} groot, zodat $\sigma_s = f_y$. Voor een lage maximale steundruk ($K_{conf}/f_{co} < 3$) blijkt het versterkings-effect nagenoeg verwaarloosbaar ($f_{cc} \approx f_{co}$) en is $\sigma_s = E_s \varepsilon_{c1} \leq f_y$ met $\varepsilon_{c1} = 2$ mm/m. De druksterkte f_{cc} van het beton omwikkeld met FRP kan bepaald worden aan de hand van het model van Spoelstra en Monti. Ongeacht het volledige spanning-vervorming gedrag (dat een iteratieve berekening vergt), kan f_{cc} op eenvoudige wijze berekend worden zoals aangegeven in paragraaf 7.6.1.1.

Resultaten van de analytische verificatie zijn weergegeven in Tabel S-16. Een relatief nauwkeurige voorspelling van de bezwijkbelasting wordt bekomen indien de effectieve breukrek in rekening gebracht wordt.

6.4 Besluiten

Uit de studie naar het omwikkelen van beton met FRP wapening kan het volgende besloten worden:

- Inrijgen van beton met FRP omwikkelingswapening is een efficiënte techniek om de sterkte en ductiliteit van kolommen te verhogen. De bekomen efficiëntie hangt in belangrijke mate af van de configuratie van de omwikkelingswapening en de kolomvorm.

Tabel S-16 *Analytische verificatie van de bezwijklast*

Proefstuk	**Experimenteel**		$\varepsilon_{fu} = f_f/E_f$			$\varepsilon_{fu,eff} = \eta_e f_f/E_f$			
	Q_{exp} [kN]	f_{co} [N/mm^2]	f_{cc} [N/mm^2]	Q_{cal} [kN]	Q_{cal}/Q_{exp} [-]	η_e [-]	f_{cc} [N/mm^2]	Q_{cal} [kN]	Q_{cal}/Q_{exp} [-]
Ref.	616	34.8	-	615	1.00	-	-	615	1.00
C240b[(1)]	814	34.8	52.7	931	1.14	0.48	45.7	806	0.99
C640b[(1)]	809	34.8	52.8	933	1.15	0.73	47.8	843	1.04
K1 (Ø/Ref.)	4685	34.6	-	4761	1.02	-	-	4761	1.02
K2 (Ø/C240/#5/volledig)	7460	33.6	66.1	8938	1.20	0.57	57.2	7657	1.03
K3 (Ø/C640/#4/volledig)	7490	33.6	57.8	7897	1.05	0.81	53.2	7288	0.97
K4 (Ø/G/#6/volledig)	7580	36.1	67.2	9068	1.20	0.56	58.2	7773	1.03
K5 (Ø/G/#2/volledig)	5325	36.1	44.1	6197	1.16	0.42	39.7	5620	1.06
K6 (Ø/G/#4/deels-cirk.)	5000	35.5	35.9	5173	1.03	0.36	35.5[(2)]	4873	0.97
K7 (Ø/G/#4/deels-helic.)	4810	35.5	35.5[(2)]	4873	1.01	0.35	35.5[(2)]	4873	1.01
K8 (Ø/H/#4/full)	6230	34.1	45.7	6397	1.03	0.45	40.6	5689	0.92
K9 (sq./r30/G/#2/full)	5810[(3)]	34.1	35.5	5095	0.88[(3)]	0.36	34.1[(2)]	4722	0.81[(3)]
K10 (sq./r15/G/#2/full)	5140	36.0	36.0[(2)]	4978	0.97	0.35	36.0[(2)]	4978	0.97
K11 (rect./r30/G/#2/full)	4990	36.0	36.0[(2)]	4920	0.99	0.34	36.0[(2)]	4920	0.99

[(1)] Met uitsluiting van de omwikkelde cilinders met meer dan 5 % holten

[(2)] $f_{cc} = f_{co}$ en $\varepsilon_{c1} = 2$ mm/m (verwaarloosbare versterking)

[(3)] De belasting nam plots toe tot breuk na het activeren van een tweede belastingspomp

- Voor een gegeven configuratie, hangt de sterktetoename voornamelijk af van de hoeveelheid en van de treksterkte van de FRP wapening.
- Voor de modellering van beton omwikkeld met FRP, is het belangrijk dat rekening gehouden wordt met de toenemende steundruk uitgeoefend door de FRP wapening en met de effectieve breukrek van de omwikkelingswapening.
- Van de onderzochte modellen bleek het model van Spoelstra en Monti [34] het meest veelzijdig en nauwkeurig te zijn voor de voorspelling van het spanning-vervorming gedrag van beton omwikkeld met FRP. Op basis van dit model (dat complex is om te berekenen) kan de druksterkte van het omwikkeld beton op eenvoudige wijze bekomen worden.
- Een indicatieve vergelijking voor het berekenen van de effectieve breukrek van de FRP omwikkelingswapening werd voorgesteld.

7 Ontwerprichtlijnen

7.1 Algemeen

Op basis van het experimenteel en analytisch onderzoek (paragrafen 3 t.e.m. 6) werden ontwerprichtlijnen opgesteld voor de dimensionering van uitwendig gelijmde FRP wapening voor de versterking in buiging en dwarskracht van gewapend betonelementen en voor het omwikkelen van axiaal belaste kolommen [16,17,37-39]. Deze worden in hetgeen volgt samengevat. Voor meer gedetailleerde informatie en de bijhorende formules wordt verwezen naar Hoofdstuk 7.

7.2 Verloop van het ontwerp

In vergelijking met het ontwerp van nieuwe betonconstructies, is dat van betonconstructies versterkt met uitwendig gelijmde wapening meer gecompliceerd. Om te beginnen, moet de bestaande toestand en het draagvermogen van de te versterken constructie nagegaan en geverifieerd worden. Oorzaken van gebreken moeten gekend zijn (zo zal bijvoorbeeld de corrosie van wapening niet gestopt worden de versterking met FRP) en de nodige herstellingen moeten voorzien worden. Vervolgens kan dan de initiële toestand van de (herstelde) constructie, voorafgaand aan het aanbrengen van de versterking, nagerekend worden. Immers, in het verder ontwerp dient rekening gehouden te worden met de belasting van de constructie voorafgaand (en tijdens) het aanbrengen van de uitwendige wapening. Op basis van deze voorafgaande studie, kan dan het eigenlijke ontwerp van de uitwendige FRP wapening gebeuren. Hierbij worden de diverse bezwijk- en gebruikgrensstoestanden die kunnen optreden geverifieerd [19]. Bijkomend dienen eventueel een aantal bijzondere ontwerpaspecten (zoals brand, impact, vandalisme, enz.) en de accidentele ontwerptoestand nagegaan te worden. In deze laatste ontwerptoestand, wordt het accidenteel verlies van de FRP wapening verondersteld, wat overeenstemt met een onversterkte constructie onderworpen aan de belastingen van de versterkte constructie. Deze ontwerptoestand gaat de bezwijkgrens na indien geen of gereduceerde veiligheidscoëfficiënten toegepast worden.

7.3 Opvatting van het ontwerp met betrekking tot veiligheid

7.3.1 Bezwijkgrenstoestand

In de bezwijkgrenstoestand (BGT), is de modellering gerelateerd tot de diverse breukvormen die kunnen optreden. Brosse breukvormen (zoals dwarskracht) dienen niet bepalend te zijn voor het ontwerp. In verband hiermee, dient er ook voor gezorgd te worden dat de inwendige staalwapening in de BGT voldoende vloeit (paragraaf 7.3.3). In dit geval bezwijkt de versterkte constructie, ondanks de brosse aard van verbrijzeling van beton, FRP breuk of onthechting, op een wijze die samengaat met waarschuwende plastische vervormingen.

Hieruit volgt dat de bepalende bezwijkmode in het ontwerp van elementen onderworpen aan buiging, hetzij vloeien van de wapening is gevolgd door verbrijzeling van het beton (zone B in Fig. S-30), hetzij vloeien van de wapening is gevolgd door FRP breuk of onthechting (zone A in Fig. S-30). In Fig. S-30, is ε_o de initiële rek in de uiterste getrokken vezel voorafgaand aan de versterking, $\varepsilon_{f,min}$ de minimum FRP rek nodig in verband met de ductiliteit (paragraaf 7.3.3) en $\varepsilon_{fu,c}$ de uiterste FRP rek in de kritieke doorsnede. Deze rek is, in het geval van FRP breuk, gelijk aan de rekenwaarde van de FRP breukrek ε_{fud}. In het geval van FRP onthechting, wordt een lagere waarde van $\varepsilon_{fu,c}$ bekomen, die correspondeert met onthechting op een mogelijk ander plaats dan de kritieke doorsnede voor het nazicht van het draagvermogen in buiging. Onthechting kan enkel toegelaten worden voor $\varepsilon_{fu,c} \geq \varepsilon_{f,min}$.

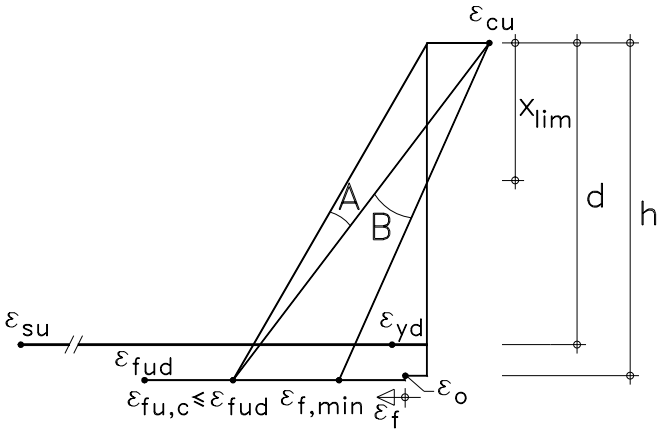

Fig. S-30 *Vervormingstoestand in de BGT van versterkte buigingselementen*

7.3.2 Accidentele ontwerptoestand

Het wordt soms gesuggereerd dat de FRP wapening enkel als zogenaamde secundaire wapening moet dienen, zodat bij accidenteel verlies van de FRP wapening de constructie niet (volledig) bezwijkt. Indien aan deze accidentele ontwerptoestand wordt voldaan is de veiligheid het grootst en dient veelal minder aandacht besteed te worden aan de bijzondere ontwerpaspecten zoals brand en impact. Dit betekent echter ook dat de maximale versterkingsfactor gelimiteerd wordt, terwijl reeds voldoende aangetoond werd dat FRP ook als volwaardige wapening kan aangewend worden. In dit geval dient echter extra aandacht besteed te worden aan de bijzondere ontwerpaspecten.

7.3.3 Ductiliteit

Het bezwijken van de versterkte constructie dient voorafgegaan te worden door voldoende grote vervorming, welke bekomen worden na het vloeien van de inwendige wapening. Op basis van Eurocode 2 [19, item 2.5.3.4.2 (5)], kunnen de vereisten weergegeven in Tabel S-17 bekomen worden. In deze tabel is $\delta_{1/r}$ de krommingsindex, gedefinieerd als de kromming bij bezwijken gedeeld door de kromming waarbij het betonstaal begint te vloeien.

Tabel S-17 *Ductiliteitsvereisten*

Betonklasse	**ξ = x/d** [-]	**$\varepsilon_{f,min}$** [mm/m]	**$\varepsilon_{s,min}$** [mm/m]	**$\delta_{1/r,min}$** [-]
C35/45 of lager	≤ 0.45	$5.0 - \varepsilon_o$	4.3	$\approx 0.0043/\varepsilon_{yk}$
Hoger dan C35/45	≤ 0.35	$7.5 - \varepsilon_o$	6.5	$\approx 0.0065/\varepsilon_{yk}$

7.4 Versterking in buiging

7.4.1 Initiële toestand

Uitgaande van een klassieke elastische berekening en het gebruiksmoment M_o (geen veiligheidscoëfficiënten op de belastingen) dat aangrijpt voorafgaand aan de versterking, kan

de initiële vervormingstoestand van het te versterken element eenvoudig bepaald worden. Indien M_o kleiner is dan het scheurmoment, is de invloed van de initiële toestand verwaarloosbaar.

7.4.2 Nazicht in de BGT bij volledige composietwerking

Het gedrag van het versterkt element in de BGT kan, indien volledige composietwerking tussen de FRP wapening en de betonconstructie verondersteld wordt, klassiek berekend worden op basis van beschouwing van de evenwichtsvergelijkingen en de compatibiliteit van de vervormingen (Fig. S-31).

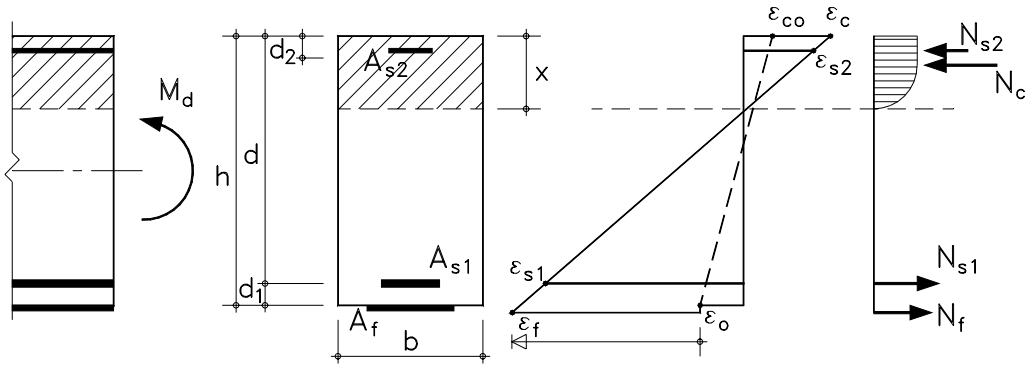

Fig. S-31 *Nazicht in de BGT voor een versterkte rechthoekige doorsnede*

7.4.3 Nazicht in de BGT van FRP onthechting

7.4.3.1 Algemeen

Indien de hechtschuifspanningen in het contactvlak tussen het beton en de FRP wapening een kritieke waarde overschrijden, dan treedt FRP onthechting op. Aangezien de sterkte van de lijmen die normaal aangewend worden, zal deze onthechtingsbreuk zich voordoen in het beton en is de kritieke schuifspanning gerelateerd tot de treksterkte van het beton.

Oorzaken van onthechting en de bijhorende bezwijkvormen kunnen als volgt beschouwd worden:

- *Lage uitvoeringskwaliteit*. De toelaatbare hechtsterkte kan in belangrijke mate afnemen door een onvoldoende kwaliteit van de uitvoering (bijvoorbeeld lage hechtsterkte door een onvoldoende oppervlakte voorbereiding, afpelwerking t.g.v. oneffenheden (Fig. S-32a), enz.). Deze onthechtingsvormen kunnen vermeden worden door een goede uitvoering en de nodige kwaliteitscontrole op de uitvoering.
- *Verankeringszone*. Startend van het vrij uiteinde dient de kracht in de FRP wapening opgebouwd te worden. Zoals aangegeven in Fig. S-32b, treden in deze verankeringszone spanningconcentraties op. Bij aanwezigheid van een dwarskrachtscheur aan het FRP-uiteinde kan een zogenaamde ‘concrete rip-off’ breuk bekomen worden (Fig. S-32c).

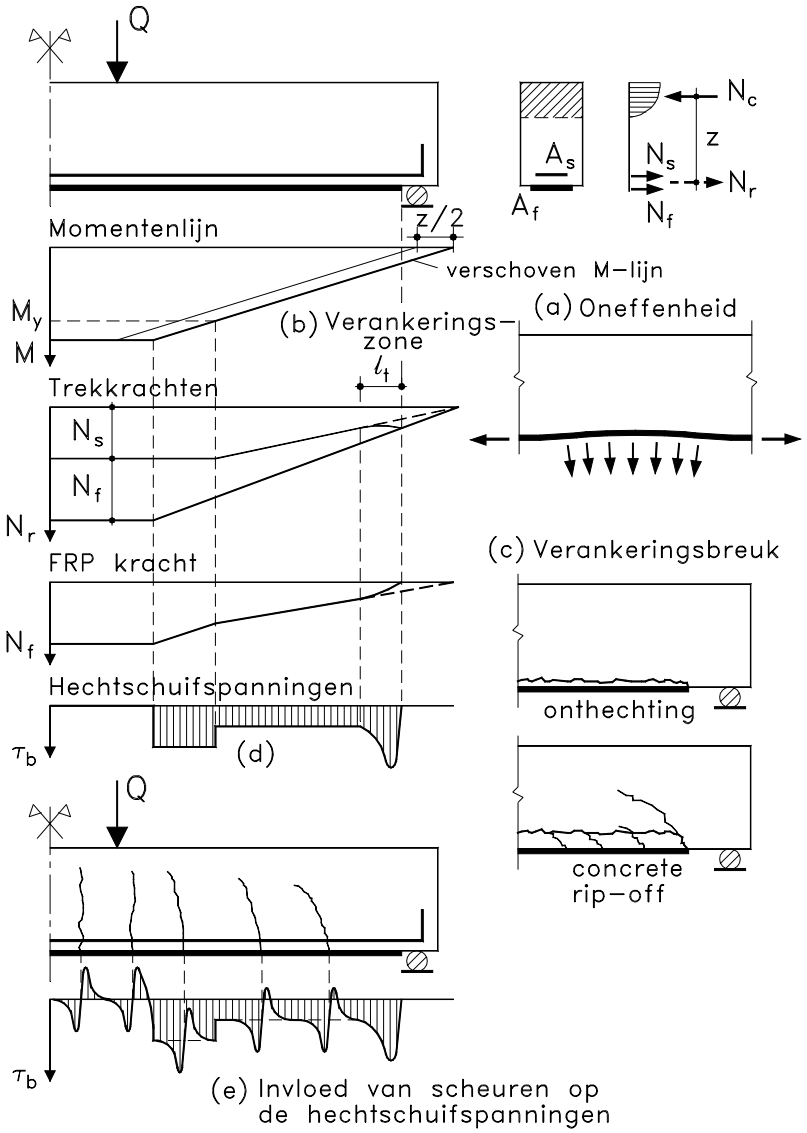

Fig. S-32 *Hechtschuifspanningen en onthechtingsbreuk*

- *Krachtsoverdracht*. T.g.v. de composietwerking tussen het beton en de FRP wapening treden er hechtspanningen op in het contactvlak (Fig. S-32d). Deze zijn evenredig met de variatie van de FRP kracht langsheen zijn lengte.
- *Scheuroverbrugging.* Ter plaatse van scheuren ontstaan eveneens extra hechtspanningen (Fig. S-32e). Onderscheid kan gemaakt worden tussen buig- en dwarskrachtscheuren. In het laatste geval wordt ook een vertikale verplaatsing van de scheurvlakken bekomen, welke een rechtstreekse en zeer nadelige afpelwerking met zich meebrengt.

7.4.3.2 Verankeringslengte

Langsheen de lengte van de balk of de plaat, dient de weerstandbiedende trekkracht in de wapeningen kleiner te zijn dan de aangrijpende trekkracht. Uitgaande hiervan kan nagegaan worden op welke plaats de FRP wapening theoretisch geschorst kan worden en welke de bijhorende kracht N_{fa} in de FRP wapening is. Deze wordt dan verankerd over een lengte ℓ_t

nodig om de kracht N_{fa} af te bouwen. De maximale kracht $N_{fa,max}$ die kan verankerd worden en de bijhorende verankeringslengte $\ell_{t,max}$, worden gevonden uit modellen zoals bijvoorbeeld het model in [30]. Het verband tussen N_{fa} en ℓ_t, in relatie tot deze maximale waarden, wordt parabolisch verondersteld:

$$N_{fa} = N_{fa,max} \frac{\ell_t}{\ell_{t,max}} \left(2 - \frac{\ell_t}{\ell_{t,max}} \right) \tag{S-21}$$

Bovendien dient nagegaan te worden dat geen 'concrete rip-off' verankeringsbreuk bekomen wordt. Dit nazicht kan gebeuren volgens [40]

7.4.3.3 Scheuroverbrugging

De invloed van scheuren op het aanhechtingsgedrag is schematisch weergegeven in Fig. S-33. Bij buigingsscheuren ontstaat bij overschrijding van de hechtsterkte een lokale onthechting, die een herverdeling van de rek in de wapening met zich meebrengt (Fig. S-33a). Deze heeft een positieve invloed op de hechtspanningen in het contactvlak zodat geen progressieve onthechtingsbreuk bekomen wordt. In het geval van dwarskrachtscheuren of buigscheuren in zones met belangrijke dwarskrachtwerkingen, ontstaat er zowel een horizontale als een vertikale verplaatsing van de scheurvlakken. De vertikale verplaatsing veroorzaakt een rechtstreekse afpelwerking (Fig. S-33b) en is zeer nadelig. Het nazicht van dit breukfenomeen kan gebeuren overeenkomstig het model besproken in paragraaf 3.3.1.

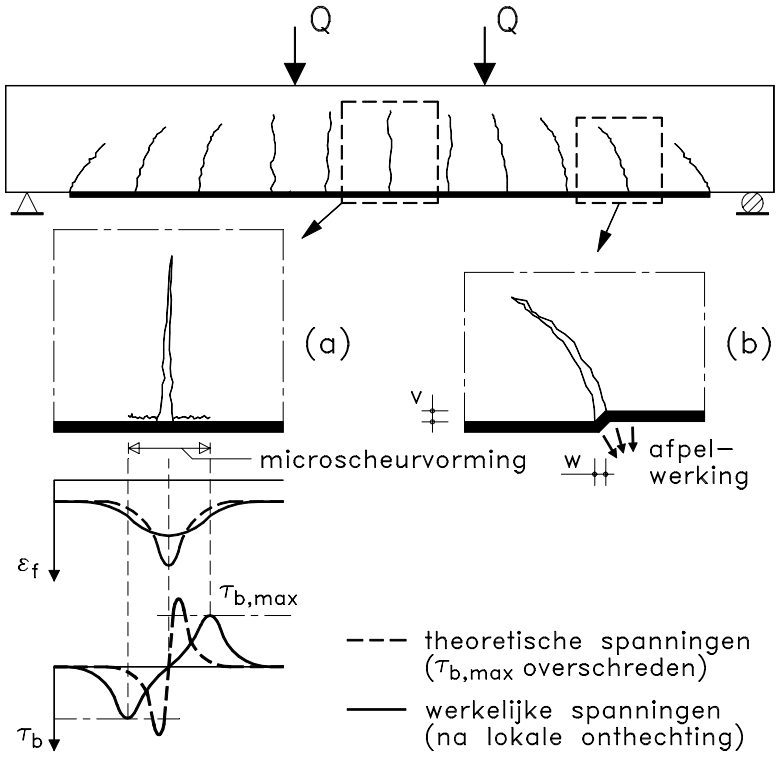

Fig. S-33 *Scheuroverbrugging*

7.4.4 Nazicht van de gebruikgrenstoestand (GGT)

De redenen om een constructie te versterken kunnen sterk verschillen, doch zijn gerelateerd aan sterkte- of gebruikscriteria. In het laatste geval zal de gebruikgrenstoestand (GGT) bepalend zijn voor het ontwerp. Echter, ook bij versterkingen om aan sterktecriteria te voldoen zal dikwijls blijken dat de GGT bepalend is. Dit komt o.a. omdat met een geringe hoeveelheid FRP wapening aanzienlijke versterkingsfactoren kunnen bekomen worden. De bijkomende wapeningsdoorsnede blijkt echter meestal onvoldoende om ook aan de GGT te voldoen, zeker indien FRP types gebruikt worden met een lage elasticiteitsmodulus.

Onder de gebruiksbelasting dienen de spanningen in het beton, het betonstaal en de FRP beperkt te worden (o.a. om kruipvervormingen tegen te gaan). Aangezien onder gebruikslast de rekken in de FRP wapening relatief klein zijn, is het FRP spanningsnazicht weinig kritiek. Dit geldt echter niet voor het beton en het betonstaal. Immers, door het toevoegen van de FRP wapening en gezien steeds een krachtenevenwicht geldt, nemen de spanningen in het beton en mogelijk ook in het betonstaal toe. Voor deze materialen gelden de spanningsbeperkingen opgegeven in [19].

Om de inwendige wapening te beschermen en om lokale onthechting t.p.v. scheuren te vermijden dienen de scheuropeningen in de GGT beperkt te worden. Dit nazicht kan gebeuren overeenkomstig het model besproken in paragrafen 3.3.4 en 5. Echter, voor elementen met uitwendige FRP wapening wordt een dicht scheurpatroon bekomen van fijne scheuren, zodat dit nazicht meestal niet kritiek is.

Doorbuigingen in de GGT dienen eveneens beperkt te zijn [19]. Deze kunnen nagerekend worden aan de hand van klassieke modellen die het tension stiffening effect in rekening brengen (zie paragrafen 3.3.3 en 5).

7.4.5 Parameterstudie en berekeningsprogramma

Om een beter inzicht te bekomen in de diverse ontwerpaspecten werd een parameterstudie uitgevoerd. Hieruit bleek dat de GGT veelal bepalend is voor het ontwerp, evenals onthechting ter plaatse van scheuren met een vertikale verplaatsing van de scheurvlakken. Op basis van deze inzichten werd een meest aangewezen verloop voor de ontwerp- en verificatieberekeningen opgesteld evenals een berekeningsprogramma.

7.5 Versterking in dwarskracht

Om een brosse dwarskrachtbreuk te vermijden van gewapend betonelementen met een gebrekkige dwarskrachtsterkte, kan uitwendig gelijmde FRP dwarskrachtwapening aangebracht worden. Hierbij kunnen diverse versterkingsconfiguraties gehanteerd worden (Fig. S-34). De grootste efficiëntie wordt bekomen indien de FRP wapening wordt aangebracht onder 45° en indien ze goed verankerd is. Uit praktisch oogpunt wordt de FRP dwarskrachtwapening echter dikwijls loodrecht op de langsas van de balk geplaatst en niet steeds verankerd.

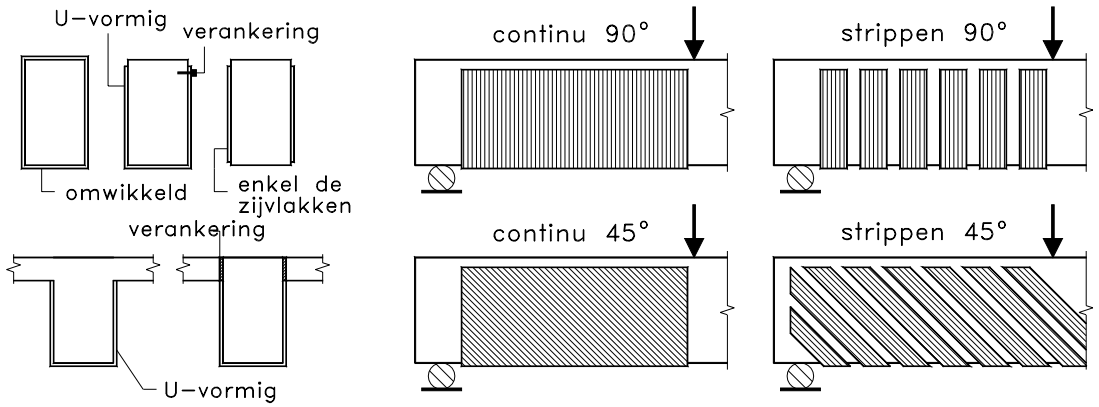

Fig. S-34 *Dwarskrachtversterking van balken*

Het nazicht van de dwarskrachtsterkte in de BGT gebeurt volgens de veralgemeende vakwerkanalogie zoals uiteengezet in paragraaf 4.3.1. De effectieve FRP breukrek die in rekening gebracht wordt, is gegeven in paragraaf 4.3.2.

Om de eventuele dwarskrachtscheuropeningen te verifiëren in de GGT (deze dienen o.a. beperkt te worden om locale FRP onthechting in de GGT te vermijden) werd een berekeningsmodel voorgesteld.

7.6 Kolommen omwikkeld met FRP

7.6.1 Nazicht van de bezwijkgrenstoestand (BGT)

7.6.1.1 Druksterkte van het omwikkeld beton

Zoals besproken in paragraaf 6.3.1, kan voor beton omwikkeld met FRP niet uitgegaan worden van de klassieke modellen voor beton ingeregen met staalwapening. Deze veronderstellen immers een constante steundruk van de omwikkelingswapening hetgeen, gezien het lineair elastisch gedrag van FRP, niet het geval is. Uitgaande van een vergelijkende studie, bleek dat het spanning-vervorming gedrag van beton omwikkeld met FRP op een goede wijze kan voorspeld worden d.m.v. het model beschreven in [34]. Dit iteratief model vergt een enigszins omslachtige berekening.

Echter, voor het praktisch ontwerp is het meestal voldoende om enkel de rekenwaarde f_{ccd} van het omwikkeld beton te kennen. Deze kan bepaald worden aan de hand van enkele eenvoudige betrekkingen die bekomen werden (zoals schematisch aangeduid in Fig. S-35) uit het voornoemd model. Hierbij dien uitgegaan te worden van de rekenwaarde van de maximale laterale steundruk $\sigma_{\ell ud}$.

7.6.1.2 Maximale steundruk

Voor cirkelvormige kolommen wordt de rekenwaarde van de maximale laterale steundruk $\sigma_{\ell ud}$ bekomen als (Fig. S-36):

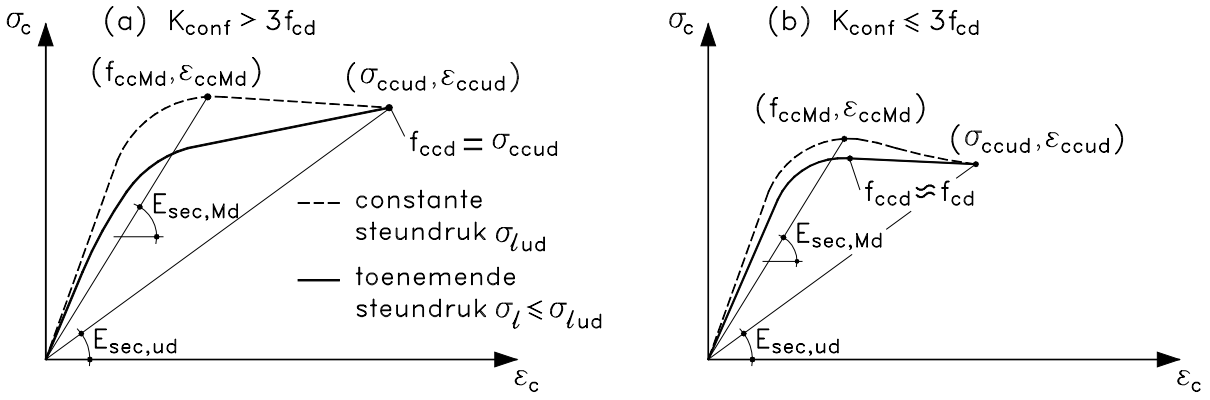

Fig. S-35 *Druksterkte van het omwikkeld beton in de BGT*

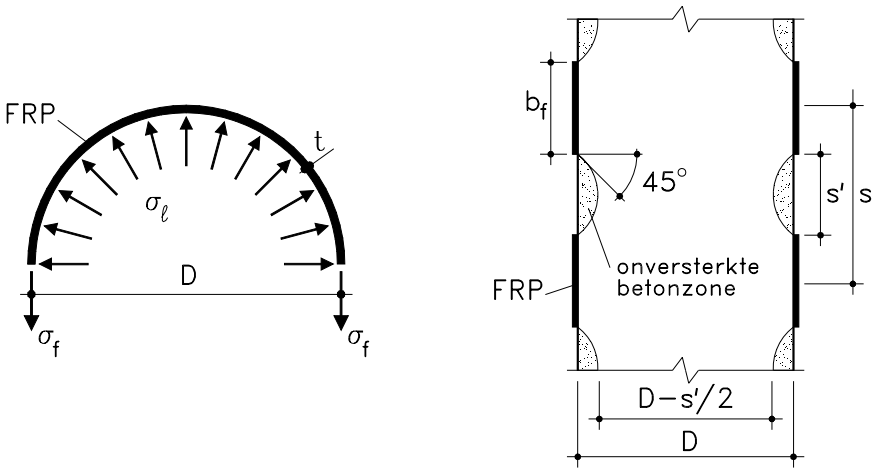

Fig. S-36 *Laterale steundruk*

$$\sigma_{\ell ud} = K_{conf}\frac{\eta_e f_{fd}}{E_f} \quad \text{met} \quad K_{conf} = \frac{1}{2}\rho_f k_e E_f \tag{S-22}$$

waarin ρ_f de volumetrische wapeningsverhouding is van de FRP omwikkelingswapening, gedefinieerd als:

$$\rho_f = \frac{4 b_f t}{D s} \tag{S-23}$$

en met $k_e = k_{e1}k_{e2}$ een efficiëntiefactor voor de invloed van deels omwikkelen (k_{e1}) en de oriëntatie van de vezels (k_{e2}):

$$k_{e1} = \frac{\left(1-\frac{s'}{2D}\right)^2}{1-\rho_{sg}} \quad \text{en} \quad k_{e2} = \frac{1}{1+\left(\frac{p}{\pi D}\right)^2} \tag{S-24}$$

met s, s' en D zoals aangegeven in Fig. S-36, p de spoed van de helicoïdaalvormige omwikkeling ($p = \pi D tg(\alpha_f)$, α_f de hoek van de vezelrichting t.o.v. de horizontale) en ρ_{sg} de hoeveelheid langswapening t.o.v. de globale kolomdoorsnede. De reductiefactor η_e wordt gegeven door de betrekking bekomen in paragraaf 6.3.4.

Analoog zoals voor cirkelvormige kolomdoorsneden, kunnen eveneens betrekkingen vooropgesteld worden voor de rekenwaarde van de maximale laterale steundruk voor kolommen met een rechthoekige of vierkante doorsnede. Een efficiëntiefactor k_{e3} op basis van de afrondingsstraal en de zijdelingse kolomafmetingen wordt hierbij in rekening gebracht.

7.6.1.3 Verankering

Er dient in de detaillering erop gelet te worden dat de omwikkelingswapening voldoende verankerd is, door het voorzien van de nodige overlappingslengte. Waarden hiervoor worden bekomen uit trekproeven op een overlappingsnaad.

7.6.2 Nazicht van de gebruikgrenstoestand (GGT)

Aangezien de FRP omwikkelingswapening slechts ten volle begint te werken eens de sterkte van het niet omwikkeld beton overschreden is (en de laterale uitzetting van het beton sterk toeneemt), zijn de FRP spanningen in de GGT bij passieve (niet-voorgespannen) omwikkelingswapening klein. Het nazicht van deze spanningen in de GGT is dan ook niet kritiek.

7.7 Bijzondere aspecten van het ontwerp

Bijzondere ontwerpaspecten zoals wisselende belastingen, extra hechtspanningen t.g.v. belemmerde temperatuursuitzettingen, impact, brand, vandalisme en specifieke duurzaamheidsaspecten kunnen relevant zijn. Deze aspecten zijn sterk afhankelijk van de specifieke situatie en de aard van de constructie en beïnvloeden zowel het ontwerp als de praktische uitvoering (detaillering). Opgemerkt kan worden dat brand en impact kunnen beschouwd worden als een accidentele ontwerptoestand, dan wel als een bijzonder ontwerpaspect. Het is enkel in het laatste geval dat de weerstand van de uitwendig gelijmde wapening bij impact of brand expliciet in rekening gebracht wordt.

8 Besluiten

Het versterken van gewapend betonelementen is van groot belang. Het gebruik hiervoor van uitwendig gelijmde vezelcomposietwapening (FRP EBR) is efficiënt en economisch aantrekkelijk, vanwege de flexibiliteit en eenvoud van deze versterkingstechniek. Commerciële toepassingen op basis van deze techniek nemen wereldwijd exponentieel toe. Er is dan ook een grote vraag naar ontwerprichtlijnen voor betonconstructies versterkt met FRP EBR.

In het kader van dit doctoraatsonderzoek werden, op basis van experimenteel en analytisch onderzoek, diverse aspecten van het structureel gedrag van gewapend betonelementen versterkt in buiging en dwarskracht en van axiaal belaste kolommen omwikkeld met FRP bestudeerd. Op basis hiervan werden bovendien concrete ontwerprichtlijnen geformuleerd.

Op basis van het uitgevoerd onderzoek kan besloten worden dat de versterking van betonelementen met uitwendig gelijmde vezelcomposietwapening een efficiënte techniek is om de buigings- en dwarskrachtcapaciteit van gewapend betonelementen te verhogen, evenals de draagkracht van axiaal belaste kolommen omwikkeld met FRP. Er werd aangetoond dat het versterkend effect zowel de bezwijktoestand als de gebruikstoestand gunstig beïnvloedt.

Uitgaande van de analytische verificaties, blijkt dat het constructief gedrag van de versterkte betonelementen op een goede wijze kan voorspeld worden. In het kader hiervan, werden diverse modellen geëvalueerd en werden berekeningsmodellen vooropgesteld.

Aan de hand van de experimentele en analytische studies werden ontwerprichtlijnen geformuleerd voor gewapend betonbalken versterkt in buiging en dwarskracht en voor het omwikkelen van axiaal belaste kolommen. Deze richtlijnen betreffen het verloop en de opvatting van het ontwerp, de procedures en modellen voor het ontwerp en enkele bijzondere ontwerpaspecten. Vergeleken met het ontwerp van nieuwe constructies, is het ontwerp van betonelementen versterkt met uitwendig gelijmde wapening meer gecompliceerd.

Om een beter inzicht te bekomen in de diverse ontwerpaspecten werd een parameterstudie uitgevoerd en werd een berekeningsprogramma opgesteld.

9 Referenties

1. ACI (1999), “FRP Around the World”, Concrete International, American Concrete Institute, Vol. 21, No. 10, 76 pp.
2. Matthys S, Taerwe L. (2000), “Use of advanced composites in concrete construction”, Proc. International Conference on Technology Watch and Innovation in the Construction Industry, Brussels, Belgium, pp. 177-184.
3. Clarke J.L., Ed. (1993), “Alternative materials for the reinforcement and prestressing of concrete”, Chapman & Hall, London, U.K., 204 pp.
4. Nanni A., Ed. (1993), “Fibre-reinforced-plastic (FRP) reinforcement for concrete structures: properties and applications”, Developments in Civil Engineering 42, Elsevier Science, Amsterdam, The Netherlands, 450 pp.
5. Taerwe L., Ed. (1995), “Non-Metallic (FRP) Reinforcement for Concrete Structures (FRPRCS-2)”, Proceedings 2nd. Intern. Symp, Ghent, RILEM Proc. 29, E & FN Spon, London, 714 pp.
6. JCI (1997), “Non-Metallic (FRP) Reinforcement for Concrete Structures (FRPRCS-3)”, Proceedings 3rd. Intern. Symp. (2 volumes), Sapporo, Japan Concrete Institute, Tokyo, Japan, 1541 pp.
7. Dolan C.W., Rizkalla S.H., Nanni A., Eds. (1999), “Fiber Reinforced Polymer Reinforcement for Reinforced Concrete Structures (FRPRCS-4)”, Proceedings 4th. Intern. Symp., Baltimore, ACI SP-188, American Concrete Institute, Michigan, USA, 1182 pp.
8. ACI (1996), “State-of-the-Art Report on Fibre Reinforced Plastic Reinforcement for Concrete Structures”, ACI Report 440R-96, American Concrete Institute, ACI Committee 440, Detroit, Michigan, USA, 153 pp.

9. JSCE (1997), “Recommendation for design and construction of concrete structures using continuous fiber reinforcing materials”, Ed. A. Machida, Concrete Engineering Series 23, Japan Society of Civil Engineers, Committee on continuous fiber reinforcing materials, Tokyo, Japan, 325 pp.
10. fib Task Group 9.3 (2000), “FRP Reinforcement for Concrete Structures”, International Federation for Structural Concrete, Commission 9, Task Group 9.3, http://allserv.rug.ac.be/~smatthys/ fibTG9.3.
11. L’hermite R.L., Bresson J. (1967), “Béton armé par collage des armatures”, Rilem International Symposium on Synthetic Resins in Building Construction, Paris, pp. 175-203.
12. Swami R.N, Gaul R., Eds. (1996), “Repair and Strengthening of Concrete Members with Adhesive Bonded Plates”, ACI SP-165, American Concrete Institute, Michigan, 264pp.
13. Meier U., Deuring M., Meier H., Schwegler G. (1993), “FRP Bonded Sheets”, in Fiber-Reinforced-Plastic (FRP) Reinforcement for Concrete Structures: Properties and Applications, Elsevier, pp. 423-434.
14. Matthys S., Taerwe L. (1996), “Versterking van beton met hoogwaardige vezelcomposietlaminaten”, Bouwkroniek, Extra editie : Betondag 24-10-1996, pp. 55-57.
15. Depla J. (1996), “Aanwending van composietmaterialen voor de versterking en de herstelling van betonconstructies”, Afstudeerwerk, Universiteit Gent, Vakgroep Bouwkundige Constructies, Laboratorium Magnel voor Betononderzoek, 152 pp.
16. Matthys S. (1997), “Versterking van structurele betonelementen met opgelijmde vezelcomposietlaminaten”, Infrastructuur in het Leefmilieu, Departement Leefmilieu en Infrastructuur, Ministerie van de Vlaamse Gemeenschap, nr. 4/97, pp. 274-298.
17. Matthys S. (1998), “Vezelcomposietlaminaten: Uitwendige versterking van constructieve betonelementen”, Cement, 50° jaargang, nr. 2, pp. 50-58.
18. Matthys S., Taerwe L., Khalil H. (1998), “Strengthening by means of externally bonded FRP reinforcement”, Proceedings of the XIIIth. FIP Congress 1998 on Challenges for Concrete in the Next Millennium, Amsterdam, The Netherlands, Eds. D. Stoelhorst, G.P.L. den Boer, Betonvereniging, published by A.A. Balkema, Vol. 2, pp. 643-647.
19. CEN (1991), “Eurocode 2: Design of concrete structures – Part 1-1: General rules and rules for buildings”, ENV 1992-1-1, Comité Européen de Normalisation (CEN), Brussels, Belgium, 263 pp.
20. Deuring M. (1993), “Verstärken von Stahlbeton mit gespannten Faserverbund-werkstoffen”, EMPA Bericht, No 224, Swiss Federal Laboratories for Materials Testing and Research, Dübendorf, Switzerland, 279 pp.
21. Taerwe L., Khalil H., Matthys S. (1997), “Behaviour of RC Beams Strengthened in shear by external CFRP sheets”, Proceedings 3rd. Int. Symp. on Non-Metallic (FRP) Reinforcement for Concrete Structures, Japan Concrete Institute, Sapporo, Japan, Vol. 2, pp. 559-566.
22. Triantafillou T.C. (1997), “Shear strengthening of concrete members using composites”, Proceedings 3rd. Int. Symp. on Non-Metallic (FRP) Reinforcement for Concrete Structures, Japan Concrete Institute, Sapporo, Japan, Vol. 1, pp. 523-530.

23. Triantafillou T.C. (1998), “Shear strengthening of Reinforced Concrete Beams Using Epoxy-Bonded FRP Composites”, ACI Structural Journal, Vol. 95, No. 2, March-April 1998, pp. 107-115.
24. Khalifa A., Gold W.J., Nanni A., Aziz A. (1998), “Contribution of Externally Bonded FRP to Shear Capacity of RC Flexural Members”, ASCE Journal of Composites for Construction, Vol. 2, No. 4, November 1998, pp. 195-201.
25. De Meyer P. (1998), “Studie van de aanhechting en de krachtswerking van op beton gelijmde vezelcomposietlaminaten”, Afstudeerwerk, Universiteit Gent, Vakgroep Bouwkundige Constructies, Laboratorium Magnel voor Betononderzoek, 184 pp.
26. Matthys S., Taerwe L., De Meyer P. (1999), “Effect of externally bonded fibre reinforced polymers on the tension stiffening behaviour of concrete members”, Proceedings 2nd. International Symposium on Adhesion Between Polymers and Concrete (ISAP'99), Dresden, Germany, pp. 363-374.
27. Lambotte H., Taerwe L. (1990), “Deflection and Cracking of High-Strength Concrete Beams and Slabs”, Proceedings of the High-Strength Concrete Second International Symposium, Ed. W.T. Hester, ACI SP-121, American Concrete Institute, Detroit, U.S.A, pp. 109-128.
28. CEB (1993), “CEB-FIP Model Code 1990, Design Code”, Comité Euro-International du Béton, Lausanne, Switzerland, Thomas Telford, 437 pp.
29. Rostásy F.S., Holzenkämpfer P., Hankers Ch. (1996), “Geklebte Bewehrung für die Verstärkung von Betonbauteilen”, Betonkalender 1996, Vol. II, pp. 547-576.
30. Holzenkämpfer P. (1994), “Ingenieurmodelle des Verbunds geklebter Bewehrung für Betonbauteile”, Doctoral thesis, Vol. 108, , Technical University Braunschweig, Germany, 214 pp.
31. Matthys S (1997), “Invloed van het inrijgen van gewapend betonkolommen met vezelcomposietlaminaten op het bezwijkgedrag”, Proceedings 4° Nationaal Congres over Theoretische en Toegepaste Mechanica, Leuven, pp. 445-448.
32. Audenaert K. (1999), “Inrijgen van betonkolommen met vezelcomposietlaminaten”, Afstudeerwerk, Universiteit Gent, Vakgroep Bouwkundige Constructies, Laboratorium Magnel voor Betononderzoek, 262 pp.
33. Matthys S., Taerwe L., Audenaert K. (1999), “Tests on axially loaded concrete columns confined by FRP sheet wrapping”, Proceedings 4th. Int. Symp. on FRP for Reinforced Concrete Structures (FRPRCS-4), Baltimore, USA, Eds. C.W. Dolan, S.H. Rizkalla, A. Nanni, ACI SP-188, pp. 217-228.
34. Spoelstra M.R., Monti G. (1999), “FRP-Confined Concrete Model”, ASCE, Journal of Composites for Construction, Vol. 3, No. 3, pp. 143-150.
35. Toutanji H. A. (1999), “Stress-Strain Characteristics of Concrete Columns Externally Confined with Advanced Fiber Composite Sheets”, ACI Materials Journal, Vol. 96, No. 3, pp. 397-404.
36. Samaan M., Mirmiran A., Shahawy M. (1999), “Model of Concrete Confined by Fiber Composites”, ASCE Journal of Structural Engineering, Vol. 124, No. 9, pp. 1025-1031.

37. Matthys S. (1997), “Versterking van structurele betonelementen met opgelijmde vezelcomposietlaminaten”, Proceedings studiedag over ‘Versterking van constructies met gekleefde composietlaminaten’, Belgische Betongroepering, Brussel, 37 pp.
38. Taerwe L., Matthys S. (1999), “Some aspects of the structural behaviour of RC beams strengthened with FRP”, in ‘Construction Materials - Theory and Applications’, Commemorative volume in honour of Prof. Reinhardt, ibidem-Verlag, Stuttgart, Germany, pp. 563-572.
39. S. Matthys, L. Taerwe, H. Blontrock (2000), “Strengthening of Concrete Structures with Externally Bonded FRP Reinforcement”, Proceedings 3th. Int. Conf. on Advanced Composite Materials in Bridges and Structures, Eds. J. Humar, A.G. Razaqpur, The Canadian Society of Civil Engineers, Montréal, Canada, pp. 497-504.
40. Jansze W. (1997), “Strengthening of Reinforced Concrete Members in Bending by Externally Bonded Steel Plates – Design for Beam Shear and Plate Anchorage”, Doctoral Thesis, Delft University of Technology, The Netherlands, pp. 205.

Chapter 1
INTRODUCTION

This chapter gives an introduction to fibre reinforced polymer (FRP) materials as structural reinforcement for concrete and more specifically as externally bonded reinforcement to strengthen existing structures. Briefly, the use of FRP in concrete construction, its history, benefits and some particular aspects of using this novel reinforcing material are mentioned. Repair and strengthening with externally bonded FRP reinforcement (FRP EBR) is discussed, among which the advantages and disadvantages of this technique. The problem statement and consequently the aim and the outline of this thesis are presented.

1 Advanced composites as structural reinforcement

Even if well designed, constructed and maintained, the service life of a concrete structure (which equals 50 years or more) is often shorter than planned for. This is due to durability problems which may occur, such as steel corrosion of reinforced concrete elements in an aggressive environment. Also, this may be due to a change in the use and function of the structure, originally not foreseen. Hence, there is a considerable interest in new reinforcing materials which can be applied as non-metallic reinforcement (non-susceptible to classical types of corrosion) for building more durable concrete members or which can be used as a means for repair and strengthening of existing structures. With this respect, advanced composites or fibre reinforced polymers as structural reinforcement gain more and more interest in construction practice worldwide [1-4]. As a result and due to the continuing research efforts, strongly linked to engineering practice, FRP reinforcement can be regarded today as a viable alternative to classical reinforcement, offering many potentials [1-6].

1.1 Fibre reinforced polymers

With the development of fibres with high strength and stiffness and low density in the 1940's, and originally used within the space and aircraft industry, fibre reinforced polymers have become an important material group in several sectors of the industry, among which concrete construction [5,6]. The FRP (Fibre Reinforced Polymer) materials consist of a high number of small, continuous, directionalized, non-metallic fibres with advanced characteristics, embedded in a polymer matrix. Used as structural reinforcement for concrete, FRP elements are mostly based on aramid (AFRP), carbon (CFRP) or glass (GFRP) fibres in combination with a thermoset resin such as epoxy, vinylester or unsaturated polyester. Fibre volume fractions up to about 60 to 70 % are common. As they occupy the largest volume fraction and share the major portion of the acting load, fibres are the principal stress bearing constituent, while the resin transfers stresses among fibres and protects them. An enlarged view of a carbon fibre reinforced polymer is shown in Fig. 1-1.

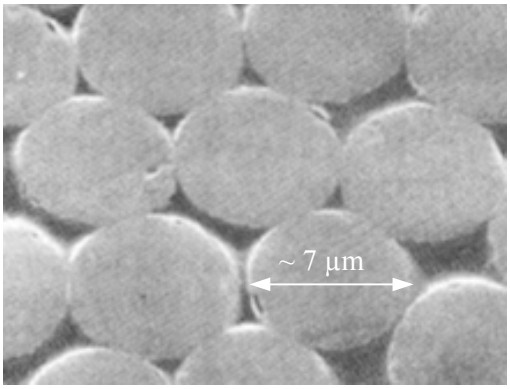

Fig. 1-1 *Enlarged view of a CFRP element*

1.2 FRP reinforcement

As structural reinforcement for concrete members, FRP elements are made available in the form of bars, tendons, ropes, grids, strips, sheets or fabrics, as illustrated in Fig. 1-2. For new structures, they are used to reinforce and prestress concrete elements. In the repair sector, they are used to strengthen existing structures e.g. by means of external post-tensioning, externally bonded reinforcement or in combination with shotcrete. Also, they are used as stay cables, ground anchors, structural shapes, etc. [1-6].

FRP reinforcement forms a group of products rather than being one reinforcement type, as its characteristics depend on fibre and resin type and properties, volume fractions, production parameters, shape and surface texture. The stress-strain behaviour of some FRP elements, compared with reinforcing and prestressing steel is shown in Fig. 1-3. Similar to the behaviour of the fibres and unlike steel, FRP do not experience any yield but rather a linear elastic behaviour nearly up to failure. The modulus of elasticity ranges between about 50 and 250 GPa and is for most FRP elements lower than steel. At the other hand, FRP's are characterized by a high tensile strength which is close or higher than that of prestressing steel. Being an anisotropic material, the mechanical properties of unidirectional (linear) FRP elements in transverse direction are inferior to those parallel to the fibres. More details on the characteristics of FRP materials are given in Chapter 2.

The application of FRP reinforcement is, due to the often high material cost, related to the utilisation of the specific material properties of FRP. Therefore, it has to be used as a specific alternative for common steel reinforcement, rather than a general substitute for it. Compared to steel, the general advantages of FRP reinforcement are:

- High axial strength.
- Low weight
- Excellent corrosion resistance and non susceptibility to a wide range of aggressive media.
- Electromagnetic neutrality.
- Excellent fatigue characteristics for CFRP and AFRP.
- Low axial coefficient of thermal expansion.

Disadvantages related to the use of structural FRP reinforcement include:

- High material cost for most FRP materials.
- Relatively low failure strain.
- High ratio of axial-to-transverse strength.
- Relatively low long-term to short-term static strength for GFRP and AFRP.
- Specific durability problems may occur for GFRP and AFRP (UV light, alkalis, etc).

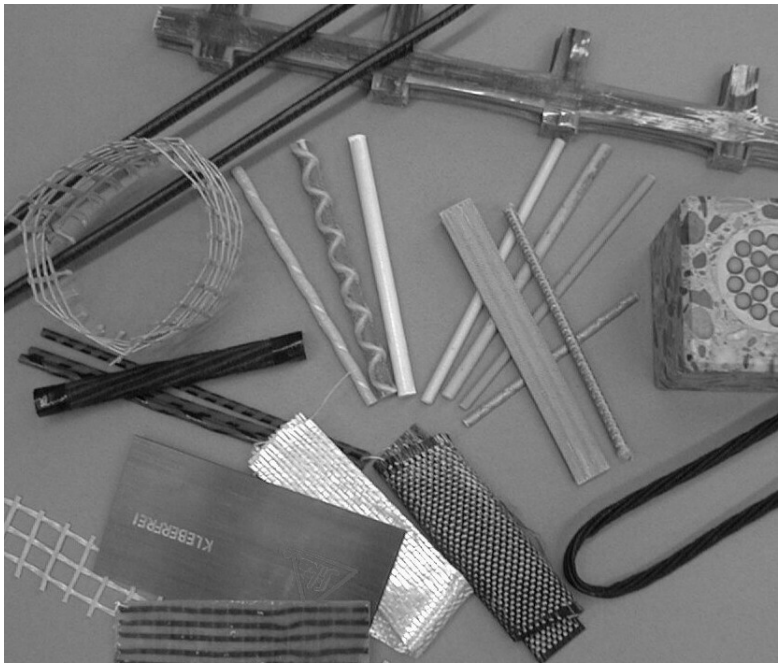

Fig. 1-2 *Examples of various FRP reinforcing elements*

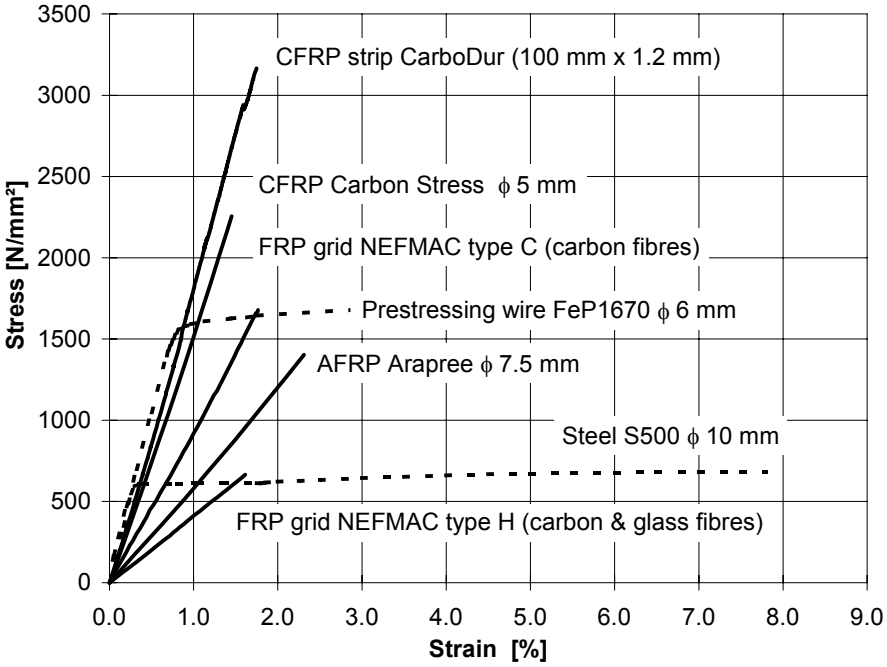

Fig. 1-3 *Stress-strain behaviour of some FRP elements compared to steel*

1.3 FRP as structural reinforcement for concrete construction

1.3.1 History and benefits of FRP reinforcement

In the 1970's, research and development of FRP reinforcement started in Europe, as well as in North-America and Japan. Commercial products became gradually available since the late 70's, followed by the first practical applications in the early 80's (demonstration projects). Since then, the use of FRP reinforcement gained more and more interest, as demonstrated by numerous research projects, practical applications and demonstration projects [1-13]. Especially, the use of FRP as externally bonded reinforcement to strengthen existing structures has become commercially of considerable importance, with each year hundreds of projects executed worldwide.

Given the advantages of FRP (Section 1.2), the use of FRP reinforcement is beneficial with respect to the following issues:

- The sustainability of concrete structures, which has become of major concern over the last decades as social and economical necessities demand a reliable and durable infrastructure. Yet many durability problems occur, related to the numerous ageing structures (expanded construction activities after World War II), the more aggressive environment (e.g. buildings in marine and industrial environments, road bridges subjected to de-icing salts), the slenderness of many structures (modern calculation techniques and concrete technology) and the sometimes poor quality of execution (due to high construction speed and short-term economical considerations). The use of FRP reinforcement, which is not susceptible to the classical types of corrosion, may offer a viable alternative to prevent some of the durability issues.
- The interest to incorporate more efficient construction materials and techniques, also with respect to maintenance, repair and strengthening of existing structures. The advantages of FRP and the fact that FRP products are available in a variety of forms, characteristics and shapes, provide an attractive and economical solution for structural engineering. For example, considerable efficiency and cost effectiveness are obtained in case of strengthening by means of externally bonded FRP reinforcement, due to the flexibility and the ease-of-application of this strengthening technique in addition to the advanced material characteristics provided by FRP. For new concrete structures, the efficiency and cost effectiveness of FRP (prestressing) reinforcement are mainly related to life-cycle considerations as demonstrated in Fig. 1-4 or to the utilisation of specific FRP material properties (e.g. insensitivity to electromagnetic fields).

1.3.2 Particular aspects related to the use of FRP reinforcement

In view of the above considerations, FRP as structural reinforcement is of special interest. Nevertheless, compared to steel reinforcement, the properties of FRP differ to a certain extent (e.g. see Fig. 1-3). As a result, the use of FRP reinforcement involves some particular aspects.

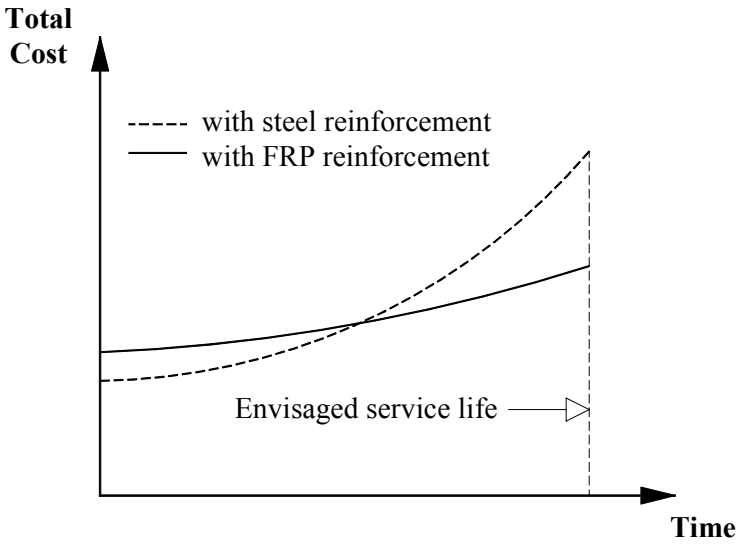

Fig. 1-4 *Life-cycle cost of a steel and FRP reinforced or prestressed structure*

1.3.2.1 Reinforced concrete

Given the high strength of FRP, relatively small cross-sectional areas are needed to reinforce concrete elements with respect to the ultimate limit state (strength considerations). On the other hand, to fulfil serviceability criteria, sufficient flexural stiffness should be available. Once cracked, the stiffness of a reinforced concrete (RC) section significantly depends on the stiffness of the reinforcement. Due to the small cross-sectional area needed for strength considerations and the generally lower modulus of elasticity of most FRP materials in comparison with steel, serviceability problems may arise when the design is based on the ultimate limit state only. This is also illustrated by the load-deflection diagrams shown in Fig. 1-5. Designing a FRP RC member with similar strength as a steel RC member (curves 1 and 2), the obtained service load of the FRP RC member is lower as a result of the lower flexural stiffness. To obtain a similar service load, the stiffness should be increased by taking a larger FRP cross-sectional area or by increasing the member depth (curve 3). In this case, the ultimate load will generally be significantly higher. Hence, the high strength of the composite is not efficiently utilised.

Another aspect concerns the linear elastic behaviour of FRP reinforcement up to failure. Although, a FRP RC member shows sufficient deformability before failure, the major part of the stored energy is elastic, as shown by the shaded area in Fig. 1-6. Hence, at ultimate load quite sudden and explosive failures may occur. Accordingly, properly designed FRP reinforced members exhibit a high safety margin in terms of deformability and ratio of ultimate to service load, while almost no ductility is obtained. For applications where there is an explicit need for ductility, specific structural measures have to be taken [14].

From these aspects, it seems that FRP reinforcement is less suitable than steel, so that its use will only be justified in specific cases, where advantages such as non-susceptibility to classical types of corrosion and insensitivity to electromagnetic fields can be fully utilised.

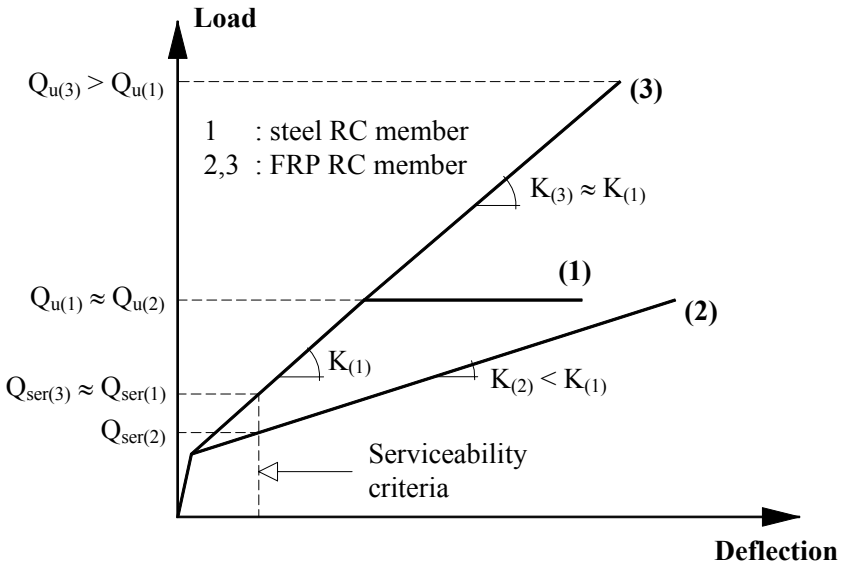

Fig. 1-5 *Steel versus FRP reinforced concrete members*

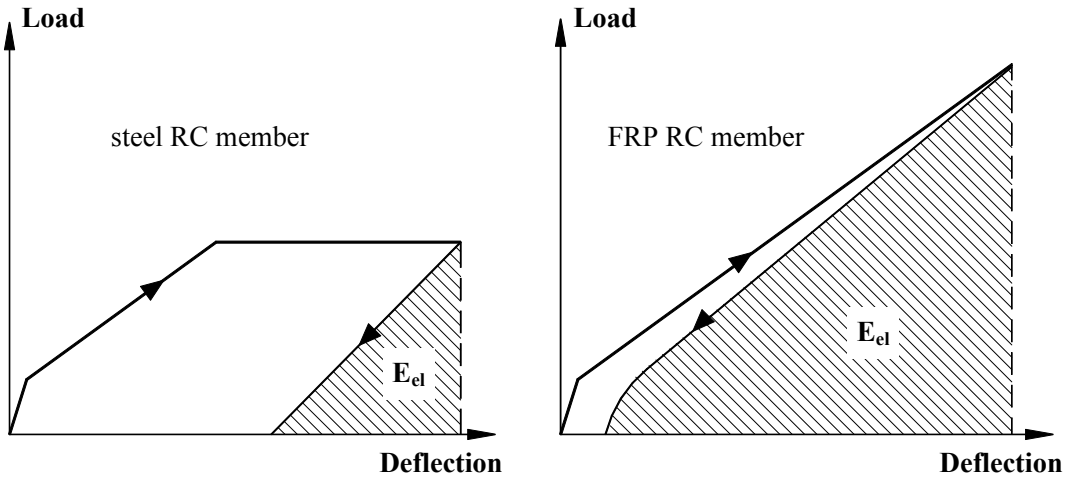

Fig. 1-6 *Elastic deformation energy of steel and FRP reinforced members*

1.3.2.2 Prestressed concrete

By prestressing, serviceability criteria can easily be satisfied and the FRP strength can be utilised in a more optimum way. Furthermore, it is noted that a low modulus of elasticity of the FRP prestressing reinforcement is beneficial in terms of long-term prestressing losses due to creep and shrinkage of the concrete. Hence, from a structural point of view, FRP is more suitable for prestressed concrete than for reinforced concrete. Nevertheless, structural measures with respect to ductility may still be needed. Also, due to relaxation and stress rupture, the initial stress level of some FRP types can be substantially lower than for prestressing steel. As the transverse strength of FRP is considerably lower than its axial strength, special anchorage devices have to be used as well.

Hence, similar to reinforced concrete (but in a lesser extent), FRP prestressing reinforcement can not be regarded as a substitute for steel tendons. Its use will mainly be related to those situations were durability and maintenance costs are of major concern.

1.3.2.3 Externally bonded FRP reinforcement

As in the case of RC members internally reinforced with FRP, the high strength of the externally bonded FRP reinforcement can not be efficiently used when serviceability criteria are governing the design. Furthermore, it should be noted that the FRP stresses, which are transferred to the concrete member through the bond interface, initiate bond shear stresses. These are limited by the concrete or adhesive shear strength. As a result, very large FRP stresses can often not be generated, unless an additional anchorage is used. Nevertheless, the use of FRP offers many advantages compared to steel plate bonding, as discussed in Section 2.3. Basically, the considerable flexibility and ease-of-application of externally bonded FRP reinforcement make this strengthening technique economical and applicable in a broader number of cases. Nevertheless, as for a lot of repair and strengthening techniques, it should be kept in mind that quality control is very important with respect to the integrity of the strengthening system.

Given the above considerations, it is clear that where the use of FRP reinforcement for new structures is limited to particular cases, its use as externally bonded reinforcement for strengthening is more general. As a result, strengthening with externally bonded FRP reinforcement is becoming well documented and a more or less standard technique in a fast way.

2 FRP as externally bonded reinforcement for strengthening

2.1 General

Each year, considerable investments in construction engineering are related to the maintenance, repair (retrofit) and strengthening (upgrading) of infrastructure. The need for repair and strengthening follows from several reasons:

- Changes in the use and the functionality of structures, such as the introduction of openings (e.g. for pipes and elevators), reallocation of rooms, increased loading and increased frequency of use.
- Damage due to mechanical actions (impact, explosions, earthquakes, vibrations from nearby constructions sites, unforeseen cutting of reinforcement, etc.) or due to environmental influences (steel corrosion, freeze-thaw action, fire, alkali-silica reaction, use of acids, etc.).
- The need to extend the service life of a structure, while minimising costs, environmental impact and disrupt in economical activity.
- More restrictive design guidelines, so that structural safety is no longer regarded to be sufficient.
- Lack of detailing, design and construction errors.

Several techniques for repair and strengthening are available [15,16], among which the use of externally bonded reinforcement (EBR). In this efficient and frequently applied method,

developed in the late 1960's, steel plates were originally used [17]. A state-of-the-art overview on steel plate bonding is given in [18]. In Belgium, pioneering work on steel plate bonding has been performed by Van Gemert [19]. Alternatively, the application of steel plates can be extended to FRP reinforcement, as the latter shows several advantages (Section 2.3). Pioneering work on the use of FRP for EBR has been performed at EMPA [20]. This research resulted in more than thousand applications in Switzerland alone. Internationally, many research projects and applications have been conducted and several FRP systems for strengthening have become commercially available. Nevertheless, design guidelines are yet scarce.

2.2 Strengthening with FRP EBR

By means of structural strengthening with externally bonded FRP reinforcement, additional reinforcement is provided to a structure to restore or increase its load bearing capacity or to fulfil certain serviceability criteria. The FRP reinforcement is fixed externally to the structure with an adhesive (mostly epoxy), although (if needed) an extra anchorage may be applied as well. An example of a FRP EBR strengthened structure is shown in Fig. 1-7.

In the case of externally bonded reinforcement, the FRP elements generally consist of either thin prefab strips and laminates, which are pre-cured, or wet lay-up sheets and fabrics, which are cured in situ. The fibres are predominantly oriented in one direction. However, FRP elements with fibres in two or more directions are also used (e.g. woven fabrics). Typical stress-strain curves of FRP and steel reinforcement for external bonding are shown in Fig. 1-8. Often CFRP is used, because of its superior material characteristics. However, products based on AFRP, GFRP or HFRP (hybrid use of fibres) also apply. More details on the different FRP EBR systems, their characteristics and the application techniques are provided in Chapter 2.

Fig. 1-7 *Strengthening with FRP EBR of the Tannberg bridge in Austria*

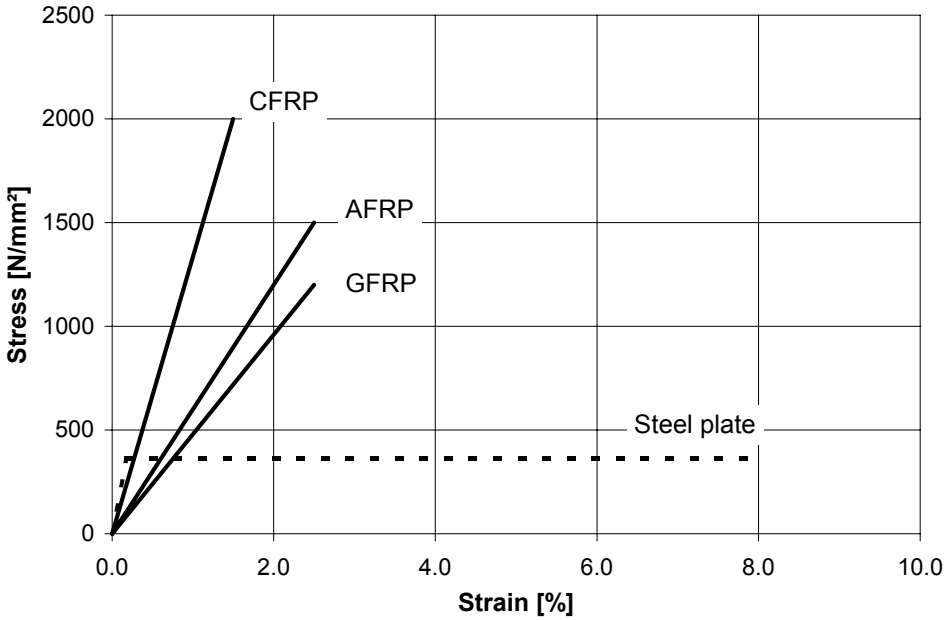

Fig. 1-8 *Stress-strain behaviour of reinforcement for external bonding*

2.3 Advantages and disadvantages of FRP EBR

The selection of a proper repair and strengthening technique is closely related to the state of the structure to be strengthened, the aimed effects, the environmental conditions, etc. Between alternatives, the final evaluation is mainly driven by the cost effectiveness, where it is not only of interest to minimise initial costs, but also the future maintenance costs. In addition, it is also of considerable importance to minimise consequential costs such as loss of production, traffic delay and disrupt during maintenance.

Given the similarity of both techniques, the advantages of FRP EBR mentioned hereafter are evaluated by comparing FRP EBR with steel plate bonding. Nevertheless, it should be noted that FRP EBR is not simply an improved form of steel plate bonding. Indeed, where the versatility of FRP EBR may result in a larger applicability of the EBR strengthening technique, steel plate bonding will remain the best solution in some case (e.g. when there is no risk for steel corrosion and the application conditions are not very labour and consequential cost driven).

Advantages of FRP EBR are given in the following list:

– Steel plates need protection against corrosion. Nevertheless, corrosion often occurs at the interface between the steel plate and the adhesive. This may result in loss of bond. FRP on the contrary exhibits excellent corrosion resistance.
– FRP elements have low weight and can be made available in continuous lengths. This makes their use very easy and more flexible (e.g. applicability in confined spaces), especially in the case of wet lay-up systems which are most versatile. Compared to that, steel plates are relatively heavy so that they are only applicable in short lengths (about 6 m). Hence, for steel plate bonding the manipulation is generally more difficult, expensive scaffolding is needed and often connections, which demand for proper detailing, have to

be executed. Connections between steel plates can not be done by in-situ welding (as this damages the bond interface) and involves expensive overlap joints. As FRP elements are very thin, joints (only rarely needed) and crossings can be easily executed.

- To assure adequate bonding, it is important that surfaces are prepared in a proper manner. For steel plates this requires grit blasting followed by careful protection until shortly before installation. In the case of FRP, surface preparation is less time consuming, as most FRP EBR systems are provided with a protective sheet which is peeled off just before application.
- Because FRP elements for EBR are much thinner than steel plates and allow for a large bond width over thickness ratio, bond interface stresses may be kept low. As a result FRP EBR can be applied in many cases without mechanical anchorage.
- FRP elements (mostly CFRP and AFRP) have an excellent fatigue behaviour.
- Given the flexibility and ease-of-application, construction periods in the case of FRP EBR will generally be smaller than for steel plate bonding. Also, the disrupt in activities close to the construction site are often less (e.g. no or light scaffolding so that traffic still can continue).
- The application of FRP EBR is, even more than for bonded steel (smaller thickness, no mechanical anchorage, etc.), aesthetically attractive. Different types of finishing and protective layers are available if needed.
- Also prestressed FRP EBR can be applied. In this way crack widths and deflections can be reduced. However, this technique is still in an experimental stage.

Disadvantages of strengthening with externally bonded FRP reinforcement are:

- Compared to steel, FRP materials cost more. CFRP for example, which is often used as EBR, can be at least 6 times more expensive than steel plates. Although the FRP material cost may still decrease in the future as these materials become more used, most FRP materials will remain more expensive than steel. Nevertheless, as the material cost normally represents a limited fraction of the total construction costs, while labour and consequential costs may be reduced significantly, FRP EBR appears very cost-effective in many cases, even without considering the advantages with respect to durability.
- The transverse strength of FRP is fairly low compared to steel. This makes FRP EBR more vulnerable to direct impact action, vandalism or determined attack. Therefore, it may sometimes be needed to provide a protective render and (additional) mechanical anchorage to the FRP EBR. On the other hand, repair of damaged areas is more easy in the case of FRP than for steel plates.
- Although FRP materials are not susceptible to the classical types of corrosion and are inert to various aggressive solutions, they may be negatively affected by some environmental conditions. For example AFRP appears to be moisture sensitive and GFRP is not very resistant against alkalis. CFRP materials are regarded to be very inert in an overall way.

3 Problem statement

As may appear from the previous sections, the use of FRP as structural reinforcement is viable and attractive, especially in the case of externally bonded reinforcement. A lot of research is conducted internationally [7-13], so that the use of FRP for concrete construction becomes more and more documented. Nevertheless, the considerable interest in FRP reinforcement will only successfully result in practical applications if the structural behaviour of concrete structures reinforced, prestressed or strengthened by FRP is sufficiently understood and if design guidance and finally code regulations are available. Initiatives to develop design guidelines have been taken in Japan, North-America and more recently also in Europe [21-23]. These initiatives tend to take some time and depend to a large extent on the research community who has to provide calculation models.

For repair and strengthening of concrete structures by means of externally bonded FRP reinforcement, the number of applications is increasing in a fast way, due to the effectiveness and ease-of-application of this technique. As a result, in this field of application, the demand for (unified) design tools and guidelines is very high, especially as design guidelines for steel plate bonding and jacketing are scarce as well. Hence, their is a considerable interest in research concerning calculation models and design criteria for FRP EBR.

4 Aim and outline of the study

4.1 Research objective and aim of the thesis

The main objective of the research project is to study the structural behaviour of reinforced concrete elements strengthened with externally bonded FRP reinforcement (so-called FRP EBR) and to investigate and develop calculation models. Related to the problem statement given in the previous section, this thesis finally aims at providing detailed design guidance concerning the use of this novel reinforcing material for the repair and strengthening of concrete structures.

4.2 Scope of the study

Although FRP EBR is applicable to structures made out of concrete, masonry, wood, steel, cast iron, etc., the study is limited to the use of fibre reinforced polymers as externally bonded reinforcement for structural concrete.

Furthermore, it should be clear that the study does not tend to cover all the different design aspects which may possibly occur when using FRP EBR in practice. Given the available time, the scope of this thesis has been restricted to those aspects which form the majority of the design problems:

- Strengthening of reinforced concrete (RC) elements (for prestressed concrete additional aspects need to be considered).
- Non-prestressed FRP elements, glued to the concrete by means of a polymer adhesive.

- Flexural and shear strengthening of RC members such as beams and slabs.
- Confinement of axially loaded concrete columns.
- Strengthening of RC tensile members.

4.3 Outline of the thesis

Subsequent to this introductory chapter, in Chapter 2 a description is given of FRP materials and their characteristics, the FRP systems available for externally bonded reinforcement and the techniques to apply them to the concrete.

The structural behaviour of concrete elements strengthened with FRP EBR is studied experimentally and analytically in Chapters 3 till 6. In Chapter 3, FRP EBR strengthening of RC beams with an insufficient flexural capacity is investigated. A similar study with respect to shear strengthening is reported in Chapter 4. Based on the conducted experiments an insight is given in the structural behaviour of the strengthened beams under different conditions (e.g. pre-cracking and strengthening under high initial load). Prediction models for the structural behaviour of RC members strengthened in flexure and shear with FRP EBR are investigated and proposed. The serviceability behaviour of the FRP EBR strengthened members is further investigated in Chapter 5, by means of experiments on strengthened tensile members. In this chapter, the tension stiffening and cracking behaviour is discussed and calculation models are provided. In Chapter 6, the structural behaviour of axially loaded concrete columns wrapped with FRP is investigated for different column shapes and strengthening configurations. The modelling of FRP confined concrete is investigated.

Based on the derived models and a literature review with respect to the models for FRP bond failure, Chapter 7 gives detailed provisions for the design of the strengthened members. In this chapter, the basis of the design, the safety concept, the design models and procedures and some special design considerations are provided for concrete members strengthened in flexure and shear, axially loaded confined columns and strengthened tensile members.

Finally, Chapter 8 deals with the concluding remarks and briefly gives an outlook on the development of the FRP EBR technique, as well as future research needs.

5 References

1. ACI (1999), “FRP Around the World”, Concrete International, American Concrete Institute, Vol. 21, No. 10, 76 pp.
2. Taerwe L., Matthys S. (1999), “FRP Reinforcement for Concrete Structures: State-of-the-Art”, Proceedings (abstracts printed, full paper on CD-Rom) 1999 IABSE Symposium on Structures for the Future - The Search for Quality, Rio de Janeiro, Brazil, pp. 158-159 (abstract) & pp. 578-585 (paper).
3. Taerwe L., Matthys S. (1999), “FRP For Concrete Construction: Activities In Europe”, ACI - Concrete International, October 1999, Vol. 21, No. 10, pp.33-36.

4. Matthys S, Taerwe L. (2000), "Use of advanced composites in concrete construction", Proc. International Conference on Technology Watch and Innovation in the Construction Industry, Brussels, Belgium, pp. 177-184.
5. Clarke J.L., Ed. (1993), "Alternative materials for the reinforcement and prestressing of concrete", Chapman & Hall, London, U.K., 204 pp.
6. Nanni A., Ed. (1993), "Fibre-reinforced-plastic (FRP) reinforcement for concrete structures: properties and applications", Developments in Civil Engineering 42, Elsevier Science, Amsterdam, The Netherlands, 450 pp.
7. Neale K.W., Labossière P., Eds. (1992), "Advanced Composite Materials in Bridges and Structures (ACMBS-1)", Proceedings 1st. Intern. Conf., Sherbrooke, Canadian Society for Civil Engineering, Montréal, Canada, 705 pp.
8. Nanni A., Dolan C.W., Eds. (1993), "Fibre-Reinforced-Plastic Reinforcement for Concrete Structures (FRPRCS-1)", Proceedings 1st. Intern. Symp., Vancouver, ACI SP-138, American Concrete Institute, Detroit, USA, 977 pp.
9. Taerwe L., Ed. (1995), "Non-Metallic (FRP) Reinforcement for Concrete Structures (FRPRCS-2)", Proceedings 2nd. Intern. Symp, Ghent, RILEM Proc. 29, E & FN Spon, London, 714 pp.
10. El-Badry M.M., Ed. (1996), "Advanced Composite Materials in Bridges and Structures (ACMBS-II)", Proceedings 2nd. Intern. Conf., Montréal, Canadian Society for Civil Engineering, Montréal, Canada, 1027 pp.
11. JCI (1997), "Non-Metallic (FRP) Reinforcement for Concrete Structures (FRPRCS-3)", Proceedings 3rd. Intern. Symp. (2 volumes), Sapporo, Japan Concrete Institute, Tokyo, Japan, 1541 pp.
12. Benmokrane B., Rahman H., Eds. (1998), "Durability of Composites for Construction (CDCC 98)", Proceedings 1st. Intern. Conf., Sherbrooke, Departement of Civil Engineering, University of Sherbrooke, Canada, 706 pp.
13. Dolan C.W., Rizkalla S.H., Nanni A., Eds. (1999), "Fiber Reinforced Polymer Reinforcement for Reinforced Concrete Structures (FRPRCS-4)", Proceedings 4th. Intern. Symp., Baltimore, ACI SP-188, American Concrete Institute, Michigan, USA, 1182 pp.
14. Naaman A.E., Jeong S.M. (1995), "Structural Ductility of Concrete Beams Prestressed with FRP Tendons", Proceedings 2nd. Intern. Symp. on Non-Metallic (FRP) Reinforcement for Concrete Structures (FRPRCS-2), Ed. Taerwe L., RILEM Proceedings 29, E & FN Spon, London, U.K., pp. 379-386.
15. FIP (1991), "Repair and strengthening of concrete structures", Fédération Internationale de la Précontrainte, FIP Guide to good practice, Thomas Telford, London, 37 pp.
16. Schäfer H.G., Ed. (1996), "Verstärken von Betonbauteilen – Sachstandbericht" (in German), Deutscher Ausschuss für Stahlbeton, Heft 467, Beuth, Berlin, 85 pp.
17. L'hermite R.L., Bresson J. (1967), "Béton armé par collage des armatures" (in French), Rilem International Symposium on Synthetic Resins in Building Construction, Paris, pp. 175-203.
18. Swami R.N, Gaul R., Eds. (1996), "Repair and Strengthening of Concrete Members with Adhesive Bonded Plates", ACI SP-165, American Concrete Institute, Michigan, 264pp.

19. Van Gemert D., Vanden Bosch M. (1982), "Dimensionering van gelijmde wapeningen bij op buiging belaste elementen" (in Dutch), Tijdschrift der Openbare Werken van België, No. 1, February 1982, pp. 7-24.
20. Meier U., Deuring M., Meier H., Schwegler G. (1993), "FRP Bonded Sheets", in Fiber-Reinforced-Plastic (FRP) Reinforcement for Concrete Structures: Properties and Applications, Elsevier, pp. 423-434.
21. ACI (1996), "State-of-the-Art Report on Fibre Reinforced Plastic Reinforcement for Concrete Structures", ACI Report 440R-96, American Concrete Institute, ACI Committee 440, Detroit, Michigan, USA, 153 pp.
22. JSCE (1997), "Recommendation for design and construction of concrete structures using continuous fiber reinforcing materials", Ed. A. Machida, Concrete Engineering Series 23, Japan Society of Civil Engineers, Committee on continuous fiber reinforcing materials, Tokyo, Japan, 325 pp.
23. fib Task Group 9.3 (2000), "FRP Reinforcement for Concrete Structures", International Federation for Structural Concrete, Commission 9, Task Group 9.3, http://allserv.rug.ac.be/~smatthys/ fibTG9.3.

Chapter 2
MATERIAL CHARACTERISTICS, FRP EBR SYSTEMS AND TECHNIQUES

In this chapter the constituent materials for externally bonded FRP reinforcement (FRP EBR) are described, as well as their function and interaction. Furthermore, the chapter deals with the material shapes, the manufacturing process and the FRP EBR systems commonly used. An overview of the techniques for strengthening with FRP EBR is given, followed by a discussion on the practical application. Finally, the material characteristics of (externally bonded) FRP reinforcement are covered.

1 Constituent materials for FRP EBR

1.1 General

Fibre reinforced polymer (FRP) materials are composites which consist of organic or inorganic fibres embedded in a matrix. The matrix, sometimes referred to as binder, is a polymer resin, often with some fillers and additives of various nature. Externally bonded FRP reinforcement (FRP EBR) can be regarded as a system of FRP reinforcement and a bonding agent to glue the FRP to the structure.

The suitability of FRP materials as load bearing component is related to the efficient use of small fibres with high strength and stiffness by embedding them in a relatively ductile polymer binder. The small diameter fibres achieve their strong material properties due to the highly oriented and pure (defect free) microstructure of the fibres. The binder or matrix allows for a good transfer of forces between the fibres as well as a smooth transfer of load from a broken fibre to nearby intact fibres. Hence, by virtue of the matrix, local stress concentrations decrease and a higher unidirectional composite strength can be achieved. In addition, the matrix protects the fibres to a certain extent against mechanical damage and environmental attack. For the use of FRP as externally bonded reinforcement, an adhesive (bonding agent) is applied as well. With the adhesive the FRP is attached to the structure and, after curing, it assures the composite action between the FRP reinforcement and the concrete element.

Several FRP EBR systems have become available for repair and strengthening of concrete structures. These systems, designed to act as a composite in an optimum way, are based on different fibre configurations, types of constituent materials, application techniques, etc. As the components of a system are carefully chosen to interact jointly, each FRP EBR system is unique. This means that for example the bonding agent of one FRP EBR system is not automatically applicable for another system or that a polymer binder for the fibres is not necessarily suitable as adhesive for FRP bonding.

In the following the constituent materials of FRP EBR are discussed [1-5]. Shapes of FRP, manufacturing of FRP elements and FRP EBR systems are discussed in Section 2.

1.2 Fibres

Various fibres (sometimes referred to as filaments) are commercially available, with a wide range of material properties. In continuous lengths and with small diameter, relatively stiff and strong fibres are very efficient to reinforce polymer matrix materials, allowing efficient load transfer between the fibres and hence utilising the excellent fibre properties. The suitability of the fibres mainly depends on the composite properties which are needed. For FRP reinforcement this means that selection is related to characteristics such as corrosion resistance, high tensile strength, sufficient failure strain, fatigue resistance and dimensional stability. With this respect, mainly three types of fibres are currently used for FRP reinforcement in concrete construction: aramid, carbon and glass. These fibres have a tensile strength which is higher than that of steel and are linear elastic up to tensile failure. The physical and mechanical properties vary considerably between the different fibre types and may vary significantly for a given type of fibre as well. Some typical properties are given in Table 2-1. The tensile stress-strain behaviour of the fibres is shown in Fig. 2-1.

Table 2-1 *Typical properties of fibres*

Fibre type	**Tensile strength** [N/mm^2]	**Modulus of elasticity** [kN/mm^2]	**Ultimate strain** [%]	**Density** [kg/m^3]	**Fibre diameter** [μm]
Aramid – IM	2700-4500	60-80	4.0-4.8	1400-1450	12-15
Aramid – HM	2700-4500	115-130	2.5-3.5	1400-1450	12-15
Carbon – Pitch HM	3000-3500	400-800	0.4-1.5	1900-2100	9-18
Carbon – PAN HM	2500-4000	350-700	0.4-0.8	1800-2000	5-8
Carbon – PAN HT	3500-5000	200-260	1.2-1.8	1700-1800	5-8
E-glass(1)	1800-2700	70-75	3.0-4.5	2550-2600	5-25
S-glass	3400-4800	85-100	4.5-5.5	2550-2600	5-25

IM: intermediate modulus, HM: high modulus, HT: high tensile strength

(1) Properties of AR-glass fibres are similar to those of E-glass

1.2.1 Aramid fibres

Aromatic polyamide or aramid fibres are produced from para-phenylene-terephthalamid by extrusion as a liquid crystal polymer and by fibre stretching. These organic fibres have an anisotropic fibrillar structure. In the fibre axis direction they consist of aligned molecular chains with strong covalent bond. In transverse direction these chains are cross-linked by weaker hydrogen bridges, so that higher tensile strength and stiffness are obtained in the longitudinal direction.

Besides the high tensile strength, aramid fibres show high energy absorption and toughness (as no other fibres), good vibration damping and fatigue resistance, low thermal conductivity, good thermal stability, moderate to fairly good chemical resistance, low compressive strength and moderate adhesive properties. The aramid fibres respond elastically in tension but exhibit non-linear and ductile behaviour under compression.

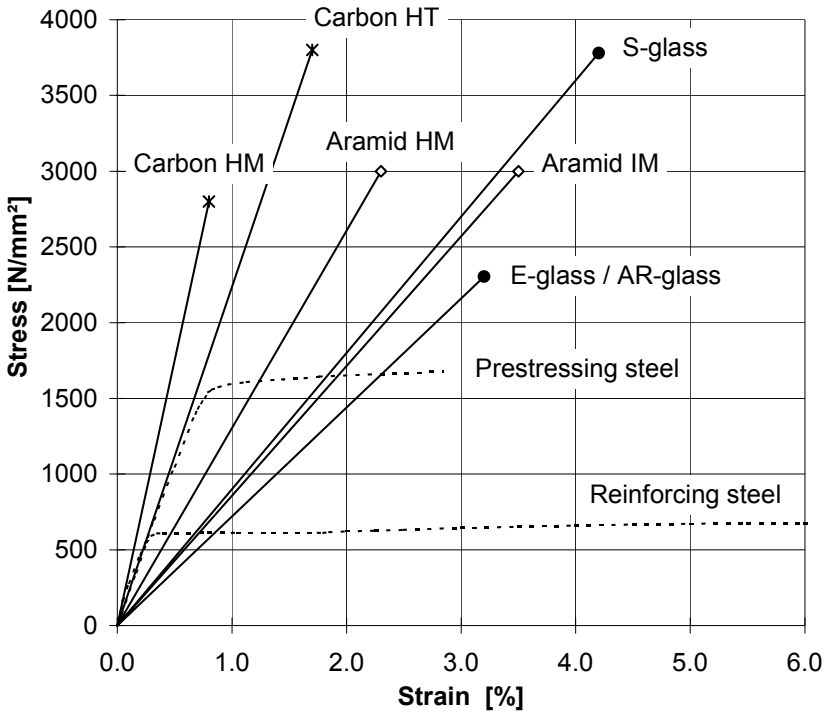

Fig. 2-1 *Tensile stress-strain behaviour of reinforcing fibres*

With respect to durability, aramid fibres generally exhibit a low or moderate resistance against acids, a moderate resistance against alkalis and a poor resistance against ultraviolet radiation. Due to the interaction of water with the polymer structure, they are sensitive to moisture as well. Because of these aspects, the fibres should be embedded in a matrix which is carefully chosen to provide additional protection. To improve the bond between fibres and matrix, surface treatments may be used.

1.2.2 Carbon fibres

Carbon and graphite fibres are produced from polyacrylnitrile (PAN), pitch or rayon. Isotropic pitch and rayon are used to produce low modulus carbon fibres ($E_{fib} \approx 50000$ N/mm^2). High modulus/high strength carbon and graphite fibres (Table 2-1), more of interest for FRP reinforcement, are made from PAN or liquid crystalline pitch. PAN fibres are obtained by separating a chain of carbon atoms from polyacrylnitrile through heating and oxidation. Pitch fibres are fabricated by using refined petroleum or coal pitch that is passed through a thin nozzle and stabilised by heating. The molecular structure consists of graphene (hexagonal) layer networks ordered in two or three dimensions. The former is defined as carbon, the latter as graphite. Typically, graphite has a higher tensile modulus than carbon. Although this difference, the term carbon fibre is often used irrespective of the graphitization.

Carbon fibres are the stiffest and strongest reinforcing fibres for polymer composites. They are very resistant against creep and fatigue and have a very good chemical, UV light and moisture resistance. Hence, carbon fibres are very durable and have excellent mechanical properties. As the fibres are electrically conducting, they can give galvanic corrosion in

contact with metals. The wetting of the fibres by resins is not easy, so that surface treatments are normally needed. In this respect, carbon fibres are often provided with an epoxy size treatment which protects the fibres against abrasion (improved handling) and offers an epoxy matrix compatible interface.

1.2.3 Glass fibres

Glass fibres are made of silicon oxide with the addition of small amounts of other oxides and are formed by extruding molten glass and fibre stretching. As glass fibres are very surface active and hydrophilic, individual fibres are generally coated by a sizing agent immediately after fibre forming. The sizing also acts to minimize abrasion damage and to aid coupling with polymer matrices. Depending on their chemical composition glass fibres can be divided into groups. Most general-purpose and widely used are E-glass fibres, which are based on calcium-aluminoborosilicate glass. These low cost fibres have a good electrical resistance and strength. S-glass is a magnesium-aluminosilicate formulation which has higher strength, stiffness and thermal stability. C-glass has a soda-lime-borosilicate composition that is used for its higher chemical stability against acids. AR or alkali-resistant glass fibres contain a considerable amount of zirconium oxide to increase resistance against alkalis from cement matrices.

Yet characterized by high tensile strength, good electrical resistivity, good thermal resistance and low price (especially E-glass fibres), glass fibres are known to degrade in the presence of water, acid and alkaline solutions. Also, they exhibit a considerable creep or stress rupture behaviour, meaning that the tensile strength gradually decreases under constant stress. Given the low durability of glass fibres, it is important to select a suitable and protective matrix. The use of AR-glass fibres with higher chemical resistance is of interest as well.

1.3 Polymer matrices

The polymer matrix of a FRP material consists of a resin binder (polymer binder) and normally some fillers and additives. Primarily the matrix has to bind the fibres together, provide lateral support to the fibres, protect the fibres from their surroundings, offer a load transfer medium and may beneficially influence some FRP material properties. In addition, the matrix selection is also important with respect to composite processability and cost.

1.3.1 Resins

Polymer matrices can be either based on thermosetting or thermoplastic polymers. Thermosetting resins, when cured, are characterized by a high degree of cross-linking of molecules (polymerisation) so that it solidifies or ‘sets’ irreversibly. Upon heating, these cured resins show no melting (at high temperature decomposition occurs). On the other hand, thermoplastic polymers are characterized by more linear macromolecules and can be repeatedly softened when heated and hardened when cooled.

Thermosetting polymer matrices allow for a good fibre wet-out without applying high pressure or temperature, which makes them very attractive with respect to processability. Compared to thermoplastics, thermosets also offer better thermal stability and chemical resistance, as well as reduced creep and stress relaxation. Disadvantages are their limited storage life and failure strain. Because thermoplastic polymers are more ductile and tough, they have higher impact strength, fracture resistance and micro-cracking resistance than thermosetting polymers. Other potential advantages of thermoplastics are the post-formability, the shorter fabrication time and the long storage life. However, as they are very viscous, incorporation of continuous fibres to thermoplastic matrices and hence composite production is difficult.

Polymer matrix materials are highly viscoelastic. Upon loading they exhibit elastic deformations, while under constant load slow viscous deformations occur. At increased temperature, low loading rates or long-term loading their response tends to be more ductile, while low temperature and high loading rate result in a rigid and more brittle behaviour. The mechanical properties of the polymer materials drop drastically when reaching the glass transition temperature T_g. At this temperature the polymer softens, meaning that it changes from a hard (often brittle) solid state to a more rubber like (soft and though) solid state. Upon further heating thermoplastics reach a highly viscous liquid state before decomposition, while thermosets degrade (char at very high temperature) before rubbery flow can be achieved.

For structural fibre composites, among which FRP reinforcement for concrete, unsaturated polyester, vinyl ester and epoxy are often used as polymer binder. From these thermosetting resins, polyesters are most general-purpose and frequently applied, given the good processability, fairly good properties and low cost. Vinyl esters process essentially like polyesters, but provide improved mechanical and chemical performance. Epoxy resins are more expensive than polyesters and vinyl esters, but are largely used in high-performance composites as they generally have the best mechanical properties, good adhesion properties and excellent resistance to chemicals and solvents. Some typical properties of these polymers, according to [2], are given in Table 2-2.

Table 2-2 *Typical properties of resins according to [2]*

Resin type	**Tensile strength** [N/mm^2]	**Modulus of elasticity** [kN/mm^2]	**Density** [kg/m^3]	**Cure shrinkage** [%]
Polyester	35-104	2.1-3.5	1100-1400	5-12
Vinyl ester	73-81	3.0-3.5	1100-1300	5-10
Epoxy	55-130	2.8-4.1	1200-1300	1-5

1.3.1.1 Unsaturated polyester

Thermosetting polyesters consist of an unsaturated ester polymer (a condensation polymerisation product of dihydroxyl derivatives and dibasic acids or anhydrides), dissolved in a cross-linking monomer such as styrene. By adding a free-radical initiator (for elevated temperature cure) or a promoter (for room temperature cure), a non-reversible chain

polymerisation reaction is initiated which yields a cross-linked styrene-polyester copolymer (cured polyester resin). To prevent premature cure during storage of the unsaturated polyester, an inhibitor may be added.

Polyester resins can be formulated to provide a wide variety of properties. Formulations which result in a higher cross-link density improve stiffness, glass transition temperature and thermal stability, but lower ductility. Given their low cost, good properties (Table 2-2), reasonable chemical resistance, good processability (low viscosity, fast cure time) and dimensional stability, polyesters are widely used for polymer matrix materials. The main disadvantage of polyesters is their high volumetric cure shrinkage, which promotes residual stresses in the composite.

1.3.1.2 Vinyl ester

Vinyl esters are produced from an unsaturated carboxylic acid (usually methacrylic acid) and an epoxy resin. Like unsaturated polyester, they are mixed with styrene for cross-linking. Hence, vinyl esters process and cure essentially as polyesters.

Compared to polyesters, vinyl esters have better chemical and temperature resistance, but are more expensive. As their molecular structure is characterized by fewer cross-links, they are more resilient, which makes them easier to handle during processing and provides higher fracture toughness. Furthermore, their chemical structure promotes hydrogen bonds with the surface of glass fibres, resulting in excellent wet-out and good adhesion with these fibres. As epoxy resins are used for the production, vinyl esters exhibit improved heat resistance and thermal stability, although tensile strength is not significantly influenced. Like unsaturated polyester they exhibit low viscosity and short curing time, as well as the disadvantage of a high volumetric shrinkage during cure.

1.3.1.3 Epoxy

Epoxy resins are made of low-molecular weight organic liquid resins containing epoxide groups (rings of two carbon and one oxygen atom). The most widely used epoxy resins are based on diglycidyl ethers of bisphenol A (DGEBA). Formulation may also include mixing of diluents to reduce viscosity and flexibilizers to improve impact strength of the cured epoxy. The cross-linking or curing of the epoxy is initiated by adding a hardener. The latter is a reactive curing agent of the amine, anhydride or Lewis acid type. Commonly used is diethylene triamine (DETA). For amine type of curing agents, hydrogen atoms in the amine groups react with the epoxide groups of the DGEBA, enabling the epoxy molecules to cross-link in a three-dimensional network.

Due to the diversity of input materials, epoxy resins have a very wide range of mechanical and physical properties, as well as processing conditions. As a result, they are the most versatile polymer binder for fibre composites, although more expensive than polyester and vinyl ester resins. Main advantages of epoxies are the excellent strength, the good creep resistance, the strong adhesion to fibres, the good resistance to chemicals and solvents and the

low cure shrinkage. Disadvantages are the relative high cost, the long curing time and the need for careful processing to maintain moisture resistance.

1.3.2 Fillers and additives

Fillers may be used to reduce matrix costs but also to control shrinkage, improve certain material properties, improve the load transfer capability of the matrix, control the thixotropy of the resin, etc. They are available in a variety of forms. Examples of some fillers are clay (alumina silicate), calcium carbonate, wollastonite and glass microspheres.

To enhance the resistance of the matrix and to improve processing of FRP manufacturing, additives of various nature may be used, such as UV inhibitors, flame retardants, anti-oxidants, initiators (catalysts), wetting agents, colour pigments, mold release materials, etc.

1.4 Adhesives

1.4.1 General considerations

By means of an adhesive two materials can be connected to each other, so that full composite action can be developed. In the case of FRP EBR, the adhesive is used to glue the FRP reinforcement onto the concrete surface and to provide a load path between these two materials. The load transfer is normally achieved by stressing the adhesive in shear (stresses in the plane of the bond interface), although peel stresses (normal to the bonded surface) may occur as well. The choice of the adhesive depends on several factors, such as the type of substrates, the required performance, the environmental conditions and the possibilities with respect to application. Furthermore, the adhesive must be able to provide excellent bond over a long period of time, even when exposed to e.g. moisture and variable temperatures.

Structural adhesives, which need to be strong, are generally based on thermosetting polymers. Different types of thermosetting adhesives can be used, among which epoxies, polyesters, cross-linkable acrylics and polyurethanes. Most widely used and accepted as structural adhesive are epoxies.

1.4.2 Adhesive requirements

To obtain a good performance of concrete structures strengthened with externally bonded FRP reinforcement, adhesives should meet certain requirements. Although detailed studies on the influence of material properties of adhesives on the performance of FRP EBR are rather limited, the following is generally required (as a result also of experience with steel plate bonding) [3,6]:

– Working characteristics with respect to mixing, application and curing should allow excellent joint quality, adequate adhesion to the concrete and the FRP (wetting ability), gap-filling properties, workability on overhead surfaces, etc. The adhesive should also be able to attach FRP without the need for temporary fixings.

- Bond quality and workability should not be unduly sensitive to limited variations in the quality of the prepared surfaces or the environmental conditions.
- With respect to durability, the adhesive should exhibit good moisture resistance, low creep, thermal stability and resistance to the alkaline nature of the concrete.
- The glass transition temperature of the adhesive should be significantly higher than the service temperature.
- The flexural modulus (E-modulus in bending) should fall within a specified range, generally taken as 2000 to 15000 N/mm^2. The lower limit relates to a restriction of creep, the upper to minimize stress concentrations. Also, the fracture toughness of the adhesive should be sufficiently high.
- The minimum shear strength of the adhesive should be 12 N/mm^2 (at 20 °C).
- The permeability of the adhesive and its maximum moisture absorption should be limited. Generally, it is required that the equilibrium moisture content should not exceed 3 % by weight after immersion in distilled water at 20 °C.
- Depending on the use of the strengthened structure and the environmental conditions, specific aspects of influence on the adhesive may be of concern. The material properties of the adhesive should also be considered in relation to those of the concrete and the FRP.

Requirements and conformity criteria for the identification, performance (including durability aspects) and safety of adhesives for structural bonding of construction materials to a concrete structure are provided in [6].

1.4.3 Epoxy as structural adhesive

As already stated in Section 1.3.1.3, epoxies can be modified for a wide range of material properties and have several advantages over other polymers. As adhesive for civil engineering they offer high surface activity and good wetting properties for a variety of substrates, high cohesion (failure in the adhesive) and adhesion (failure in the bond interfaces) strength so that debonding is governed by the adherent strength, low shrinkage and low creep. Furthermore, they can be toughened and made thixotropic. Related to the latter aspect, epoxy adhesives allow bonding of relatively large areas with only contact pressure (even on overhead surfaces) and are to a certain extent able to accommodate irregular or thick bond layers.

Given the numerous possibilities with respect to formulation, only epoxy adhesives should be used which are specifically produced for the construction industry. Generally, the formulations are complex as they are a blend of the epoxy resin, the hardener, fillers and additives. Used in construction, epoxy adhesives are normally based on DGEBA and an aliphatic polyamine hardener. The latter is often modified to obtain a more convenient mixing ratio, less hazardous handling and reduced moisture sensitivity. Fillers are used to reduce cost, assist gap-filling, reduce creep, etc. Diluents can be applied to reduce viscosity and may influence the pot life, flexibility and glass transition temperature. Flexibilisers can be used to improve impact resistance, peel strength and ductility, while toughers improve fracture energy and fracture toughness. Sometimes adhesion promoters are used to increase adhesion

to fillers and certain surfaces. Some typical values of the mechanical properties of epoxy adhesive, compared to those of concrete and steel, are given in Table 2-3. For properly formulated epoxy adhesives, generally no primer on the FRP or the concrete surface is required (for steel plate bonding a primer is normally applied on the steel).

In addition to the use of a suitable adhesive, it is very important that the gluing is performed in an appropriate manner and that quality control is provided. Techniques for the application of the FRP EBR and practical execution aspects are discussed in Section 3.

Table 2-3 *Typical properties of epoxy adhesive compared to concrete and steel, based on [7]*

Property		**Epoxy adhesive**	**Concrete**	**Steel**
Compressive strength	[N/mm^2]	55-100	25-150	200-2000
Tensile strength	[N/mm^2]	9-20	1-6	200-2000
Modulus of elasticity	[N/mm^2]	500-20000	20000-50000	≈ 200000
Coefficient of thermal expansion	[$10^{-6}/°C$]	25-30	8-12	≈ 10
Density	[kg/m^3]	1450-1550	≈ 2400	≈ 7800
Poisson ratio	[-]	≈ 0.30	0.15-0.20	0.30

2 Material shapes, manufacturing and FRP EBR systems

2.1 FRP reinforcement shapes

As structural reinforcement, FRP composites are made available in various shapes as discussed in Chapter 1, Section 1.2. Typically, these FRP products function as tensile members, so that they are usually produced as linear elements. In this respect, the FRP consists of large volume fractions of continuous, mostly unidirectional fibres (incorporated in a matrix), which function as principal stress bearing component.

To be used as externally bonded reinforcement, the FRP is made available in the shape of thin linear elements. The reinforcement is either provided as ‘pre-cured’ or as ‘in-situ curing’. Whereas the former is a FRP composite to be glued to the concrete, the latter is a fibre product to be formed into a FRP composite and to be glued to the concrete upon application. Examples of these FRP elements are shown in Fig. 2-2.

Pre-cured types are typically made available in the shape of thin unidirectional strips manufactured by pultrusion. Alternatively, strips can be produced by FRP moulding, in which case they form an arrangement of laminas (thin layers of unidirectional tape or woven fabric). These strips are referred to as laminates and can be uni- or multidirectional. Strips and laminates are delivered as:

- Pre-manufactured cured straight thin strips that may be delivered in a rolled coil.
- Pre-manufactured cured shells, jackets or angles, which are factory-made curved or shaped elements.

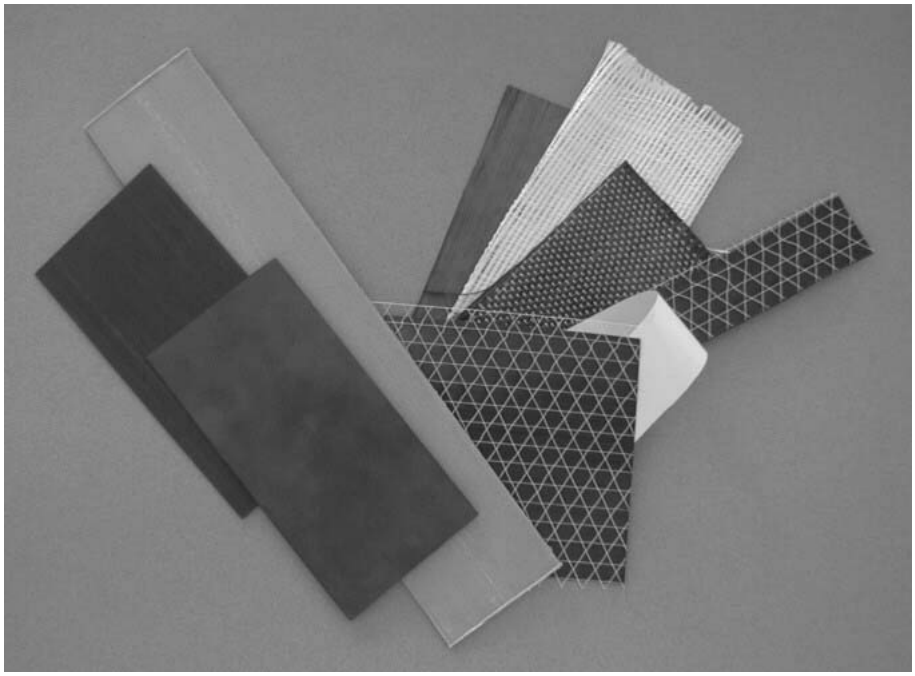

Fig. 2-2 *'Pre-cured' (left) and 'in-situ curing' (right) types of FRP EBR*

Fibre products for in-situ impregnation and curing may be of various kinds. In the most basic form, they are provided as tows or strands (untwisted bundles of parallel fibres), yarns (assemblies of twisted fibres) and rovings (tows or yarns collected in a bundle with little or no twist). More practical are unidirectional sheets (or tapes) and fabrics. These fibre products can be provided as 'dry fibre' or 'prepreg' (pre-impregnated) and are normally delivered for externally bonded reinforcement as:

- Dry unidirectional fibre sheet and semi-unidirectional or multidirectional fabric.
- Resin pre-impregnated uncured unidirectional or multidirectional sheet or fabric.
- Dry fibre or pre-impregnated tows to be wound or otherwise mechanically placed onto the concrete surface.

2.2 Manufacturing

Several manufacturing methods exist for the production of FRP composites, among which lay-up techniques, moulding techniques (e.g. injection, compression, resin transfer, vacuum bag and autoclave moulding), pultrusion and filament winding. In the following, some typical manufacturing methods for 'pre-cured' and 'in-situ curing' types of externally bonded FRP reinforcement are briefly discussed.

2.2.1 Manufacturing of strips by means of pultrusion

Pultrusion is a continuous moulding process that combines fibres and a thermosetting matrix to form straight composite parts which have a constant cross-section. The fibres, mostly in the shape of rovings, are drawn through a resin bath where they are thoroughly impregnated with the polymer matrix. The wetted fibres then enter a heated metal die, which

determines the dimensions and shape of the FRP element. The die is heated by precise temperature control to allow the curing (polymerisation) of the matrix. The FRP is continuously pulled through the pultrusion machine and exits the die with already a high degree of cure. The process is driven by a system of pullers located between the die exit and the cut-off mechanism. In Fig. 2-3 the process is schematically illustrated.

Given the nature of the process, pultrusion is dominated by the use of unidirectional fibres and allows the manufacturing of FRP elements with high fibre content. The production unit is characterized by relatively high starting costs and by low processing costs for high volumes. Major process parameters are machine speed, die temperature and resin reactivity. A peel-ply fabric or sheet may be incorporated on the surface(s).

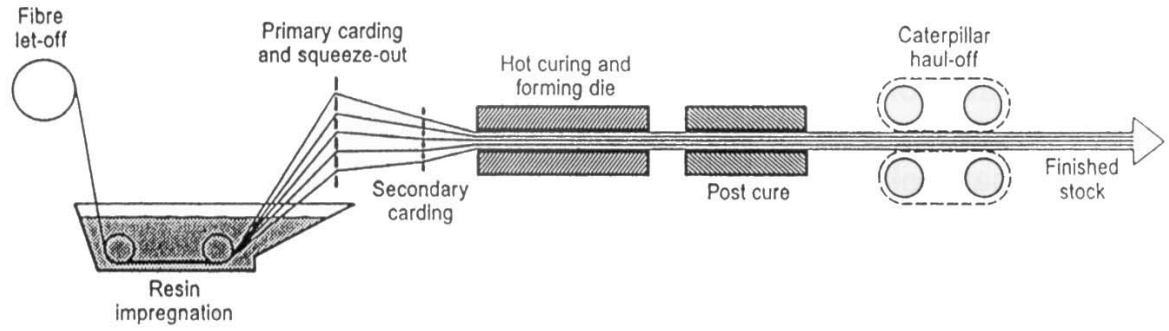

Fig. 2-3 *Pultrusion process [3]*

2.2.2 Manufacturing of laminates by means of moulding

Several moulding techniques exist for the production of FRP composites. Most simple is the open-mould technique, which consists of (manual) lay-up, consolidation and curing of laminas in a one-sided mould. More complex moulding methods are of various kind and can be divided in vacuum/pressure compacting processes and matched mould processes. The latter processes (compression moulding, resin transfer moulding, injection moulding, etc.) typically apply for quasi-isotropic (short) fibre arrangements and are not further discussed here.

Vacuum/pressure compacting processes typically compress and compact the uncured laminate by evacuation of entrapped air, densify the resin at the start of curing and cure the laminate by one of a number of methods. The process does not require a moulding press. Compared to pultrusion, these methods are more versatile and do not necessarily require high production volumes. On the other hand, the laminates can not be delivered in quasi-continuous lengths. The following vacuum/pressure compacting methods are often used. A schematic illustration is given in Fig. 2-4.

– In the case of *vacuum bag moulding*, layers of prepreg are placed underneath an air-tight bag, which is sealed at its borders. Vacuum is drawn within the covered area to compact the uncured laminate. The mould is then placed in an oven where heat is applied to cure the laminate. As an alternative to prepreg, dry-fibre laminas can be used, which are impregnated with resin on the mould. In this case, also a cold cure resin system may be applied, so that a heat source is no longer needed.

– Nearly the same as vacuum bag moulding is *autoclave moulding*. In this case the bagged laminate is placed in an autoclave which applies both heat and pressure and allows production of FRP laminates with a very high quality.
– *Pressure bag moulding* is similar to vacuum bag moulding, but applies pressure to the outside surface of the bag. Generally, this results in a better consolidation.
– Also very suitable for flat FRP elements is the *pressing technique*. Depending on the resin system, a cold or hot press consisting of two flat and parallel plates is used to apply pressure (and temperature). If needed, a vacuum bag may be used to aid the extraction of volatile substances.

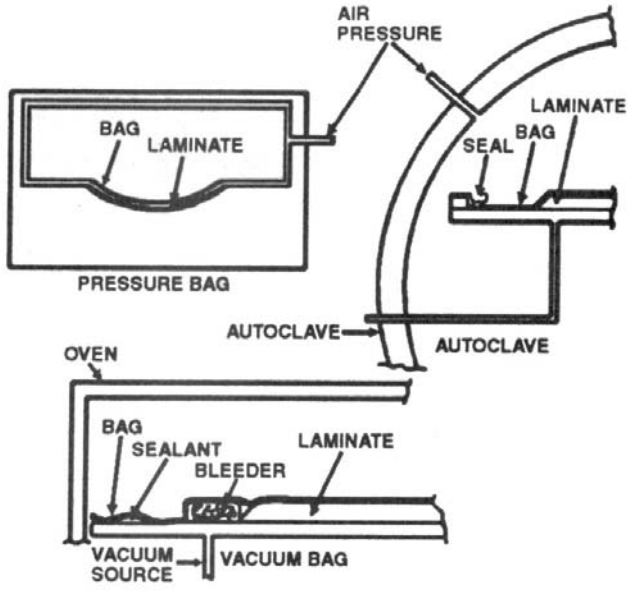

Fig. 2-4 *Vacuum bag, autoclave and pressure bag moulding [8]*

2.2.3 Manufacturing of dry-fibre sheets and fabrics

Unidirectional dry-fibre tapes or sheets consist of parallel fibres, tows, yarns or rovings, which are aligned in one direction and straightened. The sheets are very thin and available in various widths. For FRP EBR, they are normally provided with a peel-ply backing. Compared to fabrics, unidirectional sheets are characterized by a high degree of fibre alignment.

Multidirectional fabrics are produced by weaving, knitting, stitching or braiding continuous fibres (tows, yarns) into a fabric. The fabrics should be stable enough for easy handling, yet allowing quick fibre wet out and wet through with resin. Typically, these fabrics are available in various patterns, having precise fibre placement in different orientations. Woven fabrics provide fibres in the 0° (wrap) and 90° direction (weft or fill) and may be produced with different weave patterns. The basic pattern, plain weave, is most interlaced. In this weave, each weft yarn alternately crosses over and under each warp yarn. As a result, fibres are crimped (sinusoidal) and not straight. Stitched or knitted fabrics on the other hand are non-crimped, which optimizes their strength properties. Stitched fabrics are produced by assembling successive layers of aligned fibres. Often, fibre orientation includes two or more of the following directions: 0°, 90° and ±45° (bias). Braided fabrics consist of two or more

fibre yarns intertwined so that the fibres are interlocked. Typically, braided fabrics have fibres in the bias direction only (biaxial braids), where fibre angles are possible from about ±15° to ±75°. Additional fibres in the axial direction (0°) may be incorporated to obtain triaxial braids. Similar to woven fabrics, fibres in braids are crimped.

Quasi-unidirectional fabrics are obtained in a similar way as multidirectional fabric, whereas only a small amount of fibres is provided perpendicular to the axial direction. These fabrics are of interest as alternative to unidirectional sheets.

2.2.4 Manufacturing of prepreg

The dry-fibre sheets and fabrics discussed in the previous section can also be provided as prepreg. In the latter case, the polymer matrix is already impregnated into the fibres and often partially cured to a tack-free state, the so-called B-stage. This is an intermediate stage in the polymerisation reaction of a thermosetting resin, in which the material softens with heat and is plastic and fusible. The production process is schematically illustrated in Fig. 2-5. Prepreg is a fibre material form which allows storage (normally at low temperature) for later use. Final cure of the prepreg is obtained by heat, so that the thermosetting resin hardens irreversibly (C-stage).

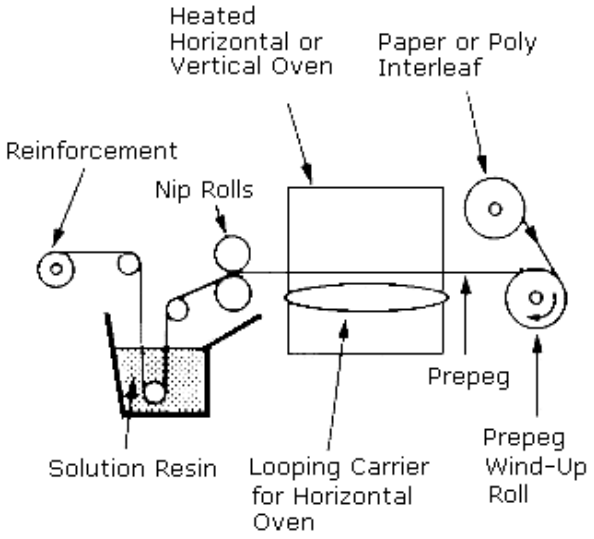

Fig. 2-5 *Solution prepregging [9]*

2.3 FRP EBR systems

FRP EBR systems consist of both the FRP reinforcement to be applied to the concrete and the bonding agent which will be used to glue the FRP. Given the various possibilities with respect to the constituent materials, the shape of the FRP and the technique for application, different systems of externally bonded FRP reinforcement exist. Similar to the material shape (Section 2.1), these systems can be subdivided in either 'prefab' ('pre-cured') or 'wet lay-up' ('in-situ curing') [10]. The main characteristics and some typical aspects of the two systems are summarized in Table 2-4. An overview is also given in the following.

Table 2-4 *Typical aspects of FRP EBR systems*

	PREFAB (PRE-CURED)	**WET LAY-UP (IN-SITU CURING)**
Shape of FRP	Strips or laminates	Sheets or fabrics
Thickness	About 1.0 to 1.5 mm	About 0.1 to 0.5 mm
Bonding agent	Thixotropic adhesive for bonding	Low viscosity resin for bonding and impregnation
Fibre volume	About 70 %	About 30 % (after impregnation)
Application	Simple bonding of the factory made elements with adhesive	Bonding and impregnation of the sheets or fabrics with resin (shaped and cured in-situ)
Applicability	If not pre-shaped only for flat surfaces	Regardless of the shape, sharp corners should be rounded
Number of layers	Normally 1 layer, multiple layers possible	Often multiple layers
Surface unevenness	Stiffness of strip and use of thixotropic adhesive allow for certain surface unevenness	Often a putty is needed to prevent debonding due to unevenness
Ease-of-application	Simple in use, higher quality guarantee (prefab system)	Very flexible in use, needs rigorous quality control
Quality control	Wrong application and bad workmanship = loss of composite action between FRP EBR and substrate/structure, lack of long term integrity of the system, etc.	

2.3.1 Prefab or pre-cured systems

The prefab FRP strips or laminates are provided as a fully cured composite, which has its final shape, strength and stiffness. Typically the strips have a fibre volume fraction of about 70 % and a thickness of about 1.0 to 1.5 mm. The latter thickness refers to the global thickness of the strip.

The FRP strips are installed through the use of an adhesive as explained in Section 3.2, whereas the adhesive provides the bond between the FRP and the concrete only. Compared to wet lay-up types, prefab strips assure a higher level of quality control as only the bonding part takes place in-situ. The application is generally more simple than in the case of wet lay-up types, but to a certain extent also less flexible as the prefab elements have already their final shape upon application.

2.3.2 Wet lay-up or in-situ curing systems

FRP wet lay-up types, provided as dry-fibre or prepreg sheets and fabrics, generally have very small thickness. The thickness after in-situ curing may vary and is difficult to determine. Therefore, reference is made to a nominal thickness, which is often taken as the equivalent dry-fibre thickness. This thickness equals the ratio of the fibre mass per area (kilogram of fibres provided per unit area) and the fibre density. Sheets and fabrics are available with an equivalent dry-fibre thickness of about 0.1 to 0.5 mm. After impregnation wet lay-up types

generally have a much smaller fibre volume fraction (magnitude of about 30 %) than prefab types.

Installation of dry-fibre elements requires a saturating resin for both impregnation and bonding. In the case of prepreg, often an insufficiently small amount of resin is already inside the element, so that also these elements require a saturating resin. For prepregs with a large amount of uncured resin inside the element before application, the installation can be executed without additional resin for impregnation, but requires heating devices. Installation of dry-fibre or prepreg sheets and fabrics is executed by wet lay-up (hand lay-up) as discussed in Section 3.2.

3 Techniques, practical application and quality control

3.1 FRP EBR strengthening techniques

3.1.1 Basic technique

With the basic technique, reference is made to the manual application of the FRP reinforcement by gluing it onto the concrete member, whereby the bonding is acheived through polymerisation of a two-part cold cured bonding agent (normally epoxy based). Besides the FRP, this technique involves the concrete substrate and the bonding agent. The concrete substrate is the (prepared) surface of the existing structure to which the FRP reinforcement is bonded to. The bonding agent is a polymer adhesive, specifically formulated to be used as structural adhesive for concrete construction and to function in an optimum way with the FRP reinforcement type and form under consideration.

In Fig. 2-6 and Fig. 2-7 an illustration is given of the application of prefab and wet lay-up FRP EBR systems according to the basic technique. More details on the practical application are provided in Section 3.2 and Appendix A.

Fig. 2-6 *Application of a prefab FRP EBR system*

Fig. 2-7 *Application of a wet lay-up FRP EBR system*

3.1.2 Other techniques

Besides the basic technique, most-widely applied, also other application techniques exist. These special techniques are more used for particular cases and resemble the basic technique in many ways. Some examples of special techniques are:

- The use of heating devices, which allow fast curing of the bond interface and wet lay-up (prepreg) FRP types. The technique makes use of heating blankets, electrical heaters or infrared (IR) heaters. In the case of CFRP the heat may even be generated by an electric current, as CFRP is electrically conducting (and yet resistant against an electric current). By applying heat to the FRP EBR the curing time may be considerably reduced, a higher glass transition temperature is obtained and the application is possible in cold regions or during cold seasons.
- Automated application of the FRP EBR for standard elements such as columns and chimneys. With this technique, FRP tows or sheets are applied to the concrete, mostly through winding, by means of an automated machine (robot). This method aims at a high degree of quality control and a reduced execution time.
- The application of prefab FRP in slits cut out in the concrete. In this way the FRP EBR can be regarded as internal reinforcement near the surface, with the advantages of being well protected and having a higher bond capacity.
- Prestressed FRP EBR, which calls for special detailing and execution techniques with respect to tensioning and anchoring of the FRP. Advantages of this technique are mentioned in Chapter 1, Section 2.3. If no extra mechanical anchorage is provided, only low prestress levels (for CFRP, about 5-6 % of the tensile strength) are feasible. To obtain a more significant effect and to be economically rational, much higher prestressing levels are needed, which requires extra fixings at the FRP ends.

3.2 Practical execution and quality control

3.2.1 Practical execution

In many respects, strengthening of concrete structures with externally bonded FRP reinforcement will stand or fall with the solidity of the practical execution. Indeed, where it is of importance to use FRP EBR systems with good quality, this does not guarantee that the system will work efficiently unless applied in an appropriate and qualified manner. Hence, the practical application should be executed by sufficiently skilled workers, according to proper procedures, under specified application conditions and subjected to quality control.

Although various FRP EBR systems are commercially available, the procedure for the practical application is often very similar. This especially holds for the basic technique, defined in Section 3.1.1. In Fig. 2-8 an overview is given of this widely used application technique. More details are provided in Appendix A. Hereby, it is noted that the application of the FRP EBR system is generally not intended to confine or arrest defects, such as steel corrosion. Hence, existing or potential damage and deterioration should be identified and causes of deficiencies should be known. This implies that the state of the member to be strengthened should be investigated in terms of concrete strength, imperfections (weak zones), corrosion of internal steel reinforcement, level of chloride ions, carbonation depth, etc. Based on this information, it can be decided if repair is needed preceding the FRP EBR application. More detailed information on repair techniques can be found in e.g. [11].

PRECEDING REPAIR
→ MEMBER TO BE STRENGTHENED
- Remove weak concrete, check for defects and potential damage mechanisms, etc.
- Repair if needed (flaws, corrosion, large cracks, etc.)

SURFACE PREPARATION
→ CONCRETE
- Remove contamination, roughen surface and round corners
- Verify unevenness and apply putty if needed
- Make dust free, the concrete should be sufficiently dry

→ FRP REINFORCEMENT
- Clean surface (e.g. carbon dust), cut to size and check for flaws

FRP EBR APPLICATION
→ PREFAB (PRE-CURED) TYPE
- Adhesive (thixotropic) application to the concrete
- Adhesive application on the FRP (roof shape)
- FRP application, squeezing out extra adhesive

→ WET LAY-UP (IN-SITU CURING) TYPE
- Adhesive application to the concrete (UNDERCOATING)
- FRP application
- FRP impregnation (OVERCOATING)

FINISHING (OPTIONAL)

QUALITY CONTROL

Fig. 2-8 *Schematic overview of the practical execution*

3.2.2 Quality control

Quality control is required to verify that proper materials are used, that the execution is performed according to the specified provisions, the design drawings and the rules for good practice, that the conditions assumed in the design are met and that no damage occurs during use. Especially, as the quality of the practical execution has a considerable impact on the bond and hence the overall performance of the strengthened element, quality control procedures are very important. More details on these procedures are given in Appendix A, Section 3.

Although a lot of consideration may be given to quality control, in the first place the quality remains a matter of skilled people performing proper design and practical execution. Hence, the design should be executed by a project engineer with experience in structural repairs and familiarity with FRP EBR systems, while the practical execution should be performed by trained workers.

4 Material characteristics of FRP EBR systems

4.1 General

With regard to design and detailing of a FRP EBR strengthening, knowledge of the material characteristics of FRP EBR systems is required. Hereby, properties of both the FRP reinforcement and the adhesive are relevant.

In structural engineering, normally the materials dealt with are basically isotropic. This is no longer the case for FRP materials, which are orthotropic due to the mostly unidirectional orientation of the continuous fibres. When the fibres are made available in multiple directions, the FRP can be assumed as quasi-isotropic. Because of the anisotropy, the various possibilities with respect to constituent materials and the influence of the production process, material properties of FRP EBR systems depend on a lot of factors. Therefore, material properties are preferably determined on the final products (the FRP reinforcement and the adhesive) by standard testing. In the following the main properties of FRP EBR systems are briefly discussed [4,5,12].

4.2 Type of FRP EBR system and dimensions

As a first characterization, the type and the dimensions of a FRP EBR system are of interest to know. This data deals with fibre type, adhesive type, system type (prefab or wet lay-up), fibre orientation(s), width, length and nominal thickness. The definition of the nominal thickness may be as follows.

For prefab FRP types, which are produced with small tolerances on the dimensions, the nominal thickness is generally taken as the global thickness. Alternatively, referring to the fibres as principle stress bearing component, the equivalent dry fibre thickness can be used. This nominal thickness is obtained as the ratio of the fibre mass per area (kilogram of fibres per unit area) and the fibre density.

In the case of wet lay-up FRP types, the final thickness after in-situ impregnation may vary considerably and is difficult to determine. Therefore, generally reference is made to the equivalent dry-fibre thickness, which is related to the fibre orientation. For sheets or fabrics with multiple fibre directions, where the weight by unit area is different depending on the fibre direction, more than one equivalent dry fibre thickness is obtained.

As demonstrated in for example Fig. 2-10(a), the FRP properties differ significantly from the properties of the fibres. Hence, using the equivalent dry fibre thickness to characterize composite properties is rather confusing. Moreover, for fibre composites, this definition of the nominal thickness results in unrealistically high values of the modulus of elasticity and the tensile strength, as reference is made to a nominal thickness which is considerably lower than the actual thickness of the cured FRP. This is illustrated in Fig. 2-9, which compares a prefab and wet lay-up FRP type with the same fibre type and fibre mass per area M_{fib}, hence with the same equivalent dry-fibre thickness t_{df}. Assuming that the tensile force is basically carried by the fibres (a more complete discussion on this aspect can be found in Section 4.4.1.1), the load-strain behaviour of the two specimens will be approximately equal. However, the stress-strain behaviour differs upon the definition of the nominal thickness. Referring to the dry-fibre thickness yields a stress-strain curve which approximates that of the fibres and is equal for the two FRP elements. By referring to the global thickness t, the fibre volume fraction is taken into consideration and the obtained stress-strain curves represent the actual composite behaviour. Hence, it may be suggested to define the nominal thickness as the global thickness in any case.

Given the fibre volume fraction v_{fib} (ratio of fibre volume to global volume), the relationship between the global thickness t and the equivalent dry-fibre thickness t_{df} is given by:

$$t = \frac{t_{df}}{v_{fib}} \tag{2-1}$$

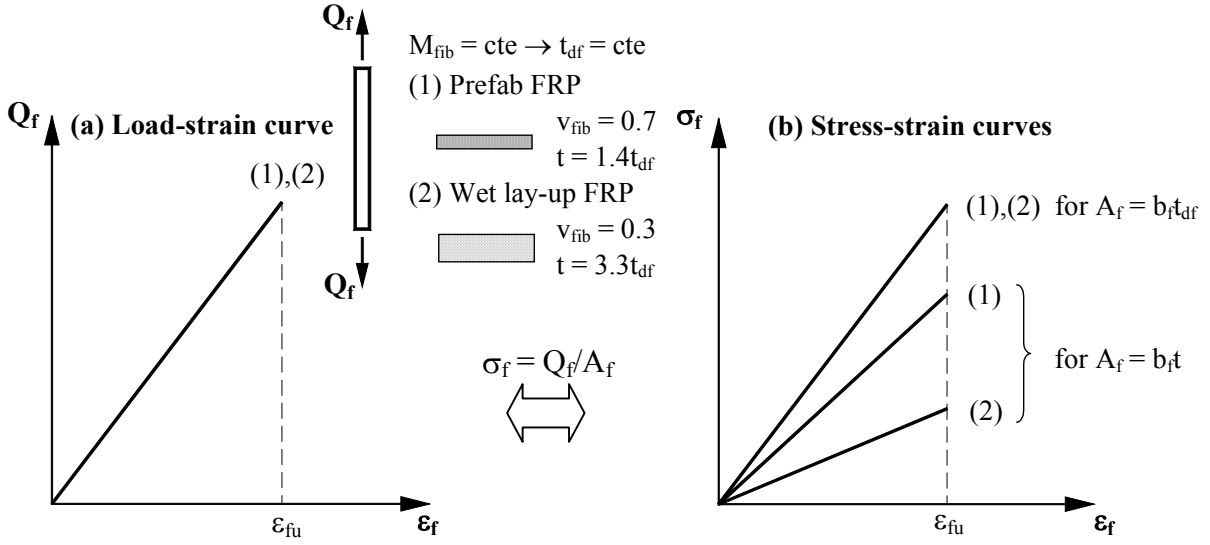

Fig. 2-9 *Influence of the definition of the nominal thickness*

For wet lay-up FRP types a nominal value of the fibre volume fraction can be determined on test specimens which are impregnated with resin in a similar way as would occur on construction site. The amount of polymer binder needed to impregnate the dry-fibre element can be derived from a saturation test.

As design verifications are based on equilibrium of forces, the definition of the nominal thickness (as far as used in a consistent way) does not influence the outcome of the design (Fig. 2-9). However, if data sheets of FRP EBR systems are compared, the possible difference in defining the nominal thickness should be considered.

4.3 Physical properties

4.3.1 FRP reinforcement

4.3.1.1 Constituent material fractions and density

FRP elements consist of fibres and matrices, which are provided in certain quantities. The fraction of a constituent can be defined as the ratio of the constituent quantity to the total quantity of the composite. Constituent material fractions can either be given by mass (weight) or by volume. The mass fractions are obtained from tests. As the volume equals the mass divided by the density, the volume fraction follows from the mass fraction as:

$$v_i = \frac{\rho_f}{\rho_i} m_i \tag{2-2}$$

where, v_i and m_i are respectively the volume and the mass fraction of constituent i. The density ρ_f of the fibre composite may be derived by applying the rule of mixture, often used for predicting unidirectional continuous fibre composite properties. Hereby, the composite property is estimated as the sum of the constituent responses weighted by the component volume fractions. Accordingly, the density is given as:

$$\rho_f = \sum \rho_i v_i \tag{2-3}$$

or also, from Equation (2-2) and given the fact that Σv_i equals 1:

$$\rho_f = \frac{1}{\sum \frac{m_i}{\rho_i}} \tag{2-4}$$

Typically, the density of FRP reinforcement equals 1400 to 2200 kg/m^3. Compared to steel, FRP is about 4 times lighter.

4.3.1.2 Coefficient of thermal expansion

The coefficient of thermal expansion (CTE) of steel and concrete are about the same and equal roughly 12 10^{-6}/°C. As a result, thermal stresses at the bond interface of the steel reinforcement and the concrete are generally not significant. Values of the CTE for FRP reinforcement are mentioned in Table 2-5. Given the anisotropy, different values are obtained in the longitudinal and the transverse direction. Compared to the value for concrete, the

longitudinal CTE of FRP differs significantly. As a result, temperature changes may unfavourably influence the bond between the FRP EBR and the concrete. Although an even larger difference is found for the transverse CTE, in the case of externally bonded reinforcement, this is of no influence as the transverse thermal expansion is not restrained. A further discussion on the influence of the CTE is given in Section 4.5.1.2.

Table 2-5 *Coefficient of thermal expansion (CTE)*

FRP type	**Longitudinal CTE** [10^{-6}/°C]	**Transverse CTE** [10^{-6}/°C]
AFRP	≈ - 2	≈ 30
CFRP	≈ 0	≈ 25
GFRP	≈ 5	≈ 25

4.3.1.3 Glass transition temperature

The glass transition temperature T_g is of particular importance, as it reflects the change of molecular mobility of polymer materials. This change significantly influences the mechanical properties of a composite material when subjected to an elevated temperature (Section 4.5.1.1). At the glass transition temperature, the amorphous regions of polymers change from hard (glass like) to rubbery (viscous) or vice versa. Compared to the fibres, the glass transition temperature of the matrix is lower, so that the latter is determining for the behaviour of FRP elements at elevated temperature. For factory processed FRP elements, the matrix generally has a T_g in the range of 130 to 140 °C. As discussed in Section 4.3.2.4, the T_g of cold-cured adhesives/saturating resins may be even lower.

4.3.1.4 Moisture absorption and chemical stability

With regard to the durability of fibre composite materials, the chemical stability of FRP elements and their constituent materials subjected to moist, solvents, alkalis, acids or ultraviolet (UV) light is of interest. Generally, it can be assumed that moisture absorption and chemical reactions may occur over time, resulting in a certain material degradation. The rate and significance of the deterioration is to be evaluated against the envisaged service life and will depend on both mechanical and environmental loading. Although specific durability problems may arise, such as degradation of glass fibres under alkaline environment, fibre composite materials generally have a good to excellent durability in various environments. A more detailed discussion on durability and long-term behaviour is given in Section 4.5.

4.3.2 Adhesive

4.3.2.1 Viscosity and thixotropy

Depending on the type of adhesive, the formulation and the temperature, the viscosity of adhesives will vary significantly. To obtain a good workability, thorough wetting of the adherents and hence quality of execution, adhesives with an optimum viscosity should be

used. Thixotropy may be required if a high viscosity is wanted yet with sufficient wetting ability during spreading. Different grades of an adhesive, each applicable within a certain working temperature range, may be made available.

4.3.2.2 Workable life and open time

After mixing, sufficient time should be available to spread out the adhesive onto the adherents. Practically, this implies that the workable or usable life (also called pot life) inside the mixing vessel should exceed preferably 30 to 40 min while the allowable joint open time preferably exceeds 20 min. Application of the adhesive beyond the workable life will result in poor wetting of the adherents.

4.3.2.3 Curing rate, temperature and humidity conditions

Under extreme conditions the adhesive will not be applicable or cure in a proper way. A maximum temperature is often specified in relation with the workable life and the viscosity, which are both temperature dependent. The minimum temperature at which curing is still possible generally equals 5 °C. The maximum relative humidity, above which insufficient adhesion is obtained, normally equals 80 %. If needed, special adhesive formulations or heating devices and dehumidifiers may be required.

The curing time depends on the type of adhesive and the ambient temperature. Often epoxy adhesive requires 6 to 12 h tack free curing, while at least 12 h is needed for nearly full curing. On curing, the shrinkage of the adhesive should be negligible (less than 0.1 %).

4.3.2.4 Glass transition temperature

The glass transition temperature of adhesives mainly depends on the type and formulation of the adhesive and the way (degree) of curing. Furthermore, it appears that the glass transition temperature may change in course of time, e.g. as a result of moisture absorption. Epoxies for structural bonding generally have a T_g of about 40 to 60 °C under ambient temperature curing (cold-cure). By means of additional heat curing the T_g value may be increased significantly.

Of all the constituent materials of externally bonded FRP reinforcement, the adhesive has the lowest T_g and is therefore the weak link with respect to the behaviour at elevated temperature. In [6] it is specified that the glass transition temperature should exceed 45 °C or the maximum shade air temperature at service + 20 °C, whichever is the higher.

4.3.2.5 Moisture absorption and chemical stability

For structural adhesives, durability is a basic requirement to guarantee adequate long-term bond performance. As a result, the resistance of adhesives against moisture and certain chemicals should be sufficiently high as further discussed in Section 4.5.1.

4.4 Mechanical properties and behaviour under short-term loading

4.4.1 FRP reinforcement

4.4.1.1 Tensile strength and stress-strain behaviour

FRP elements primarily act as tensile reinforcement, so that the tensile stress-strain behaviour is of basic interest for design. Given the mechanical characteristics and volume fractions of the constituent materials, it is possible to estimate the basic properties of unidirectional FRP elements based on the rule of mixture simplification. The FRP tensile stress (based on the global thickness) is given as:

$$\begin{aligned}\sigma_f &= \sigma_{fib} v_{fib} + \sigma_{mat} v_{mat} \\ &= \sigma_{fib} v_{fib} + \sigma_{mat} (1 - v_{fib})\end{aligned} \tag{2-5}$$

where, the fibre and matrix stress are taken at the same strain level, hence assuming that fibres, matrix and fibre composite undergo identical axial strain. The modulus of elasticity and Poisson ratio are obtained as:

$$E_f = E_{fib} v_{fib} + E_{mat} (1 - v_{fib}) \tag{2-6}$$

$$\nu_f = \nu_{fib} v_{fib} + \nu_{mat} (1 - v_{fib}) \tag{2-7}$$

The stress-strain behaviour of FRP, with σ_f according to Eq. (2-5), is shown in Fig. 2-10(a). As the fibres are the main tensile stress bearing element and as the fibre volume fraction is relatively high, the axial response of the FRP in tension is basically a reflection of that of the fibres. Compared to the fibres, the axial strength and modulus of elasticity of the FRP are lower.

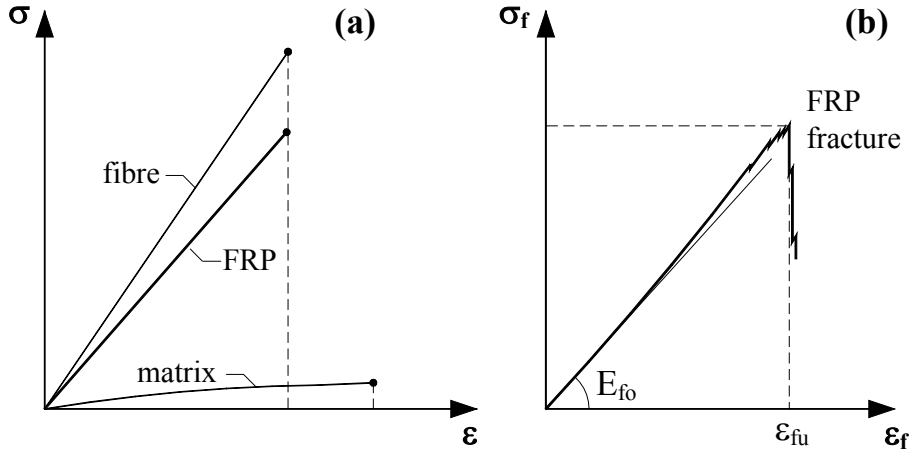

Fig. 2-10 *Tensile stress-strain behaviour, (a) rule of mixture, (b) actual*

As the rule of mixture is an approximation of the micro-mechanical behaviour of fibre composites, a more detailed prediction of the stress-strain behaviour (especially near ultimate load) should be obtained through tensile testing [13-15]. Reflecting the fibre and matrix characteristics as well as micro-structural aspects such as fibre diameter, distribution and parallelism of fibres, local defects, volume fractions and fibre-matrix interfacial properties,

the stress-strain behaviour of FRP (as generally obtained through tensile testing) is shown in Fig. 2-10(b). Under increasing tensile load, it appears that the FRP stress-strain response stiffens and hence is not perfectly linear elastic. This is because the fibres are initially lightly crimped and not fully aligned, so that they straighten and become more effective under higher loads. Near ultimate load the stiffness decreases again, as fibres start to fracture. Due to the load transfer from broken to intact fibres by the matrix, this does not immediately result in FRP fracture. Eventually, the FRP fails by fibre fracture and/or fibre delamination. Based on Eq. (2-5) and because the contribution of the matrix to the axial strength is generally negligible, the axial FRP tensile strength equals about:

$$f_f \approx f_{fib} v_{fib} \tag{2-8}$$

with, f_f and f_{fib} the tensile strength of the FRP and the fibres, respectively.

In Table 2-6 and Table 2-7 typical values of the tensile strength, modulus of elasticity and ultimate strain of commercial FRP products for externally bonded reinforcement are given. The values, which were found in various product data sheets, referred to the global FRP thickness for prefab types and the equivalent dry-fibre thickness for wet lay-up types. To make the data more comparable, values for both these definitions of the nominal thickness were calculated. Hereby, a fibre volume fraction v_{fib} of 70 % and 30 % was assumed for prefab and wet lay-up types, respectively. Referring to the equivalent dry-fibre thickness, it can be noted from Table 2-7 that the tensile strength and modulus of elasticity of both prefab and wet lay-up FRP types are similar. However, making reference to the global thickness and hence taking into account that prefab FRP types contain much higher fibre volume fractions than wet lay-up FRP types, a more realistic picture of the fibre composite strength and stiffness is obtained (Table 2-6).

Table 2-6 and Table 2-7 refer to the short-term static strength under normal laboratory conditions. The influence on the strength (and stiffness) of aspects such as sustained loading, temperature, moisture and UV radiation is discussed in Section 4.5.

Table 2-6 *Typical properties of FRP EBR, based on the global thickness*

FRP type		**Tensile strength f_f** [N/mm^2]	**Modulus of elasticity E_f** [kN/mm^2]	**Ultimate strain ε_{fu}** [%]
Prefab (v_{fib} = 0.7):	CFRP IM	2000-3000	160-250	1.2-1.8
	CFRP HM	1300	300	0.5
Wet lay-up ($v_{fib} \approx 0.3$):	CFRP IM	1050-1200	60-75	1.5-1.8
	CFRP HM	750-900	90-195	0.4-0.8
	GFRP	240-510	20-25	1.8-2.8
	AFRP	630-900	25-40	1.8-3.0

IM: intermediate modulus, HM: high modulus

Table 2-7 *Typical properties of FRP EBR, based on the equivalent dry-fibre thickness*

FRP type		**Tensile strength f_f** [N/mm^2]	**Modulus of elasticity E_f** [kN/mm^2]	**Ultimate strain ε_{fu}** [%]
Prefab (v_{fib} = 0.7):	CFRP IM	2850-4300	230-360	1.2-1.8
	CFRP HM	1850	430	0.5
Wet lay-up ($v_{fib} \approx 0.3$):	CFRP IM	3500-4000	200-250	1.5-1.8
	CFRP HM	2500-3000	300-650	0.4-0.8
	GFRP	800-1700	60-75	1.8-2.8
	AFRP	2100-3000	80-125	1.8-3.0

IM: intermediate modulus, HM: high modulus

4.4.1.2 Compressive strength and modulus of elasticity

The compressive strength and modulus of elasticity of FRP elements is smaller than their counterparts in tension. A poor compressive strength is especially obtained for AFRP, while GFRP has a moderate and CFRP has a fairly high compressive strength. Indicative values, obtained from tests on FRP bars, are reported in Table 2-8 [16].

As concrete members generally have to be strengthened in the tension region, the compressive strength of FRP is often of no relevance. Nevertheless, it may occur that certain zones of the FRP EBR, normally subjected to tension, are also subjected to compression. This depends on the load distribution and the member configuration. In [17], it has been demonstrated that prefab CFRP can successfully act as externally bonded reinforcement in compression, whereas no local buckling or peeling was obtained before concrete crushing.

Table 2-8 *Compressive properties [16]*

FRP type	**$f_{f,comp}/f_{f,tens}$** [-]	**$E_{f,comp}/E_{f,tens}$** [-]
CFRP	0.78	0.85
GFRP	0.55	0.80
AFRP	0.20	1.00

4.4.1.3 Multiaxial strength

Although primarily subjected to axial tension, the application of FRP EBR requires transfer of the tensile force to the concrete, resulting in multiaxial stresses (especially in the anchorage zones). Due to this load transfer, mainly shear stresses are generated, which act on the interior of the FRP as well as on the bond interface. In general, the shear strength of the FRP (as well as the adhesive) is superior to that of the concrete. For wet lay-up FRP types with a large number of layers, the inter-laminar shear strength may be critical.

As the shear and transverse strength of unidirectional FRP elements mainly depend on the matrix, these strengths are low compared to the axial tensile strength. As a result FRP elements are generally very vulnerable to e.g. gripping forces and direct impact loading. By orienting fibres also in the off-axis direction(s), the multiaxial strength properties can be

significantly improved. However, at the same time the strength in the main direction will be reduced.

Given the low FRP strength with respect to gripping, special provisions are required when tensile testing is performed. Test results may highly depend on the way of testing, so that the use of standard tests is very important.

4.4.2 Adhesive

Structural adhesives can be formulated for a wide range of properties. Due to the complex nature of these formulations, estimation of the mechanical properties is difficult and hence requires material testing. With this respect, in [6] various normative references are provided.

In principle, the adhesive provides a shear load path between the concrete and the FRP. As a result, the shear and adhesion strength of the adhesive are of mayor concern. For structural adhesives it is generally required to have a shear strength of at least 12 N/mm^2 and an adhesion strength in terms of pull-off tensile strength of at least 15 N/mm^2 [6]. In the case of a FRP/concrete joint, the latter condition means that adhesion is stronger than the concrete tensile strength.

For cold cured epoxy adhesives, often used for structural bonding, the shear strength equals 15 to 35 N/mm^2 [3]. As also discussed in Section 1.4.3, the flexural modulus of epoxy adhesives should be within the 2000 to 15000 N/mm^2 range.

4.5 Durability and long-term behaviour

The durability and long-term behaviour of concrete structures strengthened with FRP EBR depends on the original concrete structure, the FRP reinforcement as well as the bonded joint. In the following, the influence of temperature, moisture, chemical attack and load are discussed for the FRP and the adhesive joint only. A discussion on the durability and long-term behaviour of FRP EBR strengthened concrete members is provided in Chapter 7, Section 7. Furthermore, it is assumed that proper concrete repair is conducted preceding the FRP EBR application, so that the influence of concrete deterioration on the adhesive joint durability and long-term behaviour can be disregarded.

4.5.1 Environmental durability

4.5.1.1 Temperature and fire

Although fibres exhibit relatively high thermal stability, polymer resins are strongly affected by temperature. As a result, the material properties of FRP EBR are influenced by temperature and decrease drastically when reaching the glass transition temperature T_g. As adhesive joints have the lowest T_g and hence determine the susceptibility of FRP EBR to elevated temperature, only structural adhesives should be used with a glass transition temperature in excess of the maximum service temperature.

In the event of fire, the glass transition temperature of the adhesive is reached very quickly and as the temperature further increases the adhesive strength is completely lost. Due to the

resulting loss of bond, the fire resistance of FRP EBR systems is generally poor, although this may strongly depend on the extension and location of the debonding zones.

A further discussion on the fire behaviour with respect to the design is given in Chapter 7, Section 7.3. More details on the influence of elevated temperature and fire on the mechanical properties of fibres and fibre composites is provided in [4,18].

4.5.1.2 Thermal stresses and freeze-thaw action

Subjected to a temperature change ΔT, thermal stresses are initiated in the FRP and the concrete. These stresses are due to the – by virtue of the bond interface – restraint difference in thermal expansion (Section 4.3.1.2). In the interface, thermal bond stresses are generated, which may become critical (especially in the anchorage zone) for high values of ΔT [19]. Moreover, small defects such as microcracks and voids are generally present in the bond layer, which may further deteriorate under thermal cycling. The most critical condition is obtained in the case of wet freeze-thaw action, where also the expansion of freezing water is involved.

Durability with respect to wet freeze-thaw action has been investigated experimentally in [19-24]. Based on these tests the following can be concluded:

- Direct pull-off tensile testing of CFRP sheets bonded to concrete after 300 cycles (freeze in air at -30 °C/thaw in water at 9 °C) gave no reduction of the bond strength [20]. Also, no change in failure mode (concrete tensile failure) occurred.
- For 3 or 4-point bending tests on RC beams strengthened in flexure with CFRP and subjected to freeze-thaw cycles, no negative effects were found on the structural behaviour. Tests took into account freezing in air (minimum temperature -10 °C to -25 °C), thawing in water (maximum temperature 15 °C to 20 °C), effect of pre-cracking, FRP bonding only in the anchorage zone, presence of voids (outside the anchorage zone) and number of cycles 50, 100 or 150 [19,21,22].
- Significant degradation in the compression strength of both CFRP and GFRP wrapped cylinders can be obtained after freeze-thaw cycles in wet conditions [23,24]. GFRP wrapped specimens exhibit the highest degree of degradation (based on limited results and after 300 cycles: more than 25 % strength reduction for GFRP versus less than 20 % for CFRP). Compared to unconditioned or wet/dry conditioned specimens, a more catastrophic failure behaviour is obtained for specimens subjected to freeze-thaw.
- From the above mentioned test results it may appear that the freeze-thaw resistance is mainly related to the concrete, rather than the FRP. Indeed, in [23] the decrease in strength of unwrapped cylinders subjected to freeze-thaw appears about twice as large as that of wrapped cylinders.

4.5.1.3 Influence of moisture

Whereas carbon and glass fibres are relatively inert to water, damage may occur to the resin-glass fibre interface of GFRP due to the intrusion of moisture. In a similar way, a negative effect on the tensile strength and resin-fibre interface of AFRP may be expected, as

aramid fibres tend to absorb moisture up to 4 % by weight (8 % if stored under water) [4]. Matrix and adhesive materials absorb moisture as well, resulting in a reduction of the glass transition temperature and a stiffening of the resin. To deal with the negative influence of moisture, permeability and allowable water absorption of matrices and adhesives are generally restricted (Section 1.4.2).

Natural (outdoor exposure) and accelerated weathering tests (wet-dry cycles at a certain temperature) taking into account both fresh and salt water are reported in [20,24]. These tests indicate no tensile strength reduction of CFRP, whereas GFRP and AFRP show a significant decrease in the tensile strength. After 10000 h wet-dry cycles at 65 °C (assumed equivalent to about 50 years exposure) and based on limited test results a 35 % and 30 % tensile strength reduction was found for AFRP and GFRP, respectively. These test results should however be considered with caution as no indication was given on the T_g value. For the bond strength (direct pull-off tensile strength) of CFRP to concrete no negative influence of wet-dry cycles was found. In the case of CFRP wrapped cylinders, exposure to a wet-dry environment appeared to have only little effect on the compressive strength. For GFRP wrapped specimens, a reduction in strength of about 10 % (300 cycles at 35 °C) was found.

4.5.1.4 Chemical resistance

The chemical resistance of FRP materials against acids, alkalis and organic solvents mainly depends on the type of fibre, the resin system and the mechanical loading (which may cause matrix microcracking), whereas increased temperature is used as a means to accelerate testing. In general, FRP materials appear to have a good to excellent chemical resistance against chemical attack, although specific problems may occur.

As discussed in Section 1.2, glass and aramid fibres generally have a low acid resistance, whereas the alkali resistance is moderate for aramid fibres and generally low for glass fibres. Carbon fibres have high chemical resistance. With respect to the resins, vinyl esters show superior resistance compared to polyesters, while epoxies are regarded to be very inert (Section 1.3).

For concrete construction applications, given the alkaline environment of concrete, mainly the alkali resistance is of importance:

- Extensive deterioration in mechanical properties has been found for GFRP in alkaline solutions, especially at elevated temperatures and high mechanical stresses [25-27]. AFRP materials are less affected by alkaline solutions than GFRP. Nevertheless, combined with high tensile stresses, the life time of AFRP may considerably shorten [26,28]. CFRP with a proper fibre-resin system do not exhibit significant durability problems [25].
- Vinyl ester has a better resistance against alkaline environment than polyester [27]. Epoxy is regarded to be very inert [3].
- Exposure to natural concrete environment appears considerably less severe than exposure to alkaline solutions (which simulate the concrete pore solution) [28]. In the case of FRP EBR, there is even no direct contact between the FRP and the concrete due to the adhesive

interface layer. Also, as the FRP EBR is mostly applied on aged concrete structures, the outermost concrete layer is normally carbonated, so that alkalinity is low.

4.5.1.5 UV radiation

Ultra violet (UV) rays are known to affect fibre composites, although the effects are mainly limited to the surface of the composite [29]. Tests on fibres [30] demonstrated almost no tensile strength reduction for carbon fibres, while glass and especially aramid fibres appear susceptible to UV radiation. The tensile strength of matrix materials is only affected in a limited way [30], although colour changes and reduced light transmissibility may occur. These latter aspects may be perceived by the public as an indication of loss of integrity of the composite. UV radiation on the surface of a composite may also lead to for example increased moisture absorption.

In the case of external FRP reinforcement, degradation due to UV light is of concern and can be solved by appropriate additives to resin systems or by protective paint.

4.5.2 Mechanical behaviour under sustained loading

4.5.2.1 FRP creep and creep rupture

FRP reinforcement combines elastic fibres, which have excellent resistance to creep, with a viscoelastic polymer matrix, which may show significant creep deformations. Consequently, FRP creep will be mainly due to the creep of the matrix and the time-dependent growth of fibre-matrix debonds and resin microcracking [31]. As FRP tensile members normally have a high degree of fibre orientation, large fibre volume fractions and a high ratio of fibre over matrix stiffness, the tensile force shared by the matrix is extremely low. Because of this and provided that the glass transition temperature is well above the service temperature, FRP creep is generally negligible. Tests on FRP rods, at load levels in the range of 70 to 90 % of the tensile capacity, are reported in [32]. No significant creep was found for CFRP. For GFRP almost no and for AFRP very small creep was found, however sudden jumps in the creep strain occurred after some time, which may correspond to the onset and growth of microstructural damage prior to creep rupture.

Whereas creep basically influences the long-term deformations, sustained stresses may also reduce the short-term tensile strength of FRP. This phenomenon, which occurs for most structural materials, is referred to as creep or stress rupture. The higher the sustained stress, the lower the endurance time (time under constant load after which creep rupture occurs). For low sustained loads, creep rupture may become irrelevant. Generally, CFRP can withstand stress levels up to at least 80 % of its short term strength, while considerably lower stress levels apply for AFRP (≈ 50 % on a 50 years basis) and GFRP (≈ 30 % on a 50 years basis) [4,32]. The permissible stress level can strongly depend on the fibre/resin system, the alignment of the fibres and the fibre volume fraction. In addition, creep rupture is generally adversely influenced by the environmental conditions discussed in Section 4.5.1.

4.5.2.2 Creep and creep rupture in the case of FRP EBR

In the case of externally bonded reinforcement, also the creep and creep rupture behaviour of the adhesive is relevant as this may significantly influence the stress transferring ability of the adhesive. As demonstrated in Chapter 7, Section 7.4, the sustained stress level in adhesive joints of externally bonded reinforcement is low, so that bonded joints may be designed to withstand low stresses for a long period of time with minimized creep effects. In [31], based on a review of creep tests, it is suggested that the sustained stress in an adhesive joint should be limited to 25 % of the short term strength.

4.5.3 Cyclic loading

High modulus fibre (e.g. aramid and carbon) composites have superior fatigue resistance, as has been demonstrated in research for aerospace applications. The cyclic tension fatigue of resin impregnated fibres, loaded in tension-tension with a minimum to maximum stress ratio of 0.1, is given in Table 2-9 [16]. In terms of stress-range versus number of load cycles until failure (S-N curves), the fatigue strength of unidirectional AFRP and CFRP exceeds that of prestressing steel, while that of GFRP is lower [4]. As the fatigue limit of the matrix is lower than that of the fibres, fatigue failure is usually governed by damage in the matrix and at the fibre-matrix interface [31]. Consequently, the influence of environmental exposure on the fatigue behaviour is basically related to the sensitivity of the matrix against environmental conditions. Furthermore, as high modulus fibres and large fibre volume fractions result in low matrix strains, this has a beneficial influence on the fatigue resistance.

With respect to externally bonded reinforcement, also the fatigue performance of adhesive bonded joints is of importance. Compared to metals, the S-N curves of adhesive joints are relative flat, meaning that a small reduction in the stress range gives a large improvement of the fatigue endurance. In [31] it is concluded that the stress range of cold cured epoxies, not subjected to service temperatures above 45 °C, should be limited to 4 N/mm^2. As bond shear stresses in the serviceability limit state of concrete structures strengthened with EBR are considerably lower than the concrete shear strength (which also equals about 4 N/mm^2), fatigue of adhesives joints is unlikely to occur.

Table 2-9 *Fatigue strength of FRP [16]*

FRP type	Degradation of initial static strength per decade of logarithmic lifetime
CFRP	≈ 5 %
GFRP	≈ 10 %
AFRP	≈ 5 to 6 %

5 Conclusions

The design and application of externally bonded reinforcement for the repair and strengthening of concrete structures requires adequate knowledge of FRP materials, FRP EBR

systems and their characteristics. From the overview presented in this chapter it follows that FRP reinforcement forms a group of materials, with high performance characteristics which strongly depend on the assembly of constituent materials. In the case of externally bonded reinforcement, the FRP has to act together with a properly formulated structural adhesive, so that they can be regarded as a system. Depending on the components and the application technique, various FRP EBR systems are commercially available. In general these can be referred to as 'prefab' or 'wet lay-up' types. The former refers to the application of pre-fabricated strips and laminates, while the latter involves the bonding and in-situ impregnation of sheets and fabrics.

Although the selection of suitable materials and systems is very important, also the practical execution has a considerable influence on the bond quality and hence on the integrity of the strengthening system. Therefore, practical execution has to be related to quality control of the supplied materials, the application conditions, the practical execution process and the strengthening system after finishing application.

From the literature overview on physical and mechanical characteristics of fibres, matrices, fibre composites and adhesives, it can be concluded that FRP EBR systems are generally very strong and durable. Nevertheless, like any structural material their performance may be negatively influenced by certain environmental and loading conditions. Evaluating the properties of AFRP, CFRP and GFRP, CFRP EBR systems will exhibit generally the best performance. This explains why externally bonded CFRP reinforcement is used for the majority of the practical applications and research, worldwide. Nevertheless, also AFRP and GFRP have strong potentials to be used as externally bonded reinforcement.

6 References

1. Bakis E.B (1993), "FRP Reinforcement: Materials and Manufacturing", in Fibre-Reinforced-Plastic (FRP) Reinforcement for Concrete Structures: Properties and Applications, Developments in Civil Engineering 42, Ed. A. Nanni, Elsevier Science, Amsterdam, The Netherlands, pp. 13-58.
2. Malek A.M., Saadatmanesh H. (1996), "Physical and mechanical properties of typical fibres and resins", Proceedings 1st. Intern. Conf. on Composites in Infrastructure, Eds. H. Saadatmanesh, M.R. Ehsani, University of Arizona, Tucson, Arizona, USA, pp. 68-79.
3. Hutchinson A.R., Quinn J. (1999), "Materials", Chapter 3 in Strengthening of Reinforced Concrete Structures Using Externally Bonded FRP Composites in Structural and Civil Engineering, Eds. L.C. Hollaway, M.B. Leeming, Woodhead Publishing, UK & CRC Press, USA, pp. 46-82.
4. Rostásy F.S., Ed. (1992), "Evaluation of potentials and production technologies of FRP", Report No. BREU 1-92, BRITE Project 4142/BREU-CT 91 0515, Fibre Composite Elements and Techniques as Non-Metallic Reinforcement of Concrete, 95 pp.
5. ACI (1996), "State-of-the-Art Report on Fibre Reinforced Plastic Reinforcement for Concrete Structures", ACI Report 440R-96, American Concrete Institute, ACI Committee 440, Detroit, Michigan, USA, 153 pp.

6. CEN (1999), "Products and systems for the protection and repair of concrete structures: Definitions – Requirements – Quality control and evaluation of conformity, Part 4: Structural bonding", prEN 1504-4, Comité Européen de Normalisation (CEN), Brussels, Belgium, 18 pp.
7. Shaw J.D.N. (1982), "A review of resins used in construction, Types of resin – applications – case histories", Int. Journal Adhesion and adhesives, April 1982, pp. 77-83.
8. Schwarz M.M. (1992), "Composites Materials Handbook", McGraw-Hill, Inc., New York, USA.
9. Lubin G., Ed. (1982), "Handbook of Composites", Van Nostrand Reinhold Co., New York, USA.
10. Matthys S. (1997), "Versterking van structurele betonelementen met opgelijmde vezelcomposietwapening" (in Dutch), Infrastructuur in het Leefmilieu, Ministerie van de Vlaamse Gemeenschap, No. 4/97, pp. 274-298.
11. FIP (1991), "Repair and strengthening of concrete structures", Fédération Internationale de la Précontrainte, FIP Guide to good practice, Thomas Telford, London, 37 pp.
12. Bank L.C. (1993), "Properties of FRP reinforcements for concrete", in Fibre-Reinforced-Plastic (FRP) Reinforcement for Concrete Structures: Properties and Applications, Developments in Civil Engineering 42, Ed. A. Nanni, Elsevier Science, Amsterdam, The Netherlands, pp. 13-58.
13. ASTM (1995), "Standard test method for tensile properties of polymer matrix composite materials", D 3039/D 3039M, Annual book of ASTM Standards, Vol. 15.03, American Society for Testing and Materials (ASTM), Philadelphia, USA.
14. CEN (1996), "Aeronautical- Plastics reinforced with carbon fibres – Unidirectional laminates – Tensile test parallel to the fibre direction", EN 2561, Comité Européen de Normalisation (CEN), Brussels, Belgium.
15. CEN (1997), "Plastics, determination of tensile properties (UD laminate)", EN ISO 527:5, Comité Européen de Normalisation (CEN), Brussels, Belgium.
16. ACI (1998), "Provisional design recommendations for concrete reinforced with FRP bars", ACI Committee 440, Draft Report, Draft 2, September 1998, American Concrete Institute, Detroit, Michigan, USA, 216 pp.
17. Deuring M. (1993), "Verstärken von Stahlbeton mit gespannten Faserverbund-werkstoffen" (in German), EMPA Bericht, No 224, Swiss Federal Laboratories for Materials Testing and Research, Dübendorf, Switzerland, 279 pp.
18. Blontrock H., Taerwe L., Matthys S. (1999), "Properties of Fibre Reinforced Plastics at Elevated Temperatures with Regard to Fire Resistance of Reinforced Concrete Members", Proceedings 4th. Int. Symp. on Fibre Reinforced Polymer Reinforcement for Reinforced Concrete Structures, Eds. C.W. Dolan, S.H. Rizkalla, A. Nanni, American Concrete Institute, Mitchigan, USA, pp. 43-54.
19. Kaiser H. (1989), "Bewehren von Stahlbeton mit kohlenstoffaserverstärkten Epoxidharzen" (in German), Doctoral thesis, Technical University of Zürich, Switzerland, 224 pp.

20. Yagi K., Tanaka T., Sakai H., Otaguro H. (1997), "Durability of carbon fiber sheet for repair and retrofitting", Proceedings 3rd. Int. Symp. on Non-Metallic (FRP) Reinforcement for Concrete Structures, Japan Concrete Institute, Sapporo, Japan, Vol. 2, pp. 259-266.
21. Green M.F., Bisby L.A., Beaudoin Y., Labossière P. (1998), "Effects of Freeze-Thaw on the Bond of FRP Sheets to Concrete", Proceedings 1st. Int. Conf on Durability of Fibre Reinforced Polymer (FRP) Composites for Construction, Eds. B. Benmokrane, H. Rahman, Sherbrooke, Canada, pp. 179-190.
22. Tysl S. R., Imbrogno M., Miller B.D. (1998), "Effect of surface delamination on the freeze-thaw durability of CFRP-reinforced concrete beams", Proceedings 1st. Int. Conf. on Durability of Fibre Reinforced Polymer (FRP) Composites for Construction, Eds. B. Benmokrane, H. Rahman, Sherbrooke, Canada, pp. 317-324.
23. Soudki K. A. and Green M. F. (1997), "Freeze-thaw response of CFRP wrapped concrete", ACI Concrete International, Vol. 19, No. 8., pp. 64-72.
24. Toutanji H., Rey F. (1997), "Durability characteristics of concrete columns wrapped with FRP tow sheets", Proceedings 3rd. Int. Symp. on Non-Metallic (FRP) Reinforcement for Concrete Structures, Japan Concrete Institute, Sapporo, Japan, Vol. 2, pp. 251-258.
25. Porter M.L., Mehus J., Young K.A., O'neil E.F., Barnes B.A (1997), "Ageing for fibre reinforcement in concrete", Proceedings 3rd. Int. Symp. Non-Metallic (FRP) Reinforcement for Concrete Structures, Japan Concrete Institute, Sapporo, Japan, Vol 2, pp. 59-66.
26. Uomoto T., Nishimura T. (1997), "Development of new alkali resistant hybrid AGFRP rod", Proceedings 3rd. Int. Symp. Non-Metallic (FRP) Reinforcement for Concrete Structures, Japan Concrete Institute, Sapporo, Japan, Vol 2, pp. 67-74.
27. Gangarao H.V.S. and Vijay P.V. (1997), "Ageing of Structural Composites Under Varying Environmental Conditions", Proceedings 3rd. Int. Symp. Non-Metallic (FRP) Reinforcement for Concrete Structures, Japan Concrete Institute, Sapporo, Japan, Vol 2, pp. 91-98.
28. Scheibe M., Rostasy F.S. (1998), "Stress-Rupture Behaviour of AFRP-Bars in Concrete and Under Natural Environment", Proceedings 2nd. Intern. Conf. on Fibre Composites in Infrastructure, Vol. 2, Tucson, pp. 138-151.
29. Bank L.C., Gentry T.R. (1995), "Accelerated Test Methods to Determine the Long-Term Behavior of FRP Composite Structures: Environmental Effects", Journal of Reinforced Plastic and Composites, Vol. 14, June 1995, pp. 558-587.
30. Kato Y., Nishimura T., Uomoto T. (1998), "The effect of ultraviolet rays to FRP rods", Proceedings 1st. Int. Conf. on Durability of Fibre Reinforced Polymer (FRP) Composites for Construction, Eds. B. Benmokrane, H. Rahman, Sherbrooke, Canada, pp. 487-497.
31. Barnes R.A., Garden H.N. (1999), "Time-dependent behaviour and fatigue", Chapter 7 in Strengthening of Reinforced Concrete Structures Using Externally Bonded FRP Composites in Structural and Civil Engineering, Eds. L.C. Hollaway, M.B. Leeming, Woodhead Publishing, UK & CRC Press, USA, pp. 183-221.

32. Yamaguchi T., Nishimura T., Uomoto T. (1998), “Creep Model of FRP Rods Based on Fibre Damaging Rate”, Proceedings 1st. Int. Conf. On Durability of Fibre Reinforced Polymer (FRP) Composites for Construction, Eds. B. Benmokrane, H. Rahman, Sherbrooke, Canada, pp. 427-437.

Chapter 3
STRUCTURAL BEHAVIOUR OF RC BEAMS STRENGTHENED IN FLEXURE

This chapter reports on the performed experimental and analytical study concerning the structural behaviour of reinforced concrete (RC) beams strengthened in flexure with externally bonded CFRP reinforcement. Based on the experimental work, existing models for the structural behaviour of RC beams are verified and extended with respect to externally bonded FRP reinforcement (FRP EBR). The efficiency of flexural strengthening with FRP EBR is demonstrated. Moreover, a good correspondence between the experimental and the analytical results is obtained.

1 Introduction

In order to investigate the feasibility of strengthening concrete members by means of externally bonded FRP reinforcement (FRP EBR) and to study the structural behaviour of the strengthened elements, several test series have been conducted. These tests aimed at obtaining an understanding of the mechanisms and problems related to this strengthening technique and to find or verify appropriate mechanical and design models. In this chapter, the tests and analytical verification concerning reinforced concrete (RC) beams strengthened in flexure are reported. Further tests and verifications with respect to RC beams strengthened in shear, strengthened tension members and axially loaded confined columns are discussed in Chapters 4, 5 and 6, respectively.

To study the behaviour of steel reinforced concrete beams strengthened in flexure with externally bonded CFRP reinforcement, 4-point bending tests were performed on beams with a rectangular cross-section [1-5]. The tests were conducted in 1996 and were the first of this type performed in Belgium. Although some experiments were already reported in the literature at that time, it appeared that these experiments were mostly based on rather small specimens, which were not always sufficiently representative for real structures. In the test programme performed, it was decided to consider:

- large scale test specimens (span of 3.8 m and total depth of 0.45 m), representative for real structures
- prefab and wet lay-up CFRP types
- different amounts of internal and external reinforcement
- various load histories.

Although this study is limited to reinforced concrete members and non-prestressed FRP EBR, it is worthwhile to mention that this strengthening technique also applies to prestressed concrete or allows the application of prestressed FRP EBR. More information on these aspects can be found in [6-8].

2 Outline of the experiments

2.1 Test specimens and material properties

Test specimens comprised 9 RC beams with rectangular cross-section, two of which were reference specimens and the others were strengthened in flexure. The beams have a width of 200 mm, a total depth of 450 mm, a span of 3.8 m and a total length of 4.0 m. The dimensions of the beams and the test set-up are shown in Fig. 3-1. The test parameters are given in Table 3-1. Assuming full composite action between the FRP and the concrete, the beams were designed in such a way that they would fail in bending by yielding of the internal steel followed by concrete crushing and, except for BF9, before fracture of the FRP.

A first series of beams (BF1 till BF6) is characterized by a steel reinforcement ratio $\rho_s = A_s/bd$ of 0.96 % and is strengthened, except for the reference beam BF1, with one layer of CFRP. These beams allowed the investigation of the variability of the strengthening effect (BF2/BF3), the influence of pre-cracking (BF4) and load application prior to strengthening (BF5). The load level for pre-cracking and pre-loading (point loads Q equal to 110 kN), was taken equal to the service load of the unstrengthened beam (based on the resisting design moment and taken into account proper load safety factors following EC2). For beam BF6, an extra FRP-end anchorage was provided to verify if the FRP debonding failure, obtained for the tested beams, initiated at the FRP ends or not.

In a second series of beams (BF7 till BF9), half the amount of longitudinal steel reinforcement of the first series was provided (2 Ø16 in stead of 4 Ø16). Beam BF7 is the reference specimen, while beams BF8 and BF9 are strengthened in flexure by means of two different types of CFRP (prefab and wet lay-up CFRP).

For the internal reinforcement deformed steel bars S500 were used, with a guaranteed characteristic yield stress of 500 N/mm^2 and a diameter of 16 mm. The externally bonded reinforcement consisted of 1 layer prefab CFRP strip (CarboDur, width 100 mm, thickness 1.2 mm), except for beam BF9 for which 2 layers wet lay-up CFRP sheet (Replark, width 100 mm, nominal thickness of one layer 0.111 mm) were used. The length of the FRP EBR was taken as 3.66 m (maximum practically possible between the supports). The extra anchorage provided for BF6, consisted of 1 layer Replark (width 330 mm). The main characteristics of the reinforcement, obtained by tensile testing (Appendix B), are summarized in Table 3-2. The stress-strain behaviour of the reinforcement is shown in Fig. B-2.

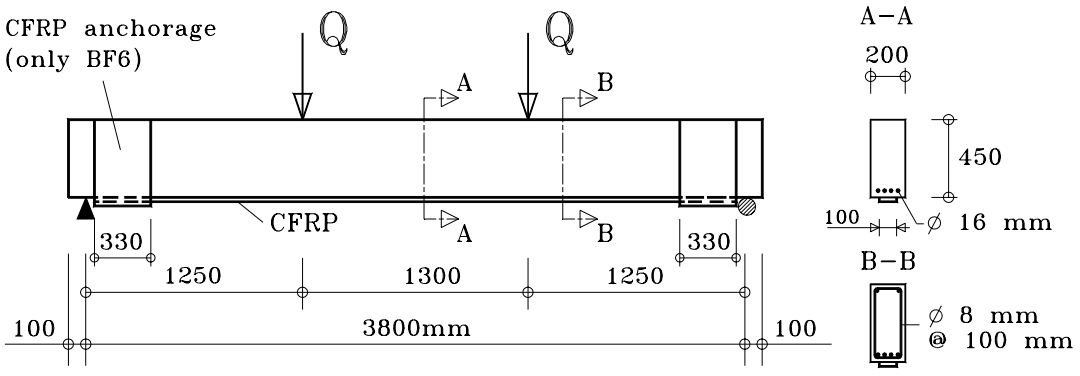

Fig. 3-1 *Test set-up and specimen dimensions*

For all beams the same concrete type was used, showing a mean compressive cylinder strength f_{cm} at 28 days of 32.8 N/mm^2. The compressive strength f_{cm} at the age of testing is given in Table 3-1. Detailed information on the material properties of the reinforcement, fresh and hardened concrete can be found in Appendix B.

Table 3-1 *Test parameters RC beams strengthened in flexure*

Spec.	Type of strengthening	Age at test [days]	f_{cm} [N/mm^2]	ρ_s [%]	ρ_f [%]	Pre-loading [kN]	Load during strengthening [kN]
BF1	Unstrength. (ref.)	56	33.7	0.96	-	-	Self weight
BF2	Strengthened(1)	56	36.5	0.96	0.14	-	Self weight
BF3	Strengthened(1)	56	34.9	0.96	0.14	-	Self weight
BF4	Pre-cracked/strength.(1)	61	30.8	0.96	0.14	110	Self weight
BF5	Strength.(1) while loaded	65	37.4	0.96	0.14	110	110
BF6	Strength.(1) & anchored(2)	72	35.9	0.96	0.14	-	Self weight
BF7	Unstrength. (ref.)	105	38.5	0.48	-	-	Self weight
BF8	Strengthened(1)	107	39.4	0.48	0.14	-	Self weight
BF9	Strengthened(3)	59	33.7	0.48	0.026	-	Self weight

(1) CarboDur 100 mm x 1.2 mm, (2) Replark 330 mm x 0.111 mm, (3) 2 layers Replark 100 mm

Table 3-2 *Mean properties obtained by tensile testing*

Type	Nominal dimensions [mm]	Yield strength [N/mm^2]	Tensile strength [N/mm^2]	Ultimate strain [%]	E-modulus [N/mm^2]
Rebar S500	Ø 16	590	690	12.4	200000
CarboDur S1012	100 x 1.2(1)	-	3200	1.85	159000(3)
Replark MRK-M2-20	100 x 0.111(2)	-	3500	1.25	233000(3)

(1) Global thickness, (2) Equivalent dry-fibre thickness, (3) Tangent modulus at the origin

2.2 Specimen preparation and test procedure

During the first 7 days after casting the specimens remained covered with a plastic foil. The formwork (side faces) was removed after 1 day. At an age of 7 days, the beams were placed on supports and stored (uncovered) in the laboratory until testing.

The external CFRP reinforcement was applied to the beams at least 7 (CarboDur) or 14 (Replark) days before testing, according to the procedures specified in Appendix B, Section 3.2. Preparation of the concrete surface included sand blasting for beams BF2 till BF5, while grinding was used for beams BF6, BF8 and BF9. Before strengthening, beam BF4 was loaded up to a point load of 110 kN and unloaded. For beam BF5, a point load of 110 kN was applied prior to strengthening and curing. The extra anchorage at the ends of the CFRP strip, provided for beam BF6, was obtained by means of U-shaped wrapping around the soffit and side faces of the beam with a CFRP sheet. In this way, the fibre direction of the latter is perpendicular to that of the CFRP strip used for flexural strengthening (Fig. 3-1). Preparation for the wrapping included rounding of the corners with a radius of 30 mm.

The beams were tested in 4-point bending as shown in Fig. 3-1. The load was applied by means of two hydraulic jacks with a capacity of 500 kN. The load was increased stepwise (to allow for manual measurements) until yielding of the internal steel, after which the load was gradually increased until failure. Mostly, point load increments of 4 kN were used until first cracking, while thereafter increments of 10 kN were applied. An unloading-reloading cycle was incorporated in the loading scheme of the reference beam BF1 at 70 kN, and at 110 kN for beams BF2, BF3, BF4 and BF6. The other beams were loaded without a reloading cycle.

During the tests, both manual and electronic measurements were taken as shown Fig. 3-2. Deflections were measured at midspan, under the point loads and at the supports, using dial gauges (manual measurements) and potentiometric displacement transducers (electronic measurements). Mechanical deformeters with a gauge length of 200 mm were used to measure manually concrete and FRP deformations in the central zone of the beam, according to the arrangement shown in Fig. 3-2. This arrangement allows to take an average of five (one side face) or ten (two side faces) measurements at several levels over the beam depth. Some of these deformations were also recorded electronically by means of so-called strain stirrups (U-shaped stirrups instrumented with strain gauges) with a gauge length of 200 mm (Fig. 3-2). Strains of the internal steel and the FRP at midspan were recorded by means of strain gauges. The strain distribution of the FRP along one half of the beam was measured by means of mechanical deformeters with a gauge lengths of 200 or 50 mm, as well as with strain gauges for beams BF3 and BF9 (Fig. 3-2). At each load interval, the appearance and development of cracks were indicated after visual inspection. Crack widths were recorded by means of a small microscope.

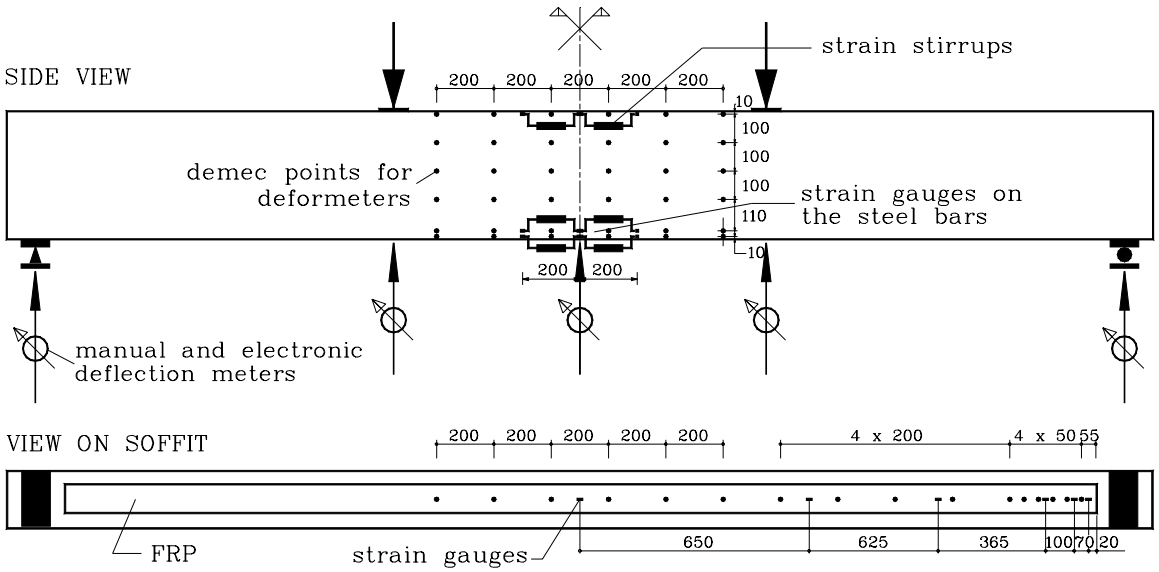

Fig. 3-2 *Measurements on beams strengthened in flexure*

3 Test results

3.1 Behaviour at ultimate load

3.1.1 Failure mode

The reference beams failed by yielding of the steel followed by concrete crushing. The strengthened beams failed by FRP debonding, as shown in Fig. 3-3 (left), after the internal steel had already yielded. The steel yielding/FRP bond failure was, except for beam BF8, directly followed by concrete crushing. This indicates that the premature debonding occurred (for most of the beams) close to the expected failure assuming full composite action between FRP and concrete.

FRP bond failure occurred along more than half of the beam length. Except for the end of the FRP strip, the bond failure occurred in the concrete, where a few millimetres of concrete remained attached to the debonded FRP. At the FRP end, over about 300 mm, debonding occurred at the interface between the FRP and the adhesive (Fig. 3-3, right). As the debonding failure happened in a very fast way, it was not possible to find out where it initiated. Given the high bond strength characteristics of the adhesive used, bond failure is expected to occur in the concrete. This may indicate that debonding did not initiate at the FRP end, but rather ran towards it, where the failure plane shifted to the FRP-adhesive interface. This hypothesis was confirmed by testing of beam BF6, for which an extra anchorage was provided at the FRP ends. The failure load and mode of this beam basically remained the same as for the previous beams. Also the analytical verification (Section 4.1) indicates, for the specimens of this test programme, that the most critical bond stresses did not occur in the anchorage zone.

Fig. 3-3 *Typical debonding failure mode of the strengthened beams*

3.1.2 Strengthening effect, ultimate FRP strain and ductility.

The test results in terms of ultimate load Q_u, ultimate deflection at midspan y_u and ultimate FRP strain at midspan ε_{fQu} are given in Table 3-3. In this table also the obtained failure mode is repeated.

Table 3-3 *Test results at ultimate load of RC beams strengthened in flexure*

Spec.	Type of strength.	Q_u [kN]	Failure mode	Q_u/Q_{ref} [-]	y_u [mm]	y_u/y_{ref} [-]	ε_{fQu} [mm/m]	$\varepsilon_{fQu}/\varepsilon_{fum}$ [-]
BF1	Unstrength. (ref.)	144.2	YS/CC	1.00	43	1.00	-	-
BF2	Strengthened(1)	185.0	BF(YS)/CC	1.28	33	0.76	6.7	0.36
BF3	Strengthened(1)	186.0	BF(YS)/CC	1.29	37	0.87	7.2	0.39
BF4	Pre-cracked/strength.(1)	184.2	BF(YS)/CC	1.28	36	0.84	6.8	0.37
BF5	Strength.(1) while loaded	177.0	BF(YS)/CC	1.23	42	0.97	5.7	0.31
BF6	Strength.(1) & anchored(2)	183.0	BF(YS)/CC	1.27	32	0.74	7.1	0.38
BF7	Unstrength. (ref.)	80.7	YS/CC	1.00	65	1.00	-	-
BF8	Strengthened(1)	111.3	BF(YS)	1.38	25	0.38	5.8	0.31
BF9	Strengthened(3)	95.8	BF(YS)/CC	1.19	41	0.63	10.0	0.80

(1) CarboDur 100 mm x 1.2 mm, (2) Replark 330 mm x 0.111 mm, (3) 2 layers Replark 100 mm
YS/CC: yielding of the steel followed by concrete crushing
BF(YS): bond failure of the FRP (after yielding of the steel)

Strength increases between 1.2 and 1.4 were obtained for the different beams. Beams BF2 and BF3, with identical characteristics, gave almost exactly the same failure load. This failure load is also found for beam BF4, which was pre-cracked before strengthening, and for beam BF6 with the extra anchorage. Beam BF5, which was loaded during strengthening gave only a slightly lower (4 %) failure load. The largest relative strength increase is found for beam BF8. Although influenced by the FRP debonding failure, this is basically due to the lower reinforcement ratio of the internal steel which allows the FRP to contribute to a larger extent before concrete crushing is reached (in the ideal situation of avoiding debonding failure). Comparing the failure loads of beams BF8 and BF9, the lowest value is found for the latter which had a smaller amount of externally bonded reinforcement.

Given the design concept of the beams (for most of the beams steel yielding/concrete crushing before FRP fracture) and given the debonding failure, the ratio of the recorded ultimate FRP strain ε_{fQu} to the mean ultimate FRP strain ε_{fum} (obtained from tensile testing) is considerably smaller than one (Table 3-3). Roughly the same FRP strain ε_{fQu} is found for beams BF2 till BF6 and BF8. The failure strain for beam BF9 is significantly larger. This beam is strengthened with a different type of CFRP.

Whereas the strengthened beams show a considerable increase of the failure load, this corresponds to a decrease in ductility (plastic deformations). This aspect is quantified in Table 3-3 by means of the ratio of the ultimate deflection at midspan y_u of the strengthened beams to that of the reference beams. Decreases of y_u between 3 and 62 % were obtained. The decrease in ultimate deflection considerably influenced by a premature bond failure.

3.2 Load-deflection behaviour

A comparison of the load-deflection response of the beams is shown in Fig. 3-4 and Fig. 3-5. In these figures, the curve for beam BF3 is not shown as it almost exactly matches that of beam BF2. The unloading/reloading branch tested for some of the beams is also not shown,

except for beam BF4 which was strengthened after unloading. The load-deflection curves of the beams, including the unloading/reloading branch are given in Appendix C. The recorded load-deflection curves clearly show the strength increase, the ductility reduction and the increase of the stiffness in the cracked state.

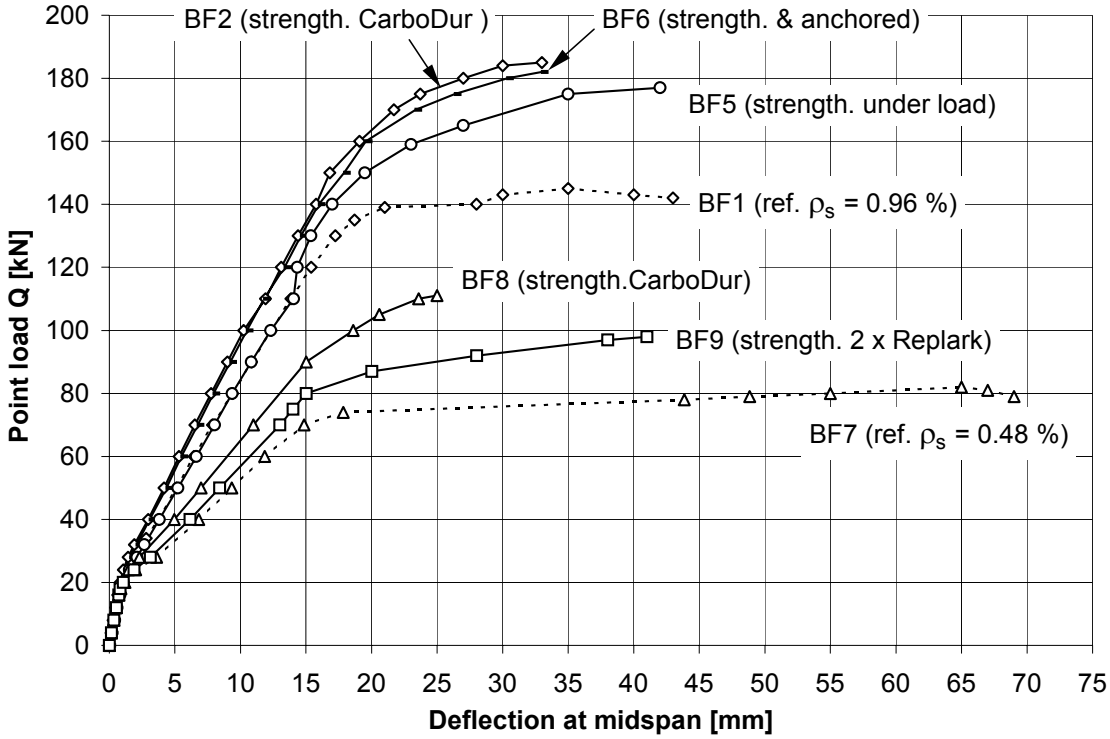

Fig. 3-4 *Load-deflection behaviour of beams BF1, BF2, BF5, BF6, BF7-BF9*

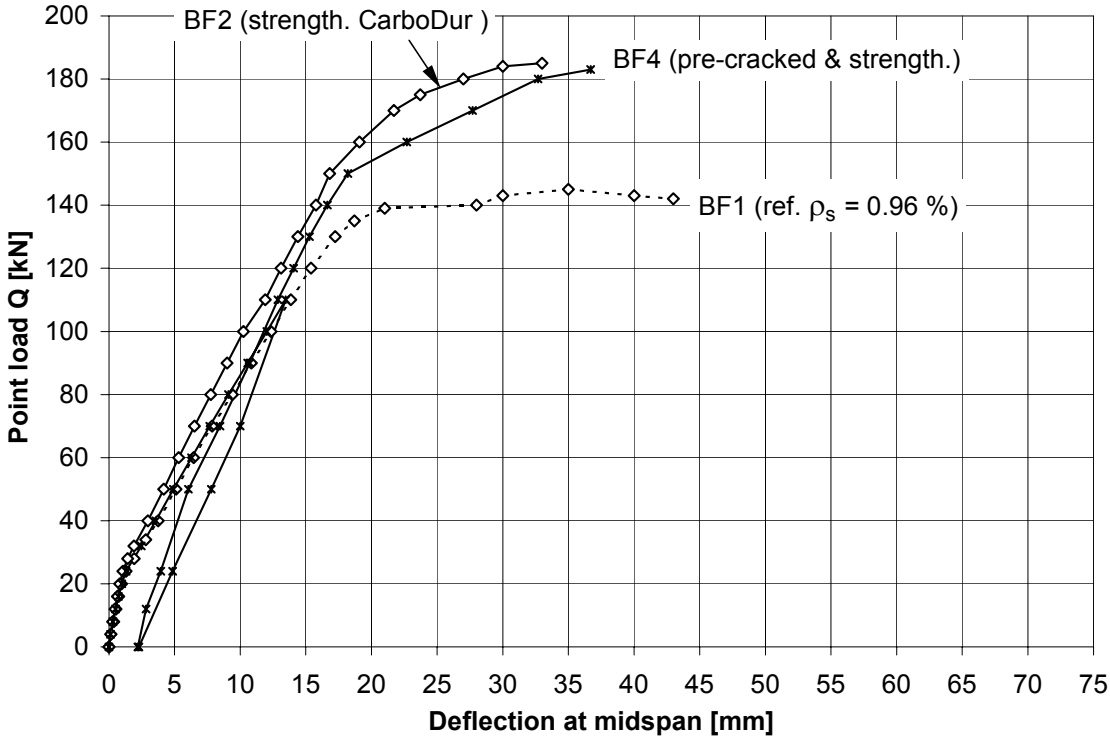

Fig. 3-5 *Load-deflection behaviour of beams BF1, BF2 and BF4*

3.3 Cracking behaviour

All beams started cracking at about the same load level $Q_{cr} \approx 18$ kN. The recorded crack pattern at ultimate load is given in Fig. 3-6. Although the higher failure load of the strengthened beams, their crack pattern at ultimate load is very similar compared to the reference beams. The mean crack widths of beams BF1, BF2, BF4, BF7, BF8 and BF9 are compared in Fig. 3-7. From this figure, the restraining effect of the CFRP strengthening on the crack width is noted. For beams BF4 (which was pre-cracked) and BF9 (with a very low FRP reinforcement ratio), this restraining effect is rather limited. The favourable influence of FRP EBR on the cracking behaviour is in agreement with the increased stiffness in the cracked state of the strengthened beams (see previous section).

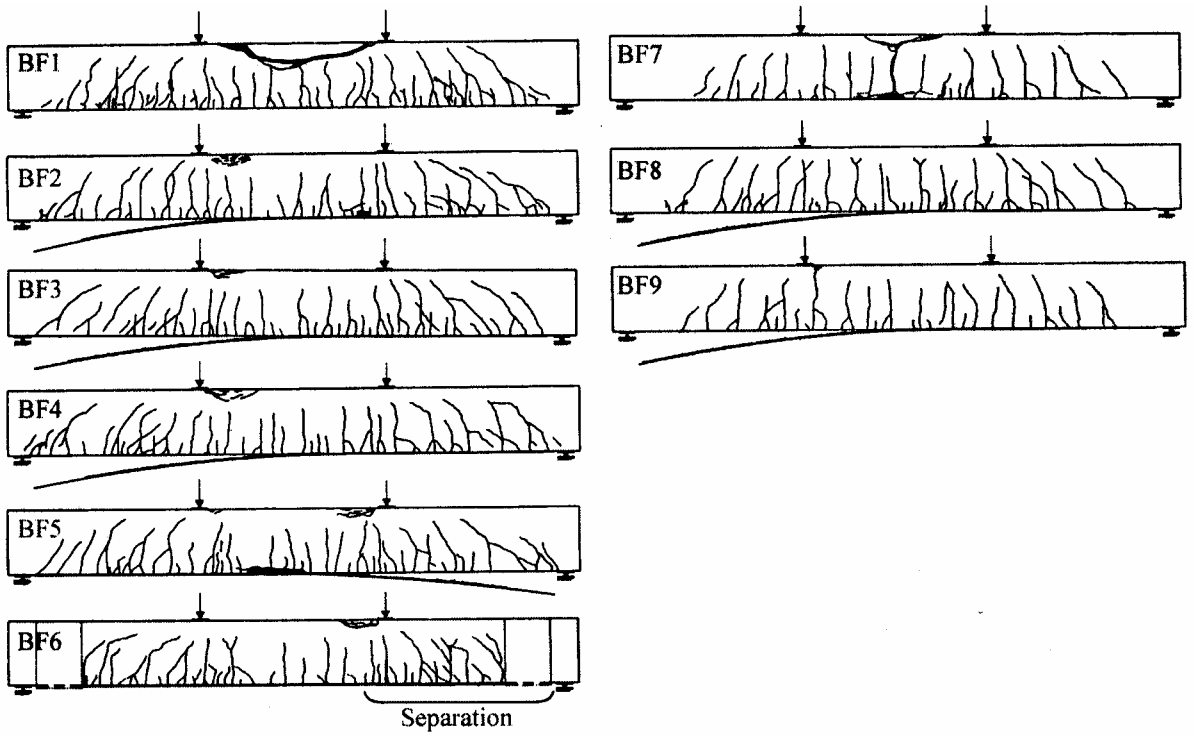

Fig. 3-6 *Crack pattern of (strengthened) RC beams at ultimate load*

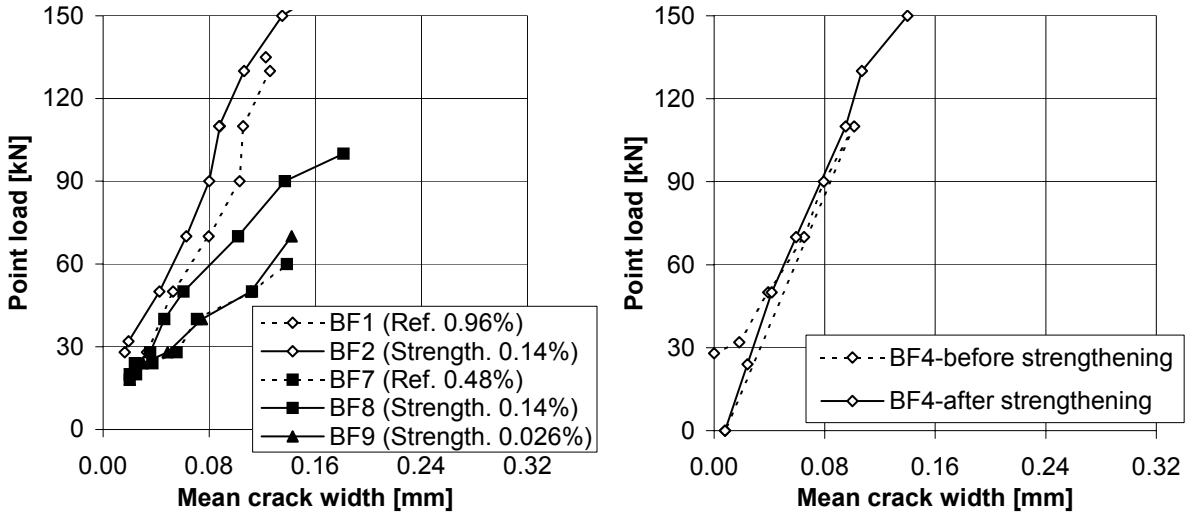

Fig. 3-7 *Mean crack width of unstrengthened and strengthened beams*

3.4 FRP strain distribution

The strain distribution of the FRP along its length, based on the manual measurements (thus before yielding of the internal steel), is shown in Fig. 3-8. At the FRP end the strain starts at zero and increases to build up the force in the FRP. Beyond this initial zone (transfer or anchorage zone) of about 150 to 300 mm, the FRP strain (and hence the FRP force) is proportional to the moment line of the beam, and reaches a plateau in between the point loads (constant moment region). Comparing Fig. 3-8 left and right, the anchorage zone of beams BF2-BF6 appears shorter and steeper than for beams BF8 and BF9. This may be due to the larger length of the cracked zone of beams BF2-BF6, which reaches about the total FRP length (Fig. 3-6). For beams BF8 and BF9, at the FRP end the beam is uncracked so that the FRP force is very small and only needs to be build up in a considerable way when reaching the cracked zone.

The strain distribution of beams BF2, BF3 and BF6 (Fig. 3-8, left) are almost identical. For beam BF4 which was pre-cracked the strains are only slightly less. The strains for beam BF5 are considerably lower, as the beam was already loaded (Q = 110 kN) before strengthening. For a given load level, higher strains are measured for beams BF8 and BF9 than for beam BF2 (Fig. 3-8, right). Indeed, the beams BF8 and BF9 have a lower amount of steel reinforcement, so that the FRP has to act in a larger extent to build up the same total (steel and FRP) tensile force in the section as for beam BF2.

For load levels above yielding of the internal steel reinforcement, the tensile force in the section can only further increase thanks to the FRP (the tensile force in the steel remains constant after yielding). As a result, FRP strains shall increase in a larger extent, as illustrated in Section 4.5.

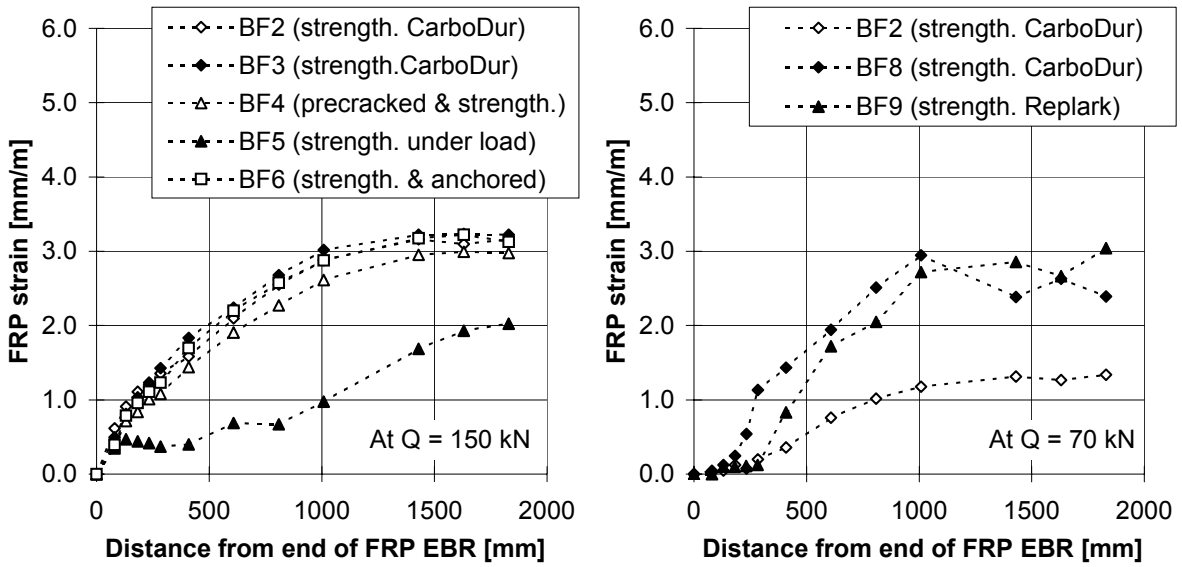

Fig. 3-8 *FRP strain distribution*

4 Analytical verification

4.1 Prediction of the failure load and failure mode

4.1.1 Verification assuming full composite action

As a first verification, the failure load and failure mode of the beams were calculated assuming full composite action between the FRP and the concrete. The calculation is performed according to EC2 [9], similar as normally done for steel reinforced concrete beams and as explained in Section 4.2 as well as in Chapter 7, Section 3.3. For the verification, the experimentally obtained material properties were considered (Appendix B) and all material safety factors were taken equal to one. The initial strains before strengthening were taken into consideration. Results of this calculation are given in Table 3-4. From this table it is noted that the FRP bond failure, experimentally obtained, happened close to the expected failure load assuming full composite action (except for BF8).

Table 3-4 *Analytical verification assuming full composite action*

Spec.	Experimental		Analytical verification		
	Q_u [kN]	Failure mode	Q_u [kN]	Failure mode	Q_{exp}/Q_{ana} [-]
BF1	144.2	YS/CC	141.8	YS/CC	1.02
BF2	185.0	DB(YS)/CC	200.2	YS/CC	0.92
BF3	186.0	DB(YS)/CC	196.7	YS/CC	0.95
BF4	184.2	DB(YS)/CC	187.3	YS/CC	0.98
BF5	177.0	DB(YS)/CC	191.8	YS/CC	0.92
BF6	183.0	DB(YS)/CC	198.9	YS/CC	0.92
BF7	80.7	YS/CC	78.2	YS/CC	1.03
BF8	111.3	DB(YS)	165.8	YS/CC	0.67
BF9	95.8	DB(YS)/CC	97.0	YS/FF	0.99

YS/CC: yielding of the steel followed by concrete crushing
YS/FF: yielding of the steel and fracture of the FRP
DB(YS): debonding of the FRP (after yielding of the steel)

4.1.2 Verification of anchorage failure

In addition to the calculation of the previous section, loss of composite action between the FRP and the concrete should be verified. With this aim, a literature study on bond failure modes and models was performed as reported in Chapter 7, Section 3.4. From this study it appeared that critical bond stress concentrations occur at the FRP ends (anchorage zones) and at the location of cracks. Although the experimental results indicate that FRP bond failure did not occur in the anchorage zone, this is verified analytically in the following. Verification of bond failure due to crack bridging is performed in Section 4.1.3.

According to [10-12], the maximum FRP force $N_{fa,max}$ which can be anchored and the corresponding transfer or anchorage length $\ell_{t,max}$ are given by (Chapter 7, Section 3.4.4):

$$N_{fa,max} = \alpha k_b b_f \sqrt{2 c_F f_{ctm} E_f t} \tag{3-1}$$

$$\ell_{t,max} = 1.57 \alpha \sqrt{\frac{c_F E_f t}{f_{ctm}}} \tag{3-2}$$

where, f_{ctm} is the mean tensile strength, E_f is the modulus of elasticity of the FRP, b_f and t are the width and thickness of the FRP, c_F = 0.202 mm is a factor which is related to the fracture energy, α = 0.9 is a reduction factor to account for the influence of inclined cracks on the bond strength [12] and k_b is a size factor given by:

$$k_b = 1.06 \sqrt{\frac{2 - b_f/b}{1 + b_f/b_o}} \geq 1.0 \tag{3-3}$$

where, b is the width of the beam, b_o = 400 mm and b_f/b should not to be taken less than 0.5.

To verify anchorage failure, $N_{fa,max}$ should be compared with the acting force $N_{fQu}(\ell_{t,max})$ at a distance $\ell_{t,max}$ from the end of the FRP, when reaching ultimate load. This force can be calculated from (Chapter 7, Section 3.4.4.2):

$$N_f(x) \approx \frac{M(x)}{z\left(1 + \frac{A_s E_s}{A_f E_f}\right)} \qquad \text{for} \qquad M(x)/z \leq A_s f_y \tag{3-4}$$

where, M(x) is the moment at a distance x from the FRP end, z is the lever arm between the total tensile force and the compression force and f_y is the yield stress of the steel. For the calculation of $N_{fQu}(\ell_{t,max})$, z was taken equal to 0.95d and the moment line corresponding to Q_u was shifted over a distance z/2 to consider the increase in the tension force due to inclined cracking. As demonstrated in Table 3-5, $N_{fa,max}$ is substantially larger than the acting force $N_{fQu}(\ell_{t,max})$. Hence, anchorage failure did not occur according to this model.

Table 3-5 *Verification of anchorage failure*

Spec.	$Q_{u,exp}$ [kN]	$N_{fa,max}$ [kN]	$\ell_{t,max}$ [mm]	$N_{fQu}(\ell_{t,max})$ [kN]	$N_{fa,max}/N_{fQu}(\ell_{t,max})$ [-]
BF2	185.0	48.5	166	21.4	2.27
BF3	186.0	47.6	169	21.7	2.19
BF4	184.2	45.1	179	21.9	2.05
BF5	177.0	49.0	164	20.4	2.40
BF6	183.0	> 48.2	-	-	-
BF8	111.3	50.1	161	23.0	2.18
BF9	95.8	24.4	89	5.2	4.68

4.1.3 Verification of bond failure due to crack bridging

As cracks are bridged by the FRP, bond stress concentrations occur at both sides of the cracks (Chapter 7, Section 3.4.6). In the case of shear cracks or flexural cracks in regions with significant shear forces, a relative displacement of the crack faces occurs both horizontally

and vertically. As a result of the vertical crack displacement, the FRP is submitted to a peeling action which is very unfavourable (Fig. 3-9, left) and may result in bond failure when reaching a critical value of the vertical crack width. This crack width is related to the internal forces transferring shear across the crack, as shown in Fig. 3-9 (right). In this figure, V_{cz} is the shear in the compression zone, V_a is the vertical component of the aggregate interlock shear contribution and V_d is the dowel action by the longitudinal reinforcement (steel and FRP).

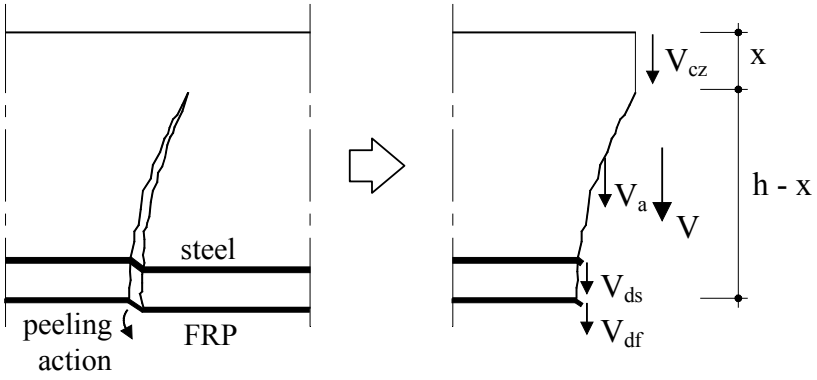

Fig. 3-9 *Peeling at a shear crack or a flexural crack with high shear forces*

Based on this approach, the following model is proposed in [7] for the resisting shear force V_{Rp} at which shear crack peeling initiates:

$$V_{Rp} = \tau_{cza} b\left(x + (h - x)\left(1 - \frac{w}{w_{crit}} \right) \right) + \chi \Sigma(EA) \tag{3-5}$$

where,

- τ_{cza} represents the shear stress transferred by the compression zone and by aggregate interlock, when peeling occurs,
- x is the depth of the compression zone,
- $\Sigma(EA) = E_s A_s + E_f A_f$ is the axial stiffness of the tension reinforcement,
- χ is coefficient relating the dowel action to the axial stiffness of the reinforcement and which is assumed to be:

$$\chi = \frac{v}{w}\left(\sqrt{1 + \frac{v^2}{w^2}} - 1 \right) \approx \text{constant} \tag{3-6}$$

- v and w are the vertical and horizontal crack displacements respectively,
- w/w_{crit} is the ratio of the horizontal crack width to the critical crack width at which there is no longer an aggregate interlock contribution and can be expressed as:

$$\frac{w}{w_{crit}} \approx \frac{\varepsilon_o + \varepsilon_f}{\varphi} \tag{3-7}$$

- $(\varepsilon_o + \varepsilon_f)$ is the strain at the extreme tension fibre (FRP strain taking into account the initial strain ε_o before strengthening),
- $\varphi = w_{crit}/s_{mr}$ is the ratio of the critical crack width at which there is no longer an aggregate interlock contribution to the mean crack spacing.

For the calculation of V_{Rp} according to Eq. (3-5), x and $(\varepsilon_o + \varepsilon_f)$ can be determined based on equilibrium of forces and strain compatibility (Section 4.2) and depend on the acting load. Hence, Eq. (3-5) should be solved by iteration. In [7], by means of an experimental calibration, the model parameters were determined as $\tau_{cza} = 2.2$ N/mm^2, $\varphi = 6.06\ 10^{-3}$ and $\chi = 1.03\ 10^{-3}$ and refer to a concrete grade C25/30, prefab CFRP, $E_f = 120000 \sim 150000$ N/mm^2 and $t = 0.5 \sim 1.0$ mm.

Results of the calculation according to Eq. (3-5) are given in Table 3-6. Except for beam BF9, for which a wet lay-up CFRP type was used, an accurate prediction of the failure load is obtained. Nevertheless, evaluating the calculation of the tested beams according to Eq. (3-5) and the model parameters proposed in [7], it appeared that the term $(1 - (\varepsilon_o + \varepsilon_f)/\varphi)$ is smaller than 0, which would correspond to a negative aggregate interlock contribution. This inconsistency results from the original calibration in [7], where the restriction $(1 - (\varepsilon_o + \varepsilon_f)/\varphi) \geq 0$ has probably not been taken into account.

To derive improved values for τ_{cza}, φ and χ, Eq. (3-5) was re-evaluated based on the experimental data given in Appendix C, Section 1. First, the factor χ was determined from the slope of the τ_{Rp}-ρ_{eq} relationship:

$$\tau_{Rp} = \tau_{cza}\left(\frac{x}{d} + \frac{h-x}{d}\left(1 - \frac{\varepsilon_o + \varepsilon_f}{\varphi}\right)\right) + \chi E_s \rho_{eq} \qquad (3\text{-}8)$$

where, $\tau_{Rp} = V_{Rp}/bd$ is the nominal shear stress corresponding to V_{Rp} and $\rho_{eq} = \rho_s + \rho_f E_f/E_s$ is the equivalent reinforcement ratio. In Fig. 3-10, the shear stress τ_{Rp} according to Eq. (3-8), with $\tau_{cza} = 2.2$ N/mm^2, $x/d = 0.3$, $(1 - (\varepsilon_o + \varepsilon_f)/\varphi) = 0$, $\chi = 1.03\ 10^{-3}$ and $E_s = 200000$ N/mm^2, is compared with the experimental data. From this comparison it follows that the contribution of the axial stiffness of the reinforcement (slope of the curve) is overestimated and hence that χ should decrease. A linear regression of the test data yields:

$$\tau_{Rp} = (0.54 + 151\rho_{eq}) \qquad [\text{N/mm}^2] \qquad (3\text{-}9)$$

which corresponds to a value $\chi = 0.75\ 10^{-3}$. Next, based on a curve fitting of Eq. (3-8) and the experimental data, $\tau_{cza} = 0.71$ N/mm^2 and $\varphi = 25.1\ 10^{-3}$ were derived.

Table 3-6 *Verification of peeling at shear cracks*

Spec.	Experimental		Analytical $V_{Rp} = Q_p$							
	Q_u [kN]	ε_{fQu} [mm/m]	$Q_p^{(1)}$ [kN]	$\varepsilon_{fp}^{(1)}$ [mm/m]	$Q_u/Q_p^{(1)}$ [-]	$Q_p^{(2)}$ [kN]	$\varepsilon_{fp}^{(2)}$ [mm/m]	$Q_u/Q_p^{(2)}$ [-]	$Q_p^{(3)}$ [kN]	$Q_u/Q_p^{(3)}$ [-]
BF2	185.0	6.7	186.5	8.0	0.99	185.9	7.7	1.00	180.0	1.03
BF3	186.0	7.2	186.2	8.1	1.00	185.8	7.8	1.00	180.0	1.03
BF4	184.2	6.8	185.1	8.4	1.00	185.5	8.2	0.99	180.0	1.02
BF5	177.0	5.7	174.7	5.7	1.01	182.2	6.9	0.97	180.0	0.98
BF6	183.0	7.1	186.3	8.0	0.98	185.9	7.7	0.98	180.0	1.02
BF8	111.3	5.8	113.3	6.8	0.98	122.3	8.0	0.91	119.5	0.93
BF9	95.8	10.0	83.7	7.3	1.14	96.9	14.5	0.99	108.4	0.88

(1) Eq. (3-5), with $\tau_{cza} = 2.2$ N/mm^2, $\chi = 1.03\ 10^{-3}$ and $\varphi = 6.06\ 10^{-3}$

(2) Eq. (3-5), with $\tau_{cza} = 0.71$ N/mm^2, $\chi = 0.75\ 10^{-3}$ and $\varphi = 25.1\ 10^{-3}$

(3) Eq. (3-9)

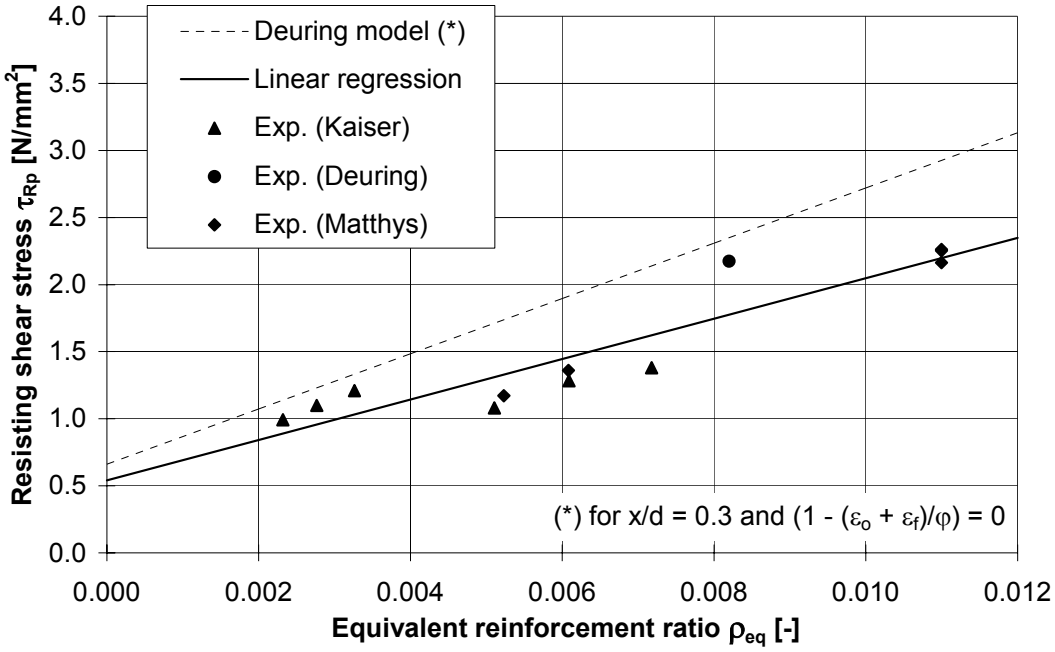

Fig. 3-10 *Verification of shear crack bridging*

Results of the analytical verification according to the re-calibrated model are shown in Table 3-6. Fairly accurate predictions are obtained. The improved model parameters apply for a concrete grade C25/30 and externally bonded CFRP reinforcement.

Alternatively, as Eq. (3-8) is rather complex to calculate, the resisting shear force at which shear crack peeling initiates can be obtained form Eq. (3-9). In this case (Table 3-6, Fig. 3-10) still fairly accurate predictions are obtained, although subject to a larger scatter

4.2 Moment-strain behaviour

The behaviour of the beams under increasing load can be evaluated as classically done, based on strain compatibility and equilibrium of forces (EC2 [9]). Fig. 3-11 shows the principle of the calculation. The following assumptions are made:

- The stress-strain behaviour of the constituent materials is modelled as shown in Fig. 3-12.
- The tensile strength of the concrete is neglected.
- Strains are proportional along the depth of the section.
- Slip at the concrete-steel and concrete-FRP interfaces are ignored.
- The FRP thickness is small so that the effective depth of the FRP reinforcement may be taken equal to the total beam depth h.

Taking the concrete strain ε_c at the top fibre as a parameter, the strain in the steel ε_s, the strain in the FRP ε_f and the moment M, can be derived as follows. Defining the parameter λ, equal to:

$$\lambda = \frac{0.002}{\varepsilon_c} \tag{3-10}$$

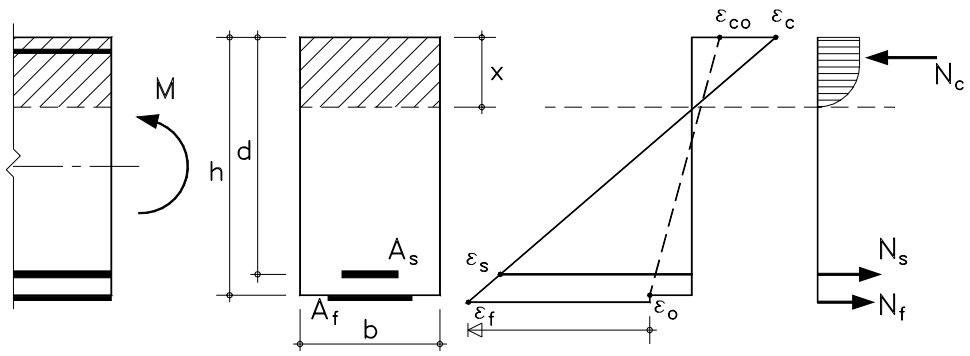

Fig. 3-11 *Principle of calculation*

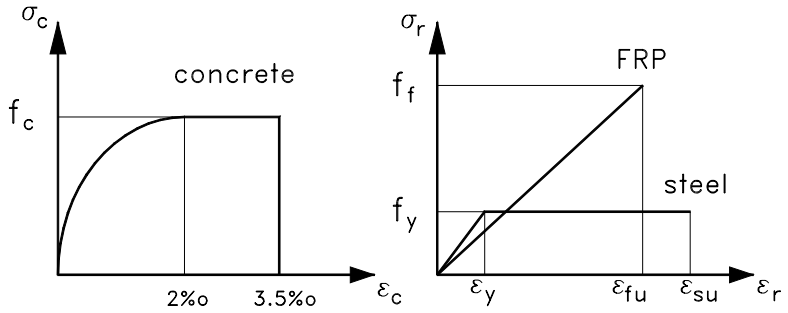

Fig. 3-12 *Stress-strain models of constituent materials*

the following coefficients related to the concrete stress block can be defined [14]:

$$\begin{aligned} &\lambda \geq 1: \quad \psi = \frac{3\lambda - 1}{3\lambda^2} \quad \delta_G = \frac{4\lambda - 1}{4(3\lambda - 1)} \\ &\lambda \leq 1: \quad \psi = 1 - \frac{\lambda}{3} \quad \delta_G = \frac{\lambda^2 - 4\lambda + 6}{4(3 - \lambda)} \end{aligned} \tag{3-11}$$

with, ψ the ratio of the average over the maximum concrete compressive stress (stress block area coefficient) and δ_G the distance from the compression face to the compression force divided by the depth of the compression zone (stress block centroid coefficient).

The depth of the compression zone x and the strains ε_s and ε_f can be evaluated based on the equilibrium of forces ($\Sigma N = 0$) and strain compatibility:

$$\psi b x f_c = A_s E_s \varepsilon_s + A_f E_f \varepsilon_f \tag{3-12}$$

where,

$$\begin{aligned} &\varepsilon_s = \varepsilon_c \frac{d - x}{x} \quad \text{with} \quad \varepsilon_s \leq \frac{f_y}{E_s} \\ &\varepsilon_f = \varepsilon_c \frac{h - x}{x} - \varepsilon_o \end{aligned} \tag{3-13}$$

and with ε_o the initial strain of the extreme tension fibre before strengthening. From the equilibrium of moments ($\Sigma M = 0$), the bending moment is obtained as:

$$M = \psi b x f_c (d - \delta_G x) + A_f E_f \varepsilon_f (h - d) \tag{3-14}$$

Before strengthening Eqs. (3-12) and (3-14) are applied with $A_f = 0$. When reaching the moment M_o at which the FRP EBR is applied, the strain ε_o follows from:

$$\varepsilon_o = \varepsilon_{co} \frac{h - x}{x} \tag{3-15}$$

with $\varepsilon_c = \varepsilon_{co}$ the concrete strain at the top fibre corresponding to M_o.

According to the above equations the behaviour of the beams was verified analytically. The concrete strain ε_c (and hence M) was increased step wise until reaching the failure load derived in the previous section. Results of the calculation, compared with the recorded strains, are given in Appendix C, Section 2 as well as in Fig. 3-13 for beams BF1 and BF2. Except for low moments, i.e. were the concrete is not yet cracked, fairly accurate predictions are obtained. From this comparison it can be concluded that the behaviour of the strengthened members can indeed be analysed according to the classical approach.

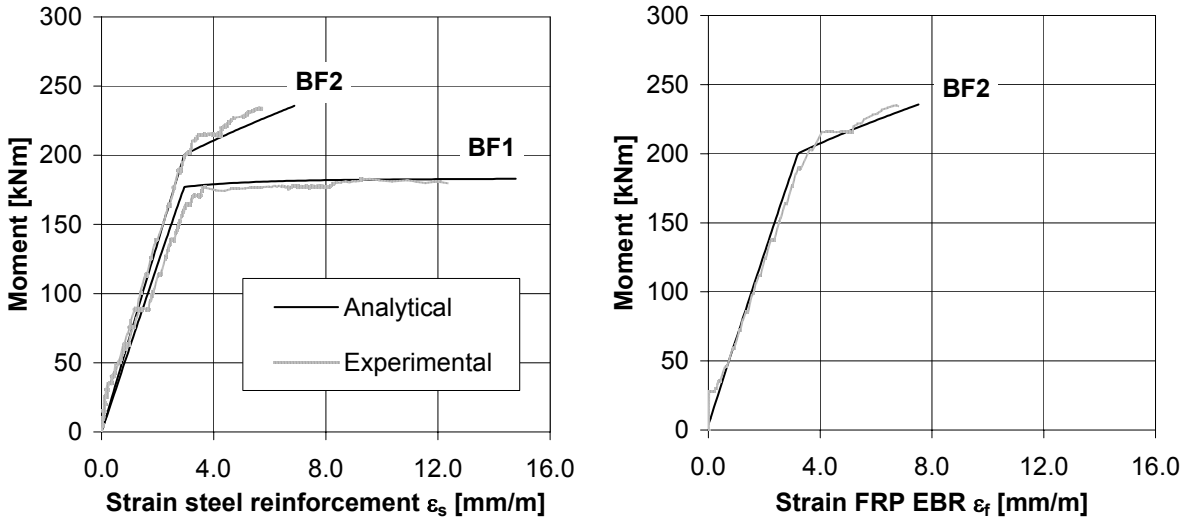

Fig. 3-13 *Reinforcement tensile strain of beams BF1 and BF2*

4.3 Moment-curvature and moment-deflection behaviour

In order to verify the beam deflections, the load-curvature behaviour at midspan was evaluated first. The curvature is calculated taking into account the tension stiffening effect (Chapter 5). Considering states 1 and 2 as the uncracked and the fully cracked state respectively, the mean curvature 1/r follows from [15]:

$$1/r = (1 - \zeta)\, 1/r_1 + \zeta\, 1/r_2 \tag{3-16}$$

with, ζ a distribution or tension stiffening coefficient defined as:

$$\begin{aligned} \zeta &= 0 && M < M_{cr} \\ \zeta &= 1 - \beta_1 \beta_2 \left(\frac{M_{cr}}{M} \right)^n && M > M_{cr} \end{aligned} \tag{3-17}$$

where, β_1 is a coefficient taking into account the bond characteristics of the reinforcement, β_2 is a coefficient taking into account the loading type, n is a power equal to 2 and M_{cr} is the cracking moment.

According to theory of elasticity the curvatures $1/r_1$ and $1/r_2$ follow from:

$$1/r_1 = \frac{M}{E_c I_1} \qquad 1/r_2 = \frac{M}{E_c I_2} \tag{3-18}$$

with, I_1 and I_2 the moment of inertia of the uncracked and cracked section respectively:

$$I_1 = \frac{b x_{e1}^3}{3} + \frac{b(h - x_{e1})^3}{3} + (\alpha_s - 1)A_s(d - x_{e1})^2 + \alpha_f A_f (h - x_{e1})^2 \tag{3-19}$$

$$I_2 = \frac{b x_{e2}^3}{3} + \alpha_s A_s (d - x_{e2})^2 + \alpha_f A_f (h - x_{e2})^2 \tag{3-20}$$

where, x is the depth of the compression zone, α_s equals E_s/E_c and α_f equals E_f/E_c. The depth of the compression zone follows from the equilibrium of forces:

$$\frac{b x_{e1}^2}{2} = \frac{b(h - x_{e1})^2}{2} + \alpha_s A_s (d - x_{e1}) + \alpha_f A_f \left(h - x_{e1}\left(1 + \varepsilon_o/\varepsilon_c\right)\right) \tag{3-21}$$

$$\frac{b x_{e2}^2}{2} = \alpha_s A_s (d - x_{e2}) + \alpha_f A_f \left(h - x_{e2}\left(1 + \varepsilon_o/\varepsilon_c\right)\right) \tag{3-22}$$

and depends on the ratio $\varepsilon_o/\varepsilon_c$ (ε_o is the initial strain at the extreme tension fibre before strengthening and ε_c the concrete strain at the extreme compression fibre). As this ratio is not constant, x and I depend on the acting load level. However, it was verified that the influence of $\varepsilon_o/\varepsilon_c$ on the calculation of I is limited (e.g. for the beams in this test programme, I_2 varied with 0.2 % maximum) so that $\varepsilon_o/\varepsilon_c$ may be assumed 0. Based on the geometrical characteristics the cracking moment is given as:

$$M_{cr} = f_{ctm} \frac{I_1}{h - x_{e1}} \tag{3-23}$$

where, f_{ctm} is the mean concrete tensile strength.

The above equations are valid for strengthened and unstrengthened members, where in the latter case $A_f = 0$. In reality, to account for the moment at which the strengthening is applied, a combination of both should be considered. Accordingly, the curvature in the cracked state is given as:

$$\begin{aligned} 1/r_2 &= \frac{M}{E_c I_{o2}} && M \le M_o \\ 1/r_2 &= \frac{M - M_o}{E_c I_2} + \frac{M_o}{E_c I_{o2}} && M > M_o \end{aligned} \tag{3-24}$$

where, I_o is the moment of inertia before strengthening. The curvature $1/r_1$ may be calculated in a similar way. However, as $I_{o1} \approx I_1$, Eq. (3-18) may still be applied.

Furthermore, it is noted that Eq. (3-22) and hence the flexural stiffness $E_c I_2$ only apply as long as $M \le M_y$, with M_y the moment at which the internal steel starts yielding.

To allow the calculation of the curvature for moments larger than M_y and to increase the accuracy, in stead of a linear elastic analysis the curvature in the cracked state can be calculated based on a non-linear analysis:

$$1/r_2 = \frac{\varepsilon_c}{x} \tag{3-25}$$

where, the concrete strain ε_c at the extreme compression fibre and the depth x of the compression zone are obtained according to Section 4.2.

The moment-curvature behaviour of the beams was verified according to the above two methods (linear and non-linear, taking into account the tension stiffening). As it is difficult to differentiate the influence of the bond behaviour of the internal steel and the external FRP reinforcement on the tension stiffening effect, it was assumed that the coefficients β_1 and β_2 as defined in EC2 [9] and the power n equal to 2 remain valid. This assumption gave a good agreement between experimental results and analytical verification. Accordingly, $\beta_1\beta_2$ was taken equal to 1 (short term loading, deformed steel). The calculation of the cracking moment M_{cr} was based on a concrete tensile strength [13]:

$$f_{cr} = 0.62\sqrt{f_{cm}} \tag{3-26}$$

with, f_{cr} and f_{cm} in N/mm^2. This gives the most accurate predictions (Table 3-7). Also in [14] the use of Eq. (3-26) in stead of f_{ctm} is recommended for the calculation of M_{cr}.

Results of the calculation are given in Appendix C, Section 3 as well as in Fig. 3-14. Both methods almost exactly match each other (for $M < M_y$) and give accurate predictions.

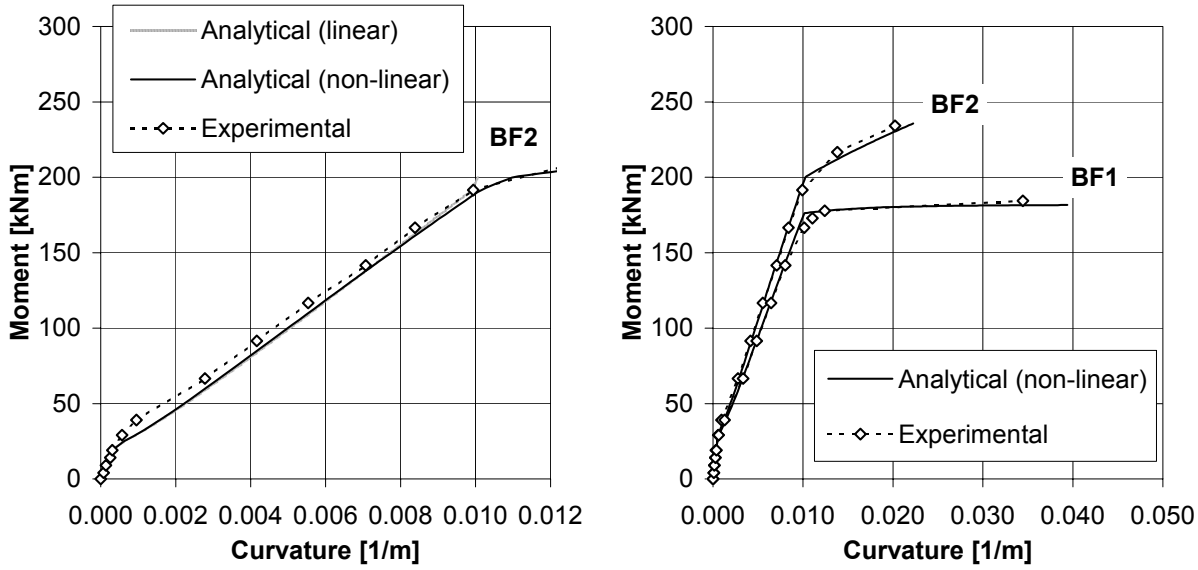

Fig. 3-14 *Curvature of beams BF1 and BF2*

In addition to the moment-curvature, also the moment-deflection behaviour of the beams was verified. Based on the method of virtual work, the deflection at midspan is derived as:

$$a = \int (1/r)\,\overline{M}\,dx \tag{3-27}$$

with, $\overline{M}$ the moment line of a beam with a point load Q = 1 at midspan and 1/r the curvature according to Eq. (3-16), calculated either linear, Eq. (3-24), or non-linear, Eq. (3-25). In the latter case, Eq. (3-27) has to be solved by numerical integration.

As an alternative, which is more simple to calculate, the mean deflection can be derived according to the so-called CEB bilinear method [16]:

$$a = (1 - \zeta_b)\, a_1 + \zeta_b a_2 \tag{3-28}$$

with, a_1 and a_2 the deflections in respectively the uncracked and the fully cracked state and ζ_b the distribution (tension stiffening) coefficient:

$$\begin{aligned} \zeta_b &= 0 && M < M_{cr} \\ \zeta_b &= 1 - \beta_1\beta_2\left(\frac{M_{cr}}{M}\right)^{n/2} && M > M_{cr} \end{aligned} \tag{3-29}$$

The deflection in the uncracked state a_1 and in the fully cracked state a_2 can be calculated by theory of elasticity, referring to a flexural stiffness in respectively the uncracked state E_cI_1 and the fully cracked state E_cI_2. In the case of the tested beams and taking into account the load Q_o at which the FRP EBR is applied:

$$a_g = \frac{5}{384}\frac{g\ell^4}{E_c I_1} \tag{3-30}$$

$$a_{1Q} = \frac{Q}{24E_c I_1}\ell_1\left(3\ell^2 - 4\ell_1^{\,2}\right) \tag{3-31}$$

$$\begin{aligned} a_{2Q} &= \frac{Q}{24E_c I_2}\ell_1\left(3\ell^2 - 4\ell_1^{\,2}\right) && Q \le Q_o \\ a_{2Q} &= \frac{1}{24}\left(\frac{Q_o}{E_c I_{o2}} + \frac{Q - Q_o}{E_c I_2}\right)\ell_1\left(3\ell^2 - 4\ell_1^{\,2}\right) && Q > Q_o \end{aligned} \tag{3-32}$$

where, a_g is the midspan deflection due to self weight g, a_Q is the midspan deflection due to the point loads Q, ℓ is the span of the beam and ℓ_1 is the distance between the point load Q and the support.

The moment-deflection behaviour of the beams was verified according to the above three methods (linear/integration, non-linear/numerical integration and bi-linear method). Results of the calculation are given in Appendix C, Section 4 and in Fig. 3-15 for beams BF1 and BF2.

4.4 Cracking

As also applied in the two previous sections, the cracking moment of the beams can be calculated according to Eq. (3-23) or simplified as:

$$M_{cr} = f_{ctm}\frac{bh^2}{6} \tag{3-33}$$

Furthermore, as also suggested in [13,14], more accuracy may be obtained when the concrete tensile strength f_{ctm} is replaced by f_{cr} according to Eq. (3-26). A comparison between the calculated cracking load and the obtained experimental load is given in Table 3-7. From this table it follows that Q_{cr} is underestimated when reference is made to f_{ctm}, while better predictions are obtained when using f_{cr}. With f_{cr}, both Eq. (3-23) and Eq.(3-33) (simplified calculation) give fairly accurate results, although subject to a significant scatter.

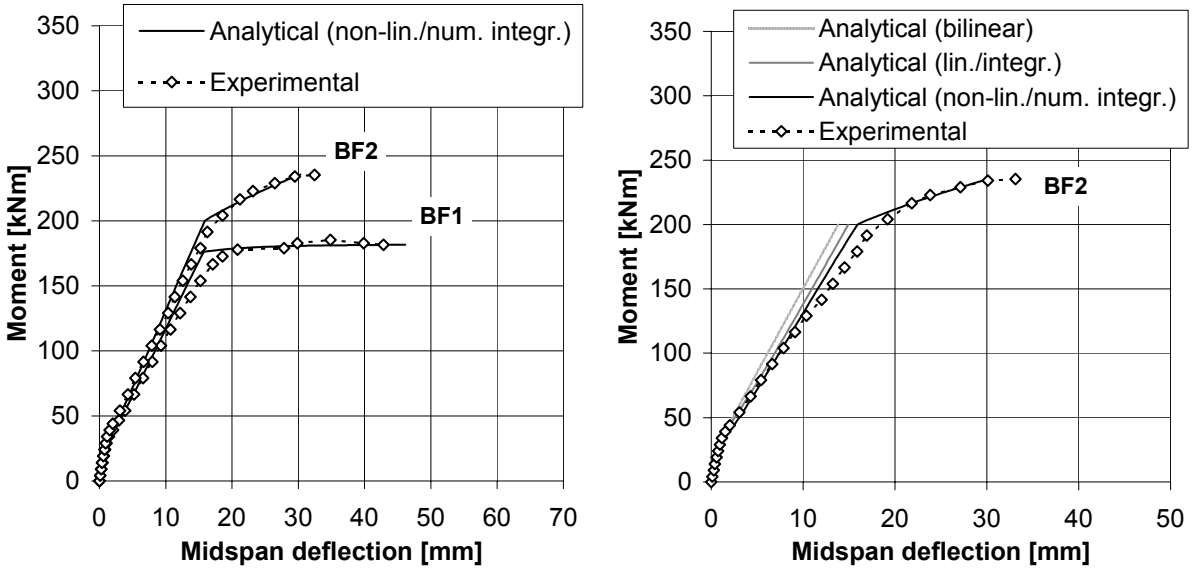

Fig. 3-15 *Deflection of beams BF1 and BF2*

Table 3-7 *Verification of the cracking load*

Spec.	$Q_{cr,exp}$ [kN]	f_{cm} [N/mm^2]	f_{ctm} [N/mm^2]	f_{cr} [N/mm^2]	$Q_{cr}^{(1)}$ [kN]	$Q_{cr}^{(2)}$ [kN]	$Q_{cr}^{(3)}$ [kN]	$Q_{cr,exp}/Q_{cr}^{(1)}$ [-]	$Q_{cr,exp}/Q_{cr}^{(2)}$ [-]	$Q_{cr,exp}/Q_{cr}^{(3)}$ [-]
BF1	16	33.7	2.61	3.60	13.1	19.3	16.2	1.22	0.83	0.99
BF2	16	36.5	2.80	3.75	14.6	20.7	17.0	1.10	0.77	0.94
BF3	16	34.9	2.69	3.66	14.0	20.2	16.5	1.14	0.79	0.97
BF4	20	30.8	2.41	3.44	11.9	18.4	15.3	1.68	1.09	1.31
BF5	20	37.4	2.86	3.79	14.6	20.4	17.2	1.37	0.98	1.16
BF6	28	35.9	2.76	3.71	14.4	20.5	16.8	1.94	1.37	1.60
BF7	18	38.5	2.93	3.85	15.0	20.7	17.5	1.20	0.87	1.03
BF8	20	39.4	2.99	3.89	15.7	21.5	17.8	1.27	0.93	1.12
BF9	18	33.7	2.61	3.60	13.5	19.8	16.2	1.33	0.91	1.11

(1) Eq. (3-23), f_{ctm}; (2) Eq. (3-23), f_{cr}; (3) Eq.(3-33), f_{cr}

In addition to the cracking load, also the crack width is verified analytically. For the modelling of the crack width, reference is made to Chapter 5. In this chapter, a model for the calculation of the mean crack width is derived based on experiments on strengthened tension members. As will be demonstrated in the following, the derived model is also applicable to strengthened flexural members.

Assuming stabilized cracking, the mean crack width is given by [9]:

$$\begin{aligned} w_m &= s_{rm}\varepsilon_{rm,r} \\ &= s_{rm}\zeta\,\varepsilon_{r2} \end{aligned} \tag{3-34}$$

with, s_{rm} the mean crack spacing, $\varepsilon_{rm,r}$ the mean strain of the reinforcement with respect to the surrounding concrete, ζ the tension stiffening coefficient according to Eq. (3-17) and ε_{r2} the reinforcement strain in the cracked section. Assuming $\varepsilon_{r2} \approx \varepsilon_s \approx \varepsilon_f + \varepsilon_o$, the latter strain can be obtained according to Section 4.2 or also, with $N_r = \varepsilon_s A_s E_s + \varepsilon_f A_f E_f$:

$$\varepsilon_{r2} = \frac{N_r + E_f A_f \varepsilon_o}{E_s A_s + E_f A_f} \tag{3-35}$$

where, $N_r = M/z_e$ is the total tensile force and $z_e \approx 0.9d$. Before strengthening, Eq. (3-35) can be applied with $A_f = 0$.

The mean crack spacing s_{rm}, for the unstrengthened reference specimens, is taken according to EC2 [9] as:

$$s_{rm} = 50\,\text{mm} + 0.25 k_1 k_2 \, Ø/\rho_r \tag{3-36}$$

with, $k_1 = 0.8$ for deformed steel, $k_2 = 0.5$ for bending, Ø the (mean) diameter of the steel reinforcement and $\rho_r = A_s/A_{c,eff}$. The effective concrete area in tension $A_{c,eff}$ is taken as the smaller of 2.5(h - d)b and (h - x)b/3. Based on Chapter 5, the mean crack spacing for the strengthened members is given as:

$$s_{rm} = \frac{2 f_{ctm} A_{c,eff}}{\tau_{sm} u_s} \frac{E_s A_s}{E_s A_s + \xi_b E_f A_f} \qquad \text{with} \qquad \xi_b = \frac{\tau_{fm} E_s Ø}{\tau_{sm} E_f 4t} \tag{3-37}$$

where, $\tau_{sm} = 1.8 f_{ctm}$ [15] and $\tau_{fm} = 1.25 f_{ctm}$ [17] are the mean bond stress of the steel and the FRP, u_s is the bond perimeter of the steel, ξ_b a bond parameter and t is the FRP thickness (total thickness for multiple layers).

Results of the analytical verification of the mean crack width are shown in Appendix C, Section 5, as well as in Fig. 3-16 for beams BF1 and BF2. Fairly accurate predictions are obtained. As the models for the calculation of the crack width are intended to be used at service load level, the accuracy at higher load levels is generally less.

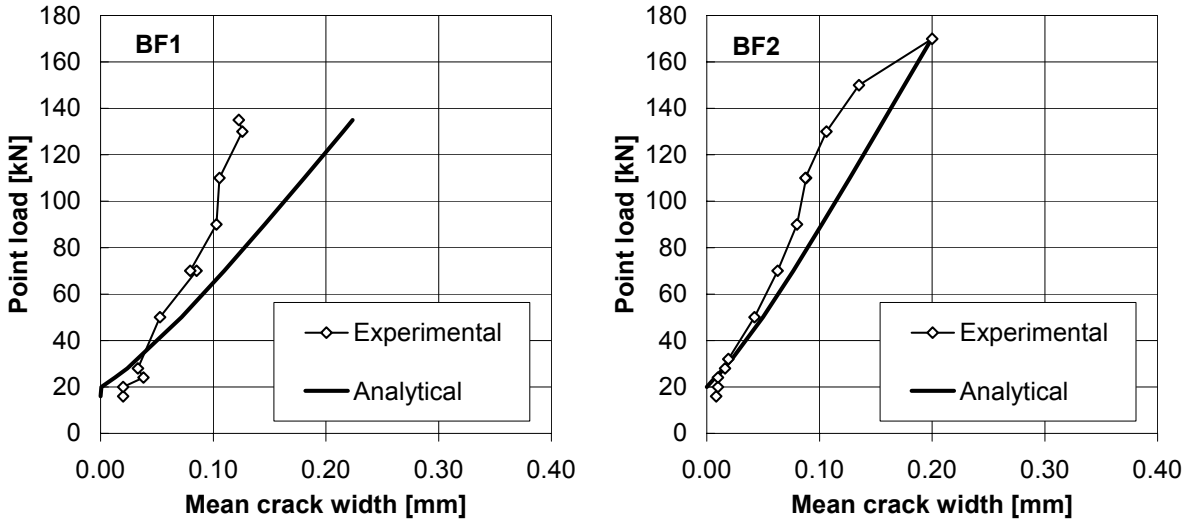

Fig. 3-16 *Verification of the mean crack width*

4.5 Strains and bond shear stresses along the FRP EBR

Based on Section 4.2, the strains along the length of the FRP can be calculated. As this calculation does not account for the transfer zone at the FRP end and for the local strain distribution at the location of cracks, it does not provide an exact representation of the FRP

strain but rather gives the overall behaviour. In the calculation reference is made to the shifted moment line (shift 0.45d, to account for the tension increase due to inclined shear cracks).

In Appendix C, Section 6, the calculated and measured strain distribution are compared for beams BF3 and BF9. For these beams the FRP strain was measured at various locations (although the measuring grid was not dense enough to detect local strain distributions at the location of cracks) up to ultimate load. The results for beam BF3 are also shown in Fig. 3-17. Except for the transfer (or anchorage) zone, the measured and calculated FRP strains correspond fairly well. Furthermore, it is noted that the FRP strain significantly increases after yielding of the internal steel (in Fig. 3-17, Q = 150 kN is just before yielding). Indeed, as also illustrated in Fig. 7-5, once the yield stress in the steel is reached, a further increase of the total tensile force (and hence the moment) is mainly related to the FRP EBR.

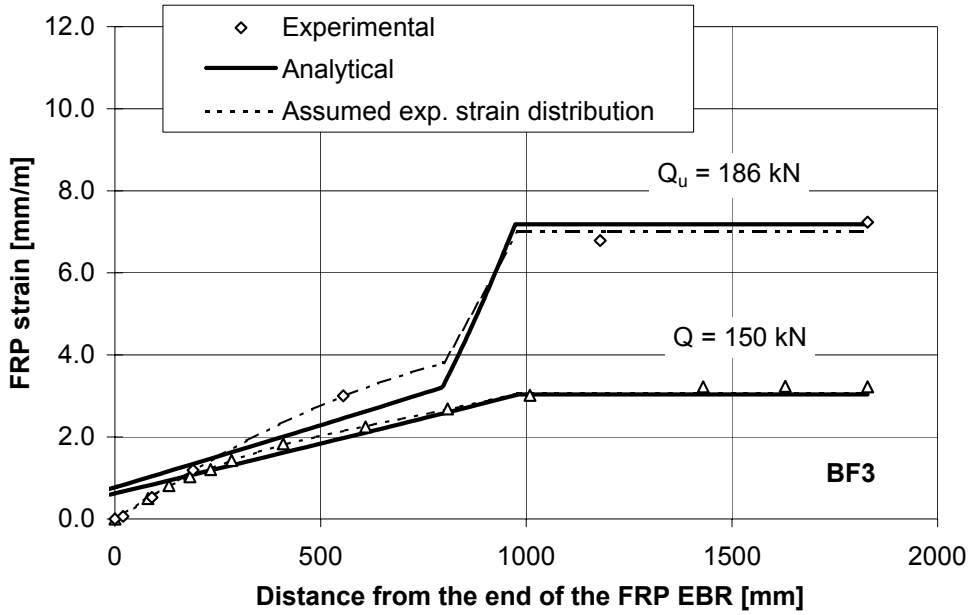

Fig. 3-17 *Verification of the FRP strain distribution for beam BF3*

Based on the FRP strain distribution an indication of the bond shear stress along the FRP EBR can be obtained. As illustrated in Fig. 3-18, the variation of the FRP force ΔN_f over a small distance Δx, initiates a bond shear stress:

$$\tau_b = \frac{\Delta N_f}{b_f \Delta x} = \frac{\Delta \varepsilon_f}{\Delta x} E_f t \tag{3-38}$$

where, b_f and t are the width and thickness of the FRP respectively. The bond shear stress τ_b is calculated, as shown in Appendix C, Section 6, based on the calculated and measured FRP strains. In the latter case, by means of curve fitting, a strain distribution was assumed as also shown for beam BF3 in Fig. 3-17. The corresponding calculated bond shear stress is shown in Fig. 3-19. A shear stress concentration is noted at the FRP end as well as near the point load after yielding of the internal steel. The calculated bond shear stress does not exceed the bond shear strength $\tau_{max} \approx 1.8 f_{ctm}$.

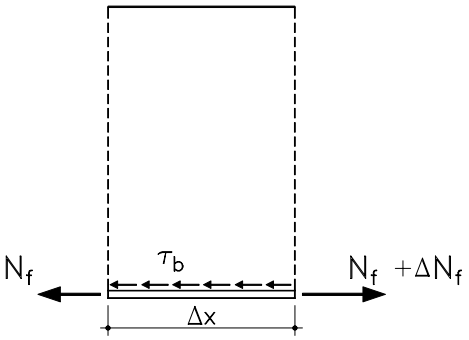

Fig. 3-18 *Bond shear stress along the FRP EBR*

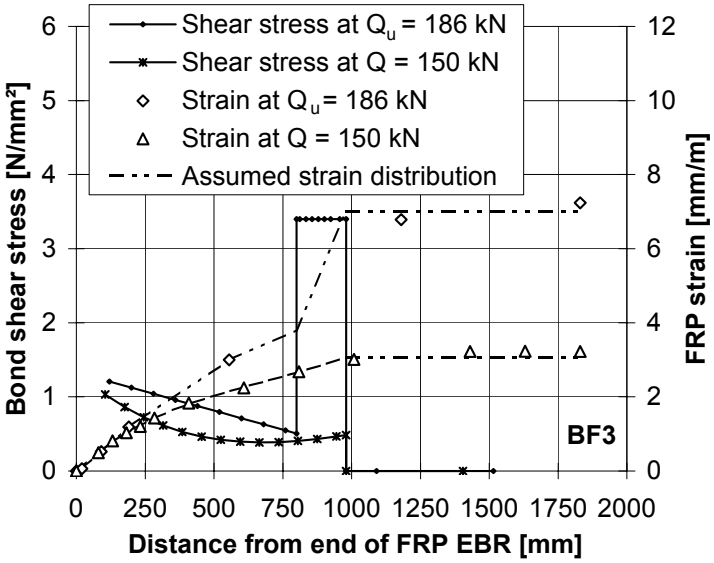

Fig. 3-19 *Calculated bond shear stress for beam BF3*

4.6 Service load, safety and ductility

4.6.1 Service load

In Table 3-8, the service load of the tested beams is given based on a verification in the ultimate limit state (ULS) and the serviceability limit state (SLS). The calculation is performed according to Chapter 7. The service load Q_{ser} equals the smallest value of:

- Q_{k1}, ULS calculation assuming full composite action between the concrete and the FRP. This calculation is based on equilibrium of forces and strain compatibility, taking into account appropriate partial safety factors (Chapter 7, Section 3.3).
- Q_{k2}, ULS calculation verifying loss of composite action with respect to shear crack bridging. This calculation is performed according to Eq. (3-9), taking into account appropriate safety factors as specified in Chapter 7, Section 3.4.6.2.
- Q_{k3}, SLS calculation with respect to the stress limitations defined in Chapter 7, Section 3.5.2. From this calculation it appeared that Q_{k3} is governed by the limitation of the concrete stress under the rare load combination.
- Q_{k4}, SLS calculation with respect to an allowable deflection $a_{lim} = \ell / 250$ [9]. As also noted from Appendix C, a_{lim} is only reached for loads larger than the load Q_y at which the steel starts yielding.
- Q_{k5}, SLS calculation with respect to an allowable crack width w_{lim} = 0.3 mm [9]. As also noted from Appendix C, w_{lim} is not reached for $Q < Q_y$.

As noted from Table 3-8, the service load Q_{ser} of the reference beams is governed by the ULS. For the strengthened beams BF2-BF6, Q_{ser} is restricted by the allowable concrete compressive stress in the SLS (although almost the same service load is found with respect to bond failure in the ULS). For beams BF8 and BF9, the service load is governed by FRP bond failure in the ULS.

Table 3-8 *Service load of the tested beams*

Spec.	Exp.	ULS		SLS		Q_{ser}	Ratios	
	Q_u [kN]	Q_{k1} [kN]	Q_{k2} [kN]	Q_{k3} [kN]	$Q_{k4\&5}$ [kN]	(= $Q_{k,min}$) [kN]	Q_u/Q_{ser} [-]	$Q_{u,ref}/Q_{ser}$ [-]
BF1	144.2	63.4	-	71.6	> 137.5	63.4	2.27	2.27
BF2	185.0	77.8	74.2	74.1	> 155.8	74.1	2.50	1.95
BF3	186.0	77.8	74.2	74.1	> 155.8	74.1	2.51	1.95
BF4	184.2	77.8	74.2	74.1	> 155.8	74.1	2.49	1.95
BF5	177.0	72.3	74.2	71.6	> 142.1	71.6	2.47	2.01
BF6	183.0	77.8	74.2	74.1	> 155.8	74.1	2.47	1.95
BF7	80.7	33.2	-	56.0	> 69.8	33.2	2.43	2.43
BF8	111.3	60.9	47.2	60.3	> 88.3	47.2	2.36	1.71
BF9	95.8	44.1	42.5	58.2	> 75.7	42.5	2.25	1.90

4.6.2 Ratio of ultimate to service load

The safety of the beams against an overloading situation is evaluated based on the ratio of the ultimate to the service load (Table 3-8). A ratio Q_u/Q_{ser} between 2.25 and 2.51 is found for all the beams. In the case of the strengthened beams BF2-BF6 (for which Q_{ser} is governed by the SLS), the ratio Q_u/Q_{ser} increases with respect to that of the reference beam BF1. For beams BF8 and BF9 (Q_{ser} governed by the ULS), Q_u/Q_{ser} slightly decreases compared to the reference beam BF7.

Furthermore, it can be noted from Table 3-8 that the service loads of the strengthened beams in this test programme remain smaller than the ultimate load of the reference beams. Hence, in case of accidental loss of the FRP EBR under service load, the beams will not collapse. The safety against overloading in case of this accidental situation is given by the ratio $Q_{u,ref}/Q_{ser}$.

4.6.3 Ductility

The curvature and hence the deflection at ultimate load of the strengthened beams decrease, as demonstrated in Fig. 3-4 and Table 3-3. A curvature ductility index $\delta_{1/r}$ may be defined as the ratio of the ultimate curvature to the curvature at yielding of the internal steel. Values of $\delta_{1/r}$ for the tested beams are given in Table 3-9. A decrease of the ductility index between 25 % and 68 % is found for the strengthened beams.

To guarantee a minimum ductility of the strengthened beams, the internal steel should sufficiently yield at ultimate load. In Chapter 7, Section 2.4.3 (based on [9]) a minimum ductility index $\delta_{1/r,min}$ = 1.72 (C25/30, S500) is suggested. Although the low values of $\delta_{1/r}$, values larger than $\delta_{1/r,min}$ are found for all the tested strengthened beams.

Table 3-9 *Curvature ductility index*

Spec.	$1/r_u$ [1/m]	$1/r_y$ [1/m]	$\delta_{1/r}$ [-]	$\Delta\delta_{1/r}/\delta_{1/r,ref}$ [-]
BF1	0.0344	0.0104	3.31	-
BF2	0.0202	0.0107	1.89	0.43
BF3	0.0226	0.0107	2.11	0.36
BF4	0.0211	0.0107	1.97	0.40
BF5	0.0256	0.0103	2.49	0.25
BF6	0.0193	0.0107	1.80	0.46
BF7	0.0493	0.0085	5.80	-
BF8	0.0162	0.0088	1.84	0.68
BF9	0.0258	0.0088	2.93	0.49

5 Conclusions

From the conducted experimental and analytical study on RC beams strengthened in flexure, by means of externally bonded CFRP reinforcement, the following is concluded:

- Strengthening with external CFRP reinforcement is an efficient technique, which allows to increase the failure load and flexural stiffness of reinforced concrete beams.
- For the beams in this test programme, strength increases between 1.2 and 1.4 were obtained. All the strengthened beams failed by FRP debonding in a sudden way. Although it was difficult to find out where failure initiated, it appeared that debonding was due to vertical crack displacement (and not of anchorage failure).
- Strengthening of a pre-cracked beam did not result in a significantly lower strengthening ratio. Also the application of FRP EBR on initially loaded beams, still allows a considerable strength increase. For beam BF5, loaded prior to strengthening at 1.7 times the service load of the reference beam, only a 4 % lower failure load was obtained compared to a similar strengthened beam which was not initially loaded.
- As the FRP EBR increases the stiffness of the beams and as a denser crack pattern with smaller crack widths is obtained, also the serviceability limit state (SLS) of the beams is positively influenced. Because already small amounts of FRP increase the failure load to a large extent, the efficiency with respect to the SLS is generally less than that with respect to the ultimate limit state (ULS).
- The ductility of the strengthened beams decreased in a considerable way (between 25 % and 68 %), but remained above a minimum curvature ductility index defined in Chapter 7, Section 2.4.3.
- The service load of the strengthened beams appeared to be governed by either the SLS or FRP bond failure in the ULS. The safety against an overloading situation slightly decreased for those strengthened beams for which the design is governed by the ULS. In case the SLS governs the design, larger safety against overloading is obtained for strengthened beams compared to reference beams. The obtained ratio of the ultimate to the service load varied between 2.25 and 2.51.

- Information obtained from the analytical verification of the test results allowed to propose and evaluate calculation models. Classical calculation methods for RC beams still apply as long as full composite action between the FRP and the concrete may be assumed. Verification of the possible loss of this composite action, is the most complex aspect in the calculation. To predict FRP bond failure at the location of shear cracks or flexural cracks in regions with high shear forces, an existing models was evaluated and re-calibrated. As this model involves an iterative calculation, also a simplified equation (based on experimental curve fitting) has been proposed.
- The structural behaviour of the beams in terms of ultimate load, failure type, strains, curvatures, deflections and crack widths could be predicted in an accurate way.

6 References

1. Matthys S., Taerwe L. (1996), "Versterking van beton met hoogwaardige vezelcomposietlaminaten" (in Dutch), Bouwkroniek, Extra editie : Betondag 24-10-1996, pp. 55-57.
2. Depla J. (1996), "Aanwending van composietmaterialen voor de versterking en de herstelling van betonconstructies" (in Dutch), Graduation thesis, Ghent University, Departement of Structural Engineering, Magnel Laboratory for Concrete Research, 152 pp.
3. Matthys S. (1997), "Versterking van structurele betonelementen met opgelijmde vezelcomposietlaminaten" (in Dutch), Infrastructuur in het Leefmilieu, Departement Leefmilieu en Infrastructuur, Ministerie van de Vlaamse Gemeenschap, nr. 4/97, pp. 274-298.
4. Matthys S. (1998), "Vezelcomposietlaminaten: Uitwendige versterking van constructieve betonelementen" (in Dutch), Cement, 50° jaargang, nr. 2, pp. 50-58.
5. Matthys S., Taerwe L., Khalil H. (1998), "Strengthening by means of externally bonded FRP reinforcement", Proceedings of the XIIIth. FIP Congress 1998 on Challenges for Concrete in the Next Millennium, Amsterdam, The Netherlands, Eds. D. Stoelhorst, G.P.L. den Boer, Betonvereniging, published by A.A. Balkema, Vol. 2, pp. 643-647.
6. Hollaway L.C., Leeming M.B., Eds., "Strengthening of Reinforced Concrete Structures Using Externally-Bonded FRP Composites in Structural and Civil Engineering", Woodhead Publishing Limited, Cambridge, 1999, 327 pp.
7. Deuring M. (1993), "Verstärken von Stahlbeton mit gespannten Faserverbund-werkstoffen" (in German), EMPA Bericht, No 224, Swiss Federal Laboratories for Materials Testing and Research, Dübendorf, Switzerland, 279 pp.
8. Cha J.Y., Balaguru P., Chung L. (1999), "Experimental and Analytical Investigation of Partially Prestressed Concrete Beams Strengthened with Carbon Reinforcement", Proceedings 4th. Int. Symp. on Fibre Reinforced Polymer Reinforcement for Reinforced Concrete Structures, Eds. C.W. Dolan, S.H. Rizkalla, A. Nanni, American Concrete Institute, Mitchigan, USA, pp. 625-634.

9. CEN (1991), “Eurocode 2: Design of concrete structures – Part 1-1: General rules and rules for buildings”, ENV 1992-1-1, Comité Européen de Normalisation (CEN), Brussels, Belgium, 263 pp.
10. Rostásy F.S., Holzenkämpfer P., Hankers Ch. (1996), “Geklebte Bewehrung für die Verstärkung von Betonbauteilen” (in German), Betonkalender 1996, Vol. II, pp. 547-576.
11. Blaschko M., Niedermeier R., Zilch K. (1998), “Bond Failure Modes of Flexural Members Strengthened with FRP”, Proceedings 2nd. Int. Conf. On Composites in Infrastructure, Tucson, USA, 15 pp.
12. Neubauer U., Rostásy F.S. (1999), “Bond Failure of Concrete Fibre Reinforced Polymer at Inclined Cracks – Experiments and Fracture Mechanics Model”, Proceedings 4th. Int. Symp. on Fibre Reinforced Polymer Reinforcement for Reinforced Concrete Structures, Eds. C.W. Dolan, S.H. Rizkalla, A. Nanni, American Concrete Institute, Mitchigan, USA, pp. 369-382.
13. ACI (1983), “Building Code Requirements for Reinforced Concrete”, ACI 318-83, American Concrete Institute, Detroit, Michigan, USA, 111 pp.
14. Lambotte H., Van Nieuwenburg D. (1991), “Gewapend beton” (in Dutch), Ghent University, Faculty of Applied Science, Magnel Laboratory for Concrete Research, 546 pp.
15. CEB (1993), “CEB-FIP Model Code 1990, Design Code”, Comité Euro-International du Béton, Lausanne, Switzerland, Thomas Telford, 437 pp.
16. CEB (1985), “CEB-Manual Cracking and Deformations”, CEB Bulletin d'Information No. 158-E, Comité Euro-International du Béton, Lausanne, Switzerland, 248 pp.
17. Holzenkämpfer P. (1994), “Ingenieurmodelle des Verbunds geklebter Bewehrung für Betonbauteile” (in German), Doctoral thesis, Vol. 108, , Technical University Braunschweig, Germany, 214 pp.

Chapter 4
STRUCTURAL BEHAVIOUR OF RC BEAMS STRENGTHENED IN SHEAR

Whereas flexural strengthening of RC beams has been discussed in Chapter 3, this chapter reports on the experimental and analytical study concerning the structural behaviour of RC beams strengthened in shear. The feasibility of shear strengthening with externally bonded FRP reinforcement is demonstrated and the efficiency of different strengthening configurations is considered. To predict the contribution of the FRP to the shear capacity, a model for the effective ultimate FRP strain is proposed.

1 Introduction

Little research has been reported concerning the behaviour of RC beams strengthened in shear. Nevertheless, existing structures with a deficient shear capacity have been reported, e.g. [1]. A lack of shear capacity may also be obtained after flexural strengthening (whereas the unstrengthened beam has sufficient shear capacity, this may no longer be the case for the load capacity of the beam strengthened in flexure). To study the feasibility of shear strengthening by means of externally bonded CFRP and to derive or verify an appropriate calculation model, the test programme outlined in the previous chapter was extended. Using the same test set-up and overall specimen dimensions, seven additional beams were tested [2,3]. The main parameters considered in this test programme deal with the strengthening configuration (amount and lay-out of the externally bonded FRP reinforcement) and the amount of internal stirrups. The test programme was restricted to unidirectional CFRP sheets (wet lay-up type), applied in a vertical way (perpendicular to the beam main axis).

2 Outline of the experiments

2.1 Test specimens and material properties

Seven RC beams, 2 reference specimens and 5 specimens strengthened in shear, were manufactured. The beam overall dimensions equal those given in Chapter 3, Section 2.1. An overview of the test specimens and main characteristics is given in Table 4-1. The strengthening lay-out and test set-up are given in Fig. 4-1.

With respect to the number of internal steel stirrups, two series of beams were tested. Beams BS1-BS2, comprised 6 mm diameter stirrups, spaced 200 mm centre to centre, while 400 mm stirrup spacing was used for beams BS3-BS7. Except for the reference specimens (BS1 and BS3), the beams were strengthened in shear by means of CFRP sheets according to the strengthening lay-out shown in Fig. 4-1. To provide extra anchorage, the FRP was not

only bonded to the sides of the beam alone, but also to the top and/or bottom side. U-shaped (sides and soffit) shear strengthening was applied for beams BS4 and BS5. Combined U-shape and reversed U-shape sheets were used for beams BS2 and BS6. For beam BS7 the FRP was wrapped all around the beam, with an overlap equal to the beam width (closed-shape). Although the latter strengthening lay-outs are normally not applicable in practice, the same effect may be derived if the FRP is anchored.

For the stirrups deformed steel bars S500 were used, with a characteristic tensile strength of 500 N/mm^2 and a diameter of 6 mm. The flexural reinforcement consisted of 6 diameter 20 mm rebars (ρ_s = 2.33 %). The externally bonded reinforcement consisted of 1 layer Replark with a nominal (equivalent dry fibre) thickness of 0.111 mm. The width of the sheets, for beams BS2, 5, 6 and 7 was taken equal to 50 mm. To force the shear failure at one shear span the width was doubled at the opposite shear span for beams BS2 and BS7. For BS4, the width covered the total shear span. The main characteristics of the reinforcement, obtained by tensile testing (Appendix B), are summarized in Table 4-2. The stress-strain behaviour of the reinforcement is shown in Fig. B-2. For all beams the same concrete grade was used. The mean concrete compressive strength for the specimens at the age of testing are given in Table 4-1. The average strength at 28 days equals 35.0 N/mm^2. Detailed information on the material properties of the reinforcements, fresh and hardened concrete can be found in Appendix B.

Table 4-1 *Test parameters RC beams strengthened in shear*

Spec.	**Strengthening lay-out** (see Fig. 4-1)	**Age at test** [days]	**f_{cm}** [N/mm^2]	**Stirrups** [mm]	**FRP width** [mm]	**FRP spacing** [mm]
BS1	Unstrength. (ref.)	56	35.0	Ø 6 at 200	-	-
BS2	2 strips (∪&∩ shape)	272	33.8	Ø 6 at 200	50/100[(1)]	400
BS3	Unstrength. (ref.)	114	37.5	Ø 6 at 400	-	-
BS4	Full shear span (∪shape)	138	38.4	Ø 6 at 400	1070	-
BS5	3 strips (∪shape)	152	36.0	Ø 6 at 400	50	400
BS6	2 strips (∪&∩ shape)	189	35.8	Ø 6 at 400	50	400
BS7	3 strips (closed shape)	247	34.7	Ø 6 at 400	50/100[(1)]	200

[(1)] Different widths in both shear spans

Table 4-2 *Mean tensile properties obtained by tensile testing*

Type	**Nominal dimensions** [mm]	**Yield strength** [N/mm^2]	**Tensile strength** [N/mm^2]	**Ultimate strain** [%]	**E-modulus** [N/mm^2]
Rebar S500	Ø 6	560	590	5.1	200000
	Ø 20	530	620	11.9	200000
Replark MRK-M2-20	100 x 0.111[(1)]	-	3500	1.25	233000[(2)]

[(1)] Equivalent dry-fibre thickness, [(2)] Tangent modulus at the origin

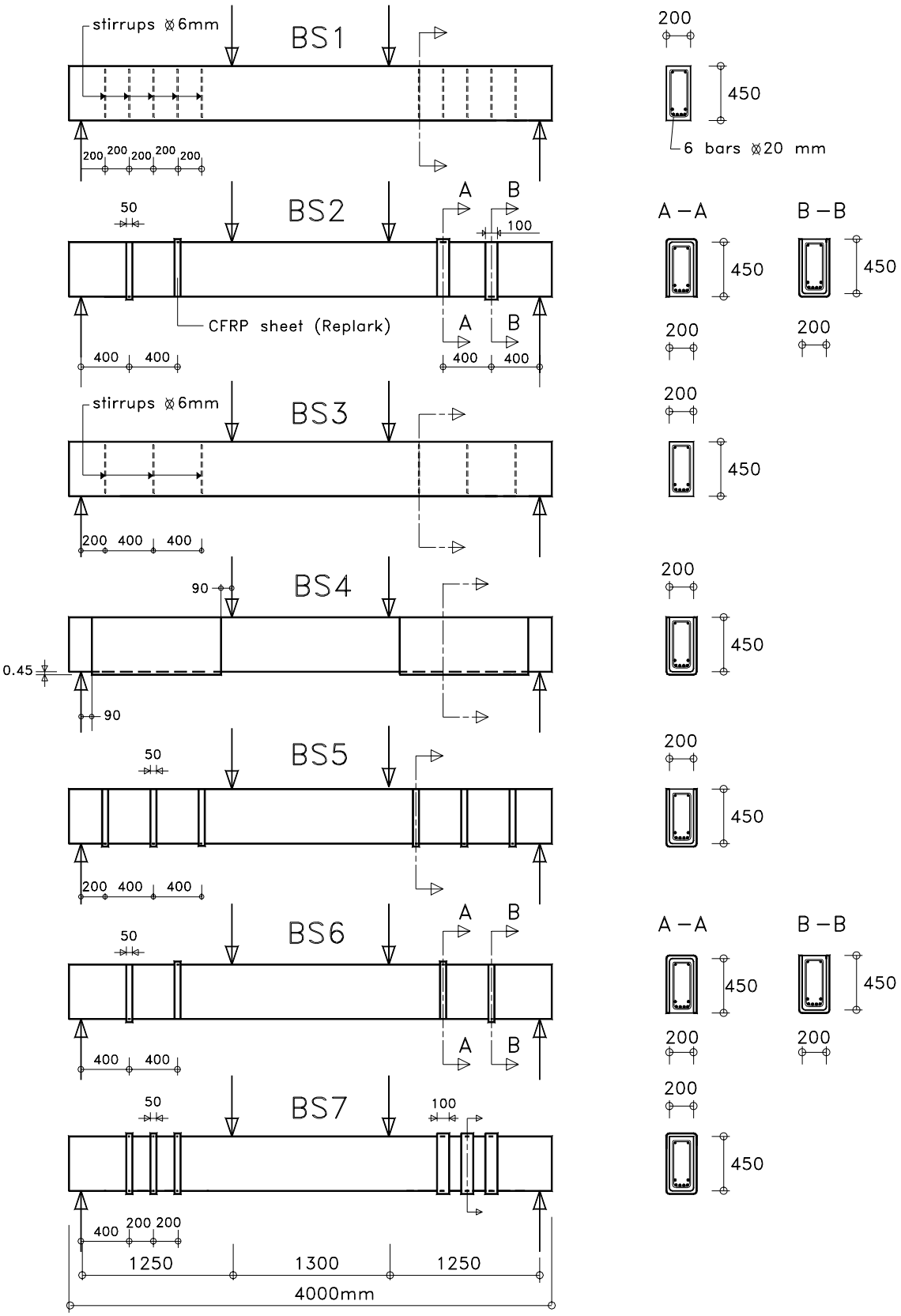

Fig. 4-1 *Test set-up and strengthening scheme*

2.2 Specimen preparation and test procedure

The specimens were prepared and tested in a similar way as described in Chapter 3, Section 2.2. Preparation of the concrete surface included sand blasting for all beams. Corners, at the location of the FRP sheets, were rounded with a diameter of 30 mm. The beams were tested in 4-point bending as shown in Fig. 4-1, with a shear span to depth ratio a/d of 3.1. The load was increased stepwise (to allow for manual measurements) for a safe part of the expected ultimate load, after which the load was gradually increased until failure. Typically, point load increments of 10 or 20 kN were chosen, except in the vicinity of the cracking load where the increments were reduced to 4 kN.

During the tests, measurements were taken in the shear spans and central zone of the beams. Deflections were measured at midspan, under the point loads and the supports, using dial gauges and potentiometric displacement transducers, similar as for the beams BF (Fig. 3-2). Mechanical deformeters with a gauge length of 200 mm and 50 mm were used to measure concrete and FRP deformations. In the central zone of the beam, concrete strains were measured at the top, at half of the beam depth and at the reinforcement level. The concrete strains at the top and at the reinforcement level were also recorded electronically by means of strain stirrups (Fig. 3-2). Mechanical deformeter measurements in the shear spans on and in between the FRP sheets gave very small strains (the shear span strains significantly increased at higher load levels at which no longer manual measurements were taken) and are not further considered. Electronic measurements (up to failure) were taken in the shear spans at various locations by means of strain gauges (60 mm gauge length). Details on the location of these measurements are given in Appendix D, Section 1. At each load interval, the appearance and the development of cracks were indicated and crack widths were measured by means of a small microscope.

3 Test results

3.1 Failure load and mode of failure

The test results of the beams, in terms of ultimate load, failure mode, strength increase and ultimate deflection at midspan are given in Table 4-3. The crack pattern at ultimate load and the failure mode of the beams is also shown in Fig. 4-2.

Depending on the amount of external shear reinforcement, strength increases between 20 % and 84 % are found. Except for beam BS4, which failed in flexure, all beams failed by means of diagonal tension. This shear failure is characterized by a large diagonal shear crack which suddenly formed at a point load of about 100 kN and which further widened and propagated until failure. In the case of the strengthened beams, the diagonal tension failure was preceded by FRP bond failure and/or FRP rupture, as illustrated in Fig. 4-2.

Table 4-3 *Test results at ultimate load of RC beams strengthened in shear*

Spec.	Type of strength.	Q_u [kN]	Failure mode	Q_u/Q_{ref} [-]	y_u [mm]	y_u/y_{ref} [-]
BS1	Unstrength. (ref.)	206.3	S(DT)	1.00	19.3	1.00
BS2	2 strips (∪&∩ shape)	247.5	S(BF/DT)	1.20	27.6	1.43
BS3	Unstrength. (ref.)	136.6	S(DT)	1.00	12.4	1.00
BS4	Full shear span (∪shape)	252.0	F(YS/CC)	1.84	23.4	1.89
BS5	3 strips (∪shape)	170.0	S(BF/DT)	1.24	15.2	1.23
BS6	2 strips (∪&∩ shape)	166.7	S(BF/DT)	1.22	16.0	1.29
BS7	3 strips (closed shape)	235.5	S(DT)	1.72	23.0	1.85

S: shear failure, F: flexural failure
DT: diagonal tension, BF/DT: bond failure of (some) of the FRP sheets, followed by DT
YS/CC: yielding of the steel followed by concrete crushing

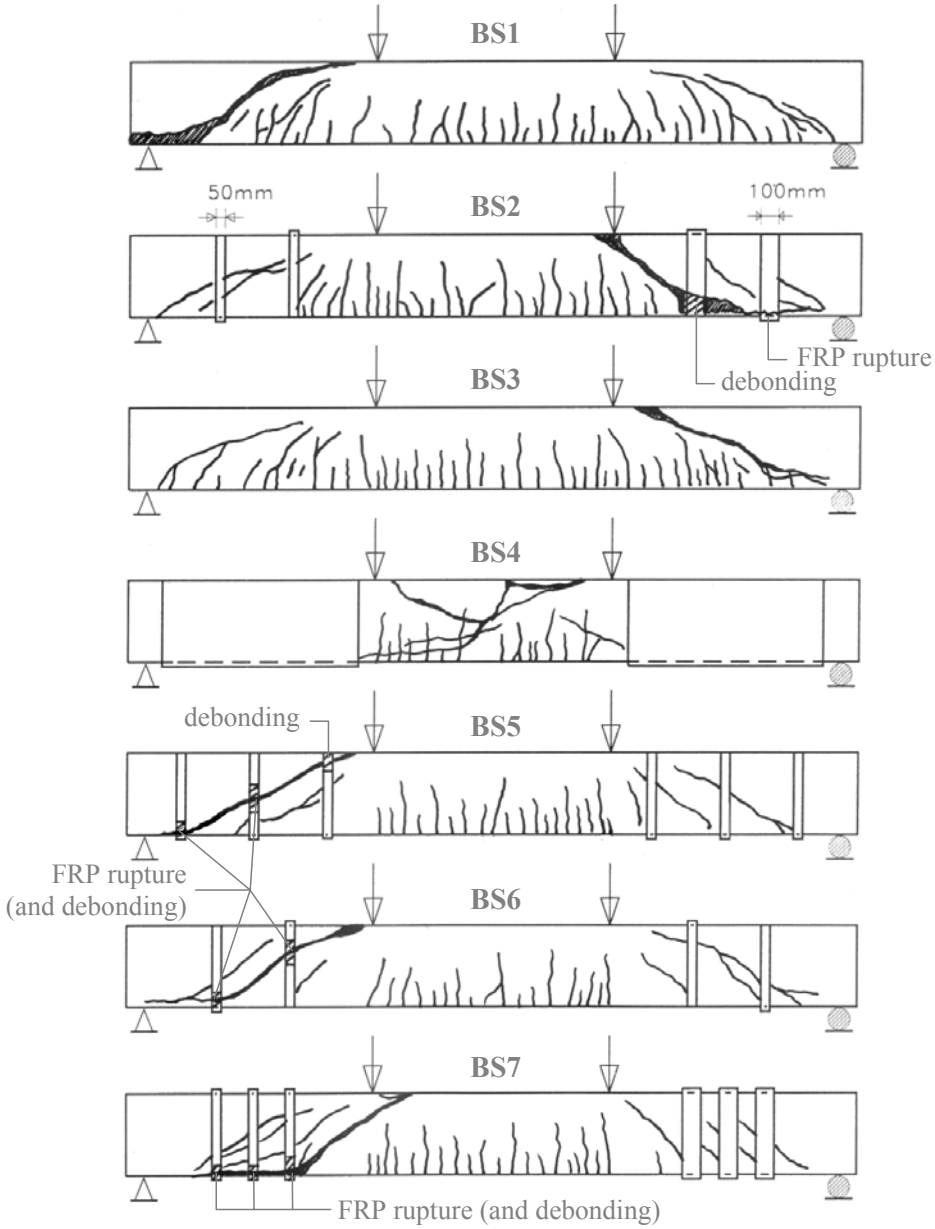

Fig. 4-2 *Crack pattern at ultimate load and failure mode*

Beam BS2 failed in the right shear span, at which wider FRP sheets (100 mm in stead of 50 mm) were provided. This particular result is due to the relatively large distance between the point load and the closest located FRP sheet. This distance, 1.1 times the effective depth of the beam, allowed the formation of a steep shear crack between the point load and the FRP sheet (Fig. 4-2). Due to variability of the concrete strength (and a possible small asymmetric loading between the left and right point load), this phenomenon appeared to be critical in the right shear span rather than in the left shear span. Other shear cracks, which appeared closer to the supports (in both shear spans) were bridged efficiently by the FRP. For beam BS4, the amount of FRP shear reinforcement was sufficient to prevent a shear failure, so that the beam failed in flexure. Due to the high reinforcement ratio of the flexural steel reinforcement, the beam failed by concrete crushing whereas the steel just started yielded (as may be noted from the recorded load-midspan deflection curve, Fig. 4-4). The failure mode of beams BS5 and BS6 is characterized by a shear crack which is bridged by the external FRP reinforcement. By bridging the shear crack, debonding occurred at both sides of the shear crack. At ultimate load and depending on the available anchorage length, the FRP failed either by bond failure or by sheet rupture. Failure of the FRP was immediately followed by diagonal tension failure. For beam BS7 the shear cracks were bridged by the FRP, so that finally (similar as for beam BS2) a diagonal tension failure occurred in the zone between the last FRP sheet and the point load. The shear crack even extended beyond the point load (Fig. 4-2). At the other end, this shear crack followed the position of the flexural steel reinforcement, where the FRP fractured.

3.2 FRP strains

By means of strain gauges the FRP strain in the shear spans was measured at different locations. The results of these measurements and the location of the strain gauges are shown in Appendix D, Section 1. The FRP strain of beam BS2 measured at the inner FRP sheet of the left shear span is also shown in Fig. 4-3. This figure clearly illustrates the variation of the FRP strain along the length of the FRP. Near the expected location of the diagonal shear crack (sg5 and sg6) the highest strain values are measured, while lower values are recorded at locations further away from the shear crack (sg7 and sg8).

3.3 Contribution of the internal and external shear reinforcement

In the test programme stirrups with a diameter of 6 mm and a yield strength of 590 N/mm^2 were used. Hence, the maximum force one stirrup can provide equals 33.4 kN. The difference in failure load between the reference beams BS1 and BS3 equals 69.7 kN. This indicates that the two additional stirrups in the critical shear span of BS1 were fully efficient (2 x 33.4 kN = 66.8 kN). The tensile strength of the CFRP sheets equals 3500 N/mm^2 (referred to a nominal thickness of 0.111 mm, Table 4-2), so that the ultimate load of a 50 mm wide CFRP sheet equals 19.4 kN (38.9 kN for a 100 mm wide sheet). As the CFRP is provided on both side faces, the maximum possible contribution of one 50 mm wide CFRP shear link equals 38.9 kN (77.8 kN for a 100 mm wide CFRP shear link).

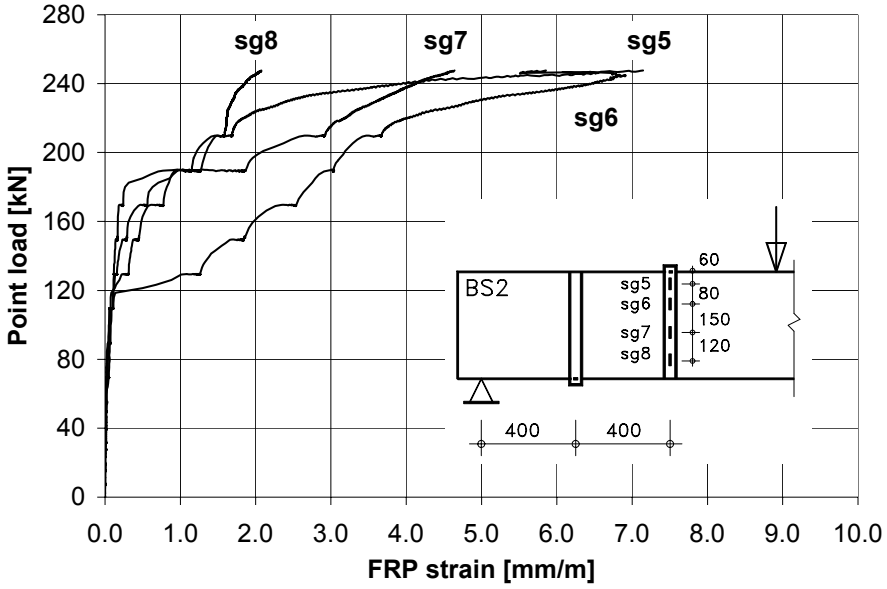

Fig. 4-3 *Measured FRP strains of beam BS2 (left shear span, inner FRP sheet)*

The actual shear contribution V_{wf} of the FRP shear links may be calculated by:

$$V_{wf} = E_f \varepsilon_{wf} A_{wf} n_a \tag{4-1}$$

where, E_f is the modulus of elasticity of the CFRP, ε_{wf} is the mean FRP strain at failure along the location of the shear crack, A_{wf} is the cross-sectional area of one CFRP shear link and n_a is the number of active shear links. The strain ε_{wf} can be estimated from the measured FRP strains (Appendix D, Section 1), by taking the mean value of the maximum recorded strain of each CFRP shear link in the critical shear span. As no measurements were performed in the critical shear span of beam BS2, for this beam the strains in the opposite shear span are considered. Calculated values of V_{wf} are given in Table 4-4. As the locations of the FRP strain measurements did not always coincide with the location of the critical shear crack, the values of V_{wf} mentioned in Table 4-4 are indicative. Nevertheless, it is of interest to compare V_{wf} with the difference in failure load between the strengthened and unstrengthened beams ($\Delta Q_u = \Delta V_u$). As noted from Table 4-4, a fairly good correspondence between V_{wf} and ΔV_u is found for beam BS2. However, this is not the case for the other beams.

For beams BS5 and BS6, significant larger values of V_{wf} are found than would be expected from the beam failure loads. This may be due to a, compared to the reference beam BS3, lower shear contribution of the steel stirrup near the support (Fig. 4-2) (a lower concrete shear contribution is unlikely, as will be demonstrated below). Furthermore, it is noted that although one more CFRP sheet is applied in each shear span of BS5, the failure loads of beams BS5 and BS6 are similar. As can be seen from Fig. 4-2, this is because the right sheet in the critical shear span of beam BS5 is not really activated.

For beam BF7, V_{wf} is significantly smaller than ΔV_u. Dividing the latter by 3 one obtains 33.0 kN, which almost equals the maximum possible contribution of one 50 mm wide CFRP shear link and which corresponds to a mean failure strain ε_{wf} of 10.6 mm/m (in stead of 8.8 mm/m estimated from the recorded strains).

Table 4-4 *Contribution of the CFRP sheets to the shear strength*

Spec.[1]	Type of strength.	V_u[2] [kN]	$V_u - V_{ref}$ [kN]	ε_{fm} [mm/m]	n_a	V_{wf} [kN]
BS1	Unstrength. (ref.)	210.6	-	-	-	-
BS2	2 strips (∪&∩ shape)	251.8	41.2	8.8	2	45.5
BS3	Unstrength. (ref.)	140.9	-	-	-	-
BS5	3 strips (∪shape)	174.3	33.4	9.9	2	51.2
BS6	2 strips (∪&∩ shape)	171.0	30.1	9.1	2	47.1
BS7	3 strips (closed shape)	239.5	98.9	8.8	3	68.3

(1) BS4 is not considered as it failed in flexure

(2) $V_u = Q_u + g\,\ell/2$, where g is the self weight of the beam

At failure of the strengthened beams, relatively large reinforcement strains and hence crack widths are obtained at the location of the critical shear crack. As a result, the question may be raised whether or not the concrete shear contribution decreases near ultimate load (due to less aggregate interlock in the wide shear crack). No visual sign of this was found during loading or from the failure mode. Based on beam BF7, for which it was demonstrated that ΔV_u equals nearly the maximum possible contribution of the CFRP sheets, it may be also be suggested that no significant decrease of aggregate interlock contribution occurred (or if so that it was compensated by a positive influence of the confining action of the external CFRP reinforcement). Also the good correspondence between V_{wf} and ΔV_u obtained for beam BS2 indicates no decrease in the concrete shear contribution.

3.4 Midspan deflection

The point load versus midspan deflection of the beams is shown in Fig. 4-4. To facilitate the comparison of the load-deflection behaviour, each successive curve in Fig. 4-4 is set off by an initial 2 mm deflection.

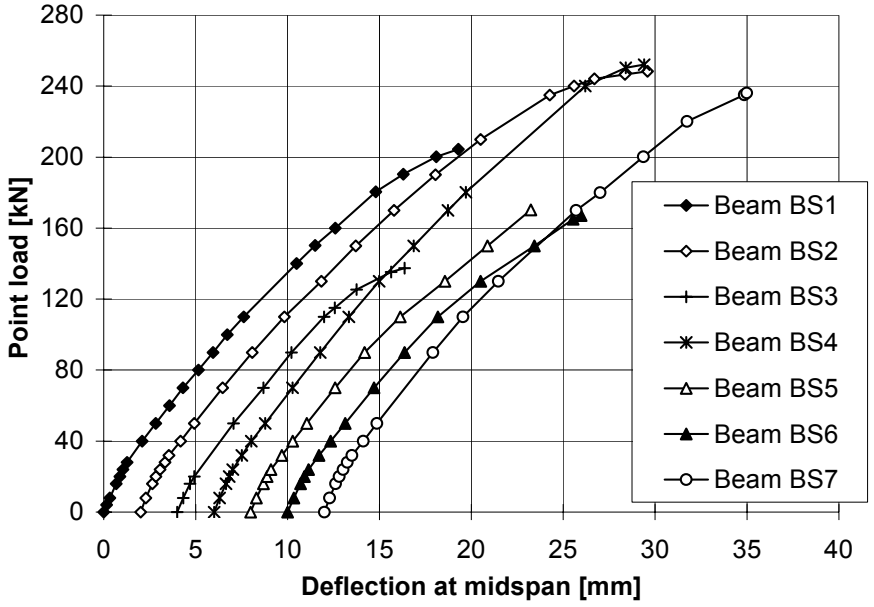

Fig. 4-4 *Deflection at midspan of the tested beams BS*

From Fig. 4-4 the strength increase is noted, whereas the flexural stiffness of the beams is almost identical (curves run parallel). The ultimate deflection at midspan y_u of the beams is given in Table 4-3. Compared to the unstrengthened reference beams, the beams strengthened in shear have a larger midspan deflection. Nevertheless, because of the shear failure the ultimate deflection at midspan remained limited. Also for beam BS4, which failed in flexure, y_u was comparable due to the high flexural steel reinforcement ratio. Hence, for none of the beams a warning in terms of a large increase of the deflection near ultimate load was obtained.

4 Analytical verification

4.1 Shear capacity of the reference beams and diagonal tension shear crack

The shear capacity of the reference beams is verified, based on a truss analogy (Mörsch), according to EC2 [4]. As the shear capacity of the concrete in diagonal compression (V_{Rd2} in EC2) is very large, the shear capacity of the reference beams is determined by that of the concrete and the internal steel stirrups:

$$V_R = V_c + V_{ws} \tag{4-2}$$

where, V_c is the shear capacity of the concrete:

$$V_c = \tau_{Rm} k(1.2 + 40\rho_l) b_w d \tag{4-3}$$

and V_{ws} is the contribution of the steel stirrups:

$$V_{ws} = \frac{A_{ws}}{s_s} 0.9 d f_{wy} (\cot\theta + \cot\alpha_s) \sin\alpha_s \tag{4-4}$$

with, $\tau_{Rm} = 0.25 f_{ctm}$ the mean shear resistance, $k = 1.6 - d \geq 1$ (d in meter), $\rho_l = A_{sl}/(b_w d) \leq 0.02$ the longitudinal reinforcement ratio, b_w the minimum width of the section, A_{ws} the cross-sectional area of the stirrups, s_s the stirrup spacing, f_{wy} the yield strength of the stirrups, θ the angle between the diagonal shear crack and the member longitudinal axis (generally assumed as 45°) and α_s the angle of the steel stirrups with respect to the member longitudinal axis (90° for the tested beams). Results of the analytical verification of the reference beams, according to Eqs. (4-2) till (4-4) and with $\theta = 45°$, are given in Table 4-5. The least accurate prediction is obtained for beam BS3. For this beam, it should be remarked that the stirrup spacing is larger than the maximum specified in EC2.

In [5] the shear force causing shear cracking is given as:

$$V_{cr} = 0.15(3d/a_v)^{1/3} \xi (100\rho_l f_{cm})^{1/3} b_w d \tag{4-5}$$

where, a_v is the distance from major load to support, $\xi = 1 + \sqrt{200/d}$ (d in mm) and $\rho_l = A_{sl}/(b_w d)$ is the longitudinal reinforcement ratio. Assuming $f_{cm} = 35.0$ N/mm^2, V_{cr} equal to 92.7 kN is obtained. This load more or less corresponds with the experimental point load at which a diagonal tension shear crack suddenly appeared.

Table 4-5 *Analytical verification reference beams*

Spec.	V_u [kN]	Failure mode	V_c [kN]	V_{ws} [kN]	V_R [kN]	V_u/V_R [-]
BS1	210.6	Diagonal tension	133.6	60.2	193.8	1.09
BS3	140.9	Diagonal tension	141.7	30.1	171.8	0.82

$V_u = Q_u + g\,\ell/2$, where g is the self weight of the beam

4.2 Shear capacity of the strengthened beams

It can be assumed that the shear capacity of the strengthened beams may be calculated in a similar way as for the reference beams:

$$V_R = V_c + V_{ws} + V_{wf} \tag{4-6}$$

where, V_{wf} is the contribution of the external FRP shear reinforcement. The FRP being a linear elastic material, its contribution depends on the FRP strain along the shear crack at ultimate load. From the experiments it follows (Section 3) that the FRP strain varies along the shear crack, that local debonding at both sides of the shear crack occurs and, depending on the available anchorage length, that a FRP bond failure may be obtained. Hence, it appears that the contribution of the FRP is limited to an effective tensile strain $\varepsilon_{f,eff}$, which is generally lower than the ultimate FRP strain ε_{fu}. Hence, based on a truss analogy:

$$V_{wf} = \frac{A_{wf}}{s_f} 0.9 d E_f \varepsilon_{f,eff} (\cot\theta + \cot\alpha_f) \sin\alpha_f \tag{4-7}$$

with, A_{wf} the cross-sectional area of the FRP shear reinforcement, s_f the spacing of the FRP sheets (for continuous FRP s_f equals b_f), $\varepsilon_{f,eff}$ the effective FRP strain according to Section 4.3 and α_f the angle of the principal FRP fibre orientation with respect to the member longitudinal axis (90° for the tested beams).

In Eq. (4-6) it is assumed that the contribution of the concrete to the shear capacity does not significantly change compared to unstrengthened members. Indeed, as demonstrated in Section 3.3, no significant reduction in the concrete shear contribution was found for the tested beams. Nevertheless, aspects related to the concrete shear contribution of strengthened RC members, such as a reduced aggregate interlock contribution near ultimate load and the influence of confining action by the FRP shear reinforcement, may be subject to further study. On the other hand, if it is assumed that a significant change in the concrete contribution did occur, this effect is incorporated in the calibration (Section 4.3) of the effective FRP strain $\varepsilon_{f,eff}$ by defining $V_{f,exp} = V_u - V_{u,ref}$. Also, it should be verified for Eq. (4-6) that the contribution of the steel stirrups may be related to a stress σ_s lower than f_{wy} in case the effective FRP strain $\varepsilon_{f,eff}$ is less than the yield strain of the stirrups.

Results of the analytical verification of the tested beams according to Eq. (4-6) (with θ = 45°), are given in Table 4-6. A spacing of the FRP sheets of 400 mm was assumed for beams BS2 and BS6, 300 mm for beam BS5 and 200 mm for beam BS7. Although, the simplified approach used for the determination of $\varepsilon_{f,eff}$, reasonably accurate predictions are obtained (similar scatter is found for the strengthened and the unstrengthened beams).

Table 4-6 *Verification of the shear capacity*

Spec.	Type of strength.	V_u [kN]	V_c [kN]	V_{ws} [kN]	$\varepsilon_{f,eff}$ [mm/m]	V_{wf} [kN]	V_R [kN]	V_u/V_R [-]
BS1	Unstrength. (ref.)	210.6	133.6	60.2	-	-	193.8	1.09
BS2	2 strips (∪&∩ shape)	251.8	129.6	60.2	8.54	24.4	214.2	1.18
BS3	Unstrength. (ref.)	140.9	141.7	30.2	-	-	171.8	0.82
BS4	Full shear span (∪shape)	256.3	F	F	F	F	F	F
BS5	3 strips (∪shape)	174.3	136.9	30.2	6.52	24.8	191.9	0.91
BS6	2 strips (∪&∩ shape)	171.0	136.2	30.2	8.56	24.4	190.8	0.90
BS7	3 strips (closed shape)	239.8	136.6	30.2	8.12	46.4	213.2	1.12

$V_u = Q_u + g\ell/2$, where g is the self weight of the beam; F: flexural failure

4.3 Effective ultimate FRP strain

From Eq. (4-7) it follows that the prediction of the shear contribution of the external FRP reinforcement basically depends on the determination of the effective FRP strain $\varepsilon_{f,eff}$. The modelling of this strain depends on several aspects, such as the crack opening along the shear crack (determining the FRP strain variation along the shear crack), the local debonding of the FRP at both sides of the shear crack and the FRP force which can be anchored. As these aspects and their interaction are very difficult to model and would need extensive and specific research data (which are currently not available), a more deterministic approach as first suggested by Triantafillou [6,7] is followed. Triantafillou argues that $\varepsilon_{f,eff}$ will mainly depend on the available development length of the FRP (force transfer zone at both sides of the shear crack) which is a function of the bond conditions and the FRP axial rigidity (area times elastic modulus). By means of an experimental data fitting, it is proposed to calibrate $\varepsilon_{f,eff}$ as a function of $E_f\rho_{wf}$, with $\rho_{wf} = A_{wf}/(s_f b_w)$. Herewith, the FRP shear contribution $V_{f,exp}$ is taken as the difference between the experimental failure load of the strengthened and unstrengthened beams. Given $V_{f,exp}$ and assuming diagonal shear cracks with $\theta = 45°$, the corresponding strain $\varepsilon_{f,eff}$ is obtained from Eq. (4-7).

According to this approach the following relationship for $\varepsilon_{f,eff}$ is suggested in [6,7]:

$$\varepsilon_{f,eff} = 0.0119 - 0.0205(E_f\rho_{wf}) + 0.0104(E_f\rho_{wf})^2 \tag{4-8}$$

for $0 < E_f\rho_{wf} \leq 1$ and with $E_f\rho_{wf}$ in kN/mm^2. In [8], using the same method but including additional experimental data a similar relationship is derived:

$$\varepsilon_{f,eff}/\varepsilon_{fu} = 0.778 - 1.2188(E_f\rho_{wf}) + 0.5622(E_f\rho_{wf})^2 \tag{4-9}$$

where it is also suggested to limit the strain ratio $\varepsilon_{f,eff}/\varepsilon_{fu}$ to 0.50 to maintain the shear integrity of the concrete. This restriction is however not logical as a possible reduction in the shear capacity of the concrete (no evidence of this was found for the tested beams) is indirectly accounted for in the calibration of $\varepsilon_{f,eff}$.

The above equations for $\varepsilon_{f,eff}$ are shown in Fig. 4-5 and Fig. 4-6. In these figures also the test results of 70 experiments are shown. These correspond with those used in [8], the test

results reported in Section 3 and additional experimental data found in the literature. Details on this experimental data base are given in Appendix D, Section 2.

From Fig. 4-5 it may be clear that Eq. (4-8) is not very accurate compared to the collected experimental data. This is due to the limited data available at the time Eq. (4-8) was derived in [6], so that one data curve fitting was reasonably accurate, irrespective of the type of FRP, the strengthening configuration (closed, U-shape, sides only) and the concrete type. A new curve fitting as shown in Fig. 4-5 could be suggested, but would not be realistic (for low values of $E_f\rho_{wf}$ the effective strain $\varepsilon_{f,eff}$ varies to a great extend with an almost insignificant change in $E_f\rho_{wf}$) as it does not account for the above mentioned aspects.

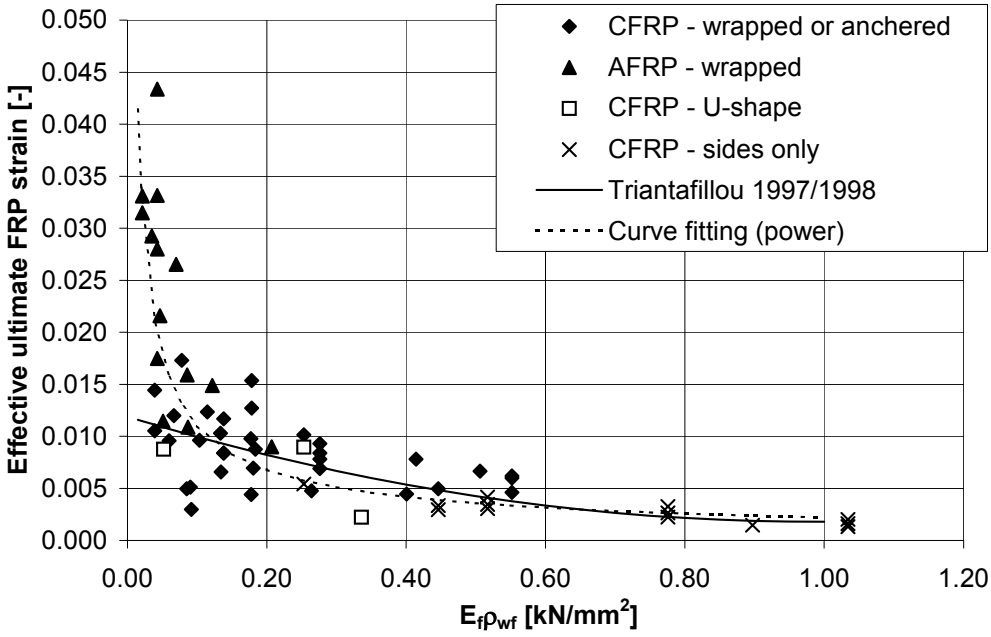

Fig. 4-5 *Effective FRP strain according to [6,7]*

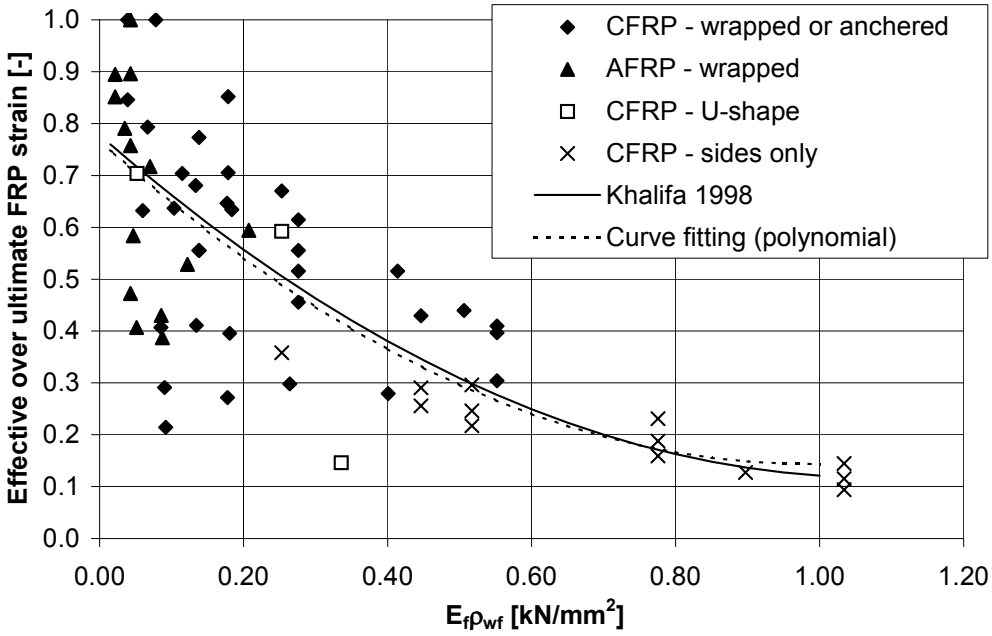

Fig. 4-6 *Effective FRP strain according to [8]*

To eliminate the effects of various types of FRP sheet, the ratio $\varepsilon_{f,eff}/\varepsilon_{fu}$ is considered in Eq. (4-9). As illustrated in Fig. 4-6 the data still follow the same trend, so that only a single curve fit was proposed in [8]. A new curve fit, similar to Eq. (4-9) but including the additionally collected experimental data (and with $\varepsilon_{f,eff}/\varepsilon_{fu} \leq 1$), almost exactly yields the original equation. Although Eq. (4-9) has been derived irrespective of the shear strengthening configuration (closed shape, U-shape or sides only), it is suggested in [8] that this equation should only be applied when the failure is governed by FRP rupture, not by FRP bond failure.

From the conducted experiments it is clear that the strengthening configuration has an important influence on the efficiency of the shear strengthening. If sufficient anchorage length is available or if closed shape wrapping is used, higher failure loads are obtained. This aspect should be reflected in the calibration of the effective FRP strain. Also, the influence of the concrete strength may be relevant. Based on suggestions by Triantafillou, this latter aspect may be taken into account by $f_{cm}^{2/3}$, which reflects the influence of the concrete tensile strength on the aforementioned transfer zone at both sides of the shear crack. Furthermore, also the shear span to effective depth ratio (a/d) may be of influence (especially with respect to the angle of the diagonal shear crack, whereas an angle $\theta = 45°$ is assumed in the calculation of the truss model). In [9], it is demonstrated that the effective strain $\varepsilon_{f,eff}$ – calculated from Eq. (4-7) with $\theta = 45°$ – will significantly increase with a/d.

According to these considerations, based on the collected experimental data base and defining the parameter:

$$\Gamma_f = \frac{E_f \rho_{wf}}{f_{cm}^{2/3}(a/d)} \tag{4-10}$$

a new curve fitting was conducted to correlate $\varepsilon_{f,eff}/\varepsilon_{fu}$ with Γ_f for different shear strengthening configurations (closed shape, U-shape or sides only). Herewith, experimental ratios $\varepsilon_{f,eff}/\varepsilon_{fu}$ larger than 1 (due to the variance of ε_{fu}) were taken equal to 1 and experiments for which $\Gamma_f > 35$ $(N/mm^2)^{1/3}$ (unrealistic cross-sectional dimensions) were omitted. An exponential curve fitting was used, as this resulted in the highest accuracy. Accordingly, the effective ultimate FRP strain in case of fully wrapped or properly anchored FRP, is given by:

$$\varepsilon_{f,eff} = 0.72\varepsilon_{fu} e^{-0.0431\Gamma_f} \tag{4-11}$$

where, f_{cm} and E_f in Γ_f are expressed in N/mm^2 (Γ_f in $(N/mm^2)^{1/3}$). For FRP bonded to the sides only, the effective ultimate FRP strain yields:

$$\varepsilon_{f,eff} = 0.56\varepsilon_{fu} e^{-0.0455\Gamma_f} \tag{4-12}$$

In case of U-shaped FRP shear reinforcement, not sufficient data were available to derive an equation, so that Eq. (4-12) should be used.

In Fig. 4-7, the ratio $\varepsilon_{f,eff}/\varepsilon_{fu}$ according to Eqs. (4-11) and (4-12) is compared to the experimental data. Although, the data follow a certain trend, large scatter is obtained and more experimental data may be required to validate these equations. The relatively large scatter also indicates that more research is needed to obtain a more fundamental understanding in the interaction of the phenomena influencing the effective FRP strain $\varepsilon_{f,eff}$.

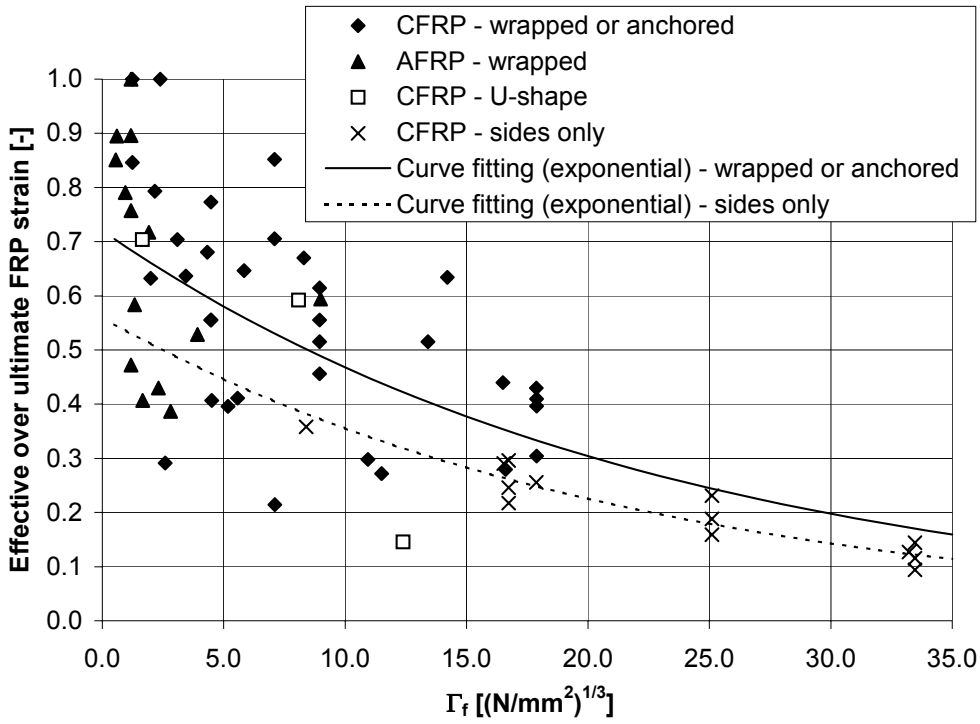

Fig. 4-7 *Proposed model for the effective FRP strain*

5 Conclusions

From the conducted experimental and analytical study on the shear strengthening of RC beams, the following is concluded:

- By means of externally bonded FRP shear reinforcement, the shear strength of the beams can be increased considerably. If sufficient FRP EBR is provided, a shear failure can be prevented, so that a flexural failure is obtained. The strengthening configuration may considerably influence the effectiveness of the shear strengthening.
- From the test results it follows that the contribution of the FRP to the shear capacity is related to an effective FRP strain which is generally lower than the ultimate FRP strain. This effective strain reflects aspects such as the crack opening along the shear crack (determining the FRP strain variation along the shear crack), the local debonding of the FRP when bridging the shear crack and the available anchorage capacity.
- Increased efficiency is obtained if FRP bond failure is avoided or delayed. This may be done by providing U-shaped or even closed shape wrapping. Although not investigated in this test programme, a mechanical anchorage may increase the efficiency as well (its effect will be similar to that of closed shape wrapping).
- The calculation of the shear capacity can be performed according to a truss analogy, whereas the FRP shear contribution is obtained in a similar way as for the steel stirrups.
- A fundamental modelling of the effective FRP strain is complex. Therefore, a model based on experimental data fitting is proposed, which takes into account the FRP reinforcement ratio, the modulus of elasticity of the FRP, the concrete strength and the shear span to effective depth ratio. Based on this model reasonably accurate predictions are obtained.

6 References

1. Alexander J.G.S., Cheng J.J.R. (1996), "Field application and studies of using CFRP sheets to strengthen concrete bridge girders" Proceedings 2nd. Int. Conf. On Advanced Composite Materials in Bridges and Structures, Ed. M. El-Badry, The Canadian Society for Civil Engineering, Montréal, Québec, Canada, pp. 465-472.
2. Taerwe L., Khalil H., Matthys S. (1997), "Behaviour of RC Beams Strengthened in shear by external CFRP sheets", Proceedings 3rd. Int. Symp. on Non-Metallic (FRP) Reinforcement for Concrete Structures, Japan Concrete Institute, Sapporo, Japan, Vol. 2, pp. 559-566.
3. Matthys S., Taerwe L., Khalil H. (1998), "Strengthening by means of externally bonded FRP reinforcement", Proceedings XIIIth. FIP Congress 1998 on Challenges for Concrete in the Next Millennium, Amsterdam, The Netherlands, Eds. D. Stoelhorst, G.P.L. den Boer, Betonvereniging, published by A.A. Balkema, Vol. 2, pp. 643-647.
4. CEN (1991), "Eurocode 2: Design of concrete structures – Part 1-1: General rules and rules for buildings", ENV 1992-1-1, Comité Européen de Normalisation (CEN), Brussels, Belgium, 263 pp.
5. CEB (1993), "CEB-FIP Model Code 1990, Design Code", Comité Euro-International du Béton, Lausanne, Switzerland, Thomas Telford, 437 pp.
6. Triantafillou T.C. (1997), "Shear strengthening of concrete members using composites", Proceedings 3rd. Int. Symp. on Non-Metallic (FRP) Reinforcement for Concrete Structures, Japan Concrete Institute, Sapporo, Japan, Vol. 1, pp. 523-530.
7. Triantafillou T.C. (1998), "Shear strengthening of Reinforced Concrete Beams Using Epoxy-Bonded FRP Composites", ACI Structural Journal, Vol. 95, No. 2, March-April 1998, pp. 107-115.
8. Khalifa A., Gold W.J., Nanni A., Aziz A. (1998), "Contribution of Externally Bonded FRP to Shear Capacity of RC Flexural Members", ASCE Journal of Composites for Construction, Vol. 2, No. 4, November 1998, pp. 195-201.
9. Miyauchi K., Inoue S., Nishibayashi S., Tanaka Y. (1997), "Shear behaviour of reinforced concrete beam strengthened with CFRP sheet", Transactions of the Japan Concrete Institute, JCI, Japan, Vol. 19, pp. 97-104.

Chapter 5
SERVICEABILITY BEHAVIOUR: TENSION STIFFENING AND CRACK BRIDGING

In Chapter 3, the positive influence of the externally bonded FRP reinforcement on the serviceability behaviour has been demonstrated. To study this aspect further with respect to tension stiffening and cracking, tests were conducted on strengthened tensile members. The performed experimental and analytical work is discussed in this chapter. Based on this work, existing models for the tension stiffening and cracking behaviour have been extended to include the influence of the externally bonded FRP reinforcement.

1 Introduction

As follows from the previous chapters, the performance of existing concrete members increases by means of the EBR method. For flexural members, it has been demonstrated that the serviceability behaviour may often govern the design. In any case, the serviceability behaviour is a crucial aspect for the further use of a construction. To understand and predict the effect of externally bonded FRP reinforcement on the serviceability, tests on strengthened tensile members were conducted [1,2]. These so-called 'tension stiffening' tests typically consist of a tensile test on a reinforcing bar embedded in a (strengthened) concrete prism. The parameters selected for the test programme included type of FRP, concrete strength and amount of internal and external reinforcement.

In order to fulfil service conditions with respect to crack widths and deflections, sufficient stiffness in the cracked state should be made available. In the case of strengthened members and depending on the amount and stiffness of the additional reinforcement, an improved serviceability behaviour will be obtained due to the following favourable aspects:

- The addition of external reinforcement causes an increase of the moment of inertia of the cracked section.
- After cracking, the tension forces in a cracked section are only balanced by the reinforcement. However, tension forces are transmitted to the surrounding concrete in between adjacent cracks by bond forces. This contributes to the stiffness in the cracked state and is called the 'tension stiffening effect'. Both the internal and external reinforcement will contribute to the tension stiffening effect, due to their capability of transferring bond forces.
- As the external reinforcement relieves some of the tensile stresses carried by the internal steel reinforcement, the bar strains and hence the crack widths are reduced for a given load level.
- The external reinforcement is bridging the cracks, causing an external restraining effect which results in denser crack spacing and smaller crack widths.

Whereas tension stiffening tests have been often used to study the crack formation, the effective stiffness of the tensile reinforcement in cracked concrete and the bond behaviour of reinforced and prestressed concrete under various conditions (e.g. [3-6]), tension stiffening tests with respect to FRP EBR have, except for [7], not been reported in the literature available to the author.

2 Outline of the test programme

2.1 Test specimens and material properties

A total of 18 concrete prisms with side length 100 mm and total length 1200 mm (1100 mm for batch T1), 14 of which strengthened with FRP EBR, were subjected to axial tension according to the test set-up shown in Fig. 5-1. Reinforcement ratios of the internal and external reinforcement, FRP type and concrete grade were considered as parameters. An overview of the different specimens, their designation and the corresponding test parameters are given in Table 5-1.

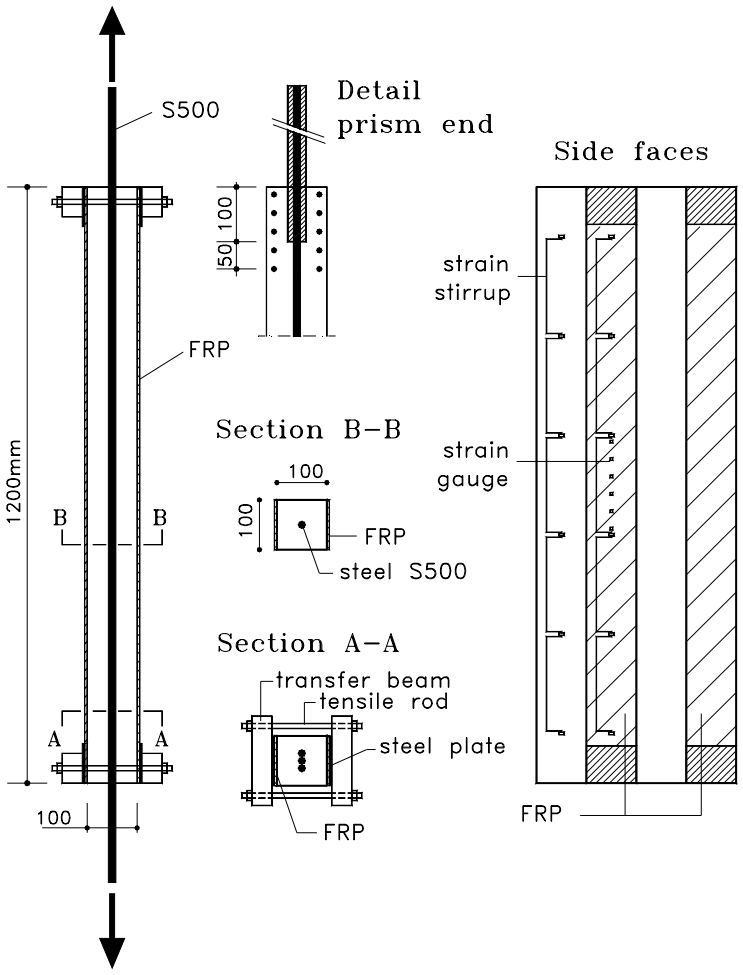

Fig. 5-1 *Tension stiffening test specimens*

Table 5-1 *Test parameters of the tension stiffening tests*

Batch	Specimen	Age at test	f_{cm} [N/mm^2]	Steel reinf.	ρ_s [%]	FRP type	FRP layers	ρ_f [%]
T1	N(T1)/100/14/Ref.	28	36.2	Ø 14 mm	1.56	-	-	-
	N(T1)/100/14/C#1	29	36.2	Ø 14 mm	1.56	CFRP	1	0.23
	N(T1)/100/14/C#2	29	36.2	Ø 14 mm	1.56	CFRP	2	0.45
T2	N(T2)/100/14/C#1	36	32.3	Ø 14 mm	1.56	CFRP	1	0.23
	N(T2)/100/14/G#2	28	32.3	Ø 14 mm	1.56	GFRP	2	0.41
	N(T2)/100/14/G#5	29	32.3	Ø 14 mm	1.56	GFRP	5	1.02
T3	N(T3)/100/10/Ref.	27	32.5	Ø 10 mm	0.79	-	-	-
	N(T3)/100/10/C#1	28	32.5	Ø 10 mm	0.79	CFRP	1	0.22
	N(T3)/100/10/G#5	28	32.5	Ø 10 mm	0.79	GFRP	5	1.01
	N(T3)/100/10/C#4	29	32.5	Ø 10 mm	0.79	CFRP	4	0.90
T4	N(T4)/100/16/Ref.	28	30.3	Ø 16 mm	2.05	-	-	-
	N(T4)/100/16/C#1	28	30.3	Ø 16 mm	2.05	CFRP	1	0.23
	N(T4)/100/16/G#5	29	30.3	Ø 16 mm	2.05	GFRP	5	1.02
	N(T4)/100/14/C#3	29	30.3	Ø 14 mm	1.56	CFRP	3	0.68
T5	H(T5)/100/14/Ref.	27	96.0	Ø 14 mm	1.56	-	-	-
	H(T5)/100/14/C#1	27	96.0	Ø 14 mm	1.56	CFRP	1	0.23
	H(T5)/100/14/G#2	28	96.0	Ø 14 mm	1.56	GFRP	2	0.41
	H(T5)/100/14/G#3	28	96.0	Ø 14 mm	1.56	GFRP	3	0.61

The internal reinforcement consisted of a centrally located deformed steel bar S500, with a characteristic yield strength of 500 N/mm^2 and a diameter of either 10 mm, 14 mm or 16 mm. The externally bonded reinforcement consisted of either CFRP sheets or GFRP fabrics. These were glued on two opposite faces of the concrete prism, impregnated and cured in-situ. For the CFRP, the Replark system (Replark Type 20 sheet/Epotherm Type XL 700 S epoxy) was used. The sheets have a width of 100 mm and the nominal thickness of one layer equals 0.111 mm. For the GFRP fabrics, Roviglas G (Roviglas G fabric/Multipox epoxy) was used, with a width of 100 mm and a nominal one layer thickness of 0.100 mm. The properties of the reinforcement are given in Table 5-2. The stress-strain behaviour of the reinforcement is shown in Fig. B-2.

For the concrete, both a normal (NSC) and a high strength concrete (HSC) with a mean compressive cylinder strength at 28 days of respectively 32.8 N/mm^2 and 96.0 N/mm^2 were used. The compressive strength f_{cm} at 28 days is also given in Table 5-1. More details on the material properties of the reinforcements, fresh and hardened concrete can be found in Appendix B.

2.2 Specimen preparation and test procedure

After casting of the specimens, the formwork was removed after 1 day. Concrete curing occurred at 20 °C/95 % R.H. during the first 7 days and at 20 °C/60 % R.H. afterwards.

Table 5-2 *Mean tensile properties obtained by tensile testing*

Type	**Nominal dimensions** [mm]	**Yield strength** [N/mm^2]	**Tensile strength** [N/mm^2]	**Ultimate strain** [%]	**E-modulus** [N/mm^2]
Rebar S500	Ø 10	590	670	-	200000
	Ø 14	550	630	-	200000
	Ø 16	590	690	-	200000
Replark MRK-M2-20	100 x 0.111[(1)]	-	3500	1.25	233000[(2)]
Roviglas G	100 x 0.100[(1)]	-	1300	2.07	57000[(2)]

[(1)] Equivalent dry-fibre thickness, [(2)] Tangent modulus at the origin

At a concrete age of about 21 days (7 days before testing) the external FRP reinforcement was bonded on two opposite side faces of the prism as shown in Fig. 5-1. The number of layers applied to one side face is given in Table 5-1. Application of the external FRP reinforcement comprised roughening of the concrete surface by means of grinding, dust removal with compressed air, FRP bonding (resin undercoating) and FRP impregnation (resin overcoating) as explained in Appendix B, Section 3.2.

The prisms were tested in a tensile testing machine with a capacity of 2500 kN in a deformation controlled way. During the tests, the movement of the actuator was 0.1 mm/min in the initial phase and 1 mm/min after the steel started yielding. The tensile force was applied by gripping of the steel reinforcement. To prevent steel yielding outside the concrete prism, three steel reinforcing bars were provided in the gripping zone. These were embedded in the concrete prisms over a distance of 100 mm, whereas only one internal bar was provided in the central zone. To account for local stresses at the prism ends, also confinement hoop reinforcement was provided over a distance of 150 mm (Fig. 5-1). For specimens of batch T2 till T5, a mechanical anchorage was applied before testing. In this way the FRP bond failure at the prism ends, obtained for specimens T1, could be prevented. The anchorage device consists of tensile rods, transfer beams and steel plates glued on the FRP reinforcement as shown in Fig. 5-1. By pre-tensioning of the rods, a transverse compressive stress of about 3.5 N/mm^2 was applied on the ends of the external FRP reinforcement.

Concrete and FRP strains, crack development and crack widths were recorded during testing as a function of the applied load. Fig. 5-1 shows the location of the strain measurements for a strengthened specimen. Strains were measured by means of 10 strain stirrups with a gauge length of 200 mm, located at 2 adjacent side faces. For the strengthened prisms, 5 of these strain stirrups were located on the FRP reinforcement. FRP strains were also recorded in the central zone of the prism by means of 6 strain gauges every 30 mm. Crack development was recorded on all sides for the reference prisms and on the opposite sides without FRP reinforcement for the strengthened prisms. This was done at a load interval of 10 kN until the internal steel started yielding and at the end of the test. At the 10 kN load intervals, also crack widths were measured by means of a small microscope. This was done on two opposite side faces (without FRP reinforcement) for batch T1. Due to the presence of the

strain stirrups on one of these side faces, crack width measurements were not always possible. As a result, crack widths were only recorded on one side face (free of stirrups and FRP reinforcement) for the remaining test specimens (batch T2 till T5).

3 Test results

3.1 Behaviour at ultimate load

The test results in terms of failure mode and ultimate load N_u are given in Table 5-3. Depending on the type and amount of externally bonded reinforcement and on the failure mode, strength increases between 1.3 and 3.0 were obtained. For the strengthened specimens of batch T1, a FRP bond failure was obtained due to high bond shear stresses at the ends of the FRP EBR. By applying a mechanical anchorage device this failure type was avoided in the next test series and fracture of the FRP reinforcement occurred, except for two specimens which failed by local pull-out, whereby a concrete pull-out cone was formed at the prism end.

Table 5-3 *Test results at ultimate load of tension stiffening tests*

Specimen	ρ_s [%]	ρ_f [%]	ρ_{eq} [%]	Failure mode	ε_{mu} [mm/m]	$\varepsilon_{mu}/\varepsilon_{fu}$ [-]	$N_{u,exp}$ [kN]	N_u/N_{ref} [-]
N(T1)/100/14/Ref.	1.56	-	-	YS [(1)]	- [(1)]	- [(1)]	87	1.00
N(T1)/100/14/C#1	1.56	0.23	1.82	DB	5.9	- [(2)]	125	1.44
N(T1)/100/14/C#2	1.56	0.45	2.08	DB	3.6	- [(2)]	128	1.47
N(T2)/100/14/C#1	1.56	0.23	1.82	FR	11.8	0.94	160	1.84
N(T2)/100/14/G#2	1.56	0.41	1.68	FR	10.3	0.50	115	1.32
N(T2)/100/14/G#5	1.56	1.02	1.85	FR	13.9	0.67	157	1.80
N(T3)/100/10/Ref.	0.79	-	-	YS [(1)]	- [(1)]	- [(1)]	43	1.00
N(T3)/100/10/C#1	0.79	0.22	1.05	FR	13.0	1.04	119	2.77
N(T3)/100/10/G#5	0.79	1.01	1.08	FR	11.5	0.56	104	2.42
N(T3)/100/10/C#4	0.79	0.90	1.82	PO	3.7	- [(2)]	131	3.05
N(T4)/100/16/Ref.	2.05	-	-	YS [(1)]	- [(1)]	- [(1)]	118	1.00
N(T4)/100/16/C#1	2.05	0.23	2.31	FR	12.6	1.01	193	1.64
N(T4)/100/16/G#5	2.05	1.02	2.34	FR	13.3	0.64	192	1.63
N(T4)/100/14/C#3	1.56	0.68	2.34	PO	6.2	- [(2)]	199	1.69
H(T5)/100/14/Ref.	1.56	-	-	YS [(1)]	- [(1)]	- [(1)]	84	1.00
H(T5)/100/14/C#1	1.56	0.23	1.82	FR	13.8	1.10	161	1.92
H(T5)/100/14/G#2	1.56	0.41	1.68	FR	12.2	0.59	120	1.43
N(T5)/100/14/G#3	1.56	0.61	1.74	FR	10.7	0.52	126	1.50

[(1)] Yielding of the steel: test stopped at about 14 mm/m, [(2)] No FRP fracture

YS: yielding of the internal steel reinforcement

DB: debonding of the FRP at one end (anchorage failure)

FR: fracture of the FRP reinforcement

PO: concrete pull-out failure at the prism end

For the prisms which failed by fracture of the FRP reinforcement, the ratio κ_f of the recorded mean tensile strain (see next section) at ultimate load ε_{mu} to the mean ultimate FRP strain ε_{fu} obtained from tensile tests can be considered, as given in Table 5-3. At failure of the FRP EBR, not much tension stiffening effect is expected as the prisms are considerably cracked. Hence, the ratio κ_f should be close to 1. However, considerably lower ratios are found for the prisms strengthened with GFRP. This can be explained as follows. Bond shear stresses at both sides of the cracks develop as a result of the crack bridging effect of the FRP EBR. Once these stresses exceed the bond shear strength of the concrete, debonding occurs between the FRP and the concrete, adjacent to the cracks. As this debonding is governed by the strength of the outer concrete layer which is not homogeneous, it occurs in a non-symmetric way at opposite side faces of the prism. Indeed, it was noticed during the tests that some of the prisms were slightly curved when reaching ultimate load. Hence, prisms failing by FRP rupture were no longer submitted to pure tension near ultimate load and their failure load was reduced by secondary effects. As debonding is related to the shear strength of the concrete and in a lesser extend to the type of FRP, roughly the same mean ultimate strain is recorded for the different prisms failing by FRP rupture, ranging between 10 and 13 mm/m (Table 5-3). The latter values are about equal to the failure strain of the CFRP but considerably lower than the failure strain of the GFRP. This explains why the above mentioned effects and low ratios κ_f were especially found for the prisms strengthened with GFRP. For three of the prisms strengthened with CFRP a ratio κ_f slightly larger than 1 is found. This can be attributed to statistical variations of the strain values used to calculate κ_f.

3.2 Mean tensile strain

The recorded mean longitudinal strains ε_m of the tested prisms are given in Appendix E, Section 1. The recorded strains of some of these prisms are also given Fig. 5-2 and Fig. 5-3. In the latter figures, ε_m represents the mean value of the strain stirrup measurements (Fig. 5-1), located on both the concrete and the FRP (for the strengthened prisms). For most of the prisms, the mean strain measured on the FRP covered side face and the mean strain of the free concrete surface were not significantly different (Appendix E, Section 1).

In Fig. 5-2 and Fig. 5-3, the load-strain behaviour is compared based on an equivalent reinforcement ratio ρ_{eq}, defined as:

$$\rho_{eq} = \rho_s + \frac{E_f}{E_s}\rho_f \tag{5-1}$$

with, $\rho_r = A_r/A_c$ the reinforcement ratio (either steel or FRP reinforcement), A_r and A_c the cross section of respectively the reinforcement and the concrete and E_r the modulus of elasticity of the reinforcement. Values of ρ_s, ρ_f and ρ_{eq} are given in Table 5-3.

Fig. 5-2 compares strengthened prisms with the same amount of internal steel and with the same equivalent reinforcement ratio (about 1.83 %). The obtained curves are close to each other. A higher stiffness in the cracked state is obtained compared to the reference prism (ρ_s = 1.56 %). Furthermore, a considerable strength increase is obtained after yielding of the

internal steel. For the prism in HSC, the cracking load is higher. In Fig. 5-3 the recorded deformations for strengthened prisms with increasing equivalent reinforcement ratio are shown. Higher stiffness in the cracked state is obtained with increasing equivalent reinforcement ratio. The slope of the last branch (stiffness in the cracked state after yielding of the steel) is almost the same for the three prisms with the same type and amount of external reinforcement, independent of the amount of internal steel reinforcement.

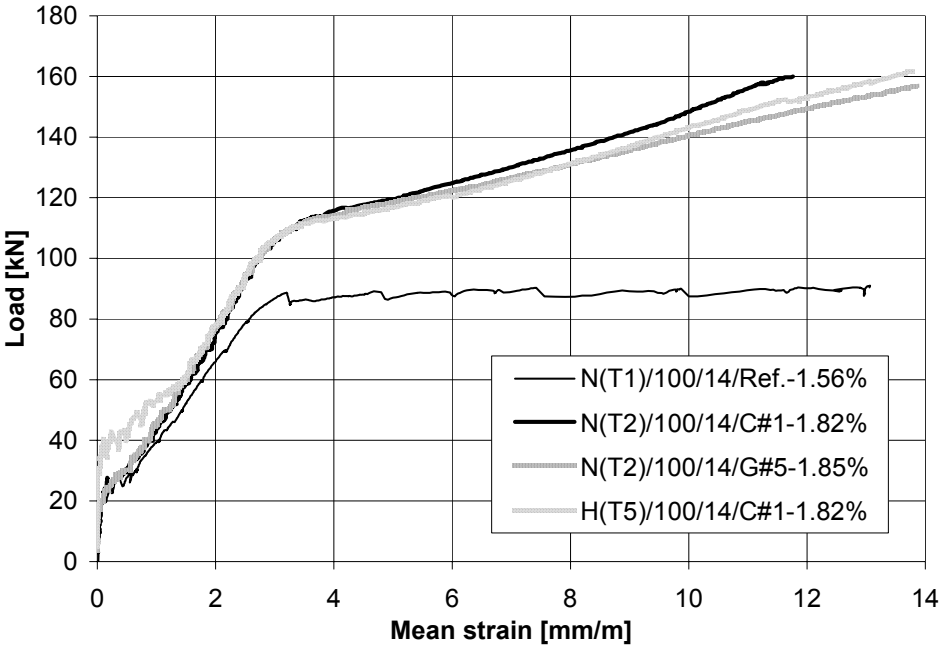

Fig. 5-2 *Load-strain behaviour of prisms with ρ_{eq} constant*

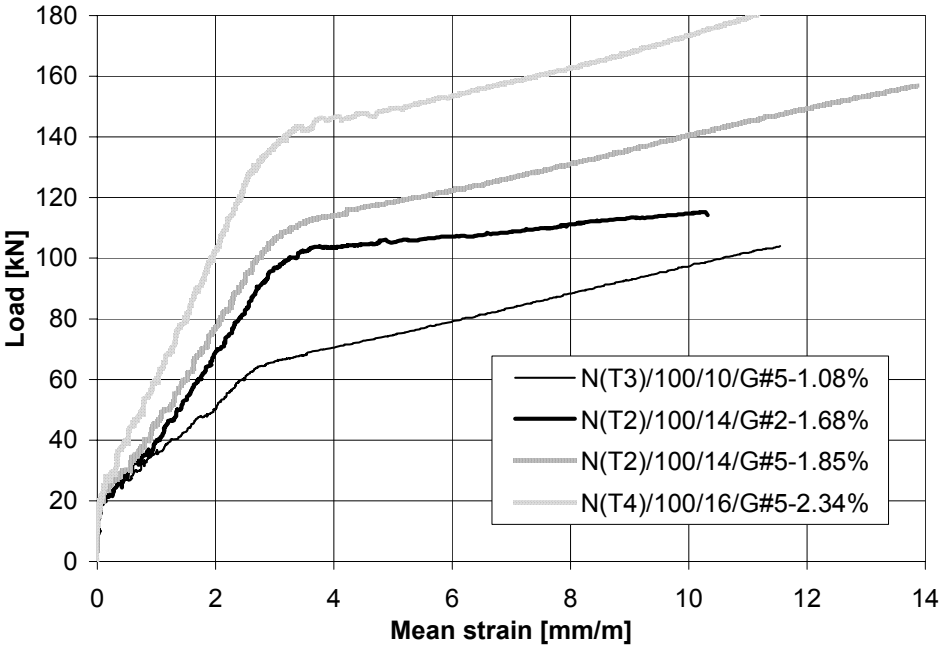

Fig. 5-3 *Load strain behaviour of prisms with increasing ρ_{eq}*

3.3 Crack pattern

In Fig. 5-4 and Fig. 5-5, the crack pattern at ultimate load, the mean crack width and the crack spacing are compared for prisms N(T4)/100/16/Ref. and N(T4)/100/16/C#1. The crack pattern and mean crack width of the tested prisms are also shown in Appendix E. From these figures it is noted that the crack pattern is influenced by both the internal steel and the external FRP reinforcement. A smaller crack spacing is obtained for an increasing amount of reinforcement, where already a small amount of external FRP reinforcement reduces the crack spacing to a great extent. The denser the crack spacing, the smaller the crack width.

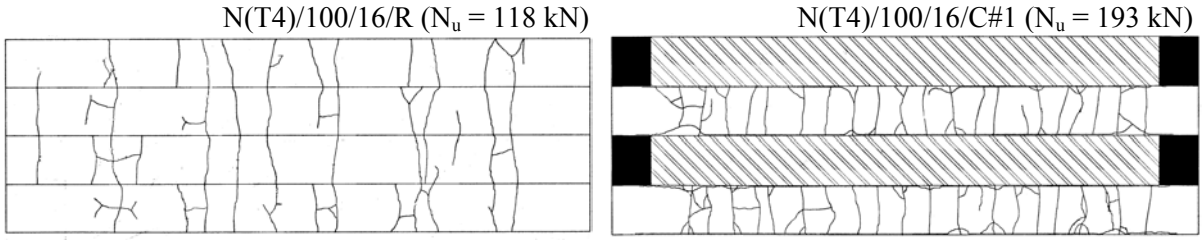

Fig. 5-4 *Crack pattern at ultimate load*

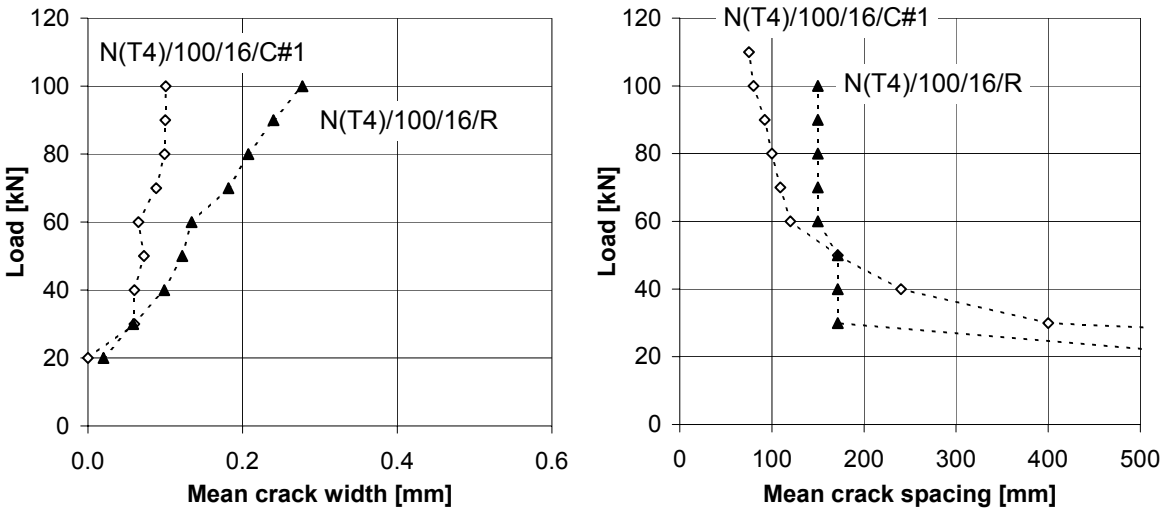

Fig. 5-5 *Mean crack width and spacing*

4 Analytical verification

4.1 Cracking load and load at which the steel starts yielding

The stiffness of the prisms significantly decreases after cracking and also after yielding of the internal steel reinforcement (Fig. 5-2 and Fig. 5-3). The corresponding loads N_{cr} and N_y can be calculated as follows:

$$N_{cr} = f_{ct} A_c \left(1 + \alpha_s \rho_s + \alpha_f \rho_f\right) \tag{5-2}$$

$$N_y = \varepsilon_y \left(E_s A_s + E_f A_f\right) \tag{5-3}$$

where, f_{ct} is the concrete tensile strength (determined by tension tests on prisms 100 mm x 100 mm x 200 mm, Appendix B) and $\varepsilon_y = f_y/E_s$ is the strain at onset of yielding.

The calculated loads N_{cr} and N_y and the experimental loads $N_{cr,exp}$ and $N_{y,exp}$ (taken from the measured load-strain curves) are given in Table 5-4. $N_{y,exp}$ is determined based on the intersection of two lines tangent to the two branches of the load-strain curves concerned.

Table 5-4 *Cracking load N_{cr} and load N_y at which the steel starts yielding*

Specimen	N_{cr} [kN]	$N_{cr,exp}$ [kN]	$N_{cr}/N_{cr,exp}$ [-]	N_y [kN]	$N_{y,exp}$ [kN]	$N_y/N_{y,exp}$ [-]
N(T1)/100/14/Ref.	27.6	22.0	1.25	89.3	89.0	1.00
N(T1)/100/14/C#1	27.9	32.5	0.86	104.1	108.0	0.96
N(T1)/100/14/C#2	28.3	33.0	0.86	118.9	123.0	0.97
N(T2)/100/14/C#1	27.1	23.0	1.18	104.1	108.0	0.96
N(T2)/100/14/G#2	26.9	19.5	1.38	95.9	99.0	0.97
N(T2)/100/14/G#5	27.2	22.5	1.21	105.8	106.0	1.00
N(T3)/100/10/Ref.	26.3	19.0	1.39	45.6	43.0	1.06
N(T3)/100/10/C#1	26.7	25.0	1.07	60.4	62.0	0.97
N(T3)/100/10/G#5	26.8	24.0	1.12	63.9	63.0	1.01
N(T3)/100/10/C#4	27.9	30.0	0.93	104.8	110.0	0.95
N(T4)/100/16/Ref.	24.3	18.0	1.35	116.6	118.0	0.99
N(T4)/100/16/C#1	24.7	16.0	1.54	313.4	136.0	0.97
N(T4)/100/16/G#5	24.7	24.0	1.03	135.0	138.0	0.98
N(T4)/100/14/C#3	24.8	30.0	0.83	133.7	138.0	0.97
H(T5)/100/14/Ref.	39.9	25.0	1.59	89.3	85.0	1.05
H(T5)/100/14/C#1	40.3	40.0	1.01	104.1	108.0	0.96
H(T5)/100/14/G#2	40.1	34.0	1.18	96.6	102.5	0.94
N(T5)/100/14/G#3	40.2	36.0	1.12	100.3	106.0	0.95
Mean value			1.16			0.98
Standard deviation			0.23			0.03

4.2 Tension stiffening effect

The load-strain behaviour of the prisms was verified according to EC2 [8], considering the tension stiffening effect. Defining states 1 and 2 as respectively the uncracked and fully cracked state, the mean tensile strain follows from:

$$\varepsilon_m = (1-\zeta)\varepsilon_1 + \zeta\varepsilon_2 \tag{5-4}$$

with, ζ a distribution or tension stiffening coefficient defined as:

$$\begin{aligned} \zeta &= 0 && N < N_{cr} \\ \zeta &= 1-\beta_1\beta_2\left(\frac{N_{cr}}{N}\right)^n && N > N_{cr} \end{aligned} \tag{5-5}$$

where, N is the applied tensile force, β_1 is a coefficient taking into account the bond characteristics of the reinforcement (1 for deformed steel) and β_2 is a coefficient taking into account the loading type (1 in case of short-term loading). According to EC2 the power n equals 2. For HSC more accuracy is obtained with n equal to 3 [9].

As it is difficult to separate the effects of the internal steel and the external FRP reinforcement, it is assumed for practical reasons that Eqs. (5-4) and (5-5) can be applied in the case of a combination of steel and FRP reinforcement. Accordingly, three branches in the load-strain curves are obtained. The first branch corresponds to state 1, in which the concrete is uncracked (concrete stress $\sigma_{ct} < f_{ct}$) or $\varepsilon_m = \varepsilon_1$:

$$\varepsilon_1 = N/(E_c A_c + E_s A_s + E_f A_f) \tag{5-6}$$

The second branch starts after cracking of the concrete and continues as long as the internal steel is not yielding. ε_m is calculated according to Eqs. (5-4) till (5-6) with:

$$\varepsilon_2 = N/(E_s A_s + E_f A_f) \quad \varepsilon_2 \le \varepsilon_y \tag{5-7}$$

The third branch corresponds to yielding of the internal steel and the additional load increase is provided by the external reinforcement only. In this case the strain in the fully cracked state becomes:

$$\varepsilon_2 = (N - A_s f_y)/E_f A_f \quad \varepsilon_2 > \varepsilon_y \tag{5-8}$$

For the reference prisms, this third branch was assumed as horizontal. In the model, failure is reached at fracture of the FRP reinforcement, this is if $\varepsilon_2 E_f$ equals the FRP tensile strength.

By means of a comparison with the experimental results, the model according to Eqs. (5-4) till (5-8) was verified. In the calculation, the material properties were taken according to Appendix B. Although the bond behaviour of FRP differs from that of steel, it was assumed that still $\beta_1 = 1$ and n = 2 (3 for HSC) could be adopted, as both materials exhibit good bond characteristics. As demonstrated in Fig. 5-6, this assumption gives a good agreement between experimental and analytical results. Due to the premature failure mode of some of the prisms and the obtained secondary effects (Section 3.1) the prediction of the third branch of the load-strain curve is less accurate for some of the prisms.

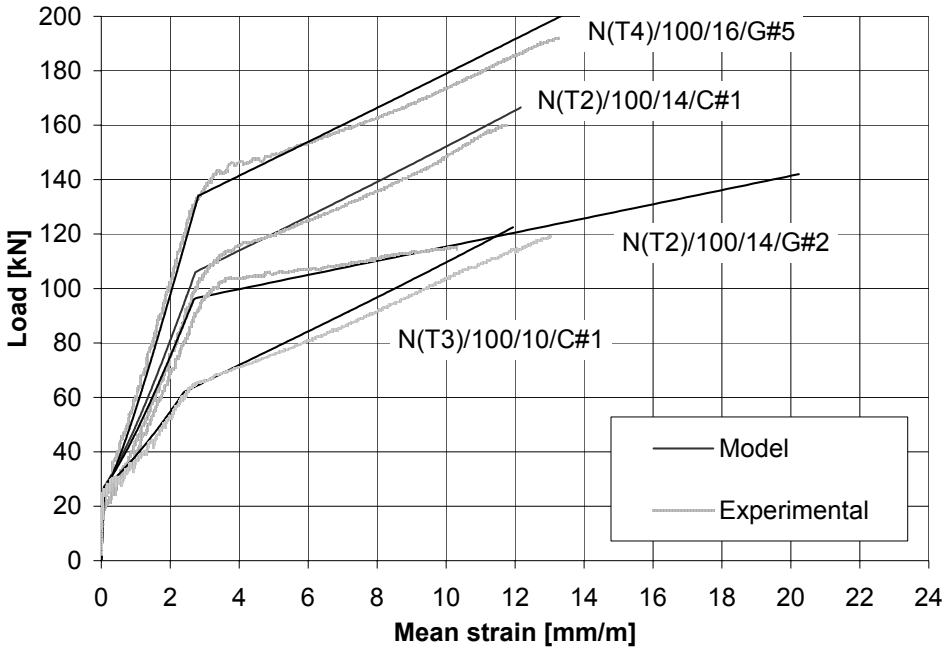

Fig. 5-6 *Load-strain behaviour*

Considering the serviceability behaviour, Fig. 5-7 and Appendix E, Section 3 focus on the load-strain behaviour of the strengthened prisms before yielding of the internal steel. In these figures the experimental values are compared with the mean strains calculated by the EC2 model and by the model given in the CEB-FIP Model Code 1990 [10]. In the latter model separate formulations are given for the crack formation phase (formation of cracks when the cracking load is exceeded) and stabilized cracking phase (at higher load levels, no new cracks appear while existing cracks widen). Accordingly, four branches in the load-strain curves are obtained. The first branch corresponds to state 1 (uncracked) or $\varepsilon_m = \varepsilon_1$. The second branch applies for $N_{cr} < N \leq N_{cr,n}$ and corresponds to the crack formation phase. As proposed in MC90, the load $N_{cr,n}$ at the last crack is taken as $1.3N_{cr}$. In the crack formation phase, the mean strain ε_m is calculated from:

$$\varepsilon_m = \varepsilon_2 - \frac{\beta_t \left(N - N_{cr}\right) + \left(N_{cr,n} - N\right)}{N_{cr,n} - N_{cr}} \left(\varepsilon_{cr2} - \varepsilon_{cr1}\right) \tag{5-9}$$

with ε_2 according to Eq. (5-7) and where ε_{cr1} and ε_{cr2} are taken according to Eqs. (5-6) and (5-7) respectively, with $N = N_{cr}$. The third branch applies for $N_{cr,n} < N \leq N_y$ and corresponds to stabilized cracking. The mean strain ε_m follows from:

$$\varepsilon_m = \varepsilon_2 - \beta_t \left(\varepsilon_{cr2} - \varepsilon_{cr1}\right) \tag{5-10}$$

and is similar to Eq. (5-4). Indeed, Eq. (5-10) can be transformed as:

$$\varepsilon_m = (1 - \zeta')\varepsilon_1 + \zeta'\varepsilon_2 \quad \text{with} \quad \zeta' = 1 - \beta_t \frac{N_{cr}}{N} \tag{5-11}$$

where, β_t is a factor taking into account the type of loading (0.40 for short-term loading). The last branch of the load-strain curve applies for $N > N_y$ (post-yielding). Here, the equation for ε_m given in MC90 is simplified by taking the factor $\delta(1 - N_{cr}/N_y)$, which does no longer apply to FRP, equal to 1. In this way, the mean strain ε_m can still be calculated from Eq. (5-11) in the post-yielding branch. In the post-yielding branch the strain ε_2 in the cracked state follows from Eq. (5-8).

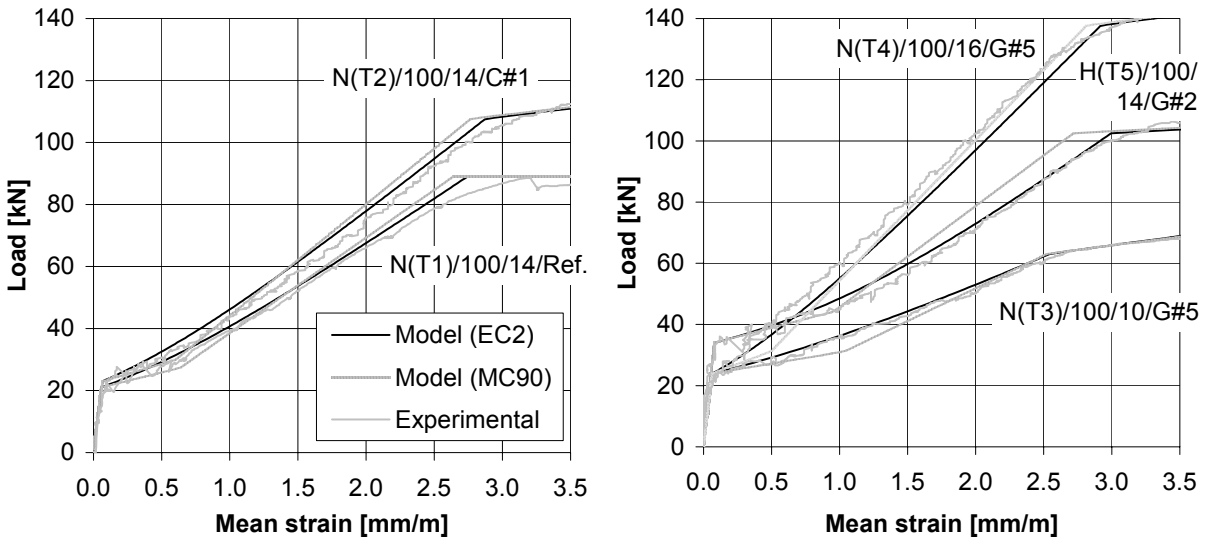

Fig. 5-7 *Load-strain behaviour at service loads*

To allow for a more accurate verification of the EC2 and MC90 model, the experimental values of the cracking load and the load at which the internal steel starts yielding were considered in the calculation.

From the analytical verification (Fig. 5-6, Fig. 5-7 and Appendix E, Section 2) the following can be concluded:

- A fairly accurate prediction is obtained for both models. The EC2 model gives the best results, whereas the MC90 model generally tends to overestimate the decrease of stiffness during crack formation and overestimates the stiffness at higher load levels.
- The crack formation happens in a smoother way for the strengthened prisms than for the reference prisms, especially in the case of low reinforcement ratios.
- For the prisms in high strength concrete the MC90 model strongly overestimates the tension stiffening effect. This is not the case for the EC2 model where a power n equal to 3 in stead of 2 was used for the tension stiffening coefficient.

4.3 Crack spacing and crack width

Assuming stabilized cracking, the mean crack width is generally calculated as [8]:

$$\begin{aligned} w_m &= s_{rm}(\varepsilon_{rm} - \varepsilon_{cm}) \\ &= s_{rm}\varepsilon_{rm,r} \end{aligned} \tag{5-12}$$

with, s_{rm} the mean crack spacing and $\varepsilon_{rm,r}$ the mean reinforcement strain with respect to the surrounding concrete. The latter equals $\varepsilon_{rm}\,\zeta$, with ε_{rm} and ζ according to Equations (5-7) and (5-5) respectively. As the model for the mean strain has been verified in Section 4.2, this section will mainly focus on the calculation of the mean crack spacing. In the following, verification between analytical and experimental results is performed with respect to the recorded crack pattern at a load level:

$$N_{cr,m} \approx \frac{N_{cr,n} + N_y}{2} \tag{5-13}$$

where, $N_{cr,n}$ is the load beyond which the concrete element is in the stabilized cracking phase and N_y is the load at which the internal steel reinforcement starts yielding. $N_{cr,n}$ is taken equal to $1.3N_{cr}$ as suggested in the MC90 [10] and rounded to the nearest 10 kN (load interval at which the crack patterns were recorded). Table 5-5 gives the experimentally obtained values of $N_{cr,m}$ and s_{rm}.

Modelling of the crack width and crack spacing of the strengthened members is more complicated due to the fact that consideration must be given to the mixed reinforcement. Regarding this aspect, different approaches are verified in the following.

In a first approach, as for steel reinforced concrete [10], the mean crack spacing s_{rm} is assumed as:

$$\begin{aligned} s_{rm} &= \frac{2}{3} s_{r\,max} \\ &= \frac{4}{3} \ell_r \end{aligned} \tag{5-14}$$

Table 5-5 *Analytical verification of the mean crack spacing*

Specimen	$N_{cr,m}$ [kN]	s_{rm}^{exp} [mm]	$s_{rm}^{exp}/s_{rmax}^{exp}$ [-]	$s_{rm}^{(a)}/s_{rm}^{exp}$ [-]	$s_{rm}^{(b)}/s_{rm}^{exp}$ [-]	$s_{rm}^{(c)}/s_{rm}^{exp}$ [-]
N(T1)/100/14/Ref.	60	122	0.51	1.36	-	-
N(T1)/100/14/C#1	80	69	0.55	0.43	0.89	0.96
N(T1)/100/14/C#2	80	79	0.65	0.38	1.12	0.85
N(T2)/100/14/C#1	70	74	0.50	0.40	0.82	0.90
N(T2)/100/14/G#2	60	104	0.52	0.29	0.38	0.64
N(T2)/100/14/G#5	70	80	0.80	0.37	0.81	0.83
N(T3)/100/10/Ref.	30	200	0.62	1.16	-	-
N(T3)/100/10/C#1	50	80	0.57	0.40	0.81	0.86
N(T3)/100/10/G#5	50	80	0.53	0.40	0.90	0.86
N(T3)/100/10/C#4	80	87	0.67	0.37	1.48	0.83
N(T4)/100/16/Ref.	70	150	0.79	0.96	-	-
N(T4)/100/16/C#1	80	87	0.75	0.33	0.68	0.76
N(T4)/100/16/G#3	80	95	0.54	0.31	0.70	0.70
N(T4)/100/14/C#5	90	69	0.60	0.43	1.53	0.98
H(T5)/100/14/Ref.	60	171	0.80	0.97	-	-
H(T5)/100/14/C#1	80	55	0.50	0.55	1.16	1.19
H(T5)/100/14/G#2	70	80	0.67	0.37	0.55	0.81
N(T5)/100/14/G#3	80	80	0.57	0.37	0.68	0.81
Mean value			0.62	0.56	0.89	0.86
Standard deviation			0.11	0.35	0.33	0.13

(a), (b) $s_{rm} = 1.33\,\ell_r$, with ℓ_r according to Eqs. (5-15) and (5-17) respectively

(c) $s_{rm} = 2\,\ell_{cr,n}$, with $\ell_{cr,n}$ according to Eq. (5-25)

with, s_{rmax} the maximum crack spacing which equals twice the transfer length ℓ_r (Fig. 5-8). As demonstrated in Table 5-5, the ratio s_{rm} to s_{rmax} experimentally obtained is subject to considerable scatter. However, the mean value equals about the ratio assumed in [10]. For the reference prisms the transfer length ℓ_r equals:

$$\ell_r = \frac{A_c}{u_s}\frac{f_{ctm}}{\tau_{sm}} = \frac{1}{4}\frac{f_{ctm}}{\tau_{sm}}\frac{Ø}{\rho_s} \tag{5-15}$$

with, $u_s = \pi Ø$ the bond perimeter, Ø the diameter of the reinforcing bar, f_{ctm} the mean concrete tensile strength, τ_{sm} the mean shear strength along the transfer length and ρ_s the reinforcement ratio. Assuming similar bond characteristics for the internal steel and the external FRP reinforcement ($\tau_{sm} = \tau_{fm} = \tau_m$), Eq. (5-15) can be applied for the strengthened prisms as:

$$\ell_r = \frac{A_c}{u}\frac{f_{ctm}}{\tau_m} \tag{5-16}$$

where, $u = \pi Ø + 2b_f$ is the total bond perimeter and b_f is the width of the FRP. Results of the analytical verification according to Eqs. (5-15) and (5-16) and with $\tau_m = 1.8\ f_{ctm}$ [10], are given in Table 5-5. For the strengthened prisms the mean crack spacing is strongly underestimated.

From Fig. 5-4 it is noted that a small amount of FRP reinforcement reduces the crack spacing to a great extend. This indicates that the crack spacing is mainly determined by the FRP reinforcement. Hence, Eq. (5-14) could be applied with respect to the transfer length ℓ_{rf} of the externally bonded FRP reinforcement. In [11] a model for the bond shear stresses of the externally bonded FRP reinforcement is presented, assuming a linear relationship between the bond stress and the slip. Based on this model (see also Chapter 7, Section 3.4.4) the following equation is derived for the transfer length:

$$\ell_{rf} = \frac{1}{\omega}\ \ln\left(\frac{\omega}{\zeta_\ell}\Delta\sigma_{f,cr}\,t\right) \tag{5-17}$$

with, t the thickness of the externally bonded reinforcement, $\Delta\sigma_{f,cr}$ the FRP stress increase at first cracking, $\zeta_\ell \approx 0$ a boundary condition and ω a parameter according to:

$$\omega^2 = \frac{G_a}{d}\left(\frac{1}{t\,E_f} + \frac{1}{h\,E_c}\right) \tag{5-18}$$

where, d is the thickness of the bond layer, h is the depth of the concrete (equal to half the prism depth as FRP reinforcement is provided at opposite sides) and G_a is the shear modulus of the adhesive. In [12], based on experimental observations, a value ζ_ℓ equal to 0.0002 N/mm^2 is proposed. Results of the analytical verification according to Eqs. (5-14), (5-17) and (5-18), with d equal to 1 mm, t equal to the nominal thickness given in Table 5-2 and G_a equal to 1150 N/mm^2, are given in Table 5-5. A better prediction is obtained compared with the previous model, however still with large scatter.

As a third approach, similar to prestressed concrete [6,10], the different bond behaviour of the mixed reinforcement is explicitly taken into account [13]. Considering a single crack, different transfer lengths ℓ_s and ℓ_f are obtained for the steel rebars and the FRP EBR respectively (Fig. 5-8):

$$\begin{aligned} \ell_s &= \frac{\sigma_s}{\tau_{sm}}\frac{A_s}{u_s} & \ell_f &= \frac{\sigma_f}{\tau_{fm}}\frac{A_f}{u_f} \\ &= \frac{\sigma_s}{\tau_{sm}}\frac{Ø}{4} & &= \frac{\sigma_f}{\tau_{fm}}t \end{aligned} \tag{5-19}$$

with, σ_s and σ_f the reinforcement stresses in the cracked section and where τ_{sm} and τ_{fm} are the mean bond shear stresses of the steel and FRP reinforcement. The mean reinforcement strain along the transfer lengths (neglecting the influence of the concrete strain) equals:

$$\varepsilon_{sm} = \frac{\sigma_s}{2E_s} \qquad \varepsilon_{fm} = \frac{\sigma_f}{2E_f} \tag{5-20}$$

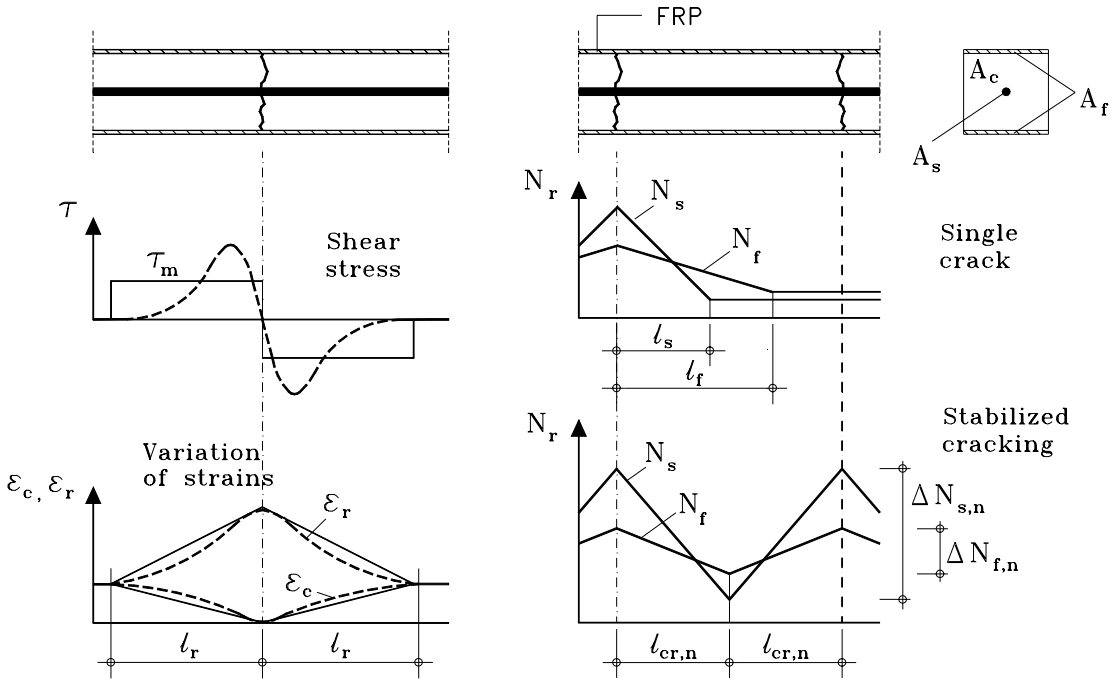

Fig. 5-8 *Behaviour at cracking*

Assuming an equal crack width $w_s = w_f = w$ where w is equal to $2\,\ell\,\varepsilon_m$, the total tensile force $N = A_s\sigma_s + A_f\sigma_f$ leads to different strains in the reinforcements:

$$\varepsilon_s = \frac{N}{E_s A_s + \sqrt{\xi_b} E_f A_f} \qquad \varepsilon_f = \frac{\sqrt{\xi_b} N}{E_s A_s + \sqrt{\xi_b} E_f A_f} \tag{5-21}$$

with,

$$\xi_b = \frac{\tau_{fm} E_s A_s u_f}{\tau_{sm} E_f A_f u_s} = \frac{\tau_{fm} E_s \varnothing}{\tau_{sm} E_f 4t} \tag{5-22}$$

At stabilized cracking and as illustrated in Fig. 5-8, the transfer lengths of both the steel and FRP reinforcement are equal to each other:

$$\ell_{cr,n} = \frac{\Delta N_{s,n}}{\tau_{sm} u_s} = \frac{\Delta N_{f,n}}{\tau_{fm} u_f} \tag{5-23}$$

With, $N_{cr} = \Delta N_{s,n} + \Delta N_{f,n}$ this yields:

$$\Delta N_{s,n} = N_{cr} \frac{E_s A_s}{E_s A_s + \xi_b E_f A_f} \qquad \Delta N_{f,n} = N_{cr} \frac{\xi_b E_f A_f}{E_s A_s + \xi_b E_f A_f} \tag{5-24}$$

from which the transfer length at stabilized cracking is derived as:

$$\ell_{cr,n} = \frac{N_{cr}}{\tau_{sm} u_s} \frac{E_s A_s}{E_s A_s + \xi_b E_f A_f} = \frac{N_{cr}}{\tau_{fm} u_f} \frac{\xi_b E_f A_f}{E_s A_s + \xi_b E_f A_f} \tag{5-25}$$

This transfer length equals half the crack spacing s_{rm}. In Table 5-5, s_{rm} according to Eq. (5-25) is given, based on the experimental values of N_{cr} and assuming mean bond stresses $\tau_{sm} = 1.80\ f_{ctm}$ [10] and $\tau_{fm} = 1.25\ f_{ctm}$ [14]. A fairly accurate prediction and the smallest scatter are obtained with this model.

Based on the latter model for the crack spacing and Eq. (5-12), Fig. 5-9 shows the recorded and calculated crack widths for some of the prisms. Results for all the prisms are given in Appendix E, Section 4. A fairly good prediction is obtained, with generally lower accuracy at higher loads (above service loads, where these equations are not intended to be used).

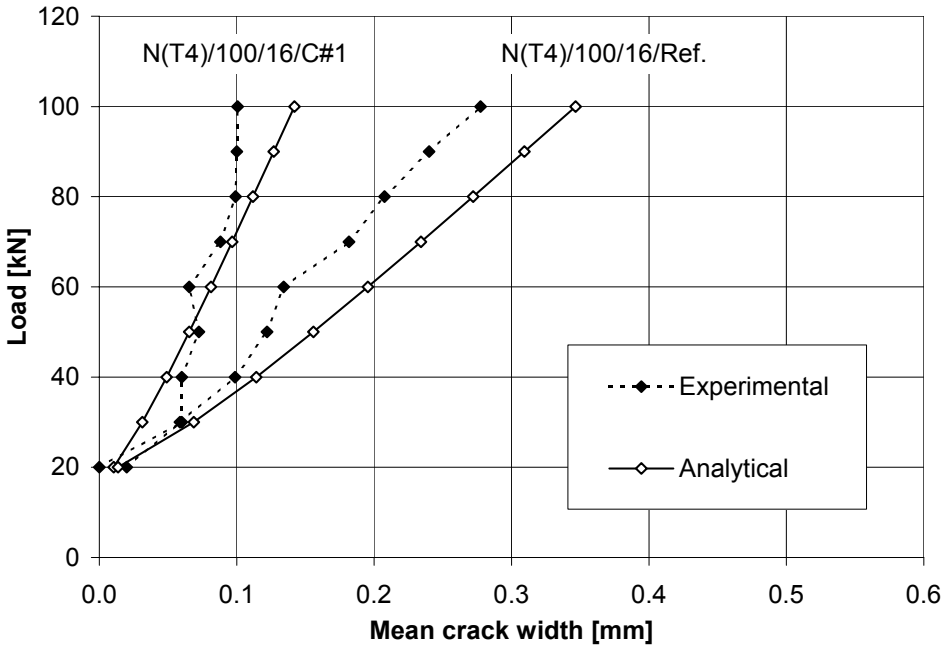

Fig. 5-9 *Analytical verification of the mean crack width*

5 Conclusions

By providing externally bonded FRP reinforcement to an existing concrete member, its performance increases in terms of strength and serviceability behaviour. Mainly focussing on the latter aspect, the following can be concluded from the performed study on strengthened tensile members:

- Compared to the reference specimens, the load carrying capacity of the strengthened prisms could be increased with a factor between 1.32 and 3.05. To prevent FRP bond failure at the prism end, a mechanical anchorage had to be applied.

- A significant increase in stiffness in the cracked state is obtained by applying externally bonded reinforcement. The magnitude of the stiffness in the cracked state strongly depends on the equivalent reinforcement ratio, hence on both the amount and stiffness of the reinforcements. The stiffness in the cracked state after yielding of the internal steel mainly depends on the amount and type of external FRP reinforcement.
- Considerably smaller crack spacing and crack widths are obtained for the strengthened prisms. Also, the crack formation happens in a smoother way compared to unstrengthened specimens.
- The load-strain behaviour of the strengthened elements, taking into account the tension stiffening effect, can be predicted in an accurate way according to EC2 [8]. Although less accurate, also according to MC90 [10] generally good predictions are obtained.
- From the different models to calculate the mean crack spacing at stabilized cracking, the model according to [13] was found to be the most accurate. This model explicitly takes into account the different bond behaviour of the mixed reinforcement.
- Based on the derived models for the mean strain and the mean crack spacing, fairly accurate predictions of the mean crack width are obtained.

As the tension zone of a flexural element can be regarded as a tensile member, the models derived in this chapter can generally be applied to RC elements strengthened in flexure as well. This has been demonstrated in Chapter 3, were the deformations and the crack widths of RC beams strengthened in flexure could be predicted in an accurate way.

6 References

1. Matthys S., Taerwe L., De Meyer P. (1999), "Effect of externally bonded fibre reinforced polymers on the tension stiffening behaviour of concrete members", Proceedings 2nd. International Symposium on Adhesion Between Polymers and Concrete (ISAP'99), Dresden, Germany, pp. 363-374.
2. De Meyer P. (1998), "Studie van de aanhechting en de krachtswerking van op beton gelijmde vezelcomposietlaminaten", Graduation thesis, Ghent University, Department of Structural Engineering, Magnel Laboratory for Concrete Research, 184 pp.
3. CEB (1985), "CEB-Manual Cracking and Deformations", CEB Bulletin d'Information No. 158-E, Comité Euro-International du Béton, Lausanne, Switzerland, 248 pp.
4. Gupta A.K., Maestrini R. (1989), "Tension stiffening model for reinforced concrete bars", Journal of Structural Engineering, Vol. 117, No. 3, pp. 769-790.
5. Giuriani E. (1982), "On the effective axial stiffness of a bar in cracked concrete", in Bond in Concrete, Ed. P. Bartos, Applied Science Publishers, London, UK, pp. 107-126.
6. König G., Fehling E. (1988), "Grundlagen zur Rissbreiten-beschränkung im Spannbetonbau" (in German), Beton- und Stahlbetonbau, Vol. 12, No. 83 (1988), Berlin, pp. 317-232.
7. Nanni A., Bakis C.E., Boothby T.E. (1997), "Externally bonded FRP composites for repair of RC structures", Proceedings 3rd. Int. Symp. on Non-Metallic (FRP)

Reinforcement for Concrete Structures, Japan Concrete Institute, Sapporo, Japan, Vol. 1, pp. 303-310.
8. CEN (1991), "Eurocode 2: Design of concrete structures – Part 1-1: General rules and rules for buildings", ENV 1992-1-1, Comité Européen de Normalisation (CEN), Brussels, Belgium, 263 pp.
9. Lambotte H., Taerwe L. (1990), "Deflection and Cracking of High-Strength Concrete Beams and Slabs", Proceedings of the High-Strength Concrete Second International Symposium, Ed. W.T. Hester, ACI SP-121, American Concrete Institute, Detroit, U.S.A, pp. 109-128.
10. CEB (1993), "CEB-FIP Model Code 1990, Design Code", Comité Euro-International du Béton, Lausanne, Switzerland, Thomas Telford, 437 pp.
11. Kaiser H. (1989), "Bewehren von Stahlbeton mit kohlenstoffaserverstärkten Epoxidharzen", Doctoral thesis, Technical University of Zürich, Switzerland, 224 pp.
12. Deuring M. (1993), "Verstärken von Stahlbeton mit gespannten Faserverbund-werkstoffen" (in German), EMPA Bericht, No 224, Swiss Federal Laboratories for Materials Testing and Research, Dübendorf, Switzerland, 279 pp.
13. Rostásy F.S., Holzenkämpfer P., Hankers Ch. (1996), "Geklebte Bewehrung für die Verstärkung von Betonbauteilen", Betonkalender 1996, Vol. II, pp. 547-576.
14. Holzenkämpfer P. (1994), "Ingenieurmodelle des Verbunds geklebter Bewehrung für Betonbauteile", Doctoral thesis, Vol. 108, , Technical University Braunschweig, Germany, 214 pp.

Chapter 6
CONFINEMENT OF AXIALLY LOADED COLUMNS

This chapter describes the experimental and analytical work concerning axially loaded columns, confined with external FRP wrapping reinforcement. The study especially focussed on some specific problems in the modelling of FRP confined concrete, i.e. the effective circumferential FRP failure strain and the effect of increasing confining action. Based on an analytical verification, different models for the prediction of the stress-strain behaviour of FRP confined concrete have been evaluated. Closed form equations for design practice are proposed.

1 Introduction

Concrete columns have an important function in the structural concept of many structures. Often, these columns are vulnerable to exceptional loads (such as impact, explosion or seismic loads), load increase (increasing use or change of function of structures, etc.) and degradation (corrosion of steel reinforcement, alkali silica reaction, etc.). On the other hand, confinement of concrete is an efficient technique to enhance the structural behaviour of concrete members primarily subjected to compression. Since the introduction of FRP as externally bonded reinforcement, confinement by means of FRP wrapping has been of considerable interest for the upgrading of columns, piers, chimneys, etc. and several research programmes have been conducted internationally [1-7]. This research mainly focused on small cylinders and on columns subjected to seismic action.

To verify the effectiveness of FRP confinement with respect to real scale axially loaded columns, to study the structural behaviour of FRP wrapped compression members and to investigate some specific aspects of the modelling of FRP confined concrete (Section 4.1), compression tests on cylinders and columns wrapped with FRP have been executed [8-10]. The variables considered in the test programme included FRP type, bonded or unbonded wrapping application, column shape (circular, square or rectangular), full or partial wrapping, fibre orientation (circular or helicoidal) and radius of rounded corners.

2 Outline of the experiments

2.1 Test specimens and material properties

Both small and large scale specimens were manufactured, comprising 15 cylinders and 11 columns. The plain concrete cylinders had a diameter of 150 mm and a depth of 300 mm and were (except for the 3 reference specimens) circularly wrapped with one layer of CFRP, providing an overlap length of 150 mm. Two types of CFRP sheet (C240 and C640) were used, either bonded (b) or not bonded (nb) to the concrete. The latter case is achieved by

attaching a foil on the concrete before FRP application. An overview of the test parameters is given in Table 6-1.

In addition to the compression tests on wrapped cylinders, large-scale testing on confined columns subjected to axial loading was performed as outlined in Table 6-2. The specimen dimensions and the wrapping configuration are shown in Fig. 6-1. The columns had a total length of 2 m, a longitudinal steel reinforcement ratio of 0.9 % and 8 mm diameter stirrups spaced every 140 mm. Extra stirrup reinforcement was provided at the column ends. Columns K1 through K8 have a 400 mm circular cross-section, while columns K9 through K11 are square or rectangular with the same gross cross-section A_g as the circular columns. Different types of FRP sheet or fabric and number of layers were used as indicated in Table 6-2. Except for columns K6 and K7, the FRP is applied over the total area (full wrapping) in a circular way, providing 200 mm overlap length in the circumferential direction (no overlap was provided in the longitudinal direction). For columns K6 and K7 partial wrapping is applied, either in a circular way with a clear spacing of 200 mm (K6) or in a helicoidal way with a pitch of 400 mm and a clear spacing of 200 mm (K7). For the latter column, anchorage of the FRP confining reinforcement is provided by means of extra circular wrapping at the column ends. Corners of square or rectangular columns are rounded with a radius of 30 mm or 15 mm (Table 6-2). For all strengthened columns, wrapping of the FRP was applied with bond between the FRP and the concrete.

Table 6-1 *Test parameters of wrapped cylinders Ø150 mm x 300 mm*

Spec.	**Age at test** [days]	**f_{cm} (28 days)** [N/mm^2]	**FRP type** [mm]	**No. of layers**	**Width** [mm]	**Wrapping** [mm]
R1-R3	28-29	34.8	-	-	-	-
C240b1-C240b3	28-30	34.8	C240	1	300	full, bonded
C240nb1-C240nb3	28-30	34.8	C240	1	300	full, not bonded
C640b1-C640b3	28-30	34.8	C640	1	300	full, bonded
C640nb1-C640nb3	28-30	34.8	C640	1	300	full, not bonded

Table 6-2 *Test parameters of wrapped columns*

Spec.	**Column shape** [mm]	**Age at test** [days]	**f_{cm} (28 days)** [N/mm^2]	**FRP type** [mm]	**No. of layers**	**Width** [mm]	**Clear spacing** [mm]	**Pitch** [mm]	**Wrapping** [mm]
K1	Ø 400	29	31.8	-	-	-	-	-	-
K2	Ø 400	28	34.3	C240	5	300	0	0	full
K3	Ø 400	29	34.3	C640	4	300	0	0	full
K4	Ø 400	29	39.3	TU600/20	6	200	0	0	full
K5	Ø 400	32	39.3	TU600/20	2	200	0	0	full
K6	Ø 400	28	35.8	TU600/20	4	200	200	0	partial
K7	Ø 400	28	35.8	TU600/20	4	200	200	400	partial
K8	Ø 400	32	39.1	TU360G160C/27G	4	50	0	0	full
K9	355x355/r30	29	39.1	TU600/20	2	200	0	0	full
K10	355x355/r15	28	37.7	TU600/20	2	200	0	0	full
K11	250x500/r30	29	37.7	TU600/20	2	200	0	0	full

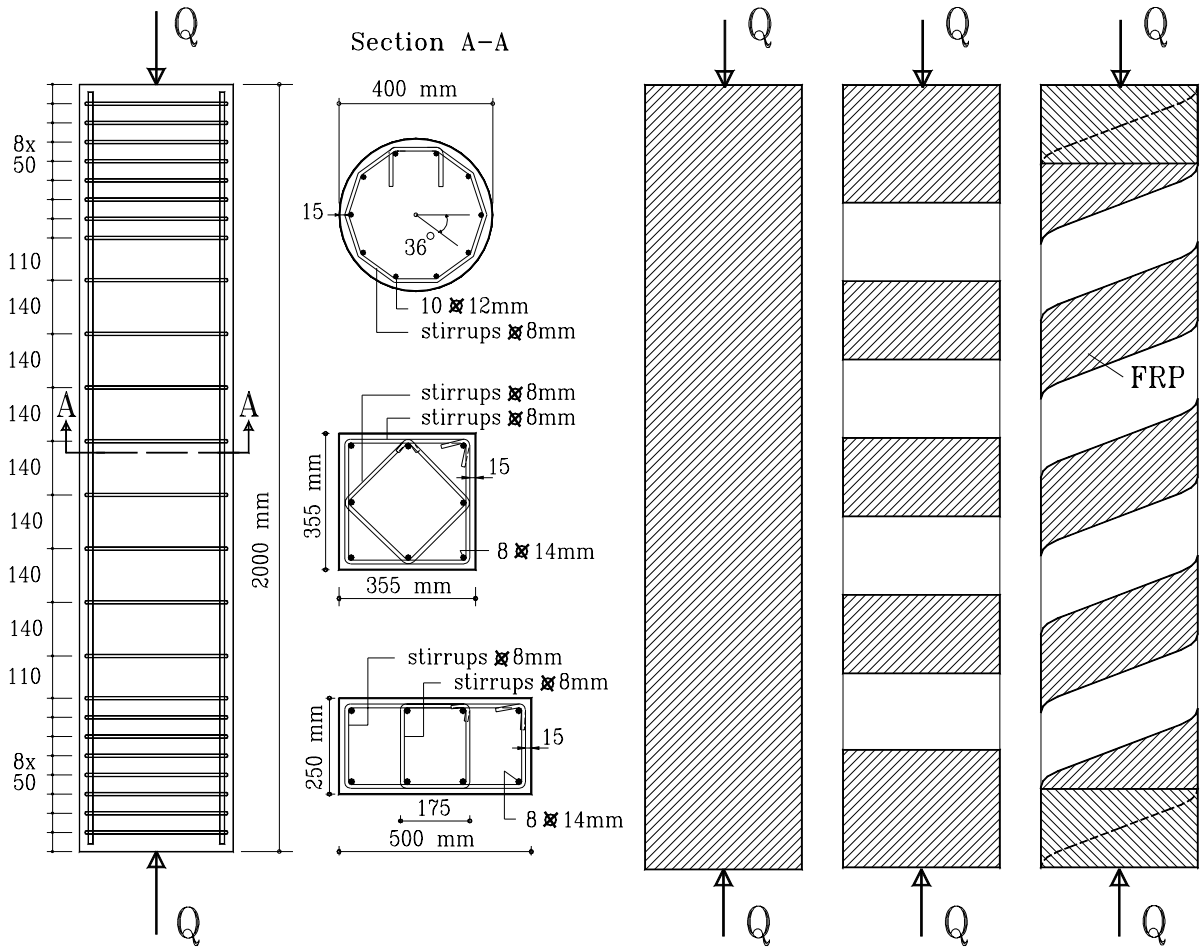

Fig. 6-1 *Column dimensions and wrapping configuration*

Different types of FRP reinforcement, consisting of CFRP sheets, GFRP fabrics and HFRP (hybrid FRP) fabric, have been used to confine the specimens. These 'wet lay-up' FRP types are glued, impregnated and cured in-situ. For the CFRP, the C-sheet system (C240 or C640 unidirectional sheet/Multipox T epoxy) was used, with a width of 300 mm and a nominal (dry fibre) thickness of 0.117 mm (C240) or 0.235 mm (C640). The GFRP consisted of the SyncoTape system, comprising a quasi unidirectional fabric TU600/25 (600 g/m^2 fibres in main direction and 25 g/m^2 in opposite direction) and PC5800 epoxy. The fabric has a width of 200 mm and a nominal thickness of 0.300 mm. For the HFRP, a hybrid type of fabric TU360G160C/27G (360 g/m^2 glass fibres and 160 g/m^2 carbon fibres in the longitudinal direction and 27 g/m^2 in the transverse direction) and PC5800 epoxy was used, with a width of 50 mm and a nominal thickness of 0.123 mm. For the columns, also internal steel reinforcement, type S500 deformed steel, was used (Fig. 6-1). The properties of the reinforcement are given in Table 6-3. The stress-strain behaviour of the reinforcement is shown in Fig. B-2. Concrete used for the specimens had a mean compressive cylinder strength at 28 days of 36.1 N/mm^2. The compressive strength f_{cm} at 28 days is also given in Table 6-1 and Table 6-2. More details on the material properties of the reinforcements, fresh and hardened concrete can be found in Appendix B.

Table 6-3 *Mean tensile properties obtained by tensile testing*

Type	**Nominal Dimensions** [mm]	**Yield strength** [N/mm^2]	**Tensile Strength** [N/mm^2]	**Ultimate strain** [%]	**E-modulus** [N/mm^2]
Rebar S500	Ø 8	560	610	2.77	200000
	Ø 12	620	720	8.73	200000
	Ø 14	560	630	9.97	200000
C-sheet 240 - Multipox T	300 x 0.117[(1)]	-	2600	1.19	198000[(2)]
C-sheet 640 - Multipox T	300 x 0.235[(1)]	-	1100	0.22	471000[(2)]
TU600/25 - PC5800	200 x 0.300[(1)]	-	780	1.30	60000[(2)]
TU360G160C/27G - PC5800	50 x 0.123[(1)]	-	1100	0.96	97000[(2)]

[(1)] Equivalent dry-fibre thickness, [(2)] Tangent modulus at the origin

2.2 Specimen preparation and test procedure

The test specimens and concrete quality control specimens were cast in the laboratory. Formwork was removed after 1 day and concrete curing occurred under a plastic foil during the first 7 days and under laboratory environment afterwards. The FRP was applied minimum 7 and maximum 9 days before the loading test. Application of the FRP was performed as described in Appendix B, Section 3.2. Concrete preparation included roughening by means of grinding.

After curing of the FRP, the presence of voids in the bond layer was verified by tapping on the surface. Voids were detected for some of the cylinders (bonded type). These were due to lack of accuracy of the practical execution. The voids content varied between 0 % and 22 % of the surface area. No significant defects could be detected for the wrapped columns.

The wrapped cylinders were tested, at a concrete age of 28 to 30 days (see Table 6-1), in a compression machine with a capacity of 6000 kN. The load was applied at 0.3 mm/min in a deformation controlled way. On each cylinder 2 strain gauges were used to measure the circumferential strain and 2 strain stirrups (gauge length 80 mm) to measure the axial deformations. The measurements were located in the region where the FRP did not overlap.

The columns were tested in a compression testing machine with a capacity of 10000 kN at the concrete age indicated in Table 6-2 (normally 28 days). The load was increased stepwise, with a load interval of 400 kN (100 kN for column K1), to allow for manual measurements. Near ultimate strength, the load was gradually increased until failure. For columns K1 till K4, an unloading-reloading branch was incorporated in the loading scheme at 1400 kN and 5600 kN for K1 and K2-K4 respectively. The load was applied in a displacement controlled way at 0.5 mm/min. Due to problems with the loading control unit, the displacement rate of column K2 decreased after reaching maximum load. Another problem occurred for column K9. In this case, the load reached a constant level near failure while the displacement rate decreased. After activating a second actuator pump to maintain the imposed displacement rate, the load suddenly increased and the column failed.

Axial and circumferential deformations of the columns were measured both manually and electronically. Manual measurements comprised dial gauges with a gauge length of 1 m and

mechanical deformeters with a gauge length of 200 mm or 50 mm. For the electronic measurements, both strain stirrups (gauge length 200 mm or 80 mm) and strain gauges have been used. The configuration of the strain measurements is schematically shown in Fig. 6-2.

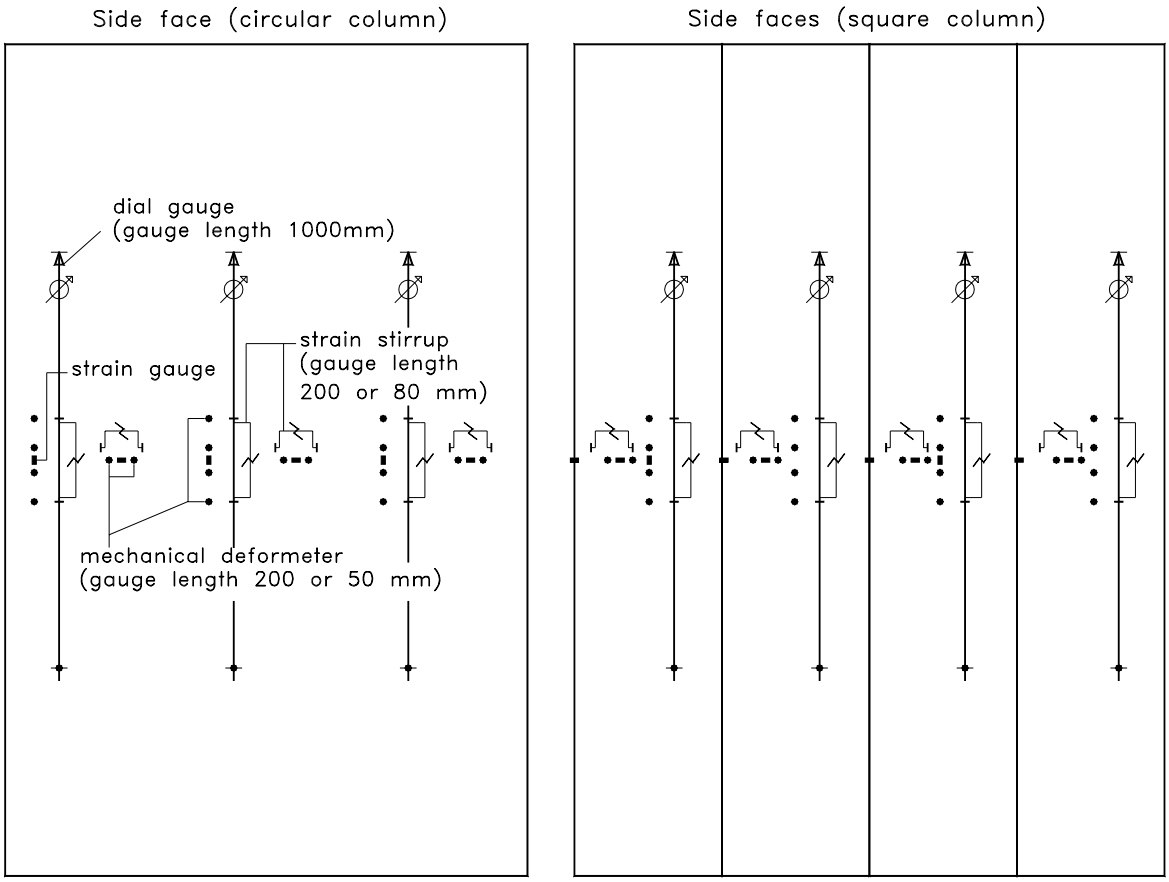

Fig. 6-2 *Typical configuration of the strain measurements of the columns*

3 Test results

3.1 Compression tests on wrapped cylinders

3.1.1 Behaviour at ultimate load

The obtained test results in terms of ultimate strength and strains are given in Table 6-4. A strength increase between 1.17 and 1.32 is found. Roughly the same strength increase is obtained for cylinders wrapped with FRP types C240 and C640. Indeed, one layer of both materials can resist about the same force, as also appears from the product $\varepsilon_{c\ell u} E_f t$ (with $\varepsilon_{c\ell u}$ the ultimate circumferential strain) which equals 266 N/mm and 250 N/mm for specimens C240b and C640b, respectively. Compared to the bonded type, the strength increase is lower for unbonded type of wrapping and for cylinders with a large amount of voids.

Whereas typically an axial strain at maximum load ε_{c1} of about 2 mm/m is found for the unconfined concrete, much higher values are obtained for the wrapped cylinders. Also the circumferential strain at maximum load $\varepsilon_{c\ell 1}$ increased for the wrapped cylinders. Except for

the cylinder with 22 % voids, the maximum load was equal to the ultimate load. Hence, strains at maximum load (ε_{c1} and $\varepsilon_{c\ell 1}$) equal those at ultimate load (ε_{cu} and $\varepsilon_{c\ell u}$). The ratio of the ultimate circumferential strain $\varepsilon_{c\ell u}$ over the FRP failure strain ε_{fum} (obtained from tensile testing, Table 6-3) equals more than 1.0 for the bonded specimens, while somewhat lower values are found in case of unbonded wrapping or in case voids are present. Values of $\varepsilon_{c\ell u}/\varepsilon_{fum}$ larger than 1.0 are in principle not possible, but may be due to statistical variation of the measured strains. Also, this ratio may depend on the way the reference tensile tests on the FRP are performed (e.g. due to the low transverse FRP strength the type of anchorage is of influence).

All FRP confined specimens failed by fracture of the FRP reinforcement, in the central zone of the cylinders, as illustrated in Fig. 6-3.

Table 6-4 *Test results of compression tests on cylinders*

Specimen		**Strength** [N/mm^2]	**Increase** [-]	ε_{c1} [mm/m]	ε_{cu} [mm/m]	$\varepsilon_{c\ell 1}$ [mm/m]	$\varepsilon_{c\ell u}$ [mm/m]	$\varepsilon_{c\ell u}/\varepsilon_{fum}$ [-]
R1-R3		34.9 ± 0.8	1.00	2.1	3.5[(1)]	1.2	3.7[(1)]	-
C240b1-C240b3	I	44.3 ± 3.0	1.27	8.5	8.5	11.5	11.5	0.97
	II	46.1 (± 0.9)	1.32	9.0	9.0	12.6	12.6	1.07
C240nb1-C240nb3		42.2 ± 1.5	1.21	7.2	7.2	10.8	10.8	0.92
C640b1-C640b3	I	41.3 ± 3.9	1.19	4.0	4.4	1.9	2.2	0.99
	II	45.8 (± ?)	1.31	6.0	6.0	3.1	3.1	1.41
C640nb1-C640nb3		40.7 ± 2.7	1.17	3.6	3.6	1.8	1.8	0.82

I: mean value of 3 specimens, II: wrapped cylinders with more than 5 % voids excluded
(1) Test stopped at an axial strain of about 3.5 mm/m

Fig. 6-3 *Failure aspect of the wrapped cylinders C240nb*

3.1.2 Stress-strain behaviour

The measured strains in axial and circumferential direction of some of the test specimens (one for each series of 3 specimens) are shown in Fig. 6-4 till Fig. 6-6 as a function of the axial stress. Once the cylinders are loaded above the strength of the unconfined concrete, the stiffness decreases to a large extent. Nevertheless, the load can be further increased in a considerable way. As a result, a combination of increase in load capacity and increase in ductility is obtained. The higher the stiffness of the FRP wrapping reinforcement the lesser the ductility increases (Fig. 6-4). No significant increase of the stiffness in the first branch of the curves could be noted. In the case of unbonded FRP, when the strength of the unconfined concrete is reached, strains initially increase with only a little strength increase (Fig. 6-5). This indicates a certain transverse expansion of the concrete before the unbonded reinforcement starts acting efficiently. A similar, however more pronounced effect, is obtained in case of low quality bonding (Fig. 6-6) where fibres are stretched first at the location of voids. For the unbonded FRP or low quality bonding, also the lower circumferential strain at ultimate load is noted, compared to that of the bonded FRP.

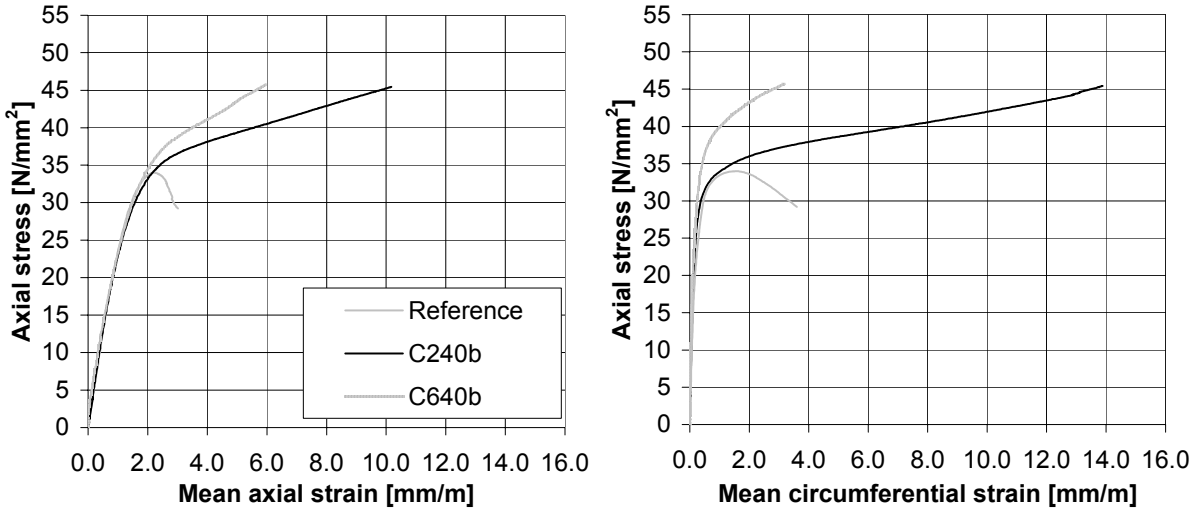

Fig. 6-4 *Stress-strain behaviour of wrapped cylinders with bonded FRP*

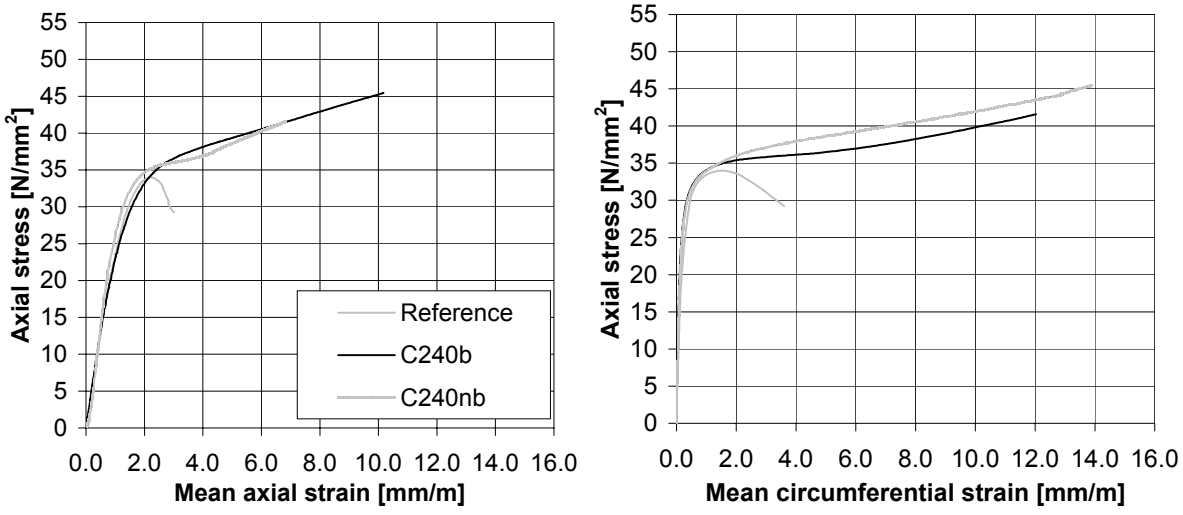

Fig. 6-5 *Stress-strain behaviour of wrapped cylinders with bonded and unbonded FRP*

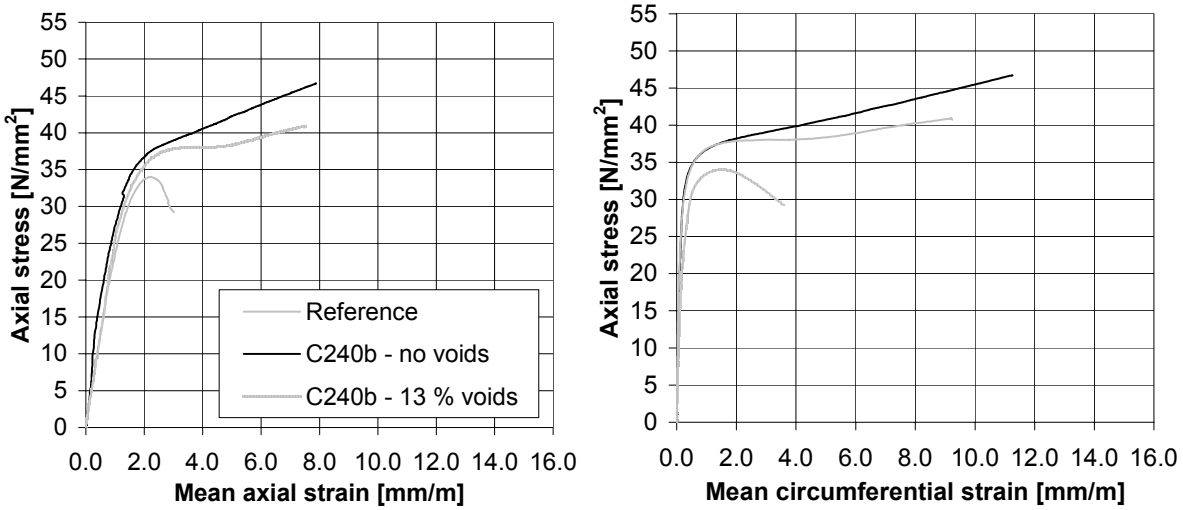

Fig. 6-6 *Stress-strain behaviour of wrapped cylinders, influence of voids*

3.2 Tests on confined columns

3.2.1 Behaviour at ultimate load

The test results of the columns in terms of maximum load Q_{max}, axial stress Q_{max}/A_g, strength increase, axial (ε_{c1} and ε_{cu}) and circumferential strains ($\varepsilon_{c\ell 1}$ and $\varepsilon_{c\ell u}$) at maximum and ultimate load respectively and ratio of the circumferential strain $\varepsilon_{c\ell u}$ over the FRP failure strain ε_{fum} are given in Table 6-5. The mentioned strains are the mean values of the strain gauge measurements.

Table 6-5 *Test results of compression tests on columns*

Specimen	Q_{max} [kN]	Q_{max}/A_g [N/mm^2]	Q/Q_{ref} [-]	ε_{c1} [mm/m]	ε_{cu} [mm/m]	$\varepsilon_{c\ell 1}$ [mm/m]	$\varepsilon_{c\ell u}$ [mm/m]	$\varepsilon_{c\ell u}/\varepsilon_{fum}$ [-]
K1 (Ø/Ref.)	4685	37.3	1.00	2.8	3.1[(1)]	1.7	1.8[(1)]	-
K2 (Ø/C240/#5/full)	7460	59.4	1.59	11.1	(12.0)[(2)]	6.9	(7.3)[(2)]	(0.61)[(2)]
K3 (Ø/C640/#4/full)	7490	59.6	1.60	4.3	4.3	2.5	2.5	1.14
K4 (Ø/G/#6/full)	7580	60.3	1.62	6.9	6.9	7.5	7.5	0.58
K5 (Ø/G/#2/full)	5325	42.4	1.14	3.8	3.8	6.8	8.0	0.62
K6 (Ø/G/#4/partial-circ.)	5000	39.8	1.07	2.8	3.3	1.6	3.3	0.25
K7 (Ø/G/#4/partial-helic.)	4810	38.3	1.03	2.2	2.2	3.1	3.3	0.25
K8 (Ø/H/#4/full)	6230	49.6	1.33	5.9	6.0	5.3	5.3	0.55
K9 (sq./r30/G/#2/full)	5810[(3)]	46.1	(1.24)[(3)]	(5.1)[(3)]	(5.1)[(3)]	(2.1)[(3)]	(2.1)[(3)]	(0.16)[(3)]
K10 (sq./r15/G/#2/full)	5140	40.8	1.10	3.2	4.2	1.8	3.4	0.26
K11 (rect./r30/G/#2/full)	4990	39.9	1.07	1.8	(1.9)[(4)]	0.6	(0.9)[(4)]	(0.07)[(4)]

[(1)] Test stopped at an axial strain of about 3.1 mm/m

[(2)] Problems with the load control unit of the actuator in the post peak region

[(3)] The load suddenly increased to failure after activating a 2nd pump

[(4)] Failure of the FRP at the column end (strain measurements located in central zone)

A strength increase up to 1.62 is found for the different columns and strongly depends on the column shape and wrapping configuration (wrapping lay-out, FRP type and amount). A further discussion on the effectiveness of the wrapping configuration in terms of strength increase and ductility is given in Section 3.2.2.

The confined concrete columns failed by fracture of the FRP reinforcement, as illustrated in Fig. 6-7. Except for column K11, the fracture occurred in the central zone of the specimens. Due to local contact between the FRP and the compression plate of the testing machine at one of the corners, the FRP fracture occurred at the column top for K11. For the fully wrapped circular columns at ultimate load, when confinement action was no longer provided due to FRP fracture, the internal steel started buckling and the crushed concrete fell down between the fractured FRP. Hence, this indicates that the concrete core is significantly damaged (but yet confined) even before reaching ultimate load. For the partially wrapped columns it was noted that the unconfined zones started crushing when reaching the strength of the plain concrete. For these columns, buckling of the internal steel occurred in the unconfined zones, after FRP failure. The square and rectangular columns failed by FRP fracture just beside one or more of the rounded corners. The failure aspect was similar as for the fully wrapped circular columns, although the concrete seemed less damaged. This may be related to the considerably lower failure loads of the square and rectangular columns. For none of the wrapped columns FRP failure at the overlap or anchorage zones occurred.

3.2.2 Stress-strain behaviour and effectiveness of wrapping configuration

Based on the stress-strain behaviour and the ratio $\varepsilon_{c\ell u}/\varepsilon_{fum}$, the influence of the type and amount of FRP and the effectiveness of the wrapping configuration are discussed in the following. It is remarked that the stress-strain behaviour of the columns, shown in Fig. 6-8 till Fig. 6-11, is based on the strain gauge measurements and does not show the unloading-reloading branch. More details on the measured stress-strain behaviour of the columns are provided in Appendix F.

3.2.2.1 Fully wrapped circular columns

Comparing the fully wrapped circular columns with the reference column (Table 6-5, Fig. 6-8 and Fig. 6-9), an increase in strength and ductility is noted. The strength increase basically depends on the amount and tensile strength of the FRP wrapping. The higher the axial stiffness (amount and E-modulus) of the FRP wrapping, the lower the ultimate axial strain and hence the lower the increase in ductility.

Although a ratio $\varepsilon_{c\ell u}/\varepsilon_{fum}$ close to or higher than 1.0 was found for the wrapped cylinders (Section 5.3.1), this is (except for K3) no longer the case for the fully wrapped circular columns. For these columns a ratio of about 0.6 is found. This may indicate that secondary effects near failure, such as stress concentrations in the FRP due to non-homogenous deformations of the damaged but yet confined concrete, have a more pronounced effect compared to tests on small scale specimens.

Fig. 6-7 *Failure aspect of the confined columns*

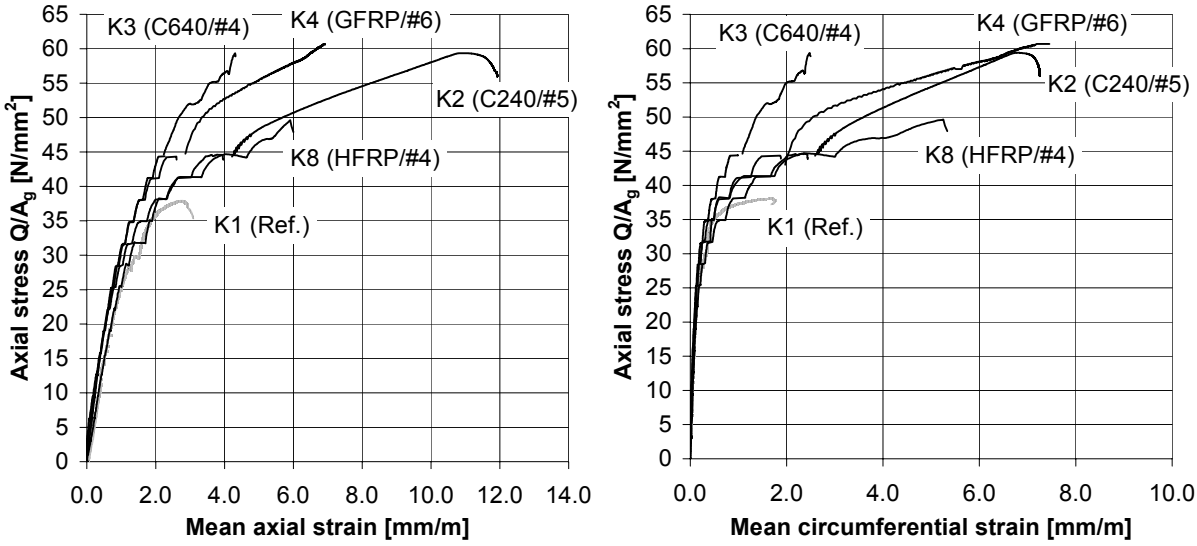

Fig. 6-8 *Stress-strain behaviour of fully wrapped circular columns, different types of FRP*

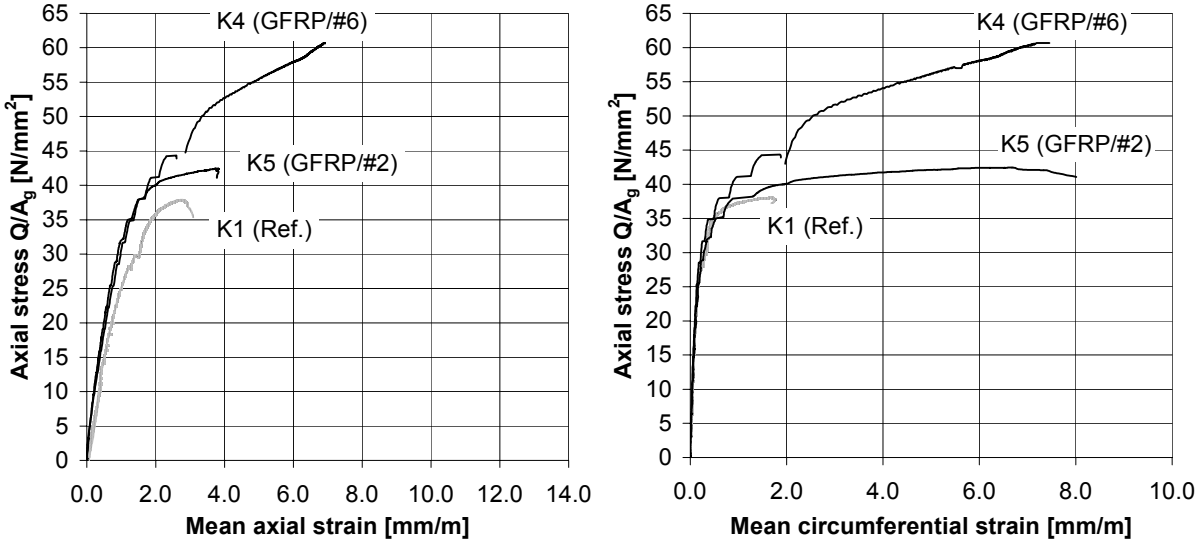

Fig. 6-9 *Stress-strain behaviour of circular columns fully wrapped with GFRP*

3.2.2.2 Partial wrapping

Comparing fully and partially wrapped columns with the same type and total amount of FRP (Table 6-5 and Fig. 6-10), less efficiency is obtained in case of partial wrapping as part of the concrete is unconfined. Furthermore, helicoidal wrapping results in a lower strength increase and axial strain compared to circular wrapping. This is due to the fact that the fibres are no longer aligned in an optimum way to restrain the lateral expansion of the concrete. The ratio $\varepsilon_{c\ell u}/\varepsilon_{fum}$ obtained for the partially wrapped columns (K6 and K7) equals 0.3, which is lower than the fully wrapped circular columns.

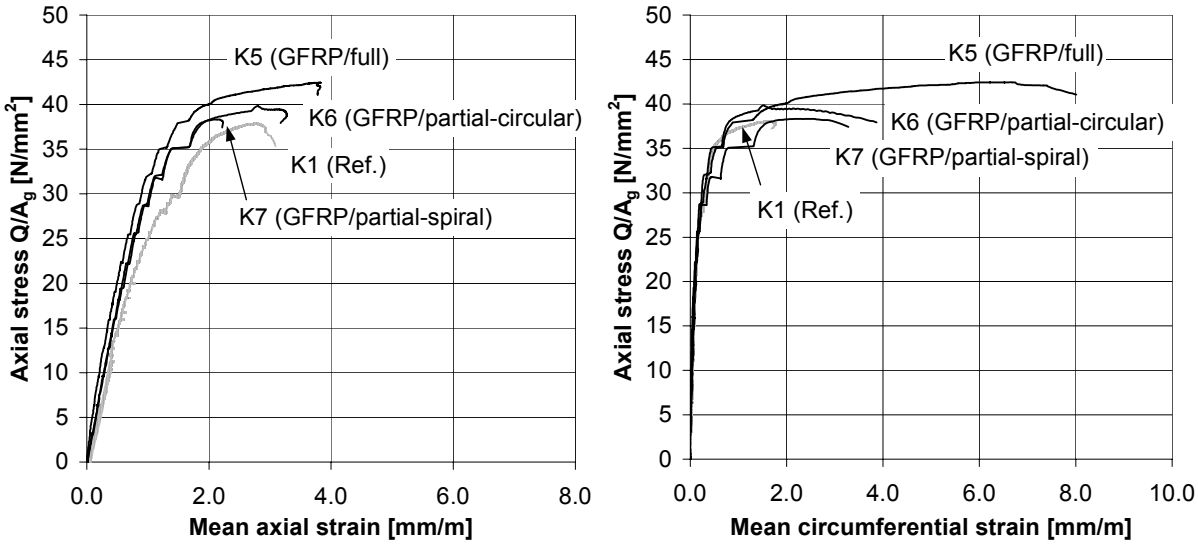

Fig. 6-10 *Partial versus full wrapping of circular columns*

3.2.2.3 Column shape

In Fig. 6-11 the influence of the column shape on the stress-strain behaviour is shown. From this figure as well as Table 6-5 it is noted that, except for column K9, a lower strength increase is obtained for the non-circular columns. The higher failure load of K9 (square) compared to K5 (circular) contradicts this trend and may be due to the problem with the test equipment while loading K9. As a result of this problem a very high loading rate was obtained at failure, which probably resulted in a higher failure load than would normally be the case. Considering a square or rectangular section and the radius at which the corners are rounded, it follows from the test results that the wrapping becomes more efficient as the cross-section approaches a circular section. Indeed, the confining action is mainly provided at the rounded corners, so that the radius should be as large as possible and the corners should be close to each other. Similar to partial wrapping, lower values of the ratio $\varepsilon_{c\ell u}/\varepsilon_{fum}$ are found for the non-circular columns compared to the fully wrapped circular columns.

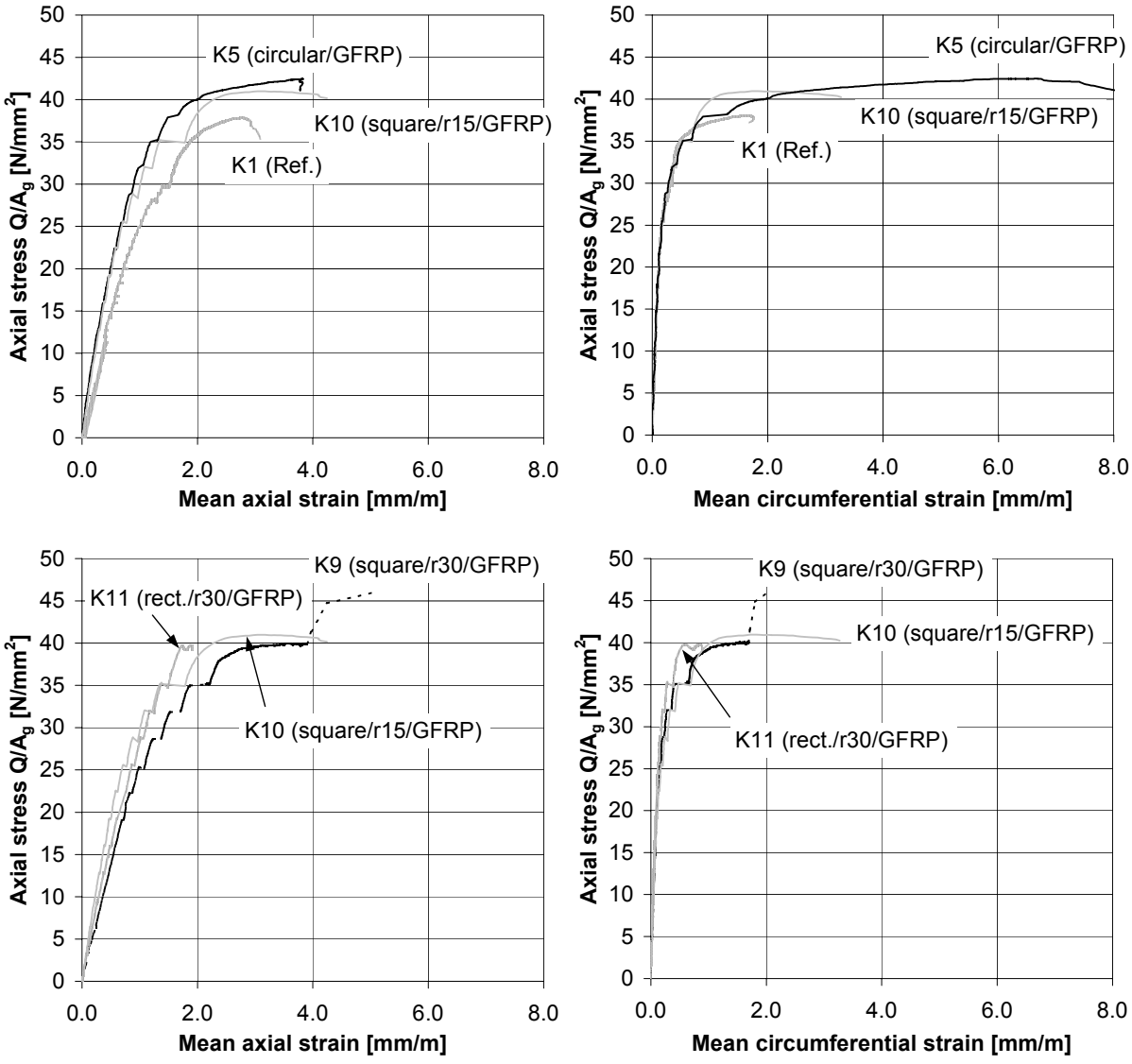

Fig. 6-11 *Stress-strain behaviour of fully wrapped circular and non-circular columns*

4 Analytical verification

4.1 Problem statement

Various models for confinement of concrete have been developed, primarily for steel wrapping reinforcement [11-19]. As also illustrated in Fig. 6-12, these models basically provide an equivalent uniaxial stress-strain relationship for confined concrete, a relationship for the strength of the confined concrete and an indication of the axial failure strain of the confined concrete. Applying these models in the case of FRP wrapping, the following specific aspects are encountered, which make these models less suitable in their present form [4,8,10].

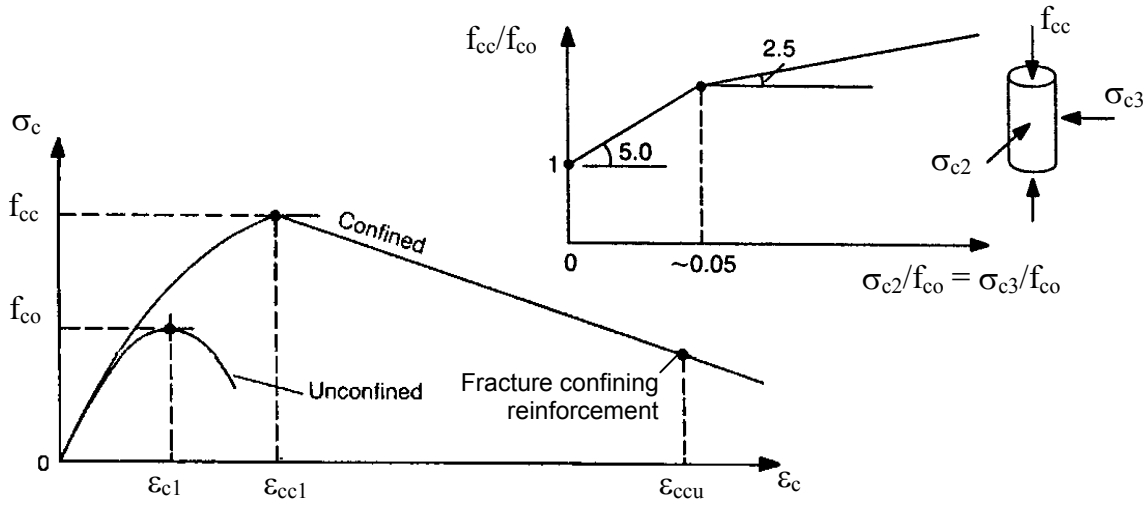

Fig. 6-12 *Model for confined concrete (constant confining action) [15]*

4.1.1 Constant versus increasing confining action

Whereas the models for steel wrapping reinforcement (Fig. 6-12) assume a constant confining pressure, in reality confinement action increases as concrete expands, its magnitude depending on the stress-strain law of the confining device. For steel transverse reinforcement, the constant confining pressure assumption is realistic when the steel is in the yield phase.

On the contrary, FRP behaves linear elastically until failure and the inward radial pressure increases with the lateral expansion of the concrete, so that the assumption of a constant confining pressure is no longer valid. Therefore, it is suggested that the confined concrete should be modelled more explicitly as a restraint sensitive material.

4.1.2 Effective circumferential failure strain

The ultimate strength of FRP confined concrete is strongly related to the in-situ failure strain of the FRP wrapping reinforcement. Experimental evidence shows that this circumferential failure strain is mostly smaller than the ultimate strain obtained from standard tensile testing of the FRP reinforcement. This reduction can be attributed to several causes:

- The FRP reinforcement basically provides transverse confinement action, but is at the same time submitted to axial loading as typically some degree of bonding is provided between the concrete and the FRP.
- Although confined and still able to resist loads, near failure the concrete is internally cracked and non-homogenous deformations occur. Due to these non-homogenous deformations, local stress concentrations may occur in the FRP reinforcement.
- As the concrete is damaged internally and given the high load levels, the longitudinal steel reinforcement tends to buckle, which is prevented by the FRP wrapping. Nevertheless, this initiates additional stress concentrations.
- The curved shape of the wrapping reinforcement, especially at corners with a small radius (wrapping of square or rectangular columns), the presence of voids or protrusions, misalignment of fibres, etc. may reduce the FRP axial strength.
- Size effects, for example in case of multiple layers.

4.1.3 Axial failure strain

The axial failure strain of the confined concrete is related to fracture of the confining reinforcement and hence should meet the strain compatibility in circumferential direction. Models based on a constant confining action do not consider this aspect, but provide other means such as the energy balance approach suggested by Mander [14]. Herewith, the strain energy stored in the confining reinforcement is set equal to the difference between the axial strain energy of the confined and unconfined concrete. In the case of FRP confined concrete it was found that this method yields unrealistic results compared to the experiments. This may be due to the fact that the energy balance approach neglects the lateral strain energy stored in the concrete.

Another aspect concerns the relation between the failure (ultimate) point and the peak strength. For steel confined concrete, generally a softening branch is observed which means that the axial failure strain is obtained after reaching the maximum strength of the confined concrete. The test results in Section 3 suggest that this is mostly not the case for FRP confined concrete, where (except for very low ultimate confining pressures) no softening branch was obtained.

4.2 Lateral confining pressure exerted by the FRP

4.2.1 Fully wrapped cylindrical specimens with fibres perpendicular to longitudinal axis

For uniaxially loaded cylindrical concrete specimens confined with FRP reinforcement, with fibres aligned according to the circumferential direction and covering the total concrete surface, the lateral confining pressure may be found by considering Fig. 6-13 (left). Assuming uniform tension in the FRP, a uniform lateral pressure is exerted on the concrete core, whereby the equilibrium of forces requires that:

$$2\sigma_f A_f = \sigma_\ell s D \tag{6-1}$$

where, σ_f is the stress in the FRP, $A_f = b_f t$ is the area of the FRP wrapping reinforcement, b_f is the width of the FRP, t is the FRP thickness (total thickness in case of multiple layers), σ_ℓ is the lateral confining pressure on the concrete, s is the centre to centre spacing of the FRP (s = b_f for fully wrapped cylinders) and D is the diameter of the cylindrical specimen. Considering the ratio of the volume of confining FRP to the volume of confined concrete core:

$$\rho_f = \frac{A_f \pi D}{\frac{\pi D^2}{4} s} = \frac{4 b_f t}{D s} \quad \left(= \frac{4t}{D} \quad \text{when} \quad b_f = s \right) \tag{6-2}$$

Eq (6-1) can be rewritten as:

$$\sigma_\ell = \frac{1}{2} \rho_f \, \sigma_f \tag{6-3}$$

or, also:

$$\sigma_\ell = K_{conf} \varepsilon_{c\ell=f} \quad \text{with} \quad K_{conf} = \frac{1}{2} \rho_f E_f \tag{6-4}$$

where, K_{conf} represents the stiffness of the FRP confinement, ρ_f is the volumetric ratio of the FRP wrapping reinforcement and $\varepsilon_{c\ell=f}$ is the circumferential strain of the concrete. In the case of proper and bonded FRP wrapping, the latter equals the FRP strain.

Hence, the lateral confining pressure σ_ℓ exerted by the FRP is calculated based on its current stress $\sigma_f = E_f \, \varepsilon_f \le f_{f,eff}$. The maximum lateral confinement pressure $\sigma_{\ell u}$ is obtained as:

$$\sigma_{\ell u} = \frac{1}{2} \rho_f \, E_f \varepsilon_{fu,eff} \tag{6-5}$$

with $\varepsilon_{fu,eff}$ the effective failure strain of the FRP wrapping reinforcement as discussed in Section 4.4.

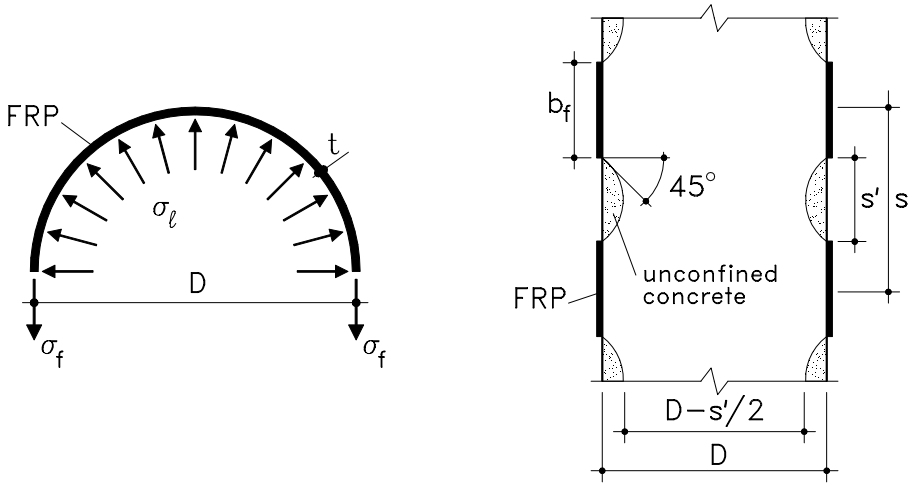

Fig. 6-13 *Confining pressure exerted by the FRP*

4.2.2 Influence of partial wrapping

If the concrete is partly wrapped, less efficiency is obtained as both confined and unconfined zones exist (Fig. 6-13, right). In this case, the effective lateral confining pressure is obtained from Eq. (6-4) by introducing a confinement effectiveness coefficient $k_e \leq 1$, so that:

$$K_{conf} = \frac{1}{2} k_e \rho_f E_f \tag{6-6}$$

The effectiveness coefficient is obtained by considering that the transverse pressure from the confining device is only effective on that part of the concrete where the confining pressure has fully developed due to arching action [14]. As illustrated in Fig. 6-13, the arching effect is assumed according to a parabola with an initial slope of 45°. Midway between two successive FRP wraps, the area of effectively confined concrete core A_e is the smallest:

$$A_e = \frac{\pi}{4}\left(D - \frac{s'}{2}\right)^2 \tag{6-7}$$

where, $s' = s - b_f$ is the clear spacing between the FRP wrapping reinforcement. The confinement effectiveness coefficient k_e is then obtained by considering the ratio A_e/A_c, with $A_c = A_g - A_s$ the area of concrete (gross cross-sectional area minus area of longitudinal steel reinforcement):

$$k_e = \frac{\left(1 - \frac{s'}{2D}\right)^2}{1 - \rho_{sg}} \tag{6-8}$$

where, $\rho_{sg} = A_s/A_g$ is the reinforcement ratio of the longitudinal steel reinforcement with respect to the gross cross-sectional area.

4.2.3 Influence of fibre orientation

If the fibres are applied in a helicoidal way, the fibre alignment is less efficient to restrain the lateral expansion of the concrete. Similar to the previous section, this effect can be considered by introducing a corresponding confinement effectiveness coefficient.

Assuming a uniform tension force N_f in the FRP, the confinement pressure exerted by the helicoidal FRP wrapping reinforcement is given by:

$$\sigma_{\ell,h} = \frac{N_f}{b_f R} \tag{6-9}$$

where, R is the curvature of the helix, given as:

$$R \approx \frac{k^2 + r^2}{r} \tag{6-10}$$

with, $k = p/2\pi$, p the pitch (vertical separation of the helix hoops) and $r = D/2$ the radius. In a similar way, the confinement pressure per unit width exerted by circular FRP wrapping reinforcement is obtained as:

$$\sigma_{\ell,c} = \frac{N_f}{b_f r} \tag{6-11}$$

Based on Eqs. (6-9) till (6-11), the confinement effectiveness coefficient can be defined as:

$$k_e = \frac{\sigma_{\ell,h}}{\sigma_{\ell,c}} = \frac{1}{1+\left(\frac{p}{\pi D}\right)^2} \tag{6-12}$$

4.2.4 Influence of column shape

For a square or rectangular section wrapped with FRP (Fig. 6-14) and with corners rounded with a radius r_c, the parabolic arching action [14] is again assumed for the concrete core where the confining pressure is fully developed. Unlike a circular section, for which the concrete core is fully confined, a large part of the cross-section remains unconfined.

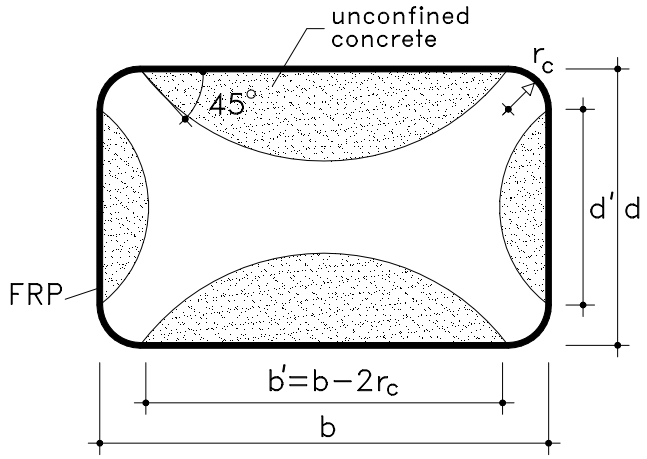

Fig. 6-14 *Effectively confined core for non-circular sections*

Taking the sum of the different parabolas, the total plan area of unconfined concrete is obtained as:

$$A_u = \sum_{i=1}^{4} \frac{(w_i')^2}{6} = \frac{b'^2 + d'^2}{3} \tag{6-13}$$

where, w'_i is the clear distance between the rounded corners. Considering the ratio $(A_c - A_u)/A_c$, the confinement effectiveness coefficient k_e is given by:

$$k_e = 1 - \frac{b'^2 + d'^2}{3A_g(1-\rho_{sg})} \tag{6-14}$$

Similar to Eq. (6-4) (circular section), the lateral confining pressures induced by the FRP wrapping reinforcement on a square or rectangular cross-section are given as:

$$\sigma_{\ell x} = K_{confx}\,\varepsilon_f \quad \text{with} \quad K_{confx} = \rho_{fx}\,k_e E_f$$
$$\sigma_{\ell y} = K_{confy}\,\varepsilon_f \quad \text{with} \quad K_{confy} = \rho_{fy}\,k_e E_f \tag{6-15}$$

where, the ratios ρ_{fx} and ρ_{fy} represent the quantities of transverse confining reinforcement in the x and y direction and are given by:

$$\rho_{fx} = \frac{2b_f t}{s\,d} \quad \text{and} \quad \rho_{fy} = \frac{2b_f t}{s\,b} \tag{6-16}$$

4.3 Stress-strain relationship of FRP confined concrete

4.3.1 General

Taking into account the considerations of Section 4.1, Fig. 6-15 schematically illustrates a calculation model for the stress-strain behaviour of FRP confined concrete submitted to an increasing load. Given the circumferential strain and the corresponding FRP confining pressure, the stress-stain response of the confined concrete is obtained. In fact, this method is based on a combination of different models for the uniaxial stress-strain response of confined concrete, the lateral expansion of the concrete, the confining pressure exerted by the FRP wrapping reinforcement and a failure criterion taking into account the effective FRP failure strain. The basic aspect in the modelling is that the increasing confining action by the FRP should be taken into account.

In the literature, three recent models have been proposed for FRP confined concrete [17-19], which are verified in the following. Details on these models (approach, background, equations and calculation procedure) are given in Appendix F, Section 1.

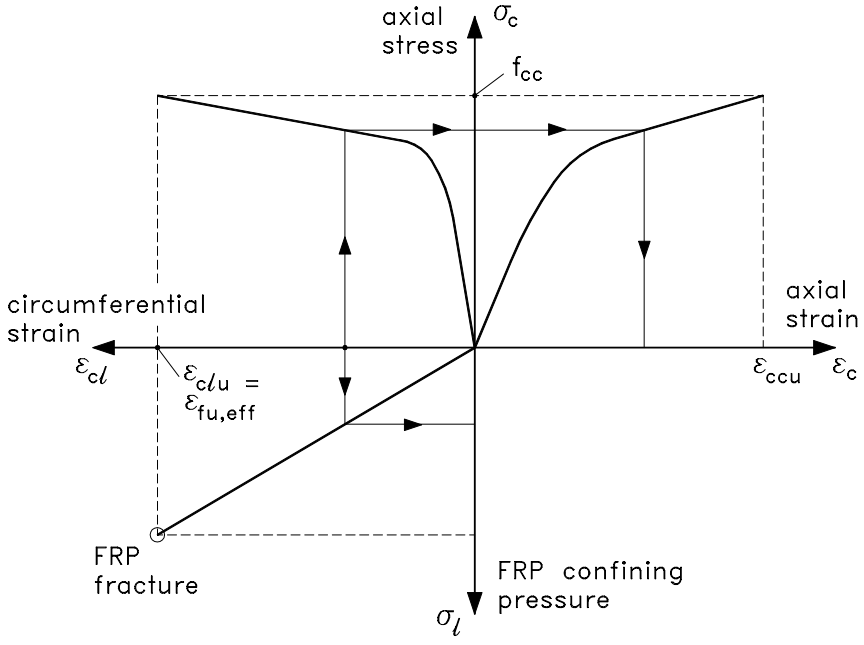

Fig. 6-15 *FRP confined concrete (incremental confining pressure)*

In the model developed by Spoelstra and Monti [17] an incremental-iterative calculation is proposed which combines the often applied steel confinement model of Mander et al [14] with a model linking the axial and the circumferential strain by Pantazopoulou and Mills [20]. An incremental approach is also followed by Toutanji [18], which can be solved without iteration. The model considers an initial region of the stress-strain behaviour which is similar to that of unconfined concrete, since lateral expansion of the concrete is small. The second region, where the FRP confinement is fully activated, is calculated based on the confinement model by Richart et al [11], whereas model coefficients are experimentally calibrated. Yet another approach is suggested by Samaan et al [19]. This model assumes a simplified bilinear relationship for the stress-strain behaviour by Richard and Abbot [21] and is based on the observation that the dilation rate (change of circumferential strain with respect to the axial strain) of FRP confined concrete approaches an asymptotic value. Hence, it is suggested to model the restraining action of the FRP by taking into account the ultimate confining pressure and the stiffness of the FRP wrapping only, without further need for an incremental approach. Model parameters of the stress-strain relationship are experimentally calibrated.

More details on the approach and background of these models can be found in Appendix F, Section 1. An overview of the basic differences in approach of these models is given in Appendix F, Section 1.4.

4.3.2 Analytical verification

A comparison between these models and the recorded stress-strain behaviour is shown, for some of the cylindrical specimens, in Fig. 6-16 and Fig. 6-17. The measured axial concrete stress was obtained from the measured load as:

$$\sigma_{c,exp} = \frac{Q_{exp}}{A_c} - \sigma_s \frac{A_s}{A_c} \quad \text{with} \quad \sigma_s = \min\left(\varepsilon_{c,exp} E_s , f_y\right) \tag{6-17}$$

The calculations have been performed according to Appendix F, Section 1, with experimental material properties according to Appendix B. The ultimate stage was assumed to occur when reaching the FRP failure strain $\varepsilon_{fu} = f_f/E_f$. For the columns, instead of the compressive cylinder strength f_c, the compressive strength $f_{c,prism}$ measured on prisms 200 mm x 200 mm x 500 mm was introduced for the strength of the plain concrete. This was done because:

- a considerable variance was found for the measured values of f_c, which was significantly higher than the variance of $f_{c,prism}$ or $f_{c,cube}$ (Table B-7)
- $f_{c,prism}$ gives a better estimation of the plain concrete compressive strength of the columns.

From the analytical verification (Fig. 6-16 and Fig. 6-17) the following is concluded:

- A considerable difference is found between the different models. In general the best predictions are obtained with the model by Spoelstra and Monti.
- For a given load level, the model by Samaan et al tends to overestimate the axial and circumferential strains in a considerable way. Also, the initiation and slope of the second

branch of the stress-strain curves is often not accurately predicted. Although the model may be subject to improvement (as it strongly depends on experimental calibration [19]), it is probably not versatile enough to be generally applicable.

- For the fully wrapped specimens, the circumferential strain is predicted in a fairly accurate way for both the Spoelstra and Toutanji model. On the contrary, for a given load level, the Toutanji model considerably underestimates the axial strain response.
- The models by Samaan et al and Toutanji can only predict an increasing load-strain response. Although this is often the case for FRP confined concrete, the conducted tests reported in Section 3 show that a decreasing (post-peak) branch may be obtained as well in particular cases. The model by Spoelstra and Monti allows the prediction of a post-peak response.
- Making reference to a failure criterion based on $\varepsilon_{fu} = f_f/E_f$, the ultimate strain of the wrapped specimens is overestimated, often in a considerable way. As a result, also the maximum load is not always accurately predicted. Hence, it is important that a reduced FRP failure strain, due to the effects discussed in Section 4.1.2, is taken into account.

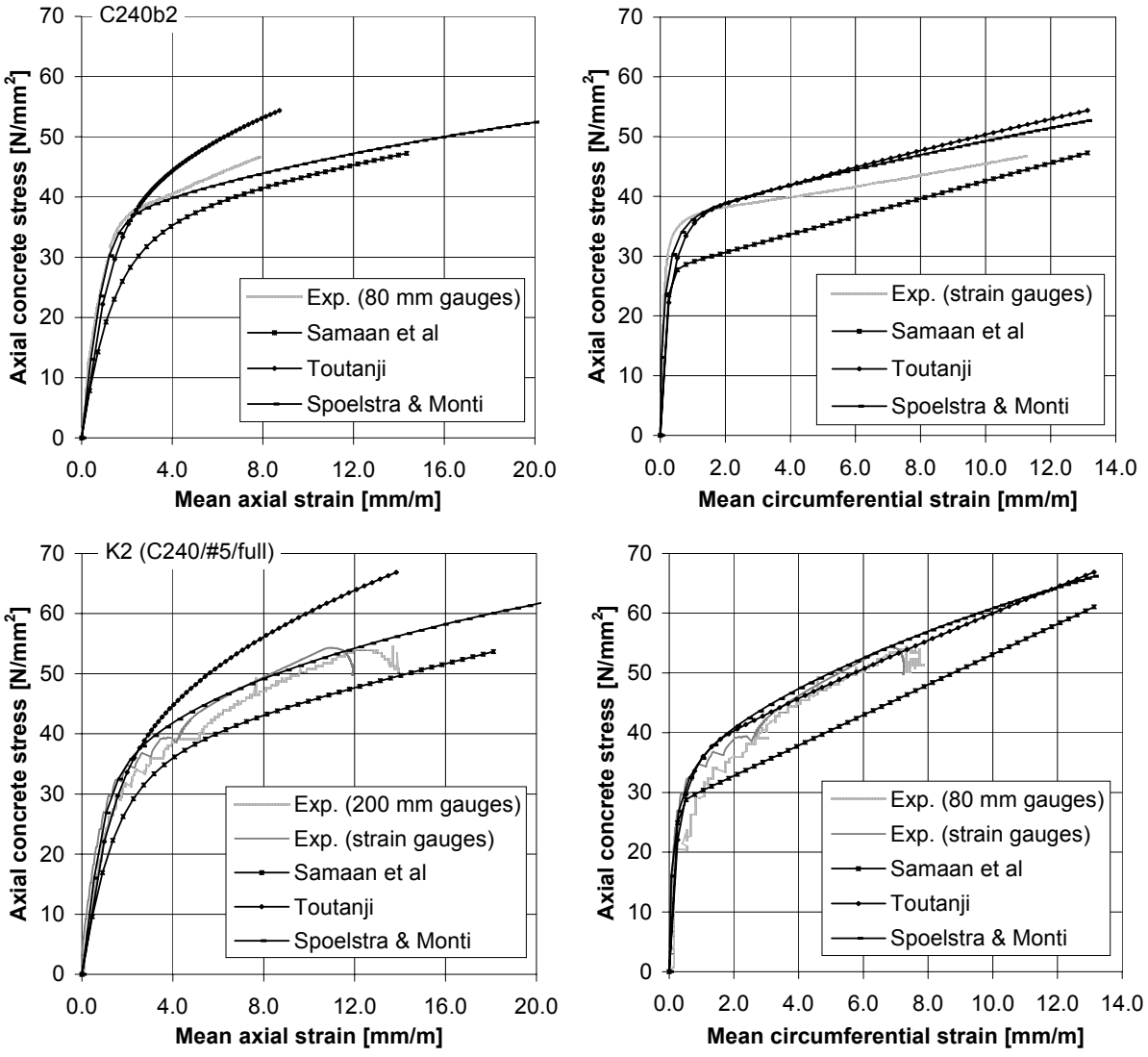

Fig. 6-16 *Analytical verification for cylinder C240b2 and column K2 (fully wrapped)*

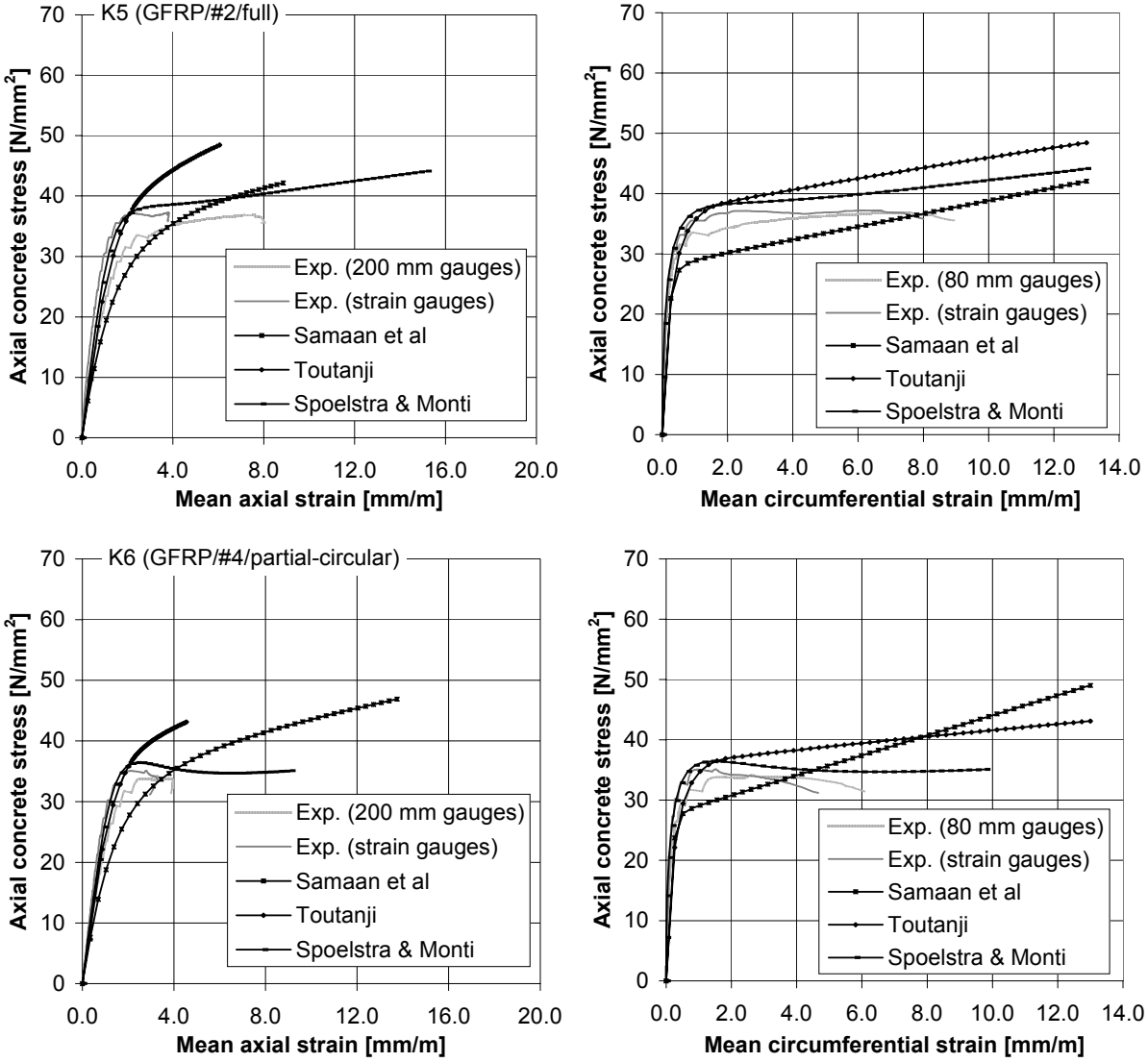

Fig. 6-17 *Analytical verification for columns K5 and K6 (fully and partially wrapped)*

– The modelling of the stress-strain response of FRP confined concrete, taking into account an increasing confining pressure, is more complex than in the case of steel confined concrete where a constant confining pressure may be assumed. From the three proposed models investigated, only the incremental-iterative approach by Spoelstra and Monti resulted in accurate predictions of the stress-strain behaviour.

Based on the model by Spoelstra and Monti and taking into account the failure criterion discussed in the following section, a comparison between the experimental and modelled stress-strain response, for all the FRP confined specimens, is shown in Appendix F, Section 2. A good correspondence between the experimental results and the analytical verification, for both the stress-strain response and the ultimate load (see also Section 4.5), are found.

4.4 Confined concrete strength and ultimate strain

Although the model by Spoelstra and Monti was found to be accurate for the prediction of the stress-strain response, it is rather complex to apply. Moreover, for design practice, it is mostly sufficient to know the compressive strength and ultimate strain of the confined concrete and not the complete stress-strain response.

4.4.1 Ultimate state

Irrespective of the complete stress-strain response, the ultimate state can be derived directly from the maximum confinement pressure, as illustrated in Fig. 6-18 (left) [17]. The ultimate compressive stress σ_{ccu} and strain ε_{ccu} are found from the intersection between the stress-strain curve assuming a constant confining pressure $\sigma_{\ell u}$ and the straight line with slope $E_{sec,u}$. For the former, the confinement model by Mander et al [14] is used, as given by Eqs. (F-1) and (F-2) in Appendix F, Section 1.1.2. The secant modulus of elasticity at failure $E_{sec,u}$ follows from Eq. (F-4) as [20]:

$$E_{sec,u} = \frac{E_c}{1 + 2\beta\varepsilon_{c\ell u}} \quad \text{with} \quad \beta = \frac{E_c}{f_{co}} - \frac{1}{\varepsilon_{c1}} \tag{6-18}$$

where, E_c is the tangent modulus of elasticity of the concrete at the origin, $\varepsilon_{c\ell u} = \varepsilon_{fu,eff}$ is the ultimate circumferential concrete strain, $\varepsilon_{fu,eff}$ is the effective FRP failure strain as defined in Section 4.4.3, f_{co} is the unconfined concrete strength and $\varepsilon_{c1} \approx 2$ mm/m is the compressive strain corresponding to f_{co}. The point of intersection (Fig. 6-18, left) yields:

$$\varepsilon_{ccu} = \varepsilon_{cc1M}\left(\frac{E_{sec,M}(E_c - E_{sec,u})}{E_{sec,u}(E_c - E_{sec,M})}\right)^{1-E_{sec,M}/E_c} \tag{6-19}$$

$$\sigma_{ccu} = E_{sec,u}\varepsilon_{ccu} \tag{6-20}$$

where, $E_{sec,M} = f_{ccM}/\varepsilon_{cc1M}$, f_{ccM} is the confined concrete strength assuming constant confining pressure $\sigma_{\ell u}$ and ε_{cc1M} is the corresponding axial strain. These parameters are given by [14,16]:

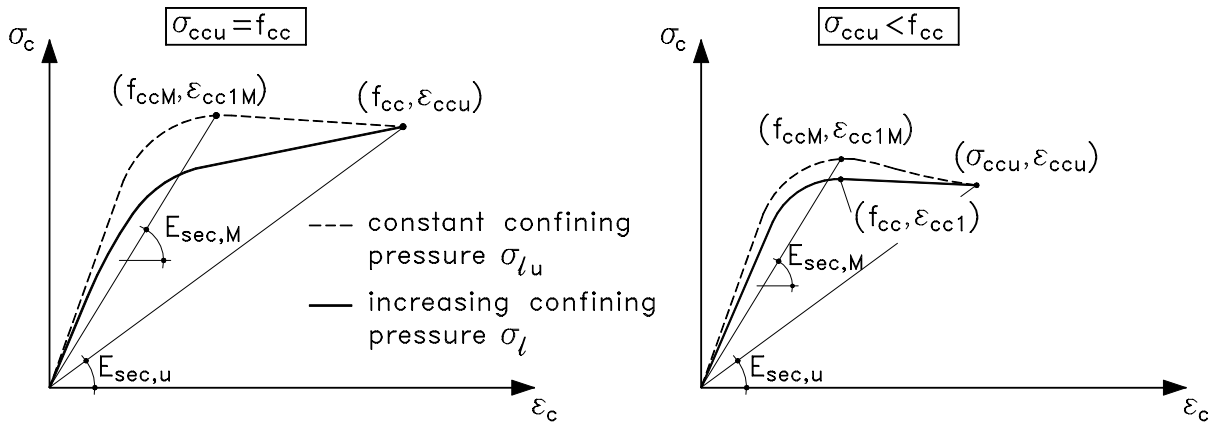

Fig. 6-18 *Modelling of the ultimate compressive strength and strain*

$$f_{ccM} = \alpha_1 \alpha_2 f_{co} \quad \text{and} \quad \varepsilon_{cc1M} = \varepsilon_{c1}\left(1 + 5\left(\alpha_1 \alpha_2 - 1\right)\right) \tag{6-21}$$

with,

$$\alpha_1 = 2.254\sqrt{1 + 7.94\frac{\sigma_{\ell ux}}{f_{co}}} - 2\frac{\sigma_{\ell ux}}{f_{co}} - 1.254 \tag{6-22}$$

$$\alpha_2 = 1 - \left(0.6\left(\frac{\sigma_{\ell uy}}{\sigma_{\ell ux}}\right)^2 - 1.4\frac{\sigma_{\ell uy}}{\sigma_{\ell ux}} + 0.8\right)\sqrt{\frac{\sigma_{\ell ux}}{f_{co}}} \tag{6-23}$$

where, $\sigma_{\ell ux} = \sigma_{\ell uy} = \sigma_{\ell u}$ (and hence $\alpha_2 = 1$) given by Eq. (6-5), is the maximum FRP confining pressure for circular cross-sections and $\sigma_{\ell ux} \geq \sigma_{\ell uy}$ given by Eq. (6-15), is the maximum FRP confining pressure in the case of square or rectangular cross-sections. These confining pressures correspond to the effective FRP failure strain $\varepsilon_{fu,eff}$ given in Section 4.4.3.

4.4.2 Confined concrete strength

Often, the compressive strength f_{cc} of the confined concrete is obtained at failure of the FRP wrapping reinforcement, as illustrated in the left part of Fig. 6-18. In this case, the confined concrete strength f_{cc} equals the ultimate stress σ_{ccu}, given by Eq. (6-20).

On the contrary, for low amounts of FRP wrapping reinforcement or low efficiency (square or rectangular cross-sections, partial wrapping), it appears from the test results and the analytical modelling that the stress-strain behaviour may be characterized by a decreasing (post-peak) branch near failure, as shown in the right part of Fig. 6-18. In this case ,the confined concrete strength f_{cc} is larger than the ultimate stress σ_{ccu}. This is also noted from the normalised axial stress σ_c/f_{co} versus circumferential strain $\varepsilon_{c\ell}$ curves shown in Fig. 6-19, calculated according to Appendix F, Section 1.1. From these curves it follows that $\sigma_{ccu} < f_{cc}$ occurs for FRP wrapped members for which the parameter K_{conf}/f_{co} is smaller than 3 (or 2 for HSC). In this situation, the normalised peak stress f_{cc}/f_{co} equals 1.00 to 1.02 and corresponds to a circumferential strain $\varepsilon_{c\ell 1} \approx 0.0012$.

From these observations it can be concluded that a low ($K_{conf}/f_{co} < 3$) ultimate confining pressure $\sigma_{\ell u}$ results in an almost negligible strength increase, so that the confined concrete strength f_{cc} can be obtained according to Section 4.4.1 as:

$$f_{cc} = E_{sec,u}\varepsilon_{ccu} \geq f_{co} \tag{6-24}$$

The normalised peak stress f_{cc}/f_{co} according to this equation, compared to Eq. (6-22) (which gives f_{cc}/f_{co} for cylindrical members in case of a constant confining pressure $\sigma_{\ell u}$), is given in Fig. 6-20.

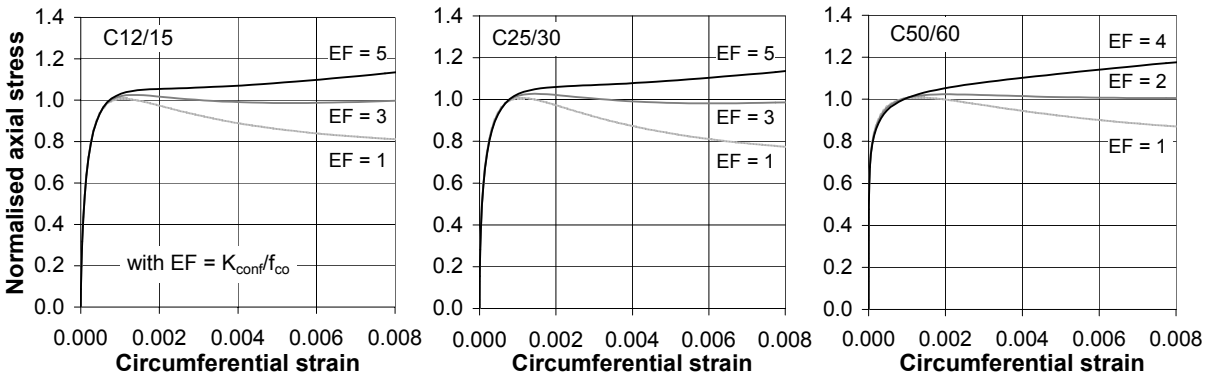

Fig. 6-19 *Influence of confinement stiffness parameter on stress-strain behaviour*

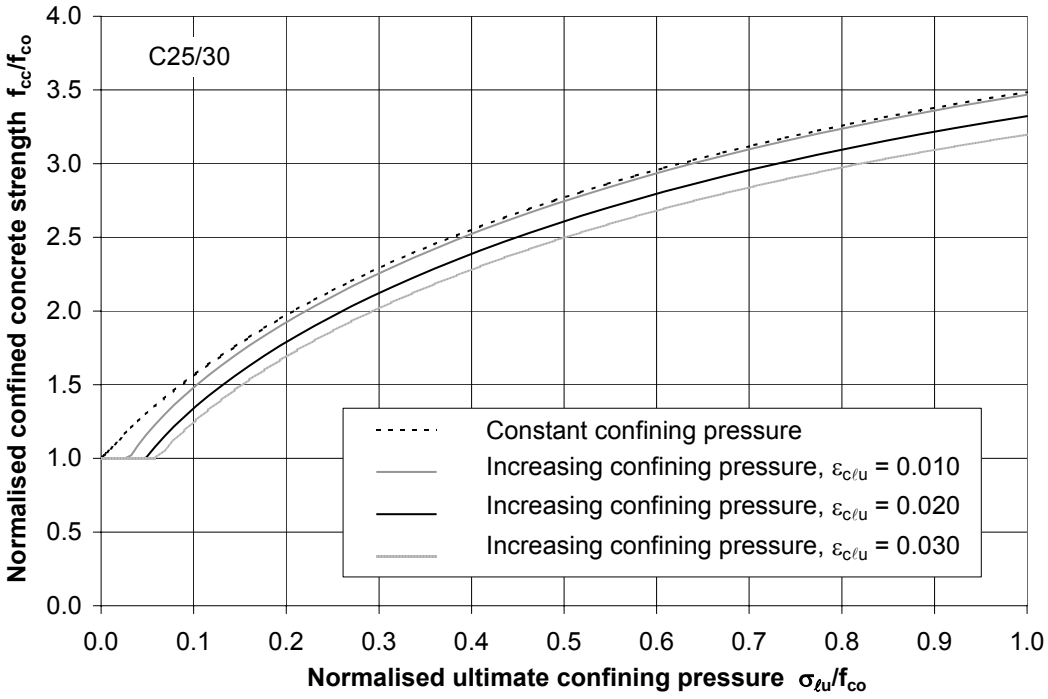

Fig. 6-20 *Confined concrete strength*

4.4.3 Effective FRP failure strain

According to the obtained test results and as discussed in Section 5.4.1.2, the mean effective FRP failure strain $\varepsilon_{fu,eff}$ when reaching the ultimate state of the wrapped members is lower than the ultimate FRP strain $\varepsilon_{fu} = f_f/E_f$. This aspect is introduced in the calculations by means of the ratio $\eta_e = \varepsilon_{fu,eff}/\varepsilon_{fu}$, so that the maximum lateral confinement pressure $\sigma_{\ell u}$ is obtained as:

$$\sigma_{\ell u} = K_{conf} \frac{\eta_e f_f}{E_f} \tag{6-25}$$

where, K_{conf} is given by Eq. (6-6) for circular cross-sections and by Eq. (6-15) for square or rectangular cross-sections.

As the effective FRP failure strain depends on various aspects, for which the influence and interaction are difficult to quantify analytically, an experimental relationship for η_e is tentatively proposed in the following. From the ratio $\varepsilon_{c\ell u} / \varepsilon_{fum}$ experimentally obtained (Table 6-4 and Table 6-5), it follows that the effective FRP failure strain decreases for large size specimens, partial wrapping and in case of square or rectangular cross-sections. Based on these observations, it was decided to express the effective FRP failure strain and hence the ratio η_e as a function of the parameter K_{conf}, which represents both the confining stiffness and effectiveness. For rectangular columns, the mean value $(K_{confx} + K_{confy})/2$ is considered. First, a curve fitting based on the ($\varepsilon_{c\ell u} / \varepsilon_{fum}$, K_{conf}) data points was performed. This approach was however abandoned, as the experimental ratio $\varepsilon_{c\ell u} / \varepsilon_{fum}$ may be considerably influenced by the location and number of strain measurements. Secondly, the curve fitting was based on the ($\varepsilon_{c\ell u,fit} E_f / f_f$, K_{conf}) data points, where $\varepsilon_{c\ell u,fit}$ is the circumferential strain taken so that the analytical verification according to Section 4.4.1 corresponds to the ultimate load of the tested specimens. The considered data base is given in Appendix F, Section 3. Only data was used for which $K_{conf} > 5f_c$ (if not, the strengthening ratio is very small so that the prediction of η_e becomes highly sensitive to the accuracy of f_c). The obtained data points and resulting curve fitting are shown in Fig. 6-21. The obtained expression equals:

$$\eta_e = 0.105(K_{conf})^{0.266} \tag{6-26}$$

with K_{conf} in N/mm^2 (η_e non-dimensional). As η_e is related to f_f/E_f, the strength and stiffness of the FRP should be known. Because the characterization of the tensile properties of FRP is influenced by the way of testing and because a detailed standard test is not available, f_f and E_f are often not known in an accurate or uniform way. This makes it very difficult to calibrate or verify the relationship for η_e.

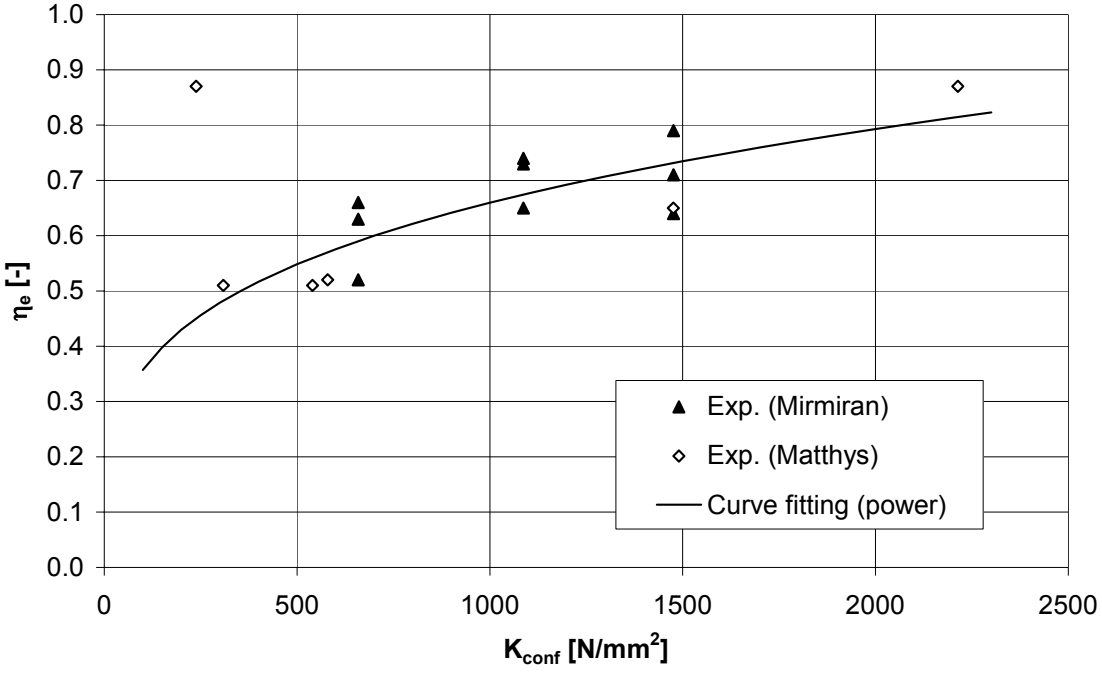

Fig. 6-21 *Effective FRP failure strain*

4.5 Load carrying capacity of the wrapped members

Based on the FRP confined concrete strength f_{cc}, obtained according to Section 4.4, the load carrying capacity of the wrapped specimens is calculated by:

$$Q_{max} = f_{cc} A_c + \sigma_s A_s \tag{6-27}$$

where, $\sigma_s = E_s \varepsilon_{cc1} \leq f_y$ is the stress in the longitudinal steel reinforcement, ε_{cc1} is the concrete axial strain corresponding to f_{cc} and f_y is the yield stress of the internal steel reinforcement. In Eq. (6-27), $\sigma_s = f_y$ may be assumed as generally large strains ε_{cc1} are obtained for confined members. However, in case of a small lateral confining pressure $\sigma_{\ell u}$, so that $\sigma_{ccu} < f_{cc}$ (Fig. 6-18, right), this assumption may no longer be valid. As in this case the strength increase is negligible ($f_{cc} = f_{co}$), $\sigma_s = E_s \varepsilon_{c1} \leq f_y$ with $\varepsilon_{c1} = 2$ mm/m can be assumed.

The load carrying capacity of the tested specimens, calculated according to Eq. (6-27), is given in Table 6-6 and Table 6-7. In Table 6-6, the ultimate state of the wrapped specimens is assumed for $\varepsilon_{fu} = f_f/E_f$. As the effective FRP failure strain $\varepsilon_{fu,eff}$ is lower than f_f/E_f (Section 4.1.2), the maximum load of the tested specimens is overestimated. Hence, more accurate predictions of the load carrying capacity are obtained taking into account $\varepsilon_{fu,eff} = \eta_e f_f/E_f$ (Table 6-7). The good results obtained in Table 6-7 follow of course from the fact that η_e has been partly calibrated based on the conducted tests. Therefore, it should be kept in mind that the equation proposed for η_e is based on limited data and needs further verification by other researchers.

Table 6-6 *Analytical verification of load carrying capacity for $\varepsilon_{fu} = f_f/E_f$*

Specimen	Q_{exp} [kN]	f_{co} [N/mm^2]	ε_{fu} [mm/m]	f_{cc} [N/mm^2]	ε_{cc1} [mm/m]	Q_{cal} [kN]	Q_{cal}/Q_{exp} [-]
Ref.	616	34.8	-	-	2.0	615	1.00
C240b[(1)]	814	34.8	13.1	52.7	20.4	931	1.14
C640b[(1)]	809	34.8	2.3	52.8	5.0	933	1.15
K1 (Ø/Ref.)	4685	34.6	-	-	2.0	4761	1.02
K2 (Ø/C240/#5/full)	7460	33.6	13.1	66.1	26.5	8938	1.20
K3 (Ø/C640/#4/full)	7490	33.6	2.3	57.8	5.6	7897	1.05
K4 (Ø/G/#6/full)	7580	36.1	13.0	67.2	23.1	9068	1.20
K5 (Ø/G/#2/full)	5325	36.1	13.0	44.1	15.2	6197	1.16
K6 (Ø/G/#4/partial-circ.)	5000	35.5	13.0	35.9	12.0	5173	1.03
K7 (Ø/G/#4/partial-helic.)	4810	35.5	13.0	35.5[(2)]	2.0[(2)]	4873	1.01
K8 (Ø/H/#4/full)	6230	34.1	11.3	45.7	15.1	6397	1.03
K9 (sq./r30/G/#2/full)	(5810)[(3)]	34.1	13.0	35.5	13.3	5095	(0.88)[(3)]
K10 (sq./r15/G/#2/full)	5140	36.0	13.0	36.0[(2)]	2.0[(2)]	4978	0.97
K11 (rect./r30/G/#2/full)	4990	36.0	13.0	36.0[(2)]	2.0[(2)]	4920	0.99

[(1)] Wrapped cylinders with more than 5 % voids excluded

[(2)] $f_{cc} = f_{co}$ and $\varepsilon_{cc1} = 2$ mm/m (low ultimate confining pressures so that $f_{ccu} < f_{cc}$)

[(3)] The load suddenly increased to failure after activating a 2nd pump

Table 6-7 *Analytical verification of load carrying capacity for* $\varepsilon_{fu,eff} = \eta_e f_f / E_f$

Specimen	Q_{exp} [kN]	f_{co} [N/mm^2]	η_e [-]	$\varepsilon_{fu,eff}$ [mm/m]	f_{cc} [N/mm^2]	ε_{cc1} [mm/m]	Q_{cal} [kN]	Q_{cal}/Q_{exp} [-]
Ref.	616	34.8	-	-	-	2.0	615	1.00
C240b[(1)]	814	34.8	0.48	6.3	45.7	8.9	806	0.99
C640b[(1)]	809	34.8	0.73	1.7	47.8	3.6	843	1.04
K1 (Ø/Ref.)	4685	34.6	-	-	-	2.0	4761	1.02
K2 (Ø/C240/#5/full)	7460	33.6	0.57	7.5	57.2	13.6	7657	1.03
K3 (Ø/C640/#4/full)	7490	33.6	0.81	1.9	53.2	4.5	7288	0.97
K4 (Ø/G/#6/full)	7580	36.1	0.56	7.3	58.2	12.1	7773	1.03
K5 (Ø/G/#2/full)	5325	36.1	0.42	5.4	39.7	6.6	5620	1.06
K6 (Ø/G/#4/partial-circ.)	5000	35.5	0.36	4.7	35.5[(2)]	2.0[(2)]	4873	0.97
K7 (Ø/G/#4/partial-helic.)	4810	35.5	0.35	4.6	35.5[(2)]	2.0[(2)]	4873	1.01
K8 (Ø/H/#4/full)	6230	34.1	0.45	5.1	40.6	6.9	5689	0.92
K9 (sq./r30/G/#2/full)	(5810)[(3)]	34.1	0.36	4.7	34.1[(2)]	2.0[(2)]	4722	(0.81)[(3)]
K10 (sq./r15/G/#2/full)	5140	36.0	0.35	4.5	36.0[(2)]	2.0[(2)]	4978	0.97
K11 (rect./r30/G/#2/full)	4990	36.0	0.34	4.4	36.0[(2)]	2.0[(2)]	4920	0.99

[(1)] Wrapped cylinders with more than 5 % voids excluded

[(2)] $f_{cc} = f_{co}$ and $\varepsilon_{cc1} = 2$ mm/m (low ultimate confining pressures so that $f_{ccu} < f_{cc}$)

[(3)] The load suddenly increased to failure after activating a 2nd pump

5 Conclusions

Based on the conducted tests on wrapped cylinders and columns and the performed analytical verification, the following conclusions may be drawn:

- Confinement of concrete by means of FRP wrapping is an efficient technique to increase strength and ductility. However, the quality of execution and the wrapping configuration have a considerable influence on the effectiveness of the FRP wrapping. Low effectiveness and hence low ultimate confining pressures result in a negligible strength increase. This is especially the case for members with a square or rectangular cross-section.
- Beside the effectiveness (influence of partial wrapping, fibre orientation and shape of cross-section), the strength increase basically depends on the amount and tensile strength of the FRP wrapping. The increase in ductility (ultimate axial strain) is inversely proportional to the stiffness (amount and E-modulus) of the FRP wrapping. Hence, for a given type of FRP, the higher the strength increase the lower the increase in ductility.
- For the modelling of FRP confined concrete, the following two aspects are of considerable importance. As the FRP behaves linear elastic, it exerts an increasing confinement pressure, corresponding to the increase in lateral expansion of the concrete. Although, the ultimate state of a wrapped member coincides with FRP fracture, the mean effective FRP failure strain appears to be lower than f_f/E_f. These aspects make the existing models for steel confinement less suitable in their present form.

– From the models for FRP confined concrete found in the literature, only the model by Spoelstra and Monti [17] was found to be versatile enough to predict the stress-strain behaviour of FRP confined concrete accurately under different conditions. As this model follows an incremental-iterative approach it is somewhat complex to calculate. Based on this model, a more practical engineering model for the maximum strength and ultimate state of FRP confined members is proposed as well. Also for this model good predictions are obtained.
– Due to several influencing factors, among which the local stress concentrations near failure, a reduced mean FRP failure strain is found for the wrapped specimens. To model this aspect an equation for the effective FRP failure strain is tentatively proposed as a function of the parameter K_{conf}, which takes into account the stiffness and effectiveness of the FRP confining device.

6 References

1. Nanni A., Ed. (1993), "Fiber-Reinforced-Plastic (FRP) Reinforcement for Concrete Structures: Properties and Applications", Developments in Civil Engineering 42, Elsevier Science, Amsterdam, The Netherlands, 450 pp.
2. Ballinger C., Maeda T., Hoshijima T. (1993), "Strengthening of Reinforced Concrete Chimneys, Columns and Beams with Carbon Fiber Reinforced Plastics", Proceedings 1st. Int. Symp. on Fiber-Reinforced-Plastic Reinforcement for Concrete Structures, Eds. A. Nanni A., C.W. Dolan, Vancouver, ACI SP-138, American Concrete Institute, Detroit, USA, pp. 233-248.
3. Saadatmanesh H., Ehsani M.R., Li M.W. (1994), "Strength and Ductility of Concrete Columns Externally Reinforced with Fiber Composite Straps", ACI Structural Journal, Vol. 91, No. 4, pp. 434-447.
4. Mirmiran A., Kargahi M., Samaan M., Shahawy M. (1996), "Composite FRP-concrete column with bi-directional external reinforcement", Proceedings 1st. Int. Conf. On Composites in Infrastructure, Eds. H. Saadatmanesh and M.R. Ehsani, Tucson, Arizona, USA, pp. 888-902.
5. Mirmiran A., Shahawy M., Samaan M., El Echary H., Mastrapa J.C., Pico O. (1998), "Effect of column parameters on FRP-confined concrete", ASCE, Journal of Composites for Construction, Vol. 2., No. 4, pp. 175-185.
6. Demers M., Naele K.W. (1999), "Confinement of reinforced concrete columns with fibre-reinforced composite sheets – an experimental study", Canadian Journal of Civ. Eng., NRC Canada, Vol. 26, pp. 226-241.
7. Dolan C.W., Rizkalla S.H., Nanni A., Eds. (1999), "Chapter 13 – Seismic rehabilitation with fibre reinforced polymer systems", in Fiber Reinforced Polymer Reinforcement for Reinforced Concrete Structures (FRPRCS-4)", Proceedings 4th. Intern. Symp., Baltimore, ACI SP-188, American Concrete Institute, Michigan, USA, pp. 865-932.

8. Matthys S (1997), “Invloed van het inrijgen van gewapend betonkolommen met vezelcomposietlaminaten op het bezwijkgedrag” (in Dutch), Proceedings 4° Nationaal Congres over Theoretische en Toegepaste Mechanica, Leuven, Belgium, pp. 445-448.
9. Audenaert K. (1999), “Inrijgen van betonkolommen met vezelcomposietlaminaten”, Graduation thesis, Ghent University, Department of Structural Engineering, Magnel Laboratory for Concrete Research, 262 pp.
10. Matthys S., Taerwe L., Audenaert K. (1999), “Tests on axially loaded concrete columns confined by FRP sheet wrapping”, Proceedings 4th. Int. Symp. on FRP for Reinforced Concrete Structures (FRPRCS-4), Baltimore, USA, Eds. C.W. Dolan, S.H. Rizkalla, A. Nanni, ACI SP-188, pp. 217-228.
11. Richart F.E., Brandtzaeg A, Brown R.L. (1929), “The Failure of Plain and Spirally Reinforced Concrete in Compression”, Bulletin 190, University of Illinois Engineering Experimental Station, Champaign, Illinois, USA.
12. Ahmad S.H., Shah S.P. (1982), “Stress-Strain Curves of Concrete Confined by Spiral Reinforcement”, ACI Structural Journal, Vol. 79, No. 6, pp. 484-490.
13. CEB (1983), “Concrete under multiaxial states of stress, constitutive equations for practical design”, CEB Bulletin d'Information No. 156, Comité Euro-International du Béton, Lausanne, Switzerland, 149 pp.
14. Mander J.B., Priestley M.J.N., Park R. (1988), “Theoretical stress-strain model for confined concrete”, Journal of Structural Engineering, ASCE, Vol. 114(8), pp. 1804-1826.
15. CEB (1993), “CEB-FIP Model Code 1990, Design Code”, Comité Euro-International du Béton, Lausanne, Switzerland, Thomas Telford, 437 pp.
16. Restrepol J.L., De Vino B. (1996), “Enhancement of the axial load carrying capacity of reinforced concrete columns by means of fibreglass-epoxy jackets”, Proceedings 2nd. Int. Conf. On Advanced Composite Materials in Bridges and Structures, Ed. M. El-Badry, The Canadian Society for Civil Engineering, Montréal, Québec, Canada, pp. 547-554.
17. Spoelstra M.R., Monti G. (1999), “FRP-Confined Concrete Model”, ASCE, Journal of Composites for Construction, Vol. 3, No. 3, pp. 143-150.
18. Toutanji H. A. (1999), “Stress-Strain Characteristics of Concrete Columns Externally Confined with Advanced Fiber Composite Sheets”, ACI Materials Journal, Vol. 96, No. 3, pp. 397-404.
19. Samaan M., Mirmiran A., Shahawy M. (1999), “Model of Concrete Confined by Fiber Composites”, ASCE Journal of Structural Engineering, Vol. 124, No. 9, pp. 1025-1031.
20. Pantazopoulou S.J., Mills R.H. (1995), “Microstructural aspects of the mechanical response of plain concrete”, ACI Materials Journal, Vol. 92, Nov.-Dec. 95, pp. 605-616.
21. Ritchard R.M., Abbott B.J. (1975), “Versatile elastic-plastic stress-strain formula”, ASCE Journal of Engineering Mechanics, Vol. 101, No. 4., pp.511-515.

Chapter 7
DESIGN OF CONCRETE MEMBERS STRENGTHENED WITH EXTERNALLY BONDED FRP REINFORCEMENT

In this chapter, design guidelines are proposed for flexural and shear strengthening of reinforced concrete elements, confinement of axially loaded concrete columns and strengthening of tensile members. The calculation models presented are those derived or verified by means of the experimental and analytical work described in Chapters 3 till 5. The elaboration of these guidelines is based on the Eurocode 2 design philosophy. Details of the design procedures are discussed.

1 Introduction

It has been demonstrated in Chapter 1, Section 2 as well as by the conducted experiments (Chapters 3 till 6), that strengthening of concrete members with FRP EBR is an attractive and efficient technique. Worldwide, practical applications are increasing exponentially and FRP EBR is becoming well documented and a state-of-the-art technique in a fast way [1,2]. Nevertheless, design guidelines for FRP EBR are still not available at the moment of this study, although several initiatives in that direction are ongoing [2-5]. In this chapter the author aims at contributing to these initiatives by discussing some design aspects, limited to flexural and shear strengthening of RC elements and to confinement of axially loaded concrete columns [6-10]. The discussion is mainly based on the experimental and analytical study reported in Chapters 3 till 5, as well as on the literature available to the author. In this study the design philosophy of Eurocode 2 (EC2) [11] has been followed.

2 Basis of design

2.1 General

The design of concrete members strengthened with FRP EBR has to address the effects of the additional reinforcement provided to the section (design assuming full composite action) as well as the ability of transferring forces by means of the bond interface (verification of debonding). To guarantee the overall structural safety of the strengthened member it is important that also attention is paid to detailing, the practical execution and the proper selection of a FRP EBR system.

As a reference for the design of the FRP EBR, the state of the structure prior to strengthening should be known. Often this will be a repaired structure, as the application of the FRP EBR system is not intended to confine or arrest defects such as e.g. steel corrosion.

Also the initial load level prior to strengthening should be known or decided on as a part of the design process. Hence, the design will be preceded by an initial situation verification (which is often an extension of the feasibility study).

Similar as for new reinforced concrete structures, the design will be based on limit states verifications and should consider all relevant design situations, as discussed in Section 2.2. Stress-strain models for the constituent materials are given in Section 2.3. To assure structural safety and ductility, the provisions given in Section 2.4 are proposed.

2.2 Limit states and design situations

2.2.1 Ultimate and serviceability limit state (persistent situation)

For persistent situations (corresponding with the normal use of the strengthened structure), both the ultimate limit state (ULS) and the serviceability limit state (SLS) should be verified. In the ULS, it is verified that the probability of reaching a failure (or excessive deformations) is acceptably small. The different failure modes which may occur have to be considered. These failure modes can be subdivided in those assuming full composite action between the RC member and the FRP EBR (adequate bonding) and those verifying the different debonding mechanisms which may occur. In the SLS, it should be demonstrated that the strengthened member performs adequately (functionality, durability and appearance) in normal use. This verification normally concerns limitation of deformations, crack widths and material stresses.

Although the reasons for strengthening may differ considerably, they are either related to serviceability or to strength increase considerations. In the former case, the SLS will govern the design, rather than the ULS. In the latter case, for flexural members, it may appear that the SLS is governing as well. Indeed, as FRP materials have high strength, small cross-sectional areas of FRP are needed for ULS. This cross-section will generally be insufficient to meet the serviceability criteria of the strengthened element, especially as the modulus of elasticity of the FRP can be relatively low. For shear strengthening and for confinement of axially loaded columns the amount of FRP EBR is mainly dictated by strength considerations, and does not considerably affect the stiffness of the member. In these cases the design is often governed by the ULS.

2.2.2 Accidental situation

The accidental design situation is a verification in which unforeseen loss of the FRP due to e.g. impact, vandalism or fire is assumed. The unstrenghtened member is submitted to all relevant load combinations of the strengthened member. This verification is performed in the ULS, considering the partial safety factors for the materials to be 1.0 and considering reduced partial safety and combination factors for the loads, as provided in Eurocode 1 (EC1) [12].

2.2.3 Special design considerations

Special design considerations such as cyclic loading, extra bond stresses due to the difference in thermal expansion between FRP and concrete, impact and fire resistance may be relevant. These aspects strongly depend on the in-situ situation and may influence both the design and the practical execution. More details are given in Section 7.

It may be noted that impact and fire can be regarded as an accidental situation as well as a special design consideration. It is only in the latter case that the resistance of the FRP EBR under impact or fire loading is considered explicitly.

2.3 Models for the constituent materials and partial safety factors

For the design verification, the stress-strain models and associated material safety factors given hereafter can be assumed. For load safety and load combination factors reference is made to EC1[12] and EC2 [11].

2.3.1 SLS verification

For the SLS, a linear stress-strain response is considered for the concrete, the steel and the FRP:

$$\sigma_c = E_c \varepsilon_c \qquad \sigma_s = E_s \varepsilon_s \qquad \sigma_f = E_f \varepsilon_f \tag{7-1}$$

and the partial safety factors of the materials γ_M are taken equal to 1.0.

In the calculation often reference is made to the ratios $\alpha_s = E_s/E_c$ and $\alpha_f = E_f/E_c$, with E_c, E_s and E_f the modulus of elasticity of the concrete, the steel and the FRP respectively. For long-term loading the creep of the concrete should be taken into consideration ($E_{c\infty} = E_c/(1+\phi)$, with ϕ the creep coefficient). For practical calculations, $\alpha_s = 15$ and $\alpha_f = 15E_f/E_s$ can be assumed.

In reality, the stress-strain response of FRP is not perfectly linear elastic (Chapter 2, Section 4.4.1.1). As the fibres, which are not perfectly aligned initially, straighten under higher loads, the stiffness of the FRP increases. Therefore, it is suggested to consider E_f for SLS verifications as the secant modulus of elasticity determined between 10 % and 50 % of the FRP tensile strength [13,14]. As this secant modulus may be subject to significant variance, the characteristic value $E_{fk0.05}$ (5 % fractile) should be considered rather than a mean value. In some verifications, when a higher E-modulus results in lower reliability, it is necessary to refer to the upper bound value $E_{fk0.95}$ (95 % fractile).

2.3.2 ULS verification, full composite action between concrete and FRP EBR

For the ULS verification, reference is made to the design stress-strain curves of the constituent materials, as shown in Fig. 7-1. According to EC2, a parabolic-rectangular stress block can be used for the concrete and a bilinear relationship for the steel reinforcement. For the FRP reinforcement a linear stress-strain relationship may be assumed.

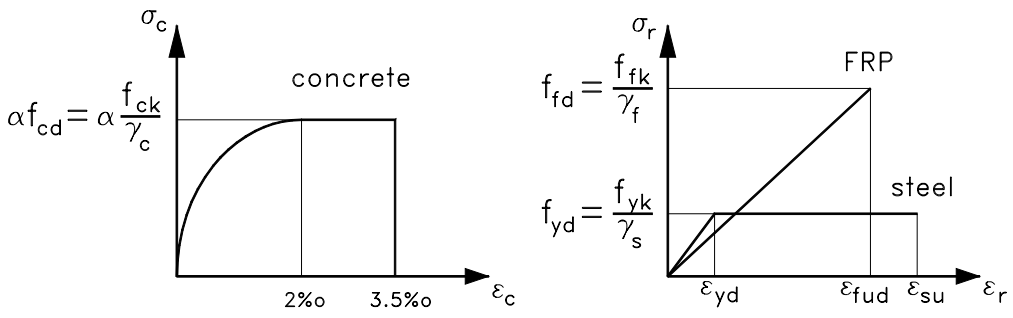

Fig. 7-1 *Design stress-strain curves of the constituent materials in ULS*

The design compressive strength of the concrete and yield strength of the steel are based on the respective characteristic values (5 % fractiles) and partial safety factors $\gamma_c = 1.5$ and $\gamma_s = 1.15$. To account for the reduced compressive strength under long-term loading, a reduction factor $\alpha = 0.85$ is applied to the design value of the compressive strength.

The design tensile stress-strain curve of the FRP is given by:

$$\sigma_f = E_{fu}\varepsilon_f \qquad \leq f_{fd} \tag{7-2}$$

where $E_{fu} = f_{fk}/\varepsilon_{fuk}$ is the modulus of elasticity at ultimate state, based on the characteristic values of the FRP tensile strength and ultimate strain (5 % fractiles), $f_{fd} = f_{fk}/\gamma_f$ is the FRP design tensile strength and γ_f is the material safety factor for the FRP.

In most cases, the failure mode of the strengthened member is not determined by FRP rupture, so that the FRP stress σ_f at ULS is generally lower than the design tensile strength f_{fd}. This means that the specific value of the partial safety factor γ_f (within a reasonable range) will mostly not be critical regarding the design calculations. In those cases where the ULS is determined by FRP tensile failure anyway, reference should be made to a proper value for γ_f. Values for the partial safety factor γ_f are still under discussion and may be based on the statistical variation, the observed differences in the long-term behaviour of FRP (basically depending on the type of fibres), as well as on the influence of the application method. In [15], a general value $\gamma_f = 1.3$ is suggested. For CFRP, which exhibits the best properties compared to other types of FRP and which is often used for strengthening, a value lower than 1.3 may probably be suggested if proper quality control on the application is provided.

In particular cases, it may be necessary to further restrict the design value of the FRP tensile strength to $f_{fd}\varepsilon_{fue}/\varepsilon_{fum}$, with ε_{fue} a nominal value for the effective ultimate FRP strain and ε_{fum} the mean ultimate FRP strain (obtained through tensile testing). Indeed, ε_{fum} refers to uniaxial loaded straight specimens, while the effective failure strain may be lower as a result of wrapping of FRP around sharp corners, application of a large number of layers, multi-axial states of stress, etc. A limited value of the FRP failure strain may also be considered as a simplified design alternative. In this case, the ULS verification restricts excessive FRP deformations, rather than verifying particular failure modes.

To assure sufficient ductility the FRP strain in the critical section at ULS should not be smaller than the minimum values given in Section 2.4.3.

2.3.3 ULS verification of bond failure

Given the high shear strength of structural adhesives, the bond failure will normally occur in the concrete. Hence, for the ULS verification, reference will be made to the design tensile or shear strength of the concrete. According to EC2, these design values can be based on γ_c = 1.5. However, to account for the bond model uncertainties, the variance in the preparation of the concrete substrate and the possible micro-defects in the bond line, it may be suggested to use a somewhat higher partial safety factor (e.g. γ_c = 1.8). Information on bond models is provided in Section 3.4.2.

2.4 Safety concept

2.4.1 Safety concept with respect to the ultimate limit state

The design should be such that brittle failure modes, such as shear, are not critical. If needed, shear strengthening should be applied. Also, it should be guaranteed that the internal steel is sufficiently yielding in ULS (see Section 2.4.3), so that the strengthened member will fail in a ductile manner despite the brittle nature of concrete crushing, FRP rupture or bond failure. Hence, the governing failure mode of a flexural member should be either steel yielding/concrete crushing (before FRP rupture or bond failure) corresponding with zone B in Fig. 7-2, or steel yielding/FRP failure (either FRP rupture or bond failure) corresponding with zone A in Fig. 7-2. In this figure, ε_o is the initial strain at the extreme tensile fibre before strengthening, $\varepsilon_{f,min}$ is the minimum required FRP strain at failure to assure sufficient ductility and $\varepsilon_{fu,c}$ is the ultimate FRP strain in the critical section. In case of FRP fracture, $\varepsilon_{fu,c}$ equals the design value of the ultimate FRP strain ε_{fud}. In case of bond failure, $\varepsilon_{fu,c}$ equals the FRP strain in the critical section when debonding occurs. This debonding may initiate at another location than the critical section which is considered for the verification of the flexural capacity. Bond failure can only be allowed if $\varepsilon_{fu,c} \geq \varepsilon_{f,min}$. Optimum design will correspond with simultaneous concrete crushing (ε_{cu} = 3.5 mm/m) and FRP tensile failure (ε_{fud}).

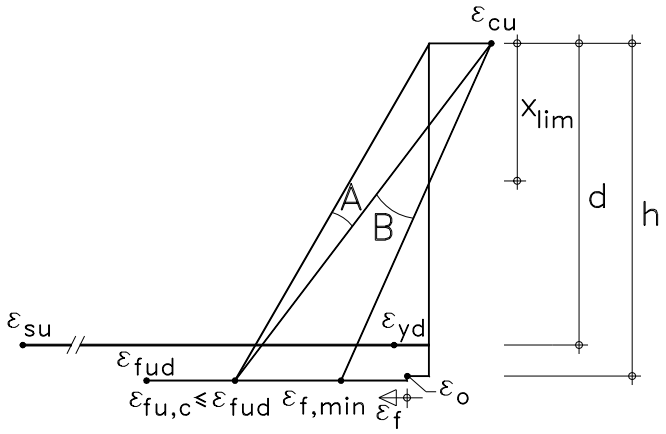

Fig. 7-2 *Strain distribution at ULS in the critical section of strengthened flexural members*

For flexural members often the SLS governs the design (see Section 2.2.1). This implies that larger amounts of FRP will be applied than needed for ULS. Generally, this will positively influence the ratio of ultimate load to service load. This also means that the section will be over-reinforced, resulting in small FRP strains at failure (zone B in Fig. 7-2). It may even appear that the FRP strain becomes smaller than $\varepsilon_{f,min}$, so that the ductility is no longer guaranteed. In this case, FRP types with a higher E-modulus should be used.

2.4.2 Safety concept with respect to accidental situation

The strength increase of properly designed strengthened members will be limited by ductility, ultimate and serviceability limit state requirements. As an additional limitation, it may be suggested that the FRP EBR should only serve as secondary reinforcement, so that in the case of accidental loss of the FRP strengthening, the existing structure does not (totally) collapse. Hence, if the accidental design situation is fulfilled, structural safety is maximized with respect to loss of the externally bonded reinforcement. In this case, special design considerations such as vandalism, impact or fire are generally no longer of concern, or they are of minor importance. On the other hand, it can be argued that sufficient evidence is available to rely on the FRP EBR not only as secondary reinforcement. In this case, extra attention should be paid to the special design considerations (Section 7).

2.4.3 Ductility

As demonstrated in Chapter 3, Sections 3.1 and 3.2, flexural strengthening decreases the ductility. Especially this will be the case for premature debonding failures and high strengthening ratios, as small FRP strains and hence small curvatures are obtained at ultimate load. To guarantee adequate ductility of a strengthened member, the internal steel should sufficiently yield at failure, i.e. curvature or deflection at ultimate load should be large enough. With respect to this issue, EC2 [11, Section 2.5.3.4.2 (5)] gives a limitation on the depth of the compression zone (Table 7-1). Based on this limitation and Fig. 7-2, with an ultimate concrete strain $\varepsilon_{cu} = 3.5$ mm/m and $h/d \approx 1.1$, values for the FRP ($\varepsilon_{f,min}$) and the steel strain ($\varepsilon_{s,min}$) can be derived as given in Table 7-1. Defining a ductility curvature index $\delta_{1/r}$ equal to the curvature at failure $1/r_u$ divided by the curvature at yield $1/r_y$ and assuming in both cases the same depth of the compression zone, the minimum curvature ductility index $\delta_{1/r,min}$ (Table 7-1) can be approximated by $\varepsilon_{s,min}/\varepsilon_{yk}$.

To guarantee sufficient ductility of strengthened tensile members, strains ($\varepsilon_f + \varepsilon_o = \varepsilon_s$) should be larger than $\varepsilon_{s,min}$ (Table 7-1). For confined columns, an increase in ductility is obtained, so that no further ductility requirements are needed.

It should be noted that the ductility requirements are only effective if a minimum amount of steel flexural reinforcement is available, so that brittle failure at first cracking is prevented. When the design is governed by the SLS, the resisting design moment may be considerably higher than the acting design moment. In this case, it may be difficult to fulfil the ductility requirement (high strengthening ratio), yet a large safety margin is obtained between the acting M_{Sd} and the resisting design moment M_{Rd}. Hence, if M_{Rd} is considerably larger than M_{Sd}, the ductility requirement could be ignored.

Table 7-1 *Ductility requirements*

Concrete grade	**ξ = x/d** [-]	**$\varepsilon_{f,min}$** [mm/m]	**$\varepsilon_{s,min}$** [mm/m]	**$\delta_{1/r,min}$** [-]
C35/45 or lower	≤ 0.45	$5.0 - \varepsilon_o$	4.3	$\approx 0.0043/\varepsilon_{yk}$
Higher than C35/45	≤ 0.35	$7.5 - \varepsilon_o$	6.5	$\approx 0.0065/\varepsilon_{yk}$

3 Flexural strengthening

3.1 General

Reference is made to RC elements, such as beams or slabs in one-way bending, which are strengthened in flexure by means of FRP EBR in the tension zone of the member. The direction of the fibres runs parallel to that of the member longitudinal axis. The analysis of the elements can be based on classical (well-established) procedures for reinforced concrete structures, provided that the contribution of external FRP reinforcement is taken into account properly and that special consideration is given to the issue of bond between the concrete and the FRP EBR.

3.2 Initial situation

The effect of the initial load prior to strengthening should be considered in the calculation of the strengthened member. Based on the theory of elasticity and with M_o, the service moment (no load safety factors are applied) acting on the RC section during strengthening, the strain distribution of the member can be evaluated. As M_o is mostly larger than the cracking moment M_{cr}, the calculation is based on a cracked section (Fig. 7-3). If M_o is smaller than M_{cr}, its influence on the calculation of the strengthened member may easily be neglected.

Based on the transformed cracked section (concrete in compression plus α times reinforcement), the neutral axis depth x_o can be solved from:

$$1/2bx_o^2 + (\alpha_s - 1)A_{s2}(x_o - d_2) = \alpha_s A_{s1}(d - x_o) \tag{7-3}$$

The concrete strain ε_{co} at the top fibre can be expressed as:

$$\varepsilon_{co} = \frac{M_o x_o}{E_c I_{co}} \tag{7-4}$$

where, I_{co} is the moment of inertia of the transformed cracked section:

$$I_{co} = bx_o^3/3 + (\alpha_s - 1)A_{s2}(x_o - d_2)^2 + \alpha_s A_{s1}(d - x_o)^2 \tag{7-5}$$

Based on strain compatibility, the concrete strain ε_o at the extreme tension fibre can be derived as:

$$\varepsilon_o = \varepsilon_{co}\frac{h - x_o}{x_o} \tag{7-6}$$

This strain equals the initial axial strain at the level of the FRP EBR, needed for the evaluation of the strengthened member.

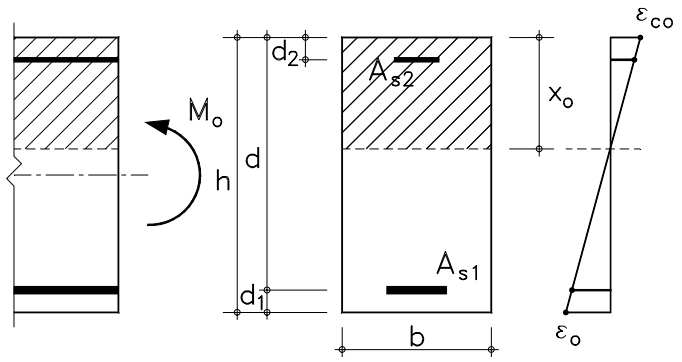

Fig. 7-3 *Initial situation*

3.3 ULS verification assuming full composite action

3.3.1 Principle of calculation and basic assumptions

The behaviour of the elements can be evaluated as classically done, based on strain compatibility and equilibrium of forces (Fig. 7-4). In the calculation the following assumptions are made:

- Idealised stress-strain diagrams as provided in Section 2.3.2 apply.
- The tensile strength of the concrete is neglected.
- Strains are proportional along the depth of the section.
- Slip at the concrete-steel and concrete-FRP interfaces may be ignored.
- The FRP thickness is small so that the effective depth of the FRP reinforcement may be taken equal to the total beam depth h.

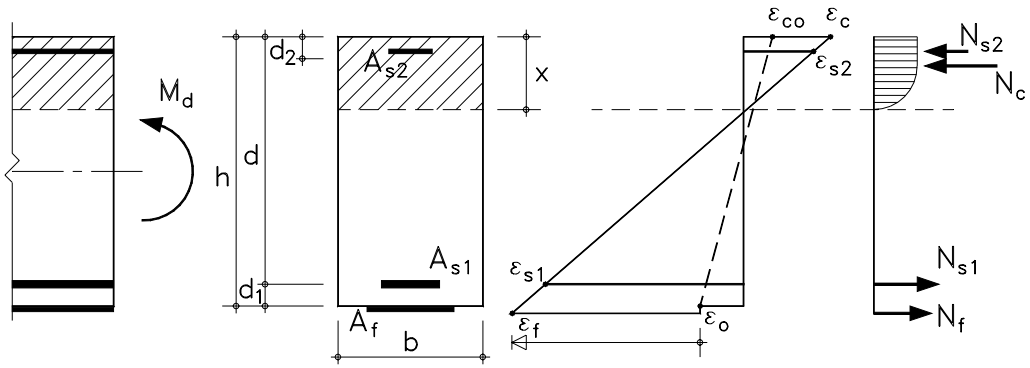

Fig. 7-4 *ULS analysis for a strengthened rectangular section*

Based on the design stress-strain curves of the constituent materials, the following failure modes can be considered for the ULS verification:

- Yielding of the steel followed by concrete crushing and before FRP failure.
- Yielding of the steel followed by FRP failure (FRP fracture or bond failure, whereas the latter may initiate at another location than the critical section) before concrete crushing.
- Concrete crushing or FRP failure without yielding of the internal steel reinforcement.
- Rupture of the steel reinforcement, before concrete crushing or FRP failure.

– Brittle failure at first cracking.
– Shear failure.

In practice, only the two first failure modes are relevant or allowed. Indeed, to guarantee ductility it should be verified that the internal steel is sufficiently yielding. Furthermore, given the limited failure strain of the FRP, rupture of the steel reinforcement will always be preceded by failure of the FRP EBR. Because of their brittle nature, it should be verified in the design that also the two last failure modes are not critical.

3.3.2 Steel yielding/concrete crushing

According to this failure mode, the strengthened member will fail by yielding of the internal steel reinforcement followed by concrete crushing, while the FRP remains intact (zone B in Fig. 7-2). The ultimate concrete strain ε_{cu} at the extreme compression fibre equals 3.5 mm/m and the parameters of the concrete stress block are:

$$\psi = 0.81 \qquad \delta_G = 0.416 \tag{7-7}$$

with, ψ the ratio of the average to the maximum concrete compressive stress (stress block area coefficient) and δ_G the distance from the compression face to the centroid of the compression force divided by the depth of the compression zone (stress block centroid coefficient).

The depth of the compression zone x can be evaluated based on the equilibrium of forces ($\Sigma N = 0$), with the concrete area in compression assumed as bx (instead of $bx - A_{s2}$):

$$0.85\psi b x f_{cd} + A_{s2}\sigma_{s2} = A_{s1}f_{yd} + A_f E_f \varepsilon_f \tag{7-8}$$

where,

$$\begin{aligned} \sigma_{s2} &= \min\left(E_s \varepsilon_{cu} \frac{x - d_2}{x}, f_{yd} \right) \\ \varepsilon_f &= \varepsilon_{cu} \frac{h - x}{x} - \varepsilon_o \quad \text{with} \quad \varepsilon_{f,min} \le \varepsilon_f \le \varepsilon_{fu,c} \end{aligned} \tag{7-9}$$

From the equilibrium of moments ($\Sigma M = 0$), the design bending moment capacity is obtained as:

$$M_{Rd} = 0.85\psi b x f_{cd}(d - \delta_G x) + A_f E_f \varepsilon_f (h - d) + A_{s2} E_s \varepsilon_{s2} (d - d_2) \tag{7-10}$$

For the above equations it should be verified that the ductility requirement is fulfilled ($\varepsilon_f \ge \varepsilon_{f,min}$, Section 2.4.3). From this requirement it also follows that the tensile steel is yielding. In addition, it should be verified that the FRP strain ε_f does not exceed the ultimate FRP strain $\varepsilon_{fu,c}$ in the critical section.

3.3.3 Steel yielding/FRP fracture

In this case, the ULS is reached by yielding of the steel followed by FRP failure, before crushing of the concrete (zone A in Fig. 7-2). The ultimate FRP strain in the critical section equals $\varepsilon_{fu,c}$ and corresponds with either FRP fracture ($\varepsilon_{fu,c} = \varepsilon_{fud}$) or bond failure ($\varepsilon_{fu,c} < \varepsilon_{fud}$).

Defining the parameter λ, equal to:

$$\lambda = \frac{0.002}{\varepsilon_{fu,c} + \varepsilon_o} \frac{h - x}{x} \tag{7-11}$$

the parameters of the concrete stress block follow from [16]:

$$\begin{aligned} &\lambda \geq 1: \quad \psi = \frac{3\lambda - 1}{3\lambda^2} \quad \delta_G = \frac{4\lambda - 1}{4(3\lambda - 1)} \\ &\lambda \leq 1: \quad \psi = 1 - \frac{\lambda}{3} \quad \delta_G = \frac{\lambda^2 - 4\lambda + 6}{4(3 - \lambda)} \end{aligned} \tag{7-12}$$

The depth of the compression zone and the design moment capacity can be calculated based on Eqs. (7-8) and (7-10), with:

$$\begin{aligned} &\varepsilon_{s2} = (\varepsilon_{fu,c} + \varepsilon_o) \frac{x - d_2}{h - x} \leq \frac{f_{yd}}{E_s} \\ &\varepsilon_f = \varepsilon_{fu,c} \end{aligned} \tag{7-13}$$

To guarantee sufficient ductility, it should be kept in mind that $\varepsilon_{fu,c} \geq \varepsilon_{f,min}$ (Section 2.4.3).

3.3.4 Brittle failure at first cracking

In order that the ductility requirements of Section 2.4.3 be effective, it is important that sufficient steel reinforcement is available to prevent brittle failure at first cracking, even in the absence of the FRP EBR (accidental situation). This requirement is fulfilled if $M_{Rd} = A_s f_{yd} z \geq M_{cr}$. Assuming a cracking moment $M_{cr} \approx f_{ct} b h^2/6$, the lever arm $z \approx 0.95d$ (corresponding with low reinforcement ratio's) and $h/d \approx 1.1$, the minimum reinforcement ratio of the internal steel can be approximated by:

$$\rho_{s,min} = 0.21 \frac{f_{ct}}{f_{yd}} \tag{7-14}$$

where an upper bound value for the concrete tensile strength $f_{ctk0.95} = 0.39 f_{ck}^{2/3}$ [14] should be used. With a design yield strength $f_{yd} = f_{yk}/1.15$, Eq. (7-14) becomes:

$$\rho_{s,min} = 0.095 \frac{f_{ck}^{2/3}}{f_{yk}} \tag{7-15}$$

3.3.5 Shear failure

As the flexural load capacity of the strengthened member increases, it should also be verified that the shear capacity of the member is still sufficient. If not, flexural strengthening should be combined with shear strengthening.

3.4 ULS verification with respect to loss of composite action

3.4.1 Bond failure modes

Strengthening by means of externally bonded reinforcement relies on the ability of transferring forces between the EBR and the concrete. Hence, loss of composite action between the FRP and the concrete, i.e. bond failure, is a crucial aspect in the verification.

Bond failure occurs if the bond stresses exceed a critical value (related to the bond shear strength of the materials) and if the debonding propagates so that the FRP EBR is no longer able to carry loads (debonding may be local and does not necessarily result in a bond failure). Different bond failure modes can be distinguished, depending on the debonding interface and the location along the FRP EBR where debonding initiates. The latter aspect is basically related to the cause of the bond failure.

With respect to the debonding interface, bond failure may occur in the concrete substrate, at the concrete/adhesive interface, in the adhesive, at the adhesive/FRP interface or inside the FRP. Given the high shear strength of the structural adhesives, debonding will normally occur in the concrete. Only in the case of high strength concrete or at elevated temperatures, a failure in the adhesive may become crucial. Because of the high adhesion strength of the adhesives compared to their cohesion strength and assuming proper surface preparation, bond failures in the interface with the concrete or the FRP are unlikely. Also inter-laminar shear failure (bond failure inside the FRP) is unlikely given the high shear strength of the polymer matrices. Based on these consideration it will be assumed in the following that debonding is localized inside the concrete.

Causes of debonding and related failure modes can be identified as follows:

- *Low quality of EBR application*. The allowable bond strength is strongly reduced in case of inadequate FRP EBR execution. Weak bond zones may occur due to inadequate repair of concrete, insufficient preparation of the concrete surface, holes, etc. Peeling stresses may also occur due to unevenness, as shown in Fig. 7-5a. Debonding of the FRP EBR with respect to these issues can be avoided by adopting certain rules for the practical application (Appendix A).
- *Anchorage zone*. Starting from the free end, the force in the EBR has to be built up. Herewith, extra bond stresses are introduced in the interface (Fig. 7-5b). If critical shear stresses are exceeded, anchorage failure will occur. Normally this results in a peeling failure (Fig. 7-5c). In case of shear cracking, the debonding failure plane moves inwards with a concrete rip-off failure at the level of the internal steel reinforcement (Fig. 7-5c). To prevent anchorage failure, reference is made to the design provisions of Section 3.4.4.
- *Transfer of forces*. Composite action between the EBR and the concrete results in shear stresses in the interface. These stresses are proportional with the variation of force in the EBR, as shown in Fig. 7-5d and as further explained in Section 3.4.5.
- *Crack bridging*. At the location of cracks extra shear stresses are initiated (Fig. 7-5e). Herewith, difference should be made between flexural cracks (only horizontal crack opening) and shear (or combined shear-flexural) cracks. In the latter case, the crack faces displace both horizontally and vertically, initiating direct peeling action. More details on crack bridging are given in Sections 3.4.6. and 3.5.4.

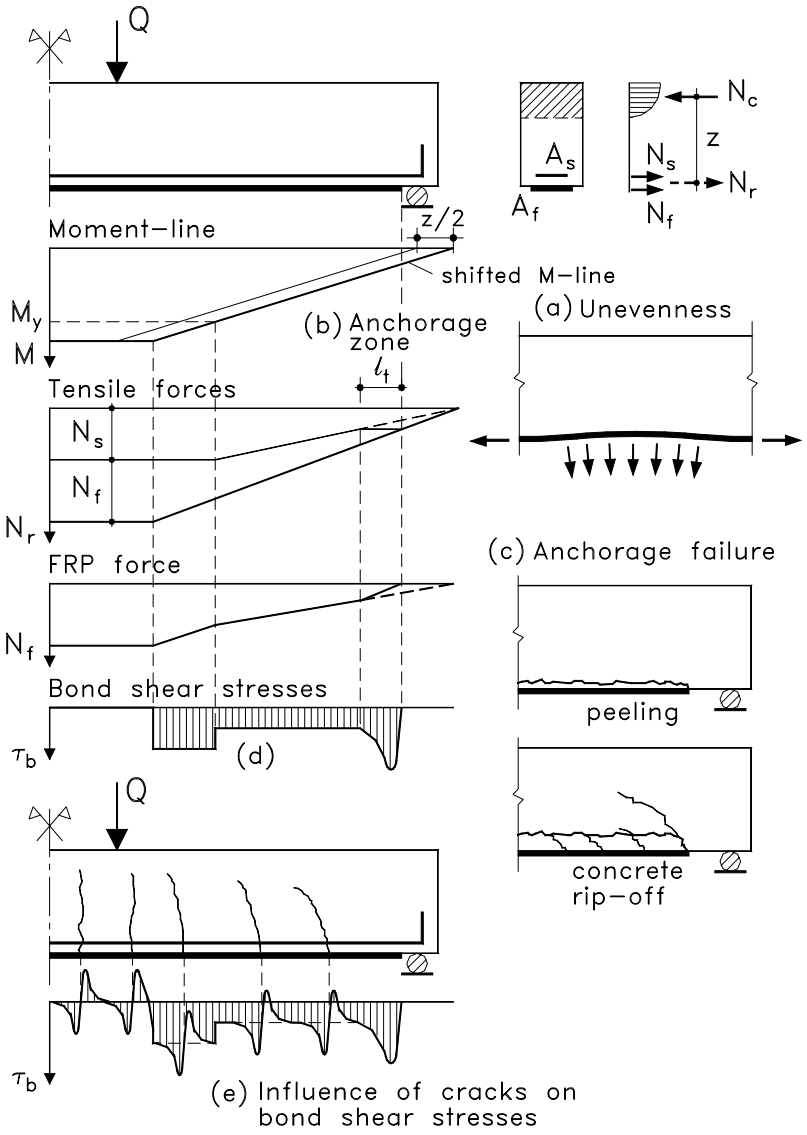

Fig. 7-5 *Causes of bond shear stresses (bond failure modes)*

3.4.2 Bond behaviour

The static bond behaviour between the FRP EBR and the concrete has been studied by many researchers [17-34]. A typical relationship between the bond shear stress τ_b and the slip s is shown in Fig. 7-6 (left) [24]. Near the origin a linear response is obtained, corresponding with the behaviour of the adhesive. Under increasing load micro-cracks start to develop, which initiate near the adhesive at the interface between cement paste and aggregates (proper surface preparation makes that the aggregates are anchored in the adhesive). This micro-cracking further increases until maximum shear stress $\tau_{b,max}$ is reached. The descending branch of the τ-s relationship corresponds to initiation and further development of horizontal cracks between the aggregates a few millimetres above the adhesive, finally resulting in total bond failure.

Typical bond behaviour of a bond shear test specimen, in terms of slip and shear stress along the EBR, is shown in Fig. 7-6 (right). Characteristic for the behaviour is the peak shear

stress which arises and moves inwards as bond cracking propagates under increasing load. Left from the peak stress ($s < s_1$), the slip is almost reversible ('elastic'). At the right ($s_1 < s < s_u$), the slip is mainly related to interface cracking and hence is not reversible ('plastic'). The maximum load which can be anchored is reached when the slip exceeds s_u, and depends on the available anchorage or transfer length ℓ_t. Experiments demonstrate that the maximum bond force increases with increasing transfer lengths, but reaches a maximum value for a certain value of the transfer length $\ell_{t,max}$ (Fig. 7-10).

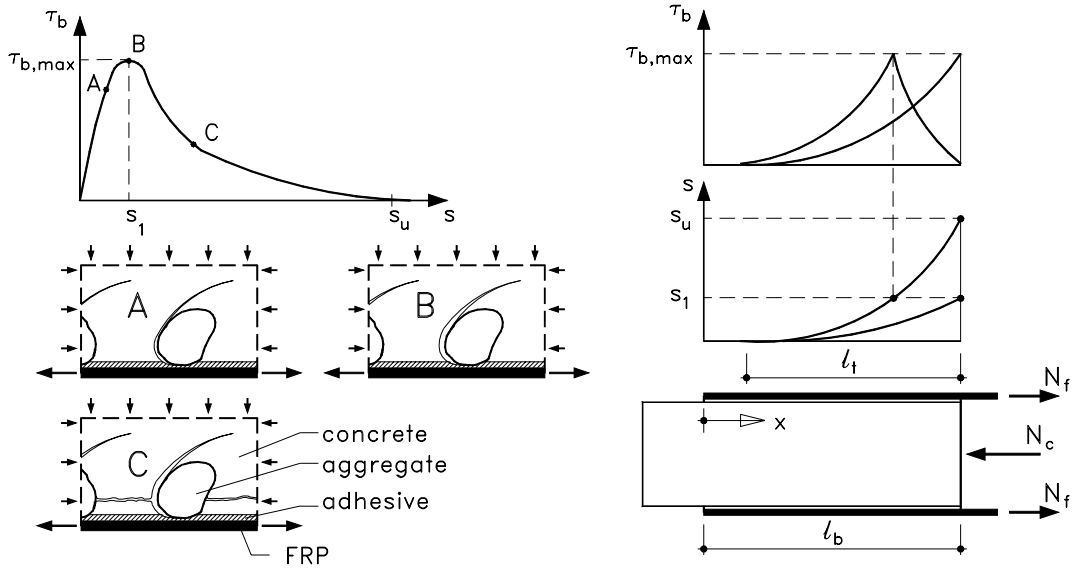

Fig. 7-6 *Bond mechanism (left) and experimental bond behaviour (right)*

3.4.3 Design bond shear strength

For the ULS verification of bond failure, reference is made to the design value of the maximum bond shear stress $\tau_{b,max}$. In most cases (see Section 3.4.1) $\tau_{b,max}$ will equal the bond shear strength of the concrete f_{cb}. Based on the Mohr-Coulomb failure criterion (Fig. 7-7), and in case the normal stress is zero, the bond strength f_{cb} equals about 1.8 times the tensile strength f_{ct}. As a result, the design shear strength can be defined as:

$$f_{cbd} = 1.8\frac{f_{ctk}}{\gamma_c} \tag{7-16}$$

where, f_{ctk} is the characteristic tensile strength. Preferably, reference is made to the surface tensile strength of the concrete, determined by pull-off tensile tests. Assuming proper surface preparation, the latter strength will equal the concrete tensile strength $f_{ctm} = 0.30 f_{ck}^{2/3}$ [11]. The lower bound characteristic tensile strength may be estimated as $f_{ctk0.05} = 0.7 f_{ctm}$ [11].

3.4.4 Anchorage zone

3.4.4.1 Overview of bond models

Several bond models for the determination of peak stresses, transfer lengths and anchorage forces have been proposed [17-34].

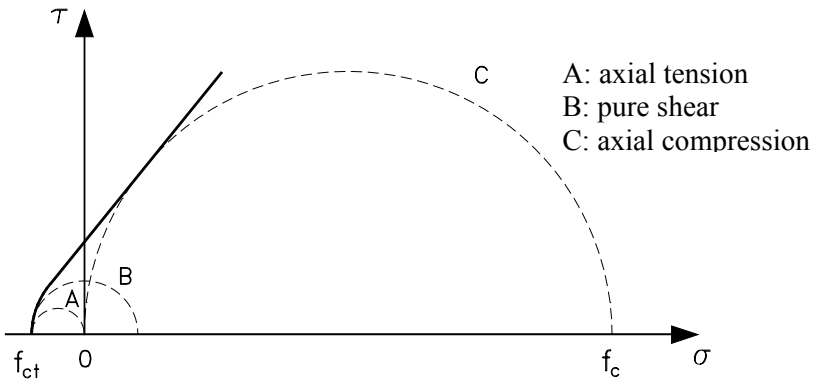

Fig. 7-7 *Mohr-Coulomb failure criterion*

(a) Based on a mean bond stress

Assuming a mean bond stress τ_{bm} along a the transfer length ℓ_t, a simple expression is derived for the force N_{fa} which can be anchored:

$$N_{fa} = \tau_{bm} b_f \ell_t \tag{7-17}$$

with, b_f the width of the FRP and τ_{bm} to be determined experimentally for a given type of FRP as a function of the concrete tensile strength f_{ct} and the transfer length ℓ_t. As Eq. (7-17) strongly simplifies the actual behaviour, it is of limited use. Also, it should be kept in mind that with this equation an unlimited increase of N_{fa} is obtained with increasing transfer length ℓ_t. This is clearly not the case, given the consideration that after a certain value $\ell_{t,max}$ the anchorage force N_{fa} will no longer increase (Fig. 7-10).

(b) Linear elastic τ-s relationship, joint subjected to pure shear

For a more detailed calculation of glued joints, often a linear elastic τ-s relationship is assumed. Based on this assumption the bond stresses for FRP glued on concrete can be modelled, as demonstrated in Fig. 7-8. Assuming pure shear Fig. 7-8 (left), the following relationship has been derived by several authors [e.g. 18,21]:

$$\tau(x) = \omega \frac{N_{fa}}{b_f} \frac{\cosh(\omega x)}{\sinh(\omega \ell_t)} \tag{7-18}$$

where,

$$\omega^2 = \frac{G_a}{s}\left(\frac{1}{E_f t} + \frac{1}{E_c h}\right) \tag{7-19}$$

with, G_a the shear modulus of the adhesive and s, t and h from Fig. 7-8 (left). For a given anchorage length ℓ_t, the peak shear stress $\tau(\ell_t)$ is limited to $\tau_{b,max}$, or:

$$N_{fa} = \frac{\tau_{b,max} b_f}{\omega} \tanh(\omega \ell_t) \tag{7-20}$$

Eq. (7-20) is maximized for large values of the transfer length ℓ_t:

$$N_{fa,max} = \frac{\tau_{b,max} b_f}{\omega} \quad \ell_t \geq \ell_{t,max} \tag{7-21}$$

The maximum transfer length $\ell_{t,max}$ corresponds to $\tau(0) = 0$, which is theoretically obtained for $\ell = \infty$. For practical calculations $\tau(0) = 2\zeta_\ell \approx 0$ can be assumed, or based on Eqs. (7-18) and (7-21), with $\sinh(\omega\ell) \approx e^{\omega\ell}/2$ ($\omega\ell > 0$):

$$\ell_{t,max} \approx \frac{1}{\omega} \ln\left(\frac{\tau_{b,max}}{\zeta_\ell}\right) \tag{7-22}$$

where a boundary condition ζ_ℓ equal to 0.0002 N/mm^2 is proposed in [20].

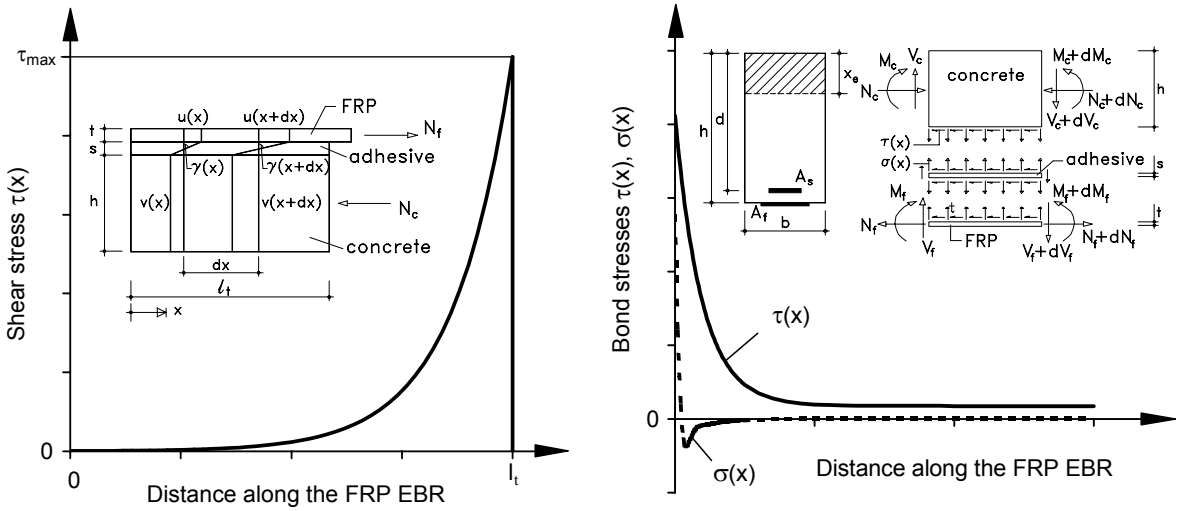

Fig. 7-8 *Linear elastic analysis of bond stresses - pure shear (left), loaded beam (right)*

(c) Linear elastic τ-s relationship, joint on the soffit of a beam subjected to bending

Based on a linear elastic analysis, it is also possible to derive expressions for the shear and normal (peeling) stresses in the glued joint of EBR bonded to the soffit of a concrete beam, as demonstrated in Fig. 7-8 (right). Different models based on this approach have been proposed [17,19,21,26], resulting in rather complex equations which can be simplified if only the maximum stresses at the end of the EBR have to be known. E.g. Roberts [19] derived the following equations for the stress concentrations at the end of the EBR:

$$\begin{aligned} \tau_{max} &= \left(V_{x=0} + \left(\frac{G_a}{E_f s\ t}\right)^{1/2} M_{x=0}\right) \frac{t(h - x_e)}{I_c} \\ \sigma_{max} &= \tau_{max} t \left(\frac{E_a b_f}{4 E_f I_f s}\right)^{1/4} \end{aligned} \tag{7-23}$$

where, $V_{x=0}$ and $M_{x=0}$ are the shear force and moment acting on the section corresponding to the end of the EBR, x_e and I_c are the depth of the compression zone and the moment of inertia about the neutral axis of the assumed uncracked section, I_f is the moment of inertia about the centroid of the FRP EBR, G_a and E_a the shear and elastic modulus of the adhesive and s, t and h according to Fig. 7-8 (right). The stresses τ_{max} and σ_{max} should be limited according to a

failure criterion for a bi-axial state of stress, as shown in Fig. 7-7. Assuming the unfavourable condition that the magnitude of σ_{max} is similar as for τ_{max} (typically σ_{max} is significantly smaller than τ_{max}), the verification can be simplified by only checking $\tau_{max} \le f_{ct}$ (Fig. 7-7).

From the models assuming a linear elastic τ-s relationship, it appears that the stress concentrations can be reduced by decreasing the thickness of the EBR, minimising the distance from the end of the EBR to the support and decreasing the stiffness of the adhesive.

(d) Models based on fracture mechanics

As been demonstrated in Fig. 7-6, the slip between the concrete and the EBR is not only the result of linear elastic deformations of the adhesive, but is also influenced by micro cracking in the concrete a few millimetres above the adhesive layer. Hence, it can be argued that models based on a linear elastic τ-s relationship only approximate the bond behaviour. In the literature also models are proposed, based on τ-s relationships which try to idealise the bond behaviour in a more realistic manner and which are often based on linear or non-linear fracture mechanics [18,21-24,28,31-33]. In the following, the model by Holzenkämpfer [23] is presented. This model, based on fracture mechanics for concrete failure, appears rather simple to apply and has been verified with extensive test data by Rostásy et al [28,31,33]. For a given geometry of the glued joint and a certain tensile strength, it is shown that the bond strength, governed by the fracture energy G_F (area enclosed by the τ-s curve), is limited to a distinct maximum independent of the transfer length. The τ-s relationships is assumed bilinear, as shown in (Fig. 7-9). The maximum force which can be anchored $N_{fa,max}$ and the maximum transfer or anchorage length $\ell_{t,max}$ are obtained as [28,33]:

$$\begin{aligned} N_{fa,max} &= \alpha k_c b_f \sqrt{2 G_F E_f t} \\ &= \alpha k_c k_b b_f \sqrt{2 c_F f_{ctm} E_f t} \end{aligned} \tag{7-24}$$

$$\begin{aligned} \ell_{t,max} &= 2\alpha \sqrt{\frac{2 G_F E_f t}{\tau_{max}^2}} \\ &= 1.57 \alpha \sqrt{\frac{c_F E_f t}{f_{ctm}}} \end{aligned} \tag{7-25}$$

with, $G_F = k_b^2 c_F f_{ctm}$, $\tau_{max} \approx 1.8 k_b f_{ctm}$ and the factor $c_F = 0.202$ mm ([33], based on 70 bond tests with CFRP). The influence of inclined cracks on the bond strength is considered by a reduction factor $\alpha = 0.9$ [33]. For FRP bonded on concrete faces with low compaction (e.g. faces which are not in contact with the formwork during casting) a factor $k_c = 0.87$ is proposed in [31]. The geometry of the anchorage zone is accounted for by means of a size factor k_b [32]:

$$k_b = 1.06 \sqrt{\frac{2 - b_f / b}{1 + b_f / b_o}} \ge 1.0 \tag{7-26}$$

with, b the width of the concrete member or the centre to centre spacing of the EBR, b_f/b not to be taken smaller than 0.5 and $b_o = 400$ mm.

The force N_{fa} corresponding to a transfer length smaller than $\ell_{t,max}$, is given by:

$$N_{fa} = N_{fa,max} \frac{\ell_t}{\ell_{t,max}} \left(2 - \frac{\ell_t}{\ell_{t,max}} \right) \tag{7-27}$$

where, N_{fa} equals $N_{fa,max}$ for transfer lengths $\ell_t \geq \ell_{t,max}$.

A comparison between experiments conducted at the Technical University of Braunschweig and the Holzenkämpfer model is given in Fig. 7-10 [31]. A fairly good prediction is obtained. In Fig. 7-11, a comparison is made between the non-linear model (Eqs. (7-24) till (7-27)) and the linear elastic model according to Eqs. (7-19) till (7-22). A considerable difference is found in the prediction of the anchorage force N_{fa}, whereas the largest forces are obtained for the model taking into account the non-linear bond-slip behaviour. From this figure, it can be concluded that the ultimate load (predicted by the non-linear model) is several times higher than the load at which micro-cracking initiates (predicted by the linear elastic model).

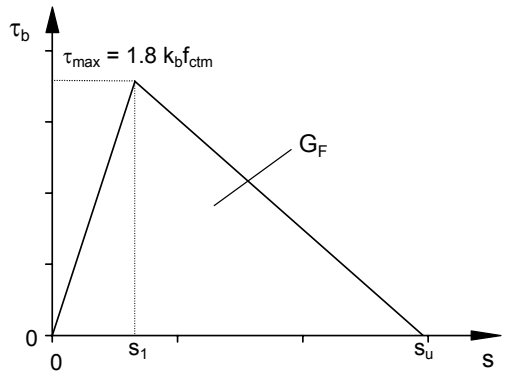

Fig. 7-9 *Bilinear τ-s relationship*

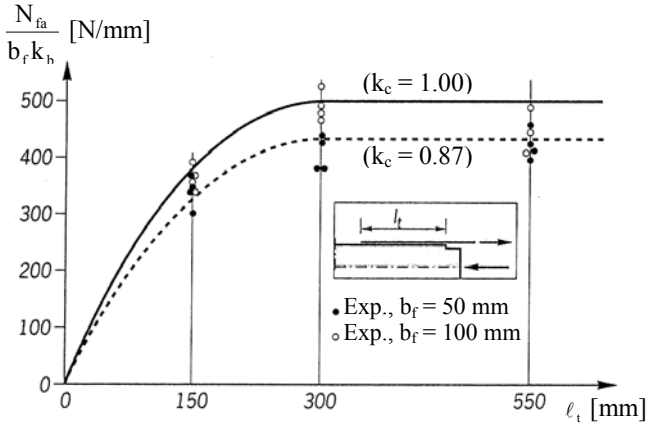

Fig. 7-10 *Anchorage force [31]*

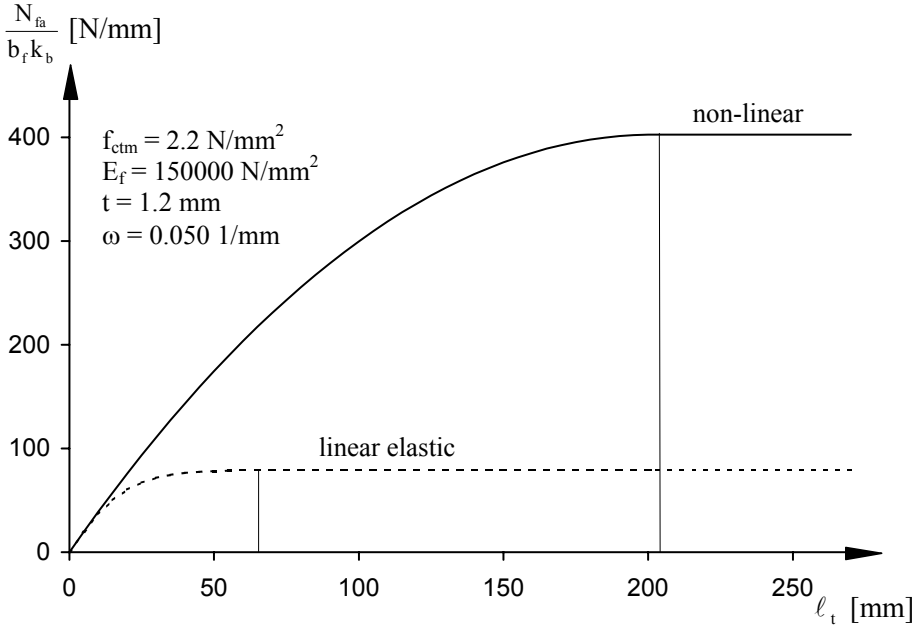

Fig. 7-11 *Non-linear versus linear elastic approach*

3.4.4.2 ULS verification with respect to anchorage length

Along the length of the beam, it should be ensured that the resisting tensile force in the reinforcements is larger than the acting tensile force $N_{Srd} = M_{Sd}/z$. Where, for the calculation of the envelope line of the total tensile force, reference is made to the shifted moment line (to consider both the tension due to the bending moment and that resulting from the truss analogy for shear). Hence, the envelope is shifted over a horizontal distance a_ℓ (as specified in EC2 [11]). For vertical shear links and assuming a 45° shear crack, this distance equals z/2. The lever arm z, for sections with externally bonded reinforcement, can be approximated as 0.95d.

Based on this concept, the theoretical point at which the FRP EBR may be curtailed is given by (Fig. 7-12a):

$$\frac{M_{Sd}(x)}{z} = N_{Rsd} \tag{7-28}$$

where, $N_{Rsd} = A_s f_{yd}$ is the resisting tensile force of the internal steel. The corresponding FRP force N_{fad} to be anchored (Fig. 7-12a) can be calculated based on equilibrium of forces and compatibility of strains (Section 3.3) or, if $\varepsilon_s \le \varepsilon_{yd}$, approximated as:

$$\begin{aligned} \frac{M_{Sd}(x)}{z} &= N_{fad}(x)\left(1+\frac{A_s E_s \varepsilon_s}{A_f E_{fu} \varepsilon_f}\right) \\ &\approx N_{fad}(x)\left(1+\frac{A_s E_s}{A_f E_{fu}}\right) \end{aligned} \tag{7-29}$$

where, $\varepsilon_s/\varepsilon_f$ is assumed equal to about 1.

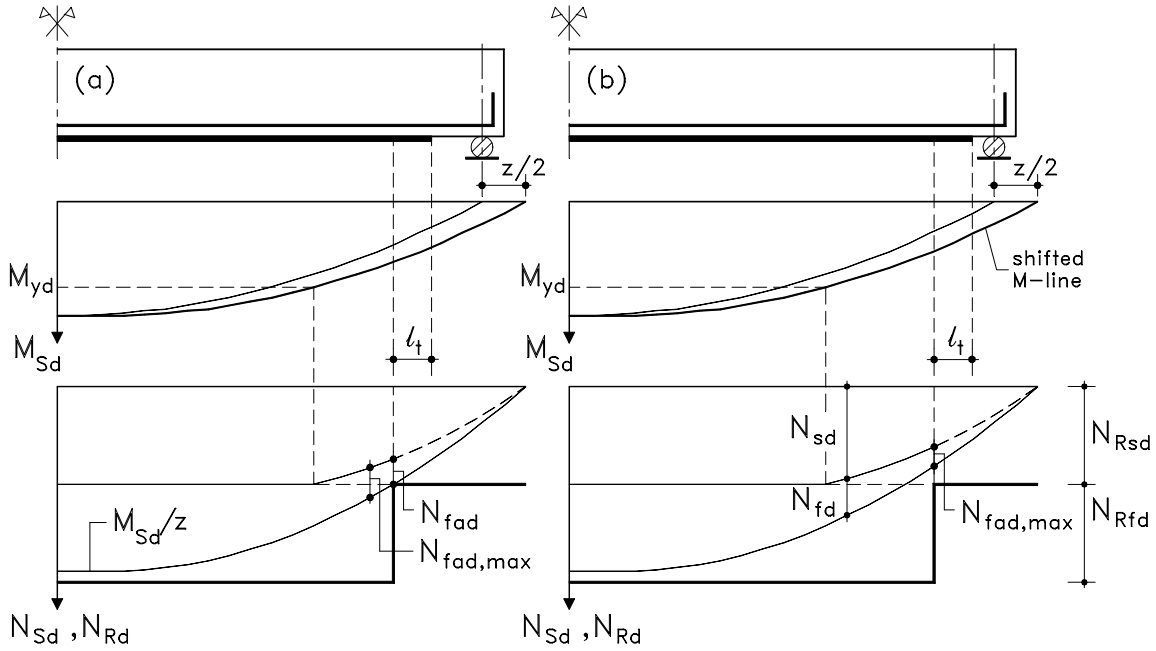

Fig. 7-12 *Curtailment and anchorage length*

The curtailed FRP must be anchored over a distance ℓ_t. It should however be verified that N_{fad} is smaller than $N_{fad,max}$ and that sufficient place is available to provide the anchorage length ℓ_t. If this is not the case, the cut-off point can be located further so that N_{fad} becomes smaller than (or equal to) $N_{fad,max}$ (Fig. 7-12b) or so that smaller transfer lengths are needed (from Fig. 7-11 it can be noted that, near $N_{fad,max}$, a small reduction of N_{fad} corresponds to a large reduction of ℓ_t). In case the available transfer length is still not sufficient, FRP with a larger width and a smaller thickness should be used or an extra end-anchorage can be provided. The anchorage length ℓ_t and maximum anchorage force $N_{fad,max}$ can be calculated according to Eqs. (7-24) and (7-27), where E_f and f_{ctm} are replaced by E_{fu} and f_{ctk}/γ_c respectively.

3.4.4.3 ULS verification for concrete rip-off

If the FRP EBR is curtailed at a certain distance from the support, a vertical crack may initiate at the end of the FRP and propagate as an inclined shear crack [27,29,30,32]. Although this shear crack is bridged by the internal stirrups, it may initiate debonding at the level of the longitudinal steel reinforcement under the form of a concrete cover rip-off failure (Fig. 7-5c). If no stirrups are provided, an EBR-end shear failure is obtained (shear failure where the shear crack initiates at the end of the EBR).

Concrete rip-off is mainly due to the vertical shift between the internal steel and the external FRP tensile forces, as illustrated (based on a truss system) in Fig. 7-13. Also the location of the EBR-end is of importance, as bond shear and normal (peeling) stresses at the end of the EBR increase with increasing distance L between the support and the EBR end point.

As concrete rip-off failure is preceded and dominated by the formation of an EBR-end shear crack, it is suggested in [30] that the modelling should be related to EBR-end shear. This modelling can be based on an analogy between an unstrengthened and a strengthened member, as illustrated in Fig. 7-14. The EBR-end shear crack occurs at a distance L from the support, analogous to the length a_c governing the critical flexural shear crack of an unstrengthened RC member. Where the length a_c is related to the shear span a, analogous a fictitious shear span a_L may be defined in relation to the length L [30].

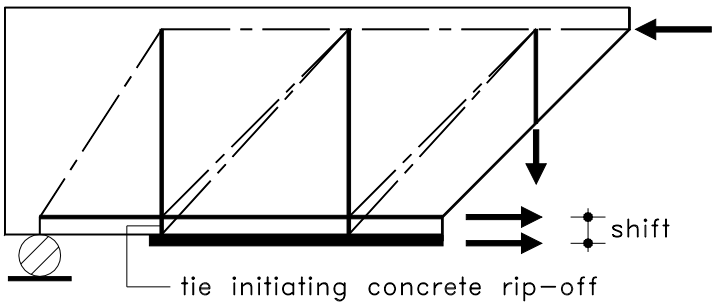

Fig. 7-13 *Vertical shift between tension forces, initiating concrete rip-off*

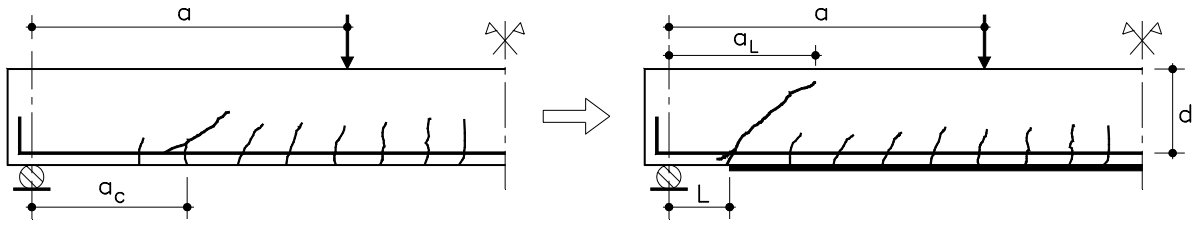

Fig. 7-14 *Modelling analogy of EBR-end shear failure*

Based on this concept of a fictitious shear span the EBR-end shear resistance can be calculated along the lines of MC90 [35]:

$$\begin{aligned} V_{Sd} &\le V_{Rd1} \\ &\le \tau_{Rd1} bd \end{aligned} \tag{7-30}$$

with, the design value of the nominal maximum shear stress is given as:

$$\tau_{Rd1} = 0.15\left(3\frac{d}{a_L}\right)^{1/3}\left(1+\sqrt{\frac{200}{d}}\right)\left(100\rho_s f_{ck}\right)^{1/3} \tag{7-31}$$

where all units are function of N and mm, and with the fictitious shear span [30]:

$$a_L = \left(\frac{\left(1-\sqrt{\rho_s}\right)^2}{\rho_s} L^3 d\right)^{1/4} \tag{7-32}$$

In the above equations, only the internal reinforcement is considered, by means of $\rho_s = A_s/bd$. The model is only valid for $a > L + d$ and $a_L < a$.

This EBR-end shear model has been extensively verified in [30] for both steel and FRP externally bonded reinforcement, where it is concluded that the EBR-end shear model is a fairly accurate lower bound model for the prediction of concrete ripp-off failure.

3.4.4.4 Extra end anchorage

To overcome the peak stresses at the end of the FRP EBR, an extra anchorage may be applied. Also, for safety reasons it is sometimes suggested to use an anchorage (not necessarily to prevent debonding but to prevent falling down of the EBR after bond failure). Different anchorage systems can be thought of, like for example extending the FRP into the concrete by means of a flexible FRP fabric bonded in a slit cut out in the concrete cover, U-shaped wrapping around the beam at the location of the EBR-end or the use of (tensioned) bolts. As fibres run unidirectional and parallel with the longitudinal axis, anchorage bolts are of no use, unless special provisions are taken such as special end zones with fibres in multiple directions. Indicative tests conducted at the Magnel Laboratory for Concrete Research on special FRP laminates which can be bolted, showed that this anchorage system can be very efficient [36,37]. More information on this issue can be found in [20,22,28,30].

3.4.5 Force transfer between FRP and concrete

Considering two sections at a distance Δx, subjected to M_d and $M_d + \Delta M_d$ respectively, the shear stress τ_b along the FRP EBR can be verified based on the equilibrium of forces as illustrated in Fig. 7-15:

$$\tau_b = \frac{\Delta N_{fd}}{b_f \Delta x} \tag{7-33}$$

where, b_f is the width of the FRP. In Eq. (7-33), the distance Δx should to be taken sufficiently small.

For the verification of the ULS, the shear stress τ_b should be restricted to the design bond shear strength f_{cbd} (Section 3.4.3). Furthermore, Eq. (7-33) can be simplified based on $N_{rd} = M_d/z$, with $N_{rd} = N_{fd} + N_{sd}$. Depending on the stress in the internal steel, that is if the steel is yielding or not, N_{rd} and ΔN_{fd} can be approximated as:

$$\begin{aligned}
&\varepsilon_s < \varepsilon_{yd}: \quad N_{rd} = N_{fd}\left(1 + \frac{A_s E_s \varepsilon_s}{A_f E_f \varepsilon_f}\right) \\
&\qquad\qquad \approx N_{fd}\left(1 + \frac{A_s E_s}{A_f E_f}\right) \quad \text{or} \quad \Delta N_{fd} \approx \frac{\Delta M_d}{z\left(1 + \frac{A_s E_s}{A_f E_f}\right)} \\
&\varepsilon_s \geq \varepsilon_{yd}: \quad N_{rd} = N_{fd} + A_s f_{yd} \qquad \text{or} \quad \Delta N_{fd} = \frac{\Delta M_d}{z}
\end{aligned} \tag{7-34}$$

With $\Delta M_d/\Delta x \approx V_d$ and $z = (z_s + z_f)/2 \approx 0.95d$, this gives the following conditions:

$$\begin{aligned}
&\varepsilon_s < \varepsilon_{yd}: \quad \frac{V_d}{b_f (0.95d)\left(1 + \frac{A_s E_s}{A_f E_f}\right)} \leq f_{cbd} \\
&\varepsilon_s \geq \varepsilon_{yd}: \quad \frac{V_d}{b_f (0.95d)} \leq f_{cbd}
\end{aligned} \tag{7-35}$$

In Eq. (7-34) it has been assumed that $\varepsilon_s/\varepsilon_f \approx 1$. From Eq. (7-35) it can be noted that this assumption is at the safe side.

Due to the considerable width of the bond interface normally available, the verification according to Eq.(7-35) is mostly not critical. Only in case the internal steel is yielding or for high shear forces, bond problems may occur.

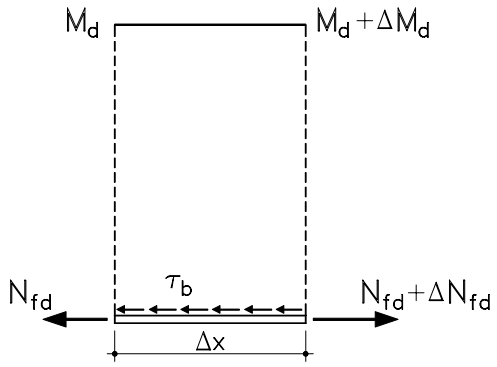

Fig. 7-15 *Shear stresses along the FRP EBR*

3.4.6 Crack bridging

In Fig. 7-5e, the influence of cracks on the bond shear stresses is schematically shown. As cracks are bridged by the EBR, bond stress concentrations occur at both sides of the crack. These stress concentrations may differ, depending on the type of crack (flexural or shear), as illustrated in Fig. 7-16.

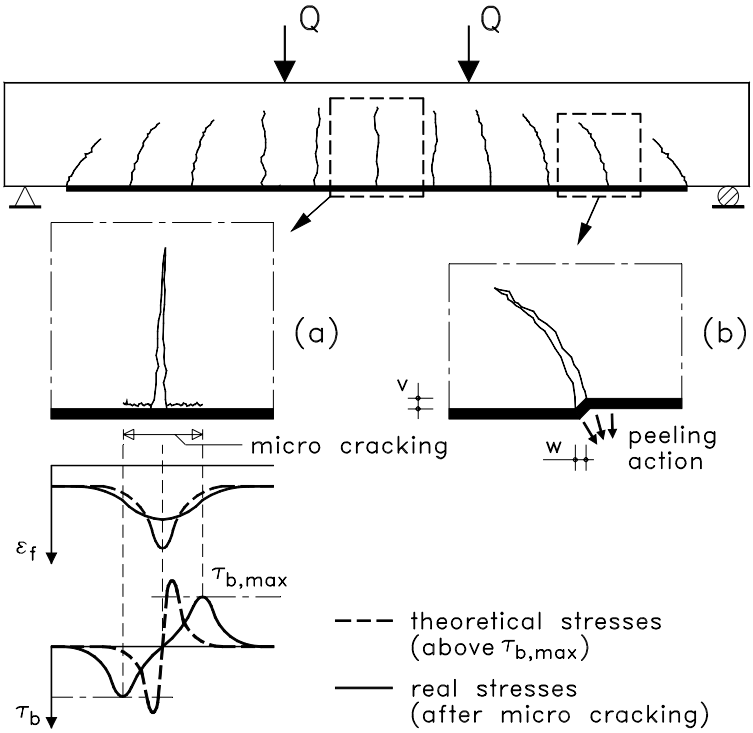

Fig. 7-16 *Bridging of flexural (a) and shear cracks (b).*

3.4.6.1 Flexural cracks

Flexural cracks are characterized by widening in the horizontal direction. At the location of the crack an increased tensile stress (and hence tensile strain) is obtained, which decreases at both sides of the crack due to the bond interaction between reinforcement and concrete (Fig. 7-16a). If the bond shear stress exceeds a critical value, interface cracking and hence redistribution of the reinforcement strain occurs, as illustrated in Fig. 7-16a. From this figure it can be noted that the shear stress concentrations decrease, meaning that the debonding is not progressive and remains local. Also, a beneficial effect is obtained from the curvature of the member. As this curvature is convex, this results in normal stresses which press the FRP to the soffit of the beam.

Provided that the provisions in Sections 3.4.4 and 3.4.5 are fulfilled, it may be concluded that crack bridging of flexural cracks will not result in a bond failure (although local debonding will occur).

3.4.6.2 Shear cracks

A different situation is obtained in the case of shear cracks or for flexural cracks in regions with significant shear forces. Indeed, as these types of cracks are characterized by both a

horizontal and vertical crack opening, a direct peeling action is initiated, as illustrated in Fig. 7-16b. In [20] it is demonstrated that already small vertical crack displacements result in debonding. Thus, compared to flexural crack bridging, shear crack bridging is far more critical and has (due to the peeling effect) a progressive tendency, which may result in bond failure. To prevent this bond failure mode it should be verified for a given horizontal crack opening w, that the vertical crack opening v is limited. The latter aspect, mainly depends on the depth of the compression zone, the aggregate interlock in the shear crack and the dowel action by the reinforcement. Based on these observations, the following model has been proposed in [20] (see also Chapter 3, Section 4.1.3):

$$V_{Rp} = \tau_{cza} b\left(x + (h - x)\left(1 - \frac{\varepsilon_o + \varepsilon_f}{\varphi} \right) \right) + \chi\Sigma(EA) \tag{7-36}$$

where,

- V_{Rp} is the resisting shear at which shear crack peeling initiates,
- τ_{cza} is the shear stress transferred in the compression zone and in the shear crack (aggregate interlock),
- x is the depth of the compression zone,
- $(\varepsilon_o + \varepsilon_f)$ the strain at the extreme tension fibre (FRP strain taking into account the initial strain ε_o before strengthening),
- $\varphi = w_{crit}/s_{rm}$ the ratio of the critical crack width at which there is no longer an aggregate interlock contribution over the mean crack spacing,
- χ is a coefficient relating the dowel action to the axial stiffness of the reinforcement,
- $\Sigma(EA) = E_sA_s + E_fA_f$ is the axial stiffness of the tension reinforcement.

For the calculation of V_{Rp} according to Eq. (7-36), x and $(\varepsilon_o + \varepsilon_f)$ depend on the acting load and can be determined based on equilibrium of forces and strain compatibility (Section 3.3). Hence, Eq. (7-36) is to be solved by iteration. The parameters τ_{cza}, φ and χ, derived in Chapter 3, Section 4.1.3, are given in Table 7-2.

Table 7-2 *Model parameters for the calculation of V_{Rp}*

τ_{cza} [N/mm^2]	χ [10^{-3}]	φ [10^{-3}]	**Remarks**
0.71	0.75	25.1	Based on experimental calibration (concrete grades C25/30 and C30/37, CFRP prefab or wet lay-up type)

Alternatively, as Eq. (7-36) is rather complex to calculate, Eq. (7-37) has been derived in Chapter 3, Section 4.1.3 through experimental data fitting (concrete grades C25/30 and C30/37, CFRP prefab or wet lay-up type):

$$V_{Rp} = \tau_{Rp} bd \quad \text{with} \quad \tau_{Rp} = (0.54 + 151\rho_{eq})\ \text{N/mm}^2 \tag{7-37}$$

with, $\rho_{eq} = \rho_s + \rho_f E_f/E_s$ the equivalent reinforcement ratio. This equation is shown in Fig. 7-17.

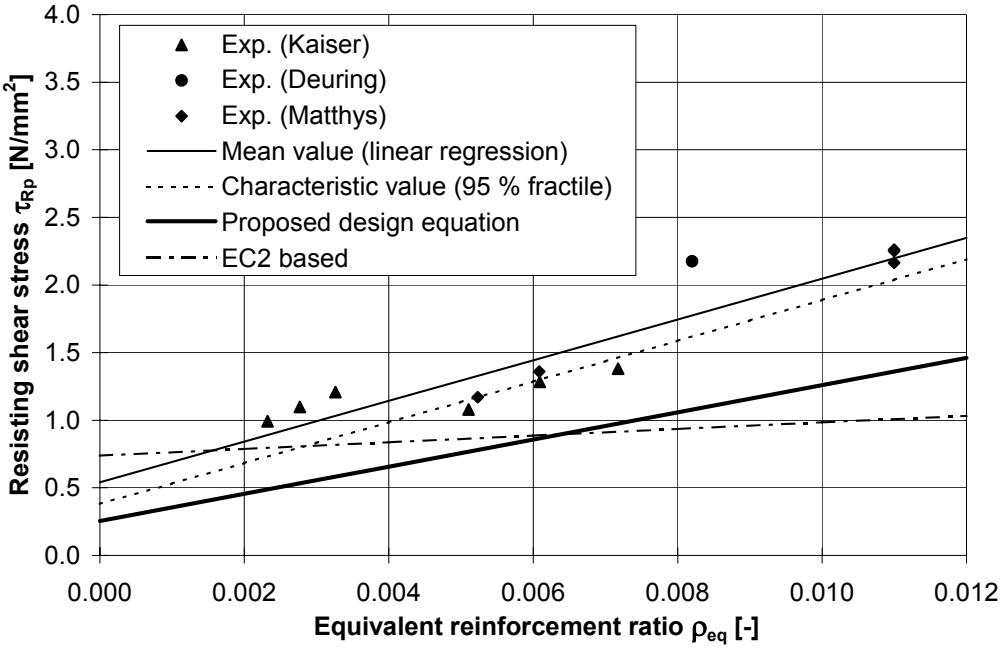

Fig. 7-17 *Resisting shear stress τ_{Rp} for the verification of shear crack bridging*

In [32], it is proposed to prevent peeling at shear crack bridging by limiting the shear force with respect to the shear resistance V_{Rd1} of RC members without shear reinforcement. This can be done according to EC2 [11], with ρ_s replaced by ρ_{eq}. As shown in Fig. 7-17 (based on f_{cm} = 33 N/mm^2 and d = 400 mm), this proposal tends to be unsafe for small values of ρ_{eq} and rather conservative for large values of ρ_{eq}.

Given the considerations presented in this section (and until improved models become available), it is proposed to use Eq. (7-37) as a basis for the ULS verification of peeling at shear crack bridging (Fig. 7-17):

$$\tau_{Rpd} = \tau_{Rpk} / \gamma_c \quad \text{with} \quad \tau_{Rpk} = (0.38 + 151\rho_{eq}) \quad [\text{N/mm}^2] \tag{7-38}$$

where, τ_{Rpk} is the 95 % fractile corresponding to Eq. (7-37) (determined by statistical interpretation [38] and linearization of the slightly curved confidence limit considered). Eq. (7-38), for γ_c = 1.5, is shown in Fig. 7-17.

3.5 SLS verification

3.5.1 Basis of calculation

Calculations to verify the serviceability limit state may be performed according to a linear elastic analysis (Section 2.3.1). Reference will be made to both uncracked (state 1) and cracked sections (state 2).

Whereas the neutral axis depth of RC members, according to a linear elastic calculation, is independent from the acting moment (e.g. Eq. (7-3)), this is no longer the case for a strengthened section as a result of the initial strains before strengthening. Assuming linear elastic material behaviour and that the concrete does not sustain tension, the cracked section

analysis can be based on Fig. 7-18. From the equilibrium of forces and strain compatibility, the depth of the neutral axis x_e is given as:

$$1/2bx_e^2 + (\alpha_s - 1)A_{s2}(x_e - d_2) = \alpha_s A_{s1}(d - x_e) + \alpha_f A_f\left(h - \left(1 + \frac{\varepsilon_o}{\varepsilon_c}\right)x_e\right) \tag{7-39}$$

where, ε_o is the initial concrete strain at the extreme tension fibre determined according to Section 3.2. For small values of ε_o, the term $(1+\varepsilon_o/\varepsilon_c)$ equals about 1, so that Eq. (7-39) can be directly solved. For large values ε_o compared to the acting concrete strain ε_c at the extreme compression fibre, the neutral axis depth x_e should be solved from both Eqs. (7-39) and (7-40):

$$E_c\varepsilon_c = \frac{M_k}{1/2\,bx_e\left(h - \frac{x_e}{3}\right) + (\alpha_s - 1)A_{s2}\frac{x_e - d_2}{x_e}(h - d_2) - \alpha_s A_{s1}\frac{d - x_e}{x_e}(h - d)} \tag{7-40}$$

Neglecting the steel reinforcement in compression ($A_{s2} = 0$) and assuming $h/d \approx 1.1$ (mean effective depth of the steel and FRP reinforcement $\approx 1.05d$), Eq. (7-40) can be written as:

$$E_c\varepsilon_c = \frac{M_k}{1/2\,bx_e\left(1.05d - \frac{x_e}{3}\right)} \tag{7-41}$$

or, based on the equations in Section 3.2,

$$\frac{\varepsilon_o}{\varepsilon_c} \approx \frac{M_o}{M_k}\frac{x_e}{x_o} \tag{7-42}$$

with, M_o the service moment prior to strengthening and x_o the corresponding neutral axis depth, calculated from Eq. (7-3). The moment of inertia of the cracked section is given by:

$$I_2 = bx_e^3/3 + (\alpha_s - 1)A_{s2}(x_e - d_2)^2 + \alpha_s A_{s1}(d - x_e)^2 + \alpha_f A_f(h - x_e)^2 \tag{7-43}$$

and depends, similar as for x_e, on the acting moment M_k.

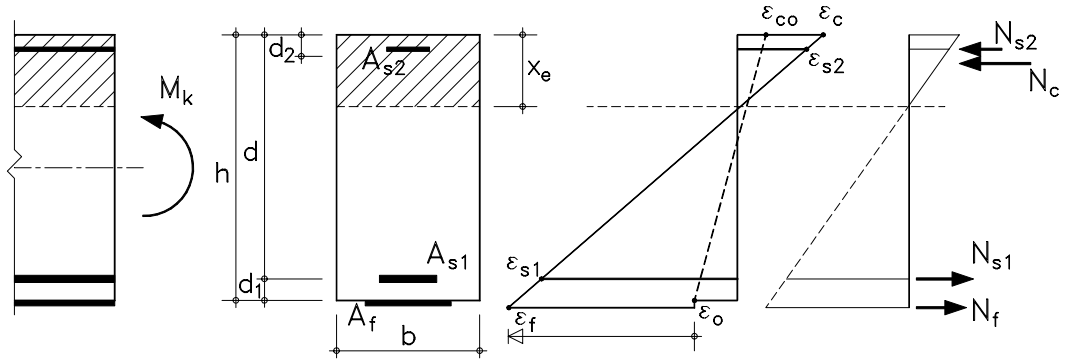

Fig. 7-18 *Linear elastic analysis of cracked section*

The uncracked section analysis can be performed in a similar way as the above mentioned cracked section analysis. However, as M_o is mostly larger than the cracking moment M_{cr} and as the influence of the FRP reinforcement is limited anyway, the geometrical characteristics

of the uncracked section before strengthening apply. Neglecting also the contribution of the steel reinforcement, the moment of inertia can be approximated as:

$$I_1 \approx \frac{bh^3}{12} \tag{7-44}$$

and the cracking moment M_{cr} as:

$$M_{cr} \approx f_{ctm} \frac{bh^2}{6} \tag{7-45}$$

where, according to [11], reference is made to the mean concrete tensile strength f_{ctm}.

3.5.2 Stress limitation

Under service load conditions it is required to limit stresses in the concrete, steel and FRP to prevent damage or excessive creep of the concrete, steel yielding and excessive creep or creep rupture of the FRP.

If external tensile reinforcement is added and as the compression force equals the total tensile force, a significant change in the state of concrete stress may be expected. To prevent excessive compression, producing longitudinal cracks and irreversible strains, the following limitations for the concrete compressive stress apply [11]:

$$\begin{aligned} &\sigma_c \le 0.60 f_{ck} && \text{under the rare load combination} \\ &\sigma_c \le 0.45 f_{ck} && \text{under the quasi - permanent load combination} \end{aligned} \tag{7-46}$$

where, $\sigma_c = E_c \varepsilon_c$ is obtained from Eq. (7-40).

To prevent yielding of the steel at service load, [11] specifies:

$$\sigma_s = E_s \varepsilon_c \frac{d - x_e}{x_e} \le 0.80 f_{yk} \quad \text{under the rare load combination} \tag{7-47}$$

In a similar way, the FRP stress under service load should be limited as:

$$\sigma_f = E_f \left(\varepsilon_c \frac{h - x_e}{x_e} - \varepsilon_o \right) \le \eta f_{fk} \quad \text{under the quasi - permanent load combination} \tag{7-48}$$

where, $\eta < 1$ is the FRP stress limitation coefficient. This coefficient depends on the type of FRP and should be obtained through experimental evidence. Based on creep rupture tests reported in [39,40], indicative values $\eta = 0.8$, 0.5 and 0.3 may be suggested for CFRP, AFRP and GFRP, respectively. As the SLS is often governing the design, relative low FRP strains at service load may be expected, so that FRP creep rupture is mostly not of concern.

3.5.3 Verification of deflections

As already a small amount of external FRP significantly increases the failure load, small cross-sectional areas A_f are needed for the ULS. As also the modulus of elasticity of FRP can be relatively low, this results in a low axial stiffness $E_f A_f$. The latter stiffness is often insufficient to limit curvatures and deflections of the strengthened beam under service load, and may need to be increased to fulfil the SLS.

In Chapter 5, Section 2.4.3, different methods for the prediction of the maximum deflection were verified. The highest accuracy is obtained for calculations based on numerical integration of the curvature, where the latter is determined taking into account tension stiffening and a non-linear analysis of the cracked section. A more simplified calculation can be performed according to the so-called CEB bilinear method [42]. This method still gives reasonably accurate predictions at the SLS. The mean deflection is calculated from:

$$a = a_1(1-\zeta_b) + a_2\zeta_b \tag{7-49}$$

with, a_1 and a_2 the deflections in respectively the uncracked and the fully cracked state and ζ_b a distribution (tension stiffening) coefficient:

$$\begin{aligned} \zeta_b &= 0 && M_k < M_{cr} \\ \zeta_b &= 1-\beta_1\beta_2\left(\frac{M_{cr}}{M_k}\right)^{n/2} && M_k > M_{cr} \end{aligned} \tag{7-50}$$

where, β_1 is a coefficient taking into account the bond characteristics of the reinforcement and β_2 is a coefficient taking into account the loading type. According to MC90 [35] the power n equals 2. For HSC more accuracy is obtained with n equal to 3 [41]. Although the bond behaviour of FRP differs from that of steel, a good agreement between experimental and analytical results is reported in Chapter 5, if β_1 and β_2 are taken as specified in EC2 [11] (β_1 = 0.5 and 1 for smooth and deformed steel respectively; β_2 = 0.5 and 1 for long-term and short-term loading respectively). The deflection in the uncracked state a_1 and in the fully cracked state a_2 can be calculated by classical elasticity analysis, referring to a flexural stiffness in respectively the uncracked state E_cI_1 and the fully cracked state E_cI_2. Taking into account the moment M_o at which the FRP EBR is applied, this yields:

$$a_1 = k_M \ell^2 \frac{M_k}{E_c I_1} \tag{7-51}$$

$$a_2 = k_M \ell^2 \left(\frac{M_o}{E_c I_{o2}} + \frac{M_k - M_o}{E_c I_2}\right) \qquad M_k > M_o \tag{7-52}$$

where, k_M is a coefficient depending on the loading type and I_{o2} is the moment of inertia in the cracked state before strengthening.

3.5.4 Verification of crack widths

To protect the internal steel and to guarantee functionality of the member, crack widths should be limited. For RC beams strengthened with EBR, new cracks will appear in between existing cracks. Hence, more dense cracking and smaller crack widths are obtained, which often makes the verification of crack widths not necessary.

In Chapter 5, Sections 2.4.3 and 4.4.3, the calculation of mean crack widths has been investigated for strengthened members. Assuming stabilized cracking, the characteristic value of the crack width is calculated as [11]:

$$\begin{aligned} w_k &= \beta s_{rm} \varepsilon_{rm,r} \\ &= \beta s_{rm} \zeta \varepsilon_2 \end{aligned} \tag{7-53}$$

where, $\beta = 1.7$ is a coefficient which relates the mean and characteristic value of the crack width, s_{rm} is the mean crack spacing, $\varepsilon_{sm,r}$ is the mean strain of the steel reinforcement with respect to the surrounding concrete, ζ is a tension stiffening coefficient similar to Eq. (7-50):

$$\begin{aligned} \zeta &= 0 && M_k < M_{cr} \\ \zeta &= 1 - \beta_1 \beta_2 \left(\frac{M_{cr}}{M_k} \right)^n && M_k > M_{cr} \end{aligned} \tag{7-54}$$

and ε_2 is the reinforcement strain in the fully cracked state. Assuming $\varepsilon_2 \approx \varepsilon_{s1} \approx \varepsilon_f + \varepsilon_o$ and with $N_{rk} = N_{s1} + N_f$ (Fig. 7-18), ε_2 is given as:

$$\varepsilon_2 = \frac{N_{rk} + E_f A_f \varepsilon_o}{E_s A_s + E_f A_f} \tag{7-55}$$

with, $N_{rk} = M_k / z_e$ and z_e the lever arm between the total tensile force ($N_{s1} + N_f$) and the compression force ($N_c + N_{s2}$).

The mean crack spacing s_{rm}, taking into account the effect of both the internal and external reinforcement, can be calculated as derived in Chapter 5, Section 4.4.3:

$$\begin{aligned} s_{rm} &= \frac{2 f_{ctm} A_{c,eff}}{\tau_{sm} u_s} \frac{E_s A_s}{E_s A_s + \xi_b E_f A_f} \\ &= \frac{2 f_{ctm} A_{c,eff}}{\tau_{fm} u_f} \frac{\xi_b E_f A_f}{E_s A_s + \xi_b E_f A_f} \end{aligned} \tag{7-56}$$

with, $A_{c,eff}$ the effective area in tension taken as the lesser of $2.5(h - d)b$ and $(h - x)b/3$ [11], $\tau_{sm} = 1.8 f_{ctm}$ [35] and $\tau_{fm} = 1.25 f_{ctm}$ [23] the mean bond stress of the steel and the FRP, u_s and u_f the bond perimeter of the steel and FRP reinforcement and ξ_b a bond parameter given as:

$$\begin{aligned} \xi_b &= \frac{\tau_{fm} E_s A_s u_f}{\tau_{sm} E_f A_f u_s} \\ &= \frac{\tau_{fm} E_s Ø}{\tau_{sm} E_f 4t} \end{aligned} \tag{7-57}$$

where, $Ø$ is the (mean) diameter of the steel bars and t is thickness of the FRP.

Neglecting the tension stiffening effect ($\zeta = 1$) and assuming $\varepsilon_o \approx 0$, the crack width is derived from Eqs. (7-53) till (7-57) as:

$$w_k = 2.1 \rho_{c,eff} \frac{M_k}{E_s d \rho_{eq}} \frac{1}{(u_s + 0.694 u_f)} \tag{7-58}$$

with, $\rho_{c,eff} = A_{c,eff}/bd$ the ratio of the effective area in tension and $\rho_{eq} = \rho_s + \rho_f E_f / E_s$ the equivalent reinforcement ratio. Specifying $w_k \leq 0.3$ mm [11, 42], the following condition is obtained for the FRP bond width $u_f = b_f$ (b_f total width of the bonded FRP):

$$u_f \geq 10.1 \rho_{c,eff} \frac{M_k}{E_s d \rho_{eq}} - 1.44 u_s \tag{7-59}$$

Eq. (7-59) expresses that sufficient bond area should be provided to bridge the cracks in such a way that the crack width is limited under service load (for a constant value of ρ_f and hence ρ_{eq}, crack widths will be smaller for FRP with large width and small thickness). For very deep beams it may appear that the required bond width u_f is larger than the available width b of the beam. In this case ρ_f should be increased by considering also a larger FRP thickness.

3.5.5 Verification of bond interface cracking

As illustrated in Fig. 7-5, stress concentrations are especially obtained at the FRP end and at the location of cracks. At service load, bond interface crack initiation at the FRP curtailment should be prevented as it may reduce the long-term integrity of the anchorage zone under e.g. cyclic loading and freeze/thaw action. To fulfil this requirement it should be verified (SLS, quasi-permanent load combination) that the shear stress concentration τ_{max} at the FRP end, calculated according to a linear elastic analysis, Eq. (7-23), is smaller than f_{ctk}. In the case that an extra anchorage is provided at the FRP end (Section 3.4.4.4), this verification is no longer necessary.

In Section 3.4.6, it is argued that local debonding at the location of cracks can be allowed in ULS as far as no bond failure is obtained. This local debonding should however be avoided at service load to guarantee the long-term integrity of the bond interface. From Fig. 7-9, it follows that local debonding occurs if the slip is larger than s_u:

$$s_u = \frac{2G_F}{\tau_{max}} \tag{7-60}$$

With $G_F = c_F f_{ctm}$, $\tau_{max} = 1.8 f_{ctm}$ and $c_F = 0.202$ mm [33], the ultimate slip s_u equals 0.224 mm, which corresponds to a crack width $2s_u = 0.45$ mm. As the characteristic value of the crack width under service load is limited to a maximum of 0.30 mm (mean crack width of 0.18 mm), it appears that no local debonding will occur in the SLS.

3.6 Influence of design parameters and governing design aspects

To study the influence of the design parameters and to gain knowledge about the aspects which typically govern the design, a parametric study was conducted with respect to FRP strengthened singly reinforced RC members subjected to bending.

3.6.1 Influence of characteristics of the existing RC element

In principle, the strength increase is determined by the amount of externally bonded FRP reinforcement provided to the RC member. Nevertheless, for a given amount of FRP the strength increase will largely depend on the characteristics of the existing RC element, such as the amount of steel reinforcement, the concrete grade, the FRP type, the load level prior to strengthening and the shape (rectangular or T-section) and dimensions of the cross-section of the RC element.

To study the influence of these parameters, the ratio η_S of the resisting design moment M_{RdS} of the strengthened member to the resisting design moment M_{RdU} of the unstrengthened member was determined as a function of the FRP reinforcement ratio ρ_f. The analysis is based on the following assumptions:

- Bond failure modes are not considered (this aspect will be analysed in Section 3.6.2). Hence, M_{Rd} can be calculated according to Section 3.3 (assuming full composite action between the FRP EBR and the RC member). The ultimate limit state (ULS) is either governed by yielding of the steel followed by fracture of the FRP reinforcement (YS/FR) or by yielding of the steel followed by concrete crushing (YS/CC). The calculation is stopped when, for increasing ρ_f, the internal steel is no longer yielding.
- The initial strains in the RC member prior to strengthening are taken into account (Section 3.2). This is done by introducing the ratio $\eta_o = M_o/M_{serU}$, where M_o is the acting moment during strengthening (load safety factors equal to 1) and M_{serU} is the service moment of the unstrengthened beam under the rare load combination, obtained from M_{RdU}. This ratio can also be written as:

$$\eta_o = \frac{M_o}{M_{serU}} = \frac{\Phi_{rU} M_o}{M_{RdU}} \tag{7-61}$$

  where, $\Phi_{rU} = M_{RdU}/M_{serU}$ is the global load safety factor for the rare load combination. Defining the ratio $m_U = M_{kqU}/M_{kgU}$ of the moment due to live load to the moment due to dead load of the unstrengthened beam and assuming only one live load, Φ_{rU} is given by:

$$\Phi_{rU} = \frac{\gamma_g + \gamma_q m_U}{1 + m_U} \tag{7-62}$$

  where, γ_g and γ_q are the load safety factors for the dead and live load respectively.
- The ductility requirements of Section 2.4.3, which give a restriction on the depth of the compression zone (large depths result in a low ultimate curvature and hence a low ductility) are verified.
- The accidental situation (AS) (Sections 2.2.2 and 2.4.2) is verified based on the ratio $\eta_a = M_{serS}/M_{Ad}$. In this ratio, M_{serS} is the service moment of the strengthened beam under the rare load combination, obtained from M_{RdS}. The moment M_{Ad} is the resisting moment corresponding to the accidental loss of the FRP EBR and is calculated in the ULS, with material safety factors equal to 1. This ratio can also be written as:

$$\eta_a = \frac{M_{serS}}{M_{Ad}} = \frac{M_{RdS}}{\Phi_{rS} M_{Ad}} \tag{7-63}$$

  where, $\Phi_{rS} = M_{RdS}/M_{serS}$ is the global load safety factor for the rare load combination (load safety factors equal to 1). Similar to Eq. (7-62), this global load safety factor is given by:

$$\Phi_{rS} = \frac{\gamma_g + \gamma_q m_S}{1 + m_S} \tag{7-64}$$

  where, $m_S = M_{kqS}/M_{kgS}$ is the ratio of the moment due to live load to the moment due to dead load of the strengthened beam.

In the case $\eta_a \leq 1$, the FRP acts as secondary reinforcement only (meaning that the RC member will not collapse in the case of accidental loss of the FRP EBR, although it is subjected to the loads of the strengthened member).

– Also, the stress limitations in the serviceability limit state (SLS) may offer a boundary condition. This aspect is verified according to Section 3.5.2. The result of this SLS calculation can be expressed in terms of a corresponding value of the resisting design moment M_{RdS} (above this moment the design is governed by SLS stress limitation rather than by the ULS), by means of the global load safety factor Φ_{rS} (rare load combination) or Φ_{qpS} (quasi-permanent load combination). Similar to Eq. (7-64), the latter global load safety factor is given by:

$$\Phi_{qpS} = \frac{\gamma_g + \gamma_q m_S}{1 + \psi_2 m_S} \tag{7-65}$$

where, ψ_2 is the load combination factor with respect to the quasi-permanent load combination.

– For the calculation it was assumed that $m_S = 1$ and $\psi_2 = 0.4$ or $\Phi_{rS} = 1.43$ and $\Phi_{qpS} = 2.04$. As the variation of m has only a limited influence on Φ_r (3.5 % increase of Φ_r for m going from 0.5 to 2) and for simplicity, Φ_{rU} was also assumed 1.43.

Based on the above verifications and given the shape of the cross-section (rectangular or T-section), the grade of the constituent materials, the steel reinforcement ratio ρ_s and the ratio η_o (representative for the service moment prior to strengthening), the strengthening ratio $\eta_S = M_{RdS}/M_{RdU}$ can be calculated as a function of the FRP reinforcement ratio ρ_f. The calculation procedure has been programmed (using the software MathCad) and is given in Appendix G.

3.6.1.1 Amount of steel reinforcement

The influence of the amount of steel reinforcement is shown in Fig. 7-19, for a concrete grade C20, a steel grade S400, CFRP with $E_f = 165000$ N/mm^2 and $f_f = 2800$ N/mm^2, a rectangular cross-section and $\eta_o = 0.5$. From this figure it is noted that, for a given amount of FRP EBR, a larger strength increase is obtained when the steel reinforcement ratio is small. Indeed, for low steel reinforcement ratios the concrete is not fully utilized in the ULS, so that the addition of FRP tensile reinforcement has a more pronounced effect than in the case that already a large amount of steel reinforcement is initially available.

Hence, compared to rectangular beams, higher strengthening factors can be obtained for slabs (which have typically a low steel reinforcement ratio). In practice, beside slabs, mostly T-beams will occur in stead of rectangular beams. As will be demonstrated in Section 3.6.1.4, also T-beams allow for higher strengthening factors.

3.6.1.2 Grade of constituent materials

Making reference to a rectangular cross-section, a steel reinforcement ratio $\rho_s = 0.5$ % and $\eta_o = 0.5$, the influence of the concrete grade, the steel grade and the type of FRP is shown in Fig. 7-20.

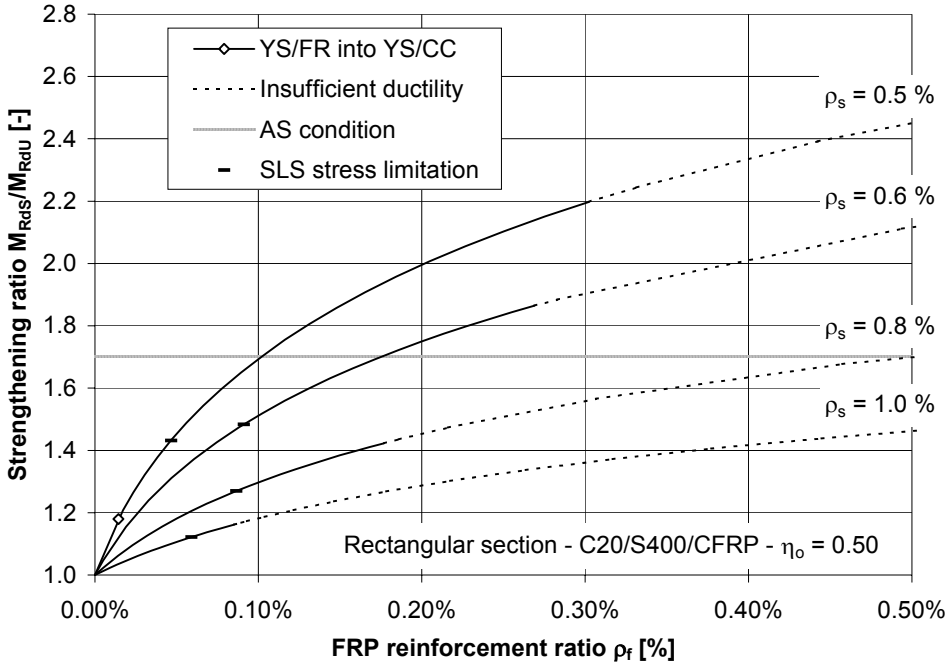

Fig. 7-19 *Influence of the amount of steel reinforcement*

From Fig. 7-20 it follows that the grade of the constituent materials has a considerable influence on the strengthening ratio. The lower the concrete strength, the lower the strength increase. Indeed, given the equilibrium between the compression and the tensile force, it is not possible to achieve high FRP tensile forces when only limited concrete strength is available. In a similar way, steel reinforcements with a low yield strength allow for a larger strengthening effect (a lower steel tensile force in the section corresponds to a lower compression force, so that the FRP can contribute in a larger extent to increase this compression force). The influence of the type of FRP depends on both the stiffness and the strength of the FRP. Indeed, as a result of the linear elastic stress-strain behaviour, for a given FRP strain, higher tensile forces are obtained for FRP types with a higher modulus of elasticity. The FRP tensile force is however also restricted by the FRP tensile strength. Hence, for low reinforcement ratios ρ_f (when the FRP is governing) the strength increase is mainly related to the strength of the FRP. For high reinforcement ratios ρ_f (when the concrete is governing), a higher strength increase is obtained for FRP types with a higher modulus of elasticity.

3.6.1.3 Service moment prior to strengthening

The influence of the service moment M_o prior to strengthening (or the ratio $\eta_o = M_o/M_{RkU}$) is shown in Fig. 7-21, for a concrete grade C20, a steel grade S400, CFRP with E_f = 165000 N/mm^2 and f_f = 2800 N/mm^2, a rectangular cross-section and a steel reinforcement ratio ρ_s = 0.5 %. The higher the ratio η_o the lower the strength increase in ULS. For low FRP reinforcement ratios, this effect of the ratio η_o is negligible.

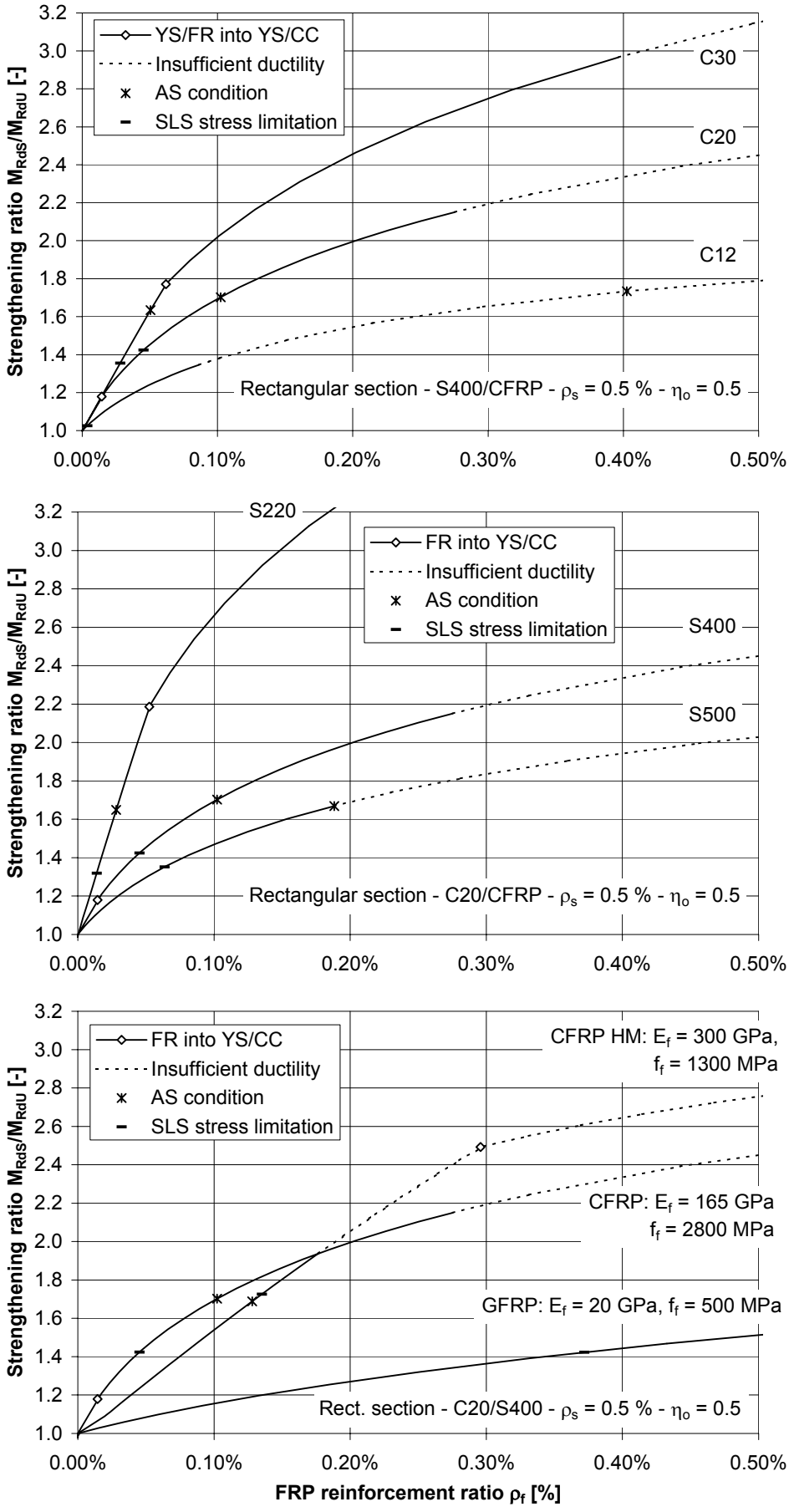

Fig. 7-20 *Influence of grade of constituent materials*

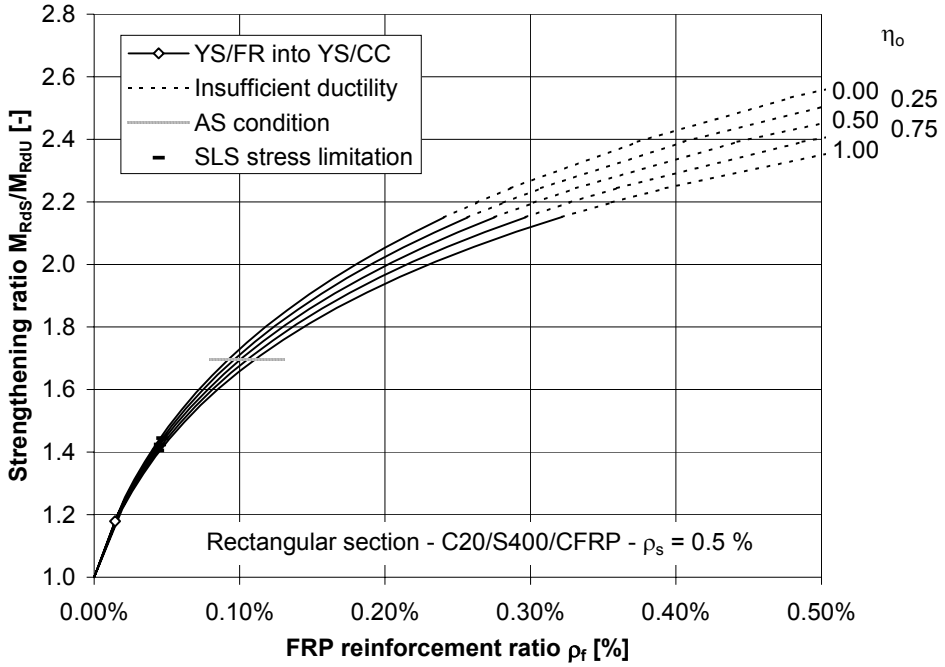

Fig. 7-21 *Influence of the ratio $\eta_o = M_o/M_{RkU}$*

3.6.1.4 Rectangular versus T-shaped cross-sections

In Fig. 7-22, for a concrete grade C20, a steel grade S400, CFRP with E_f = 165000 N/mm^2 and f_f = 2800 N/mm^2, a steel reinforcement ratio ρ_s = 1.0 % and η_o = 0.5, the influence of a rectangular versus a T-shaped cross-section is shown.

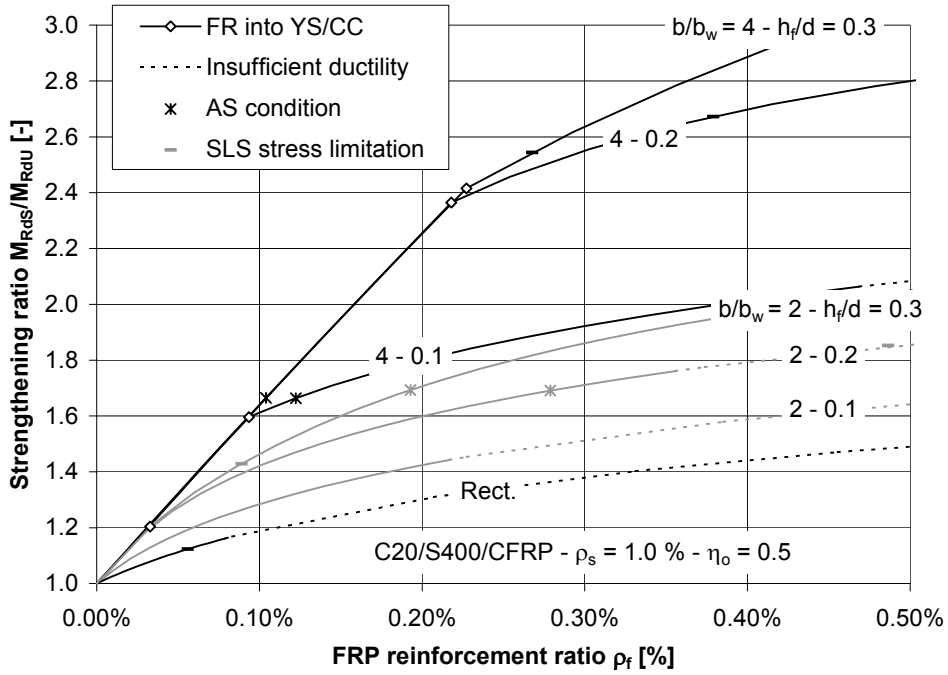

Fig. 7-22 *Influence of the shape to the cross-section*

The comparison is based on a constant width $b_{w,}$ as illustrated in Fig. 7-23. Hence, in Fig. 7-22 the reinforcement ratios ρ_s and ρ_f refer to the width b_w of the web of the T-shaped cross-section (note that in the calculation programme ρ_s and ρ_f refer to the width b, so that the ratio b/b_w was used to convert ρ with respect to b_w). As the compression zone of a T-section is larger than that of a rectangular section with the same width b_w, the strengthening effect in the ULS increases for T-shaped cross-sections. This is especially the case for large widths b and large flange depths h_f.

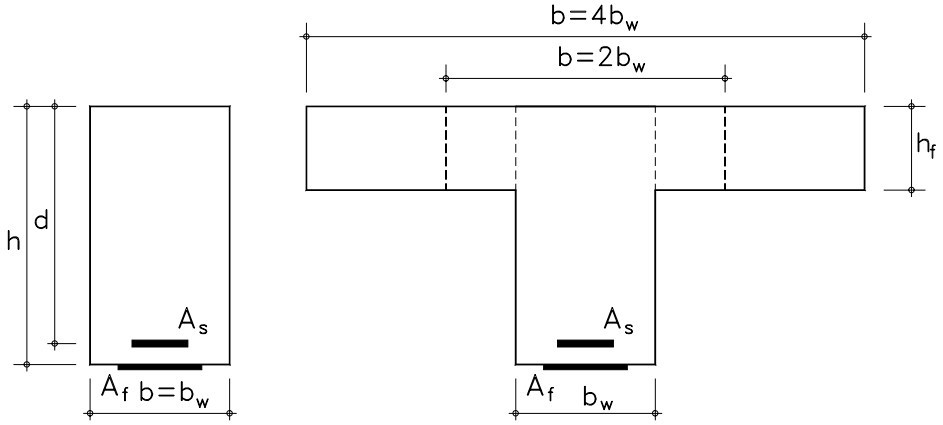

Fig. 7-23 *Rectangular versus T-shaped cross-sections*

3.6.2 Governing design aspects

As already appeared from the figures in the previous section, the maximum strength increase in the ULS is restricted by aspects such as accidental situation, ductility requirements and stress limitations. In the following a more detailed discussion on these and other aspects governing the design is given.

3.6.2.1 Failure mode assuming full composite action and ductility

Assuming full composite action the failure mode in ULS is either governed by yielding of the steel followed by FRP fracture (YS/FR) or by yielding of the steel followed by concrete crushing (YS/CC). Often the latter failure mode will be governing (Fig. 7-19), although this depends significantly on the amount of steel and FRP reinforcement and on the grade of the constituent materials (Fig. 7-20).

If high FRP reinforcement ratios are provided, strains in the steel and FRP reinforcement become rather small, so that it may occur that the steel is no longer or insufficiently yielding. To fulfil the ductility requirements (Section 2.4.3) the maximum amount of FRP and hence the maximum strength increase is restricted (Fig. 7-19 till Fig. 7-22).

3.6.2.2 FRP bond failure outside the anchorage zone

Even when properly anchored, FRP bond failure may occur outside the anchorage zone as a result of peeling initiated at vertical crack displacements (Section 3.4.6.2) or force transfer

between the FRP and the concrete (Section 3.4.5). Both these verifications are related to a restriction of the shear force.

Considering Eq. (7-38) for the verification of shear crack peeling, the strength increase at which peeling failure occurs is given by:

$$\frac{M_{Rpd}}{M_{RdU}} = \frac{\tau_{Rpk}}{f_{ck}} \frac{\upsilon}{\mu_{RdU}} \tag{7-66}$$

where, M_{Rpd} is the design moment corresponding to the critical shear force V_{Rpd} at which peeling initiates (Section 3.4.6.2), $\mu_{RdU} = M_{RdU}/(bd^2 f_{cd})$ is the reduced design moment of the unstrengthened beam and υ is a coefficient taking into account the load configuration and span of the beam ℓ:

$$\upsilon = \frac{\ell}{k_V d} \tag{7-67}$$

where, ℓ / k_V equals the ratio of the maximum moment to the maximum shear force of the RC member. The maximum shear force is to be taken within the zone where the FRP EBR is provided.

In a similar way, based on Eq. (7-35) (assuming $\varepsilon_s \geq \varepsilon_{yd}$, which corresponds to the most adverse situation), the strength increase at which bond failure occurs related to the force transfer between the FRP and the concrete (Section 3.4.5), is given by:

$$\frac{M_{Rbd}}{M_{RdU}} = \frac{f_{cbk}}{f_{ck}} \frac{\upsilon}{\mu_{RdU}} \frac{b_f}{b} \tag{7-68}$$

where, M_{Rbd} is the design moment corresponding to the critical shear force V_{Rbd} at which bond failure initiates (Section 3.4.5).

In Fig. 7-24, Eqs. (7-66) and (7-68) are compared with the strengthening ratio assuming full composite action. This is done for a rectangular cross-section, C20/S400/CFRP, $\rho_s = 0.5$ % and $\eta_o = 0.5$. It is noted that the FRP bond failure often governs the design. Provided that the width b_f of the FRP is taken sufficiently large with respect to the width b of the member, bond failure due to force transfer between the FRP and the concrete can easily be avoided. On the other hand, for members with low ratios ℓ / d (for a simply supported beam subjected to an uniform load, $\upsilon = 2.50 \sim 3.75$ corresponds with $\ell / d = 10 \sim 15$), bond failure at vertical crack displacements restricts the strengthening ratio to a large extent. Hence, this failure mode may often be a critical design criterion.

3.6.2.3 FRP anchorage failure

To prevent anchorage failure the provisions of Sections 3.4.4.2 till 3.4.4.4 may be followed, meaning that the distance L between the support and the end of the FRP should be sufficiently small or that a mechanical anchorage should be provided if needed.

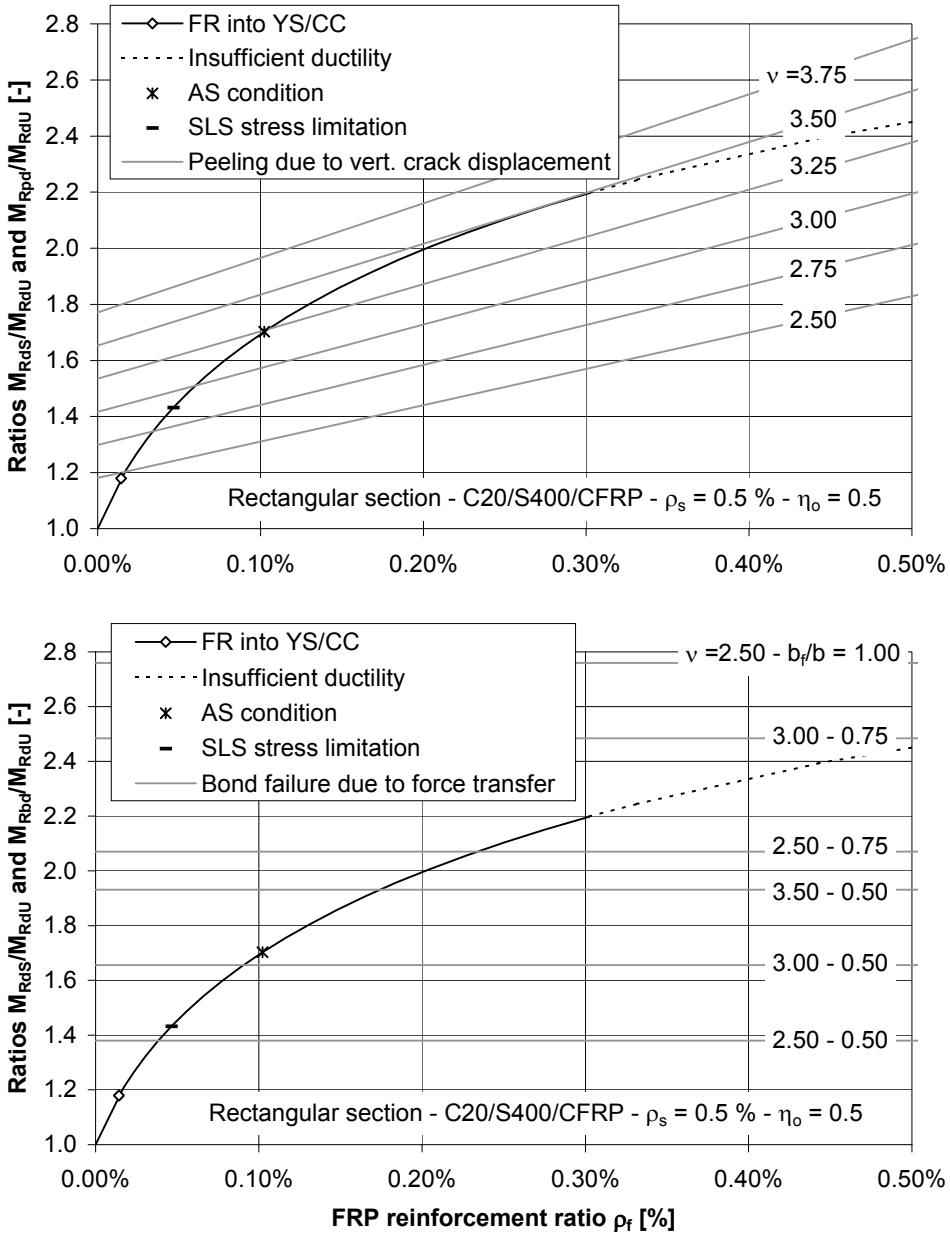

Fig. 7-24 *Bond failure outside the anchorage zone*

If insufficient anchorage length is available and no extra mechanical anchorage is provided, the ultimate FRP strain $\varepsilon_{fu,c}$ in the critical section will be smaller than the FRP failure strain ε_{fu} (Section 2.4.1). The influence of this aspect, for a rectangular cross-section (C20/S400/CFRP - ρ_s = 0.5 % - η_o = 0.5), is illustrated in Fig. 7-25. As the strain $\varepsilon_{fu,c}$ decreases, the strengthening effect becomes smaller in the zone where the failure mode is governed by yielding of the steel followed by FRP failure (in the zone corresponding with yielding of the steel followed by concrete crushing, the curves match each other). The range over which a yielding of the steel/FRP failure mode is obtained becomes larger. The lower the ratio $\varepsilon_{fu,c}/\varepsilon_{fu}$, the more pronounced the decrease in the strengthening ratio. This illustrates once more, that proper anchorage detailing is of considerable importance.

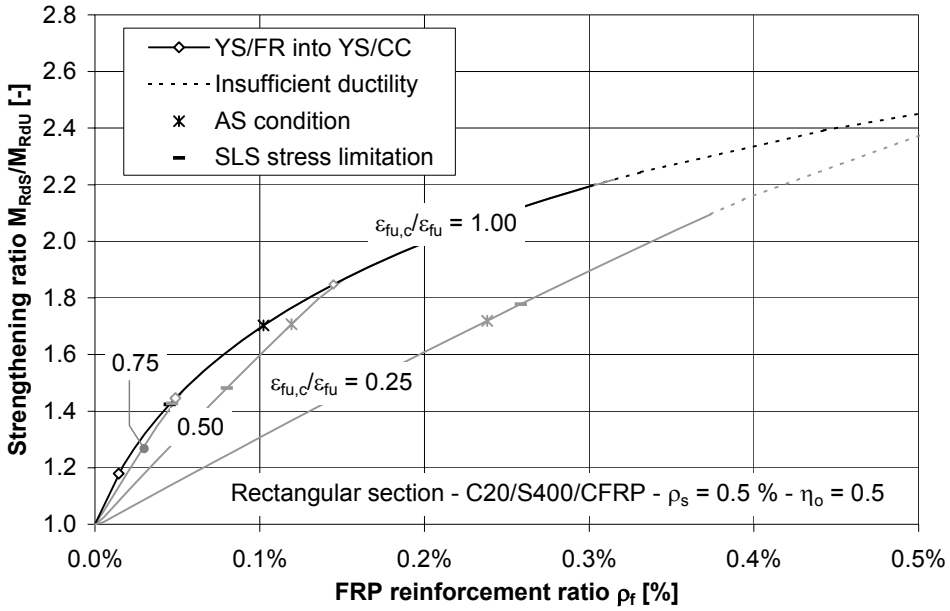

Fig. 7-25 *Influence of the ultimate FRP strain in the critical section*

3.6.2.4 SLS stress limitations

In the serviceability limit state, stresses in the concrete, steel and FRP are restricted to a fraction of the characteristic material strengths (Section 3.5.2). As demonstrated in Fig. 7-19 till Fig. 7-22, for rectangular cross-sections these stress limitations may often govern the design (for large strengthening factors, SLS stress limitations become critical). In calculating these graphs, it appeared that the steel stress limitation is governing when dealing with low steel reinforcement ratios or with high concrete strengths, while the concrete compressive stress limitation governs for low concrete strengths and high reinforcement ratios. In none of the cases, the FRP stress limitation was governing. Moreover, the FRP stress in the SLS appeared very small, meaning less than 25 % of the characteristic strength (high FRP stresses are generally obtained after the internal steel started yielding). If the allowable concrete or steel stress in the SLS is exceeded, the amount of FRP reinforcement may be increased beyond what is needed for the ULS (in which case in Fig. 7-19 till Fig. 7-22 no longer apply as such) to reduce these stresses.

For T-shaped cross-sections stress limitations in the SLS tend to be of less or no concern (Fig. 7-21).

3.6.2.5 Verification of crack widths

When concrete members are strengthened with externally bonded FRP reinforcement, typically a dense crack pattern and small crack widths are obtained. Hence, generally the crack width limitation is not governing the design.

In Section 3.5.4, a condition for the FRP bond width $u_f = b_f$ is obtained, so that unacceptable crack widths in the SLS are avoided. Assuming an effective concrete area in tension $\rho_{c,eff} \approx 2.5(\eta - 1)$, with $\eta = h/d \approx 1.1$ and a typical diameter (Ø = 20 mm) of the steel reinforcing bars, the condition for b_f given by Eq. (7-59) can be rewritten as:

$$d \le \frac{b_f}{b} \frac{1}{2.53 \dfrac{\mu_{RdS} f_{cd}}{\Phi_{qp} E_s \rho_{eq}} - 0.3\rho_s} \tag{7-69}$$

This equation is shown in Fig. 7-26, for a rectangular cross-section (C20/S400/CFRP - ρ_s = 0.5 % - η_o = 0.5). From this figure it follows that for members with a large effective depth d, the bond width of the FRP should be taken sufficiently large to control the crack widths in the SLS.

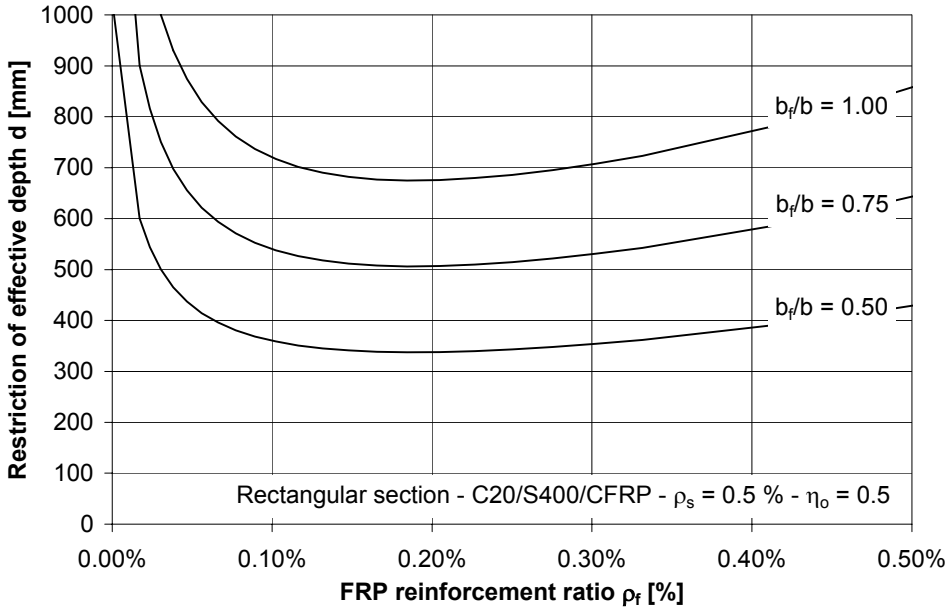

Fig. 7-26 *Restriction of the effective depth according to Eq. (7-69)*

3.6.2.6 Verification of deflections

By means of a small amount of FRP EBR, a relatively large strength increase in the ULS can be achieved. The contribution to the stiffness of the strengthened member is however of a lower magnitude, so that deflection control in the SLS may often govern the design.

In Section 3.5.3, equations for the calculation of the maximum deflection are provided. From these equations the following condition for the ratio of the span length ℓ over the effective depth d, can be obtained:

$$\frac{\ell}{d} \le \frac{(a/\ell)_{max}}{\beta k_M \dfrac{f_{ctm}\eta^2}{6E_c}\left(\dfrac{1}{\Gamma_1} - \eta_o\eta_S\dfrac{1}{\Gamma_o} - \dfrac{1-\eta_o\eta_S}{\Gamma_2}\right) + k_M \dfrac{\mu_{RdS} f_{cd}}{\Phi_{qp} E_c}\left(\eta_o\eta_S\dfrac{1}{\Gamma_o} + \dfrac{1-\eta_o\eta_S}{\Gamma_2}\right)} \tag{7-70}$$

where, $(a/\ell)_{max}$ is the ratio of the allowable deflection over the span length ℓ, $\beta = \beta_1\beta_2$ is a coefficient taken according to Section 3.5.3, k_M is a coefficient depending on the loading type, and $\Gamma = I/(bd^3)$ is the reduced moment of inertia about the neutral axis of the cross-section, respectively prior to strengthening (Γ_o), for the uncracked (Γ_1) and for the cracked strengthened cross-section (Γ_2).

The calculation of Eq. (7-70) has been programmed (using the software MathCad) as given in Appendix G. Based on this, Fig. 7-27 gives the ratio $(\ell/d)_{max}$ for a rectangular cross-section (C20/S400/CFRP - ρ_s = 0.5 % - η_o = 0.5), $(a/\ell)_{max}$ = 1/500 and k_M = 0.104 (simply supported member subjected to an uniform load). Compared to an unstrengthened member (ρ_f = 0 %), the ratio $(\ell/d)_{max}$ decreases considerably for a strengthened member. As a result, for slender RC elements (large values of ℓ/d) the allowable defection in the SLS will often govern the design. This means that, for a given design moment M_{dS} of the strengthened member, the FRP reinforcement ratio should be increased until $(\ell/d)_{max}$ equals the actual ℓ/d ratio of the strengthened member. In this case Eq. (7-70) becomes:

$$\frac{\ell}{d} \le \frac{(a/\ell)_{max}}{\beta k_M \frac{f_{ctm}\eta^2}{6E_c}\left(\frac{1}{\Gamma_1} - \eta_o\eta_S\frac{1}{\Gamma_o} - \frac{1-\eta_o\eta_S}{\Gamma_2}\right) + k_M\frac{\mu_{dS}f_{cd}}{\Phi_{qp}E_c}\left(\eta_o\eta_S\frac{1}{\Gamma_o} + \frac{1-\eta_o\eta_S}{\Gamma_2}\right)} \tag{7-71}$$

where, $\mu_{dS} = M_{dS}/(bd^2f_{cd})$ is the reduced design moment of the strengthened member and $\eta_S = M_{dS}/M_{RdU}$. The ratio $(\ell/d)_{max}$ according to Eq. (7-71) is shown in Fig. 7-27 for different values of μ_{dS}.

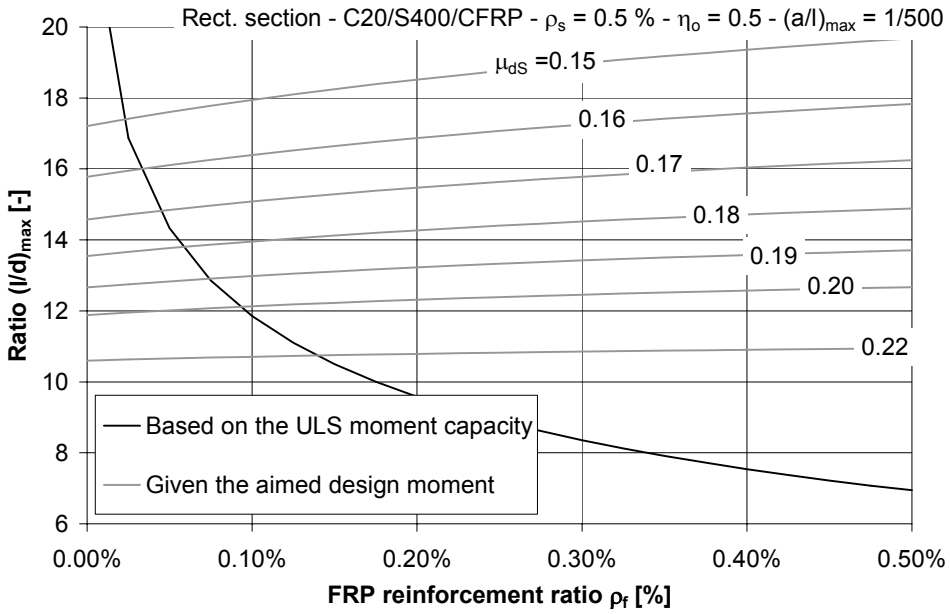

Fig. 7-27 *Ratio $(\ell/d)_{max}$ according to Eqs. (7-70) and (7-71)*

3.6.2.7 Verification of the accidental situation

When large FRP reinforcement ratios are applied, the ratio $\eta_a = M_{RkS}/M_{Ak}$ becomes larger than 1. This means that in case of accidental loss of the FRP EBR, the member will collapse. As appears from Fig. 7-19 till Fig. 7-22, η_a = 1 corresponds to a strengthening ratio η_S of about 1.7. Below this value, the RC member will not collapse in the case of accidental loss of the FRP EBR, although it is subjected to the loads of the strengthened member. In many cases (Fig. 7-19 till Fig. 7-22), the accidental situation condition is less governing than the SLS stress limitations or the ductility requirements.

3.7 Summary of design process

As appears from the previous sections, the dimensioning of externally bonded FRP reinforcement for the strengthening of flexural members, is related to various verifications. From Section 3.6, it follows that the design is likely to be governed by the SLS or by bond failure due to vertical crack displacements. The design process can be summarized as follows:

- Determine the resisting design moment of the existing member (ULS, Section 3.3 with $A_f = 0$ mm^2) and verify that a minimum amount of steel reinforcement is available to prevent brittle failure (Section 3.3.4). Check the SLS of the existing member. Although the latter aspect is not really needed for the further design, it provides valuable information with respect to the SLS criteria (these criteria are likely to govern the further design).
- Given the service moment prior to strengthening, determine the initial strain at the extreme tension fibre (Section 3.2).
- Given the design moment acting on the strengthened structure, determine the required FRP cross-section to fulfil the ULS, assuming full composite action (Section 3.3). Verify that sufficient ductility is obtained at the ULS (Section 2.4.3).
- Calculate the deflections in the SLS (Section 3.5.3). If the maximum allowable deflection is exceeded, determine the required FRP cross-section to fulfil the allowable deflection.
- Calculate the stresses in the concrete, steel and FRP in the SLS (Section 3.5.2). If allowable stresses are exceeded, determine the required FRP cross-section to fulfil the stress limitation conditions.
- Verify that the provided FRP bond width is sufficient to control the crack widths in the SLS (Section 3.5.4). Enlarge the FRP bond width if possible or, given a maximum bond width, increase the amount of FRP. Bond interface cracking in the SLS is of no concern (Section 3.5.5).
- Verify the resisting shear force at which bond failure due to vertical crack displacement occurs (ULS, Section 3.4.6.2). If this failure mode is dominant, determine a new value of the required FRP cross-section.
- Verify that the mean bond shear stress due to force transfer between the FRP and the concrete (Section 3.4.5) is not exceeded. If this is the case the FRP should be additionally fixed (mechanical anchorage).
- Detail the anchorage zone, so that anchorage and concrete ripp-off failure are avoided (Sections 3.4.4.2 till 3.4.4.4).
- Verify the accidental situation (Section 2.2.2).
- Verify the shear design resistance of the strengthened member (ULS). If needed shear strengthening should be provided (Section 4).

As the design procedure involves a relatively large number of sometimes repetitive calculations, these calculations have been programmed (using the software Mathcad) for a simply supported member subjected to a uniform load. This programme, which offers at the same time a design example, is given in Appendix H.

4 Shear strengthening

4.1 General

To avoid brittle shear failure, RC beams with an insufficient shear capacity should be strengthened. By means of externally bonded FRP reinforcement, a wide range of strengthening configurations is possible. Some examples are shown in Fig. 7-28. To allow moisture exchange of the concrete and as it is normally most practical to attach the external FRP reinforcement with the principal fibre direction perpendicular to the member longitudinal axis, the 90° strip configuration (Fig. 7-28) may often be preferable. If the FRP is aligned according to the 45° direction, more efficiency will be obtained as the fibres are provided more or less according to the principal tensile stress and as the anchorage length is longer. To avoid bond failure (given the limited anchorage length), the FRP should be totally wrapped or anchored.

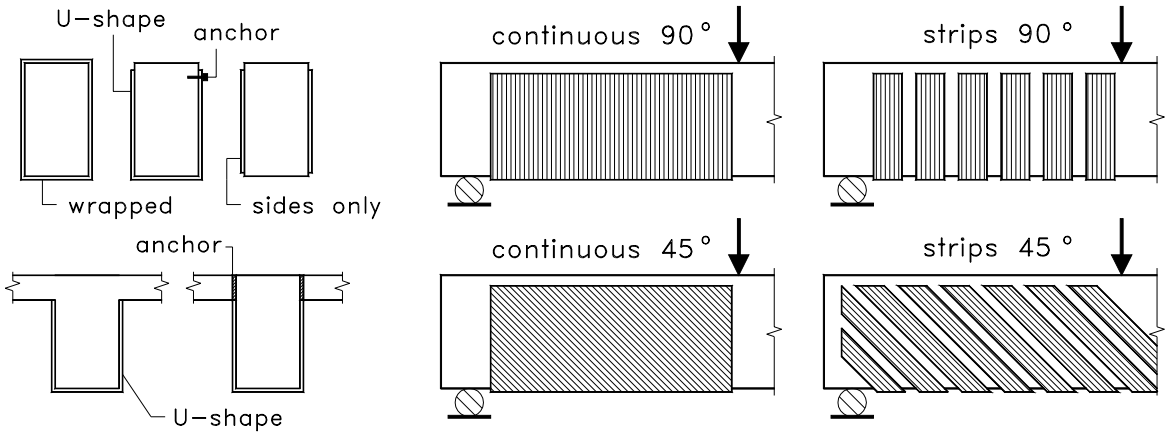

Fig. 7-28 *Shear strengthening of RC beams*

Shear failure of RC beams strengthened with FRP EBR mostly happens, in a similar way as for unstrengthened members, by diagonal tension (failure at an inclined shear crack). This failure may be initiated prematurely as a result of FRP bond failure or may correspond to fracture of the FRP. Due to strain variations along the shear crack, local debonding at both sides of the shear crack, possible bond failure, etc. it appears that the contribution of the FRP is limited to an effective tensile strain ε_{fue}, which is generally lower than the ultimate FRP strain ε_{fu}. (Chapter 4, Section 4.3).

Because of the many aspects of influence and their complexity, the prediction of the effective FRP strain ε_{fue} is rather difficult. Using the approach suggested by Triantafillou [43], simple relationships for ε_{fue} (based on experimental data fitting) have been proposed in Chapter 4, Section 4.3.

4.2 ULS verification

4.2.1 Shear capacity

It can be assumed that the ULS verification may be based on a truss analogy (Mörsch), similar as for unstrengthened RC members. Hence, the shear capacity V_{Rd} of the strengthened member can be formulated, according to the EC2 format, as:

$$V_{Rd} = \min\left(V_{Rd1} + V_{wsd} + V_{wfd}, V_{Rd2}\right) \tag{7-72}$$

where, V_{Rd1} is the shear capacity of the concrete, V_{wsd} and V_{wfd} are the contribution of the internal steel and external FRP reinforcement respectively and V_{Rd2} is the shear strength of the concrete in diagonal compression. For the design equations of V_{Rd1} and V_{Rd2}, reference is made to EC2 [11]. The contribution of the shear reinforcement is given as:

$$V_{wsd} = \frac{A_{ws}}{s_s} 0.9 d \sigma_{ws} \left(\cot\theta + \cot\alpha_s\right) \sin\alpha_s \tag{7-73}$$

$$V_{wfd} = \frac{A_{wf}}{s_f} 0.9 d E_f \varepsilon_{fue,d} \left(\cot\theta + \cot\alpha_f\right) \sin\alpha_f \tag{7-74}$$

with, A_{ws} and A_{wf} the cross-sectional area of the internal steel and external FRP shear reinforcement, s_s and s_f the steel and FRP shear reinforcement spacing (for continuous FRP s_f equals b_f), d the effective depth of the cross-section, θ the angle between the diagonal shear crack and the member longitudinal axis (generally assumed as 45°), α_s and α_f the angle of the steel stirrups and the principle FRP fibre orientation with respect to the member longitudinal axis and $\varepsilon_{fue,d}$ the design value of the effective FRP strain, given in Section 4.2.2. Mostly, $\varepsilon_{fue,d}$ will be larger than the yield strain of the steel stirrups, so that the tensile stress in the steel σ_{ws} equals the design value of the yield strength f_{wyd}. If not, σ_{ws} should be taken equal to $E_s\varepsilon_{fue,d}$.

Defining $\rho_{ws} = A_{ws}/(s_f b_w)$ and $\rho_{wf} = A_{wf}/(s_f b_w)$, the steel and FRP shear reinforcement ratio respectively and with b_w the minimum width of the member, Eqs. (7-73) and (7-74) can also be written as:

$$V_{wsd} = \rho_{ws} 0.9 d b_w \sigma_s \left(\cot\theta + \cot\alpha_s\right) \sin\alpha_s \tag{7-75}$$

$$V_{wfd} = \rho_{wf} 0.9 d b_w E_f \varepsilon_{fue,d} \left(\cot\theta + \cot\alpha_f\right) \sin\alpha_f \tag{7-76}$$

4.2.2 Effective FRP failure strain

The prediction of the effective FRP failure strain ε_{fue} is a crucial aspect in the ULS design verification for shear strengthening. Some models have been proposed [43-49]. However, more research is needed with respect to these models and the verification of their accuracy. In Chapter 4, Section 4.3, based on experimental data fitting (see also [43,47]), simple relationships for the prediction of the effective ultimate FRP strain ε_{fue} have been derived. In case of fully wrapped or properly anchored FRP, the strain ε_{fue} is given by:

$$\varepsilon_{fue} = 0.72 \varepsilon_{fu} e^{-0.0431\Gamma_f} \tag{7-77}$$

where,

$$\Gamma_f = \frac{E_f \rho_{wf}}{f_{cm}^{2/3}(a/d)} \tag{7-78}$$

with, (a/d) the shear span over the effective depth and where f_{cm} and E_f are expressed in N/mm^2 (Γ_f in (N/mm^2)$^{1/3}$). For FRP bonded to the sides only, the effective ultimate FRP strain yields:

$$\varepsilon_{fue} = 0.56\varepsilon_{fu} e^{-0.0455\Gamma_f} \tag{7-79}$$

In case of U-shaped FRP, not sufficient data was available to derive an equation, so that Eq. (7-79) should be used.

Although the above equations for ε_{fue} do not consider the strain distribution along the shear crack and the bond behaviour explicitly, it has the advantage of avoiding a complex modelling. On the other hand and as demonstrated in Fig. 7-29, a relatively large scatter is found compared to the experimental data. Hence, also this approach is subject to further improvement.

Based on Eqs. (7-77) and (7-79), the design value of the effective FRP strain at ultimate is obtained as:

$$\varepsilon_{fue,d} = \beta_{fe}\, \varepsilon_{fue} / \gamma_f \tag{7-80}$$

with, γ_f the FRP material safety factor and β_{fe} a coefficient which relates the mean and characteristic value of ε_{fue}. In Fig. 7-29, the ratio $\varepsilon_{fue,d}/\varepsilon_{fu}$ is shown for $\gamma_f = 1.3$ (Section 2.3.2) and $\beta_{fe} = 0.8$ (estimated from the variance of the regression [38]). The effective strain and hence the shear capacity are larger in case bond failure is prevented (wrapping or anchored). For increasing values of $E_f\rho_{wf}/f_{cm}^{2/3}$ the effective strain decreases.

In the literature (e.g. [47]) it is sometimes suggested that $\varepsilon_{fue,d}$ should be smaller than about 4 mm/m to insure concrete and aggregate interlock shear contribution. In Chapter 5, Section 3.4.3 it is argued that this limitation is not useful with respect to the above equations for ε_{fue}.

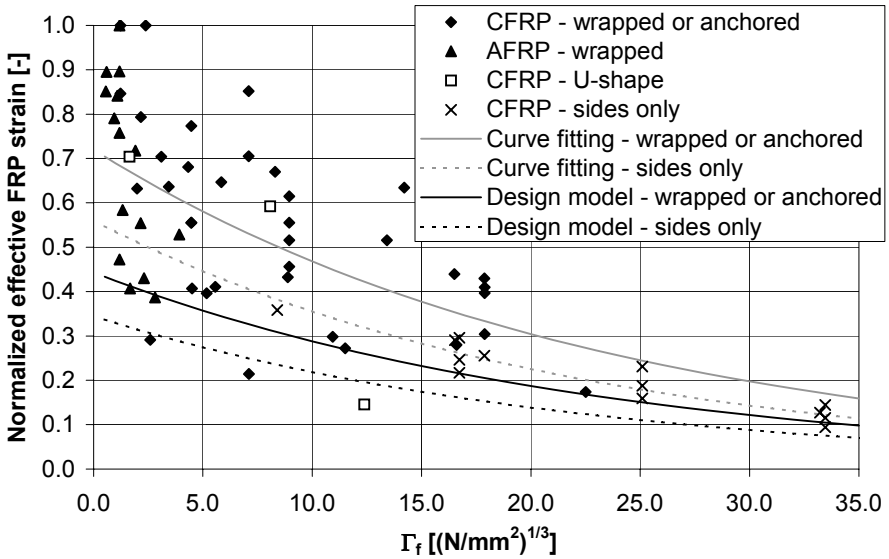

Fig. 7-29 *Effective ultimate FRP strain for shear design*

4.3 SLS verification

The risk of cracking in the SLS may be evaluated by means of the shear stress in the concrete:

$$\tau_{c,max} = \frac{V_k}{z b_w} \tag{7-81}$$

with z = 0.75d and 0.80d for rectangular or T-sections respectively [16]. If $\tau_{c,max}$ is smaller than f_{ctk} it may be assumed that there are no shear cracks at service load. Is $\tau_{c,max} \geq f_{ctk}$, shear cracking may occur and it should be verified that crack widths are restricted. As demonstrated in Section 3.5.5, by controlling the crack width also local debonding is prevented under service load.

For the calculation of the crack width, reference can be made to the behaviour of tensile members (Chapter 5, Section 4.3). In the case of a strengthened beam subjected to shear, the tensile member forms part of the truss analogy as shown in Fig. 7-30. Mostly shear cracks initiate at the location of flexural cracks. Due to the relatively high contribution of the concrete to the shear capacity at service load, no additional web shear cracks are expected at SLS. Hence, the crack spacing of the shear cracks is dictated by that of the flexural cracks (Fig. 7-30).

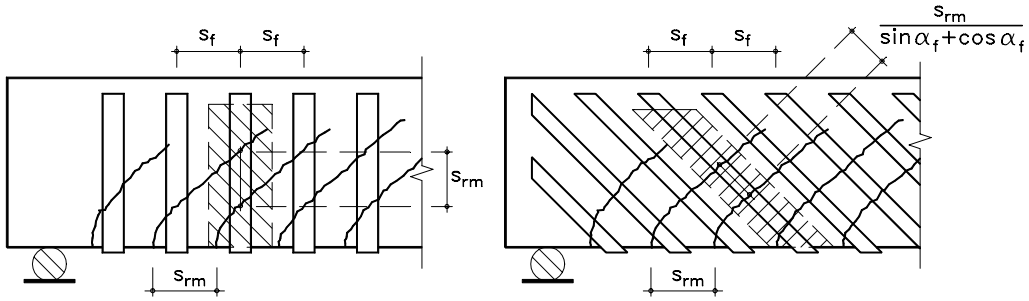

Fig. 7-30 *Principle for calculating the width of shear cracks*

In the case of vertical internal and external shear reinforcement ($\alpha_s = \alpha_f = 90°$) and 45° shear cracks, the tensile strain ε_2 in the cracked state can be obtained from:

$$\begin{aligned}(V_k - V_{ck}) &= \varepsilon_2 \, 0.9 d b_w \left(E_s \rho_{ws} + E_f \rho_{wf}\right) \\ &= \varepsilon_2 \, 0.9 d b_w E_s \rho_{w,eq}\end{aligned} \tag{7-82}$$

where, V_k is the shear force at service load, $\rho_{w,eq}$ is the equivalent shear reinforcement ratio and V_{ck} is the concrete shear contribution at service load, given by [11]:

$$V_{ck} = 0.25 f_{ctk\,0.05} k (1.2 + 40\rho) d b_w \tag{7-83}$$

where, k = 1.6 – d ≥ 1 (d in [m]) and ρ ≤ 0.02 is the longitudinal steel reinforcement ratio (ρ may be taken as ρ_{eq} when the member is strengthened with FRP EBR in flexure).

Assuming the crack width as the product of the crack spacing and the tensile strain, the characteristic value of the shear crack width is given by:

$$w_k = \beta k_\alpha s_{rm} \frac{V_k - V_{ck}}{0.9 d b_w E_s \rho_{w,eq}} \tag{7-84}$$

with, $\beta = 1.7$ a factor relating the mean and characteristic crack width [11], $k_\alpha = 1.4$ a factor relating the crack width in the assumed tensile member to the maximum crack width and s_{rm} the mean crack spacing as given in [11] or according to Eq. (7-56) for RC members strengthened in flexure. The factor $k_\alpha = 1.4$ for vertical shear reinforcement follows from the fact that the shear force is both carried by a vertical component (shear reinforcement) and a horizontal component (longitudinal reinforcement). Assuming equal crack widths $w_v = w_h$ corresponding with these two components, the maximum crack width is given as $\sqrt{2}w_v$ or $k_\alpha = \sqrt{2} \approx 1.4$.

For shear reinforcement with $\alpha_s = \alpha_f = \alpha$, the shear crack width is in a similar way obtained as:

$$w_k = \beta k_\alpha s_{rm} \frac{V_k - V_{ck}}{0.9 d b_w E_s \rho_{w,eq}} \frac{1}{(\sin\alpha + \cos\alpha)^2} \tag{7-85}$$

where, the factor k_α equals 1.0 for $\alpha \approx 45$ °. Comparing Eqs. (7-84) and (7-85) for a constant value of $\rho_{w,eq}$, the smallest crack width is obtained for $\alpha = 45°$.

In the case of different angles of the internal and external shear reinforcement, the crack width may be approximated as:

$$w_k \approx \beta k_\alpha \frac{s_{rm}}{\min(k_s, k_f)} \frac{V_k - V_{ck}}{0.9 d b_w (E_s \rho_{ws} k_s + E_f \rho_{wf} k_f)} \tag{7-86}$$

with, $k_s = (\sin\alpha_s + \cos\alpha_s)$ and $k_f = (\sin\alpha_f + \cos\alpha_f)$. The factor k_α should be taken between 1.0 and 1.4.

In the above equations it is assumed that the FRP reinforcement is wrapped or properly anchored. If this is not the case, the amount of FRP reinforcement which bridges the shear cracks in an effective way is smaller. This aspect can be taken into account by considering a reduced shear reinforcement ratio $\eta\rho_{wf}$. Based on Fig. 7-31, the reduction factor η is defined as:

$$\eta \approx \frac{L - S}{L} \tag{7-87}$$

For rectangular sections $L = 0.9d$, while $S \approx (0.50 s_{rm} - 0.1d) \le 0.25 s_{rm}$ or $0.50 s_{rm}$ for U-shaped FRP and FRP bonded to the sides only, respectively. For T-sections $L = d - h_f$ and $S \approx 0.25 s_{rm}$ or $0.50 s_{rm}$ for U-shaped FRP and FRP bonded to the side only, respectively.

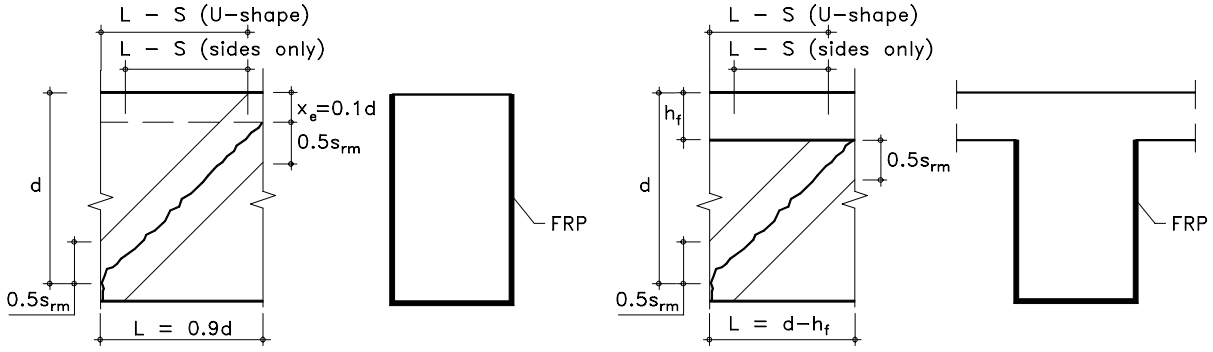

Fig. 7-31 *Available transfer zone at both sides of the shear crack*

4.4 Spacing requirements

Similar to steel shear reinforcement, the formation of a diagonal crack without intercepting FRP shear reinforcement should be avoided. For this reason, if FRP is provided strip wise (discontinuous), the spacing of the FRP shear reinforcement s_f should be less than:

$$s_{f,max} = 0.45d + b_f/2 \tag{7-88}$$

4.5 Summary of the design process

The design process for the dimensioning of the FRP EBR shear strengthening, can be summarized as follows:

- Given the acting design shear force, the design shear capacity of the concrete and that of the steel stirrups, the remaining design shear force to be taken by the FRP is obtained. Verify that the shear strength of the concrete in diagonal compression is not exceeded (Section 4.2.1).
- Assume a value for the effective FRP failure strain and determine the FRP shear reinforcement ratio ρ_{wf} needed (Sections 4.2.1 and 4.2.2). Update the value for the effective FRP failure strain and recalculate. Repeat this process until convergence is obtained.
- Choosing the amount of FRP which will be used for external shear strengthening, determine the required spacing of the FRP reinforcement $s_f = A_{wf}/(\rho_{wf} b_w)$. Verify that the spacing is smaller than the maximum specified in Section 4.4.
- Verify the crack width in the SLS (Section 4.3).

5 Confinement of axially loaded columns

5.1 General

Confinement is an efficient technique to increase the load carrying capacity and ductility of compressed concrete members. By providing lateral confining pressure, the concrete is subjected to a tri-axial state of stress, so that the compressive strength and deformability increase. Mostly, the lateral confining action is induced in a passive way, by restraining the lateral expansion of the concrete through closed spaced stirrup or hoop reinforcement. For existing structures, this can be achieved by means of externally bonded confinement reinforcement, such as a FRP wrapping. In the case the FRP wrapping is prestressed (e.g. by means of expansive mortar) an active confining pressure will be obtained. In the following, only passive confinement is dealt with.

As the range of loading conditions for columns is quite large, a wide range of models for the design of columns is available. Referring to the experimental and analytical study on FRP confined concrete described in Chapter 6, only the modelling of axially loaded columns confined with FRP EBR is discussed in the following. With respect to this loading type, EC2 [11] specifies that the uncertainty of the dimensional tolerances and the position and line of

action of the axial load should be considered in the design. This can be done by considering an equivalent geometrical imperfection (arbitrary eccentricity) as defined in [11]. As an alternative, in [50] it is allowed to still consider uniaxial compression, whereby increased material safety factors are applied:

$$\gamma_{c,axial} = 1.1\gamma_c \quad \text{and} \quad \gamma_{s,axial} = 1.1\gamma_s \tag{7-89}$$

Furthermore, it is assumed that the column slenderness is low enough to prevent buckling and that the condition with respect to the minimum amount of longitudinal steel reinforcement, as specified in [11], is satisfied. In absence of the minimum amount of longitudinal steel reinforcement, the axially loaded column should be calculated in combined bending assuming the aforementioned arbitrary eccentricity. In this way, the amount of longitudinal FRP EBR needed in addition to the FRP wrapping reinforcement can be calculated. By providing FRP wrapping reinforcement, it is no longer needed to satisfy the condition with respect to the minimum amount of internal steel stirrups specified in [11]. In this case, it should however be verified that the stiffness and possible spacing of the FRP wrapping is such that local buckling of the internal longitudinal steel is prevented.

5.2 ULS verification

5.2.1 Load carrying capacity

The resisting load carrying capacity in the ultimate limit state of axially loaded FRP confined columns is given by:

$$\begin{aligned} N_{Rd} &= 0.85 f_{ccd} A_c + f_{yd} A_s \\ &= 0.85 f_{ccd} A_g \left(1 + \left(\frac{f_{yd}}{0.85 f_{ccd}} - 1 \right) \rho_{sg} \right) \end{aligned} \tag{7-90}$$

where, f_{ccd} and f_{yd} are the design values (calculated with the increased material safety factors given by Eq. (7-89)) of the confined concrete compressive strength and the steel yield stress respectively, A_c is the cross-sectional area of the concrete, A_s is the cross-sectional area of the longitudinal steel reinforcement, A_g is the gross cross-section and $\rho_{sg} = A_s/A_g$ is the longitudinal steel reinforcement ratio.

In Eq. (7-90), it is assumed that the axial strain when reaching f_{ccd} is larger than the yield strain corresponding with f_{yd}. This assumption is valid as generally the axial strain of confined concrete is a multiple of that of unconfined concrete. Even in the case of a very low confining action, so that f_{ccd} equals about the unconfined concrete strength f_{cd} and the axial strain can be assumed 2 mm/m [11], this assumption is satisfied. Indeed, assuming a maximum steel quality S500, the yield strain $f_{yk}/(\gamma_{s,axial}E_s) \leq 2$ mm/m.

5.2.2 Stress-strain relationship and compressive strength of confined concrete

As FRP materials behave linear elastic until failure, the lateral confining stress exerted by FRP wrapping reinforcement increases with the lateral expansion of the concrete. As a result

of this aspect, classical models for steel confined concrete, which assume a constant confining action, are no longer suitable. In Chapter 6, Section 4.3, the modelling of the stress-strain behaviour of FRP confined concrete has been investigated. From this study it was concluded that the incremental-iterative stress-strain model by [51] yields accurate results. Details on this model are provided in Appendix F, Section 1.1.

For design practice, it is often only of interest to know the design value f_{ccd} of the confined concrete compressive strength. Similar to Chapter 6, Section 4.4 and given the design value of the ultimate lateral confining pressure $\sigma_{\ell ud}$ (Section 5.2.3), the confined concrete strength is derived as (Fig. 7-32) [51]:

$$f_{ccd} = E_{sec,ud}\varepsilon_{ccud} \geq f_{cd} \tag{7-91}$$

where, $E_{sec,ud}$ is the secant modulus when reaching the ultimate limit state, given as:

$$E_{sec,ud} = \frac{E_c}{1 + 2\beta\eta_e f_{fd}/E_f} \quad \text{with} \quad \beta = \frac{E_c}{f_{cd}} - \frac{1}{0.002} \tag{7-92}$$

and ε_{ccud} is the corresponding axial strain:

$$\varepsilon_{ccud} = \varepsilon_{ccMd}\left(\frac{E_{sec,Md}(E_c - E_{sec,ud})}{E_{sec,ud}(E_c - E_{sec,Md})}\right)^{1-E_{sec,Md}/E_c} \tag{7-93}$$

with, β a parameter depending on the unconfined concrete properties, $\eta_e f_{fd}$ the design value of the effective FRP strength of the confining reinforcement (Section 5.2.3) and $E_{sec,Md}$ the secant modulus defined as:

$$E_{sec,Md} = \frac{f_{ccMd}}{\varepsilon_{ccMd}} \tag{7-94}$$

where, f_{ccMd} is the confined concrete strength assuming a constant confining pressure $\sigma_{\ell ud}$ and ε_{ccMd} is the corresponding axial strain. According to the model by Mander, these parameters are given as [52,53]:

$$f_{ccMd} = \alpha_{1d}\alpha_{2d}f_{cd} \quad \text{and} \quad \varepsilon_{ccMd} = 0.002\left(1 + 5\left(\alpha_{1d}\alpha_{2d} - 1\right)\right) \tag{7-95}$$

with,

$$\alpha_{1d} = 2.254\sqrt{1 + 7.94\frac{\sigma_{\ell xud}}{f_{cd}}} - 2\frac{\sigma_{\ell xud}}{f_{cd}} - 1.254 \tag{7-96}$$

$$\alpha_{2d} = 1 - \left(0.6\left(\frac{\sigma_{\ell yud}}{\sigma_{\ell xud}}\right)^2 - 1.4\frac{\sigma_{\ell yud}}{\sigma_{\ell xud}} + 0.8\right)\sqrt{\frac{\sigma_{\ell xud}}{f_{cd}}} \tag{7-97}$$

where, $\sigma_{\ell xud} = \sigma_{\ell yud} = \sigma_{\ell ud}$ (and hence $\alpha_{2d} = 1$) is the ultimate FRP confining pressure for circular cross-sections and $\sigma_{\ell xud} \geq \sigma_{\ell yud}$ is the ultimate FRP confining stress in the case of square or rectangular cross-sections. These confining pressures, taking into account the design value of the effective FRP failure strain, are given in Section 5.2.3.

For sufficiently large confining pressures $\sigma_{\ell ud}$, the maximum and ultimate concrete stress coincide, as illustrated in Fig. 7-32(a). Hence, in this case, f_{ccd} is reached at the same moment the design value of the effective FRP strength is reached in the wrapping reinforcement. At the contrary, for low confining pressures $\sigma_{\ell ud}$, the peak stress is obtained before reaching the ultimate limit state, as shown in Fig. 7-32(b). In this case, it has been demonstrated in Chapter 6, Section 4.4 that the strength increase is negligible, so that $f_{ccd} = f_{cd}$, while the ultimate stress $\sigma_{ccud} < f_{cd}$ is given by the left part of Eq. (7-91).

To avoid confining pressures resulting in a negligible strength increase, K_{conf} should be taken larger than about $3f_{cd}$ for NSC and about $2f_{cd}$ for HSC (Chapter 6, Section 4.4), where E_{conf} is a parameter expressing the stiffness and effectiveness of the confining device as defined in the next section.

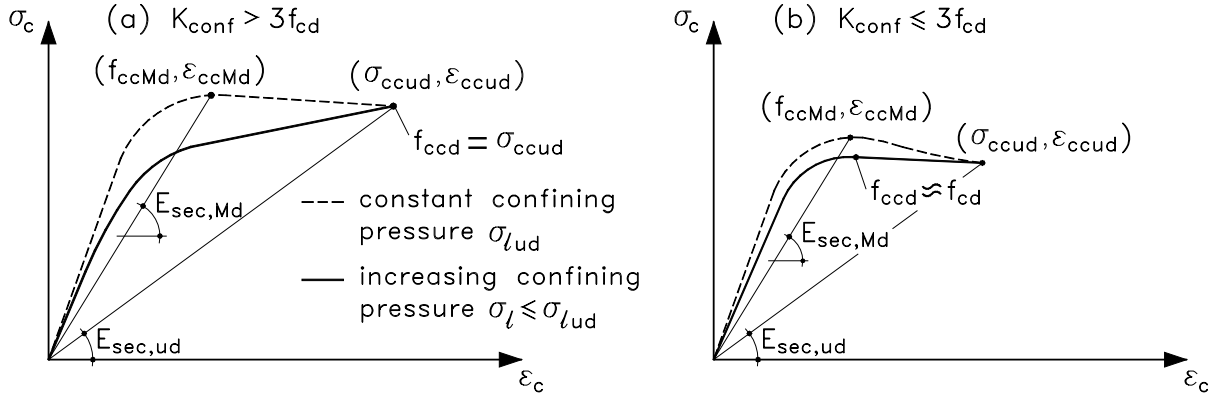

Fig. 7-32 *Ultimate limit state and confined concrete design strength*

5.2.3 Effective ultimate FRP strain and corresponding lateral confining pressure

The FRP being a linear elastic material, the design value of the maximum lateral confining pressure $\sigma_{\ell ud}$ exerted by the FRP wrapping reinforcement is obtained when reaching the design value $\eta_e f_{fd}$ of the effective FRP strength. The reduction factor η_e follows from the fact that the mean ultimate strain of the FRP wrapping reinforcement is lower than the strain $\varepsilon_{fud} = f_{fd}/E_f$. This is due to local stress concentrations in the FRP near failure, the multiaxial state of stress of the FRP, size effects when using multiple layers, etc.

5.2.3.1 Circular cross-sections

Following Chapter 6, Section 4.2, the design value of the lateral confining pressure at the ULS can be derived as (Fig. 7-33):

$$\sigma_{\ell ud} = K_{conf} \frac{\eta_e f_{fd}}{E_f} \quad \text{with} \quad K_{conf} = \frac{1}{2} \rho_f k_e E_f \tag{7-98}$$

where, ρ_f is the volumetric ratio of the FRP wrapping reinforcement given by:

$$\rho_f = \frac{4 b_f t}{D s} \tag{7-99}$$

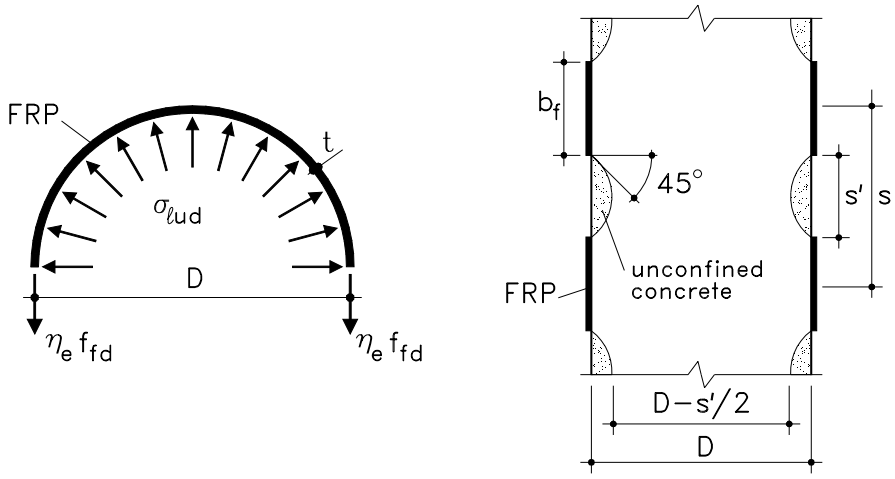

Fig. 7-33 *Design value of the maximum lateral confining stress*

and $k_e = k_{e1}k_{e2} \leq 1$ is a confinement effectiveness coefficient, taking into account partial wrapping (k_{e1}) and fibre orientation (k_{e2}):

$$k_{e1} = \frac{\left(1 - \frac{s'}{2D}\right)^2}{1 - \rho_{sg}} \quad \text{and} \quad k_{e2} = \frac{1}{1 + \left(\frac{p}{\pi D}\right)^2} \tag{7-100}$$

with, D the diameter of the column, s the centre to centre spacing of the FRP wrapping, s' the clear spacing and p the pitch of the spiral wrapping ($p = \pi D tg(\alpha_f)$, α_f the fibre orientation with respect to the circumferential direction). The influence of the effectiveness coefficient k_e is shown in Fig. 7-34, from which it is noted that the efficiency considerably decreases in case of spiral wrapping and for partial wrapping with a large clear spacing.

The reduction factor η_e should be based on relevant experimental evidence, or is tentatively suggested as (Chapter 6, Section 4.4.3):

$$\eta_e = 0.105(K_{conf})^{0.266} \tag{7-101}$$

where, K_{conf} is expressed in [N/mm^2].

5.2.3.2 Square or rectangular cross-sections

Similar to circular cross-sections, the design value of the lateral confining pressure on a square or rectangular cross-section is given at the ULS by (Fig. 7-35):

$$\begin{aligned} \sigma_{\ell xud} &= K_{confx} \frac{\eta_e f_{fd}}{E_f} \quad \text{with} \quad K_{confx} = \rho_{fx}\, k_e E_f \\ \sigma_{\ell yud} &= K_{confy} \frac{\eta_e f_{fd}}{E_f} \quad \text{with} \quad K_{confy} = \rho_{fy}\, k_e E_f \end{aligned} \tag{7-102}$$

where, η_e follows from Eq. (7-101) taking into account a mean value for K_{conf}. The ratios ρ_{fx} and ρ_{fy} represent the quantities of transverse confining reinforcement in the x and y direction and are given by:

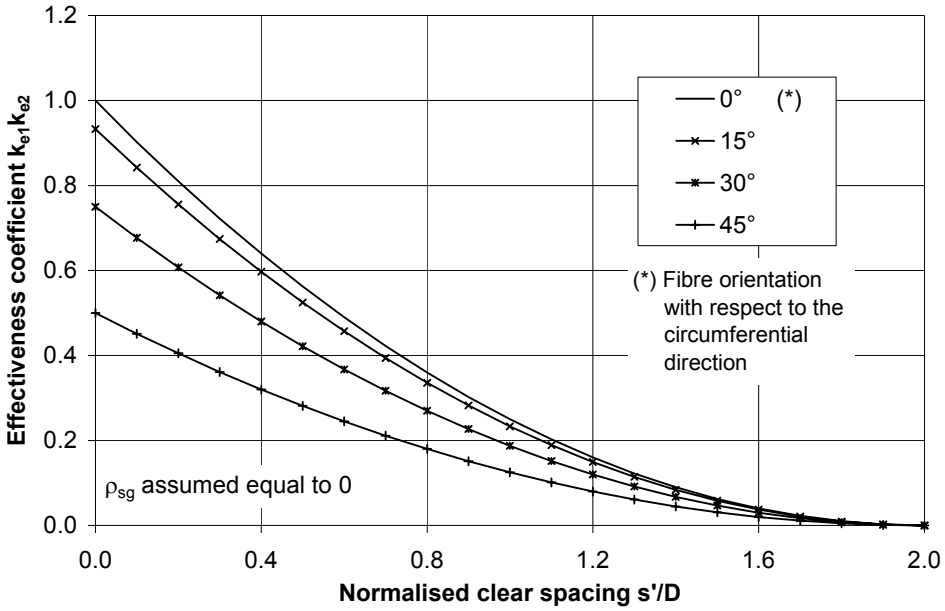

Fig. 7-34 *Influence of partial wrapping and fibre orientation on confinement effectiveness*

$$\rho_{fx} = \frac{2b_f t}{s\,d} \quad \text{and} \quad \rho_{fy} = \frac{2b_f t}{s\,b} \tag{7-103}$$

The confinement effectiveness coefficient $k_e = k_{e1}k_{e2}k_{e3} \leq 1$, takes into account partial wrapping (k_{e1}) and fibre orientation (k_{e2}) according to Eq. (7-100), while the influence of the shape of the cross-section (k_{e3}) is given by:

$$k_{e3} = 1 - \frac{b'^2 + d'^2}{3A_g\left(1-\rho_{sg}\right)} \tag{7-104}$$

with, $b' \geq d'$ the clear distance between the rounded corners (Fig. 7-35). Assuming a constant gross cross-sectional area A_g, Fig. 7-36 shows the influence of the column shape and the radius r_c at which the corners are rounded. Hereby, r_c is normalised with respect to the maximum radius R, corresponding to a circular cross-section. Assuming that the corners of square or rectangular cross-sections can be rounded up to about 20 mm and depending on the column size, the magnitude of r_c/R will be about 0.1. From Fig. 7-36 it is noted that in this case the effectiveness of the wrapping is extremely low. Hence, before wrapping square or rectangular columns, if possible they should be reshaped to obtain a more circular cross-section.

5.2.4 Anchorage and bond quality

It should be assured that the FRP wrapping is properly anchored, so that no anchorage failure is obtained in the ultimate limit state. For circular wrapping, this means that sufficient overlap length should be provided. In the case of continuous wrapping (spiral wrapping), a circular wrapping at the column ends can be provided as anchorage. The minimum overlap length ℓ needed to anchor the FRP is based on experimental evidence. According to lap shear tests [54] (Fig. 7-37), the overlap length is derived as:

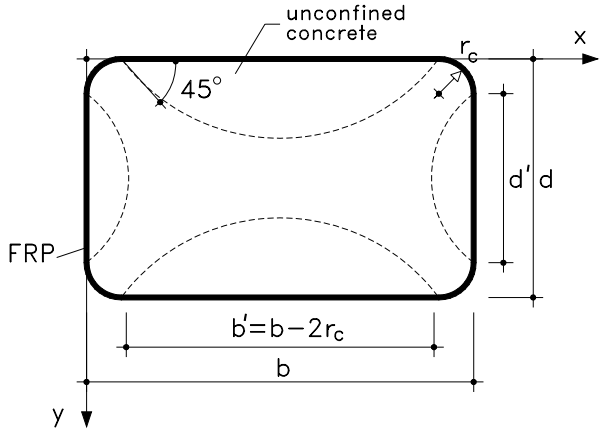

Fig. 7-35 *Wrapping of square or rectangular cross-sections*

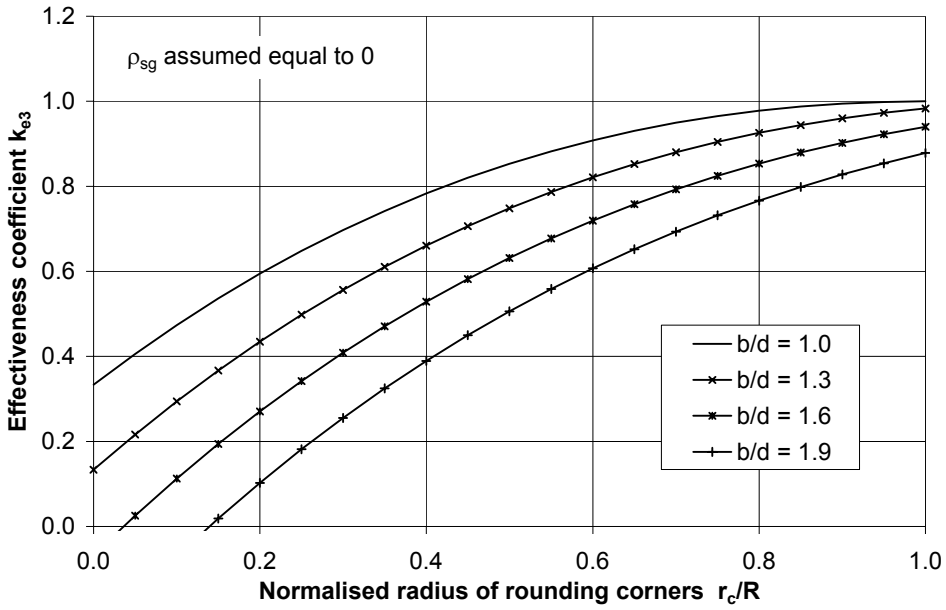

Fig. 7-36 *Influence of columns shape on confinement effectiveness*

$$\ell \geq \frac{f_{fd}\, t}{\tau_{ad}} \tag{7-105}$$

where, τ_{ad} is the design value of the mean shear strength obtained through lap shear tests and which depends on the strength characteristics of the adhesive, the provided overlap length and the characteristics of the FRP. Because of the high shear and adhesion strength of the adhesives, the overlap length is generally rather small (order of magnitude about 100 mm).

If sufficient overlap length is provided, the circular wrapping forms a closed shape and the FRP EBR will act irrespective of the quality of the bond between the FRP and the concrete. However, based on this aspect, it may not be concluded that the bond quality is of minor concern. Indeed, from the conducted experiments in Chapter 6, Section 3.1, it appeared that unbonded FRP wrappings may be less efficient to some extent (the concrete needs more lateral expansion before the FRP acts efficiently). Also, it was demonstrated that the quality

of the execution is of importance (if fibres are not aligned in an optimum way due to protrusions or voids, the FRP wrapping will be less effective).

With respect to the bond quality, it should also be kept in mind that fully wrapped columns do not allow moisture exchange between the concrete and the environment in a normal way. As a result, trapped moisture may adversely affect the bond quality and hence the effectiveness of the FRP confinement.

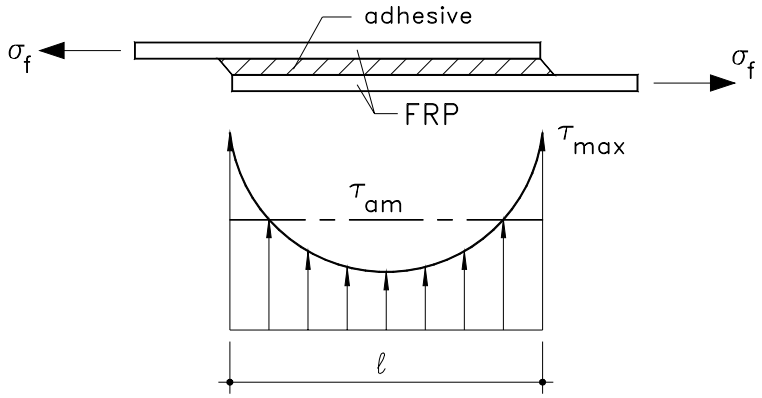

Fig. 7-37 *Overlap length of a single FRP joint*

5.3 SLS verification

As the FRP confinement is only activated in a significant way for loads above the strength of the unconfined concrete (that is when the concrete deformations increase to a large extent), FRP stresses under service conditions are very low and the behaviour of the axially loaded confined columns under service conditions is similar to that of unconfined columns. Hence, stress limitations with respect to excessive creep or creep rupture of the FRP are of no concern in the case of passive confinement (meaning that the FRP is not prestressed). For further information on the SLS verifications of unconfined columns, reference is made to [11].

5.4 Summary of the design process

The design process for the dimensioning of the FRP wrapping reinforcement can be summarized as:

- Given the acting design load, the design value of the confined concrete compressive strength, which is to be provided by the FRP wrapping, can be obtained (Section 5.2.1).
- Assume a value for the effective FRP strength of the confining reinforcement and calculate the ultimate lateral confining pressure which is needed (Section 5.2.2). Determine the amount of FRP wrapping reinforcement (taking into account the shape of the column cross-section and the wrapping configuration which will be used) (Section 5.2.3). Update the value for the effective FRP strength of the confining reinforcement and recalculate until convergence is obtained.

- Specify a minimum overlap length, to assure that the FRP wrapping is properly anchored (Section 5.2.4).
- Verify that the concrete and longitudinal steel reinforcement stresses in the SLS do not exceed the maximum allowable stresses. SLS stress limitations for the (passive) FRP confining reinforcement are of no concern (Section 5.3).

6 Strengthened tensile members

6.1 General

Given the high tensile strength of FRP, strengthening of RC tensile members by means of externally bonded FRP reinforcement is an efficient technique, especially if premature anchorage failure can be avoided or delayed. Referring to Chapter 5, also the positive influence of the FRP EBR on the serviceability behaviour of tensile members has been demonstrated.

6.2 ULS verification

From the equilibrium of forces in the cracked section, the resisting tensile force in ULS is obtained as:

$$N_{Rd} = A_s f_{yd} + A_f f_{fd,eff} \tag{7-106}$$

where, $f_{fd,eff} = E_f \varepsilon_{f,eff} / \gamma_f \leq f_{fd}$ is the effective design strength of the FRP. In case the FRP is properly anchored, premature anchorage failure is prevented, so that the design strength equals f_{fd}. At the contrary, in case no extra end anchorage is provided, a bond failure between the FRP and the concrete may be expected before reaching the full tensile capacity of the FRP. The strain $\varepsilon_{f,eff}$ at which this anchorage failure occurs, is evaluated from the maximum anchorage force given by Eq. (7-24). To assure yielding of the internal steel and hence a ductile behaviour, the FRP strain at failure should be larger than $\varepsilon_{f,min}$ given in Table 7-1. Local debonding at cracks, which will occur for high load levels and which will happen in a non-homogenous way, may reduce the effective strength of the FRP in the ULS (even if the FRP is anchored at its ends). This aspect can be considered by means of a proper effective FRP failure strain $\varepsilon_{f,eff}$, based on experimental evidence.

To prevent brittle failure at first cracking, even in the absence of the FRP EBR (accidental situation), sufficient steel reinforcement should be available. Assuming $N_{cr} \approx f_{ct} A_g$, this condition yields:

$$\rho_{sg} \geq f_{ct} / f_{yd} \tag{7-107}$$

where, f_{ct} should be taken equal to $f_{ctk0.95} = 0.39 f_{ck}^{2/3}$ [14] to maximize safety.

6.3 SLS verification

6.3.1 Stress limitation

At service load conditions, it should be prevented that the internal steel is yielding or $\sigma_s \leq 0.8f_{yk}$ under the quasi-permanent load combination [11]. With the stress in the steel reinforcement obtained from the equilibrium of forces, this yields:

$$\sigma_s = \frac{N_k}{A_s + \frac{E_f}{E_s}A_f} \leq 0.8f_{yk} \tag{7-108}$$

6.3.2 Verification of deformations

The mean deformation of the strengthened tensile member, taking into account tension stiffening, can be verified according to:

$$\varepsilon_m = (1-\zeta)\varepsilon_1 + \zeta\varepsilon_2 \tag{7-109}$$

with, ε_1 and ε_2 the deformations in respectively the uncracked and the cracked state and ζ the tension stiffening coefficient:

$$\begin{aligned} &\zeta = 0 && N_k < N_{cr} \\ &\zeta = 1-\beta_1\beta_2\left(\frac{N_{cr}}{N_k}\right)^n && N_k > N_{cr} \end{aligned} \tag{7-110}$$

where a good agreement between experimental and analytical results is reported in Chapter 5 if the coefficients β_1 and β_2 are taken according to EC2 [11] and if the power n equals 2 in the case of NSC [35] and 3 in case of HSC [41]. The strains ε_1 and ε_2 are given by:

$$\varepsilon_1 = N_k/(E_cA_c + E_sA_s + E_fA_f) \tag{7-111}$$

$$\varepsilon_2 = N_k/(E_sA_s + E_fA_f) \qquad \varepsilon_2 \leq \varepsilon_y \tag{7-112}$$

where, Eq. (7-112) only applies before yielding of the internal steel (which is the case for service conditions).

6.3.3 Verification of crack widths and bond interface cracking

Similar to Section 3.5.4 and assuming stabilized cracking, the characteristic value of the crack width is given by Eq. (7-53). Hereby, the mean crack spacing is obtained from Eq. (7-56), with $f_{ctm}A_{c,eff}$ replaced by N_{cr}.

As demonstrated in Section 3.5.5, no bond interface cracking is expected under service load conditions if the crack widths are restricted.

7 Special design considerations

7.1 General

Depending on the use of the strengthened structure and the environmental conditions, specific aspects with respect to the FRP EBR may apply and call for additional design verifications. These special design considerations (e.g. fire resistance, environmental durability, cyclic loading, long-term loading, impact, etc.) are often of a considerable importance to guarantee the structural safety of the strengthened structure. Hereby, it is of concern to evaluate the behaviour of the strengthened member rather than the FRP itself.

In the following, a number of special design verifications are briefly discussed.

7.2 Influence of environmental conditions

7.2.1 Temperature effects and freeze-thaw action

The temperature range at which concrete structures are normally subjected to, may differ significantly. In central Europe, this range may equal up to about -40 °C ≤ T ≤ +60 °C. Within this temperature interval, the following issues can be addressed. The resistance against fire is discussed in Section 7.3.

7.2.1.1 Maximum service temperature

To avoid a significant decrease in the mechanical properties of the FRP EBR, it should be clear that the maximum service temperature is significantly lower than the glass transition temperature T_g (Chapter 2, Sections 4.3.2.4 and 4.5.1.1). Hence, adhesives or resins with a sufficiently high glass transition temperature should be selected. If no cold-cure resin with a proper T_g is available, post-cure heating may be foreseen to achieve a higher glass transition temperature.

7.2.1.2 Thermal stresses

Unlike steel reinforcement, the coefficient of thermal expansion of FRP differs from that of the concrete (e.g. $\alpha_{T,CFRP} \approx 0\ 10^{-6}/°C$ versus $\alpha_{T,concrete} \approx 12\ 10^{-6}/°C$). Hence, for strengthened RC beams subjected to a certain temperature change ΔT (after curing of the FRP EBR), thermal stresses are initiated in the FRP and the concrete, due to the restraining of the different thermal expansions of both materials. These stresses may become critical for high values of ΔT (especially for decreasing ΔT, in which case the FRP is subjected to compression and as the compressive strength of some FRP types is fairly low). As the stress (or force) in the FRP is to be anchored at the FRP ends, extra bond stresses are initiated as well and should be taken into account. Calculation of these stresses may be performed according to a classical thermal dilatation analysis as e.g. in [18]. From the data available in the literature, no significant problems have been reported, within the -25 °C ≤ T ≤ +20 °C range, for RC beams strengthened in flexure (see Chapter 2, Section 4.5.1.2).

7.2.1.3 Freeze-thaw action

The bond layer between the concrete and the FRP is not perfect, due to the presence of cracks, voids or other imperfections. Hence, the effect of freeze-thaw action on the bond interface (especially under wet conditions) may be of concern. From data available in the literature (see Chapter 2, Section 4.5.1.2), it appears that the freeze-thaw resistance of elements strengthened with FRP EBR is mainly related to the freeze-thaw resistance of the concrete.

7.2.2 Moisture

The main concern with respect to moisture is the resistance of the FRP EBR system against prolonged exposure to fresh or salt water as well as the influence of trapped moisture on the bond behaviour. As indicated in Chapter 2, Section 4.5.1.3, resins and adhesives with sufficiently low moisture absorption should be used (maximum absorption of 3 % by weight). For outdoor exposure (FRP subjected to weathering), the use of CFRP is recommended.

After application of the FRP EBR, especially in the case of a wet-lay up system which may cover a large area of the concrete surface, moisture can accumulate at the bond interface as a result of entrapment, infiltration and diffusion of water. To prevent this water accumulation and hence possible damage of the bond interface, it may be needed to allow the strengthened structure to 'breathe'. This can be achieved by the use of water vapour permeable resin systems or by means of partial application of the FRP EBR to the concrete surface (e.g. leaving a gap of 50 mm every 300 mm FRP width). In the case of the first solution, the durability under harsh environmental conditions may be less obvious. These vapour permeable resins should for example not be used for GFRP, given the low resistance of glass fibres against an alkaline environment.

7.2.3 Chemical resistance

As discussed in Chapter 2, Section 4.5.1.4, the influence of the alkaline environment of the concrete is of little concern for externally bonded FRP reinforcement. Moreover, FRP materials often have a high chemical resistance (especially CFRP), although specific problems may occur.

7.2.4 UV light exposure

Often externally bonded FRP reinforcement is exposed to direct or indirect sunlight and hence to ultraviolet radiation. As demonstrated in Chapter 2, Section 4.5.1.5, degradation due to UV light is of concern. Hence, for most FRP strengthening systems it will be required to apply special UV resistant paintings. With respect to the thermal effects discussed in Section 7.2.1, preferably light colored paint (which reflects heat) will be used.

7.2.5 Lightning

In most applications, the FRP EBR is not exposed to lightning strikes as they are inside buildings, on the soffits of beams or in a box girder (which acts as a grounded cage). Nevertheless, in the case of for example wrapped outdoor columns, lightning may have to be considered as a potential risk of damage.

Provided that the structure is grounded, direct lightening strikes on GFRP and AFRP, which are insulators, can cause only local damage such as burning. At the other hand and although relative resistive to electricity, more problems may be expected in the case of CFRP, which is a conductor. As a result of a lightning strike, the CFRP will be heated over a large area and to a large extent, so that the resin vaporises and structural integrity is affected (even after the carbon fibres cooled down) [56]. In situations where lightening may be of danger, aluminium grids (which are used for this reason in aircraft design) can be used in the outermost layer to protect the composite.

7.3 Fire protection

Generally, concrete members strengthened with FRP EBR may be subjected to fire. Hence, the resistance against fire is an often raised question with respect to the use of FRP EBR. In [57] a survey is given on the limited data available on this subject. Fire tests on loaded large scale RC beams strengthened with CFRP EBR have been conducted at EMPA [56]. Comparing steel and FRP strengthened beams without protection, the latter will behave better because of the low thermal conductivity and low weight of the FRP materials. Nevertheless, the fire resistance often remains limited as the resins have low thermal stability at elevated temperature, resulting finally in a total loss of bond. A sufficiently large fire resistance may be obtained in the case the fire is local and the FRP anchorage zones remain fairly intact.

With respect to fire resistance, the design may be based on an accidental situation verification. Herewith, the FRP EBR only serves as secondary reinforcement, so that in case of loss of the FRP still a residual factor of safety remains. In other cases, insulation will have to be applied to achieve sufficient fire resistance of the strengthened member. The dimensioning of the protection will be based on a limitation of the temperature in the adhesive layer (weakest element of the cross-section) during a certain time. This temperature limit is mainly related to the glass transition temperature of the adhesive. The analysis will consist of a thermal analysis to determine temperature distributions in the element, followed by a mechanical analysis with temperature-dependent material properties [57].

7.4 Long-term loading

When submitted to a constant load, the FRP strengthened concrete member will exhibit some degree of creep deformations. This creep may even lead to a delayed fracture, so-called creep or stress rupture. Due to the viscoelastic behaviour of polymer adhesives, also the shear creep in the bond interface is of special concern.

From conducted studies as reported in e.g. [55,58], it appears that CFRP exhibits negligible creep, while the creep of GFRP is rather small and that of AFRP is significantly larger. Furthermore, the fact that unstrengthened and CFRP or GFRP strengthened beams experience similar proportional creep, suggests that the sustained load behaviour of strengthened beams is mainly governed by the compressive creep of the concrete and not by time-dependent effects of the adhesive. Indeed, at application of the externally bonded FRP reinforcement, the structure is still submitted to the mayor part of its dead load. As a result, sustained stresses in the bond interface are generally very low. As AFRP creeps itself, long-term deformations of AFRP strengthened elements will be higher. Nevertheless, as strengthening is mostly applied on aged concrete structures (most concrete creep deformations already occurred) and as the sustained FRP load level is generally low, creep is seldom a controlling factor for the dimensioning of the FRP EBR system.

Besides the creep deformations, also the stress level is of importance as FRP creep rupture failure may occur at a stress level below the FRP short-term strength. Generally, CFRP can withstand stress levels up to 80 % of its short term strength, while considerably lower stress levels apply for AFRP and GFRP [39,40]. The permissible stress level can strongly depend on the fibre/resin system, the alignment of the fibres and the fibre volume fraction. The design with respect to this issue is based on a FRP stress limitation in the SLS, as explained in e.g. Section 3.5.2. As the FRP stress level at service load is often fairly low, creep rupture is mostly not governing.

Another important aspect related to sustained loading is the environmental influence, sometimes referred to as stress corrosion. Indeed, the effects described under Section 7.2.1 till 7.2.4 are strongly affected if combined with mechanical action. Whereas, CFRP is generally very inert to combined environmental/mechanical action, AFRP and GFRP are more susceptible. Given these considerations, it is recommended to use CFRP and a suitable formulated adhesive in case the EBR has to carry a considerable sustained load under rather harsh environmental conditions.

7.5 Cyclic loading

Advanced unidirectional composites, such as CFRP, exhibit superior performance under cyclic loading compared to that of steel, as demonstrated from for example the cyclic loading tests reported in [18,20]. These tests, conducted at 4 Hz on RC beams strengthened with HFRP (hybrid glass/carbon) and CFRP, show that the dominant factor in the fatigue of FRP strengthened beams is the fatigue of the existing steel reinforcement. For part of the tests the loading conditions were taken unrealistically high, to gain also insight into the FRP failure mechanism after complete failure of the steel reinforcement. It was observed that the FRP EBR could withstand some further cyclic loading, whereas final FRP failure was related to the large crack widths which resulted in debonding or damage due to the sharp concrete edges. Also, cyclic loading under harsh environment (40 °C/95 % R.H.) gave no indication of severe strain fatigue in the joint between the CFRP and the concrete. From cyclic loading tests on RC beams strengthened with CFRP fabric reported in [59], it was concluded that the fatigue life

of the tested strengthened specimens was 600 % (2 layers CFRP) and 1000 % (3 layers CFRP) higher than that of the bare specimens. Also the fatigue life of a previously fatigued specimen (before strengthening subjected to cyclic loading for about half of the fatigue life of the bare specimen) could be considerably increased.

Given the excellent resistance of FRP materials [55], the design for cyclic loading will be related to a limitation of the stress range in the internal rebars, similar as for unstrengthened beams.

7.6 Impact and vandalism

Although having high axial tensile strength, FRP materials have generally low transverse strength. Hence, vandalism and direct impact loads on the FRP EBR may lead to significant damage (e.g. with a sharp knife the FRP can be considerably damaged in a relative easy way). If this damage occurs at critical locations such as the anchorage zone or the maximum moment region, the integrity of the FRP strengthening can no longer be guaranteed. For the design this implies that the accidental situation (Section 2.2.2) should be fulfilled, so that in case of loss of the FRP still a residual factor of safety remains. Alternatively, protective measures can be applied.

Also of interest is the impact resistance of FRP strengthened concrete members, whereas the FRP EBR is not directly hit. With regard to this aspect very limited information is available. In a recent study [60], the impact resistance of 2 steel and 2 CFRP strengthened RC beams was compared. In the performed tests, the impact load was induced by lifting one beam end and dropping it from given heights. It was concluded by the authors of the study, that the RC beams strengthened in flexure with CFRP performed well under impact loading, although they could not provide the same energy absorption as the beams strengthened with steel plates. Furthermore, they recommend the use of additional anchoring (at least at the ends of the CFRP EBR) to prevent premature debonding of the CFRP under impact loading.

8 References

1. ACI (1999), “FRP Around the World”, Concrete International, American Concrete Institute, October 1999, Vol. 21, No. 10, 76 pp.
2. JCI (1997), “State-of-the-Art Report on Retrofitting and Strengthening by Continuous Fibre”, Keynote lectures, Proceedings 3rd. Int. Symp. on Non-Metallic (FRP) Reinforcement for Concrete Structures, Japan Concrete Institute, Tokyo, Japan, pp. 3-58.
3. fib (2000), “FRP Reinforcement for Concrete Structures”, fib Task Group 9.3, International Federation for Structural Concrete, http://allserv.rug.ac.be/~smatthys/fibTG9.3
4. ACI (1996), “State-of-the-art report on fiber reinforced plastic reinforcement for concrete structures”, ACI Committee 440, American Concrete Institute, USA, 153 pp.
5. NIST (1999), “NIST Workshop on Standards Development for the Use of Fibre Reinforced Polymers for the Rehabilitation of Concrete and Masonry Structures”,

Proceedings, United States Department of Commerce Technology Administration, National Institute of Standards and Technology, Tucson, Arizona, USA, 149 pp.
6. Matthys S. (1997), "Versterking van structurele betonelementen met opgelijmde vezelcomposietlaminaten" (in Dutch), Infrastructuur in het Leefmilieu, Departement Leefmilieu en Infrastructuur, Ministerie van de Vlaamse Gemeenschap, Brussels, Belgium, No. 4/97, pp. 274-298.
7. Matthys S. (1998), "Vezelcomposietlaminaten: Uitwendige versterking van constructieve betonelementen" (in Dutch), Cement, Vol. 50, No. 2, pp. 50-58.
8. Matthys S. (1997), "Versterking van structurele betonelementen met opgelijmde vezelcomposietlaminaten" (in Dutch), Proceedings Workshop on 'Versterking van constructies met gekleefde composietlaminaten', Belgian Concrete Society, Brussels, Belgium, 37 pp.
9. Taerwe L., Matthys S. (1999), "Some aspects of the structural behaviour of RC beams strengthened with FRP", in 'Construction Materials - Theory and Applications', Commemorative volume in honour of Prof. Reinhardt, ibidem-Verlag, Stuttgart, Germany, pp. 563-572.
10. S. Matthys, L. Taerwe, H. Blontrock (2000), "Strengthening of Concrete Structures with Externally Bonded FRP Reinforcement", Proceedings 3th. Int. Conf. on Advanced Composite Materials in Bridges and Structures, Eds. J. Humar, A.G. Razaqpur, The Canadian Society of Civil Engineers, Montréal, Canada, pp. 497-504.
11. CEN (1991), "Eurocode 2: Design of concrete structures – Part 1-1: General rules and rules for buildings", ENV 1992-1-1, Comité Européen de Normalisation (CEN), Brussels, Belgium, 263 pp.
12. CEN (1994), "Eurocode 1: Basis of design and actions on structures – Part 1: Basis of design", ENV 1991-1, Comité Européen de Normalisation (CEN), Brussels, Belgium, 85 pp.
13. CEN (1996), "Aeronautical- Plastics reinforced with carbon fibres – Unidirectional laminates – Tensile test parallel to the fibre direction", EN 2561, Comité Européen de Normalisation (CEN), Brussels, Belgium.
14. CEN (1997), "Plastics, determination of tensile properties (UD laminate)", EN ISO 527:5, Comité Européen de Normalisation (CEN), Brussels, Belgium.
15. JSCE (1997), "Recommendation for design and construction of concrete structures using continuous fibre reinforcing materials", Ed. A. Machida, Concrete Engineering Series 23, Japan Society of Civil Engineers, Tokyo, Japan, 325 pp.
16. Lambotte H., Van Nieuwenburg D. (1991), "Gewapend beton" (in Dutch), Ghent University, Faculty of Applied Sciences, Magnel Laboratory for Concrete Research, 546 pp.
17. Jones R., Swamy R.N., Charif A. (1988), "Plate seperation and anchorage of reinforced concrete beams strengthened by epoxy-bonded steel plates", The Structural Engineer, Vol. 66, No. 5/1, March 1988, pp. 85-94.

18. Kaiser H. (1989), "Bewehren von Stahlbeton mit kohlenstoffaserverstärkten Epoxidharzen" (in German), Doctoral thesis, Technical University of Zürich, Switzerland, 224 pp.
19. Roberts T.M. (1989), "Approximate analysis of shear and normal stress concentrations in the adhesive layer of plated RC beams", The Structural Engineer, Vol. 67, No. 12/20, June 1989, pp.229-233.
20. Deuring M. (1993), "Verstärken von Stahlbeton mit gespannten Faserverbund-werkstoffen" (in German), EMPA Bericht, No 224, Swiss Federal Laboratories for Materials Testing and Research, Dübendorf, Switzerland, 279 pp.
21. Täljsten B. (1994), "Plate Bonding – Strengthening of Existing Concrete Structures with Epoxy Bonded Plates of Steel or Fibre Reinforced Plastics", Doctoral thesis, Luleå University of Technology, Sweden, 281 pp.
22. Pichler D., Wicke M. (1994), "Verstärken von Betonbauteilen durch angeklebte Stahllamellen mit angepreβter Endverankerung" (in German), Beton- und Stahlbetonbau 89 (1994), No. 10 and 11, pp. 261-265 and 312-314.
23. Holzenkämpfer P. (1994), "Ingenieurmodelle des Verbunds geklebter Bewehrung für Betonbauteile" (in German), Doctoral thesis, Vol. 108, , Technical University Braunschweig, Germany, 214 pp.
24. Hankers Ch. (1995), "Zum Verbundsverhalten laschenverstärkter Betonbauteille unter nicht vorwiegend ruhender Beanspruchung" (in German), Doctoral thesis, Technical University Braunschweig, Germany, 202 pp.
25. Chajes M.J., Finch W.W., Januszka T.F., Thomson T.A. (1996), "Bond and Force Transfer of Composite Material Plates Bonded to Concrete", ACI Structural Journal, Vol. 93, No. 2, pp. 208-217.
26. Malek A.M., Saadatmanesh H., Ehsani M.R. (1996), "Shear and Normal Stress Concentrations in RC Beams Strengthened with FRP Plates", Proceedings 2nd. Int. Conf. on Advanced Composite Materials in Bridges and Structures, Montréal, Québec, Canada, pp. 629-637.
27. Varastehpour H., Hamelin P. (1996), "Analysis and Study of Failure Mechanism of RC Beam Strengthened with FRP Plate", Proceedings 2nd. Int. Conf on Advanced Composite Materials in Bridges and Structures, Montréal, Québec, Canada, pp. 527-536.
28. Rostásy F.S., Holzenkämpfer P., Hankers Ch. (1996), "Geklebte Bewehrung für die Verstärkung von Betonbauteilen" (in German), Betonkalender 1996, Vol. II, pp. 547-576.
29. Raoof M., Zhang S. (1996), "Analysis of Plate Peeling Failure of RC Beams with Externally Bonded Plates", in Concrete Repair, Rehabilitation and Protection, Eds. R.K. Dhir, M.R. Jones, E&FN Spon, pp. 605-614.
30. Jansze W. (1997), "Strengthening of Reinforced Concrete Members in Bending by Externally Bonded Steel Plates – Design for Beam Shear and Plate Anchorage", Doctoral Thesis, Delft University of Technology, The Netherlands, pp. 205.
31. Rostásy F.S., Neubauer U., Hankers Ch. (1997), "Verstärken von Betontragwerken met geklebter äuβeren Bewehrung aus kohlenstoffaserversträrken Kunststoffen" (in German), Beton- und Stahlbetonbau 92 (1997), No. 5., pp. 132-138.

32. Blaschko M., Niedermeier R., Zilch K. (1998), "Bond Failure Modes of Flexural Members Strengthened with FRP", Proceedings 2nd. Int. Conf. On Composites in Infrastructure, Tucson, USA, 15 pp.
33. Neubauer U., Rostásy F.S. (1999), "Bond Failure of Concrete Fibre Reinforced Polymer at Inclined Cracks – Experiments and Fracture Mechanics Model", Proceedings 4th. Int. Symp. on Fibre Reinforced Polymer Reinforcement for Reinforced Concrete Structures, Eds. C.W. Dolan, S.H. Rizkalla, A. Nanni, American Concrete Institute, Mitchigan, USA, pp. 369-382.
34. Brosens K., Van Gemert D. (1999), "Anchorage Design for Externally Bonded Carbon Fibre Reinforced Polymer Laminates", Proceedings 4th. Int. Symp. on Fibre Reinforced Polymer Reinforcement for Reinforced Concrete Structures, Eds. C.W. Dolan, S.H. Rizkalla, A. Nanni, American Concrete Institute, Mitchigan, USA, pp. 635-646.
35. CEB (1993), "CEB-FIP Model Code 1990, Design Code", Comité Euro-International du Béton, Lausanne, Switzerland, Thomas Telford, 437 pp.
36. Matthys S., Blontrock H. (2000), "Experimenteel onderzoek op een versterkingssysteem met vezelcomposietmaterialen" (in Dutch), Bouwkroniek, 7 April 2000, pp. 26-30.
37. Matthys S., Blontrock H. (2000), "Experimenteel onderzoek op een versterkingssysteem met vezelcomposietmaterialen" (in Dutch), Proceedings Workshop on 'Toepassing Composieten in Bouw en Renovatie', Flanders Congress & Concert Centre Antwerpen, Antwerp, Belgium, 10 pp.
38. Taerwe L. (1997), "Waarschijnlijkheidsrekening en statistiek" (in Dutch), Ghent University, Faculty of Applied Sciences, Magnel Laboratory for Concrete Research, 352 pp.
39. Rostásy F.S., Ed. (1992), "Evaluation of potentials and production technologies of FRP", BRITE Project 4142/BREU-CT 91 0515, Report No. BREU 1-92, 95 pp.
40. Yamaguchi T., Nishimura T., Uomoto T. (1998), "Creep Model of FRP Rods Based on Fibre Damaging Rate", Proceedings 1st. Int. Conf. On Durability of Fibre Reinforced Polymer (FRP) Composites for Construction, Eds. B. Benmokrane, H. Rahman, Sherbrooke, Canada, pp. 427-437.
41. Lambotte H., Taerwe L. (1990), "Deflection and Cracking of High-Strength Concrete Beams and Slabs", Proceedings of the High-Strength Concrete Second International Symposium, Ed. W.T. Hester, ACI SP-121, American Concrete Institute, Detroit, U.S.A, pp. 109-128.
42. CEB (1985), "CEB-Manual Cracking and Deformations", CEB Bulletin d'Information No. 158-E, Comité Euro-International du Béton, Lausanne, Switzerland, 248 pp.
43. Triantafillou T.C. (1997), "Shear strengthening of concrete members using composites", Proceedings 3rd. Int. Symp. on Non-Metallic (FRP) Reinforcement for Concrete Structures, Japan Concrete Institute, Sapporo, Japan, Vol. 1, pp. 523-530.
44. Kamiharako A., Maruyama K., Takada K., Shimomura T., (1997), "Evaluation of shear contribution of FRP sheets attached to concrete beams", Proceedings 3rd. Int. Symp. on Non-Metallic (FRP) Reinforcement for Concrete Structures, Japan Concrete Institute, Sapporo, Japan, Vol. 1, pp. 467-474.

45. Umezu K., Fujita M., Nakai H., Tamaki, K. (1997), "Shear behaviour of RC beams with aramid fibre sheet", Proceedings 3rd. Int. Symp. on Non-Metallic (FRP) Reinforcement for Concrete Structures, Japan Concrete Institute, Sapporo, Japan, Vol. 1, pp. 491-498.
46. Triantafillou T. C. (1998), "Shear strengthening of reinforced concrete beams using epoxy-bonded FRP composites", ACI Structural Journal, 95(2), March-April, pp. 107-115.
47. Khalifa A., Gold W. J., Nanni A. and Aziz A. M. I. (1998), "Contribution of externally bonded FRP to shear capacity of rc flexural members", ASCE Journal of Composites for Construction, 2(4), pp. 195-202.
48. Hutchinson R.L., Rizkalla S.H. (1999), "Shear strengthening of AASHTO Bridge Girders Using Carbon Fibre Reinforced Polymer Sheets", Proceedings 4th. Int. Symp. on Fibre Reinforced Polymer Reinforcement for Reinforced Concrete Structures, Eds. C.W. Dolan, S.H. Rizkalla, A. Nanni, American Concrete Institute, Mitchigan, USA, pp. 945-958.
49. Kamiharako A., Maruyama K., Shimomura T. (1999), "Evaluation system of shear capacity of reinforced concrete members retrofitted with carbon fibre reinforced polymer sheets in consideration of bond-peeling characteristics", Proceedings 4th. Int. Symp. on Fibre Reinforced Polymer Reinforcement for Reinforced Concrete Structures, Eds. C.W. Dolan, S.H. Rizkalla, A. Nanni, American Concrete Institute, Mitchigan, USA, pp. 973-983.
50. BIN (1995), "Eurocode 2: Berekening van betonconstructies – Deel 1-1: Algemene regels en regels voor gebouwen [Eurocode 2: Design of concrete structures – Part 1-1: General rules and rules for buildings]", ENV 1992-1-1 and National Application Document, Belgisch instituut voor normalisatie (BIN), Brussels, Belgium, 263 pp.
51. Spoelstra M.R., Monti G. (1999), "FRP-Confined Concrete Model", ASCE, Journal of Composites for Construction, Vol. 3, No. 3, pp. 143-150.
52. Mander J.B., Priestley M.J.N., Park R. (1988), "Theoretical stress-strain model for confined concrete", Journal of Structural Engineering, ASCE, Vol. 114(8), pp. 1804-1826.
53. Restrepol J.L., De Vino B. (1996), "Enhancement of the axial load carrying capacity of reinforced concrete columns by means of fibreglass-epoxy jackets", Proceedings 2nd. Int. Conf. on Advanced Composite Materials in Bridges and Structures, Ed. M. El-Badry, The Canadian Society for Civil Engineering, Montréal, Québec, Canada, pp. 547-554.
54. CEN (1995), "Adhesives. Determination of tensile lap-shear strength of rigid-to-rigid bonded assemblies", EN 1465:1995, Comité Européen de Normalisation (CEN), Brussels, Belgium, 12 pp.
55. Hollaway L.C., Leeming M.B., Eds. (1999), "Strengthening of reinforced concrete structures using externally bonded FRP composites in structural and civil engineering", Woodhead Publishing, UK & CRC Press, USA, 327 pp.
56. Meier U. (1996), "Composites for structural repair and retrofitting", Proceedings 1st. Int. Conf. on Composites in Infrastructure, Tucson, Arizona, Eds. H. Saadatmanesh, M.R. Ehsani, University of Arizona, pp. 1202-1214.
57. Blontrock H., Taerwe L., Matthys S. (1999), "Properties of Fibre Reinforced Plastics at Elevated Temperatures with Regard to Fire Resistance of Reinforced Concrete Members",

Proceedings 4th. Int. Symp. on Fibre Reinforced Polymer Reinforcement for Reinforced Concrete Structures, Eds. C.W. Dolan, S.H. Rizkalla, A. Nanni, American Concrete Institute, Mitchigan, USA, pp. 43-54.
58. Plevris N. and Triantafillou T.C. (1994), "Time-dependent behaviour of RC members strengthened with FRP laminates", ASCE Journal of Structural Engineering, Vol. 120, No. 3, pp. 1016-1042.
59. Shahawy M., Beitelman T. (1998), "Fatigue Performance of RC Beams Strengthened with CFRP Laminates", Proceedings 1st. Int. Conf. on Durability of Fibre Reinforced Polymer (FRP) Composites for Construction, Eds. B. Benmokrane, H. Rahman, Sherbrooke, Canada, pp. 169-178.
60. Erki M.A., Meier U. (1999), "Impact loading of concrete beams externally strengthened with CFRP laminates", ASCE Journal of Composites for Construction, Vol. 3, No. 3, pp. 117-124.

Chapter 8
CONCLUSIONS AND OUTLOOK

In this last chapter the conclusions of the performed study are summarized and an outlook on the future use of externally bonded FRP reinforcement for the strengthening of structural elements is given. Suggestions with respect to future research are made.

1 General

In recent years, there is an increasing interest in FRP (fibre reinforced polymer) materials as high-performance non-metallic reinforcement for concrete structures. Used as externally bonded reinforcement (EBR) for strengthening of concrete structures, these FRP materials offer excellent durability, high structural performance and ease of application. Given the importance of repair and strengthening of concrete structures, the commercial and research interest in this novel strengthening technique is considerable. Although design guidelines are yet scarce, applications with respect to the FRP EBR technique are growing exponentially and the use of externally bonded FRP reinforcement is becoming well documented and a standard technique in a fast way.

As a result, in this field of application, the demand for (unified) design tools and guidelines is very large, especially as guidelines for steel plate bonding are scarce as well. Initiatives to develop design recommendations are currently taken by international committees and depend to a large extent on the research community who has to provide calculation models. To contribute in this respect, different research programmes have been performed in this study, concerning the structural behaviour of reinforced concrete members strengthened in flexure and shear, axially loaded confined columns and strengthened tensile members. Based on this research, the thesis provides design guidance concerning the main aspects of strengthening reinforced concrete structures with externally bonded FRP reinforcement. In developing these guidelines the Eurocode 2 design philosophy has been followed.

2 Conclusions

2.1 FRP materials and FRP EBR systems

The design and application of externally bonded reinforcement requires adequate knowledge of FRP reinforcement, FRP EBR systems and their characteristics. Typically, FRP reinforcement form a group of materials, with high performance characteristics, which strongly depend on the assembly of the constituent materials. In the case of externally bonded reinforcement, the FRP also has to act together with a properly formulated structural adhesive, so that they can be regarded as a system. Depending on the components and the application

technique, various FRP EBR systems are commercially available. In general these can be classified as 'prefab' or 'wet lay-up' types. The former refers to the application of pre-fabricated strips and laminates, while the latter involves the bonding and in-situ impregnation of sheets and fabrics. Using proper FRP EBR systems, it is also important that the practical execution takes place in a good way and that adequate quality control is provided.

In general, FRP EBR systems are very strong and durable. Nevertheless, when evaluating the properties of AFRP, CFRP and GFRP more into detail, clearly CFRP EBR systems will exhibit the best performance. This explains why externally bonded CFRP reinforcement is used for the majority of the practical applications and research, worldwide.

2.2 Structural behaviour of RC elements strengthened with FRP EBR

From the conducted experimental work, it follows that strengthening of existing concrete members by means of externally bonded FRP reinforcement is a feasible and efficient technique, which allows the enhancement of the flexural and shear capacity of RC beams as well as the load carrying capacity of axially loaded confined columns. Tests on strengthened RC beams and prisms, demonstrate that both the ultimate and serviceability limit state of strengthened beams and tensile members are positively influenced. Furthermore, it was found that also good results are obtained in case of strengthening of pre-cracked beams or of beams which are initially loaded (to a great extent) during strengthening. By increasing the strength of RC beams the ductility considerably decreases. Nevertheless, high strengthening factors are needed before the remaining ductility becomes unacceptably small. Shear failure of RC beams can be avoided if sufficient FRP shear strengthening is provided. Hereby, the strengthening configuration may considerably influence the effectiveness of the shear strengthening. Finally, from the tests on axially loaded cylinders and columns it appears that FRP wrapping is an efficient technique to confine the concrete and hence to increase both strength and ductility. These tests also demonstrate that the effectiveness is considerably influenced by partial wrapping, the shape of the cross-section and the fibre orientation. In case of a low ultimate confinement pressure, a negligible strength increase is found.

From the analytical verifications, it appears that the structural behaviour of the strengthened concrete members can be predicted in an accurate way. With this respect, calculation models for both the ultimate state and serviceability behaviour have been proposed and evaluated. For flexural strengthening of RC beams, classical calculation methods still apply as long as full composite action between the FRP and the concrete may be assumed. Possible loss of this composite action, forms a rather complex aspect of the calculation. To predict the crack width of RC beams strengthened in flexure, the influence of both the internal and external reinforcement, which have a different bond behaviour, should be taken into account. For shear strengthening of RC beams, again the classical methods apply. In this case, it is however important to accurately predict the effective FRP failure strain. Unlike the modelling of strengthened RC beams, classical calculation models were demonstrated to be no longer suitable in case of FRP confined concrete members. With this respect, an incremental-iterative model is proposed to predict the complete stress-strain behaviour of FRP confined concrete. This model gives accurate predictions. Alternatively, a

more practical engineering model for the maximum strength and ultimate state of FRP confined members is proposed as well. Also for this model good predictions are obtained.

2.3 Design guidelines for concrete structures strengthened with FRP EBR

Based on the experimental work, the analytical verifications and a literature review, guidelines are given on the main design aspect of reinforced concrete members strengthened in flexure and shear, axially loaded confined columns and strengthened tensile members. The guidelines focus on the basis of the design, the safety concept, the design models and procedures and some special design considerations.

Compared to new structures, the design of concrete members strengthened with externally bonded reinforcement is more complex. To assure structural safety, suggestions with respect to design failure modes, ductility and accidental situations have been formulated. Furthermore, it is demonstrated that the design of strengthened flexural members is often governed by the serviceability limit state and that special attention should go to the ultimate limit state verification of bond failure and the special design considerations (impact, fire, etc.).

To gain better insight in the design aspects, a parametric study concerning flexural strengthening has been conducted and a calculation programme has been developed.

3 Outlook on the use and development of the FRP EBR technique

3.1 The use of externally bonded FRP reinforcement wit respect to steel plate bonding

FRP EBR should not be regarded as a replacement for steel plate bonding, but rather as a specific alternative for it. Indeed, as FRP materials are expensive on the one hand and easy to apply on the other hand, their use is only economical for those projects were a substantial reduction in labour cost may be achieved or when the disruption (and related costs) can be minimized with this technique. Applications are also envisaged, where durability problems are expected when using steel plates. Furthermore, because of the flexibility and ease of application, the FRP EBR technique may be a solution for projects where steel plate bonding is technically not feasible.

In those applications where the above aspects are of no concern, steel plate bonding is likely to remain more cost-effective. This is especially the case if mainly an increase of the stiffness is needed (compared to most FRP elements steel plates are thicker and stiffer).

3.2 The use of externally bonded FRP reinforcement in practice

Based on social and economical necessities, maintenance, repair (retrofit) and strengthening (upgrading) of infrastructure is of great importance. Considerable investments in construction engineering are related to the repair sector and tend to increase over the years (due to ageing of structures and changes in the use of infrastructure). Hence, efficient and cost-effective techniques for the repair and strengthening are expected to gain importance. Moreover, as this trend is already ongoing today, it explains way hundreds of applications

with externally bonded FRP reinforcement are conducted worldwide, even in the absence of detailed design provisions.

Based on the positive experience of most projects conducted so far and on the various initiatives which are ongoing to develop design recommendations, it may be expected that the number of applications will further increase in a considerable way during the coming years (after which the number is expected to reach a more or less constant value).

3.3 New developments

Given the variety of possible FRP materials and FRP EBR systems, several new developments are likely to be introduced in the future. Some of these developments are already in an advanced stage of experimental testing.

On the materials side it may be expected that FRP EBR systems will be further optimized and will become even more tailor made with respect to the specific needs of a project. In this way, it is basically aimed to reduce labour costs further and to improve the quality and the applicability of the strengthening technique

- As for the basic technique the FRP EBR is applied by means of an ambient curing adhesive, in some countries the period over which construction is possible is limited. Development of systems which can cure under a broader range of conditions, which achieve a higher degree of curing or which allow a short curing time (to reduce construction time) are of special interest. This basically relates to new formulations for structural epoxy adhesives and the introduction of alternative adhesives such as polyurethanes.
- Although mostly CFRP is used so far, FRP EBR systems based on other types of fibres or the hybrid use of fibres will gain importance (for some of the envisaged applications the superior quality of the CFRP is not really needed).
- New types of application techniques may become available (curing with special heating systems, vacuum impregnation, etc.).
- Given, the increasing number of applications, it may be expected that also a wider range of products which are compatible as finishing layer (e.g. for fire protection) will become available.

Regarding the structural concept, some of the following developments are of considerable interest:

- As the maximum force which can be anchored through the bond interface is limited, often the FRP is to be provided in longer lengths (to reach zones with low moments) than needed. Moreover, in some situations, such as shear strengthening, insufficient anchorage length will be available. With this respect, the development and introduction of anchorage systems for FRP EBR are of interest, as well as FRP EBR types which can be anchored in a easier way. For example, a research project on FRP EBR types which can be bolted is ongoing at the Magnel Laboratory for Concrete Research.
- The field of application of FRP EBR may increase significantly if prestressed FRP EBR becomes practically possible. Research on this field is currently in an advanced stage and

systems to prestress and anchor the FRP are introduced. By means of prestressing, the serviceability aspects are more easily solved (for non-prestressed FRP EBR, the serviceability is often governing the design as a result of which higher amounts of FRP EBR are needed than for strength considerations).

- By means of externally bonded FRP reinforcement, a strengthening effect is achieved by simply adding additional tensile reinforcement. However, because of the equilibrium between the tensile and compression forces, the efficiency is strongly related to the concrete strength, the amount of steel reinforcement and the dimensions of the existing structure. It may for example appear that adding additional tensile reinforcement has such a low efficiency that very large (read uneconomically) amounts of FRP are needed. In this case it may be of interest, not only to provide additional tensile reinforcement, but also to increase the lever arm between the FRP reinforcement and the compression zone. In this case prefab light weight systems may be used which provide the FRP reinforcement onto the concrete structure by means of intermediate load transfer medium (e.g. wood). In Belgium, a company has developed such a system, which has been experimentally tested at the Magnel Laboratory for Concrete Research. This system has been applied for the first time in the spring of 2000 in a strengthening project in the zoological garden of Antwerp.

4 Continued research needed

Although in this thesis several design aspects have been dealt with, clearly not all aspects were covered and further research in this field is needed. This research should concentrate on the following aspects:

- Verification and optimization of models for the prediction of bond failure. Development of models for anchorage zones, when an additional mechanical anchorage is provided.
- More fundamental approaches to determine the effective FRP failure strain, e.g. for shear strengthening and confinement of columns
- Special design considerations such as torsion, impact and fire.
- Specific design aspects when using prestressed FRP EBR.
- Durability and efficiency of alternative structural adhesives and FRP EBR systems.
- The favourable or unfavourable effect of externally bonded FRP reinforcement to slow down certain durability problems (such as steel corrosion, alkali-silica reaction, etc.).
- The detailing of the FRP EBR. For example if the FRP EBR is provided on large areas, the construction will no longer ‘breath’ and moisture problems may occur.

Furthermore, co-ordinated research is urgently needed with respect to the development of detailed standard test procedures and methods to characterize the tensile properties and bond performance of externally bonded reinforcement.

Appendix A
PRACTICAL EXECUTION AND QUALITY CONTROL

1 General

Practical execution and quality control are very important for the integrity of FRP EBR strengthening systems. Indeed, to work efficiently the FRP EBR should be applied in an appropriate and qualified manner. Moreover, the application has to be related to quality control of the supplied materials, the application conditions, the practical execution process and the strengthening system after finishing.

In the following, reference is made to the practical execution and quality control of the basic technique (Chapter 2, Section 3.1.1). A schematic overview is given in Fig. A-1. Other techniques (Chapter 2, Section 3.1.2) resemble this basic technique in many ways. As various FRP EBR systems are commercially available, in any case reference is also made to the specifications by the manufacturer(s).

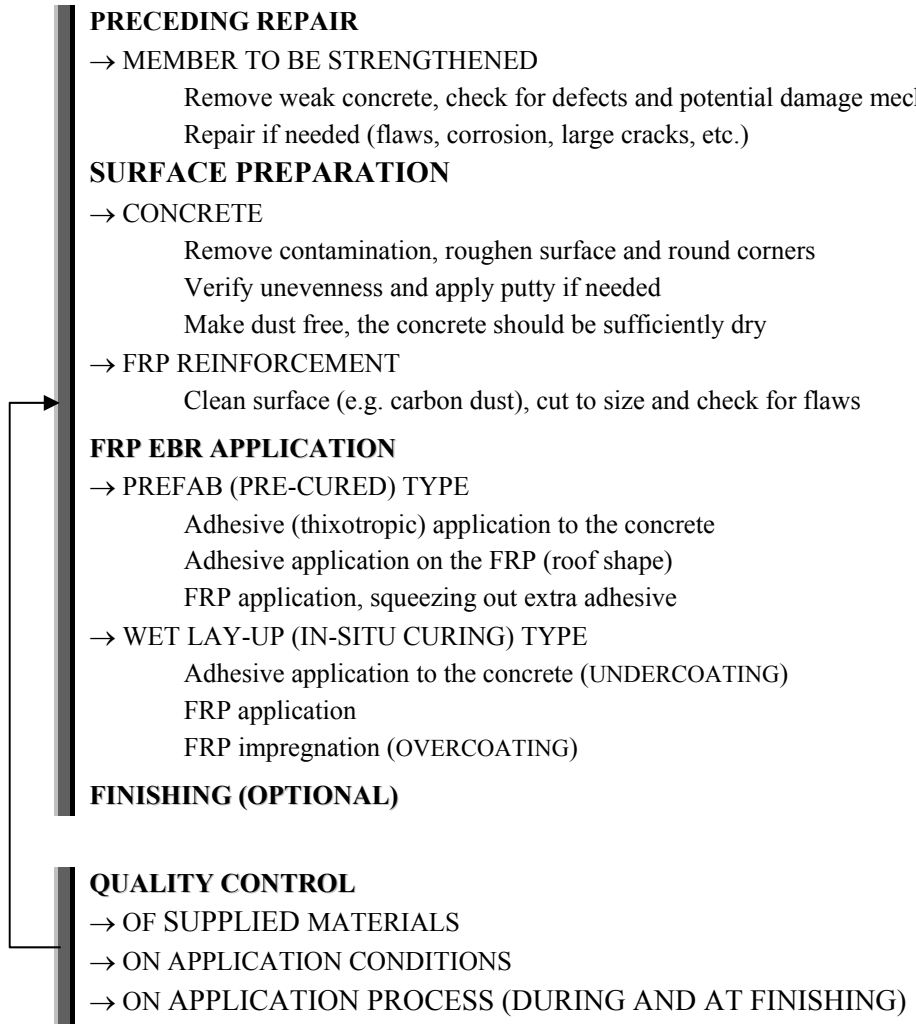

Fig. A-1 *Schematic overview of the practical execution and quality control*

2 Practical application

2.1 Preceding repair

The application of the FRP EBR system is generally not intended to confine or arrest defects, so that repair actions may be needed preceding the FRP EBR application. This repair work may include the following aspects.

- Repair of the concrete surface to restore concrete soundness. If the deteriorated or damaged concrete has reached a depth which no longer allows shallow surface repair, replacement of the concrete should be considered. Generally, it is required that the minimum concrete tensile strength is higher than 1.5 N/mm^2.
- Corrosion protection of the steel reinforcement, so that no expansive rust is formed. Although the external reinforcement may act as a (partial) replacement of the steel reinforcement, corrosion should be stopped to avoid damage to the concrete. Indeed, this damage may result in a decreased bond strength and an increased susceptibility to freeze-taw action. Protection is needed if the steel is already corroded or is likely to start corroding. For corrosion to occur, it is required that the carbonation depth has reached the reinforcement (no longer alkaline passivation of the steel) and that moisture and oxygen are present.
- Removal of chloride contamination, so that the risk of steel corrosion decreases. Generally, chloride concentrations larger than 0.3 % by weight of cement are assumed as dangerous.
- Sealing of wide cracks by means of injection, which is required to reduce the risk of reinforcing steel corrosion, to solve leakage problems, to avoid weak bond strength at horizontal cracks, etc. Often, crack widths larger than 0.2 mm are considered for sealing.
- Repair of porous concrete and joints to restore water retaining.

2.2 Surface preparation

2.2.1 Concrete

To ensure adequate bond and to allow the concrete quality to be used in an optimum way, the concrete substrate should be roughened and made laitance and contamination free. This should be done by a suitable method and in such a way that the quality of the outermost concrete is not compromised. Examples are sand or grid blasting, water jet blasting, grinding and milling (‘bouchardage’). Generally, grid blasting may be preferred, whereas the obtained surface should resemble coarse grained sand paper with exposure of minor aggregates. For wet lay-up FRP EBR systems, which require a fairly even surface, grinding may be most appropriate. For the application of FRP around sharp edges, corners shall be rounded with a specified radius (often about 20 mm).

The prepared concrete should be sufficiently sound, if not repaired as discussed in Section 2.1. Furthermore, the prepared surface should be relatively even or made so by means of the application of a putty (repair mortar to fill unevenness). The putty should be compatible with

the adhesive for FRP application and a primer may have to be applied (if specified by the manufacturer) preceding the putty application. The unevenness which can be allowed depends on the type of FRP EBR. Prefab strips and laminates have already their final stiffness before application and are applied with a high viscosity thixotropic adhesive. As a result, they are less sensitive for unevenness. Wet lay-up sheets and fabrics on the other hand are very flexible and will follow also a small unevenness. Indicative values of the allowable unevenness, expressed as the depth of protrusions and imperfections with respect to a straight ruler with a certain base length, are given in Table A-1.

Before application of the FRP, the prepared surface should be made dust free (and kept dust and contamination free). This is generally achieved by steel brushing and further cleaning with vacuum or oil free compressed air.

Table A-1 *Permissible unevenness of the concrete surface*

FRP EBR type	**2.0 m base**	**0.3 m base**
Prefab, large thickness (> 1.5 mm)	6 mm	3 mm
Prefab, small thickness (< 1.0 mm)	6 mm	2 mm
Wet lay-up	4 mm	2 mm

2.2.2 FRP reinforcement

Prefab FRP strips and laminates are delivered at the specified width and may need to be further cut to the necessary length. For proper bonding, the surface should be free from contamination such as oil, dust, carbon dust and release agents. In some cases it is also specified that the surface should be lightly sand papered for abrasion. Cleaning can be performed with an appropriate agent, such as acetone. Often however, the prefab FRP is provided with a surface ready for bonding, rather or not protected by a peel-ply.

Wet lay-up FRP types need to be cut to the necessary plan-dimensions, while cleaning is generally not required. To facilitate handling, often the sheets or fabrics are provided with a protecting foil or a peel-ply.

The FRP should be handled under dry conditions, with clean gloves and kept free from any contamination. Obviously they should not show any sign of damage (e.g. from transportation, wrong handling or cutting). If present, peel-plies should only be removed just before application.

2.3 FRP EBR application

2.3.1 General considerations

The FRP EBR application, meaning the gluing of the FRP reinforcement on the concrete substrate by means of an adhesive, differs upon the type of FRP. For prefab FRP (strips and laminates) the adhesive is basically a thixotropic resin for bonding, while in the case of wet lay-up FRP (sheets and fabrics) a low viscosity adhesive/saturating resin for both bonding and impregnation is required. In the latter case, the names adhesive and (saturating) resin are often

used interchangeably. Details on the application of prefab and wet lay-up FRP EBR types are given in Sections 2.3.3 and 2.3.4, respectively.

To obtain a good result, the practical application of the adhesive should be executed with care. This implies that proper tools are used and that the specified mixing ratio (resin and hardener), speed and time are respected. The use of modern packaging, such as pre-dosed vessels of which one can be used for mixing, is highly recommended. If the two adhesive components have different colours, the degree of mixing can be visually controlled. To avoid the formation of air bubbles, the speed of the mixer is to be limited. In rare cases it is required to apply a primer before the application of the adhesive. As the shelf life of thermosetting adhesives is restricted, the expire date of the mixing components may be of interest for verification. Furthermore, as working with adhesives is to some extend hazardous, precautions mentioned on the product safety data sheet have to be considered.

To limit the risk of FRP peeling from concave surfaces (Fig. 6-5a), the final FRP EBR unevenness should be sufficiently small. An indicative limit for the unevenness, expressed as the depth of the surface variation with respect to a straight base length of 0.3 m, is 2 mm. Assuming proper surface preparation (Section 2.2) and adhesive application, generally the unevenness requirement is fulfilled.

Given the use of cold-curing adhesives, hardening of the FRP EBR is allowed under ambient conditions, as far as the temperature does not drop below a certain minimum (given by the adhesive manufacturer, mostly 5 °C). Tack free hardening normally takes a couple of hours. Further curing takes some days, whereas a significant degree of cure and (bond) strength development is already achieved after about 12 hours. Nearly full curing is reached after 2 to 7 days. These figures however significantly depend on the type of adhesive and the ambient conditions. No pressing devices are required during adhesive curing.

2.3.2 Verification of temperature and humidity conditions

Depending on the type and the formulation of the adhesive, the manufacturer will specify a minimum and maximum application temperature, as well as a maximum relative humidity. The ambient and concrete surface temperature and relative humidity should be within these limits.

If the temperature is too low or the humidity too high, the adhesive will not cure in a proper way. Also, to prevent weak bonding between the adhesive and the substrates, wet surfaces should be avoided. Therefore, during application, the surface temperature should be in excess of the actual dew point temperature (which depends on the air humidity). If these conditions are not met, artificial heating and dehumidifiers may be required.

High temperatures will result in very fast curing and a too fluid adhesive, so that it is practically not possible to glue the FRP. The available time frame for application, at the prevailing temperature, is characterized by the pot life (workable life) and the open time of the adhesive. The former represents the time one can work with the adhesive after mixing it (time before the adhesive starts to harden in the mixing vessel). The latter is the time available, after application of the adhesive to the adherents, for making the joint.

2.3.3 Application of strips and laminates (prefab FRP)

To glue the FRP strips or laminates, adhesive is applied as a thin layer on the concrete and as a roof shaped layer on the FRP. The latter adhesive layer has slightly more thickness along the centre line, to reduce the risk of forming voids when applying the FRP. Next, the strip or laminate is applied to the concrete surface, pressing it by means of a rubber roller and squeezing out the extra adhesive along the sides. The pressure is applied from the centre to the outer to avoid voids. The final bond layer should be equal along the FRP and should have a thickness of 1.0 to 2.0 mm. Mostly, the strips are applied in one layer, although multiple layers are possible.

To make cleaning of the excess of adhesive more easy, masking tape at either side of the FRP is sometimes used. Removal of this tape after gluing the FRP should be performed with care, so that the FRP does not detach.

If the FRP strips or laminates are applied in different directions, the change in thickness of the adhesive at crossings should be gradually applied so that the unevenness requirements are fulfilled.

2.3.4 Application of sheets and fabrics (wet lay-up FRP EBR)

The application of FRP sheets and fabrics onto the prepared concrete surface is performed by means of hand lay-up. The process starts with the so-called undercoating, whereby the adhesive is applied on the concrete, generally with a roller brush. The undercoating should have sufficient thickness (about 1 mm), yet remain as an even layer. Next, the sheet or fabric is applied by pressing it manually into the adhesive in such a way that it is stretched. During the FRP hand lay-up, the fibres are aligned as good as possible and the introduction of voids should be avoided. As the last step, the overcoating is performed. This is the impregnation and further pressing of the FRP by applying adhesive, which also acts as saturating resin, on top of the sheet or fabric. The final bond layer should be of an even thickness along the FRP.

Often the sheets or fabrics need to be applied in multiple layers. Generally, this can be done before the previous layer has cured. If performed later, abrading of the resin surface by means of sand paper may be required.

2.4 Finishing

Various possibilities exist with respect to finishing. From the perspective of aesthetics, the finishing is optional. On the other hand, finishing may be required as a protection against fire, ultra violet radiation, vandalism, etc. Finishing layers such as painting, plaster, shot concrete or fire protection panels can be provided. In some cases a primer is required.

3 Quality control

3.1 On the supplied materials

The materials are delivered on the construction site in proper packaging, together with all necessary information concerning handling, transportation, storage, safety , etc. In many countries, the materials are certified in some way, implying that quality control in the factory and additional testing by independent laboratories has been executed. If this is not the case or if additional quality control on the supplied materials is requested, representative samples have to be taken for further testing. Typically the control tests may include tensile testing of the FRP reinforcement and compression testing of the adhesive. The number and type of tests may remain limited as extensive testing has already been performed with respect to the material characterization (the manufacturer should be able to provide relevant material properties, e.g. needed for the design).

The quality control of the supplied materials may also include a verification of damage to the FRP as a result of transportation, storage and handling. This visual inspection may follow the in-situ cutting (as far as needed) of the FRP reinforcement. At the same time it can be verified that the FRP dimensions correspond to those specified on the design drawings.

3.2 On the application conditions

Before the FRP EBR can be applied, certain conditions should be verified and met. To check the repair (if executed) and surface preparation of the concrete substrate, pull-off tests are usually performed. By means of these tests, an indication of the concrete bond and tensile strength is obtained. The test method involves bond testing in direct tension of a steel disk, with diameter 50 mm, adhered to the prepared concrete. Generally a saw cut by drilling is provided along the disk perimeter, a few millimetres inside the concrete. If proper surface preparation has been performed, the locus of the failure will be within the concrete. The minimum concrete tensile strength should exceed 1.5 N/mm^2.

In addition, the unevenness of the concrete substrate is to be checked with respect to the requirements specified in Table A-1. To verify the temperature and humidity conditions discussed in Section 2.3.2, necessary measurements should be performed at the start as well as during the application.

3.3 On the application process

When gluing the FRP reinforcement, quality control is advisable with respect to the proper execution procedure, the temperature and humidity conditions, the amount of materials and the FRP placement (fibre direction). After finishing, the bond layer thickness, the unevenness of the FRP EBR and the presence of imperfections should be verified. Where relevant, also the bond quality should be verified. Both non-destructive and (partially) destructive testing may be applied. In the latter case, control tests are performed on separate FRP EBR zones glued extra during the practical application.

The presence of voids can be checked in a simple way by surface tapping with a 5 mm diameter steel stick having a rounded tip. Sometimes, more objective techniques are preferred such as thermography and ultrasonic scanning. Thermography is a non-destructive testing technique, which detects flaws by recording the temperature of a homogeneously heated surface by means of infra red imaging. Typically defects are located as hot spots due to differences in thermal properties. Non-destructive testing by means of ultrasonic wave techniques is also possible, yet more time consuming. In this case, voids are detected by recording transmission speed and wave attenuation. More accurate are the ultrasonic pulse techniques, where defects are located through measurements of echoes generated by acoustic impedance mismatch. Generally, these or other non-destructive tests have significant limitations in their applicability and require well-experienced personnel.

To verify bond strength, typically destructive testing is performed such as pull-off, torque or shear tests. Most common is the pull-off test already described in Section 3.2, in this case applied on the whole FRP/adhesive/concrete assembly. To determine the shear strength a torque test may be applied on a ring disk glued on the FRP and partially cored. If a FRP test strip is glued on the concrete and extending an edge, a bond test in pure shear my be executed. A schematic illustration of the pull-off, torque and shear bond tests is given in Fig. A-2.

If large or a significant amount of voids are detected or if the bond strength appears insufficient in critical zones, repair actions may be needed. Injection of voids is questionable, due to the damage which generally occurs to the FRP. Hence, the FRP should be cut out over the damaged length and a new piece bonded over the top providing sufficient overlap length.

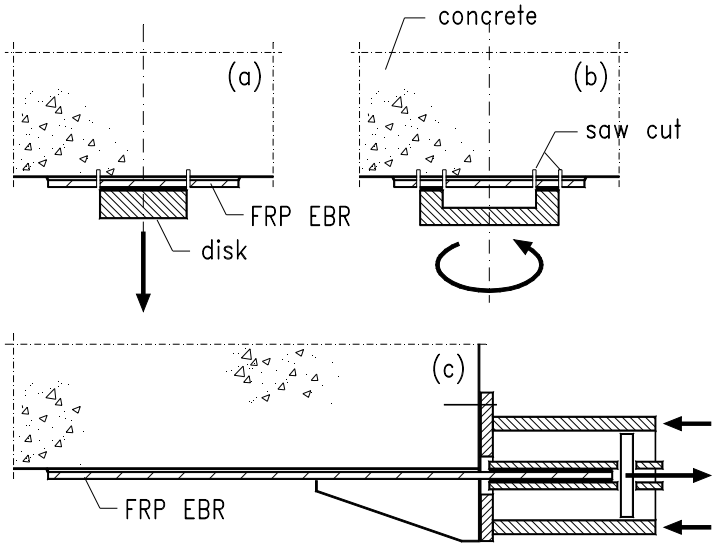

Fig. A-2 *Verification of bond by (a) pull-off, (b) torque and (c) shear test*

3.4 In-service inspection

Although FRP EBR systems are generally expected to be very durable and do not require a lot of maintenance, long-term experience with FRP EBR strengthening is limited. Also, damage may occur to the FRP EBR due to e.g. concrete deterioration, impact, etc. Hence, it may be recommended to perform in-service inspection, especially if the FRP EBR has a considerable influence on the overall safety of the structure.

Appendix B
MATERIAL PROPERTIES

1 Concrete

Two grades of concrete were used for the different experiments. A normal strength concrete (NSC) with a compressive cylinder strength f_c of about 33 N/mm^2 and a high strength concrete (HSC) with f_c equal to about 95 N/mm^2. The compositions (per m^3) are given in Table B-1. The concrete was manufactured in the laboratory.

Table B-1 *Concrete composition*

Material	**NSC**	**HSC**
Gravel 4/14	1250 kg	-
Crushed limestone 4/7	-	1065 kg
Coarse sand	665 kg	710 kg
Portland cement CEM I 42.5	300 kg	-
CEM I 52.5	-	446 kg
Water	170 kg	145 kg
Silica fume	-	40.1 kg
Superplasticizer (Rheobuild 2000)	-	12.3 l

For each concrete batch quality control tests were performed. Tested properties of the fresh concrete include slump, flow test and density. For the hardened concrete some or all of the following properties were determined:

- Compressive cylinder strength f_c on cylinders with a diameter of 150 mm and a height of 300 mm.
- Compressive strength $f_{c,cub}$ on cubes with side lengths 150 or 200 mm (e.g. $f_{c,cub200}$ corresponds with side length 200 mm).
- Compressive strength $f_{c,prism}$ on prisms with dimensions 200 mm x 200 mm x 500 mm.
- Flexural tensile strength f_{ctb} by means of 3-point bending tests on prisms 150 mm x 150 mm x 600 mm and a span of 500 mm.
- Splitting tensile strength f_{cts} by splitting tests on the remaining halves of the prisms for the bending test.
- Pure tensile strength f_{ct} on prisms 100 mm x 100 mm x 200 mm.
- Secant modulus of elasticity E_c by axial compression tests on prisms 200 mm x 200 mm x 500 mm.

Tests on the hardened concrete were performed on 3 specimens, except for the modulus of elasticity and the compressive prism strength which involved one specimen. All tests were performed according to the relevant Belgian standards.

Results of the quality control tests, for the different experimental programmes can be found in the following tables. Table B-2 till Table B-4 give the properties of the fresh concrete, while Table B-5 till Table B-7 give the properties of the hardened concrete.

Table B-2 *Fresh concrete, FRP EBR strengthened beams*

Batch	**Concrete type**	**Slump** [mm]	**Flow test**	**Density** [kg/m^3]
BF1	NSC	135	1.95	2410
BF2	NSC	105	1.85	2410
BF3	NSC	103	2.07	2410
BF4	NSC	72	1.69	2390
BF5	NSC	104	1.80	2410
BF6	NSC	90	1.94	2385
BF7	NSC	88	1.94	2390
BF8	NSC	105	1.89	2425
BF9	NSC	85	1.69	2415
BS1	NSC	143	1.83	2410
BS2	NSC	109	1.92	2390
BS3	NSC	70	1.82	2400
BS4	NSC	92	1.77	2420
BS5	NSC	105	2.07	2400
BS6	NSC	86	1.67	2400
BS7	NSC	98	1.93	2400

Table B-3 *Fresh concrete, tension stiffening tests*

Batch	**Concrete type**	**Slump** [mm]	**Flow test**	**Density** [kg/m^3]
T1	NSC	55	1.77	2385
T2	NSC	162	2.14	2415
T3	NSC	60	1.75	2395
T4	NSC	105	2.05	2400
T5	HSC	-	2.35	2450

Table B-4 *Fresh concrete, FRP confined concrete*

Batch	**Concrete type**	**Slump** [mm]	**Flow test**	**Density** [kg/m^3]
C	NSC	90	2.20	2400
K1	NSC	100	1.69	2405
K2-K3	NSC	155	2.14	2390
K4-K5	NSC	158	2.30	2430
K6-K7	NSC	76	2.23	2380
K8-K9	NSC	152	2.24	2400
K10-K11	NSC	178	2.45	2415

Table B-5 *Hardened concrete, FRP EBR strengthened beams*

Batch	Conc. type	At 28 days	At age of testing				
		f_c [N/mm^2]	Age [days]	f_c [N/mm^2]	f_{ctb} [N/mm^2]	f_{cts} [N/mm^2]	E_c [N/mm^2]
BF1	NSC	31.3	56	33.7	4.21	3.43	33900
BF2	NSC	36.0	56	36.5	5.05	1.99	31600
BF3	NSC	33.1	56	34.9	4.56	3.58	33600
BF4	NSC	30.2	61	30.8	4.48	3.30	32400
BF5	NSC	35.0	65	37.4	4.80	3.92	33600
BF6	NSC	30.1	72	35.9	4.93	3.75	31200
BF7	NSC	31.8	105	38.5	5.66	3.84	32900
BF8	NSC	35.7	107	39.4	5.42	4.17	34200
BF9	NSC	31.9	99	33.7	4.50	3.53	34700
BS1	NSC	32.7	56	35.0	4.60	3.40	32400
BS2	NSC	34.5	272	33.8	5.67	3.62	33200
BS3	NSC	34.9	114	37.5	5.04	3.53	32900
BS4	NSC	36.4	138	38.4	5.72	3.90	34100
BS5	NSC	38.2	152	36.0	4.32	3.79	31100
BS6	NSC	35.2	189	35.8	5.68	3.31	32700
BS7	NSC	33.0	247	34.7	5.97	3.57	34800

Table B-6 *Hardened concrete, tension stiffening tests*

Batch	Conc. type	At 28 days					
		f_c [N/mm^2]	$f_{c,cub150}$ [N/mm^2]	f_{ctb} [N/mm^2]	f_{cts} [N/mm^2]	f_{ct} [N/mm^2]	E_c [N/mm^2]
T1	NSC	36.2	45.4	5.10	3.48	2.57	31700
T2	NSC	32.3	37.9	3.82	3.41	2.47	31700
T3	NSC	32.5	41.8	4.04	3.74	2.53	32000
T4	NSC	30.3	39.2	4.25	3.40	2.21	29700
T5	HSC	96.0	111.2	6.64	5.59	3.76	40700

Table B-7 *Hardened concrete, FRP confined concrete*

Batch	Conc. type	At 28 days					
		f_c [N/mm^2]	$f_{c,cub150}$ [N/mm^2]	$f_{c,prism}$ [N/mm^2]	f_{ctb} [N/mm^2]	f_{cts} [N/mm^2]	E_c [N/mm^2]
C	NSC	34.8	39.5	35.5	3.98	3.32	33000
K1	NSC	31.8	-	34.6	4.14	3.76	34000
K2-K3	NSC	34.3	50.6	33.6	4.19	3.63	31900
K4-K5	NSC	39.3	46.8	36.1	4.57	3.94	31900
K6-K7	NSC	35.8	46.9	35.5	4.60	3.74	30100
K8-K9	NSC	39.1	48.5	34.1	4.03	3.36	30900
K10-K11	NSC	37.7	47.5	36.0	4.44	3.90	31700

2 Steel reinforcement

For the internal steel reinforcement, deformed bars S500 were used with a guaranteed characteristic yield strength of 500 N/mm^2. Properties of the steel were determined by means of tensile tests according to NBN-EN 10002-1. Three tests were performed for each rebar type. The properties are given in Table B-8.

Table B-8 *Mean tensile properties of the steel reinforcement*

Test programme	**Nominal diameter** [mm]	**Yield strength** [N/mm^2]	**Tensile strength** [N/mm^2]	**Ultimate strain** [%]
RC beams strengthened in flexure	16	590	690	12.4
	8	560	620	12.4
RC beams strengthened in shear	20	530	620	11.9
	6	560[(1)]	590	5.1
Tension stiffening	10	590	670	-
	14	550	630	-
	16	590	690	-
Confined columns	8	560	610	2.8
	12	620	720	8.7
	14	560	630	10.0

[(1)] 0.2 % proof stress

3 Externally bonded FRP reinforcement

3.1 FRP EBR systems

Different types of externally bonded FRP reinforcement (FRP EBR) were used, comprising both 'prefab' and 'wet lay-up' systems (see Chapter 2, Section 2.3). The following information specifically applies to the FRP EBR systems used in the test programmes. The properties according to the manufacturers, as far as available, are given in Table B-9 and Table B-10. The nominal thickness of the FRP mentioned, refers to the global thickness for prefab types and to the equivalent dry-fibre thickness for the wet lay-up types. The latter thickness is obtained as the ratio of the fibre mass per area and the fibre density.

CarboDur S system (CFRP, prefab type)

This FRP EBR combines CarboDur prefabricated strips and Sikadur-30 epoxy adhesive, manufactured by Sika. The strips consist of continuous unidirectional carbon fibres impregnated in an epoxy matrix and are available in different sizes and E-moduli. For the experimental work, type S1012 was used, with a thickness of 1.2 mm and a width of 100 mm. The designation S stands for the low modulus of elasticity type. The fibre volume fraction is at least 68 %.

C-sheet system (CFRP, wet lay-up type)

This system combines C-sheet, manufactured by S&P Clever Reinforcing Company, with Multipox T epoxy adhesive, manufactured by Resiplast. The sheets consist of continuous unidirectional carbon fibres glued onto a light textile grid as backing and protected from dust by a plastic foil. Two types, with different moduli of elasticity of the fibres, were used: type C240 with a normal and type C640 with a high modulus of elasticity. For the C240 type, the mass per area equals 200 g/m^2 and the nominal thickness 0.117 mm. For the C640 these quantities equal 600 g/m^2 and 0.235 mm. The sheets used had a width of 300 mm.

Replark system (CFRP, wet lay-up type)

The Replark system combines Replark Type 20 sheet and Epotherm Type XL 700 S epoxy adhesive, manufactured by Mitsubishi. The sheets consist of continuous unidirectional carbon fibres impregnated with a small amount of resin on a paper backing. The fibre mass per area equals 200 g/m^2, the nominal (dry fibre) thickness 0.111 mm. The sheets were delivered with a width of 330 mm.

Roviglas G system (GFRP, wet lay-up type)

This system consists of Roviglas Type G fabric and Multipox T epoxy adhesive, manufactured by Syncoglas and Resiplast respectively. In this woven quasi-unidirectional dry-fibre fabric a small amount of fibres (20 g/m^2) is provided in the transverse direction, mainly to keep the longitudinal fibres (200 g/m^2) together. The nominal thickness equals 0.100 mm. The fabric was delivered with a width of 2 m.

SyncoTape system (GFRP, wet lay-up type)

This FRP EBR type consists of SyncoTape glass fibre fabric, manufactured by Syncoglas, and PC5800 epoxy adhesive, manufactured by ECC. In this woven quasi-unidirectional fabric, 600 g/m^2 fibres are provided in the longitudinal direction and 25 g/m^2 fibres in the transverse direction. The nominal thickness of the fabric equals 0.300 mm, the width 200 mm.

TU360G160C/27G system (HFRP, wet lay-up type)

This product manufactured by ECC combines a hybrid type of fabric and PC5800 epoxy adhesive. In the longitudinal direction of this dry-fibre fabric both glass (360 g/m^2) and carbon (160 g/m^2) fibres are provided, together with a small amount of glass fibres (27 g/m^2) in the transverse direction. The nominal thickness of the fabric equals 0.123 mm, the width 50 mm.

Table B-9 *Properties of the FRP EBR according to the manufacturers*

Property	**CarboDur S**	**C sheet 240**	**C sheet 640**	**Replark 20**
Young's modulus E_f [N/mm^2]	> 155000	240000$^{(3)}$	640000$^{(3)}$	230000
Tensile strength f_f [N/mm^2]	> 2400$^{(1)}$/3100$^{(2)}$	3900$^{(3)}$	2650$^{(3)}$	3400
Failure strain ε_{fu} [%]	> 1.9	1.6$^{(3)}$	0.4$^{(3)}$	1.4

$^{(1)}$ Characteristic value, $^{(2)}$ mean value, $^{(3)}$ fibre properties

Table B-10 *Properties of the adhesive according to the manufacturers*

Property	Sikadur-30	Epotherm	Multipox T	PC5800
Mixing ratio (resin:hardener)	3:1	2:1	2:1	2:1
Pot life [min.]	40 at 35 °C	60 at 30 °C	60 at 20 °C	30 at 20 °C
Density [kg/m^3]	1770	-	1000	1300
Compressive strength [N/mm^2]	95	-	35 to 90	75
Tensile strength [N/mm^2]	30	>29	32	-
Lap shear strength [N/mm^2]	-	> 9.8	-	-
Modulus of elasticity [N/mm^2]	12800	-	-	-

3.2 Practical application

The FRP EBR was applied according to the procedures given in Appendix A and as specified by the manufacturers. The concrete surface was roughened by means of sand-blasting (until it resembled coarse sand paper) or by grinding (until removal of the outer cement skin and appearance of the aggregates) and carefully cleaned with compressed air. The prefab CFRP type used, was cleaned with an acetone agent. Before FRP bonding, adhesive was applied to both the concrete and the FRP. The wet lay-up types were clean at delivery and were only unpacked just before application. For the first practical applications of the wet lay-up system (strengthening of RC beams in flexure and shear; Chapter 3), prior to sheet application a primer and putty resin were used to smoothen the surface. This was not done for later applications, as it appeared not necessary in case of the smoothly roughened concrete surface obtained by grinding. During gluing, the external reinforcement was properly pressed to the concrete by means of a rubber (prefab type) or brush roller (wet lay-up type). Curing of the FRP EBR was allowed for at least 7 days under laboratory environment. No pressing devices were applied during curing.

3.3 Quality control tests

Tensile tests on the FRP EBR were performed on specimens with a width of 50 or 100 mm. Dimensions of the specimens and details of the gripping zone are shown in Fig. B-1. Prefab FRP types were tested as delivered, while wet lay-up FRP types were first impregnated with resin and cured under laboratory environment during at least 7 days. The tests were performed, according to ASTM Standard D3039/D3039M, in a tensile testing machine with a capacity of 1000 kN. Bonded steel plates were provided at the specimen ends to allow for a smooth introduction of the gripping forces. The tensile strain was recorded by means of two strain gauges (one at each opposite side) in the centre of the specimen. Results, in terms of mean values and standard deviations (mentioned behind the ± sign), are given in Table B-11. Because the modulus of elasticity of FRP is not constant (Chapter 2, Section 4.4.1.1 and Fig. 2-10b). It was decided to determine both a tangent modulus (slope of the stress-strain behaviour at the origin) and a secant modulus. The latter was determined between stress-strain points corresponding to 20 % and 60 % of the ultimate load. The recorded stress-strain behaviour of some of the specimens is shown in Fig. B-2.

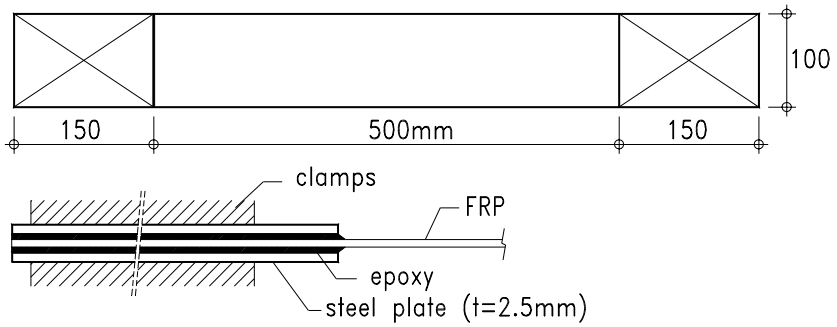

Fig. B-1 *Tensile test specimens*

Table B-11 *Mean tensile properties of the FRP EBR obtained from tensile testing*

Type	**No. tests**[(1)]	**Nominal dimensions** [mm]	**Tensile strength** [N/mm^2]	**Failure strain** [mm/m]	**$E_{f,tan}$** [kN/mm^2]	**$E_{f,secan}$** [kN/mm^2]
CarboDur S1012	3	100 x 1.2	3200 ± 80	18.5 ± 1.0	159 ± 4	179 ± 10
Replark MRK-M2-20	4	100 x 0.111[(2)]	3500 ± 140	12.5 ± 0.5	233 ± 16	281 ± 3
Roviglas G 200/20	1	100 x 0.100[(2)]	1300	20.7	57	69
C-sheet 240	2	50 x 0.117[(2)]	2600 ± 180	11.9 ± 0.4	198 ± 12	226 ± 13
C-sheet 640	3	50 x 0.235[(2)]	1100 ± 100	2.2 ± 0.2	471 ± 9	505 ± 35
SyncoTape TU600/25	3	50 x 0.300[(2)]	780 ± 110	13.0 ± 3.1	60 ± 14	73 ± 5
TU360G160C/27G	3	50 x 0.123[(2)]	1100 ± 120	9.6 ± 1.0	97 ± 8	120 ± 12

[(1)] With the failure area in between the grips, [(2)] Equivalent dry-fibre thickness

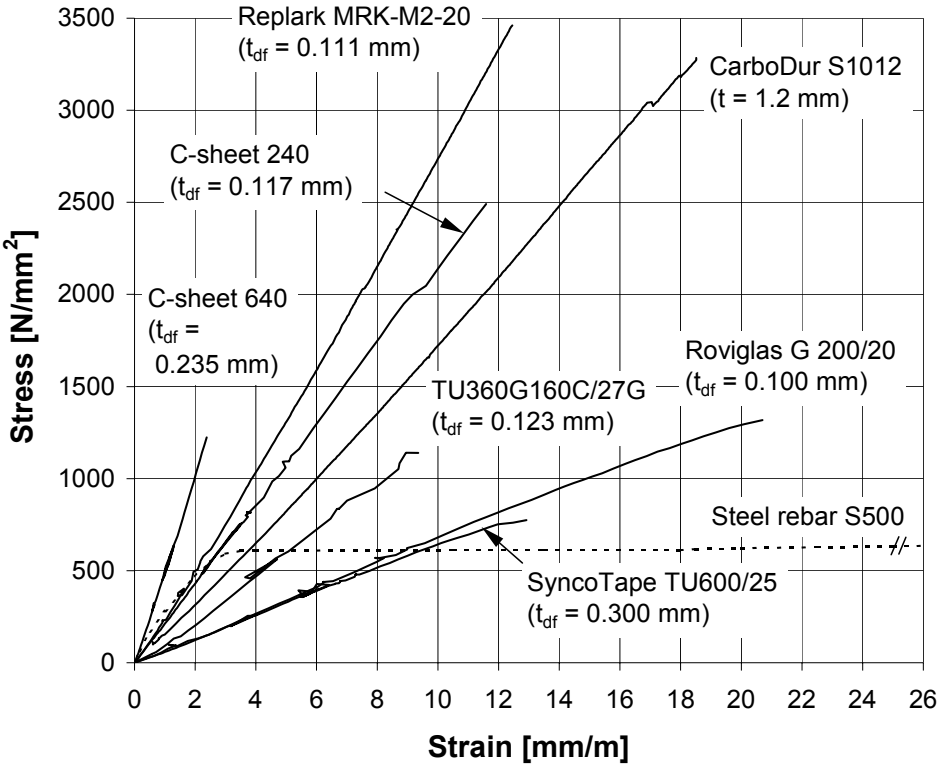

Fig. B-2 *Stress-strain behaviour of FRP EBR*

Appendix C
RC BEAMS STRENGTHENED IN FLEXURE

1 Bond failure due to vertical crack displacement: experimental data

To calibrate the model discussed in Chapter 3, Section 4.1.3, the following data was used. This data concerns 4-point bending tests on rectangular beams strengthened in flexure by means of externally bonded CFRP. All the beams failed by FRP debonding at the location of a shear crack.

No.	Designation	ℓ [mm]	ℓ_1 [mm]	b [mm]	h [mm]	d [mm]	f_{cm} [N/mm^2]	Q_u [kN]
1	M(BF2)	3800	1250	200	450	409	36.5	185.0
2	M(BF4)	3800	1250	200	450	409	30.8	184.2
3	M(BF5)	3800	1250	200	450	409	37.4	177.0
4	M(BF8)	3800	1250	200	450	409	39.4	111.3
5	M(BF9)	3800	1250	200	450	409	33.7	95.8
6	K(B10-13)	2000	660	250	150	120	37.7	32.4
7	K(B14/19-21)	2000	660	250	150	120	37.7	38.5
8	K(B15-18)	2000	660	250	150	120	37.7	41.4
9	K(GB1/2)	2000	660	300	250	220	38.2	79.8
10	K(GB3/4)	2000	660	300	250	220	38.7	72.5
11	K(GB5/6)	2000	660	300	250	220	38.9	65.5
12	D(BL02)	2000	660	300	250	210	39.0	137

D: Deuring [1], K: Kaiser [2], M: Matthys (Chapter 3)

No.	Designation	A_s [mm²]	E_s [N/mm^2]	A_f [mm²]	E_f [N/mm^2]	ρ_{eq} [-]	$\tau_p = Q_u/(bd)$ [N/mm^2]
1	M(BF2)	804	200000	120	159000	0.0110	2.26
2	M(BF4)	804	200000	120	159000	0.0110	2.25
3	M(BF5)	804	200000	120	159000	0.0110	2.16
4	M(BF8)	402	200000	120	159000	0.0061	1.36
5	M(BF9)	402	200000	22.2	233000	0.0052	1.17
6	K(B10-13)	101	210000	100	110532	0.0051	1.08
7	K(B14/19-21)	101	210000	150	114983	0.0061	1.28
8	K(B15-18)	101	210000	200	120506	0.0072	1.38
9	K(GB1/2)	101	210000	200	120506	0.0033	1.21
10	K(GB3/4)	101	210000	150	114983	0.0028	1.10
11	K(GB5/6)	101	210000	100	110532	0.0023	0.99
12	D(BL02)	402	210000	200	120100	0.0082	2.17

D: Deuring [1], K: Kaiser [2], M: Matthys (Chapter 3)

2 Moment-strain behaviour

2.1 Concrete compressive strain

In the following figures, the concrete strain ε_c at the extreme compression fibre is given. The experimental strain is the mean value of the concrete strains measured at 10 mm from the top of the beam by means of strain stirrups (Fig. 3-2). The analytical verification is performed according to Chapter 3, Section 4.2.

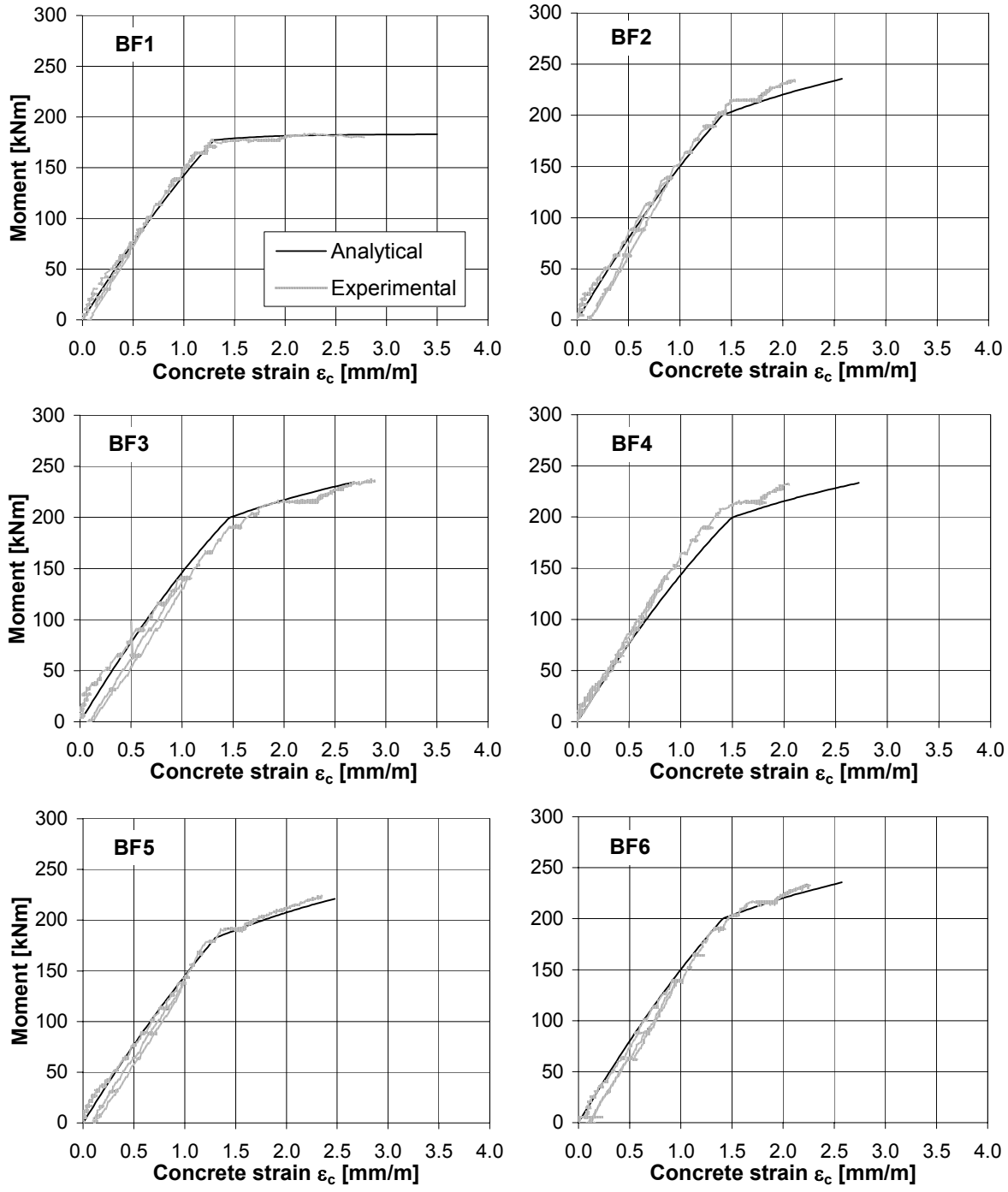

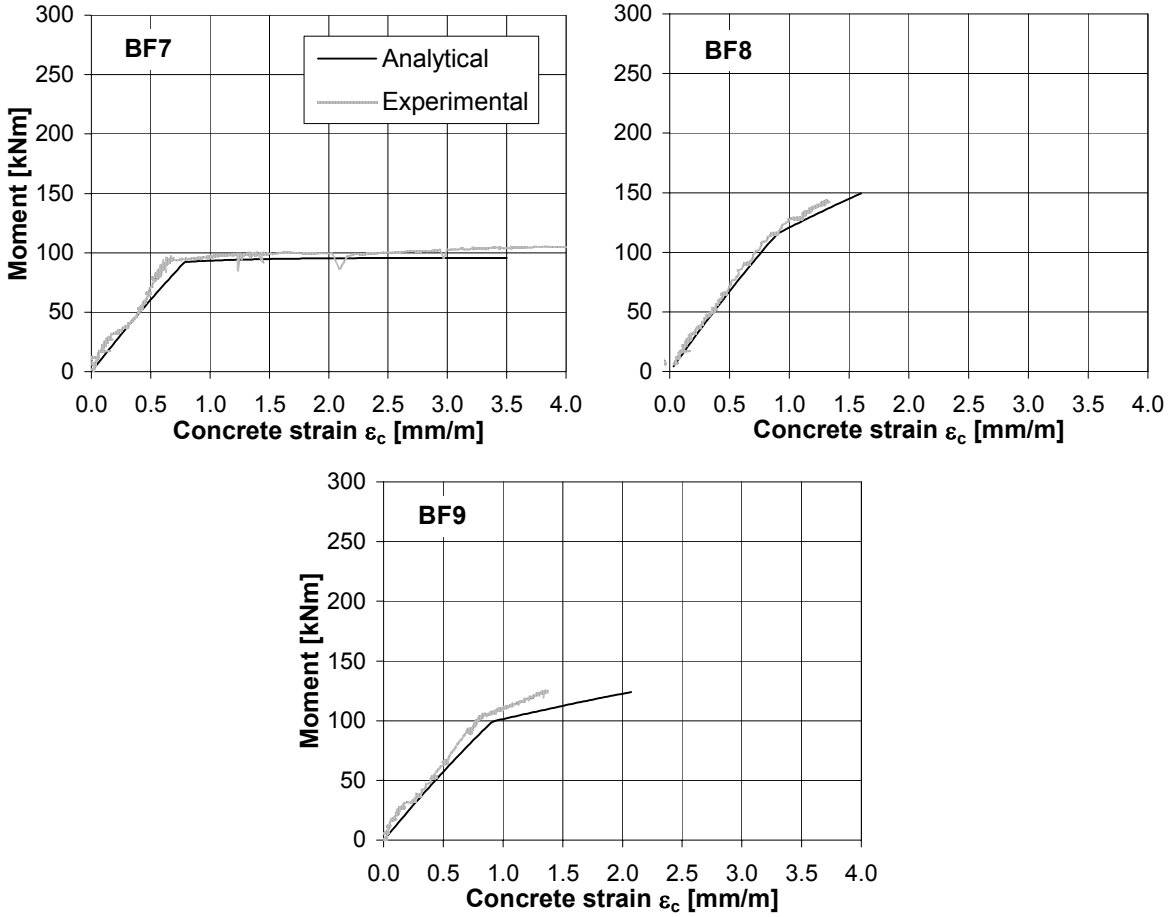

2.2 Reinforcement tensile strain

In the following figures, the tensile strain of the internal steel ε_s and the FRP EBR ε_f are given. The mean value of the concrete strains measured (by means of strain stirrups) at the reinforcement level is taken as the strain of the internal steel reinforcement. The experimental FRP strain at midspan is recorded by means of a strain gauge (Fig. 3-2). The analytical verification is performed according to Chapter 3, Section 4.2.

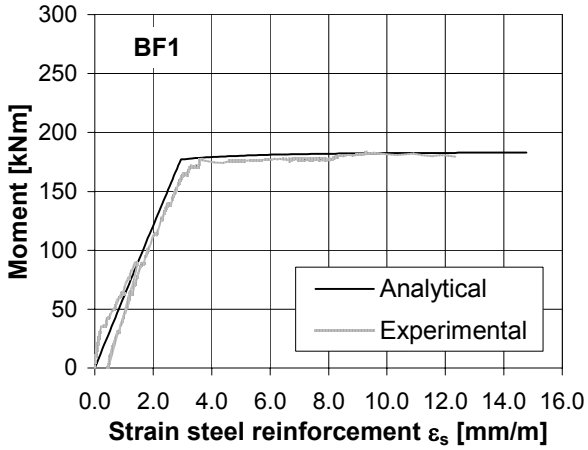

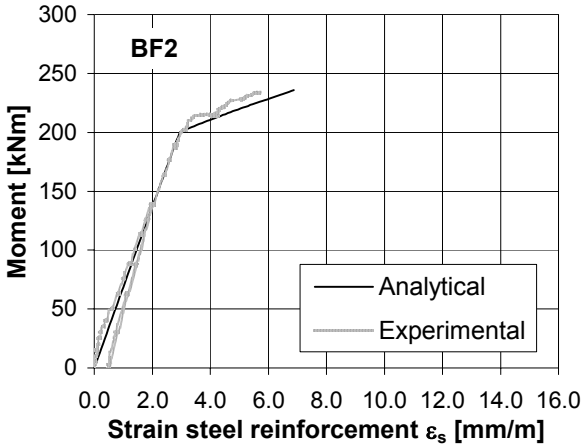
BF2
Moment [kNm]
Strain steel reinforcement ε_s [mm/m]
Analytical
Experimental

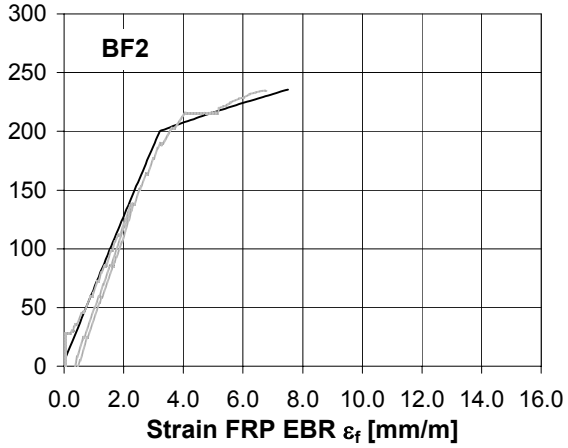
BF2
Strain FRP EBR ε_f [mm/m]

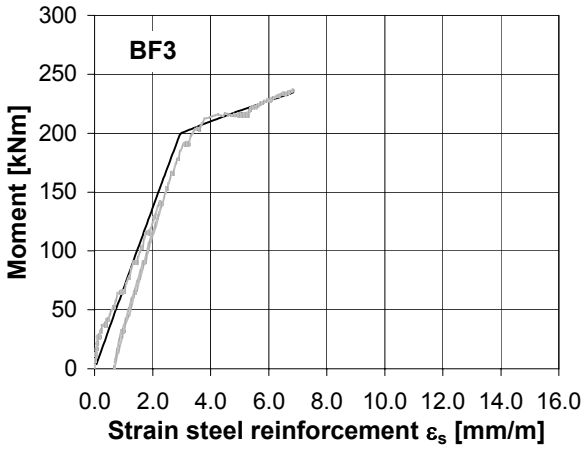
BF3
Moment [kNm]
Strain steel reinforcement ε_s [mm/m]

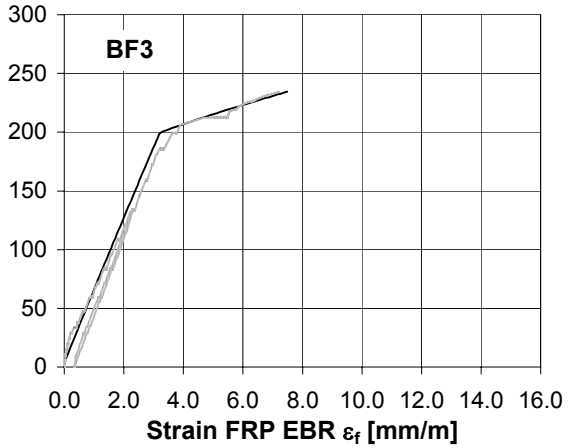
BF3
Strain FRP EBR ε_f [mm/m]

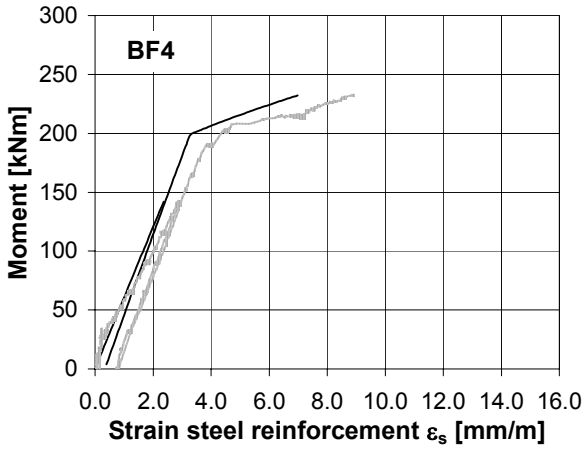
BF4
Moment [kNm]
Strain steel reinforcement ε_s [mm/m]

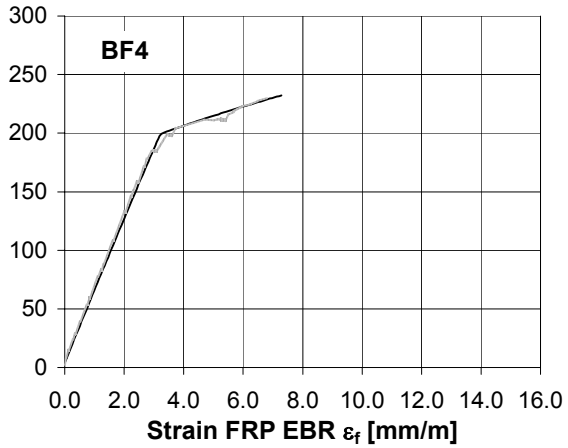
BF4
Strain FRP EBR ε_f [mm/m]

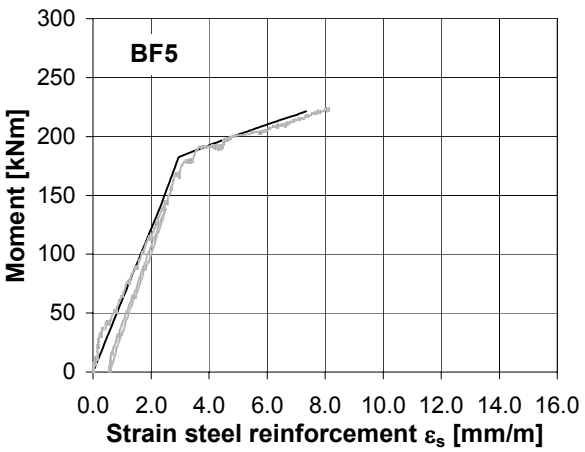
BF5
Moment [kNm]
Strain steel reinforcement ε_s [mm/m]

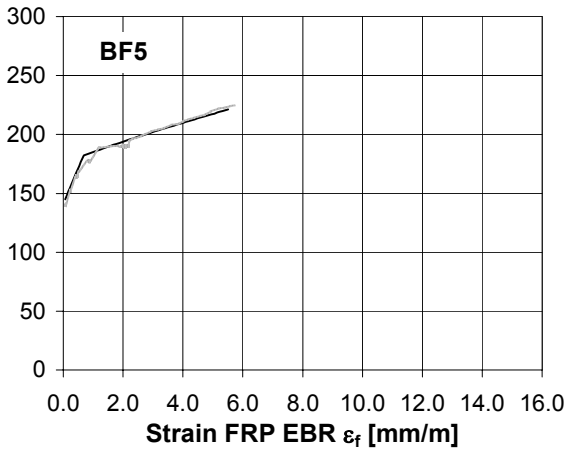
BF5
Strain FRP EBR ε_f [mm/m]

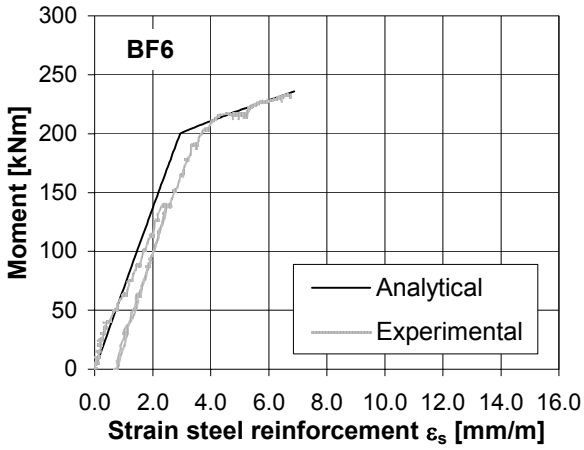
BF6
Moment [kNm]
Strain steel reinforcement εs [mm/m]
Analytical
Experimental

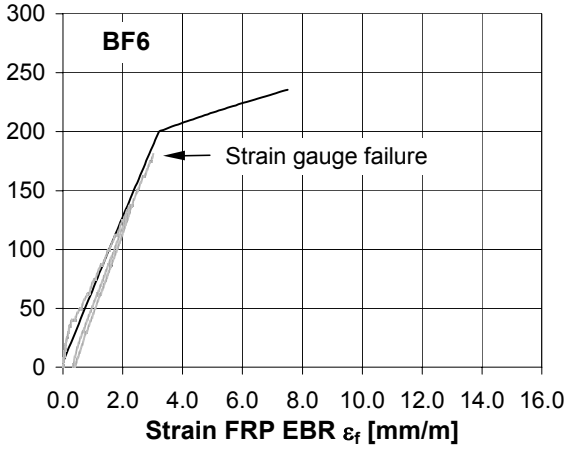
BF6
Strain gauge failure
Strain FRP EBR εf [mm/m]

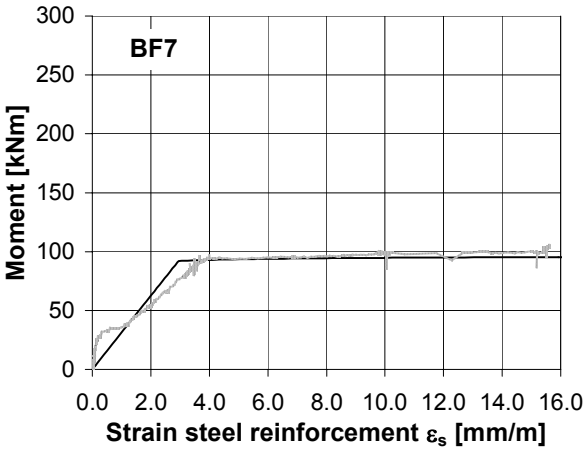
BF7
Moment [kNm]
Strain steel reinforcement εs [mm/m]

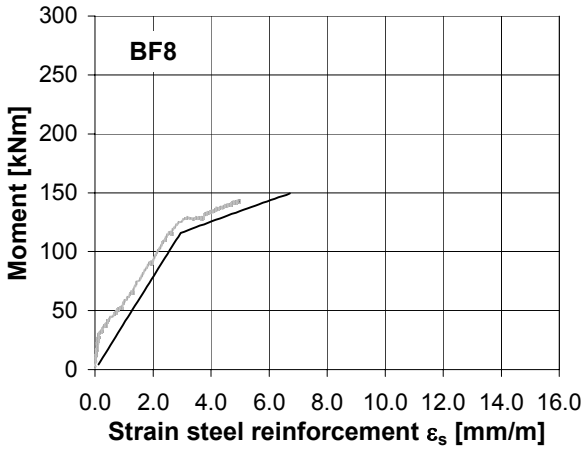
BF8
Moment [kNm]
Strain steel reinforcement εs [mm/m]

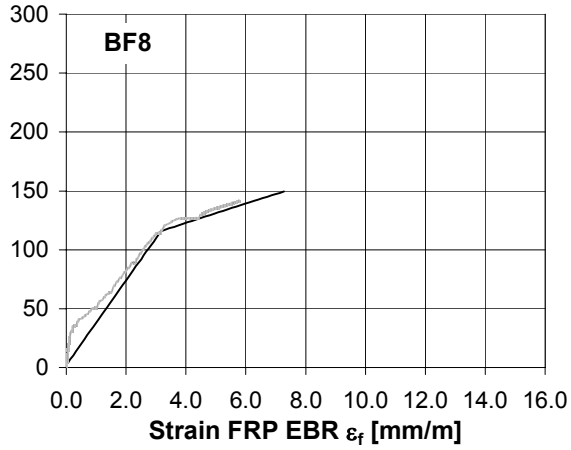
BF8
Strain FRP EBR εf [mm/m]

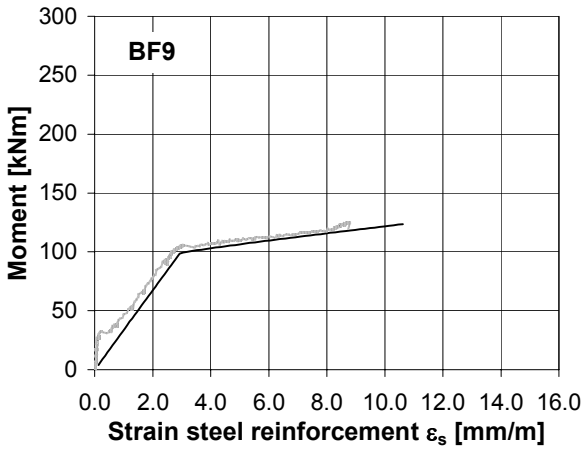
BF9
Moment [kNm]
Strain steel reinforcement εs [mm/m]

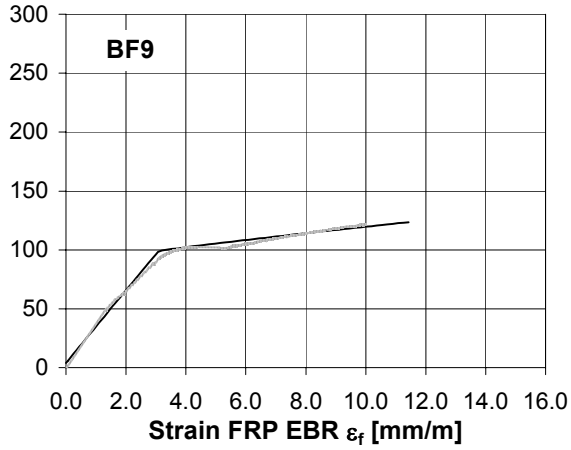
BF9
Strain FRP EBR εf [mm/m]

3 Moment-curvature behaviour

The experimental and analytical moment-curvature behaviour of beams BF1, BF2, BF4, BF5 and BF7-BF9 are given in the following figures (no figures are provided for beams BF3 and BF6, as their behaviour is almost identical to that of beam BF2 (see Section 2)). The experimental curvature is derived from the measured concrete strains at the top and bottom of the beam (Fig. 3-2). The analytical verification is performed according to Chapter 3, Section 4.3.

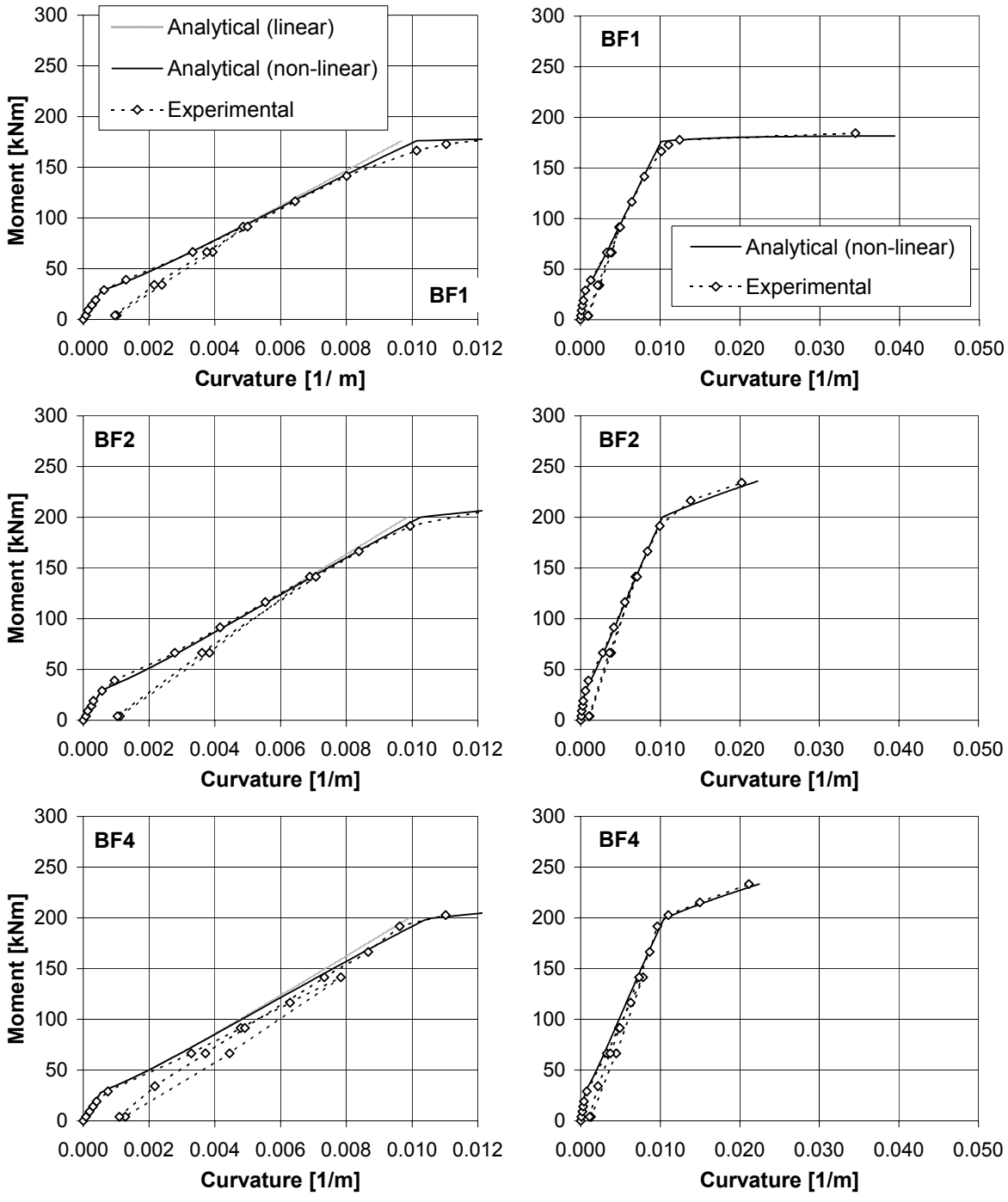

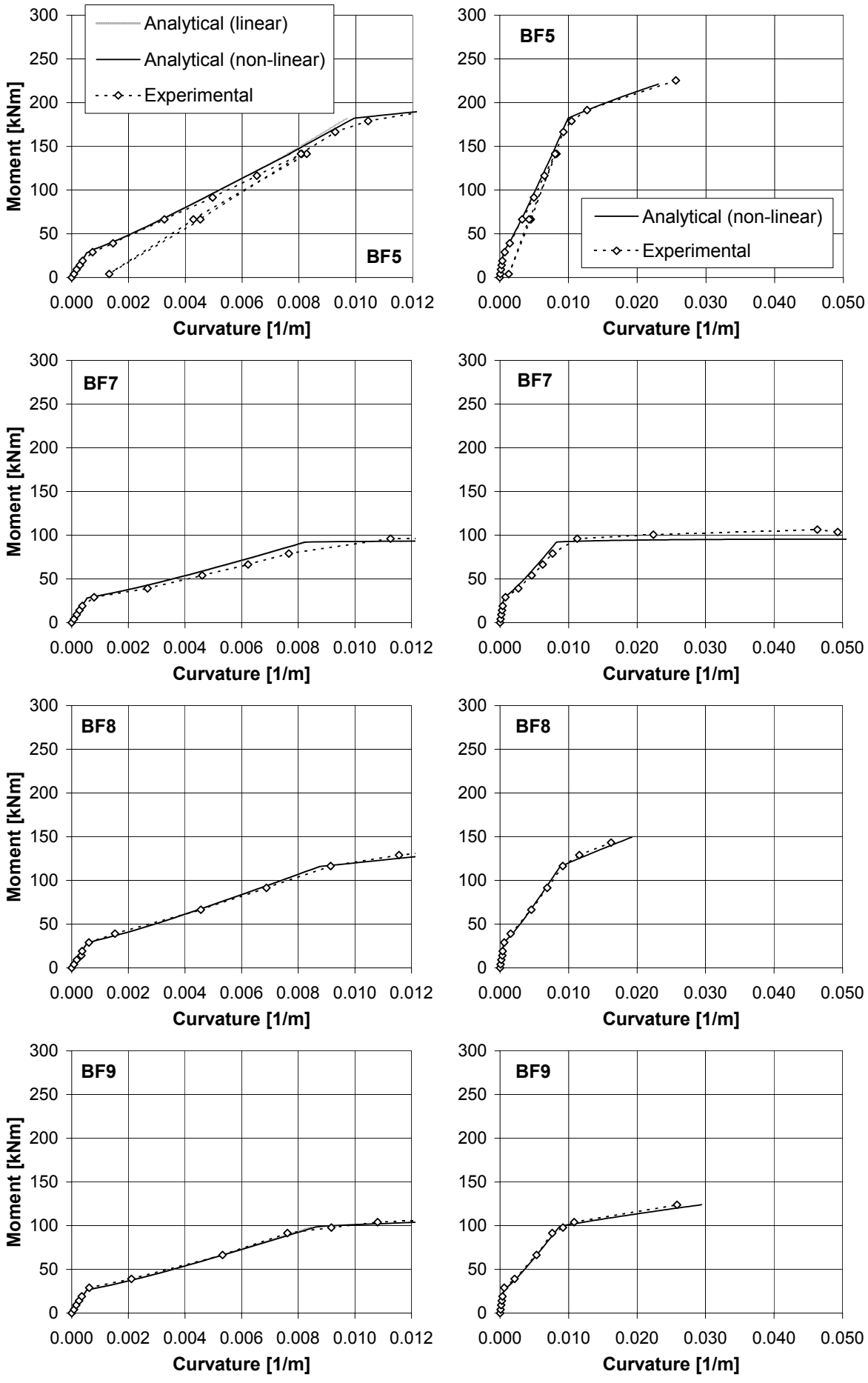
Analytical (linear)
Analytical (non-linear)
Experimental
BF5
BF5
BF7
BF7
BF8
BF8
BF9
BF9
Moment [kNm]
Curvature [1/m]
0
50
100
150
200
250
300
0.000
0.002
0.004
0.006
0.008
0.010
0.012
0.020
0.030
0.040
0.050

4 Moment-deflection behaviour

Similar to the moment-curvature behaviour (Section 3), the experimental and analytical moment-deflection behaviour of beams BF1, BF2, BF4, BF5 and BF7-BF9 is compared in the following figures. The analytical verification is performed according to Chapter 3, Section 4.3.

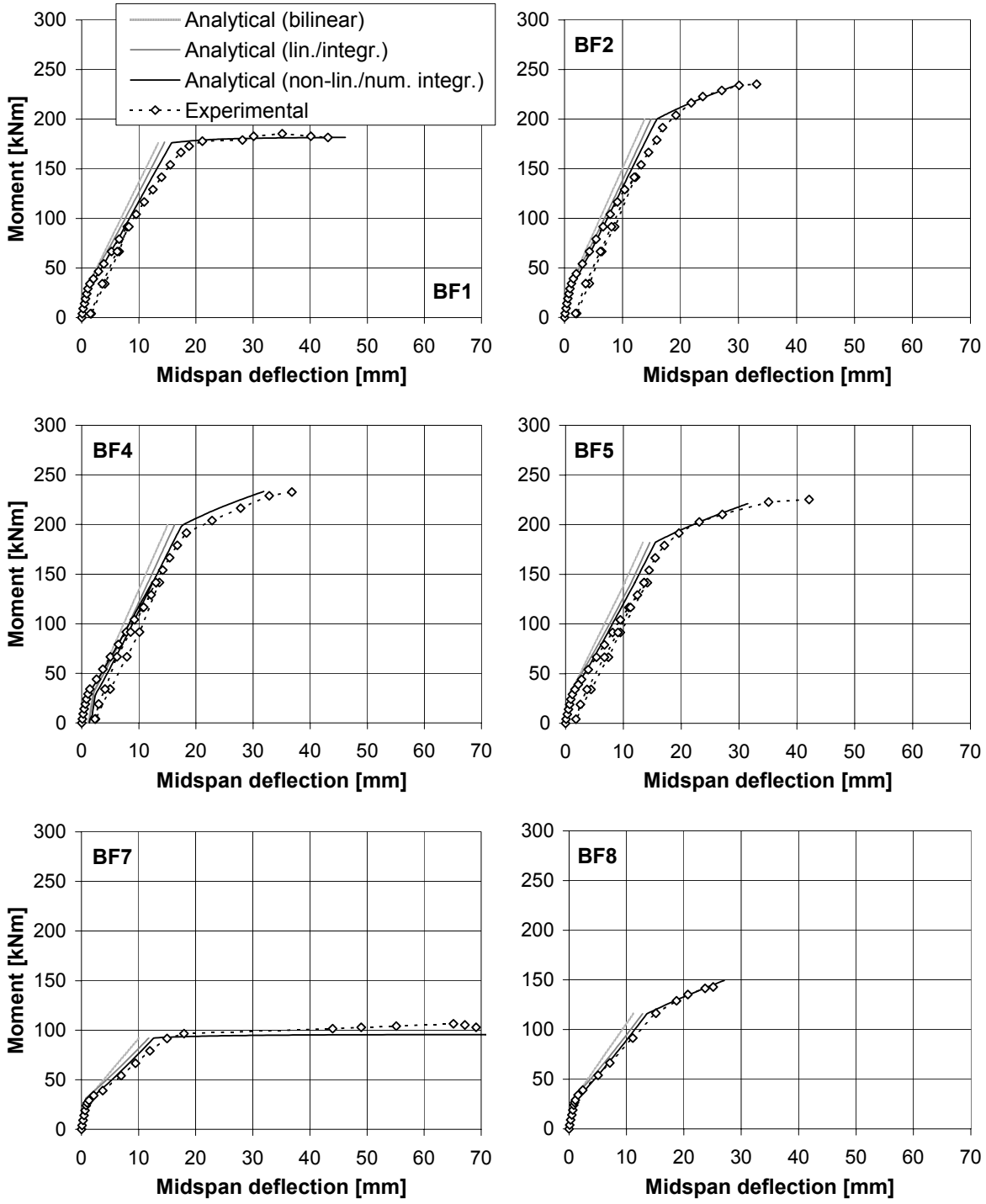

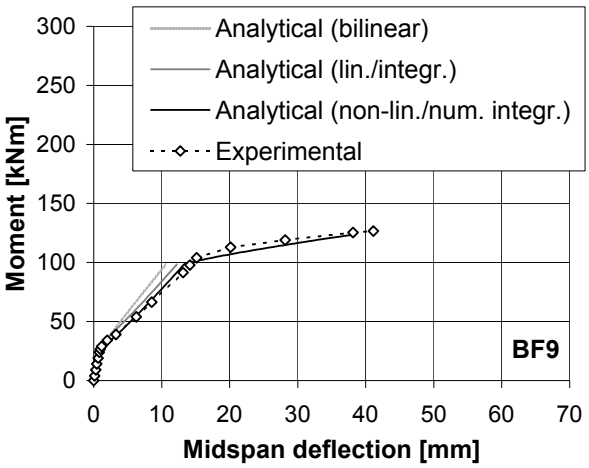

5 Cracking

The following figures give the measured mean and maximum crack width, compared to the calculated mean crack width. The analytical verification is performed according to Chapter 3, Section 4.4.

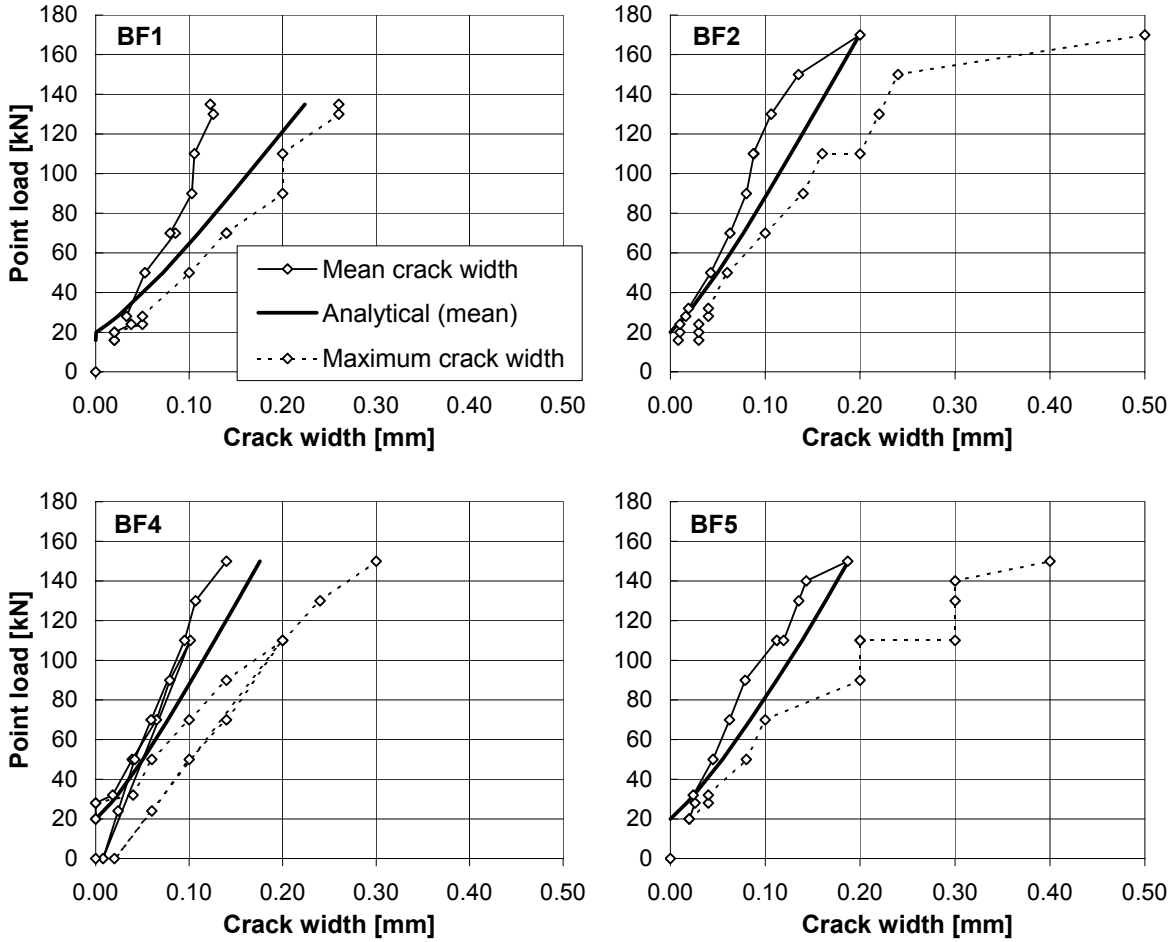

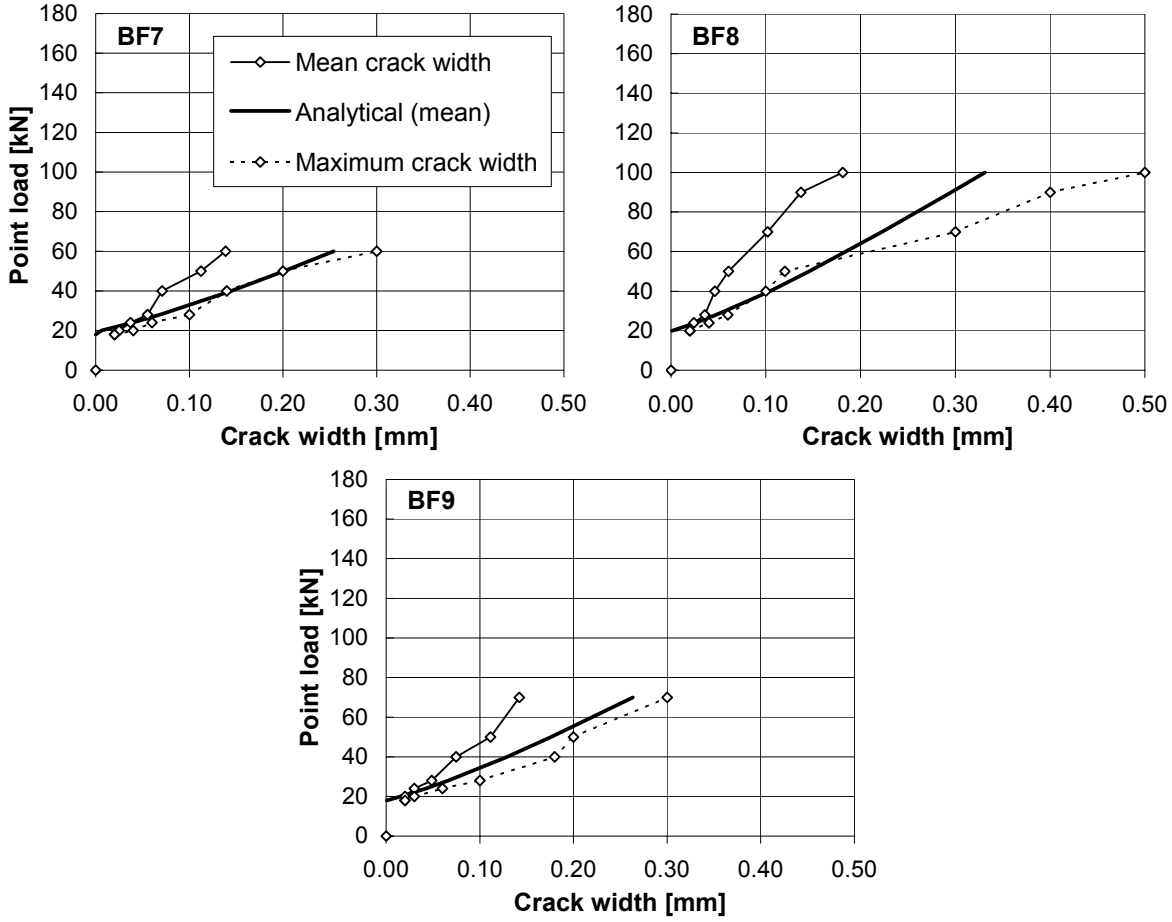

6 Strain and bond shear stress along the FRP EBR

In the following the strain and bond shear stress distribution along the length of the FRP is shown for beams BF3 and BF9 (for these beams various FRP strains were measured up to failure). The experimental strains are those recorded by mechanical deformeters (before yielding of the steel) and by strain gauges (up to failure). The analytical verification is performed according to Chapter 3, Section 4.2 (strains) and Section 4.5 (bond shear stresses).

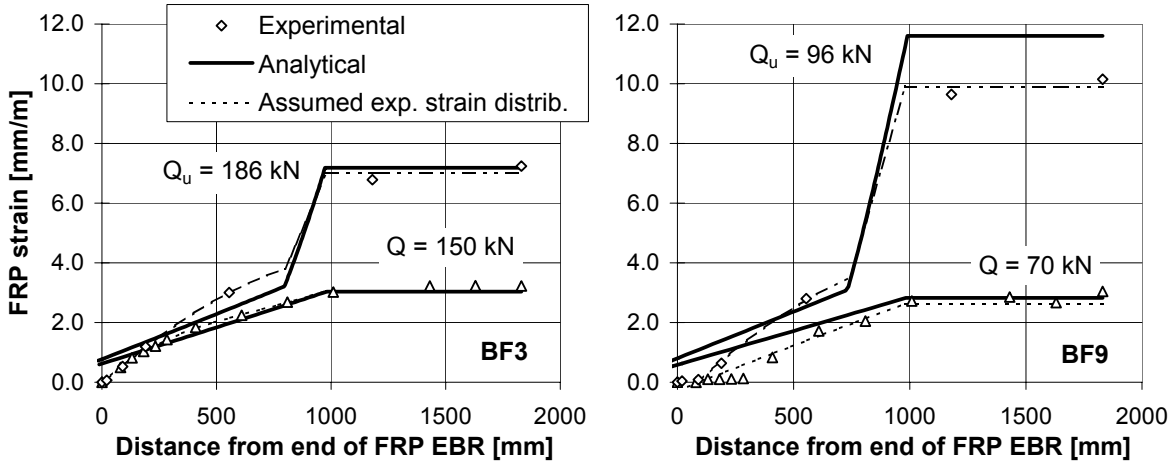

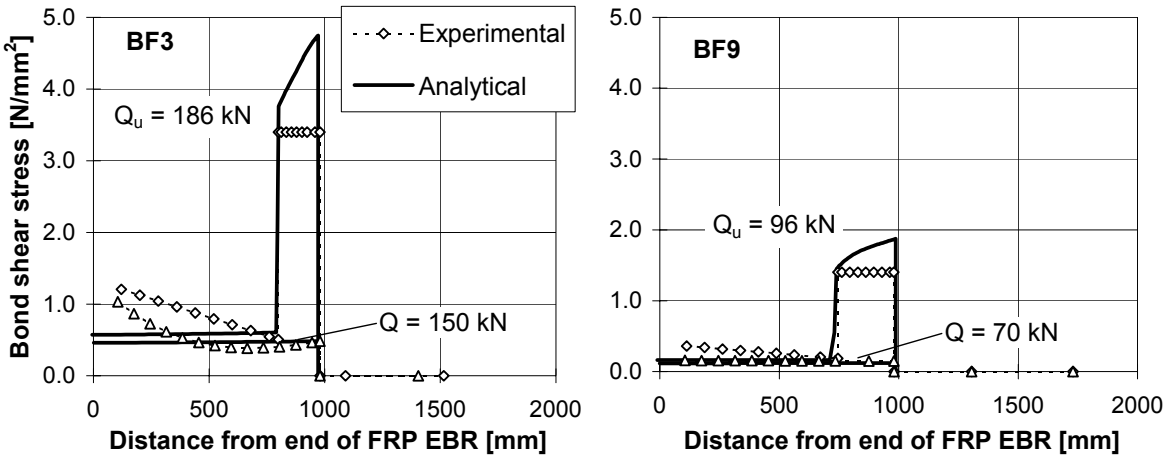

7 References

1. Deuring M. (1993), "Verstärken von Stahlbeton mit gespannten Faserverbund-werkstoffen" (in German), EMPA Bericht, No 224, Swiss Federal Laboratories for Materials Testing and Research, Dübendorf, Switzerland, 279 pp.
2. Kaiser H. (1989), "Bewehren von Stahlbeton mit kohlenstoffaserverstärkten Epoxidharzen" (in German), Doctoral thesis, Technical University of Zürich, Switzerland, 224 pp.

Appendix D
RC BEAMS STRENGTHENED IN SHEAR

1 Measured FRP strains

By means of strain gauges the FRP strain in the shear span of the strengthened beams was measured at different locations. In the following figures, the results of the strain measurements and the location of the strain gauges are shown.

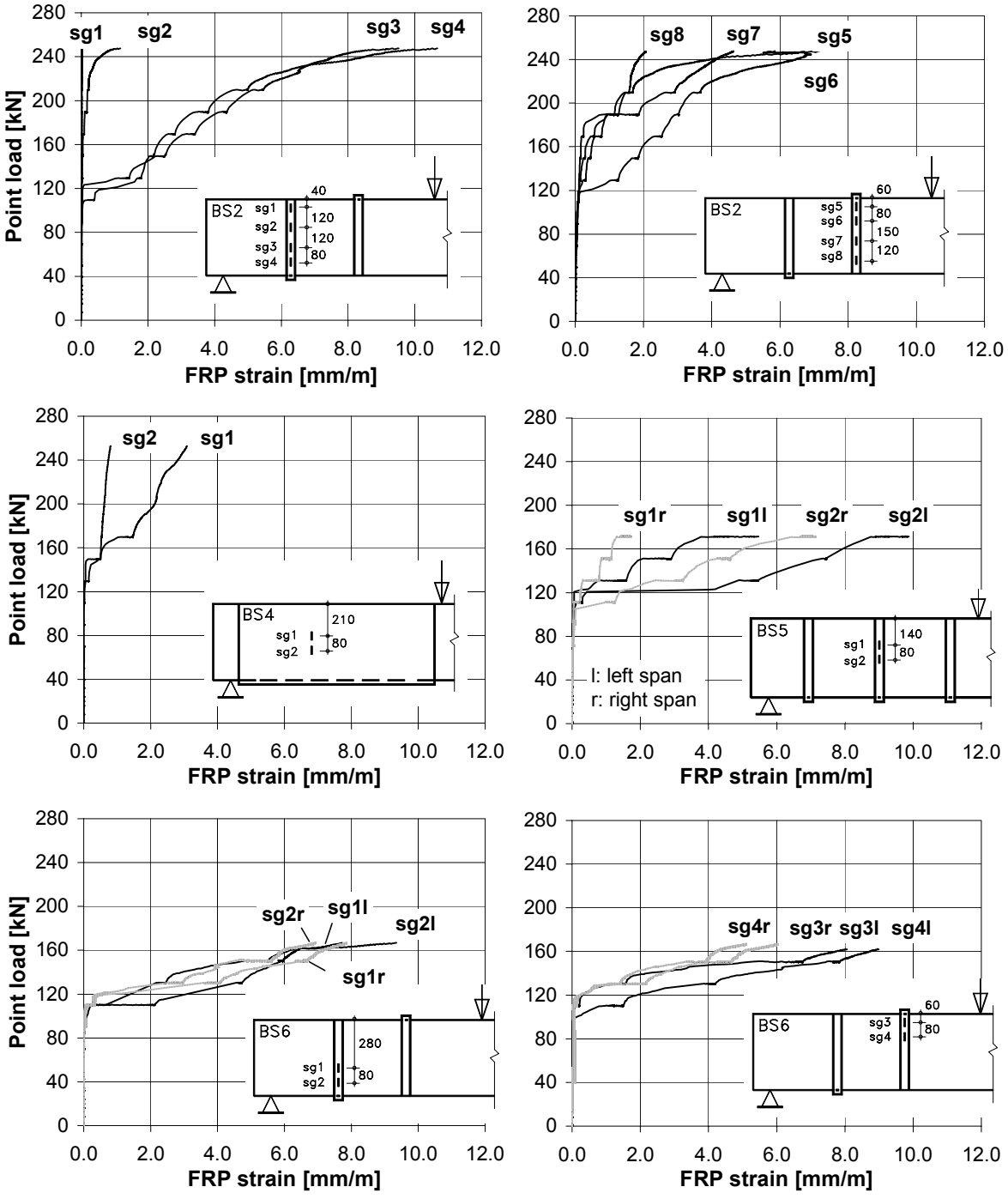

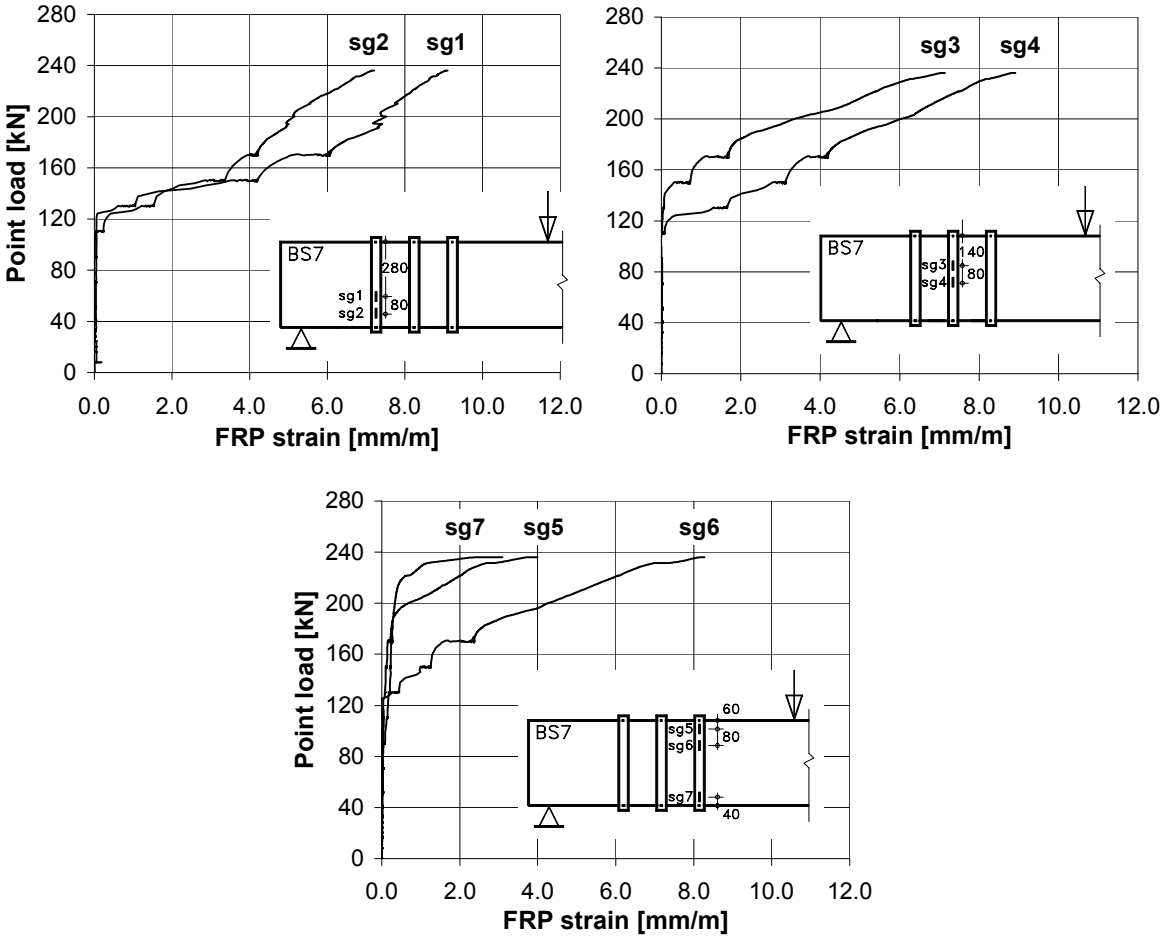

2 Experimental data base

No.	Desig-nation	FRP type	b_w [mm]	d [mm]	a/d [-]	f_{cm} [N/mm^2]	E_f [N/mm^2]	f_{fm} [N/mm^2]	ρ_f [%]	α_f [°]	V_f [kN]	$\varepsilon_{f,eff}$ [mm/m]
WRAPPED OR ANCHORED												
1	F(S-2)	CFRP	600	510	2.50	30.0	240000	3834	0.056	90	243.0	6.57
2	F(S-3)	CFRP	600	510	2.50	30.0	240000	3834	0.110	90	346.0	4.76
3	F(S-4)	CFRP	600	510	2.50	30.0	240000	3834	0.167	90	493.0	4.47
4	Um(CS1)	CFRP	300	257	2.96	40.5	244000	4280	0.074	90	87.0	6.94
5	Um(CS2)	CFRP	300	257	2.96	40.5	244000	4280	0.037	90	32.0	5.11
6	Um(CS3)	CFRP	150	272	2.94	44.8	244000	4280	0.047	90	52.0	12.35
7	Uj(3)	CFRP	100	170	-	24.0	230000	2650	0.194	90	33.8	4.95
8	A(CF045)	CFRP	200	340	3.53	24.8	230000	3480	0.026	90	35.0	9.56
9	A(CF064)	CFRP	200	340	3.53	24.9	230000	3480	0.045	90	61.0	9.63
10	A(CF097)	CFRP	200	340	3.53	25.2	230000	3480	0.077	90	106.0	9.78
11	A(CF131)	CFRP	200	340	3.53	25.4	230000	3480	0.110	90	157.0	10.14
12	A(CF243)	CFRP	200	340	3.53	25.6	230000	3480	0.220	90	206.0	6.65
13	Oh(BS12)	CFRP	180	360	-	-	230000	-	0.120	90	-	8.40
14	Oh(BS24)	CFRP	180	360	-	-	230000	-	0.240	90	-	6.20
15	Oh(BM06)	CFRP	180	360	-	-	230000	-	0.060	90	-	11.70

No.	Desig-nation	FRP type	b_w [mm]	d [mm]	a/d [-]	f_{cm} [N/mm^2]	E_f [N/mm^2]	f_{fm} [N/mm^2]	ρ_f [%]	α_f [°]	V_f [kN]	$\varepsilon_{f,eff}$ [mm/m]
16	Oh(BM12)	CFRP	180	360	-	-	230000	-	0.120	90	-	9.30
17	Oh(BM18)	CFRP	180	360	-	-	230000	-	0.180	90	-	7.80
18	Oh(BM24)	CFRP	180	360	-	-	230000	-	0.240	90	-	6.00
19	Oh(BL06)	CFRP	180	360	-	-	230000	-	0.060	90	-	8.40
20	Oh(BL12)	CFRP	180	360	-	-	230000	-	0.120	90	-	7.80
21	Oh(BLW06)	CFRP	180	360	-	-	230000	-	0.060	90	-	8.40
22	Oh(BLW12)	CFRP	180	360	-	-	230000	-	0.120	90	-	6.90
23	Oh(BLW24)	CFRP	180	360	-	-	230000	-	0.240	90	-	4.60
24	Oh(2)	CFRP	400	340	-	-	230000	-	0.029	90	-	12.00
25	Oh(3)	CFRP	400	340	-	-	230000	-	0.058	90	-	10.30
26	SK(S-3)	CFRP	300	416	2.24	37.6	241000	4350	0.074	90	255.0	12.73
27	SK(S-4)	CFRP	300	416	2.24	37.6	241000	4350	0.074	90	308.0	15.38
28	SK(M-3)	CFRP	300	420	2.24	18.1	240000	3900	0.074	90	89.0	4.42
29	Ma(BS2)	CFRP	200	407	3.07	33.0	281000	3500	0.014	90	41.2	14.42
30	Ma(BS6)	CFRP	200	407	3.07	33.0	281000	3500	0.014	90	30.1	10.54
31	Ma(BS7)	CFRP	200	407	3.07	34.7	281000	3500	0.028	90	98.9	17.31
32	On(SB2)	CFRP	300	260	1.54	24.3	248000	3430	0.037	81	22.0	2.97
33	On(SB3)	CFRP	300	260	1.54	24.3	248000	3430	0.074	90	113.0	8.77
34	On(SC2)	CFRP	600	540	2.20	25.2	230000	2803	0.037	90	123.0	4.96
35	On(SC3)	CFRP	600	540	2.20	25.2	230000	2803	0.073	90	258.0	5.27
36	On(SC4)	CFRP	600	540	2.20	25.2	230000	2803	0.185	90	263.0	2.12
37	Mi(1/5Z-3)	CFRP	125	165	3.00	35.1	230000	3480	0.040	90	18.8	10.98
38	Mi(1/2Z-3)	CFRP	125	165	3.00	32.4	230000	3480	0.090	90	29.5	7.68
39	Mi(1/2Z5-2)	CFRP	125	165	2.00	39.1	230000	3480	0.090	90	34.6	8.99
40	A(AF060)	AFRP	200	340	3.53	25.8	87000	2450	0.059	90	36.0	11.46
41	A(AF090)	AFRP	200	340	3.53	25.9	87000	2450	0.100	90	58.0	10.89
42	A(AF120)	AFRP	200	340	3.53	26.1	87000	2450	0.140	90	111.0	14.89
43	Um(AS1)	AFRP	150	272	2.94	43.0	73000	2700	0.059	90	27.5	17.48
44	Um(AS2)	AFRP	150	272	2.94	43.0	73000	2700	0.029	90	26.0	33.10
45	Um(AS3)	AFRP	150	272	3.00	44.8	73000	2700	0.117	90	50.0	15.90
46	Um(AB1)	AFRP	150	253	3.00	41.9	73000	2700	0.059	90	63.5	43.39
47	Um(AB2)	AFRP	300	253	3.00	45.6	73000	2700	0.029	90	46.0	31.48
48	Um(AB3)	AFRP	300	253	3.00	41.9	73000	2700	0.059	90	82.0	28.01
49	Um(AB4)	AFRP	300	253	3.00	41.9	73000	2700	0.059	90	97.0	33.14
50	Um(AB5)	AFRP	300	253	3.00	42.7	73000	2700	0.096	90	127.0	26.53
51	Um(AB8)	AFRP	600	253	3.00	43.5	73000	2700	0.048	90	140.0	29.24
52	Um(AB9)	AFRP	450	399	3.00	39.9	73000	2700	0.064	90	163.0	21.59
53	Um(AB10)	AFRP	550	499	3.00	39.9	73000	2700	0.052	90	294.0	31.12
54	Um(AB11)	AFRP	550	499	3.00	40.6	73000	2700	0.105	90	387.0	20.50
U-SHAPE												
1	ST(S5)	CFRP	200	260	2.69	39.7	230000	3480	0.110	90	106.1	8.96
2	SO(2)	CFRP	150	240	2.50	35.7	230000	3480	0.146	90	24.0	2.21
3	Ma(BS5)	CFRP	200	407	3.07	33.0	281000	3500	0.014	90	33.4	11.69
SIDES ONLY												
1	ST(S4)	CFRP	200	260	2.69	37.5	230000	3480	0.110	90	64.2	5.42

No.	Desig-nation	FRP type	b_w [mm]	d [mm]	a/d [-]	f_{cm} [N/mm^2]	E_f [N/mm^2]	f_{fm} [N/mm^2]	ρ_f [%]	α_f [°]	V_f [kN]	$\varepsilon_{f,eff}$ [mm/m]
2	Uj(5)	CFRP	100	170	-	24.0	230000	2650	0.194	90	20.1	2.94
3	Uj(6)	CFRP	100	170	-	27.0	230000	2650	0.194	45	32.3	3.35
4	Uj(7)	CFRP	100	170	-	27.0	230000	2650	0.390	90	20.1	1.46
5	T(S1a)	CFRP	70	100	3.20	30.0	235000	3300	0.220	90	13.6	4.16
6	T(S1b)	CFRP	70	100	3.20	30.0	235000	3300	0.220	90	11.3	3.45
7	T(S2a)	CFRP	70	100	3.20	30.0	235000	3300	0.330	90	15.9	3.24
8	T(S2b)	CFRP	70	100	3.20	30.0	235000	3300	0.330	90	12.9	2.64
9	T(S3a)	CFRP	70	100	3.20	30.0	235000	3300	0.440	90	13.2	2.03
10	T(S3b)	CFRP	70	100	3.20	30.0	235000	3300	0.440	90	10.6	1.62
11	T(S1-45)	CFRP	70	100	3.20	30.0	235000	3300	0.220	45	14.1	3.05
12	T(S2-45)	CFRP	70	100	3.20	30.0	235000	3300	0.330	45	15.5	2.24
13	T(S3-45)	CFRP	70	100	3.20	30.0	235000	3300	0.440	45	12.2	1.32

- : value not available; f_{cm} is assumed 33 N/mm^2; f_{fm} is assumed 3480 N/mm^2; a/d is assumed 3.0

A: Araki et al [1], F: Funakawa et al. [2], Ma: Matthys (Chapter 5, Section 3), Mi: Miyauchi et al. [3], Oh: Ohuchi et al. [4], On: Ono et al. [5], SK: Sato et al. [6], ST: Sato et al [7], SO: Sato et al. [8], T: Triantafillou [9], Uj: Uji [10], Um: Umezu et al. [11].

3 References

1. Araki N., Matsuzaki Y., Nakano K., Kataoka T., Fukuyama H. (1997), "Shear capacity of retrofitted RC members with continuous fiber sheets", Proceedings 3rd. Int. Symp. on Non-Metallic (FRP) Reinforcement for Concrete Structures, Japan Concrete Institute, Sapporo, Japan, Vol. 1, pp. 515-522.
2. Funakawa I., Shimono K., Watanabe T., Asada S., Ushijima S. (1997), "Experimental study on shear strengthening with continuous fiber reinforcement sheet and methyl methacrylate resin", Proceedings 3rd. Int. Symp. on Non-Metallic (FRP) Reinforcement for Concrete Structures, Japan Concrete Institute, Sapporo, Japan, Vol. 1, pp. 475-482.
3. Miyauchi K., Inoue S., Nishibayashi S., Tanaka Y. (1997), "Shear behaviour of reinforced concrete beam strengthened with CFRP sheet", Transactions of the Japan Concrete Institute, JCI, Japan, Vol. 19, pp. 97-104.
4. Ohuchi H., Ohno S., Katsumata H., Kobatake Y., Meta T., Yamagata K., Inokuma Y., Ogata N. (1994), "Seismic strengthening design technique for existing bridge columns with CFRP", in Seismic Design and Retrofitting of Reinforced Concrete Bridges, Ed. R. Park, pp. 495-514.
5. Ono K., Matsumura M., Sakanishi S., Miyata K. (1997), "Strength improvement of RC bridge piers by carbon fiber sheet", Proceedings 3rd. Int. Symp. on Non-Metallic (FRP) Reinforcement for Concrete Structures, Japan Concrete Institute, Sapporo, Japan, Vol. 1, pp. 563-570.
6. Sato Y., Katsumata H., Kobatake Y. (1997), "Shear strengthening of existing reinforced concrete beams by CFRP sheet", Proceedings 3rd. Int. Symp. on Non-Metallic (FRP)

Reinforcement for Concrete Structures, Japan Concrete Institute, Sapporo, Japan, Vol. 1, pp. 507-514.
7. Sato Y., Ueda T., Kakuta Y., Tanaka T. (1996), "Shear reinforcing effect of carbon fibre sheet attached to side of reinforced concrete beams", Proceedings 2nd. Int. Conf. on Advanced Composite Materials in Bridges and Structures, Ed. M. El-Badry, The Canadian Society for Civil Engineering, Montréal, Québec, Canada, pp. 621-627.
8. Sato Y., Ueda T., Kakuta Y., Ono S. (1997), "Ultimate shear capacity of reinforced concrete beams with carbon fiber sheets", Proceedings 3rd. Int. Symp. on Non-Metallic (FRP) Reinforcement for Concrete Structures, Japan Concrete Institute, Sapporo, Japan, Vol. 1, pp. 499-506.
9. Triantafillou T.C. (1997), "Shear strengthening of concrete members using composites", Proceedings 3rd. Int. Symp. on Non-Metallic (FRP) Reinforcement for Concrete Structures, Japan Concrete Institute, Sapporo, Japan, Vol. 1, pp. 523-530.
10. Uji K. (1992), "Improving shear capacity of existing reinforced concrete members by applying carbon fiber sheet", Japan Concrete Institute, No. 14, pp. 253-266.
11. Umezu K., Fujita M., Nakai H., Tamaki K. (1997), "Shear behaviour of RC beams with aramid fiber sheet", Proceedings 3rd. Int. Symp. on Non-Metallic (FRP) Reinforcement for Concrete Structures, Japan Concrete Institute, Sapporo, Japan, Vol. 1, pp. 491-498.

Appendix E
TENSION STIFFENING AND CRACKING BEHAVIOUR

1 Measured load-strain curves

In the following figures the recorded load-strain curves are shown. Two curves show the mean strain measured by each time five strain stirrups located on two adjacent side faces (Fig. 5-1). A third curve gives the mean value of the ten strain stirrups.

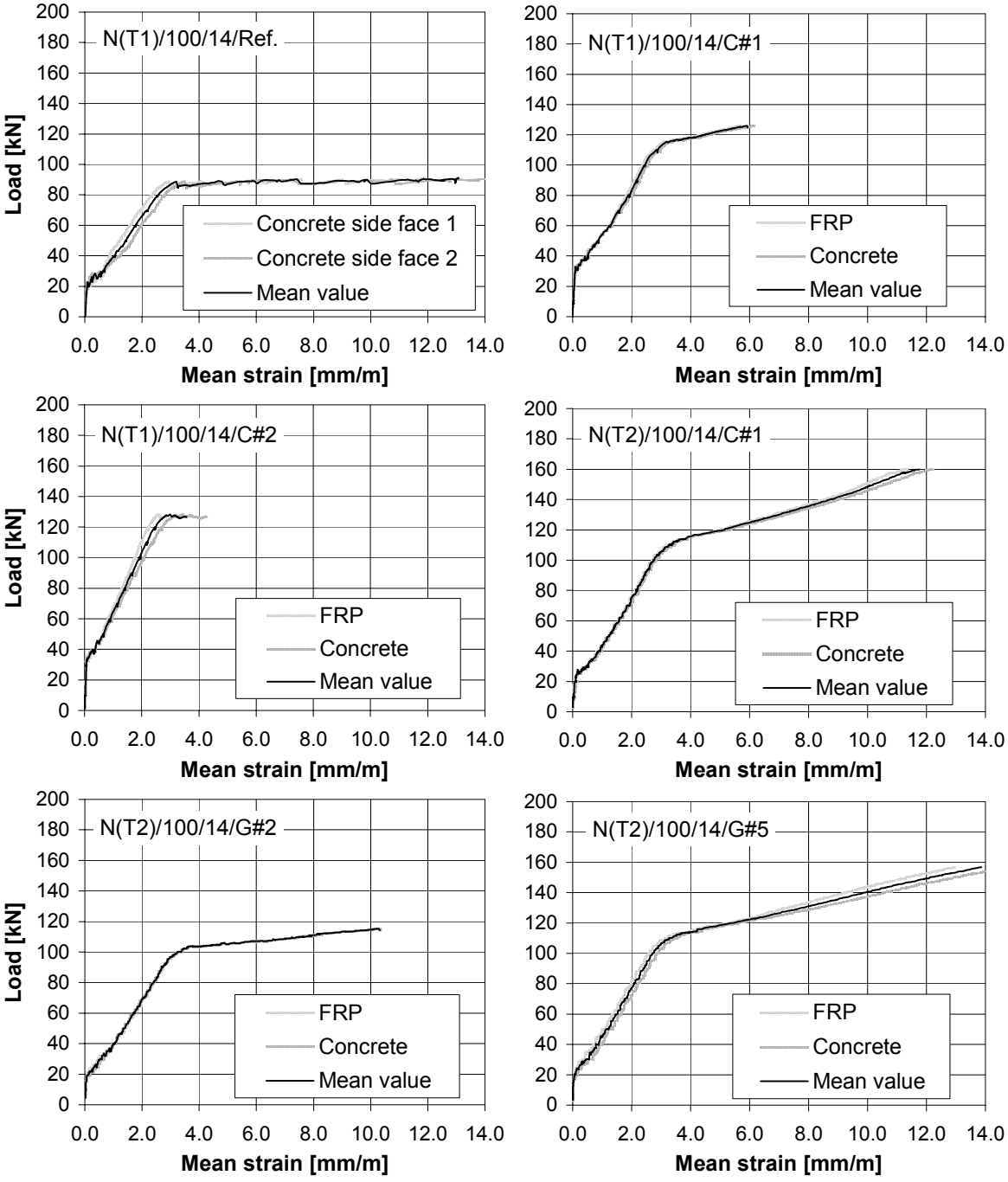

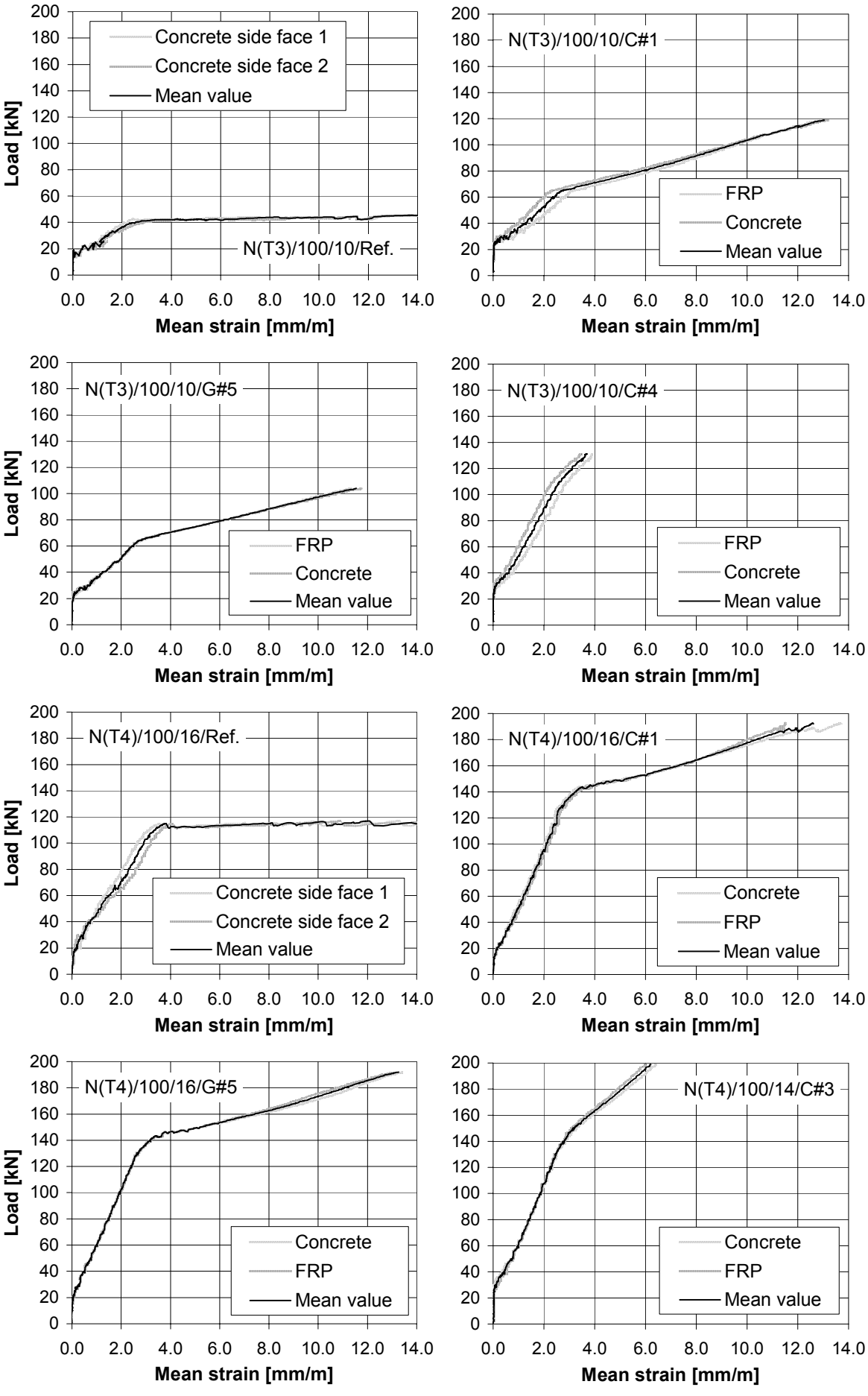
Concrete side face 1
Concrete side face 2
Mean value
N(T3)/100/10/Ref.
N(T3)/100/10/C#1
FRP
Concrete
Mean value
N(T3)/100/10/G#5
N(T3)/100/10/C#4
N(T4)/100/16/Ref.
N(T4)/100/16/C#1
N(T4)/100/16/G#5
N(T4)/100/14/C#3
Load [kN]
Mean strain [mm/m]

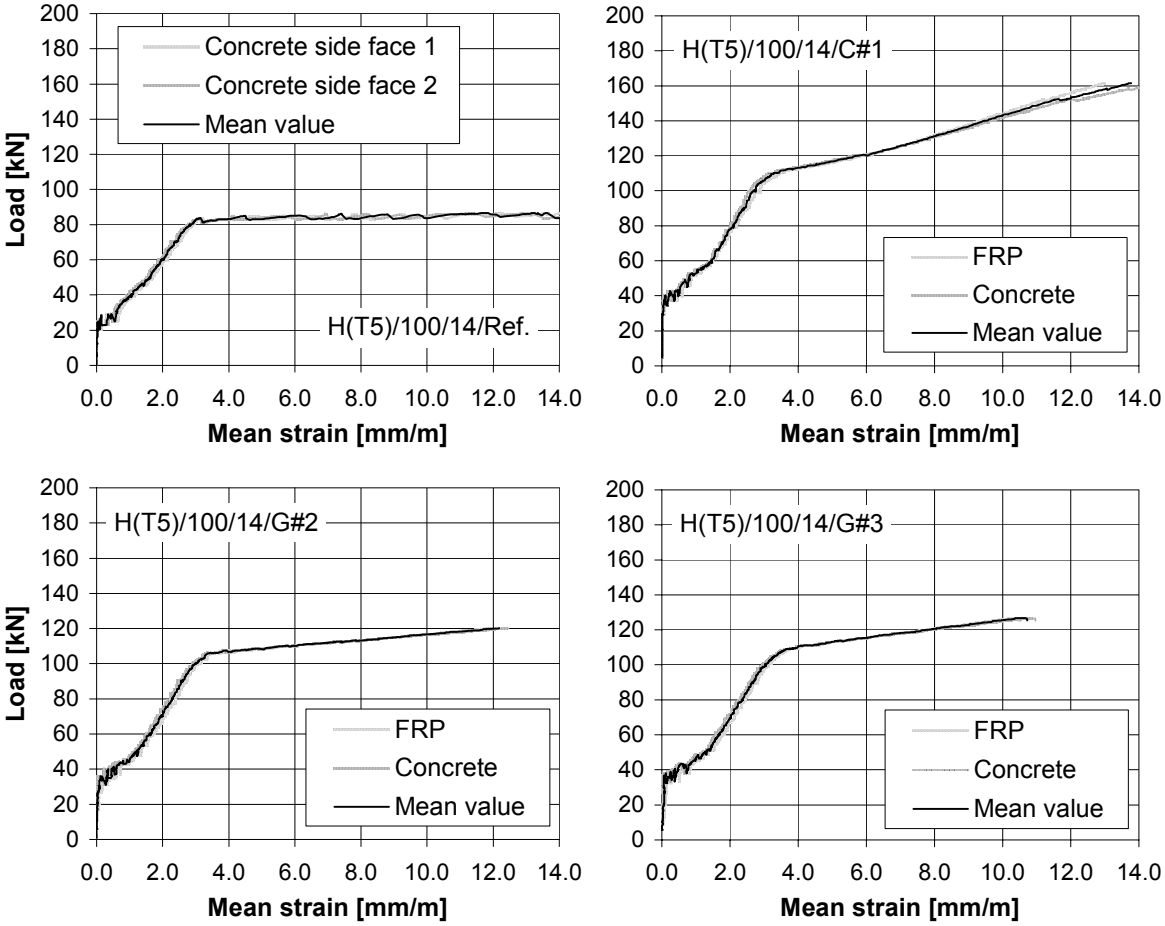

2 Crack pattern at ultimate

After testing the (strengthened) tensile members, the following crack patterns were recorded.

N(T1)/100/14/Ref. (N_u = 87 kN)

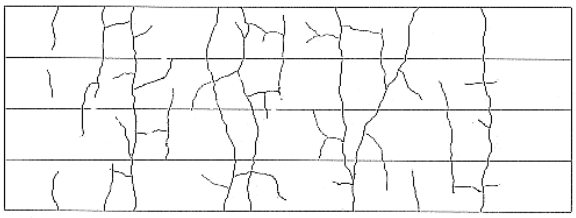

N(T1)/100/14/C#1 (N_u = 125 kN)

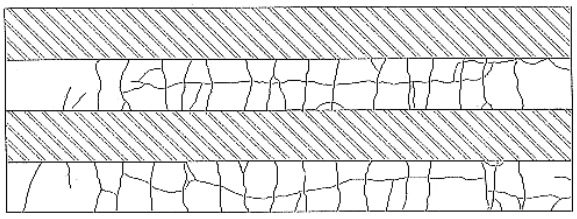

N(T1)/100/14/C#2 (N_u = 128 kN)

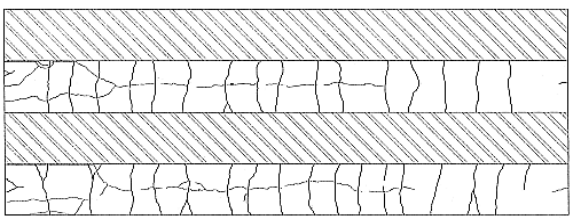

N(T2)/100/14/C#1 (N_u = 160 kN)

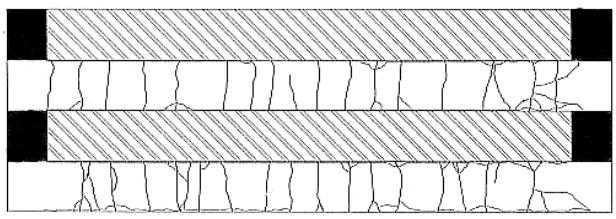

N(T2)/100/14/G#2 (N_u = 115 kN)

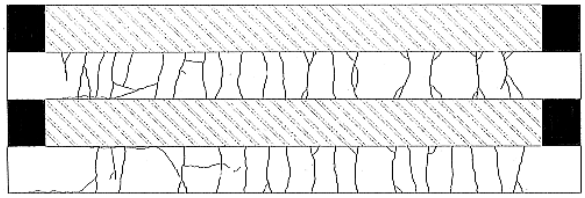

N(T2)/100/14/G#5 (N_u = 157 kN)

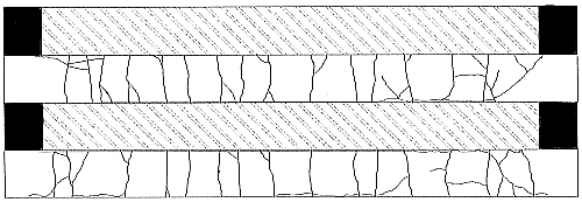

N(T3)/100/10/Ref. (N_u = 43 kN)

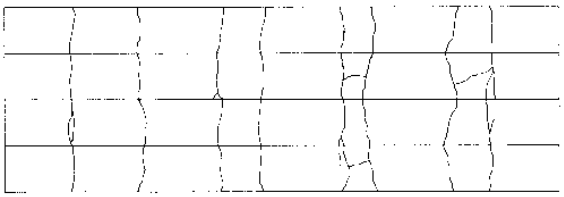

N(T3)/100/10/C#1 (N_u = 119 kN)

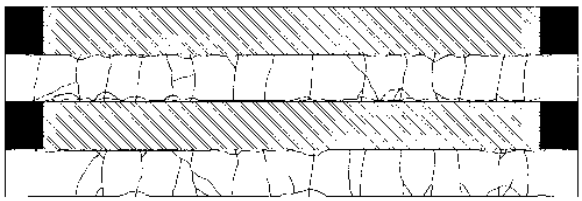

N(T3)/100/10/G#5 (N_u = 104 kN)

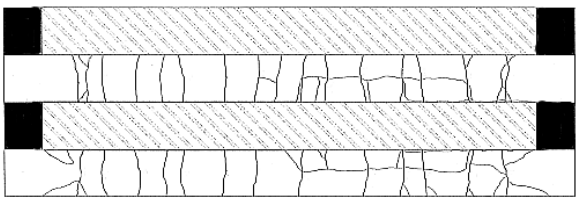

N(T3)/100/10/C#4 (N_u = 131 kN)

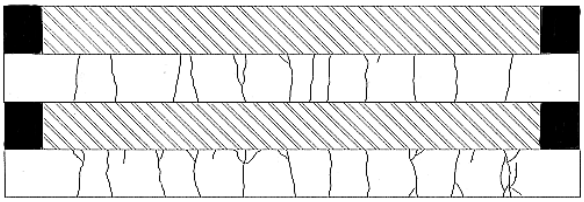

N(T4)/100/16/Ref. (N_u = 118 kN)

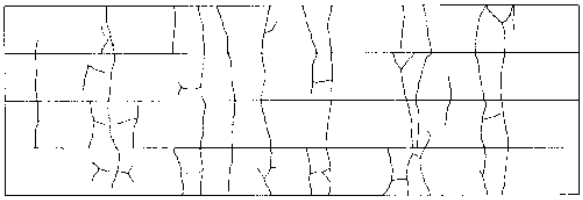

N(T4)/100/16/C#1 (N_u = 193 kN)

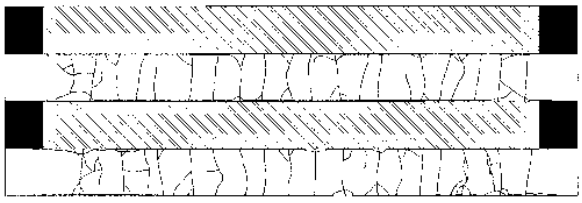

N(T4)/100/16/G#5 (N_u = 192 kN)

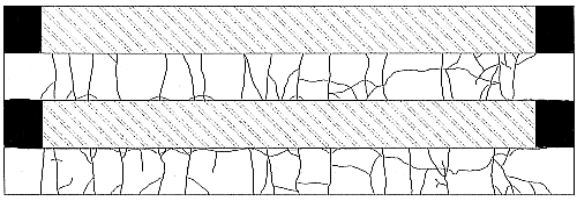

N(T4)/100/14/C#3 (N_u = 199 kN)

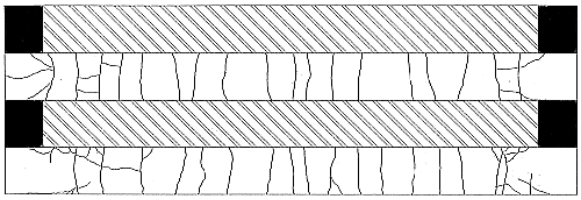

H(T5)/100/14/Ref. (N_u = 84 kN)

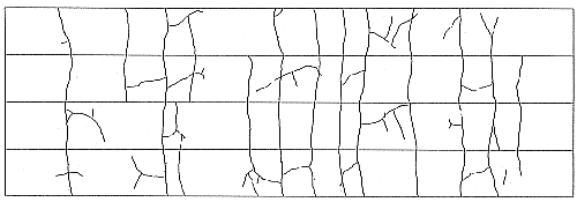

H(T5)/100/14/C#1 (N_u = 161 kN)

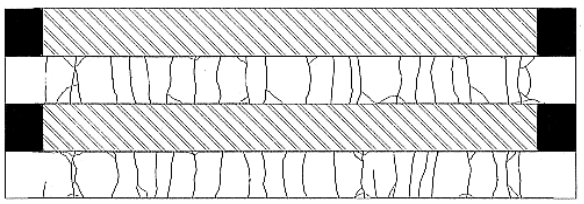

H(T5)/100/14/G#2 (N_u = 120 kN)

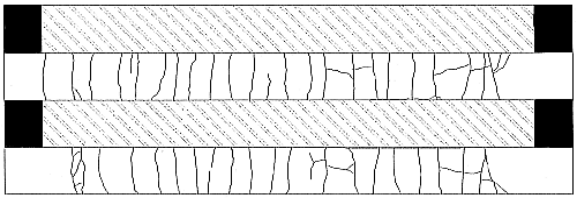

H(T5)/100/14/G#3 (N_u = 126 kN)

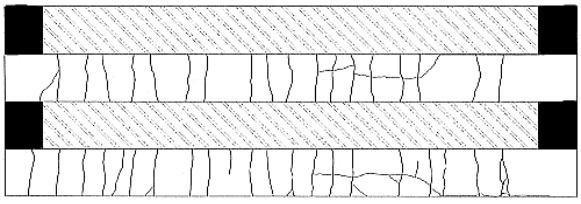

3 Analytical verification of the load-strain behaviour

The measured and calculated mean strain before post-yielding are compared in the following figures. The analytical verification has be performed according to Chapter 5, Section 4.2.

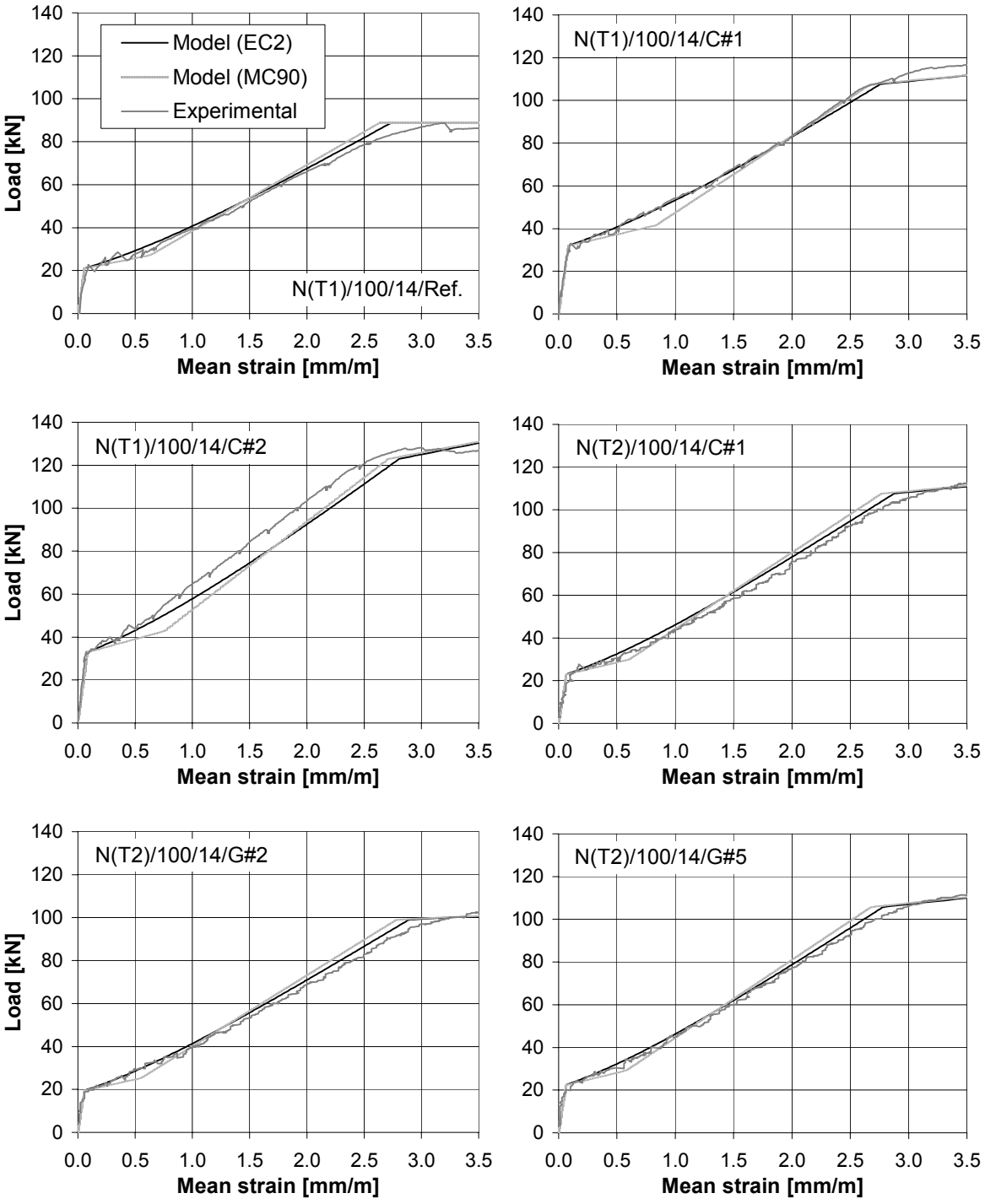

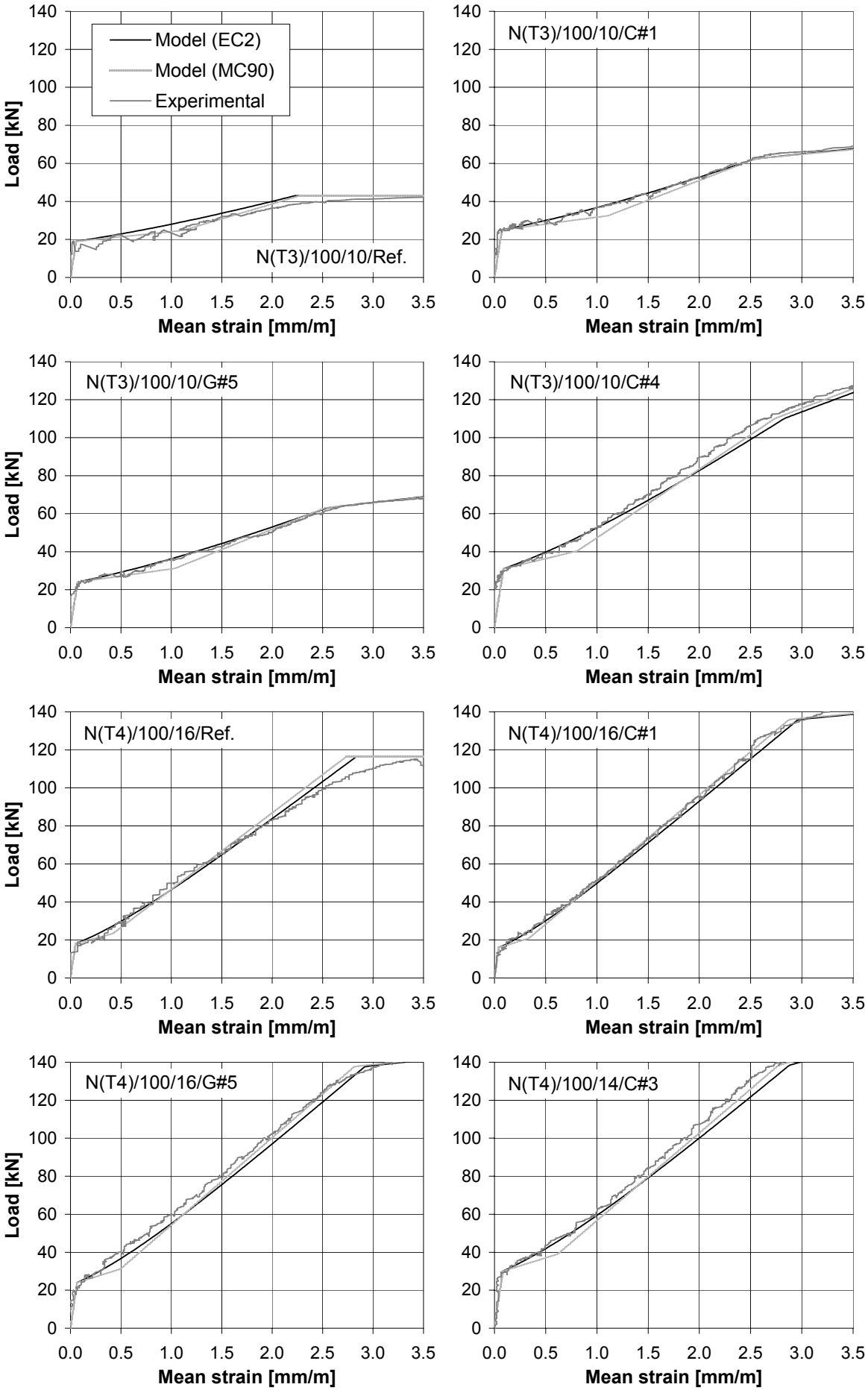
Model (EC2)
Model (MC90)
Experimental
N(T3)/100/10/Ref.
N(T3)/100/10/C#1
N(T3)/100/10/G#5
N(T3)/100/10/C#4
N(T4)/100/16/Ref.
N(T4)/100/16/C#1
N(T4)/100/16/G#5
N(T4)/100/14/C#3
Load [kN]
Mean strain [mm/m]

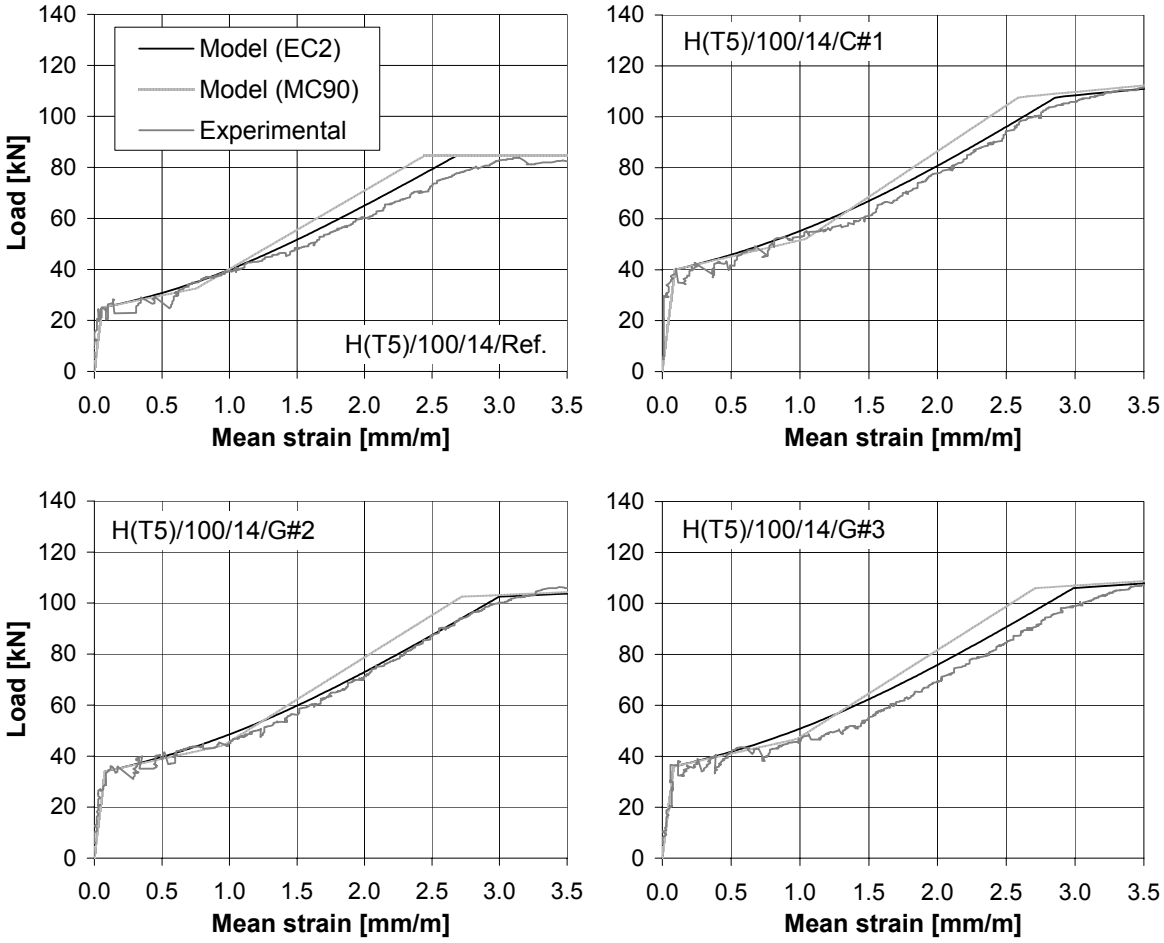

4 Analytical verification of the crack width

Based on Chapter 5, Section 4.3, the measured mean crack width has been verified analytically. Results of this calculation are shown in the following figures. The experimental crack width is the mean value of the crack widths measured between the point loads at the level of the internal steel reinforcement.

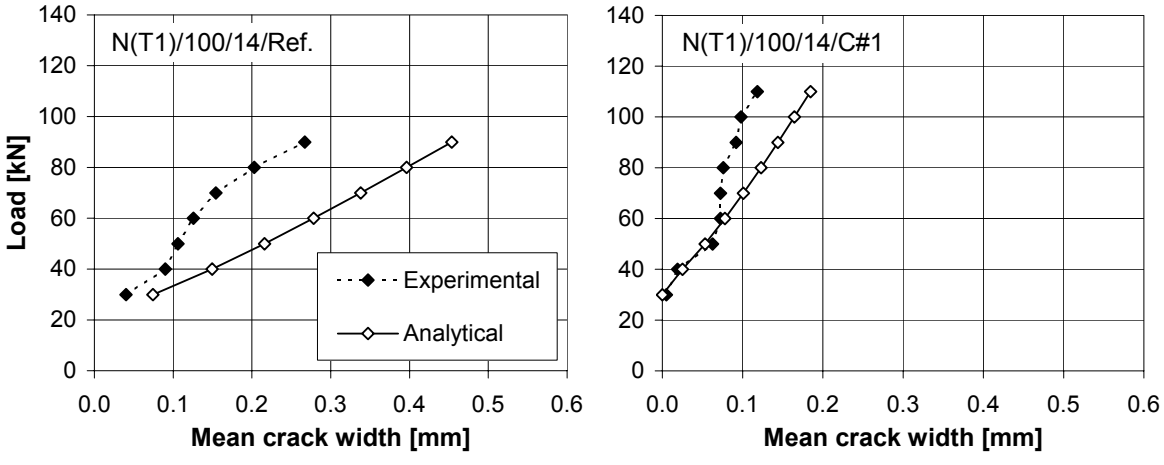

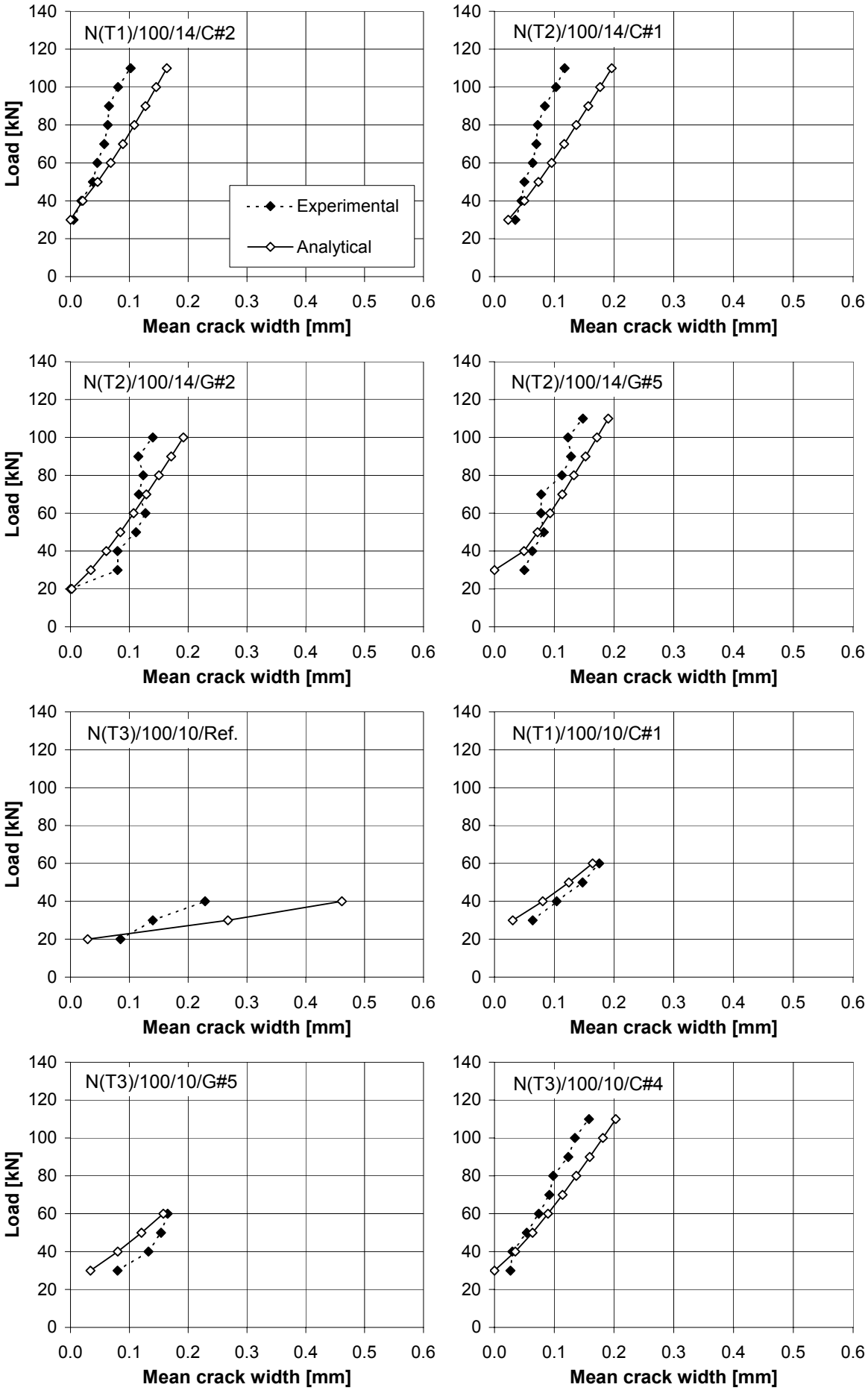
N(T1)/100/14/C#2
N(T2)/100/14/C#1
N(T2)/100/14/G#2
N(T2)/100/14/G#5
N(T3)/100/10/Ref.
N(T1)/100/10/C#1
N(T3)/100/10/G#5
N(T3)/100/10/C#4
Experimental
Analytical
Load [kN]
Mean crack width [mm]
0
20
40
60
80
100
120
140
0.0
0.1
0.2
0.3
0.4
0.5
0.6

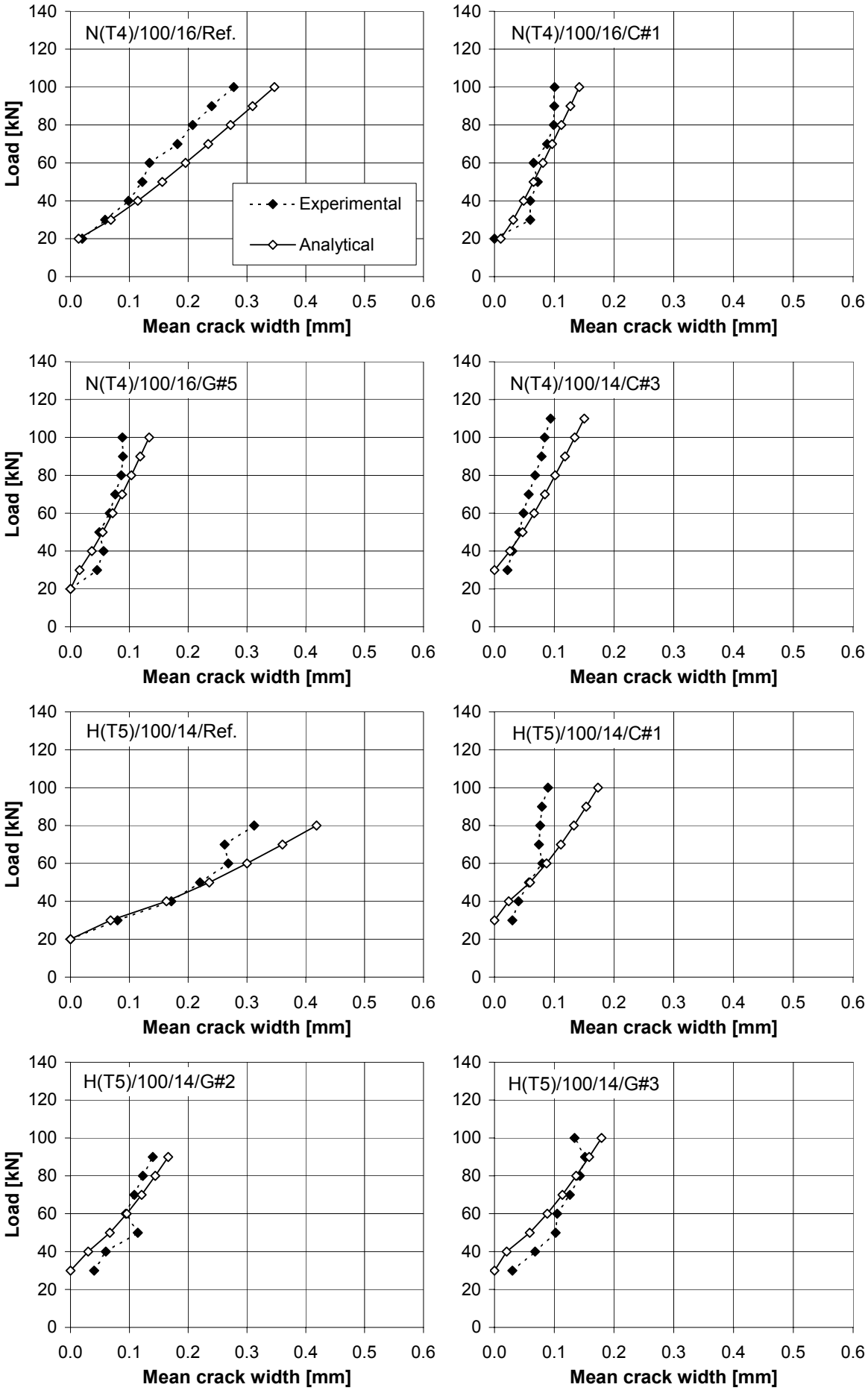
N(T4)/100/16/Ref.
N(T4)/100/16/C#1
N(T4)/100/16/G#5
N(T4)/100/14/C#3
H(T5)/100/14/Ref.
H(T5)/100/14/C#1
H(T5)/100/14/G#2
H(T5)/100/14/G#3
Experimental
Analytical
Load [kN]
Mean crack width [mm]
0
20
40
60
80
100
120
140
0.0
0.1
0.2
0.3
0.4
0.5
0.6

Appendix F
FRP CONFINED CONCRETE

1 Stress-strain behaviour of FRP confined concrete

1.1 Model by Spoelstra and Monti [1]

1.1.1 Approach and background of the model

This model uses an incremental-iterative approach to calculate the stress-strain behaviour of the FRP confined concrete. The incremental approach follows from the fact that reference is made to the axial stress-strain model by Mander et al. [2], which assumes a constant confining pressure and hence needs to be applied repeatedly, each time increasing the confining pressure. As the increase in confining pressure depends on the increase in circumferential strain, the axial and the circumferential strain response need to be linked. For this aspect of the modelling, reference is made to the volumetric strain relations of plain concrete by Pantazopoulou and Mills [3]. The resulting calculation scheme can only be solved by iteration. The Mander model used for the incremental approach, has been originally developed for concrete confined by means of steel stirrups [2]. This often applied steel confinement model is based on [4,5] and has been extensively tested against experimental data (although not for FRP).

Hence, the incremental-iterative approach by Spoelstra and Monti offers a combination of existing models, originally not developed for FRP confinement, but applied in such a way that prediction of the stress-strain response of FRP confined concrete becomes possible.

1.1.2 Equations and calculation procedure

Making reference to the Mander model [2], the axial stress-strain relationship σ_c-ε_c is given as:

$$\sigma_c = \frac{f_{cc}\ x\ r}{r - 1 + x^r} \tag{F-1}$$

where,

$$x = \frac{\varepsilon_c}{\varepsilon_{cc1}} \qquad \varepsilon_{cc1} = \varepsilon_{c1}\left(1 + 5\left(\frac{f_{cc}}{f_{co}} - 1\right)\right) \qquad r = \frac{E_c}{E_c - E_{sec1}} \qquad E_{sec1} = \frac{f_{cc}}{\varepsilon_{cc1}} \tag{F-2}$$

with, f_{co} and f_{cc} the unconfined and confined concrete peak strength, ε_{c1} and ε_{cc1} the compressive (axial) strain corresponding to these peak strengths (generally ε_{c1} is assumed as 2 mm/m) and E_c the tangent modulus of elasticity of the concrete at the origin. The confined concrete peak strength $f_{cc}(\sigma_\ell)$ for a given lateral confining pressure σ_ℓ is obtained as [2]:

$$\frac{f_{cc}(\sigma_\ell)}{f_{co}} = 2.254\sqrt{1+7.94\frac{\sigma_\ell}{f_{co}}} - 2\frac{\sigma_\ell}{f_{co}} - 1.254 \tag{F-3}$$

Based on the constitutive model for unconfined concrete by [3] and taking the area strain (which, assuming radial symmetry, only depends on the circumferential strain) as measure of internal damage of the concrete,

$$\sigma_c = E_{sec}\varepsilon_c \quad \text{with} \quad E_{sec} = \frac{E_c}{1+2\beta\varepsilon_{c\ell}} \tag{F-4}$$

the following relationship for the circumferential strain $\varepsilon_{c\ell}(\varepsilon_c, \sigma_\ell)$ is derived as a function of the axial strain ε_c and lateral confining stress σ_ℓ:

$$\varepsilon_{c\ell}(\varepsilon_c, \sigma_\ell) = \frac{E_c\,\varepsilon_c - \sigma_c(\varepsilon_c, \sigma_\ell)}{2\beta\,\sigma_c(\varepsilon_c, \sigma_\ell)} \tag{F-5}$$

with, β a constant which depends on the concrete properties. This constant may be obtained according to [1] or simplified as:

$$\beta = \frac{E_c}{f_{co}} - \frac{1}{\varepsilon_{c1}} \tag{F-6}$$

Whereas the above equations apply for a uniform lateral confining stress σ_ℓ (circular cross-section), the model can be extended towards square and rectangular cross-sections for which $\sigma_{\ell x} \geq \sigma_{\ell y}$. In this case, in stead of using Eq. (F-3), the confined concrete peak strength $f_{cc}(\sigma_\ell)$ is obtained as [6]:

$$\frac{f_{cc}(\sigma_\ell)}{f_{co}} = \alpha_1(\sigma_{\ell x})\alpha_2(\sigma_{\ell x}, \sigma_{\ell y}) \tag{F-7}$$

where,

$$\alpha_1(\sigma_{\ell x}) = 2.254\sqrt{1+7.94\frac{\sigma_{\ell x}}{f_{co}}} - 2\frac{\sigma_{\ell x}}{f_{co}} - 1.254 \tag{F-8}$$

$$\alpha_2(\sigma_{\ell x}, \sigma_{\ell y}) = 1 - \left(0.6\left(\frac{\sigma_{\ell y}}{\sigma_{\ell x}}\right)^2 - 1.4\frac{\sigma_{\ell y}}{\sigma_{\ell x}} + 0.8\right)\sqrt{\frac{\sigma_{\ell x}}{f_{co}}} \tag{F-9}$$

Based on the Eqs. (F-1) till (F-9) the stress-strain response of the confined concrete is calculated based on the following incremental-iterative procedure. The calculation is performed as a function of the axial compressive strain ε_c:

- Impose stepwise the axial strain ε_c, so that the complete σ_c-ε_c curve is covered.
- Given ε_c, assume or update a value for the lateral confining stress σ_ℓ, so that the confined concrete peak strength $f_{cc}(\sigma_\ell)$, the current axial stress $\sigma_c(\varepsilon_c, \sigma_\ell)$ and the circumferential strain $\varepsilon_{c\ell}(\varepsilon_c, \sigma_\ell)$ can be calculated from Eqs. (F-3), (F-1) and (F-5) respectively. Once $\varepsilon_{c\ell}$ is calculated, a new estimate of the confining stress σ_ℓ is obtained as (Chapter 6, Section 4.2):

$$\sigma_\ell = \frac{1}{2} k_e \rho_f E_f \varepsilon_{f=c\ell} \tag{F-10}$$

where, k_e is a effectiveness factor and ρ_f is the volumetric ratio of the FRP wrapping reinforcement, as defined in Chapter 6, Section 4.2. Compare this value with the assumed one and recalculate until σ_ℓ is converging to a single value.

– This iterative procedure, which converges in a few steps, is to be solved for each value of ε_c imposed. The calculation procedure stops when $\varepsilon_{c\ell}$ reaches the effective failure strain of the FRP (Chapter 6, Section 4.4.3).

1.2 Model by Toutanji [7]

1.2.1 Approach and background of the model

Similar to the model by Spoelstra and Monti, also for this model an incremental approach is followed to deal with the increasing confining action exerted by the FRP. As illustrated in Fig. F-1, the model considers two regions. In a first region (I), assumed for a circumferential strain $\varepsilon_{c\ell} \leq 2$ mm/m, the behaviour is similar to that of plain concrete, since the lateral expansion of the concrete is small. For this region, the stress-strain response is modelled based on [8], whereas the model parameters follow from the boundary conditions with the second region (II). In this second region ($\varepsilon_{c\ell} > 2$ mm/m), the FRP confining reinforcement is fully activated, so that the response is mainly dependent on the stiffness of the FRP. The stress-strain relationship of this region is based on the steel confined model by [9], however with the model coefficients experimentally calibrated with respect to FRP confined concrete. The model can be solved without iteration.

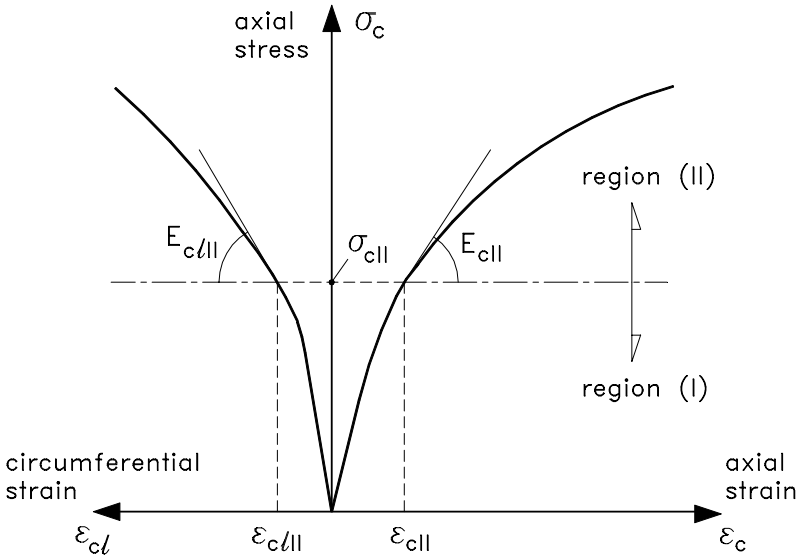

Fig. F-1 *Stress-strain model proposed by Toutanji [7]*

1.2.2 Equations and calculation procedure

Based on [8], the stress-strain response of the initial region is model as:

$$\sigma_c = \frac{E_i \varepsilon_i}{1 + C_i \varepsilon_i + D_i \varepsilon_i^{\,2}} \tag{F-11}$$

where, E_i and ε_i are the tangent E-modulus at the origin and strain of the concrete in the axial (i = c) or circumferential (i = cℓ) direction. The constants C_i and D_i follow from the boundary conditions with the second (II) region:

$$C_i = \frac{E_i}{\sigma_{cII}} - \frac{2}{\varepsilon_{iII}} + \frac{E_{iII} E_i \varepsilon_{iII}}{\sigma_{cII}^{\,2}} \quad \text{and} \quad D_i = \frac{1}{\varepsilon_{iII}^{\,2}} - \frac{E_{iII} E_i}{\sigma_{cII}^{\,2}} \tag{F-12}$$

with, σ_{cII}, ε_{iII} and E_{iII} the stress, strain and E-modulus at the origin of the second branch (see further). In [7], the tangent moduli of the concrete are calculated as:

$$E_c = 10200 (f_{co})^{1/3} \quad \text{and} \quad E_{c\ell} = 51000 (f_{co})^{1/3} \tag{F-13}$$

in which E_i and f_{co} are expressed in N/mm^2.

The second region response, based on [9], is given as:

$$\begin{aligned} \sigma_c &= f_{co} + k_1 \sigma_\ell \\ &= f_{co} \left(1 + 3.5 \left(\frac{\sigma_\ell}{f_{co}} \right)^{0.85} \right) \end{aligned} \tag{F-14}$$

with, k_1 a coefficient which decreases with an increase of the lateral stress σ_ℓ and which has been experimentally calibrated in [7]. As the lateral stress σ_ℓ follows, according to Eq. (F-10), from the circumferential strain $\varepsilon_{c\ell}$, Eq. (F-14) represents the axial stress-circumferential strain relationship of the second region. Based on [2,9], the axial stress-strain relationship of this region is obtained from:

$$\begin{aligned} \varepsilon_c &= \varepsilon_{c1} \left(1 + k_2 \left(\frac{\sigma_c}{f_{co}} - 1 \right) \right) \\ &= \varepsilon_{c1} \left(1 + (310.57 \varepsilon_{c\ell} + 1.90) \left(\frac{\sigma_c}{f_{co}} - 1 \right) \right) \end{aligned} \tag{F-15}$$

with, k_2 a coefficient which increases with increasing circumferential strain $\varepsilon_{c\ell}$ and which has been experimentally calibrated in [7].

Rewriting Eq. (F-10) as $\sigma_\ell = K_{conf} \varepsilon_{c\ell}$, with $K_{conf} = 0.5\, k_e \rho_f E_f$, from Eqs. (F-14) and (F-15) the following expressions are obtained at the origin of the second region:

$$\varepsilon_{c\ell II} = 0.002 \quad \text{and} \quad \varepsilon_{cII} = \varepsilon_{c1} \left(1 + 0.0448 \left(\frac{K_{conf}}{f_{co}} \right)^{0.85} \right) \tag{F-16}$$

$$\sigma_{cII} = f_{co} \left(1 + 0.0178 \left(\frac{K_{conf}}{f_{co}} \right)^{0.85} \right) \tag{F-17}$$

$$E_{c\ell II} = 7.557 K_{conf}^{0.85} f_{co}^{0.15} \quad \text{and} \quad E_{cII} = 0.3075 \frac{f_{co}}{\varepsilon_{c1}} \tag{F-18}$$

By imposing stepwise the circumferential strain $\varepsilon_{c\ell}$, the complete stress-strain behaviour of the FRP confined concrete can be calculated from Eqs. (F-11) till (F-18). The calculation finishes if the ultimate circumferential strain $\varepsilon_{c\ell u}$ is reached. This corresponds to failure of the confining reinforcement ($\varepsilon_{c\ell u} = \varepsilon_{fu,eff}$).

1.3 Model by Samaan et al. [10]

1.3.1 Approach and background of the model

This model is based on the observation that the dilation rate (change of circumferential strain with respect to the axial strain) of FRP confined concrete approaches an asymptotic value. Based on this dilation rate, Samaan et al. propose a model for FRP confined concrete which is not calculated by an incremental approach.

For the stress-strain behaviour a bilinear response is assumed (Fig. F-2), based on the four-parameter stress-strain relationship for concrete by Richard and Abbot [11]. The stiffness of the first branch is taken as that of unconfined concrete, while the stiffness and model parameters of the second branch are experimentally calibrated as a function of the stiffness of the confining reinforcement and the unconfined concrete strength.

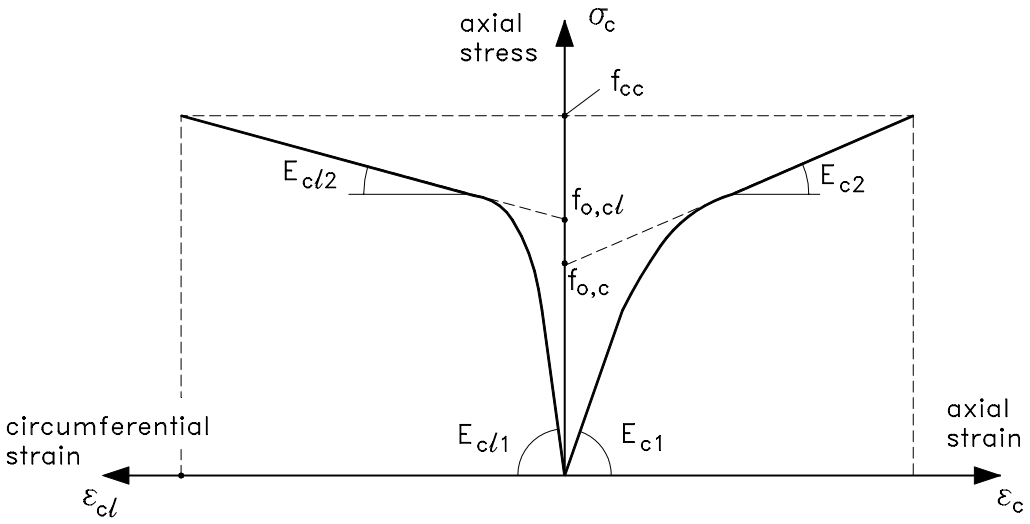

Fig. F-2 *Stress-strain model proposed by Samaan et al. [10]*

1.3.2 Equations and calculation procedure

Assuming a bilinear response of FRP confined concrete, the stress-strain relationship is taken according to [11] as:

$$\sigma_c = \frac{(E_{i1} - E_{i2})\varepsilon_i}{\left(1 + \left(\frac{(E_{i1} - E_{i2})\varepsilon_i}{f_{o,i}}\right)^{n_i}\right)^{1/n_i}} + E_{i2}\varepsilon_i \le f_{cc} \tag{F-19}$$

where, ε_i is the strain of the concrete in the axial (i = c) or circumferential (i = cℓ) direction, E_{i1} and E_{i2} are the first and second branch slopes, $f_{o,i}$ is the stress at the intercept of the second slope with the stress axis and n_i is a curve-shaped parameter that mainly controls the curvature in the transition zone between the first and second branch. The strength of the confined concrete f_{cc} is given as:

$$\begin{aligned} f_{cc} &= f_{co} + k_1 \sigma_{\ell u} \\ &= f_{co} + 6.0\, \sigma_{\ell u}^{0.7} \end{aligned} \tag{F-20}$$

with; k_1 a coefficient (similar as in Section 1.2) experimentally calibrated in [10] and $\sigma_{\ell u}$ the maximum confining stress obtained from Eq. (F-10) for $\varepsilon_{c\ell u} = \varepsilon_{fu,eff}$. The axial strain $\varepsilon_{cc1} = \varepsilon_{ccu}$ corresponding to f_{cc} follows from Eq. (F-19), or also as:

$$\varepsilon_{ccu} = \frac{f_{cc} - f_{o,c}}{E_{c2}} \tag{F-21}$$

With respect to the modelling of the axial strain response, it is proposed to take the E-modulus of the first branch according to [8]:

$$E_{c1} = 3950\sqrt{f_{co}} \tag{F-22}$$

and the E-modulus of the second branch, calibrated as a function of the stiffness of the confining reinforcement and the unconfined concrete strength, as:

$$E_{c2} = 245.61\, f_{co}^{0.2} + 1.3456\, \frac{E_f t}{D} \tag{F-23}$$

in which E_{c1}, E_{c2} and f_{co} are expressed in N/mm^2. The curve-shape parameter n_c is taken equal to 1.5, while the intercept stress $f_{o,c}$ was experimentally calibrated as:

$$f_{o,c} = 0.872\, f_{co} + 0.371\, \sigma_{\ell u} + 6.258 \tag{F-24}$$

In a similar way, the following expressions apply for the circumferential strain response:

$$E_{c\ell 1} = \frac{E_{c1}}{\nu} \quad \text{and} \quad E_{c\ell 2} = \frac{E_{c2}}{\mu_u} \tag{F-25}$$

with, μ_u the dilation rate (change of circumferential strain with respect to the axial strain) according to [10]:

$$\mu_u = -0.187 \ln\left(\frac{2E_f t}{f_{co} D}\right) + 0.881 \tag{F-26}$$

The curve-shape parameter and the intercept stress are taken as:

$$n_{c\ell} = \frac{n_c}{\mu_u} \quad \text{and} \quad f_{o,c\ell} = 0.636\, f_{co} + 0.233\, \sigma_{\ell u} + 4.561 \tag{F-27}$$

Based on the ultimate FRP confining pressure, the unconfined concrete strength and the characteristics of the FRP wrapping reinforcement, the stress-strain response of the FRP confined concrete is directly obtained from Eq. (F-19), with the model parameters according to Eqs (F-20) till (F-27).

1.4 Basic differences in approach of the three models

In the following an overview is given of the basic differences in approach of the three models. A discussion on the efficiency of the models is given in Chapter 6, Section 4.3.2.

1.4.1 Incremental confining action

To model FRP confined concrete, the incremental confining action exerted by the FRP should be taken into account. The models by Spoelstra-Monti and by Toutanji consider this aspect by means of an incremental approach, whereby the model is repeatedly applied, each time increasing the confining pressure. To simplify the calculation, in the model by Samaan et al. a constant dilation rate is assumed, so that the incremental approach is no longer needed.

1.4.2 Experimental calibration of model parameters

The model by Spoelstra and Monti only offers a combination of existing models, without further (re)calibration of model parameters with respect to FRP confined concrete. In their approach, they rely on sound models which were not developed for FRP confined concrete, but which are assumed to be applicable for FRP confinement by means of the incremental approach. On the other hand, the models by Toutanji and by Samaan et al. depend strongly on certain model parameters which have been obtained through experimental calibration with respect to concrete cylinders confined with FRP wrapping reinforcement. Although the approach of the Toutanji model is basically the same as for the Spoelstra model, it makes use of a more simple relationship for the stress-strain response of confined concrete, whereby it was needed to recalibrate the model coefficients. Due to the specific approach of the Samaan model (based on the dilation rate of FRP confined concrete) and the simplified bilinear stress-strain relationship, this model is most of all related to experimental calibration.

1.4.3 Calculation procedure and versatility of the model

Due to the incremental approach, the calculation procedures of the models by Spoelstra-Monti and by Toutanji are more complex than for the approach by Samaan et al. Moreover, the linking between axial strain, circumferential strain and FRP confining pressure results for the Spoelstra model in an iterative calculation, which makes this model even more complex. Unlike the models by Spoelstra-Monti and by Samaan et al., the model by Toutanji uses different relationships for the initial region of the stress-strain behaviour where the response is mainly that of unconfined concrete and the region where the confinement is fully activated.

Given the different nature of the stress-strain relationships used in these three models, the model by Spoelsta and Monti is the most versatile and for example allows the prediction of a

descending stress-strain branch. With its simplified bilinear relationship, the model by Samaan et al. is the least versatile.

2 Analytical verification of the stress-strain behaviour

Based on the model proposed in Section 1.1 and taking into account the failure criterion defined in Chapter 6, Section 4.4.3, a comparison between the experimental and analytical stress-strain response of the FRP confined specimens is shown in the following figures.

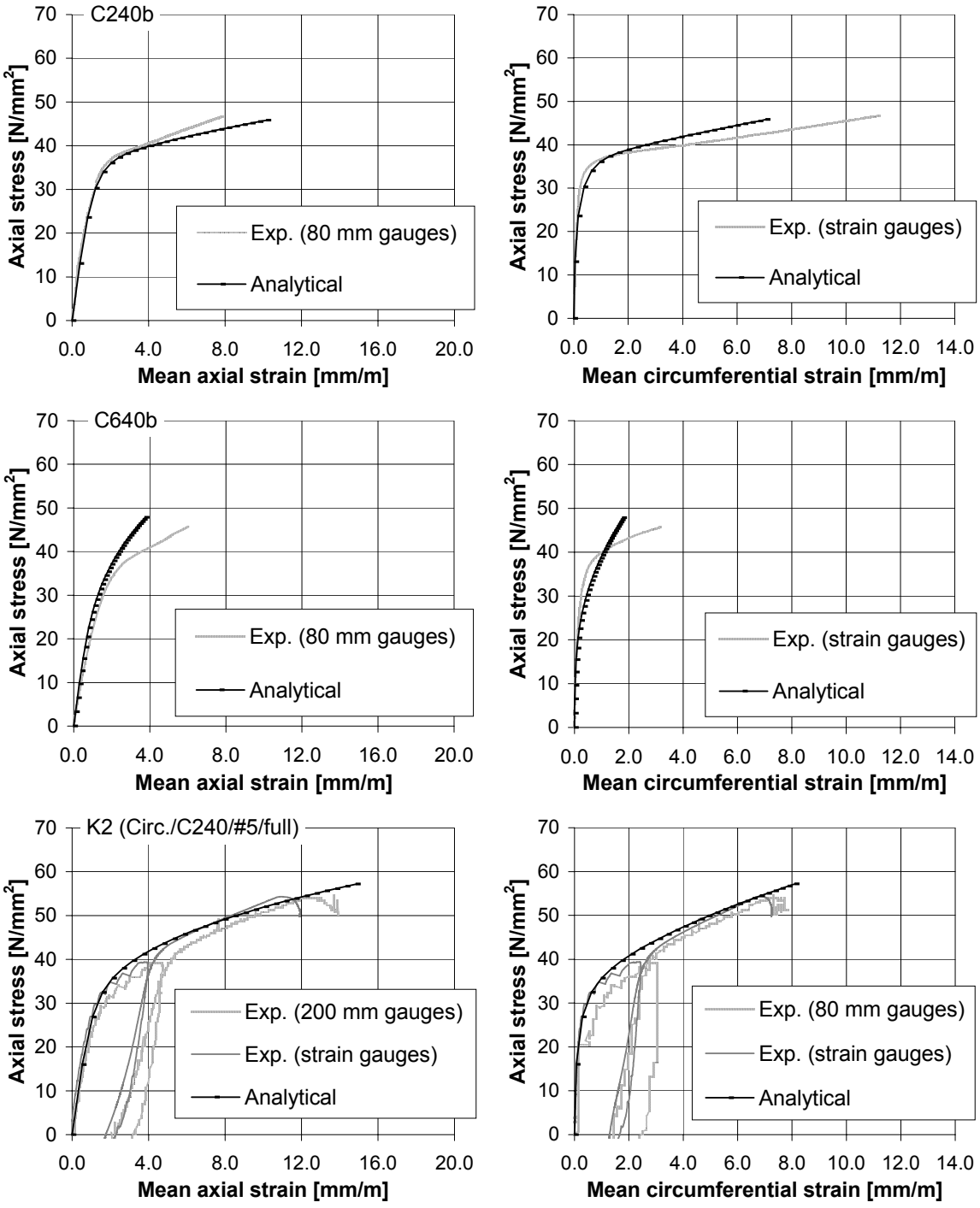

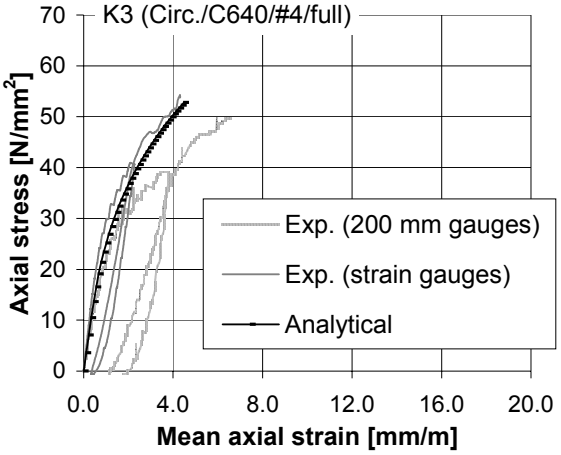
K3 (Circ./C640/#4/full)
Axial stress [N/mm²]
Mean axial strain [mm/m]
Exp. (200 mm gauges)
Exp. (strain gauges)
Analytical

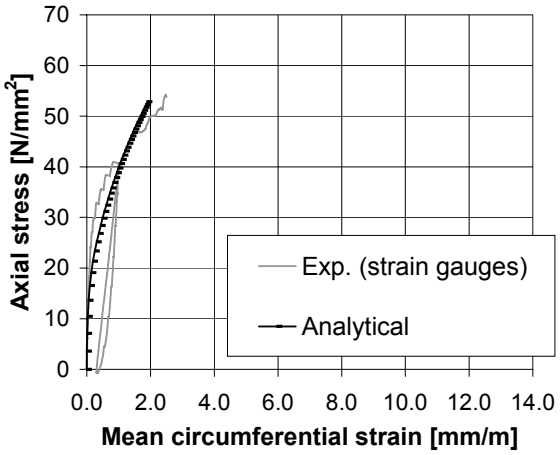
Axial stress [N/mm²]
Mean circumferential strain [mm/m]
Exp. (strain gauges)
Analytical

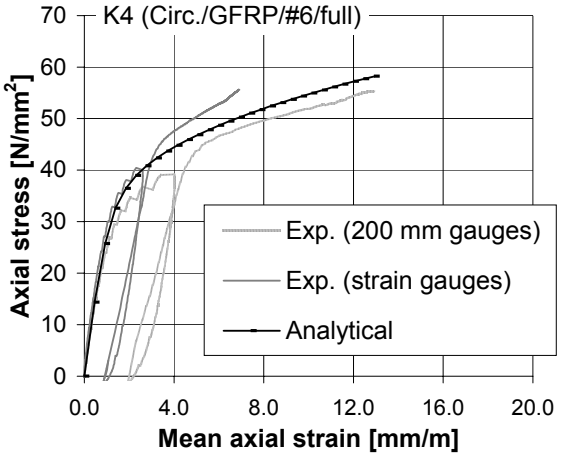
K4 (Circ./GFRP/#6/full)
Axial stress [N/mm²]
Mean axial strain [mm/m]
Exp. (200 mm gauges)
Exp. (strain gauges)
Analytical

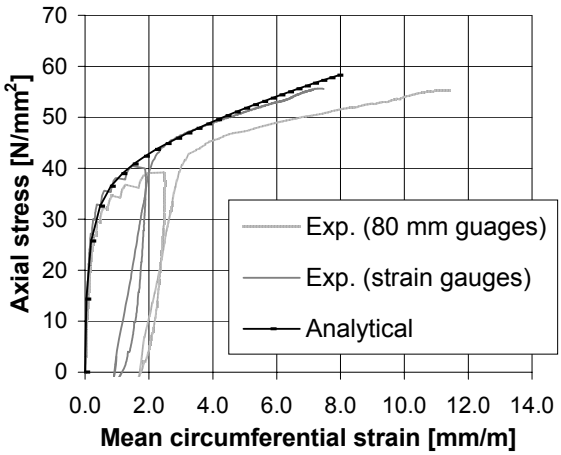
Axial stress [N/mm²]
Mean circumferential strain [mm/m]
Exp. (80 mm guages)
Exp. (strain gauges)
Analytical

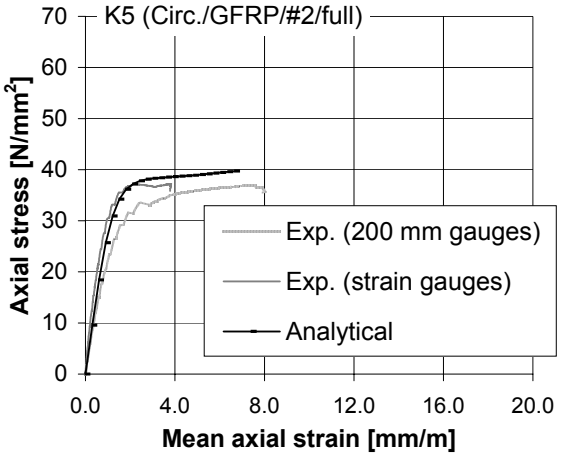
K5 (Circ./GFRP/#2/full)
Axial stress [N/mm²]
Mean axial strain [mm/m]
Exp. (200 mm gauges)
Exp. (strain gauges)
Analytical

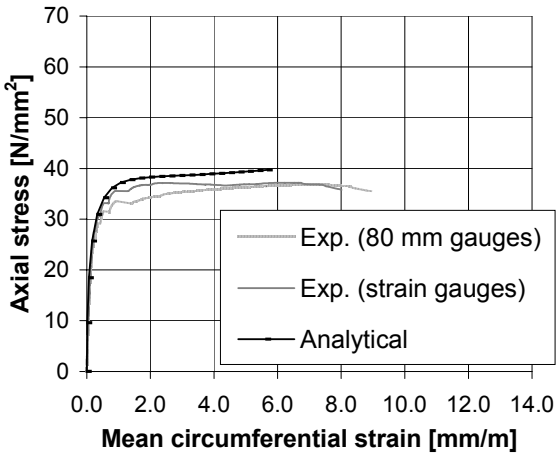
Axial stress [N/mm²]
Mean circumferential strain [mm/m]
Exp. (80 mm gauges)
Exp. (strain gauges)
Analytical

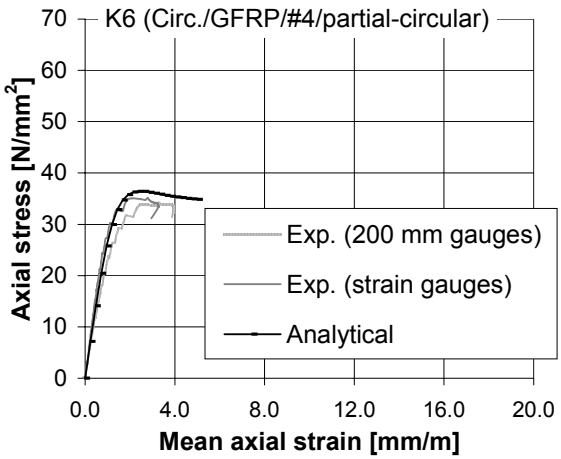
K6 (Circ./GFRP/#4/partial-circular)
Axial stress [N/mm²]
Mean axial strain [mm/m]
Exp. (200 mm gauges)
Exp. (strain gauges)
Analytical

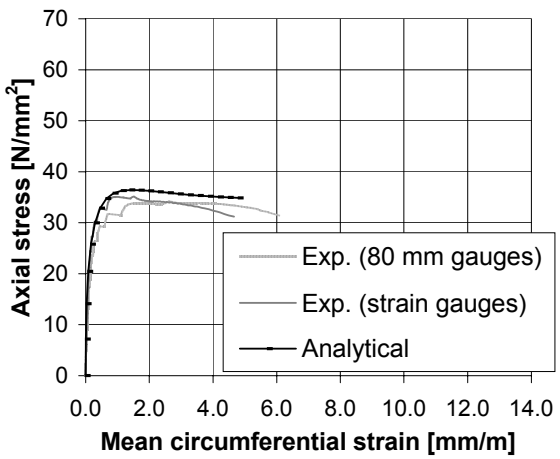
Axial stress [N/mm²]
Mean circumferential strain [mm/m]
Exp. (80 mm gauges)
Exp. (strain gauges)
Analytical

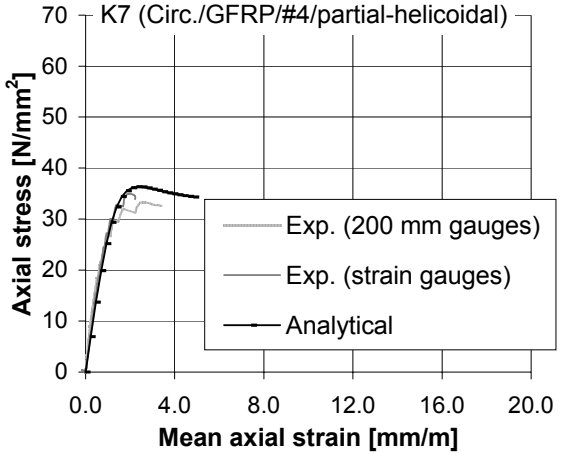
K7 (Circ./GFRP/#4/partial-helicoidal)
Axial stress [N/mm²]
Mean axial strain [mm/m]
Exp. (200 mm gauges)
Exp. (strain gauges)
Analytical

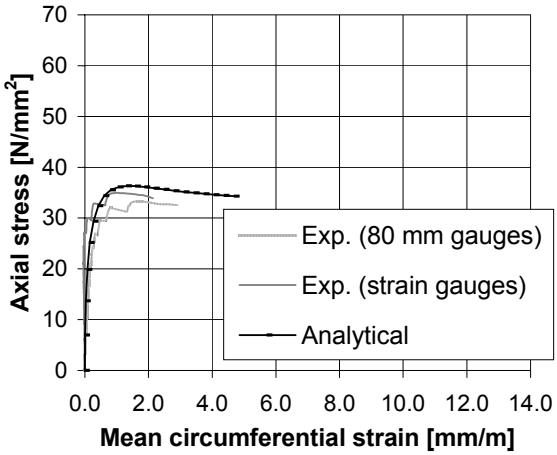
Axial stress [N/mm²]
Mean circumferential strain [mm/m]
Exp. (80 mm gauges)
Exp. (strain gauges)
Analytical

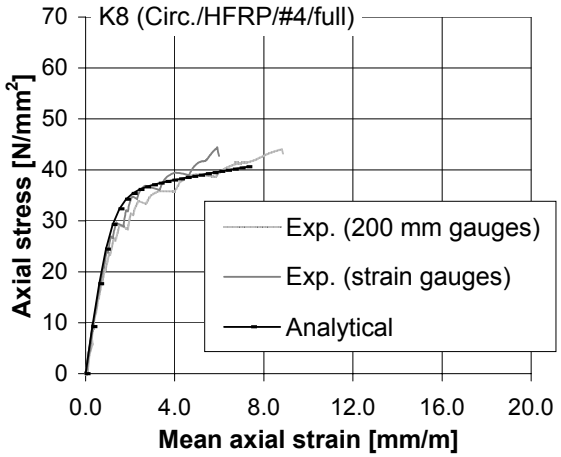
K8 (Circ./HFRP/#4/full)
Axial stress [N/mm²]
Mean axial strain [mm/m]
Exp. (200 mm gauges)
Exp. (strain gauges)
Analytical

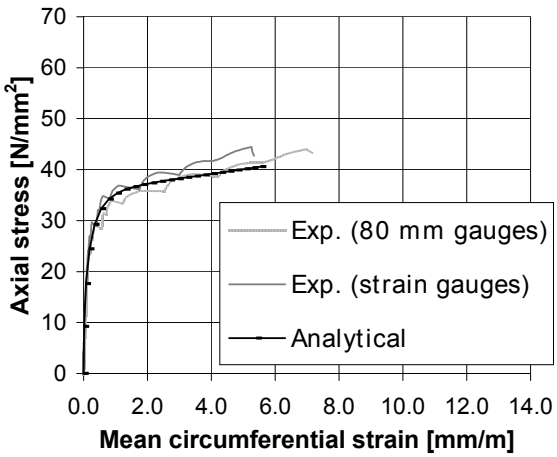
Axial stress [N/mm²]
Mean circumferential strain [mm/m]
Exp. (80 mm gauges)
Exp. (strain gauges)
Analytical

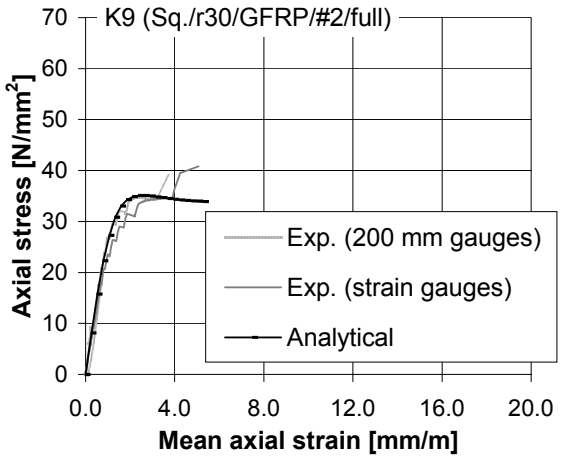
K9 (Sq./r30/GFRP/#2/full)
Axial stress [N/mm²]
Mean axial strain [mm/m]
Exp. (200 mm gauges)
Exp. (strain gauges)
Analytical

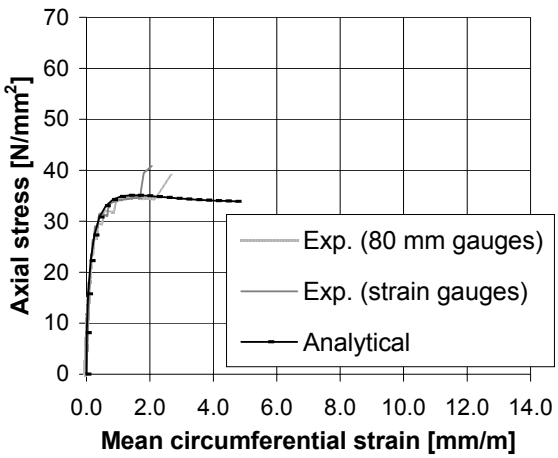
Axial stress [N/mm²]
Mean circumferential strain [mm/m]
Exp. (80 mm gauges)
Exp. (strain gauges)
Analytical

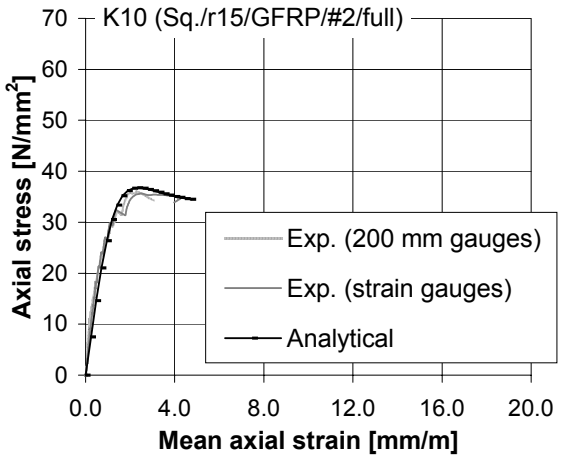
K10 (Sq./r15/GFRP/#2/full)
Axial stress [N/mm²]
Mean axial strain [mm/m]
Exp. (200 mm gauges)
Exp. (strain gauges)
Analytical

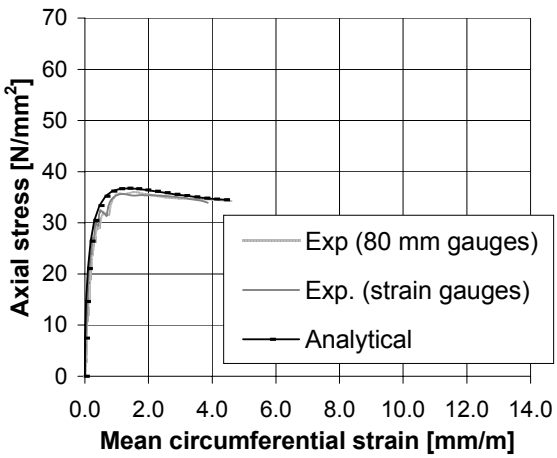
Axial stress [N/mm²]
Mean circumferential strain [mm/m]
Exp (80 mm gauges)
Exp. (strain gauges)
Analytical

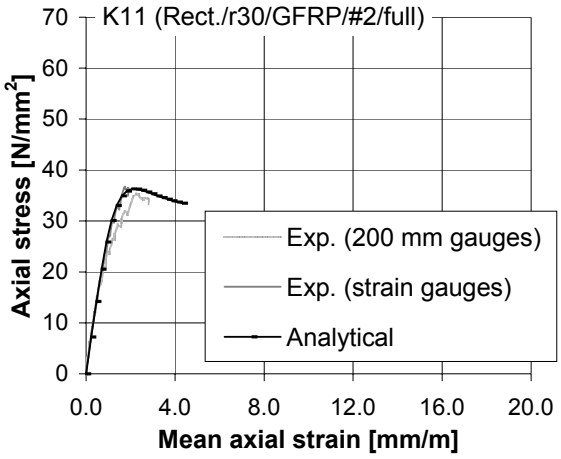

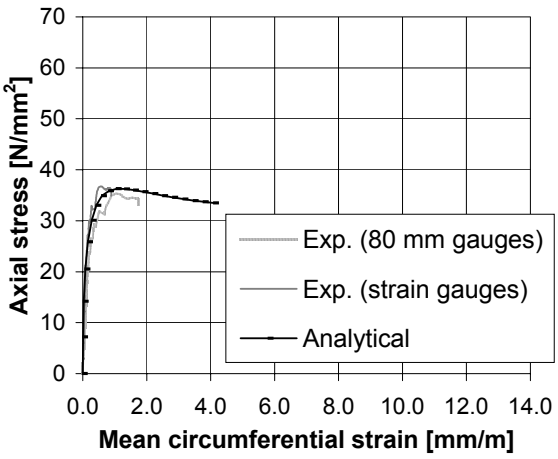

3 Effective FRP failure strain

The following data was used to determine an experimental relationship for the effective FRP failure strain $\varepsilon_{fu,eff} = \eta_e f_f / E_f$, with η_e the effectiveness factor. The curve fitting is based on (η_e, K_{conf}) data points, where η_e is taken so that the analytical verification according to Chapter 6, Section 4.4.1 corresponds to the ultimate load of the tested specimens. Only data was considered for which $K_{conf} > 5f_c$ (if not, the strengthening ratio is very small so that the prediction of η_e becomes highly sensitive to the accuracy of f_c).

No.	Desig-nation	D [mm]	b_f [mm]	t [mm]	s [mm]	f_f [N/mm²]	E_f [N/mm²]	k_e [-]	K_{conf} [N/mm²]	f_c [N/mm²]	Q_u [kN]	η_e [-]
1	Ma(C240)	150	300	0.117	300	2600	198000	1.00	309	35.5	814	0.51
2	Ma(C640)	150	300	0.235	300	1100	471000	1.00	1476	35.5	809	0.65
3	Ma(K2)	400	300	0.585	300	2600	198000	1.00	579	33.6	7460	0.52
4	Ma(K3)	400	300	0.940	300	1100	471000	1.00	2214	33.6	7490	0.87
5	Ma(K4)	400	200	1.800	200	780	60000	1.00	540	36.1	7580	0.51
6	Ma(K8)	400	50	0.492	50	1100	97000	1.00	239	34.1	6230	0.87
7	Mi(CB1-6)	152.5	305	1.450	305	524	37233	0.93	658	30.9	1006[1]	0.52
8	Mi(CB1-10)	152.5	305	2.210	305	579	40336	0.93	1087	30.9	1319[1]	0.65
9	Mi(CB1-14)	152.5	305	2.970	305	641	40749	0.93	1476	30.9	1574[1]	0.71
10	Mi(CB2-6)	152.5	305	1.450	305	524	37233	0.93	658	29.6	1056[2]	0.66
11	Mi(CB2-10)	152.5	305	2.210	305	579	40336	0.93	1087	29.6	1337[2]	0.73
12	Mi(CB2-14)	152.5	305	2.970	305	641	40749	0.93	1476	29.6	1585[2]	0.79
13	Mi(CB3-6)	152.5	305	1.450	305	524	37233	0.93	658	32.0	1094[1]	0.63
14	Mi(CB3-10)	152.5	305	2.210	305	579	40336	0.93	1087	32.0	1410[1]	0.74
15	Mi(CB3-14)	152.5	305	2.970	305	641	40749	0.93	1476	32.0	1554[1]	0.64

[1]Mean value of two tests

[2]Mean value of three tests, values diverging more than 15 % of the mean value were excluded

Ma: Matthys (Chapter 6, Section 3), Mi: Mirmiran et al. [12,13]

4 References

1. Spoelstra M.R., Monti G. (1999), "FRP-Confined Concrete Model", ASCE, Journal of Composites for Construction, Vol. 3, No. 3, pp. 143-150.
2. Mander J.B., Priestley M.J.N., Park R. (1988), "Theoretical stress-strain model for confined concrete", Journal of Structural Engineering, ASCE, Vol. 114(8), pp. 1804-1826.
3. Pantazopoulou S.J., Mills R.H. (1995), "Microstructural aspects of the mechanical response of plain concrete", ACI Materials Journal, Vol. 92, Nov.-Dec. 95, pp. 605-616.
4. Popovics S. (1973), "Numerical Approach to the Complete Stress-Strain Curves for Concrete", Cement and Concrete Research, Vol. 3, No. 5, pp. 583-599.
5. Richart F.E., Brandtzaeg A, Brown R.L. (1928), "A Study of the Failure of Concrete Under Combined Compressive Stresses", Bulletin 185, University of Illinois Engineering Experimental Station, Champaign, Illinois, USA.
6. Restrepol J.L., De Vino B. (1996), "Enhancement of the axial load carrying capacity of reinforced concrete columns by means of fibreglass-epoxy jackets", Proceedings 2nd. Int. Conf. On Advanced Composite Materials in Bridges and Structures, Ed. M. El-Badry, The Canadian Society for Civil Engineering, Montréal, Québec, Canada, pp. 547-554.
7. Toutanji H. A. (1999), "Stress-Strain Characteristics of Concrete Columns Externally Confined with Advanced Fiber Composite Sheets", ACI Materials Journal, Vol. 96, No. 3, pp. 397-404.
8. Ahmad S.H., Shah S.P. (1982), "Stress-Strain Curves of Concrete Confined by Spiral Reinforcement", ACI Structural Journal, Vol. 79, No. 6, pp. 484-490.
9. Richart F.E., Brandtzaeg A, Brown R.L. (1929), "The Failure of Plain and Spirally Reinforced Concrete in Compression", Bulletin 190, University of Illinois Engineering Experimental Station, Champaign, Illinois, USA.
10. Samaan M., Mirmiran A., Shahawy M. (1999), "Model of Concrete Confined by Fiber Composites", ASCE Journal of Structural Engineering, Vol. 124, No. 9, pp. 1025-1031.
11. Ritchard R.M., Abbott B.J. (1975), "Versatile elastic-plastic stress-strain formula", ASCE Journal of Engineering Mechanics, Vol. 101, No. 4., pp.511-515.
12. Mirmiran A., Shahawy M. (1997), "Behaviour of Concrete Columns Confined by Fibre Composites", ASCE Journal of Structural Engineering, Vol. 123, No. 5, pp. 583-590.
13. Mirmiran A., Shahawy M., Samaan M., El Echary H., Mastrapa J.C., Pico O. (1998), "Effect of column parameters on FRP-confined concrete", ASCE, Journal of Composites for Construction, Vol. 2., No. 4, pp. 175-185.

Appendix G
CALCULATION PROGRAMME USED FOR THE PARAMETRIC STUDY

To study the influence of the design parameters on the ULS and the SLS of single reinforced RC members strengthened in flexure with FRP EBR and subjected to bending, a calculation programme (using the software MathCad) has been developed. This programme makes use of the design models provided in Chapter 7, Sections 2 and 3. More details on the programme are given in Chapter 7, Section 3.6.

The calculation is based on the following non-dimensional parameters:

$\xi = \frac{x}{d}$ relative distance of the neutral axis position

$\eta = \frac{h}{d}$ relative depth of the section

$\delta = \frac{h_f}{d}$ depth of the flange over effective depth

$\beta = \frac{b_w}{b}$ width of the web over width of the flange

$\rho_s = \frac{A_s}{bd}$ steel reinforcement ratio

$\rho_s = \frac{A_s}{bd}$ FRP reinforcement ratio

$\mu_k = \frac{M_k}{bd^2 f_{ck}}$ reduced characteristic moment

$\mu_d = \frac{M_d}{bd^2 f_{cd}}$ reduced design moment

$\Gamma = \frac{I}{bd^3}$ reduced moment of inertia

$\frac{\ell}{d}$ span length over effective depth

$\frac{a}{\ell}$ maximum deflection over span length

The source code of the programme is given in the following.

ULTIMATE AND SERVICEABILITY LIMIT STATE
Single reinforced strengthened member - flexure

$kN := 1000 \cdot N$

$MPa := \frac{N}{mm^2}$

$‰ := 0.001$

Input parameters C20, S400, CFRP

Material properties

$f_{ck} := 20 \cdot MPa$ $\gamma_c := 1.5$ $f_{cd} := \frac{f_{ck}}{\gamma_c}$ $f_{ctm} := 0.3 \cdot f_{ck}^{\frac{2}{3}} \cdot MPa^{\frac{1}{3}}$

$f_{yk} := 400 \cdot MPa$ $\gamma_s := 1.15$ $f_{yd} := \frac{f_{yk}}{\gamma_s}$

$f_{fk} := 2800 \cdot MPa$ $\gamma_f := 1.3$ $f_{fd} := \frac{f_{fk}}{\gamma_f}$

$E_c := 9500 \cdot MPa^{\frac{2}{3}} \cdot \left(f_{ck} + 8 \cdot MPa\right)^{\frac{1}{3}}$ $\varepsilon_{cu} := 0.0035$

$E_c = 28848 \cdot MPa$

$E_s := 200000 \cdot MPa$ $\varepsilon_{su} := 0.025$

$E_f := 165000 \cdot MPa$ $\varepsilon_{fud} := \frac{f_{fd}}{E_f}$ $\varepsilon_{fud} = 0.0131$

Geometry $\eta := 1.1$ $\delta := 1$ $\beta := 1$

Initial state parameters $\rho_s := 0.005$ $\eta_o := 0.5$

Global load safety factors $\Phi_r := 1.43$ $\Phi_{qp} := 2.04$

E-moduli for the SLS Creep coefficient $\phi_c := 1.15$

$E_{c\phi} := \frac{E_c}{\left(1 + \phi_c\right)}$ $\alpha_s := \frac{E_s}{E_{c\phi}}$ $\alpha_s = 15$ $\alpha_f := \frac{E_f}{E_{c\phi}}$ $\alpha_f = 12$

Guess values for calculation $\xi g := 0.3$ $\rho g := 0.001$

INITIAL SITUATION - ULS UNSTRENGTHENED MEMBER

Failure modes

Mode A: Fracture of the reinforcement/no concrete crushing $0 < \xi < \xi_{lim1}$

$\xi_{lim1s} := \frac{\varepsilon_{cu}}{\varepsilon_{cu} + \varepsilon_{su}}$ $\xi_{lim1s} = 0.123$

Mode B: Yielding of the steel/concrete crushing $\xi_{lim1} < \xi < \xi_{lim2}$

$\xi_{lim2k} := \frac{\varepsilon_{cu}}{\varepsilon_{cu} + \frac{f_{yk}}{E_s}}$ $\xi_{lim2k} = 0.636$ $\xi_{lim2d} := \frac{\varepsilon_{cu}}{\varepsilon_{cu} + \frac{f_{yd}}{E_s}}$ $\xi_{lim2d} = 0.668$

Concrete stress block parameters

$$\lambda 1(\xi) := \text{if}\left(\xi < \xi_{lim1s}, \frac{0.002}{\varepsilon_{su}} \cdot \frac{1-\xi}{\xi}, \frac{0.002}{\varepsilon_{cu}}\right)$$

$$\lambda 2(\xi) := \text{if}\left(\xi < \xi_{lim1s}, \frac{0.002}{\varepsilon_{su}} \cdot \frac{\xi}{\xi-\delta} \cdot \frac{1-\xi}{\xi}, \frac{0.002}{\varepsilon_{cu}} \cdot \frac{\xi}{\xi-\delta}\right)$$

$$\psi 1(\xi) := \text{if}\left(\lambda 1(\xi) \geq 1, \frac{3\cdot\lambda 1(\xi)-1}{3\cdot\lambda 1(\xi)^2}, 1 - \frac{\lambda 1(\xi)}{3}\right)$$

$$\psi 2(\xi) := \text{if}\left(\lambda 2(\xi) \geq 1, \frac{3\cdot\lambda 2(\xi)-1}{3\cdot\lambda 2(\xi)^2}, 1 - \frac{\lambda 2(\xi)}{3}\right)$$

$$\psi(\xi) := \text{if}\left[\xi \leq \delta, \psi 1(\xi), \psi 1(\xi) - \psi 2(\xi)\cdot(1-\beta)\cdot\left(1-\frac{\delta}{\xi}\right)\right]$$

$$\delta 1_g(\xi) := \text{if}\left[\lambda 1(\xi) \geq 1, \frac{4\cdot\lambda 1(\xi)-1}{4\cdot(3\cdot\lambda 1(\xi)-1)}, \frac{\lambda 1(\xi)^2 - 4\cdot\lambda 1(\xi)+6}{4\cdot(3-\lambda 1(\xi))}\right]$$

$$\delta 2_g(\xi) := \text{if}\left[\lambda 2(\xi) \geq 1, \frac{4\cdot\lambda 2(\xi)-1}{4\cdot(3\cdot\lambda 2(\xi)-1)}, \frac{\lambda 2(\xi)^2 - 4\cdot\lambda 2(\xi)+6}{4\cdot(3-\lambda 2(\xi))}\right]$$

$$\delta_g(\xi) := \text{if}\left[\xi \leq \delta, \delta 1_g(\xi), \frac{\left[\psi 1(\xi)\cdot\delta 1_g(\xi) - \psi 2(\xi)\cdot\delta 2_g(\xi)\cdot(1-\beta)\cdot\left(1-\frac{\delta}{\xi}\right)^2 - \psi 2(\xi)\cdot(1-\beta)\cdot\left(1-\frac{\delta}{\xi}\right)\cdot\frac{\delta}{\xi}\right]}{\psi(\xi)}\right]$$

Nominal value of the strength of the unstrengthened member

$$\xi_n := \text{root}\left(\frac{\xi g\cdot\psi(\xi g)\cdot f_{ck}}{f_{yk}} - \rho_s, \xi g\right)$$

$$\mu_{nU} := \xi_n\cdot\psi\left(\xi_n\right)\cdot\left(1-\delta_g\left(\xi_n\right)\cdot\xi_n\right) \qquad \mu_{nU} = 0.095$$

ULS unstrengthened member

$$\xi_{dU} := \text{root}\left(\frac{\xi g\cdot 0.85\cdot\psi(\xi g)\cdot f_{cd}}{f_{yd}} - \rho_s, \xi g\right)$$

$$\mu_{dU} := \xi_{dU}\cdot 0.85\cdot\psi\left(\xi_{dU}\right)\cdot\left(1-\delta_g\left(\xi_{dU}\right)\cdot\xi_{dU}\right) \qquad \mu_{dU} = 0.120$$

Initial state before strengthening (linear elastic calculation)

$$\mu_o := \mu_{dU}\cdot\frac{\eta_o}{\gamma_c\cdot\Phi_r}$$

$$\xi_{oR} := \text{root}\left[\xi g - \left(2\cdot\rho_s\right)\cdot\alpha_s\cdot\frac{1-\xi g}{\xi g}, \xi g\right] \qquad \xi_{oT} := \text{root}\left[\xi g - \xi g\cdot\left[(1-\beta)\cdot\left(1-\frac{\delta}{\xi g}\right)^2\right] - 2\cdot\rho_s\cdot\alpha_s\cdot\frac{1-\xi g}{\xi g}, \xi g\right]$$

$$\xi_o := \text{if}\left(\xi_{oR} \le \delta, \xi_{oR}, \xi_{oT}\right)$$

$$\varepsilon_{co} := \frac{\mu_o \cdot \xi_o \cdot f_{ck}}{E_{c\phi} \cdot \left[\frac{\xi_o^3}{3} + \alpha_s \cdot \rho_s \cdot \left(1 - \xi_o\right)^2\right]} \qquad \varepsilon_o := \varepsilon_{co} \cdot \frac{\eta - \xi_o}{\xi_o} \qquad \varepsilon_o = 0.0007$$

ULS STRENGTHENED MEMBER

Failure modes assuming no debonding

Mode A: Steel yielding/FRP fracture/no concrete crushing $0 < \xi < \xi_{lim1}$

$$\xi_{lim1} := \frac{\varepsilon_{cu}}{\varepsilon_{cu} + \varepsilon_{fud} + \varepsilon_o} \cdot \eta$$

Mode B: Yielding of the steel/concrete crushing/no FRP fracture $\xi_{lim1} < \xi < \xi_{lim2}$

$$\xi_{lim2} := \frac{\varepsilon_{cu}}{\varepsilon_{cu} + \frac{f_{yd}}{E_s}}$$

Ductility condition (minimum amount of yielding)

$$\xi_{max} := 0.45$$

Concrete stress block parameters

$$\lambda 1(\xi) := \text{if}\left(\xi < \xi_{lim1}, \frac{0.002}{\varepsilon_{fud} + \varepsilon_o} \cdot \frac{\eta - \xi}{\xi}, \frac{0.002}{\varepsilon_{cu}}\right)$$

$$\lambda 2(\xi) := \text{if}\left(\xi < \xi_{lim1}, \frac{0.002}{\varepsilon_{fud} + \varepsilon_o} \cdot \frac{\xi}{\xi - \delta} \cdot \frac{\eta - \xi}{\xi}, \frac{0.002}{\varepsilon_{cu}} \cdot \frac{\xi}{\xi - \delta}\right)$$

$$\psi 1(\xi) := \text{if}\left(\lambda 1(\xi) \ge 1, \frac{3 \cdot \lambda 1(\xi) - 1}{3 \cdot \lambda 1(\xi)^2}, 1 - \frac{\lambda 1(\xi)}{3}\right)$$

$$\psi 2(\xi) := \text{if}\left(\lambda 2(\xi) \ge 1, \frac{3 \cdot \lambda 2(\xi) - 1}{3 \cdot \lambda 2(\xi)^2}, 1 - \frac{\lambda 2(\xi)}{3}\right)$$

$$\psi(\xi) := \text{if}\left[\xi \le \delta, \psi 1(\xi), \psi 1(\xi) - \psi 2(\xi) \cdot (1 - \beta) \cdot \left(1 - \frac{\delta}{\xi}\right)\right]$$

$$\delta 1_g(\xi) := \text{if}\left[\lambda 1(\xi) \ge 1, \frac{4 \cdot \lambda 1(\xi) - 1}{4 \cdot (3 \cdot \lambda 1(\xi) - 1)}, \frac{\lambda 1(\xi)^2 - 4 \cdot \lambda 1(\xi) + 6}{4 \cdot (3 - \lambda 1(\xi))}\right]$$

$$\delta 2_g(\xi) := \text{if}\left[\lambda 2(\xi) \ge 1, \frac{4 \cdot \lambda 2(\xi) - 1}{4 \cdot (3 \cdot \lambda 2(\xi) - 1)}, \frac{\lambda 2(\xi)^2 - 4 \cdot \lambda 2(\xi) + 6}{4 \cdot (3 - \lambda 2(\xi))}\right]$$

$$\delta_g(\xi) := \text{if}\left[\xi \le \delta, \delta 1_g(\xi), \frac{\left[\psi 1(\xi) \cdot \delta 1_g(\xi) - \psi 2(\xi) \cdot \delta 2_g(\xi) \cdot (1 - \beta) \cdot \left(1 - \frac{\delta}{\xi}\right)^2 - \psi 2(\xi) \cdot (1 - \beta) \cdot \left(1 - \frac{\delta}{\xi}\right) \cdot \frac{\delta}{\xi}\right]}{\psi(\xi)}\right]$$

ULS analysis

$$\varepsilon_f(\xi) := \text{if}\left(\xi < \xi_{lim1}, \varepsilon_{fud}, \varepsilon_{cu}\cdot\frac{\eta - \xi}{\xi} - \varepsilon_o\right)$$

$$\xi_d(\rho_f) := \text{root}\left(0.85\cdot\psi(\xi g)\cdot\xi g\cdot f_{cd} - \rho_s\cdot f_{yd} - \rho_f\cdot E_f\cdot\varepsilon_f(\xi g), \xi g\right)$$

$$\Psi(\rho_f) := \psi\left(\xi_d(\rho_f)\right)$$

$$\Delta_g(\rho_f) := \delta_g\left(\xi_d(\rho_f)\right)$$

$$\mu_d(\rho_f) := \xi_d(\rho_f)\cdot 0.85\cdot\Psi(\rho_f)\cdot\left(1 - \Delta_g(\rho_f)\cdot\xi_d(\rho_f)\right) + \rho_f\cdot\frac{E_f\cdot\varepsilon_f\left(\xi_d(\rho_f)\right)}{f_{cd}}\cdot(\eta - 1)$$

$$\eta_S(\rho_f) := \frac{\mu_d(\rho_f)}{\mu_{dU}}$$

$$\rho_f := 0, 0.0005 .. 0.005$$

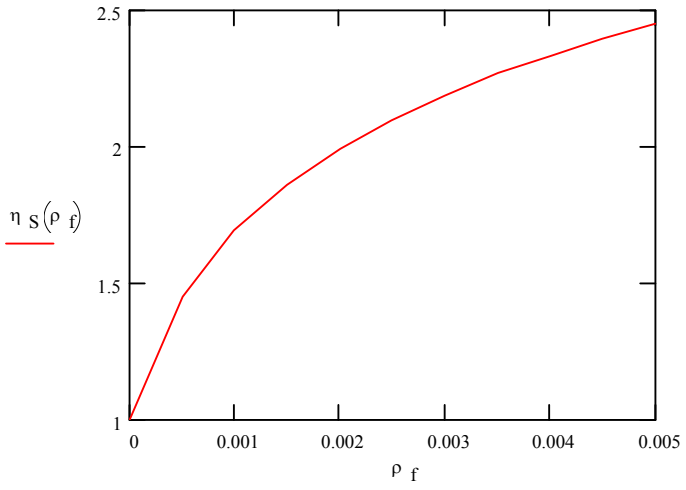

$$\rho f_{lim1} := \frac{\xi_{lim1}\cdot 0.85\cdot\psi(\xi_{lim1})\cdot f_{cd} - \rho_s\cdot f_{yd}}{E_f\cdot\varepsilon_f(\xi_{lim1})} \qquad \rho f_{lim1} = 0.0001 \qquad \eta_S(\rho f_{lim1}) = 1.18$$

$$\rho f_{max} := \frac{\xi_{max}\cdot 0.85\cdot\psi(\xi_{max})\cdot f_{cd} - \rho_s\cdot f_{yd}}{E_f\cdot\varepsilon_f(\xi_{max})} \qquad \rho f_{max} = 0.003 \qquad \eta_S(\rho f_{max}) = 2.24$$

$$\rho f_{lim2} := \frac{\xi_{lim2}\cdot 0.85\cdot\psi(\xi_{lim2})\cdot f_{cd} - \rho_s\cdot f_{yd}}{E_f\cdot\varepsilon_f(\xi_{lim2})} \qquad \rho f_{lim2} = 0.017 \qquad \eta_S(\rho f_{lim2}) = 3.04$$

Accidental situation

$$\eta_a(\rho_f) := \frac{\mu_d(\rho_f)}{\mu_{nU}}\cdot\frac{1}{\gamma_c\cdot\Phi_r}$$

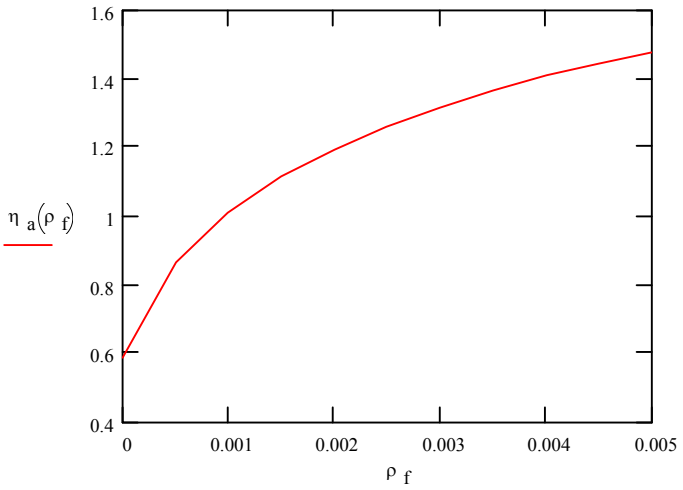

$\rho f_a := \text{root}\left(\eta_a(\rho g) - 1, \rho g\right)$ $\rho f_a = 0.001$ $\eta_S\left(\rho f_a\right) = 1.69$

Bond failure outside the anchorage zone

Parameters $\upsilon := 3.0$ $bf\_b := 0.75$

$$\eta_{Sb1}(\rho_f) := \frac{\left[0.38 + 151 \cdot \left(\rho_s + \frac{E_f}{E_s} \cdot \rho_f\right)\right] \cdot \frac{N}{mm^2}}{f_{ck}} \cdot \frac{\upsilon}{\mu_{dU}} \qquad \eta_{Sb2}(\rho_f) := \frac{0.84 \cdot f_{ctm}}{f_{ck}} \cdot \frac{\upsilon}{\mu_{dU}} \cdot bf\_b$$

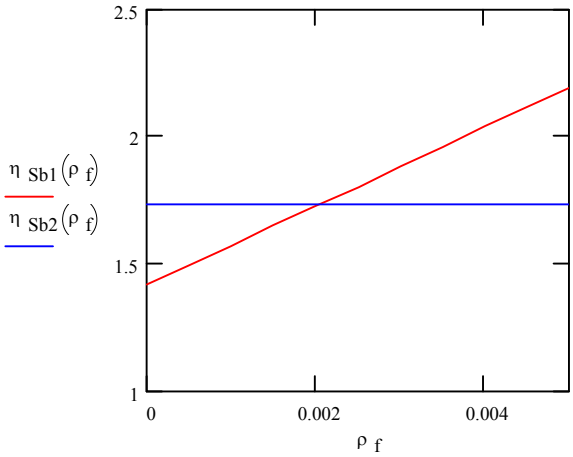

SLS STRENGTHENED MEMBER

Neutral axsis $\xi g := 0.4$

$$\xi_{e1R} := \text{root}\left[\xi g - \frac{(\eta - \xi g)^2}{\xi g} - 2 \cdot \alpha_s \cdot \rho_s \cdot \left(\frac{1 - \xi g}{\xi g}\right), \xi g\right]$$

$$\xi_{e1T} := \text{root}\left[\xi g - \frac{(1 - \beta) \cdot (\eta - \xi g)^2}{\xi g} - 2 \cdot \alpha_s \cdot \rho_s \cdot \left(\frac{1 - \xi g}{\xi g}\right), \xi g\right]$$

$\xi_{e1} := \text{if}\left(\xi_{e1R} \le \delta, \xi_{e1R}, \xi_{e1T}\right)$

$$\xi_{e2R}(\rho_f) := \text{root}\left[\xi g - 2\cdot\alpha_s\cdot\rho_s\cdot\left(\frac{1-\xi g}{\xi g}\right) - 2\cdot\alpha_f\rho_f\left[\frac{\eta-\xi g}{\xi g} - \eta_o\cdot\Phi_r\cdot\left(\frac{\xi g}{\xi_o}\right)\right], \xi g\right]$$

$$\xi_{e2T}(\rho_f) := \text{root}\left[\xi g - \xi g\cdot(1-\beta)\cdot\left(1-\frac{\delta}{\xi g}\right)^2 - 2\cdot\alpha_s\cdot\rho_s\cdot\left(\frac{1-\xi g}{\xi g}\right) - 2\cdot\alpha_f\rho_f\left[\frac{\eta-\xi g}{\xi g} - \eta_o\cdot\Phi_r\cdot\left(\frac{\xi g}{\xi_o}\right)\right], \xi g\right]$$

$$\xi_{e2}(\rho_f) := \text{if}\left(\xi_{e2R}(\rho_f)\le\delta, \xi_{e2R}(\rho_f), \xi_{e2T}(\rho_f)\right)$$

$$\zeta_{e2}(\rho_f) := \text{if}\left[\xi_{e2}(\rho_f)\le\delta, 1.05 - \frac{\xi_{e2}(\rho_f)}{3}, 1.05 - \frac{\frac{\delta^2}{\beta}\cdot\left(3\cdot\xi_{e2}(\rho_f) - 2\cdot\delta\right) + \left(\xi_{e2}(\rho_f)-\delta\right)^2\cdot\left(2\cdot\delta + \xi_{e2}(\rho_f)\right)}{3\cdot\frac{\delta}{\beta}\cdot\left(2\cdot\xi_{e2}(\rho_f) - \delta\right) + 3\cdot\left(\xi_{e2}(\rho_f)-\delta\right)^2}\right]$$

Reduced moment of inertia

$$\Gamma_{oR} := \frac{\xi_o^3}{3} + (\alpha_s)\cdot\rho_s\cdot(1-\xi_o)^2 \qquad \Gamma_{oT} := \frac{\xi_o^3}{3}\cdot\left[1-(1-\beta)\cdot\left(1-\frac{\delta}{\xi_o}\right)^3\right] + (\alpha_s)\cdot\rho_s\cdot(1-\xi_o)^2$$

$$\Gamma_o := \text{if}\left(\xi_o\le\delta, \Gamma_{oR}, \Gamma_{oT}\right)$$

$$\Gamma_{1R} := \frac{\xi_{e1}^3}{3} + \frac{(\eta-\xi_{e1})^3}{3} + (\alpha_s - 1)\cdot\rho_s\cdot(1-\xi_{e1})^2$$

$$\Gamma_{1T} := \frac{\xi_{e1}^3}{3}\cdot\left[1-(1-\beta)\cdot\left(1-\frac{\delta}{\xi_{e1}}\right)^3\right] + \frac{(1-\beta)\cdot(\eta-\xi_{e1})^3}{3} + (\alpha_s-1)\cdot\rho_s\cdot(1-\xi_{e1})^2$$

$$\Gamma_1 := \text{if}\left(\xi_{e1}\le\delta, \Gamma_{1R}, \Gamma_{1T}\right)$$

$$\Gamma_{2R}(\rho_f) := \frac{\xi_{e2}(\rho_f)^3}{3} + \left[\alpha_s\cdot\rho_s\cdot\left(1-\xi_{e2}(\rho_f)\right)^2\right] + \alpha_f\rho_f\left(\eta-\xi_{e2}(\rho_f)\right)^2$$

$$\Gamma_{2T}(\rho_f) := \frac{\xi_{e2}(\rho_f)^3}{3}\cdot\left[1-(1-\beta)\cdot\left(1-\frac{\delta}{\xi_{e2}(\rho_f)}\right)^3\right] + \left[\alpha_s\cdot\rho_s\cdot\left(1-\xi_{e2}(\rho_f)\right)^2\right] + \alpha_f\rho_f\left(\eta-\xi_{e2}(\rho_f)\right)^2$$

$$\Gamma_2(\rho_f) := \text{if}\left(\xi_{e2}(\rho_f)\le\delta, \Gamma_{2R}(\rho_f), \Gamma_{2T}(\rho_f)\right)$$

Stress limitation

$$\upsilon_c(\rho_f, \Phi) := \frac{\mu_d(\rho_f)}{\Phi\cdot\gamma_c\cdot 0.5\cdot\xi_{e2}(\rho_f)\cdot\zeta_{e2}(\rho_f)}$$ < 0.6 (rare load combination)

< 0.45 (quasi-perm. load combination)

$$\upsilon_{s2}(\rho_f) := \alpha_s\cdot\upsilon_c(\rho_f, \Phi_r)\cdot\frac{f_{ck}}{f_{yk}}\cdot\frac{1-\xi_{e2}(\rho_f)}{\xi_{e2}(\rho_f)}$$ < 0.8 (rare load combniation)

$$\upsilon_{f2}(\rho_f) := \alpha_f\upsilon_c(\rho_f, \Phi_{qp})\cdot\frac{f_{ck}}{f_{fk}}\cdot\left[\frac{\eta-\xi_{e2}(\rho_f)}{\xi_{e2}(\rho_f)} - \eta_o\cdot\Phi_r\cdot\left(\frac{\xi_{e2}(\rho_f)}{\xi_o}\right)\right]$$ < 0.8 (quasi-perm. load comb.)

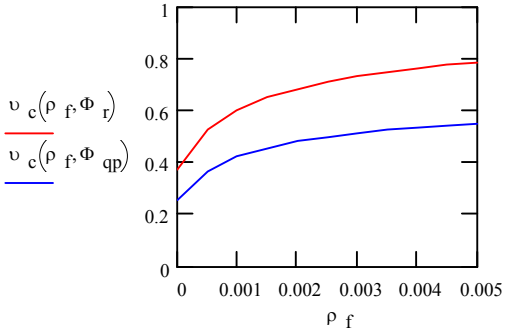

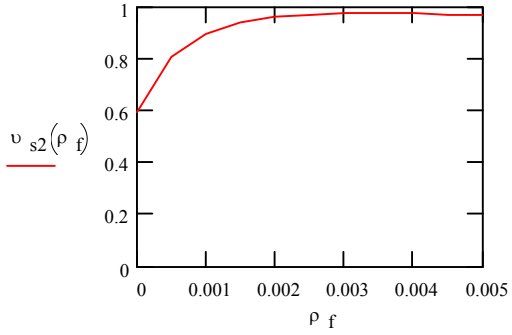

$\rho fmaxc := root\left(\upsilon_{c}(\rho g, 1.425) - 0.6, \rho g\right)$

$\rho fmaxs := root\left(\upsilon_{s2}(\rho g) - 0.8, \rho g\right)$

$\rho_{fmax} := min((\rho fmaxc\ \rho fmaxs))$

$\rho_{fmax} = 0.000455$

$\eta_{S}\left(\rho_{fmax}\right) = 1.42$

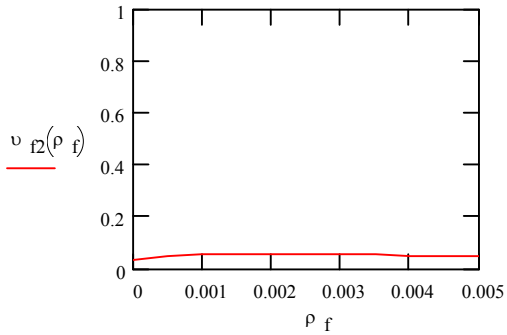

Crack limitation $bf\_b := 0.75$

$$d_{max}\left(\rho_{f}\right) := \frac{bf\_b}{2.53 \cdot \frac{\mu_{d}\left(\rho_{f}\right) \cdot f_{cd}}{\Phi_{qp} \cdot E_{s} \cdot \left(\rho_{s} + \frac{E_{f}}{E_{s}} \cdot \rho_{f}\right)} - 0.3 \cdot \rho_{s}}$$

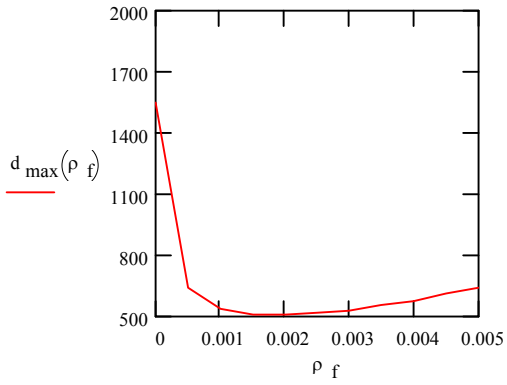

Limitation of deflection $k_{M} := \frac{1}{k}$

Parameters $k := 9.6$ $\beta 1\beta 2 := 1$ $a\_l_{max} := 0.002$

Based on the ULS moment capacity

$$l\_d1\left(\rho_{f}\right) := \frac{a\_l_{max}}{\left[\frac{1}{k} \cdot \left(\frac{\mu_{d}\left(\rho_{f}\right) \cdot f_{cd}}{\Phi_{qp} \cdot E_{c\phi} \cdot \Gamma_{1}}\right)\right]}$$

$$l\_d\zeta(\rho_f) := \frac{a\_l_{max}}{\left[\frac{\mu_d(\rho_f)\cdot f_{cd}}{k\cdot\Phi_{qp}\cdot E_{c\phi}}\cdot\left(\frac{\eta_o\cdot\eta_S(\rho_f)}{\Gamma_o}+\frac{1-\eta_o\cdot\eta_S(\rho_f)}{\Gamma_2(\rho_f)}\right)+\frac{\beta 1\beta 2}{k}\cdot\frac{f_{ctm}\cdot\eta^2}{6\cdot E_{c\phi}}\cdot\left(\frac{1}{\Gamma_1}-\frac{\eta_o\cdot\eta_S(\rho_f)}{\Gamma_o}-\frac{1-\eta_o\cdot\eta_S(\rho_f)}{\Gamma_2(\rho_f)}\right)\right]}$$

$$l\_d_{max}(\rho_f) := if\left[\left(\frac{\mu_d(\rho_f)\cdot f_{cd}}{\Phi_{qp}}\right)\le\frac{f_{ctm}\cdot\eta^2}{6}, l\_d1(\rho_f), l\_d\zeta(\rho_f)\right]$$

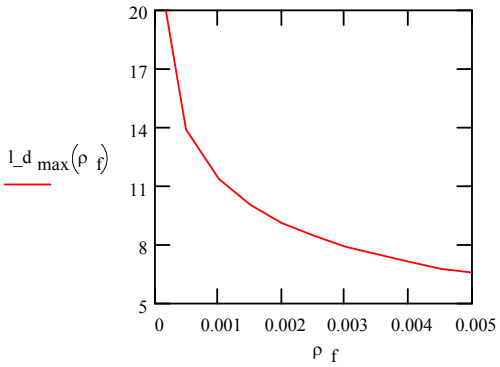

Given the acting design moment $\mu_d := 0.22$ $\eta_{Sk} := \frac{\mu_d}{\mu_{dU}}$

$$l\_d1 := \frac{a\_l_{max}}{\left[\frac{1}{k}\cdot\left(\frac{\mu_d\cdot f_{cd}}{\Phi_{qp}\cdot E_{c\phi}\cdot\Gamma_1}\right)\right]}$$

$$l\_d\zeta(\rho_f) := \frac{a\_l_{max}}{\left[\frac{\mu_d\cdot f_{cd}}{k\cdot\Phi_{qp}\cdot E_{c\phi}}\cdot\left(\frac{\eta_o\cdot\eta_{Sk}}{\Gamma_o}+\frac{1-\eta_o\cdot\eta_{Sk}}{\Gamma_2(\rho_f)}\right)+\frac{\beta}{k}\cdot\frac{f_{ctm}\cdot\eta^2}{6\cdot E_{c\phi}}\cdot\left(\frac{1}{\Gamma_1}-\frac{\eta_o\cdot\eta_{Sk}}{\Gamma_o}-\frac{1-\eta_o\cdot\eta_{Sk}}{\Gamma_2(\rho_f)}\right)\right]}$$

$$l\_d_{max}(\rho_f) := if\left[\left(\frac{\mu_d\cdot f_{cd}}{\Phi_{qp}}\right)\le\frac{f_{ctm}\cdot\eta^2}{6}, l\_d1, l\_d\zeta(\rho_f)\right]$$

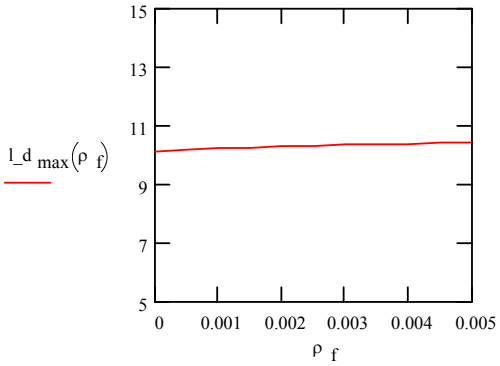

Appendix H
CALCULATION PROGRAMME FOR FLEXURAL STRENGTHENING

A design procedure for the dimensioning of FRP EBR for the flexural strengthening of reinforced concrete beams has been presented in Chapter 7, Section 3.7. As the procedure involves a relative large number of sometimes repetitive calculations, these have been programmed (using the software Mathcad) in a calculation sheet. This calculation programme is given in the following and deals with a simply supported beam strengthened in flexure and subjected to a uniform load. The cross-section of the beam is either T-shaped or rectangular (in the latter case the width b_w of the web is set equal to the width b of the beam).

The programme makes use of the design models provided in Chapter 7, Sections 2 and 3. Non-dimensional parameters used in the calculation are explained in Appendix G. To clarify some of the symbols used in the programme, reference is made to the textual comments in the programme as well as to the following figure.

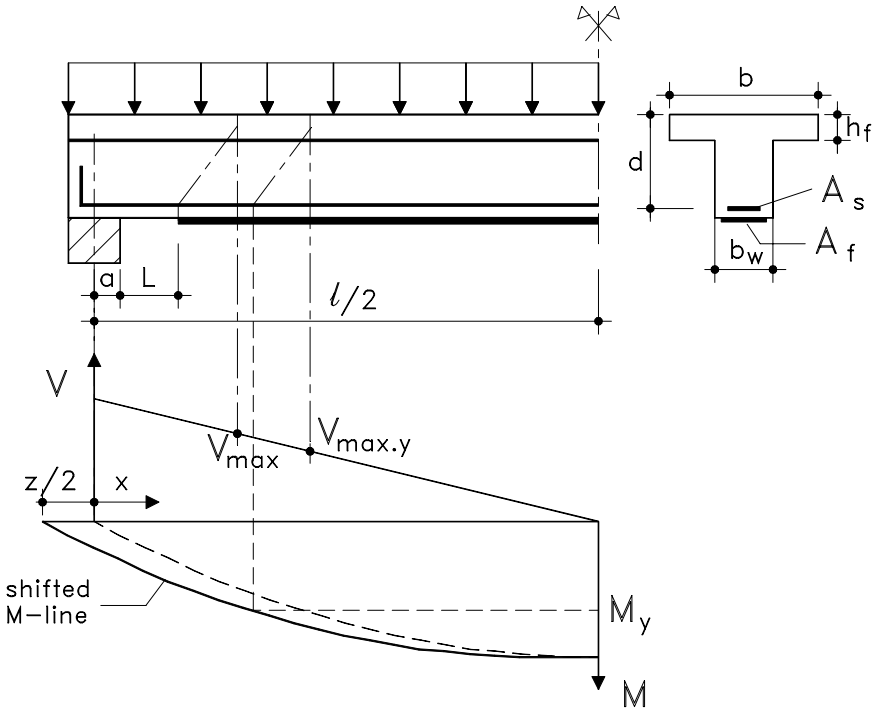

It is noted that the programme covers the design in bending. Herewith, it is assumed that the shear capacity is not critical. Of course this should be verified in addition to the flexural design calculation.

Simply supported beam, uniform load
Rectangular or T-section
Flexural strengthening

$kN := 1000 \cdot N$

$MPa := \frac{N}{mm^2}$

$‰ := 0.001$

PART A: Data and general definitions

Existing beam

Span length $l := 8 \cdot m$

Total beam depth $h := 500 \cdot mm$

Effective depth of steel reinf. $d := 435 \cdot mm$ $\eta := \frac{h}{d}$ $\frac{l}{d} = 18.4$

Width of flange $b := 800 \cdot mm$

Width of web $b_w := 250 \cdot mm$ $\beta := \frac{b_w}{b}$ $\beta = 0.31$

Depth of flange $h_f := 100 \cdot mm$ $\delta := \frac{h_f}{d}$ $\delta = 0.23$

Amount of steel reinforcement $A_s := 2454 \cdot mm^2$ $\rho_s := \frac{A_s}{b \cdot d}$ $\rho_s = 0.71 \cdot ‰$

(mean) diameter $\phi := 25 \cdot mm$ $\rho\rho_s := \frac{A_s}{b_w \cdot d}$ $\rho\rho_s = 2.26 \cdot ‰$

Half of the support width $a := 100 \cdot mm$

Safety factors

Material safety factor concrete $\gamma_c := 1.5$

Material safety factor steel $\gamma_s := 1.15$

Material safety factor FRP $\gamma_f := 1.3$

Load safety factor dead load $\gamma_g := 1.35$

Load safety factor live load $\gamma_q := 1.5$

Load combination factor for the quasi-permanetn load combination $\psi_2 := 0.4$

Concrete grade

$f_{ck} := 20 \cdot MPa$

$f_{ctm} := 0.3 \cdot MPa^{\frac{1}{3}} \cdot f_{ck}^{\frac{2}{3}}$

$f_{cd} := \frac{f_{ck}}{\gamma_c}$ $f_{cd} = 13.33 \cdot MPa$

$f_{ctk} := 0.7 \cdot f_{ctm}$

$E_c := 9500 \cdot MPa^{\frac{2}{3}} \cdot \left(f_{ck} + 8 \cdot MPa\right)^{\frac{1}{3}}$

$E_c = 28848 \cdot MPa$

$\varepsilon_{cu} := 3.5 \cdot ‰$

Steel grade

$f_{yk} := 400 \cdot MPa$ $\quad f_{yd} := \frac{f_{yk}}{\gamma_s}$ $\quad f_{yd} = 348 \cdot MPa$

$E_s := 200000 \cdot MPa$

$\varepsilon_{su} := 25 \cdot \%o$

FRP grade

$f_{fk} := 2800 \cdot MPa$ $\quad f_{fd} := \frac{f_{fk}}{\gamma_f}$ $\quad f_{fd} = 2154 \cdot MPa$

$E_f := 165000 \cdot MPa$

$\varepsilon_{fuk} := 1.65 \cdot \%$

$E_{fu} := \frac{f_{fk}}{\varepsilon_{fuk}}$ $\quad E_{fu} = 169697 \cdot MPa$ $\quad \varepsilon_{fud} := \frac{f_{fd}}{E_{fu}}$

E-moduli for the SLS

Creep coefficient $\quad \phi_c := 1.15$

$E_{c\phi} := \frac{E_c}{(1 + \phi_c)}$ $\quad \alpha_s := \frac{E_s}{E_{c\phi}}$ $\quad \alpha_s = 15$ $\quad \alpha_f := \frac{E_f}{E_{c\phi}}$ $\quad \alpha_f = 12$

Acting loads on unstrengthened beam

Dead load (self weight beam included) $\quad g_U := 15 \cdot \frac{kN}{m}$

$M_{gkU} := \frac{g_U \cdot l^2}{8}$ $\quad M_{gkU} = 120.0 \cdot kN \cdot m$

$M_{gdU} := M_{gkU} \cdot \gamma_g$ $\quad M_{gdU} = 162.0 \cdot kN \cdot m$

Live load $\quad q_U := 10 \cdot \frac{kN}{m}$

$M_{qkU} := \frac{q_U \cdot l^2}{8}$ $\quad M_{qkU} = 80.0 \cdot kN \cdot m$

$M_{qdU} := M_{qkU} \cdot \gamma_q$ $\quad M_{qdU} = 120.0 \cdot kN \cdot m$

Acting moment

$M_{kU.r} := M_{gkU} + M_{qkU}$ $\quad M_{kU.r} = 200.0 \cdot kN \cdot m$ $\quad$ (rare load comb.)

$M_{kU.qp} := M_{gkU} + \psi_2 \cdot M_{qkU}$ $\quad M_{kU.qp} = 152.0 \cdot kN \cdot m$ $\quad$ (quasi-perm load comb.)

Acting design moment

$M_{dU} := M_{gdU} + M_{qdU}$ $\quad M_{dU} = 282.0 \cdot kN \cdot m$

Acting loads on strengthened beam

Dead load (self weight beam included) $g_S := 15 \cdot \frac{kN}{m}$

$M_{gkS} := \frac{g_S \cdot l^2}{8}$ $M_{gkS} = 120.0\ kN \cdot m$ $V_{gkS} := \frac{g_S \cdot l}{2}$

$M_{gdS} := M_{gkS} \cdot \gamma_g$ $M_{gdS} = 162.0\ kN \cdot m$ $V_{gdS} := V_{gkS} \cdot \gamma_g$

Live load $q_S := 20 \cdot \frac{kN}{m}$

$M_{qkS} := \frac{q_S \cdot l^2}{8}$ $M_{qkS} = 160.0\ kN \cdot m$ $V_{qkS} := \frac{q_S \cdot l}{2}$

$M_{qdS} := M_{qkS} \cdot \gamma_q$ $M_{qdS} = 240.0\ kN \cdot m$ $V_{qdS} := V_{qkS} \cdot \gamma_q$

Acting moment

$M_{kS.r} := M_{gkS} + M_{qkS}$ $M_{kS.r} = 280.0\ kN \cdot m$ (rare load comb.)

$M_{kS.qp} := M_{gkS} + \psi_2 \cdot M_{qkS}$ $M_{kS.qp} = 184.0\ kN \cdot m$ (quasi-perm load comb.)

Acting design moment

$M_{dS} := M_{gdS} + M_{qdS}$ $M_{dS} = 402.0\ kN \cdot m$ $\frac{M_{dS}}{M_{dU}} = 1.43$

Acting design shear load

$V_{dS} := V_{gdS} + V_{qdS}$ $V_{dS} = 201.0\ kN$

Acting loads during strengthening

Dead load (self weight beam included) $g_o := 15 \cdot \frac{kN}{m}$

$M_{go} := \frac{g_o \cdot l^2}{8}$ $M_{go} = 120.0\ kN \cdot m$

Live load $q_o := 0 \cdot \frac{kN}{m}$

$M_{qo} := \frac{q_o \cdot l^2}{8}$ $M_{qo} = 0.0\ kN \cdot m$

Acting moment during strengthening

$M_o := M_{go} + M_{qo}$ $M_o = 120.0\ kN \cdot m$ $\frac{M_o}{M_{kU.r}} = 0.60$

PART B: UNSTRENGTHENED

Ultimate limit state (ULS)

Concrete stress block parameters

$$\xi_{lim1s} := \frac{\varepsilon_{cu}}{\varepsilon_{cu} + \varepsilon_{su}} \qquad \xi_{lim2d} := \frac{\varepsilon_{cu}}{\varepsilon_{cu} + \frac{f_{yd}}{E_s}}$$

$$\lambda 1(\xi) := \text{if}\left(\xi < \xi_{lim1s}, \frac{0.002}{\varepsilon_{su}} \cdot \frac{1-\xi}{\xi}, \frac{0.002}{\varepsilon_{cu}}\right)$$

$$\lambda 2(\xi) := \text{if}\left(\xi < \xi_{lim1s}, \frac{0.002}{\varepsilon_{su}} \cdot \frac{\xi}{\xi-\delta} \cdot \frac{1-\xi}{\xi}, \frac{0.002}{\varepsilon_{cu}} \cdot \frac{\xi}{\xi-\delta}\right)$$

$$\psi 1(\xi) := \text{if}\left(\lambda 1(\xi) \geq 1, \frac{3\cdot\lambda 1(\xi) - 1}{3\cdot\lambda 1(\xi)^2}, 1 - \frac{\lambda 1(\xi)}{3}\right)$$

$$\psi 2(\xi) := \text{if}\left(\lambda 2(\xi) \geq 1, \frac{3\cdot\lambda 2(\xi) - 1}{3\cdot\lambda 2(\xi)^2}, 1 - \frac{\lambda 2(\xi)}{3}\right)$$

$$\psi(\xi) := \text{if}\left[\xi \leq \delta, \psi 1(\xi), \psi 1(\xi) - \psi 2(\xi)\cdot(1-\beta)\cdot\left(1 - \frac{\delta}{\xi}\right)\right]$$

$$\delta 1_g(\xi) := \text{if}\left[\lambda 1(\xi) \geq 1, \frac{4\cdot\lambda 1(\xi) - 1}{4\cdot(3\cdot\lambda 1(\xi) - 1)}, \frac{\lambda 1(\xi)^2 - 4\cdot\lambda 1(\xi) + 6}{4\cdot(3 - \lambda 1(\xi))}\right]$$

$$\delta 2_g(\xi) := \text{if}\left[\lambda 2(\xi) \geq 1, \frac{4\cdot\lambda 2(\xi) - 1}{4\cdot(3\cdot\lambda 2(\xi) - 1)}, \frac{\lambda 2(\xi)^2 - 4\cdot\lambda 2(\xi) + 6}{4\cdot(3 - \lambda 2(\xi))}\right]$$

$$\delta_g(\xi) := \text{if}\left[\xi \leq \delta, \delta 1_g(\xi), \frac{\left[\psi 1(\xi)\cdot\delta 1_g(\xi) - \psi 2(\xi)\cdot\delta 2_g(\xi)\cdot(1-\beta)\cdot\left(1-\frac{\delta}{\xi}\right)^2 - \psi 2(\xi)\cdot(1-\beta)\cdot\left(1-\frac{\delta}{\xi}\right)\cdot\frac{\delta}{\xi}\right]}{\psi(\xi)}\right]$$

Resisting design moment

Guess values $\xi_g := 0.3$

$$\xi_{dU} := \text{root}\left(\frac{\xi_g\cdot 0.85\cdot\psi(\xi_g)\cdot f_{cd}}{f_{yd}} - \rho_s, \xi_g\right) \qquad \xi_{dU} = 0.28$$

$$x_{dU} := \xi_{dU}\cdot d \qquad x_{dU} = 121\cdot\text{mm}$$

$$\text{if}\left(\xi_{dU} \geq \xi_{lim1s}, \text{if}\left(\xi_{dU} \geq \xi_{lim2d}, \text{"CC/noYS"}, \text{"YS/CC"}\right), \text{"YS/FR"}\right) = \text{"YS/CC"}$$

$$\mu_{dU} := \xi_{dU}\cdot 0.85\cdot\psi\left(\xi_{dU}\right)\cdot\left(1 - \delta_g\left(\xi_{dU}\right)\cdot\xi_{dU}\right) \qquad \mu_{dU} = 0.163$$

$$M_{RdU} := \mu_{dU}\cdot b\cdot d^2\cdot f_{cd} \qquad M_{RdU} = 329.2\cdot\text{kN}\cdot\text{m} \qquad \frac{M_{RdU}}{M_{dU}} = 1.17$$

$$\text{if}\left(\frac{M_{RdU}}{M_{dU}} \geq 1, \text{"resisting > acting"}, \text{"resisting < acting"}\right) = \text{"resisting > acting"}$$

No brittle failure at first cracking?

$$\rho_{s.min} := 0.095 \cdot MPa^{\frac{1}{3}} \cdot \frac{f_{ck}^{\frac{2}{3}}}{f_{yk}} \qquad \rho_{s.min} = 0.17 \cdot \%$$

$$if\left(\rho_{s.min} < \rho_s, \text{"no brittle failure"}, \text{"britte failure at 1st cracking"}\right) = \text{"no brittle failure"}$$

Serviceability limit state (SLS)

Neutral axis and moment of inertia

$$\xi_{e1R} := root\left[\xi g - \frac{(\eta - \xi g)^2}{\xi g} - 2 \cdot \alpha_s \cdot \rho_s \cdot \left(\frac{1 - \xi g}{\xi g}\right), \xi g\right]$$

$$\xi_{e1T} := root\left[\xi g - \frac{(1 - \beta) \cdot (\eta - \xi g)^2}{\xi g} - 2 \cdot \alpha_s \cdot \rho_s \cdot \left(\frac{1 - \xi g}{\xi g}\right), \xi g\right]$$

$$\xi_{e1} := if\left(\xi_{e1R} \le \delta, \xi_{e1R}, \xi_{e1T}\right) \qquad \xi_{e1} = 0.57 \qquad x_{e1} := \xi_{e1} \cdot d$$

$$\xi_{e2R} := root\left[\xi g - \left(2 \cdot \rho_s\right) \cdot \alpha_s \cdot \frac{1 - \xi g}{\xi g}, \xi g\right]$$

$$\xi_{e2T} := root\left[\xi g - \xi g \cdot \left[(1 - \beta) \cdot \left(1 - \frac{\delta}{\xi g}\right)^2\right] - 2 \cdot \rho_s \cdot \alpha_s \cdot \frac{1 - \xi g}{\xi g}, \xi g\right]$$

$$\xi_{e2} := if\left(\xi_{e2R} \le \delta, \xi_{e2R}, \xi_{e2T}\right) \qquad \xi_{e2} = 0.38 \qquad x_{e2} := \xi_{e2} \cdot d$$

$$\Gamma_{1R} := \frac{\xi_{e1}^3}{3} + \frac{\left(\eta - \xi_{e1}\right)^3}{3} + \left(\alpha_s - 1\right) \cdot \rho_s \cdot \left(1 - \xi_{e1}\right)^2$$

$$\Gamma_{1T} := \frac{\xi_{e1}^3}{3} \cdot \left[1 - (1 - \beta) \cdot \left(1 - \frac{\delta}{\xi_{e1}}\right)^3\right] + \frac{(1 - \beta) \cdot \left(\eta - \xi_{e1}\right)^3}{3} + \left(\alpha_s - 1\right) \cdot \rho_s \cdot \left(1 - \xi_{e1}\right)^2$$

$$\Gamma_1 := if\left(\xi_{e1} \le \delta, \Gamma_{1R}, \Gamma_{1T}\right) \qquad I_1 := \Gamma_1 \cdot b \cdot d^3 \qquad I_1 = 7.61 \cdot 10^9 \cdot mm^4$$

$$\Gamma_{2R} := \frac{\xi_{e2}^3}{3} + \left(\alpha_s\right) \cdot \rho_s \cdot \left(1 - \xi_{e2}\right)^2$$

$$\Gamma_{2T} := \frac{\xi_{e2}^3}{3} \cdot \left[1 - (1 - \beta) \cdot \left(1 - \frac{\delta}{\xi_{e2}}\right)^3\right] + \left(\alpha_s\right) \cdot \rho_s \cdot \left(1 - \xi_{e2}\right)^2$$

$$\Gamma_2 := if\left(\xi_{e2} \le \delta, \Gamma_{2R}, \Gamma_{2T}\right) \qquad I_2 := \Gamma_2 \cdot b \cdot d^3 \qquad I_2 = 3.81 \cdot 10^9 \cdot mm^4 \qquad I_{o2} := I_2$$

Cracking load

$$M_{cr} := f_{ctm} \cdot \frac{I_1}{\left(h - x_{e1}\right)} \qquad M_{cr} = 66.5 \cdot kN \cdot m$$

$$if\left(M_{cr} \ge M_{kU.qp}, \text{"not cracked"}, \text{"cracked"}\right) = \text{"cracked"}$$

Stresses

$$\sigma_c(M) := \frac{M}{0.5 \cdot b \cdot x_{e2} \cdot \left(d - \frac{x_{e2}}{3}\right)} \qquad \sigma_c\left(M_{kU.r}\right) = 7.93 \cdot MPa \qquad \sigma_c\left(M_{kU.qp}\right) = 6.03 \cdot MPa$$

$$if\left(\sigma_c\left(M_{kU.r}\right) \le 0.6 \cdot f_{ck}, "OK", "SLS\ stress\ limit\ exceeded"\right) = "OK"$$

$$if\left(\sigma_c\left(M_{kU.qp}\right) \le 0.45 \cdot f_{ck}, "OK", "SLS\ stress\ limit\ exceeded"\right) = "OK"$$

$$\sigma_s := \frac{M_{kU.r}}{A_s \cdot \left(d - \frac{x_{e2}}{3}\right)} \qquad \sigma_s = 215 \cdot MPa$$

$$if\left(\sigma_s \le 0.8 \cdot f_{yk}, "OK", "SLS\ stress\ limit\ exceeded"\right) = "OK"$$

Crack widths

$k_1 := 0.8$ $\quad k_2 := 0.5$ $\quad \beta 1\beta 2 := 0.5$ $\quad \zeta := 1 - \beta 1\beta 2 \cdot \left(\frac{M_{cr}}{M_{kU.qp}}\right)^2$

$$h_r := \min\left[\left[2.5 \cdot (h - d) \quad \frac{h - x_{e2}}{3}\right]\right] \qquad \rho_r := \frac{A_s}{h_r \cdot b_w}$$

$$s_{rm} := 50 \cdot mm + 0.25 \cdot k_1 \cdot k_2 \cdot \frac{\phi}{\rho_r}$$

$$\varepsilon_{sm} := \zeta \cdot \frac{\sigma_s}{E_s}$$

$$w_k := 1.7 \cdot s_{rm} \cdot \varepsilon_{sm} \qquad w_k = 0.13 \cdot mm$$

$$if\left(w_k \le 0.3 \cdot mm, "OK", "SLS\ stress\ limit\ exceeded"\right) = "OK"$$

Deflections

$\beta 1\beta 2 := 0.5$ $\quad \zeta_b := 1 - \beta 1\beta 2 \cdot \left(\frac{M_{cr}}{M_{kU.qp}}\right)$

$$a_1 := \frac{5}{384} \cdot \frac{\left(g_U + \psi_2 \cdot q_U\right) \cdot l^4}{E_{c\phi} \cdot I_1} \qquad a_1 = 9.9 \cdot mm$$

$$a_2 := \frac{5}{384} \cdot \frac{\left(g_U + \psi_2 \cdot q_U\right) \cdot l^4}{E_{c\phi} \cdot I_2} \qquad a_2 = 19.8 \cdot mm$$

$$a := a_1 \cdot \left(1 - \zeta_b\right) + a_2 \cdot \zeta_b \qquad a = 17.6 \cdot mm \qquad \frac{l}{a} = 454$$

$$if\left(\frac{a}{l} \le \frac{1}{250}, "OK", "SLS\ deflection\ limit\ exceeded"\right) = "OK"$$

PART C: STRENGTHENED

Initial state

$\xi_o := \xi_{e2}$

$M_o = 120.0\ \text{kN·m}$

$\varepsilon_{co} := \frac{M_o \cdot x_{e2}}{E_c \cdot I_2}$ $\varepsilon_o := \varepsilon_{co} \cdot \frac{\eta - \xi_o}{\xi_o}$ $\varepsilon_o = 0.36\ \text{‰}$

Ulitimate limit state (ULS)

Concrete stress block parameters

$\xi_{lim1} := \frac{\varepsilon_{cu}}{\varepsilon_{cu} + \varepsilon_{fud} + \varepsilon_o} \cdot \eta$

$\lambda 1(\xi) := \text{if}\left(\xi < \xi_{lim1}, \frac{0.002}{\varepsilon_{fud} + \varepsilon_o} \cdot \frac{\eta - \xi}{\xi}, \frac{0.002}{\varepsilon_{cu}}\right)$

$\lambda 2(\xi) := \text{if}\left(\xi < \xi_{lim1}, \frac{0.002}{\varepsilon_{fud} + \varepsilon_o} \cdot \frac{\xi}{\xi - \delta} \cdot \frac{\eta - \xi}{\xi}, \frac{0.002}{\varepsilon_{cu}} \cdot \frac{\xi}{\xi - \delta}\right)$

$\psi 1(\xi) := \text{if}\left(\lambda 1(\xi) \geq 1, \frac{3 \cdot \lambda 1(\xi) - 1}{3 \cdot \lambda 1(\xi)^2}, 1 - \frac{\lambda 1(\xi)}{3}\right)$

$\psi 2(\xi) := \text{if}\left(\lambda 2(\xi) \geq 1, \frac{3 \cdot \lambda 2(\xi) - 1}{3 \cdot \lambda 2(\xi)^2}, 1 - \frac{\lambda 2(\xi)}{3}\right)$

$\psi(\xi) := \text{if}\left[\xi \leq \delta, \psi 1(\xi), \psi 1(\xi) - \psi 2(\xi) \cdot (1 - \beta) \cdot \left(1 - \frac{\delta}{\xi}\right)\right]$

$\delta 1_g(\xi) := \text{if}\left[\lambda 1(\xi) \geq 1, \frac{4 \cdot \lambda 1(\xi) - 1}{4 \cdot (3 \cdot \lambda 1(\xi) - 1)}, \frac{\lambda 1(\xi)^2 - 4 \cdot \lambda 1(\xi) + 6}{4 \cdot (3 - \lambda 1(\xi))}\right]$

$\delta 2_g(\xi) := \text{if}\left[\lambda 2(\xi) \geq 1, \frac{4 \cdot \lambda 2(\xi) - 1}{4 \cdot (3 \cdot \lambda 2(\xi) - 1)}, \frac{\lambda 2(\xi)^2 - 4 \cdot \lambda 2(\xi) + 6}{4 \cdot (3 - \lambda 2(\xi))}\right]$

$\delta_g(\xi) := \text{if}\left[\xi \leq \delta, \delta 1_g(\xi), \frac{\left[\psi 1(\xi) \cdot \delta 1_g(\xi) - \psi 2(\xi) \cdot \delta 2_g(\xi) \cdot (1 - \beta) \cdot \left(1 - \frac{\delta}{\xi}\right)^2 - \psi 2(\xi) \cdot (1 - \beta) \cdot \left(1 - \frac{\delta}{\xi}\right) \cdot \frac{\delta}{\xi}\right]}{\psi(\xi)}\right]$

Amount of FRP needed for ULS

Guess values $\xi g := 0.3$ $\rho g := 0.1 \cdot \%$

$\varepsilon_f(\xi) := \text{if}\left(\xi < \xi_{lim1}, \varepsilon_{fud}, \varepsilon_{cu} \cdot \frac{\eta - \xi}{\xi} - \varepsilon_o\right)$

$\xi_d(\rho_f) := \text{root}\left(0.85 \cdot \psi(\xi g) \cdot \xi g \cdot f_{cd} - \rho_s \cdot f_{yd} - \rho_f E_{fu} \cdot \varepsilon_f(\xi g), \xi g\right)$

$\mu_d(\rho_f) := \xi_d(\rho_f) \cdot 0.85 \cdot \psi\left(\xi_d(\rho_f)\right) \cdot \left(1 - \delta_g\left(\xi_d(\rho_f)\right) \cdot \xi_d(\rho_f)\right) + \rho_f \frac{E_{fu} \cdot \varepsilon_f\left(\xi_d(\rho_f)\right)}{f_{cd}} \cdot (\eta - 1)$

$\rho_{f.ULS} := root\left(\mu_d(\rho g) - \frac{M_{dS}}{b \cdot d^2 \cdot f_{cd}}, \rho g\right)$ $\rho_{f.ULS} = 0.06\,\%$

$A_{f.ULS} := \rho_{f.ULS} b \cdot d$ $A_{f.ULS} = 194.24\,mm^2$

Choose value based on available sizes :

Total bond width of FRP (width of FRP times number next to each other) $u_f := 200 \cdot mm$

Thickness of FRP $t_f := 1.2 \cdot mm$

Number of layers $n_f := 1$

$A_f := n_f t_f u_f$ $A_f = 240.00\,mm^2$

$\rho_f := \frac{A_f}{b \cdot d}$ $\rho_f = 0.07\,\%$ $\rho\rho_f := \frac{A_f}{b_w \cdot d}$ $\rho\rho_f = 0.22\,\%$

Resisting design moment

$x_d := \xi_d(\rho_f) \cdot d$ $x_d = 193.12\,mm$

$if(x_d \geq \xi_{lim1} \cdot d, if(x_d \geq \xi_{lim2d} d, "CC/noYS", "YS/CC"), "YS/FR") = "YS/CC"$

$\varepsilon_s := \varepsilon_{cu} \cdot \frac{d - x_d}{x_d}$ $\varepsilon_s = 4.38\,‰$

$\varepsilon_f := \varepsilon_{cu} \cdot \frac{h - x_d}{x_d} - \varepsilon_o$ $\varepsilon_f = 5.20\,‰$

$M_{RdS} := \mu_d(\rho_f) \cdot b \cdot d^2 \cdot f_{cd}$ $M_{RdS} = 410.56\,kN \cdot m$ $\frac{M_{RdS}}{M_{dS}} = 1.02$

Ductility condition

$\xi_{lim} := 0.45$

$if(x_d \geq \xi_{lim} \cdot d, "Insufficient\ ductility", "OK") = "OK"$

Serviceability limit state (SLS)

Neutral axis and moment of inertia

$$\xi_{e2R}(\rho_f, M) := \text{root}\left[\xi g - 2\cdot\alpha_s\cdot\rho_s\cdot\left(\frac{1-\xi g}{\xi g}\right) - 2\cdot\alpha_f\rho_f\left[\frac{\eta-\xi g}{\xi g} - \frac{M_o}{M}\cdot\left(\frac{\xi g}{\xi_o}\right)\right], \xi g\right]$$

$$\xi_{e2T}(\rho_f, M) := \text{root}\left[\xi g - \xi g\cdot(1-\beta)\cdot\left(1-\frac{\delta}{\xi g}\right)^2 - 2\cdot\alpha_s\cdot\rho_s\cdot\left(\frac{1-\xi g}{\xi g}\right) - 2\cdot\alpha_f\rho_f\left[\frac{\eta-\xi g}{\xi g} - \frac{M_o}{M}\cdot\left(\frac{\xi g}{\xi_o}\right)\right], \xi g\right]$$

$$\xi_{e2}(\rho_f, M) := \text{if}\left(\xi_{e2R}(\rho_f, M) \le \delta, \xi_{e2R}(\rho_f, M), \xi_{e2T}(\rho_f, M)\right)$$

$$\Gamma_{2R}(\rho_f, M) := \frac{\xi_{e2}(\rho_f, M)^3}{3} + \left[\alpha_s\cdot\rho_s\cdot\left(1-\xi_{e2}(\rho_f, M)\right)^2\right] + \alpha_f\rho_f\left(\eta-\xi_{e2}(\rho_f, M)\right)^2$$

$$\Gamma_{2T}(\rho_f, M) := \frac{\xi_{e2}(\rho_f, M)^3}{3}\cdot\left[1-(1-\beta)\cdot\left(1-\frac{\delta}{\xi_{e2}(\rho_f, M)}\right)^3\right] + \left[\alpha_s\cdot\rho_s\cdot\left(1-\xi_{e2}(\rho_f, M)\right)^2\right] + \alpha_f\rho_f\left(\eta-\xi_{e2}(\rho_f, M)\right)^2$$

$$\Gamma_2(\rho_f, M) := \text{if}\left(\xi_{e2}(\rho_f, M) \le \delta, \Gamma_{2R}(\rho_f, M), \Gamma_{2T}(\rho_f, M)\right)$$

Deflections

$$a_{max} := \frac{l}{250} \qquad \beta 1\beta 2 := 0.5 \qquad \zeta_b := 1 - \beta 1\beta 2\cdot\left(\frac{M_{cr}}{M_{kS.qp}}\right)$$

$$I_2 := \Gamma_2(\rho_f, M_{kS.qp})\cdot b\cdot d^3 \qquad I_2 = 4.14\cdot 10^9\ \text{mm}^4$$

$$a_1 := \frac{5}{384}\cdot\frac{(g_S + \psi_2\cdot q_S)\cdot l^4}{E_{c\phi}\cdot I_1} \qquad a_1 = 12.0\ \text{mm}$$

$$a_2 := \frac{5}{384}\cdot\frac{(g_o + \psi_2\cdot q_o)\cdot l^4}{E_{c\phi}\cdot I_{o2}} + \frac{5}{384}\cdot\frac{\left[(g_S + \psi_2\cdot q_S) - (g_o + \psi_2\cdot q_o)\right]\cdot l^4}{E_{c\phi}\cdot I_2} \qquad a_2 = 23.3\ \text{mm}$$

$$a := a_1\cdot(1-\zeta_b) + a_2\cdot\zeta_b \qquad a = 21.3\ \text{mm} \qquad \frac{l}{a} = 376$$

$$\text{if}\left(\frac{a}{l} \le \frac{1}{250}, \text{"OK"}, \text{"SLS deflection limit exceeded"}\right) = \text{"OK"}$$

If "OK" the following calculation may be neglected (go to next SLS verification)

Amount of FRP needed to fulfil SLS of deflections

$$a_{2max} := \frac{a_{max} - (1-\zeta_b)\cdot a_1}{\zeta_b} \qquad a_{2max} = 36.4\ \text{mm}$$

$$I_{2min} := \frac{5}{384}\cdot\frac{\left[(g_S + \psi_2\cdot q_S) - (g_o + \psi_2\cdot q_o)\right]\cdot l^4}{E_{c\phi}\cdot\left[a_{2max} - \frac{5}{384}\cdot\frac{(g_o + \psi_2\cdot q_o)\cdot l^4}{E_{c\phi}\cdot I_{o2}}\right]} \qquad I_{2min} = 1.53\cdot 10^9\ \text{mm}^4$$

$$\rho_{f.min.defl} := \text{root}\left(\Gamma_2(\rho g, M_{kS.qp}) - \frac{I_{2min}}{b\cdot d^3}, \rho g\right)$$

$A_{f.min.defl} := \rho_{f.min.defl} b \cdot d$ $A_{f.min.defl} = -1 \cdot 10^{3}\ mm^2$

Choose new value if needed:

Number of layers $n_f := 1$ $A_f := n_f t_f u_f$ $A_f = 240.00\ mm^2$

$\rho_f := \frac{A_f}{b \cdot d}$ $\rho_f = 0.07\ \%$ $\rho\rho_f := \frac{A_f}{b_w \cdot d}$ $\rho\rho_f = 0.22\ \%$

Stresses

$$\varepsilon_c(\rho_f, M) := \frac{M}{0.5 \cdot b \cdot d^2 \cdot \xi_{e2}(\rho_f, M) \cdot E_{c\phi} \cdot \left(\eta - \frac{\xi_{e2}(\rho_f, M)}{3}\right) - A_s \cdot E_s \cdot \frac{(1 - \xi_{e2}(\rho_f, M))}{\xi_{e2}(\rho_f, M)} \cdot (h - d)}$$

$\sigma_{c.r} := E_{c\phi} \cdot \varepsilon_c(\rho_f, M_{kS.r})$ $\sigma_{c.r} = 10.47\ MPa$

$\sigma_{c.qp} := E_{c\phi} \cdot \varepsilon_c(\rho_f, M_{kS.qp})$ $\sigma_{c.qp} = 6.92\ MPa$

$if(\sigma_{c.r} \le 0.6 \cdot f_{ck}, "OK", "SLS stress limit exceeded") = "OK"$

$if(\sigma_{c.qp} \le 0.45 \cdot f_{ck}, "OK", "SLS stress limit exceeded") = "OK"$

$$\sigma_{s.r} := E_s \cdot \varepsilon_c(\rho_f, M_{kS.r}) \cdot \frac{1 - \xi_{e2}(\rho_f, M_{kS.r})}{\xi_{e2}(\rho_f, M_{kS.r})} \qquad \sigma_{s.r} = 239.55\ MPa$$

$if(\sigma_{s.r} \le 0.8 \cdot f_{yk}, "OK", "SLS stress limit exceeded") = "OK"$

$$\sigma_{f.qp} := E_f \left(\varepsilon_c(\rho_f, M_{kS.qp}) \cdot \frac{\eta - \xi_{e2}(\rho_f, M_{kS.qp})}{\xi_{e2}(\rho_f, M_{kS.qp})} - \varepsilon_o\right) \qquad \sigma_{f.qp} = 104.62\ MPa$$

$if(\sigma_{f.qp} \le 0.8 \cdot f_{fk}, "OK", "SLS stress limit exceeded") = "OK"$

If "OK" the following calculation may be neglected (go to next SLS verification)

Amount of FRP needed to fulfil concrete stress

$$\rho_{f.min.c.r} := root\left(E_c \cdot \varepsilon_c(\rho_f, M_{kS.r}) - 0.6 \cdot f_{ck}, \rho g\right)$$

$A_{f.min.c.r} := \rho_{f.min.c.r} b \cdot d$ $A_{f.min.c.r} =\ mm^2$

Amount of FRP needed to fulfil steel stress

$$\rho_{f.min.c.r} := root\left(E_s \cdot \varepsilon_c(\rho_f, M_{kS.r}) \cdot \frac{1 - \xi_{e2}(\rho_f, M_{kS.r})}{\xi_{e2}(\rho_f, M_{kS.r})} - 0.8 \cdot f_{yk}, \rho g\right)$$

$A_{f.min.s.r} := \rho_{f.min.s.r} b \cdot d$ $A_{f.min.s.r} =\ mm^2$

Choose new value if needed:

Number of layers $n_f := 1$ $A_f := n_f t_f u_f$ $A_f = 240.00\ mm^2$

$\rho_f := \frac{A_f}{b \cdot d}$ $\rho_f = 0.07\ \%$ $\rho\rho_f := \frac{A_f}{b_w \cdot d}$ $\rho\rho_f = 0.22\ \%$

Cracking

$\beta 1\beta 2 := 0.5$ $\zeta := 1 - \beta 1\beta 2 \cdot \left(\frac{M_{cr}}{M_{kS.qp}}\right)^2$

$x_{e2} := \xi_{e2}(\rho_f, M_{kS.qp}) \cdot d$

$z_{e2} := 1.05 \cdot d - \frac{x_{e2}}{3}$

$h_r := \min\left[\left[2.5 \cdot (h - d) \quad \frac{h - x_{e2}}{3}\right]\right]$ $\rho_{c.eff} := \frac{h_r \cdot b_w}{d \cdot b}$ $A_{c.eff} := h_r \cdot b_w$

$\rho_{eq} := \rho_s + \frac{E_f}{E_s} \cdot \rho_f$

$n_s := \frac{4 \cdot A_s}{\pi \cdot \phi^2}$ $n_s = 5.0$ $u_s := n_s \cdot \pi \cdot \phi$ $u_s = 392.6\ mm$

$\xi_b := 0.69 \cdot \frac{E_s}{E_f} \cdot \frac{A_s}{A_f} \cdot \frac{u_s}{u_f}$

$s_{rm} := 1.11 \cdot \frac{A_{c.eff}}{u_s} \cdot \frac{E_s \cdot A_s}{E_s \cdot A_s + \xi_b \cdot E_f \cdot A_f}$ $s_{rm} = 32.94\ mm$

$\varepsilon_2 := \frac{\frac{M_{kS.qp}}{z_{e2}} + E_f \cdot A_f \cdot \varepsilon_o}{\left(E_s \cdot A_s + \xi_b \cdot E_f \cdot A_f\right)}$ $\varepsilon_2 = 0.41\ ‰$

$w_k := 1.7 \cdot \zeta \cdot s_{rm} \cdot \varepsilon_2$ $w_k = 0.02\ mm$

$\text{if}\left(w_k \le 0.3 \cdot mm, \text{"OK"}, \text{"crack limit exceeded"}\right) = \text{"OK"}$

If "OK" the following calculation may be neglected (go to next verification)

Amount of FRP needed to fulfil concrete stress. This depends on the value of u_f.

Take u_f as large as possible $u_{f.max.possible} := 200 \cdot mm$

$\rho_{f.min.w} := \text{root}\left[\left[\frac{10.1 \cdot \zeta}{mm} \cdot \rho_{c.eff} \frac{M_{kS.qp}}{E_s \cdot d \cdot \left(\rho_s + \frac{E_f}{E_s} \cdot \rho g\right)} - 1.44 \cdot u_s\right] - u_{f.max.possible}, \rho g\right]$

$A_{f.min.w} := \rho_{f.min.w} \cdot b \cdot d$ $A_{f.min.w} = \ mm^2$

Choose new value if needed:

Number of layers $n_f := 1$ $A_f := n_f \cdot t_f \cdot u_f$ $A_f = 240.00\ mm^2$

$\rho_f := \frac{A_f}{b \cdot d}$ $\rho_f = 0.07\ ‰$ $\rho\rho_f := \frac{A_f}{b_w \cdot d}$ $\rho\rho_f = 0.22\ ‰$

ULS for debonding failure

Peeling due to vertical crack displacement

Assume value for L, or update the value after the anchorage detailing calcultion (see below)

$L := 50 \cdot mm$

$\rho\rho_{eq} := \rho\rho_{s} + \frac{E_f}{E_s} \cdot \rho\rho_{f}$

$V_{max} := V_{dS} \cdot \frac{\frac{l}{2} - (a + L + 0.9 \cdot d)}{\frac{l}{2}}$ $\quad V_{max} = 177.77 \cdot kN$

$V_{Rpd} := \frac{(0.38 + 151 \cdot \rho\rho_{eq}) \cdot MPa}{\gamma_c} \cdot b_w \cdot d$ $\quad V_{Rpd} = 294.52 \cdot kN$

$if(V_{Rpd} \geq V_{max}, "OK", "risk of peeling") = "OK"$

If "OK" the following calculation may be neglected (go to next verification)

Amount of FRP needed to fulfil the peeling condition.

$$\rho\rho_{f.min.p} := root\left[V_{max} - \frac{\left[0.38 + 151 \cdot \left(\rho\rho_{s} + \frac{E_f}{E_s} \cdot \rho g \right) \right] \cdot MPa}{\gamma_c} \cdot b_w \cdot d, \rho g \right]$$

$A_{f.min.p} := \rho\rho_{f.min.p} \cdot b_w \cdot d$ $\quad A_{f.min.p} = -1166 \cdot mm^2$

Choose new value if needed:

Number of layers $n_f := 1$ $\quad A_f := n_f \cdot t_f \cdot u_f$ $\quad A_f = 240.00 \cdot mm^2$

$\rho_f := \frac{A_f}{b \cdot d}$ $\quad \rho_f = 0.07 \cdot \%$ $\quad \rho\rho_f := \frac{A_f}{b_w \cdot d}$ $\quad \rho\rho_f = 0.22 \cdot \%$

Force transfer

Guess value $tg := 0.2$

Mean lever arm of tensile reinforcements $z := 0.95 \cdot d$

$f_{cbd} := 1.8 \cdot \frac{f_{ctk}}{\gamma_c}$

$N_{yd} := A_s \cdot f_{yd}$ $\quad M_{yd} := N_{yd} \cdot z \cdot \left(1 + \frac{A_f \cdot E_f}{A_s \cdot E_s} \right)$ $\quad M_{yd} = 381.20 \cdot kN \cdot m$

$t_y := root\left[M_{yd} - 4 \cdot M_{dS} \cdot tg \cdot (1 - tg), tg \right]$

$x_y := t_y \cdot l - \frac{z}{2}$ $\quad x_y = 2883 \cdot mm$

$$V_{max.y} := V_{dS} \cdot \frac{\frac{l}{2} - \left(x_y + 0.9 \cdot d\right)}{\frac{l}{2}} \qquad V_{max.y} = 36.4 \cdot kN$$

Zone for which the steel is yielding

$$V_{Rbd1} := f_{cbd} \cdot u_f \cdot 0.95 \cdot d \qquad V_{Rbd1} = 153.5 \cdot kN$$

$$if\left(V_{Rbd1} \geq V_{max.y}, \text{"OK"}, \text{"risk of bond failure"}\right) = \text{"OK"}$$

Zone for which the steel is not yielding

$$V_{Rbd2} := f_{cbd} \cdot u_f \cdot 0.95 \cdot d \cdot \left(1 + \frac{A_s \cdot E_s}{A_f \cdot E_f}\right) \qquad V_{Rbd2} = 2055.4 \cdot kN$$

$$if\left(V_{Rbd2} \geq V_{max}, \text{"OK"}, \text{"risk of bond failure"}\right) = \text{"OK"}$$

If "risk of bond failue": maximize u_f

Curtailment and anchorage length

Theoretical point of curtailment so that internal steel can take over:

$$M_{curtail} := N_{yd} \cdot z \qquad M_{curtail} = 352.74 \cdot kN \cdot m$$

$$t := root\left[M_{curtail} - 4 \cdot M_{dS} \cdot tg \cdot (1 - tg), tg\right]$$

$$x := t \cdot l - \frac{z}{2} \qquad x = 2393 \cdot mm$$

FRP force to be anchored at that location

$$N_{fad} := \frac{M_{curtail}}{z \cdot \left(1 + \frac{A_s \cdot E_s}{A_f \cdot E_f}\right)} \qquad N_{fad} = 63.73 \cdot kN$$

Maximum force which can be anchored

$$k_b := 1.06 \cdot \sqrt{\frac{2 - if\left(\frac{u_f}{b_w} \geq 0.5, \frac{u_f}{b_w}, 0.5\right)}{1 + \frac{u_f}{400 \cdot mm}}} \qquad k_b = 0.95$$

$$N_{fa.max} := 0.9 \cdot k_b \cdot u_f \cdot \sqrt{2 \cdot 0.202 \cdot mm \cdot f_{ctm} \cdot E_f \cdot n_f \cdot t_f} \qquad N_{fa.max} = 71.76 \cdot kN$$

$$if\left(N_{fa.max} \geq N_{fad}, \text{"OK"}, \text{"not OK"}\right) = \text{"OK"}$$

If "OK", provide anchor length: Guess value $lg := 150 \cdot mm$

$$l_{t.max} := 0.7 \cdot mm^{0.5} \cdot \sqrt{\frac{E_{fu} \cdot t_f}{0.7 \cdot f_{ctm}}} \qquad l_{t.max} = 254 \cdot mm$$

$$l_t := root\left[N_{fad} - N_{fa.max} \frac{lg}{l_{t.max}} \cdot \left(2 - \frac{lg}{l_{t.max}} \right), lg \right]$$

Length FRP $l_{f.min} := l - 2 \cdot x + 2 \cdot l_t \qquad l_{f.min} = 3552 \cdot mm$

Free length $L := \frac{l - l_{f.min}}{2} - a \qquad L = 2203 \cdot mm$

$$if(L \geq 0, "OK", "apply\ mechanical\ anchor") = "OK"$$

If "not OK", calculte new theoretical point of curtailment:

$$M_{curtail} := z \cdot N_{fa.max} \cdot \left(1 + \frac{A_s \cdot E_s}{A_f \cdot E_f} \right) \qquad M_{curtail} = 397.2 \cdot kN \cdot m$$

$$t := root\left[M_{curtail} - 4 \cdot M_{dS} \cdot tg \cdot (1 - tg), tg \right]$$

$$x := t \cdot l - \frac{z}{2} \qquad x = 3356 \cdot mm$$

Length FRP $l_{f.min} := l - 2 \cdot x + 2 \cdot l_t \qquad l_{f.min} = 1626 \cdot mm$

Free length $L := \frac{l - l_{f.min}}{2} - a \qquad L = 3166 \cdot mm$

$$if(L \geq 0, "OK", "apply\ mechanical\ anchor") = "OK"$$

Choose length of FRP and corresponding value of L. $L := 2200 \cdot mm$

Concrete rip-off

$$a_L := \left[\frac{\left(1 - \sqrt{\rho\rho_s} \right)^2}{\rho\rho_s} \cdot L^3 \cdot d \right]^{\frac{1}{4}}$$

$$\tau_{R.rip} := \left[0.15 \cdot \left(3 \cdot \frac{d}{a_L} \right)^{\frac{1}{3}} \cdot \left(1 + \sqrt{\frac{200 \cdot mm}{d}} \right) \cdot \left(100 \cdot \rho\rho_s \cdot \frac{f_{ck}}{MPa} \right)^{\frac{1}{3}} \right] \cdot MPa \qquad \tau_{R.rip} = 0.65 \cdot MPa$$

$$V_{R.rip} := \tau_{R.rip} \cdot b_w \cdot d \qquad V_{R.rip} = 70.22 \cdot kN$$

$$if(V_{R.rip} \geq V_{max}, "OK", "risk\ of\ concrete\ rip\text{-}off") = "risk\ of\ concrete\ rip\text{-}off"$$

If "OK" the following calculation may be neglected

L needs to be reduced: calculation of new value for L.

Guess valu $Lg := 20 \cdot mm$

$$a_L(L) := \left[\frac{\left(1 - \sqrt{\rho\rho_s}\right)^2}{\rho\rho_s} \cdot L^3 \cdot d \right]^{\frac{1}{4}}$$

$$\tau_{R.ripp}(L) := \left[0.15 \cdot \left(3 \cdot \frac{d}{a_L(L)} \right)^{\frac{1}{3}} \cdot \left(1 + \sqrt{\frac{200 \cdot mm}{d}} \right) \cdot \left(100 \cdot \rho\rho_s \cdot \frac{f_{ck}}{MPa} \right)^{\frac{1}{3}} \right] \cdot MPa$$

$$L := root\left[\tau_{R.ripp}(Lg) \cdot b_w \cdot d - V_{dS} \cdot \frac{\frac{l}{2} - (a + Lg + 0.9 \cdot d)}{\frac{l}{2}}, Lg \right] \qquad L = 54 \cdot mm$$

Choose final value for the length of the FRP and the correspondig value for L.
Update calculation of peeling at veritcal crack displacement if needed. $L := 50 \cdot mm$

PART D: ACCIDENTAL SITUATION

Concrete stress block parameters

$$\lambda 1(\xi) := if\left(\xi < \xi_{lim1s}, \frac{0.002}{\varepsilon_{su}} \cdot \frac{1 - \xi}{\xi}, \frac{0.002}{\varepsilon_{cu}} \right)$$

$$\lambda 2(\xi) := if\left(\xi < \xi_{lim1s}, \frac{0.002}{\varepsilon_{su}} \cdot \frac{\xi}{\xi - \delta} \cdot \frac{1 - \xi}{\xi}, \frac{0.002}{\varepsilon_{cu}} \cdot \frac{\xi}{\xi - \delta} \right)$$

$$\psi 1(\xi) := if\left(\lambda 1(\xi) \geq 1, \frac{3 \cdot \lambda 1(\xi) - 1}{3 \cdot \lambda 1(\xi)^2}, 1 - \frac{\lambda 1(\xi)}{3} \right)$$

$$\psi 2(\xi) := if\left(\lambda 2(\xi) \geq 1, \frac{3 \cdot \lambda 2(\xi) - 1}{3 \cdot \lambda 2(\xi)^2}, 1 - \frac{\lambda 2(\xi)}{3} \right)$$

$$\psi(\xi) := if\left[\xi \leq \delta, \psi 1(\xi), \psi 1(\xi) - \psi 2(\xi) \cdot (1 - \beta) \cdot \left(1 - \frac{\delta}{\xi} \right) \right]$$

$$\delta 1_g(\xi) := if\left[\lambda 1(\xi) \geq 1, \frac{4 \cdot \lambda 1(\xi) - 1}{4 \cdot (3 \cdot \lambda 1(\xi) - 1)}, \frac{\lambda 1(\xi)^2 - 4 \cdot \lambda 1(\xi) + 6}{4 \cdot (3 - \lambda 1(\xi))} \right]$$

$$\delta 2_g(\xi) := if\left[\lambda 2(\xi) \geq 1, \frac{4 \cdot \lambda 2(\xi) - 1}{4 \cdot (3 \cdot \lambda 2(\xi) - 1)}, \frac{\lambda 2(\xi)^2 - 4 \cdot \lambda 2(\xi) + 6}{4 \cdot (3 - \lambda 2(\xi))} \right]$$

$$\delta_g(\xi) := if\left[\xi \leq \delta, \delta 1_g(\xi), \frac{\left[\psi 1(\xi) \cdot \delta 1_g(\xi) - \psi 2(\xi) \cdot \delta 2_g(\xi) \cdot (1 - \beta) \cdot \left(1 - \frac{\delta}{\xi} \right)^2 - \psi 2(\xi) \cdot (1 - \beta) \cdot \left(1 - \frac{\delta}{\xi} \right) \cdot \frac{\delta}{\xi} \right]}{\psi(\xi)} \right]$$

Nominal value resisting moment

$$\xi_n := \text{root}\left(\frac{\xi g \cdot \psi(\xi g) \cdot f_{ck}}{f_{yk}} - \rho_s, \xi g\right)$$

$$\mu_A := \xi_n \cdot \psi\left(\xi_n\right) \cdot \left(1 - \delta_g\left(\xi_n\right) \cdot \xi_n\right)$$

$$M_A := \mu_A \cdot b \cdot d^2 \cdot f_{ck} \qquad M_A = 425.33 \cdot \text{kN} \cdot \text{m}$$

In the case of accidental loss of the FRP EBR:

$$\text{if}\left(M_A \geq M_{kS.r}, \text{"no collapse"}, \text{"collapse"}\right) = \text{"no collapse"}$$